Neutrino Masses and Lepton Flavor Physics Beyond the Standard Model

Tesi Doctoral

Programa de Doctorat en Física - 3126

Pablo Escribano Valiente

Director: Dr. Avelino Vicente Montesinos

IFIC - CSIC/Universitat de València
Departament de Física Teòrica

València, juny de 2023

A mis padres, por su apoyo incondicional.
A mi abuelo, por su aliento constante,
aunque nunca entendiera lo que hacía.
A Paloma, por lo mismo y por todo lo
demás.

Dr. Avelino Vicente Montesinos,
Investigador Ramón y Cajal en la Universitat de València

como director de tesis y tutor,

CERTIFICA:

Que la presente memoria, *Neutrino Masses and Lepton Flavor Physics Beyond the Standard Model*, ha sido realizada bajo su dirección en el Instituto de Física Corpuscular, centro mixto de la Universitat de València y del Consejo Superior de Investigaciones Científicas, por Pablo Escribano Valiente, y constituye su Tesis para optar al grado de Doctor por la Universitat de València una vez cursados los estudios en el Doctorado en Física.

Y para que así conste, en cumplimiento de la legislación vigente, presenta en el Departament de Física Teòrica de la Universidad de Valencia la referida Tesis Doctoral, y firma el presente certificado.

Valencia, a día 12 de junio de 2023.

Avelino Vicente Montesinos

Agradecimientos

Podría comenzar este breve texto de muchas maneras, pero no encuentro ninguna mejor que citar a Gandalf, en aquel entonces conocido como *el Gris*, quien en una ocasión pronunció estas palabras: "Es peligroso... cruzar tu puerta. Pones tu pie en el camino, y si no cuidas tus pasos, nunca sabes a dónde te pueden llevar". No estoy seguro de si fui lo suficientemente cuidadoso, pero el camino me ha llevado hasta la etapa final de un doctorado que parece haber comenzado ayer. De esta manera, me encuentro escribiendo las últimas líneas de la tesis (aún apareciendo al principio) y es el momento de hacer memoria. De rememorar para agradecer a todas aquellas personas que de una manera u otra han aportado a este momento. Sin ellas, esta experiencia no habría resultado tan maravillosa.

Al plasmar estas palabras y reflexionar sobre los últimos años, soy más consciente de la función que mi familia ha desempeñado en este proceso. A pesar de no siempre ver las cosas desde la misma perspectiva, han sido un apoyo constante. Les agradezco a mis padres por todo lo que me han aportado, por sus esfuerzos, por la educación que me han proporcionado y por haberme ayudado a elegir libremente cada paso de mi camino. Igualmente, agradezco a mi hermano, que siempre estará ahí cuando necesite su ayuda.

Rápidamente me viene a la mente Avelino cuando pienso en quienes más me han ayudado en esta fase de mi vida. Todo lo que he aprendido durante estos cuatro años de tesis no habría sido posible sin la supervisión de mi director. Muchísimas gracias por siempre haber encontrado tiempo para charlar, para aconsejarme y para enseñarme, especialmente durante los meses de confinamiento en los que estuviste constantemente presente. No podría haber tenido un director mejor.

Asimismo, quisiera agrader a todos los miembros de la familia AHEP por el excepcional ambiente que han creado. Estoy especialmente agradecido con Pablo II por haberme acompañado de principio a fin. Agradezco de corazon todas las conversaciones, el intercambio de inquietudes y, en especial, la presión indirecta que me motivó a no posponer la tesis hasta el último momento. Gracias a Pablo IV, Jorge y Mario por el tiempo compartido en el despacho, actualmente conocido como *Pabloficina*. También a Omar, Rebeca, Antonio, Víctor, Gonzalo, Julio y Valentina por todos los buenos ratos. A cada uno de vosotros y a todos los demás, ha sido un auténtico placer cruzar caminos.

Por supuesto, el doctorado me ha brindado la posibilidad de entablar vínculos y colaborar con personas realmente increíbles, así como viajar mucho. Nunca olvidaré los tres meses que pasé en París (tres años desde el sistema de referencia del Colegio de España). Estoy profundamente agradecido con Asmaa por lo mucho que se involucró con mi llegada al IJCLab. También con Gio, por por su paciencia al responder mis dudas repetidas veces, y con el resto del grupo, que fue muy acogedor. Imborrable será todo lo vivido en el Colegio de España, así como las personas que tuve la fortuna de conocer. Gracias infinitas a Adri, Alberto, Carlos, Elena, Íñigo, Josemi, Josep, *Josetrón*, Maru, Rubén y Samu por hacer de París una experiancia mágica e irrepetible (también surrealista).

A vosotros, Lloria, David, Celia y Pilar, os agradezco que sigáis ahí después de tanto tiempo, que se pueda contar con vosotros para cualquier cosa y que siempre intentéis encontrar un hueco para que nos veamos. Es un auténtico privilegio teneros.

Llegar hasta aquí no habría sido posible sin la persona más importante en mi vida. Gracias Paloma por tu apoyo inagotable en todo momento. Por escucharme y aconsejarme siempre que lo he necesitado. Por todo lo vivido a lo largo de tantos años. Gracias infinitas por ser parte de mi vida.

One of the final steps of the doctoral journey is the evaluation of the manuscript by the members of the jury. Therefore, I want to thank all of them for their time and dedication. Además, agradezo al Ministerio de Ciencia, Innovación y Universidades (MICIU) por su apoyo económico mediante las ayudas para contratos predoctorales para la formación de doctores con referencia PRE2018-084599.

Me gustaría agradecerle también al COVID-19 por haberme hecho sentir como en casa durante el inicio de mi doctorado. Asimismo, doy las gracias a Lupe y Emilio por adoptarme durante esos primeros meses de pandemia.

Así pues, quisiera poner el punto final agradeciéndole a todo aquel que haya tenido el valor (o la obligación) de leerse esta tesis. ¡Gracias!

List of scientific publications

This thesis is based on the following publications:

1. ***Generalizing the Scotogenic model***
   P. Escribano, M. Reig, A. Vicente
   Journal: JHEP 07 (2020) 097
   Preprint: 2004.05172

2. ***Ultralight scalars in leptonic observables***
   P. Escribano, A. Vicente
   Journal: JHEP 03 (2021) 240
   Preprint: 2008.01099

3. $(\mathbf{g-2})_{e,\mu}$ ***in an extended inverse type-III seesaw***
   P. Escribano, J. Terol-Calvo, A. Vicente
   Journal: Physical Review D 103 (2021), 115018
   Preprint: 2104.03705

4. ***An ultraviolet completion for the Scotogenic model***
   P. Escribano, A. Vicente
   Journal: Physics Letters B 823 (2021) 136717
   Preprint: 2107.10265

5. ***Observable flavor violation from spontaneous lepton number breaking***
   P. Escribano, Martin Hirsch, Jacopo Nava, A. Vicente
   Journal: JHEP 01 (2022) 098
   Preprint: 2108.01101

6. ***Collider Searches for Heavy Neutral Leptons: beyond simplified scenarios***
   A. Abada, P. Escribano, X. Marcano, G. Piazza
   Journal: EPJ C 82, 1030 (2022)
   Preprint: 2208.13882

7. ***Neutrino masses, flavor anomalies and muon $g-2$ from dark loops***
   R. Cepedello, P. Escribano, A. Vicente
   Journal: Physical Review D 107 (2023), 035034
   Preprint: 2209.02730

8. ***Ultraviolet extensions of the Scotogenic model***
   D. Portillo-Sánchez, P. Escribano, A. Vicente
   Journal: JHEP 08 (2023) 023
   Preprint: 2301.05249

Other publications not included here:

1. ***A Scotogenic explanation for the 95 GeV excesses***
   P. Escribano, V. M. Lozano, A. Vicente
   Preprint: 2306.03735

Contents

List of Acronyms

AMM	Anomalous Magnetic Moment
ALP	Axion-Like Particle
BFB	Bounded From Below
CKM	Cabibbo-Kobayashi-Maskawa
CP	Charge Conjugation times Parity
DM	Dark Matter
EDM	Electric Dipole Moment
EW	Electroweak
HNL	Heavy Neutral Lepton
IO	Inverted Ordering
ISS1	Inverse Type-I Seesaw
ISS3	Inverse Type-III Seesaw
NO	Normal Ordering
LHC	Large Hadron Collider
LFV	Lepton Flavor Violation
LNC	Lepton Number Conservation
LNV	Lepton Number Violation
LSS	Linear Seesaw
NP	New Physics
OS	Opposite Sign
OSSF	Opposite-Sign Same-Flavor
PMNS	Pontecorvo-Maki-Nakagawa-Sakata
QCD	Quantum Chromodynamics
QED	Quantum Electrodynamics
QFT	Quantum Field Theory
RGEs	Renormalization Group Equations
SM	Standard Model
SS	Same Sign
SSSF	Same-Sign Same-Flavor
SSB	Spontaneous Symmetry Breaking

SS1	Type-I seesaw
SS2	Type-II Seesaw
SS3	Type-III Seesaw
UV	Ultraviolet
VEV	Vacuum Expectation Value
VEB	Valor d'Expectació del Buit
VL	Vector-Like
ME	Model Estàndard
BSM	Beyond the Standard Model
ISS3VL	Inverse Type-III Seesaw plus 2 Vector-Like Leptons

Introduction

The study of fundamental particles and their interactions has been one of the most fascinating and captivating fields of scientific research over the last century. Currently, our understanding of matter is described by the Standard Model of particle physics, which provides an incredibly accurate picture of Nature at the subatomic level. Nevertheless, even with its remarkable success, the model falls short of explaining certain crucial experimental results. Thus, Beyond the Standard Model physics is an active area of research where physicists are searching for a more comprehensive theory that can explain the existing discrepancies between the Standard Model predictions and the experimentally measured quantities.

One of the most notable shortcomings of the Standard Model is its prediction of massless neutrinos, which contradicts the experimental detection of neutrino oscillations. The experimental observation of this phenomenon undoubtedly confirms the existence of non-zero neutrino masses and Lepton Flavor Violation. However, whether neutrinos are Dirac or Majorana particles and which is the mechanism behind the generation of their tiny masses, remain a mystery. This motivates researchers to delve deeper and go beyond the currently established theory in order to provide an explanation to the open questions.

Moreover, it is particularly appealing to connect the neutrino mass mechanism to other unresolved questions that also deserve attention. These include the long-standing discrepancy between the Standard Model prediction for the muon anomalous magnetic moment and its experimentally determined value and the more recent deviation for the electron case, the measurements of observables involving B-meson decays that do not align with the theoretical predictions, as well as the nature of the Dark Matter of the Universe.

The work presented in the present thesis has primarily focused on studying and proposing models that include neutrino mass mechanisms. The thesis can be divided into four parts, each covering a specific aspect of the research. The first part comprises Chapters 1 and 2. Chapters 1 introduces the Standard Model, focusing on the electroweak theory and the Higgs mechanism, and discusses some of the problems of the model. In Chapter 2, neutrino flavor oscillations and the possible nature of these particles are discussed, along with a review of some of the most important neutrino mass mechanisms.

The second part begins with Chapter 3, where the possible contributions of new ultralight scalars to many leptonic observables are computed, taking a model-independent approach. In Chapters 4, 5, and 6, we propose different neutrino mass models aimed at accommodating some

of the other anomalies presented above, although the main goal of the model in Chapter 6 was to include sizable Lepton Flavor Violating signatures.

Part three includes Chapters 7 and 8, which are based on some model-building works. Chapter 7 introduces the *general Scotogenic model* with arbitrary numbers of generations of the Scotogenic states, while Chapter 8 classifies all possible ultraviolet extensions of the Scotogenic model satisfying specific requirements.

Chapter 9 constitutes the fourth part of the thesis. Here, we discuss how the available experimental bounds on the mixings of hypothetical Heavy Neutral Leptons with the Standard Model neutrinos from LHC searches can be recast when considering more generic mixing patterns.

Finally, several appendices can be found at the end of the document with details on many topics discussed throughout the whole thesis. These appendices may be valuable for readers interested in the technical details of the works.

Part I

Introduction and Motivation

Chapter 1

The Standard Model of particle physics

"Never underestimate the joy people derive from hearing something they already know."

– Enrico Fermi

1.1 Introduction

Throughout the latter half of the 20$^{\text{th}}$ century, a comprehensive theory describing the behavior of subatomic particles and the interactions among them through the exchange of other particles known as bosons was developed. This framework, known as the Standard Model of particle physics (SM) [1–3], is considered one of the most successful theories ever constructed, offering an excellent description of numerous experimental results that physicists have measured over the years. Nevertheless, the SM has some open questions that must be addressed.

The SM is the culmination of a collective effort by many researchers working in different areas, such as theoretical particle physics and experimental physics. Its construction was a gradual process that took place over several decades, arguably with its origins dating back to 1918. That was when Hermann Weyl introduced the concept of gauge symmetry [4], which played a significant role in the development of the SM. But it was not important just for the SM but also for the development of Quantum Electrodynamics (QED) [5–8]. QED is a relativistic quantum field theory (QFT) of the electromagnetic force describing how charged particles interact between them and with the electromagnetic field. Although its principles were proposed during the 1920s, it was in the late 1940s that it was fully developed and refined independently by Richard P. Feynman, Julian S. Schwinger and Shin'ichirō Tomonaga [5–8].

Later on, in the early 1950s, Chen Ning Yang and Robert Mills proposed the Yang-Mills (YM) theory [9], consisting of an extension of the QED theory. Similar to the theory of electrodynamics, where the electromagnetic interaction is mediated by photons, the YM theory allows for new interactions between subatomic particles also mediated by the exchange of other particles. These particles were named gauge bosons. This framework turned out to constitute the foundation of the SM.

In the 1970s, Sheldon Glashow, Abdus Salam, and Steven Weinberg proposed the electroweak (EW) theory, successfully unifying both electromagnetic and weak nuclear forces into a single framework [1, 2, 10, 11]. This theory is, precisely, a YM theory based on the gauge group $\mathrm{SU}(2) \times \mathrm{U}(1)$ and is generally regarded as a milestone for the development of the SM. Creating the EW theory was already a breakthrough; however, another fundamental force of Nature remained to be unified. Of course, we are talking about the strong nuclear force.

The theoretical framework describing the properties of the strong force was presented in the 1970s and received the name of Quantum Chromodynamics (QCD) [12–14]. It took nearly a decade for it to be considered complete and self-consistent. QCD was heavily influenced by other theories, such as the YM theory and QED, being itself an extension of the former based on the SU(3) gauge group. It was built upon the quark model independently developed by Murray Gell-Mann and George Zweig in the 1960s [15, 16]. [1] In summary, the model assumed that hadrons [2] are made up of combinations of more fundamental particles, the quarks. In contrast to hadrons, such as protons and neutrons, quarks have a fractional electric charge and are held together within composite particles thanks to the strong force. The model could explain the large number of baryons and mesons that experiments observed back then. It was even able to make precise predictions that were verified by comparison with experimental data.

Therefore, the SM is the unification of the electroweak theory and quantum chromodynamics as a coherent theory obeying an intricate set of symmetries. However, in the first stages of the theory, there was a big problem related to the masses of the bosons mediating the weak force, the weak gauge bosons W and Z. The model predicted both of them to be massless, in contrast with what the experiments showed. That is why Peter Higgs, Robert Brout and François Englert and Gerald Guralnik, C. Richard Hagen and Tom Kibble, independently proposed what nowadays is known as the Higgs mechanism [17–19]. The underlying idea is that particles in the SM acquire their mass by interacting with a new field called the Higgs field. Its associated particle, the so-called Higgs boson, was discovered in 2012 at CERN's Large Hadron Collider (LHC) [20, 21], completing the SM puzzle.

[1] Gell-Mann's proposal was more succesful than Zweig's, being the one adopted by the physics community. However, both physicists were considered the fathers of the model.

[2] Hadrons are particles that interact strongly. There are two types of hadrons: baryons, composed by three quarks, and mesons, composed by just two quarks.

1.2 Particle content and their interactions

The majority of what we know about matter and its interactions at the most fundamental level is summarised in the Standard Model of particle physics. This theoretical framework can describe three of the four fundamental forces present in Nature. It includes electromagnetism and weak and strong interactions, but not gravity. Being a gauge theory, the SM is based on the symmetry group

$$\mathrm{SU(3)_C} \times \mathrm{SU(2)_L} \times \mathrm{U(1)_Y}\,. \tag{1.1}$$

The forces are mediated by the exchange of spin-1 gauge bosons: the strong sector is characterized by the group $\mathrm{SU(3)_C}$ and its associated 8 massless gauge fields, the gluons, while the electroweak block relies on the $\mathrm{SU(2)_L} \times \mathrm{U(1)_Y}$ symmetry, with 3 $\mathrm{SU(2)_L}$ W gauge bosons and 1 $\mathrm{U(1)_Y}$ B gauge boson. The strong $\mathrm{SU(3)_C}$ piece is out of the scope of this thesis but a detailed discussion can be found, for instance, in Refs. [22, 23].

Regarding the matter content of the model, it includes 12 spin-1/2 fermions plus their associated antiparticles. Depending on whether they are charged under $\mathrm{SU(3)_C}$ or not, these fermions can be classified into six flavors of quarks (up u, down d, charm c, strange s, top t, and bottom b) and six flavors [3] of leptons (electron e, electron neutrino ν_e, muon μ, muon neutrino ν_μ, tau τ, and tau neutrino ν_τ). Each quark flavor can have three different colors (red, green, and blue), resulting in $3 \times 6 = 18$ types of quarks. Despite having a large number of particles, the classification can be easily simplified by casting the particles as $\mathrm{SU(2)_L}$ doublets and singlets. For quarks,

$$\begin{gathered} q_L = \begin{pmatrix} u \\ d \end{pmatrix}_L , \begin{pmatrix} c \\ s \end{pmatrix}_L , \begin{pmatrix} t \\ b \end{pmatrix}_L , \\ u_R = u_R\,,\ c_R\,,\ t_R\,, \qquad d_R = d_R\,,\ s_R\,,\ b_R\,, \end{gathered} \tag{1.2}$$

while for leptons,

$$\ell_L = \begin{pmatrix} \nu_e \\ e \end{pmatrix}_L , \begin{pmatrix} \nu_\mu \\ \mu \end{pmatrix}_L , \begin{pmatrix} \nu_\tau \\ \tau \end{pmatrix}_L , \qquad e_R = e_R\,,\ \mu_R\,,\ \tau_R\,. \tag{1.3}$$

Notice that the SM is a chiral theory, left-handed fields transform as $\mathrm{SU(2)_L}$ doublets while their right-handed partners are $\mathrm{SU(2)_L}$ singlets. Therefore, both left- and right-handed fields transform differently under the gauge group of the model. The three families encompassed in the multiplets have identical properties differing only by their masses and flavor numbers. Notice, however, that there are no right-handed neutrinos in the theory. This will have important consequencies later. In the following, we will use e_R to refer to the three generations of right-handed leptons.

[3] We will talk about flavor in Section 1.4.

Field	**Generations**	**Spin**	$SU(3)_C$	$SU(2)_L$	$U(1)_Y$
q_L	3	1/2	**3**	**2**	1/6
u_R	3	1/2	**3**	**1**	2/3
d_R	3	1/2	**3**	**1**	-1/3
ℓ_L	3	1/2	**1**	**2**	-1/2
e_R	3	1/2	**1**	**1**	-1
H	1	0	**1**	**2**	1/2
B boson	1	1	**1**	**1**	0
W bosons	1	1	**1**	**3**	0
gluons	1	1	**8**	**1**	0

Table 1.1: Lepton, scalar, and boson particle content of the SM, including the number of generations, the spin and the representations under the gauge symmetries. q_L and ℓ_L and u_R, d_R, and e_R are the SM left- and right-handed fermions, respectively, and H is the SM Higgs boson. B and W are the $SU(2)_L \times U(1)_Y$ bosons while the gluons are the $SU(3)_C$ bosons.

Finally, a well-known problem of Yang-Mills theories is that particles transforming non-trivially under the gauge group cannot have a mass in the traditional sense. Gauge invariance forbids mass terms. Instead, masses of fermions and gauge bosons arise from interactions between particles after the symmetry is broken. For this to happen, a scalar $SU(2)_L$ doublet must be added to the particle content of the model. Once it acquires a vacuum expectation value (VEV), the electroweak gauge symmetry is spontaneously broken to the electromagnetic subgroup, generating the masses of the weak gauge bosons and fermions. This mechanism is known as Spontaneous Symmetry Breaking (SSB) and the new scalar added to the model is the so-called Higgs doublet.

The complete particle content of the model as well as the quantum numbers under the SM symmetries are shown in Table 1.1.

1.2.1 Gauge Invariance

We have previously mentioned the concept of *gauge invariance* and, in this section, we will delve deeper into its meaning. Gauge invariance is a fundamental concept in physics. It refers to the symmetry of a physical system under a particular type of local transformations, known as gauge transformations. Indeed, it is a fundamental pillar for the SM. In the following, we will show how QED and the EW theory were constructed using this principle.

1.2.1.1 Quantum Electrodynamics

We will now see the method of deriving the QED Lagrangian from the current perspective, that is, through gauge symmetries. We will start from the free Dirac Lagrangian for an arbitrary

fermion

$$\mathcal{L}_\psi = \bar{\psi}(i\partial\!\!\!/ - m)\psi\,, \tag{1.4}$$

where ψ is the spinor of the fermion, m is its mass, and $\partial\!\!\!/ \equiv \gamma^\mu\partial_\mu$. Although this Lagrangian is invariant under global phase transformations, the derivative term prevents the symmetry from being local. However, it is this local symmetry that we aim to impose on our Lagrangian.

Let us hypothesize a local U(1) transformation, that is, a local phase transformation,

$$\psi(x) \to \psi'(x) = e^{-i\,Q\,\alpha(x)}\psi(x)\,, \tag{1.5}$$

where $\alpha(x)$ is an arbitrary real function and Q an arbitrary constant. After applying it to the free Lagrangian we obtain

$$\mathcal{L}_\psi \to \mathcal{L}'_\psi = \mathcal{L}_\psi + Q\,\left[\partial^\mu\alpha(x)\right]\bar{\psi}\gamma_\mu\psi\,. \tag{1.6}$$

This implies that once we choose a phase convention at a specific reference point in space-time, the same convention must be consistently applied at all space-time points for the physics of the system to be consistent. The requirement that the U(1) phase invariance should hold locally is referred to as the *gauge principle*. Therefore, if we want the transformation to leave the Lagrangian invariant, we must add an extra field transforming in such a way as to cancel the $\partial^\mu\alpha\,(x)$ in Eq. (1.6),

$$A_\mu \to A'_\mu = A_\mu + \frac{1}{e}\partial_\mu\alpha(x)\,. \tag{1.7}$$

We also define the covariant derivative

$$D_\mu \equiv \partial_\mu + i\,e\,Q\,A_\mu\,, \tag{1.8}$$

that is introduced in the free Dirac Lagrangian by replacing the usual partial derivative with the covariant derivative,

$$\mathcal{L}_\psi = \bar{\psi}(iD\!\!\!/ - m)\psi\,. \tag{1.9}$$

With the new field and its transformation, it is straightforward to check that the Lagrangian is now invariant. What happens, and that is the reason why the covariant derivative is truly useful, is that $D_\mu\psi$ transforms exactly as ψ.

This symmetry transformation is known as the gauge symmetry of the U(1) group, and the field we have introduced is a gauge field. In particular, if the constant $e\,Q$ introduced in the covariant derivative is the electric charge of the fermion ψ, the new field A_μ corresponds to the electromagnetic field, with the photon its associated particle. Note that the interaction between the Dirac fermion and the electromagnetic field, which is nothing but the usual QED vertex, has been generated by the gauge principle.

To complete the construction of the gauge invariant Lagrangian, we need to add a gauge invariant kinetic term for the gauge field,

$$\mathcal{L}_{\text{Kin}} = -\frac{1}{4} F_{\mu\nu} F^{\mu\nu} \,, \tag{1.10}$$

where $F_{\mu\nu} = \partial_\mu A_\nu - \partial_\nu A_\mu$ is the electromagnetic field tensor as in classical electrodynamics. Notice that a possible mass term for the gauge field, $\mathcal{L}_m = \frac{1}{2} m_A^2 A^\mu A_\mu$ is forbidden because it would violate the local U(1) symmetry. This feature is common to any gauge theory. [4] As a result, gauge bosons are predicted to be massless.

The complete Lagrangian of QED is then expressed as

$$\mathcal{L}_{\text{QED}} = -\frac{1}{4} F_{\mu\nu} F^{\mu\nu} + \bar{\psi}(i\partial\!\!\!/ - m)\psi - e\, Q\, \bar{\psi}\gamma^\mu \psi A_\mu \,. \tag{1.11}$$

1.2.1.2 Electroweak Theory

By the time the EW framework was established, weak charged currents were already well-known, and they hinted at the existence of a vectorial charged boson along with its conjugate, $W^\pm$, as the mediator of weak interactions. QED, mediated by the photon, a massless gauge boson, was also familiar to theoretical physicists. Therefore, to unify both the electromagnetic and weak interactions within a single theory, the simplest symmetry with three generators, SU(2), was sought. The idea was to utilize the gauge symmetry principle, which had proven successful for the electromagnetic interaction, but now with a much more ambitious goal.

Considering the Lie algebra of the group, the charges associated with the hypothesized gauge bosons should obey some specific commutation relations. This, however, was not the case and was considered as an indication for the existence of a fourth gauge boson associated with the missing charge. Notably, both weak currents were of the $V - A$ form, while the electromagnetic current was vectorial.

It is reasonable to check the next to the most straightforward option that would provide us with the four desired gauge bosons: SU(2) × U(1) [2]. However, the right-handed fields e_R, u_R, and d_R are only present in the electromagnetic current and do not interact with the SU(2) gauge fields. They are singlets under a new quantum number associated with SU(2), called *weak isospin*. On the contrary, left-handed fields should appear in doublets, as shown in Eqs. (1.2) and (1.3). On the other hand, the electric charge Q could not be the generator of the remaining gauge group U(1) because the SU(2) doublets do not possess a unique electric charge. We require a new quantum number. As seen in Table 1.2, it is clear that both components of ℓ_L and q_L, separately, share the same number of $Y = Q - T_3$, where T_3 is the weak isospin. This Y is referred to as *hypercharge* and will be the generator of the U(1) group. Then, the electroweak

[4] This is, however, strictly only true for non-Abelian gauge groups. An Abelian gauge theory can be made massive while still preserving gauge invariance by introducing a new scalar field. This is known as the Stueckelberg mechanism [24].

	Q	T_3	$\rightarrow$	$Y = Q - T_3$
$\begin{pmatrix} \nu_e \\ e \end{pmatrix}$	0	$+1/2$		$-1/2$
	-1	$-1/2$		$-1/2$
$\begin{pmatrix} u \\ d \end{pmatrix}$	$+2/3$	$+1/2$		$+1/6$
	$-1/3$	$-1/2$		$+1/6$

Table 1.2: Derivation of the U(1) quantum number. Q and T_3 are the electric charge and weak isospin of the particles, respectively.

symmetry group to consider is

$$G \equiv \mathrm{SU(2)_L} \times \mathrm{U(1)_Y}\,, \tag{1.12}$$

where the L refers to left-handed fields and Y to hypercharge.

We are now able to apply the gauge principle to the model. We will focus on a single fermion family for the sake of simplicity. The model includes two types of fields: those transforming as doublets under $\mathrm{SU(2)_L}$, and those that transform as singlets.

$$\begin{aligned} &\text{Doublets:} \quad \psi_D(x) = \begin{pmatrix} u(x) \\ d(x) \end{pmatrix}_L, \begin{pmatrix} \nu_e(x) \\ e(x) \end{pmatrix}_L, \\ &\text{Singlets:} \quad \psi_S(x) = e_R(x)\,,\ u_R(x)\,,\ d_R(x)\,. \end{aligned}$$

Following what we did for QED, we begin by constructing the free Dirac Lagrangian. Then, we impose gauge transformations for the fields according to the symmetry group,

$$\begin{aligned} \psi_D(x) \rightarrow \psi'_D(x) &= e^{iY\beta(x)} U_L(x) \psi_D(x)\,, \\ \psi_S(x) \rightarrow \psi'_S(x) &= e^{iY\beta(x)} \psi_S(x)\,, \end{aligned} \tag{1.13}$$

where $U_L = \exp\left[i\frac{\sigma_i}{2}\alpha_i(x)\right]$, σ_i being the Pauli matrices, generators of the SU(2) group.

To ensure that these transformations truly preserve the symmetry of our Lagrangian, the introduction of the covariant derivative becomes necessary once again. However, this time we will need to include four gauge fields. Also, depending on how the fields transform under the symmetries, the covariant derivatives will be different,

$$\begin{aligned} D_\mu \psi_D(x) &= \left[\partial_\mu - ig\frac{\vec{\sigma}}{2}\vec{W}_\mu(x) - ig\prime Y B_\mu(x)\right]\psi_D(x)\,, \\ D_\mu \psi_S(x) &= \left[\partial_\mu - ig\prime Y B_\mu(x)\right]\psi_S(x)\,. \end{aligned} \tag{1.14}$$

Imposing now that $D_\mu \psi_X(x)$ transforms exactly as ψ_X, it is straightforward to find what transformations the gauge fields satisfy,

$$\begin{aligned} B_\mu \to B'_\mu &= B_\mu + \frac{1}{g'}\partial_\mu \beta(x) \\ \frac{\vec{\sigma}}{2}\vec{W}_\mu \to \frac{\vec{\sigma}}{2}\vec{W}'_\mu &= U_L(x)\left[\frac{\vec{\sigma}}{2}\vec{W}_\mu\right] U_L^\dagger(x) + \frac{i}{g} U_L(x)\partial_\mu U_L^\dagger . \end{aligned} \tag{1.15}$$

Notice that $\vec{W}$ are the generators of a non-Abelian gauge group, and their transformation is not as simple as that of B.

Similar to what we have seen for QED, the kinetic terms of the gauge bosons are given by

$$\mathcal{L}_{\text{Kin}} = -\frac{1}{4} B_{\mu\nu} B^{\mu\nu} - \frac{1}{4} W^i_{\mu\nu} W_i^{\mu\nu} , \tag{1.16}$$

where

$$\begin{aligned} B_{\mu\nu} &= \partial_\mu B_\nu - \partial_\nu B_\mu , \\ W^i_{\mu\nu} &= \partial_\mu W^i_\nu - \partial_\nu W^i_\mu + g\varepsilon^{ijk} W^j_\mu W^k_\nu , \end{aligned} \tag{1.17}$$

are the field tensors. The latter is the generalization for a non-Abelian symmetry.

As a final note for this part, it is worth mentioning that not only the gauge boson mass terms violate gauge invariance, but fermionic mass terms do as well. These terms are proportional to $\bar{\psi}\psi$ and, in the SM, left- and right-handed fields transform differently. So, we have constructed a theory containing both massless vector bosons and fermions.

1.2.2 Charged and neutral vector currents

We already know that the interactions between fermions and gauge bosons are determined by the additional terms included in the covariant derivatives. For the first family of fermions, these are

$$\mathcal{L}_{\text{int}} = g \sum_D \bar{\psi}_D \gamma^\mu \frac{\sigma^i}{2} W^i_\mu \psi_D + g' B_\mu \sum_{j=S,D} Y_j \bar{\psi}_j \gamma^\mu \psi_j , \tag{1.18}$$

where S, D refer to singlet and doublet, respectively. Using the expressions of the Pauli matrices we have

$$\frac{\sigma^i}{2} W^i_\mu = \frac{1}{2}\begin{pmatrix} W^3_\mu & W^1_\mu - iW^2_\mu \\ W^1_\mu + iW^2_\mu & -W^3_\mu \end{pmatrix} \equiv \frac{1}{2}\begin{pmatrix} W^3_\mu & \sqrt{2}W^+_\mu \\ \sqrt{2}W^-_\mu & -W^3_\mu \end{pmatrix} , \tag{1.19}$$

where we have defined the fields $W^\pm_\mu \equiv \frac{1}{\sqrt{2}}\left(W^1_\mu \mp i\, W^2_\mu\right)$, which correspond to the charged bosons mediating the weak interaction. Taking just the terms with the charged weak bosons from Eq. (1.18), we can write the Lagrangian of charged currents describing the coupling between fermions and these bosons,

$$\mathcal{L}_{\text{CC}} = \frac{g}{\sqrt{2}}\left\{ W^+_\mu \left[\bar{u}\gamma_\mu (1-\gamma_5)\, d + \overline{\nu_e}\gamma_\mu (1-\gamma_5)\, e\right] + \text{h.c.}\right\} . \tag{1.20}$$

Regarding neutral currents, there is a mixing between the gauge neutral bosons W^3 and B. The mixing is described by the electroweak mixing angle, also known as the Weinberg angle, θ_W, [5]

$$\begin{pmatrix} W^3_\mu \\ B_\mu \end{pmatrix} = \begin{pmatrix} \cos\theta_W & \sin\theta_W \\ -\sin\theta_W & \cos\theta_W \end{pmatrix} \begin{pmatrix} Z_\mu \\ A_\mu \end{pmatrix} , \tag{1.21}$$

where Z_μ is the neutral weak boson and A_μ is the photon. The value of this angle determines the extent to which the weak and electromegnetic forces are mixed. Then, from the remaining terms in Eq. (1.18), we get the neutral electroweak interactions

$$\begin{aligned} \mathcal{L}^A_{NC} &= \sum_i \bar{\psi}_i(x)\gamma^\mu \left[gT_3 \sin\theta_W + g'Y\cos\theta_W\right] \psi_i(x) A_\mu(x) , \\ \mathcal{L}^Z_{NC} &= \sum_i \bar{\psi}_i(x)\gamma^\mu \left[gT_3 \cos\theta_W - g'Y\sin\theta_W\right] \psi_i(x) Z_\mu(x) , \end{aligned} \tag{1.22}$$

where $T_3 = \sigma_3/2$ when acting on the doublets, and zero when it does on the singlets. Obviously, the first interaction must be identical to that obtained in the last term of Eq. (1.11) for QED. Therefore, using the relation $Q = Y + T_3$, we identify

$$e = g\sin\theta_W = g'\cos\theta_W . \tag{1.23}$$

Finally, we can express the neutral currents in a more simplified form using the previously established relation between the coupling constants and the weak mixing angle.

$$\begin{aligned} \mathcal{L}^A_{NC} &= \sum_i \bar{\psi}_i(x)\gamma^\mu [eQ] \psi_i(x) A_\mu , \\ \mathcal{L}^Z_{NC} &= \frac{e}{\sin\theta_W \cos\theta_w} \sum_i \bar{\psi}_i(x)\gamma^\mu \left(T_3 - Q\sin^2\theta_W\right) \psi_i(x) Z_\mu(x) . \end{aligned} \tag{1.24}$$

To summarize, we have successfully unified the weak and electromagnetic interactions using the gauge principle. However, instead of a single symmetry group, we have two, each with its own independent coupling constant. And this does not consider the strong interaction represented by the QCD part. As a result, the unification is not considered entirely satisfactory. A large number of theoretical physicists are working on the search for *Grand Unified Theories*, models in which, at high energies, the three SM gauge interactions are merged into a single force, and also for the so-called *Theory of Everything*, which aims to describe not only the weak and electromagnetic interactions with a single free coupling constant but all the fundamental forces of Nature, including gravity.

We will present in the next section the Higgs mechanism of spontaneous symmetry breaking, which provides a natural explanation for the masses of the particles in the SM.

[5] Although the mixing angle is known as the Weinberg angle, it was first proposed by Sheldon Lee Glashow, Abdus Salam, and Steven Weinberg, independently, in the 1970s.

1.3 The Higgs Mechanism

So far, we have seen how QED can be incorporated into the same theoretical framework that describes weak interactions. However, the model for electroweak interactions that we constructed has very little to do with reality. Our gauge bosons do not possess a mass. While this, of course, is not a problem for the photon, which is known to be massless, the weak bosons $W^{\pm}$ and Z should be massive.

Before proceeding to the main topic of the section, the Higgs mechanism, we will introduce a crucial concept to understand the Higgs mechanism. Although symmetries play a fundamental role in particle physics, it is not always the case that they are observed in Nature. This is the case for the EW theory. In order for the gauge bosons to get a mass, we need the $\mathrm{SU(2)_L \times U(1)_Y}$ to be broken.

1.3.1 Spontaneous Symmetry Breaking

Symmetry breaking in quantum field theories can happen in two ways: explicitly or spontaneously.

Explicit symmetry breaking occurs when adding a term to the Lagrangian that does not preserve the symmetry. If that term is small, the symmetry is approximately conserved, and the violation of the associated conserved current can only be observed with high experimental precision. However, breaking a gauge symmetry explicitly can lead to several inconsistencies, such as unitarity violation and non-renormalizability. [6] [7] The former may lead to negative probabilities and non-unitary time evolution, meaning that the probability of observing a process is not conserved over time. Fortunately, there is a second possibility to break a symmetry compatible with gauge symmetries: spontaneous symmetry breaking.

Spontaneous symmetry breaking is one of the crucial concepts in the construction of the SM. Unlike explicit symmetry breaking, where there is no exact symmetry from the beginning, the Lagrangian remains invariant under the symmetry in the spontaneous breaking case, but the ground state of the theory does not. In the following, we will refer to the ground state as the *vacuum*. Depending on the nature of the symmetry, SSB may have different implications. In our case, we are interested in the spontaneous breaking of continuous symmetries.

Let us consider the presence of a continuous global symmetry in our Lagrangian. According to the *Goldstone theorem* [26, 27], if there is at least one generator, G, of the symmetry not preserving the vacuum, meaning that it does not maintain the minimum energy state ($G\,|0\rangle \neq |0\rangle$), then the symmetry is said to be spontaneously broken and one massless spin-0 particle will exist for each of the broken generators. These particles are known as Goldston bosons.

[6] A renormalizable theory is one in which the infinities that emerge during calculations can be absorbed into a finite number of parameters of the theory, such as masses and coupling constants. Therefore, one can remove the infinities just by redefining those parameters. On the contrary, a non-renormalizable theory does not allow for the absorption of the infinities in a finite number of quantities. These theories are considered effective theories and have limited validity.

[7] Note that the SM, being constructed upon a gauge symmetry with SSB, is fully renormalizable [25].

In summary, the EW symmetry must be broken to explain particle masses, and it can only be broken spontaneously. However, the experiments have not observed any of the predicted Goldstone bosons associated with the spontaneous EW symmetry breaking. As we will see below, the Higgs mechanism uses these massless scalars to give mass to some particles in the model.

1.3.2 The Higgs Mechanism

It may seem that the Goldstone theorem, far from solving the mass problem in the EW symmetry, complicates it, as it predicts new massless states rather than massive ones. However, the situation changes if the continuous global symmetry is local, that is, gauge.

We aim to give mass to the $W^{\pm}$ and Z bosons through SSB, while the photon must remain massless. Therefore, we need three degrees of freedom to become the longitudinal modes of the weak mediators. With this in mind, we introduce a new field with a scalar potential that preserves the gauge symmetry and makes the vacuum not invariant under it. We want these new degrees of freedom to have weak charge and hypercharge to break the gauge group. It should also be a neutral field that acquires a non-zero expectation value in the vacuum, breaking the $\mathrm{SU(2)_L} \times \mathrm{U(1)_Y}$ group down to electromagnetism, $\mathrm{U(1)_Q}$. The simplest way to achieve this is by defining a doublet under $\mathrm{SU(2)_L}$ with hypercharge $\mathrm{Y} = 1/2$, known as the Higgs doublet:

$$H = \begin{pmatrix} H^+ \\ H^0 \end{pmatrix} . \tag{1.25}$$

The most general Lagrangian we can build for this doublet, while ensuring that the theory remains renormalizable, is

$$\mathcal{L}_H = (D_\mu H)^\dagger (D^\mu H) - \mathcal{V}_H + \mathcal{L}_Y \quad \text{with} \quad \mathcal{V}_H = \mu^2 H^\dagger H + \lambda \left(H^\dagger H\right)^2 , \tag{1.26}$$

with λ a positive real number, $\mathcal{L}_Y$ is the Yukawa interaction Lagrangian that we will see below, and the covariant derivative is the same we defined in Eq. (1.14), substituting the hypercharge operator by its eigenvalue, 1/2,

$$D_\mu H(x) = \left[\partial_\mu - ig\frac{\vec{\sigma}}{2}\vec{W}_\mu(x) - i\frac{g\prime}{2}B_\mu(x)\right] H(x) . \tag{1.27}$$

We want the potential to be bounded from below to have a ground state. This is why $\lambda > 0$. However, for the quadratic coupling μ there are two possibilities, as shown in Fig. 1.1.

(a) $\mu^2 > 0$

This potential only has a minimum at $|H| = 0$ (Fig. 1.1a), which preserves the symmetry. This configuration describes just a massive scalar doublet with mass μ and quartic coupling λ, which does not lead to SSB.

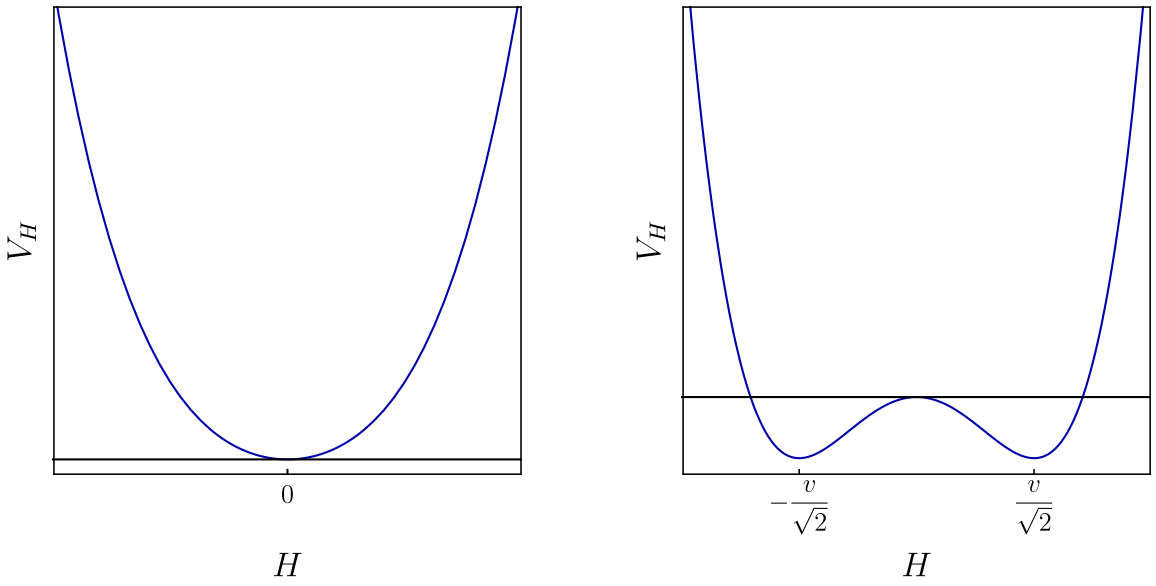

(a) $\mu^2 > 0\,,\, \lambda > 0$ (b) $\mu^2 < 0\,,\, \lambda > 0$

Figure 1.1: The well-known Higgs potential in the SM for the two possible scenarios: (a) $\mu^2 > 0$ and (b) $\mu^2 < 0$. In the former, the potential has just one minimum at $|H| = 0$, while in the latter, the minimum occurs for $|H| \neq 0$, leading to the spontaneous breaking of the gauge group of the model. λ is always taken to be positive in order for the potential to be bounded from below.

(b) $\mu^2 < 0$

In this scenario, the minimum of the potential is obtained for the field configurations satisfying

$$H^\dagger H = -\frac{\mu^2}{2\lambda} \equiv \frac{v^2}{2}, \tag{1.28}$$

where $H^\dagger$ represents the Hermitian conjugate of the field H and we have defined $v^2 = -\mu^2/\lambda$ (Fig. 1.1b).

The set of points that minimizes the potential is invariant under gauge group transformations, but if we choose one of these minima as the vacuum expectation value of $H(x)$, we will have spontaneously broken the symmetry.

Focusing on the second possibility, the most appropriate choice for the VEV is

$$\langle H \rangle \equiv \langle 0|H|0\rangle = \frac{1}{\sqrt{2}} \begin{pmatrix} 0 \\ v \end{pmatrix}. \tag{1.29}$$

This VEV keeps the photon massless as it remains invariant under the QED gauge symmetry. Using

$$Q = T_3 + Y = \frac{1}{2}\sigma_3 + \frac{1}{2}I = \begin{pmatrix} 1 & 0 \\ 0 & 0 \end{pmatrix}, \tag{1.30}$$

it is straightforward to see that electric charge is not a broken generator:

$$Q\langle H\rangle = \begin{pmatrix} 1 & 0 \\ 0 & 0 \end{pmatrix} \frac{1}{\sqrt{2}} \begin{pmatrix} 0 \\ v \end{pmatrix} = \begin{pmatrix} 0 \\ 0 \end{pmatrix}, \tag{1.31}$$

meaning that the vacuum remains invariant under $\mathrm{U(1)_Q}$ transformations and the photon will not get a mass. Therefore, the addition of the Higgs doublet breaks the symmetry $\mathrm{SU(2)_L \times U(1)_Y}$ spontaneously to $\mathrm{U(1)_Q}$. Notice that, according to the Goldstone theorem, three massless scalars should appear in the theory.

To understand how the Higgs mechanism will give masses to the W and Z bosons, it proves convenient to parametrize the scalar doublet in the general form

$$H(x) = \frac{1}{\sqrt{2}} \exp\left(i \frac{\vec{\sigma}}{2} \cdot \frac{\vec{\theta}(x)}{v} \right) \begin{pmatrix} 0 \\ v + h(x) \end{pmatrix}, \tag{1.32}$$

which makes the particle content manifest. The crucial point for this transformation is that the gauge of the theory under $\mathrm{SU(2)_L}$ allows us to eliminate any dependence on the $\theta_i(x)$ fields, which are precisely the three would-be Goldstone bosons associated with the SSB mechanism. The field $h(x)$ is the physical Higgs boson field, which stays in the particle spectrum of the model.

It is possible to eliminate the non-physical fields $\theta_i(x)$ through the gauge transformation

$$H \to H' = \exp\left(-i \frac{\vec{\sigma}}{2} \cdot \frac{\vec{\theta}(x)}{v} \right) H = \frac{1}{2} \begin{pmatrix} 0 \\ v + h(x) \end{pmatrix}, \tag{1.33}$$

which is known as the unitary gauge and can be interpreted as if the Goldstone bosons have been absorbed by the gauge bosons.

1.3.3 Masses in the Standard Model

Gauge bosons masses can be identified after substituting Eq. (1.33) into the kinetic term of the scalar potential. Starting with the covariant derivative in Eq. (1.27) we get,

$$\begin{aligned} D_\mu H &= \left[\partial_\mu - i \frac{g}{2} \begin{pmatrix} W_\mu^3 & \sqrt{2} W_\mu^+ \\ \sqrt{2} W_\mu^- & -W_\mu^3 \end{pmatrix} - i \frac{g'}{2} B_\mu \right] \frac{1}{\sqrt{2}} \begin{pmatrix} 0 \\ v + h \end{pmatrix} \\ &= \begin{bmatrix} -i \frac{g}{2} W_\mu^+ (v + h) \\ \frac{1}{\sqrt{2}} \partial_\mu h + \frac{i}{2\sqrt{2}} \left(g W_\mu^3 - g' B_\mu \right) (v + h) \end{bmatrix}. \end{aligned} \tag{1.34}$$

Then, using the weak rotation introduced in Eq. (1.21), it is not difficult to verify that the second term appearing in the lower component of the derivative is nothing else than the Z boson field,

$$Z_\mu = \cos\theta_W W_\mu^3 - \sin\theta_W B_\mu = \frac{1}{\sqrt{g^2 + g'^2}} \left(g W_\mu^3 - g' B_\mu \right). \tag{1.35}$$

Finally, the kinetic term of the Higgs boson becomes

$$(D_\mu H)^\dagger (D^\mu H) = \frac{1}{2}\partial_\mu h\, \partial^\mu h + (v+h)^2 \left(\frac{g^2}{4} W_\mu^+ W^{-\mu} + \frac{g^2+g'^2}{8} Z_\mu Z^\mu \right) . \tag{1.36}$$

This result shows that by including the Higgs boson and using spontaneous symmetry breaking, we have successfully given mass to the gauge bosons of the weak interaction, their masses being given, at tree-level, by

$$m_W = \frac{gv}{2}, \quad m_Z = \frac{\sqrt{g^2+g'^2}\, v}{2} = \frac{m_W}{\cos\theta_W} . \tag{1.37}$$

Notice that, as expected, there is no mass term for the photon.

Regarding the fermions, it is the previously introduced Yukawa interaction Lagrangian of Eq. (1.26) the one providing the masses of these particles, as well as their interaction with the Higgs boson. It is defined as

$$\mathcal{L}_Y^{\text{SM}} = -(Y_d)_{ij}\, \bar{Q}_L^i H\, d_R^j - (Y_u)_{ij}\, \bar{Q}_L^i \widetilde{H}\, u_R^j - (Y_e)_{ij}\, \bar{\ell}_L^i H\, e_R^j + \text{ h.c.} , \tag{1.38}$$

where $Y_{u,d,e}$ are 3×3 Yukawa matrices in flavor space, and we have introduced the field $\widetilde{H} \equiv i\sigma_2 H^*$, which transforms exactly as H under SU(2)_L, to construct an interaction term that leads to masses for the positively charged quarks. Note that there is only one Yukawa matrix for the lepton sector. Since right-handed neutrinos do not exist in the model, neutrinos do not get a mass from Yukawa interactions with the SM Higgs doublet.

The Yukawa matrices that appear are 3×3 complex matrices with many parameters, 54 in total, although we only want to provide masses for 9 particles: the 3 charged leptons and the 6 quarks. Fortunately, many of these parameters are unphysical, and after several changes of basis and phase transformations, as detailed in [28], the Lagrangian can be written in what is known as the mass basis,

$$\mathcal{L}_Y^{\text{SM}} = -\left(1+\frac{h}{v}\right)\left(\bar{e}_L \widehat{m}_e e_R + \bar{d}_L \widehat{m}_d d_R + \bar{u}_L \widehat{m}_u u_R\right) + \text{ h.c. } , \tag{1.39}$$

where the $\widehat{m}$ matrices are the diagonal mass matrices whose values must be measured experimentally. It follows that the strength of the interaction between the physical Higgs boson and the SM fermions is proportional to the fermion masses, such that

$$m_q = \frac{v}{\sqrt{2}} Y_q , \tag{1.40}$$

with $q = u, d, e$.

1.4 Flavor in the Standard Model

Through experiments, we have learnt that there exist three different copies, known as *flavors*, of each of the SM fermions: for the up-type quarks u, c, t; for the down-type quarks d, s, b; for the charged leptons e, μ, τ; and for the neutrinos ν_e, ν_μ, ν_τ. All of the species of the same fermion group share the same quantum numbers and only differ in their mass. Interestingly, the mass hierarchy in the families (except perhaps in the neutrino sector) is such that the third generation is much heavier than the second one, and so is the second generation with respect to the first. For instance, $m_e \ll m_\mu \ll m_\tau$. The question of why each fundamental fermion comes in three flavors together with the huge differences in the masses of the copies and in the mixings of different fermions is known as the Standard Model flavor puzzle.

In this section, we will provide more details about the derivation of the fermion mass eigenstates and the possible mixing among flavors. In the previous section, we saw that the mass matrices of the charged fermions are related to the Yukawa couplings and the Higgs VEV through Eq. (1.40). However, the Yukawa matrices are not diagonal in general, and in order to go to the mass basis, we must rotate the gauge eigenstates to the mass fields via

$$q_L^g = V_L^q \, q_L^m \,, \tag{1.41}$$

$$q_R^g = V_R^q \, q_R^m \,, \tag{1.42}$$

where, again, $q = u, d, e$ and $V_{L,R}^q$ are 3×3 unitary matrices. The superindices g and m denote gauge and mass basis, respectively. Therefore, after applying these transformations to Eq. (1.38) (where the superindex g was omitted for simplicity from all the fields), the diagonal mass matrices of the SM fermions defined in Eq. 1.39 are given by

$$\widehat{m}_q = V_L^q \, m_q \, (V_R^q)^\dagger \,. \tag{1.43}$$

The states participating in the physical processes are those with well-defined mass, that is, the mass eigenstates. This implies that the interaction eigenstates in the kinetic terms of the fermions must be rotated to the mass basis. The neutral currents given in Eq. (1.24) remain unaffected because they do not mix up- and down-type quarks nor charged and neutral leptons, and the change of basis matrices cancel due to their unitary nature. However, weak currents in Eq. (1.20) are sensitive to flavor rotations. The charged current Lagrangian in the new basis is

$$\mathcal{L}_{CC} = \frac{g}{\sqrt{2}} W_\mu^+ \left(\bar{u}_L \gamma^\mu V_{\rm CKM} d_L + \bar{\nu}_L \gamma^\mu e_L \right) + \text{ h.c. } \,, \tag{1.44}$$

where $V_{\rm CKM}$ is the famous Cabibbo-Kobayashi-Maskawa (CKM) matrix [29, 30] defined as

$$V_{\rm CKM} = V_L^u \left(V_L^d \right)^\dagger = \begin{pmatrix} V_{ud} & V_{us} & V_{ub} \\ V_{cd} & V_{cs} & V_{cb} \\ V_{td} & V_{ts} & V_{tb} \end{pmatrix} . \tag{1.45}$$

It is a 3×3 non-diagonal unitary matrix that is typically parametrized in a convenient way that is based on some mathematical considerations. Any complex $n \times n$ matrix has a total of $2\,n^2$ free real parameters. However, if the matrix is unitary, the condition $V_{\rm CKM}^{\dagger} V_{\rm CKM} = \mathbb{1}$ imposes n^2 constraints, reducing the number of independent parameters to n^2. Then, the free parameters can be split into $n(n-1)/2$ mixing angles and $n(n+1)/2$ phases. For the case of the SM, with just three quark families, this leaves us with 3 angles and 6 phases, though not all of the latter are observable. Five of these phases can be set to zero using the $\mathrm{U}(1)^6$ symmetry under which the quark masses are invariant. The non-removable phase is of great physical significance as it is capable of explaining the observed CP (charge conjugation times parity) violation in experiments. Therefore, we are left with 4 degrees of freedom: three angles and one phase. The CKM matrix can, then, be parametrized as [31]

$$V_{\rm CKM} = \begin{pmatrix} c_{12}c_{13} & s_{12}c_{13} & s_{13}e^{-i\delta} \\ -c_{12}s_{23}s_{13}e^{i\delta} - s_{12}c_{23} & c_{12}c_{13} - s_{12}s_{23}s_{13}e^{i\delta} & s_{23}c_{13} \\ s_{12}s_{23} - c_{12}c_{23}s_{13}e^{i\delta} & -c_{12}s_{23} - s_{12}c_{23}s_{13}e^{i\delta} & c_{23}c_{13} \end{pmatrix}, \tag{1.46}$$

where we have defined $s_{ij} \equiv \sin\theta_{ij}$ and $c_{ij} \equiv \cos\theta_{ij}$, and i and j are generation indices. After a global fit combining different experimental results (see [32] and references therein), the magnitude of the Cabibbo-Kobayashi-Maskawa matrix elements become

$$|V_{\rm CKM}| = \begin{pmatrix} 0.97435 \pm 0.00016 & 0.22500 \pm 0.00067 & 0.00369 \pm 0.00011 \\ 0.22486 \pm 0.00067 & 0.97349 \pm 0.00016 & 0.04182^{+0.00085}_{-0.00074} \\ 0.00857^{+0.00020}_{-0.00018} & 0.04110^{+0.00083}_{-0.00072} & 0.999118^{+0.000031}_{-0.000036} \end{pmatrix}, \tag{1.47}$$

which, as mentioned above, is non-diagonal, although it is very hierarchical. Finally, the fit result for the CP-violating phase is $\delta = 1.144 \pm 0.027$.

It is important to note that, in the SM, there is no lepton mixing matrix equivalent to the $V_{\rm CKM}$ matrix. This is due to the fact that the theory does not include right-handed neutrinos, therefore, neutrinos remain massless. We have then the freedom to redefine the neutrino fields in such a way as to eliminate the mixing in the lepton sector. Therefore, the three leptonic flavors are exactly conserved and a global accidental symmetry $\mathrm{U}(1)_{\rm e} \times \mathrm{U}(1)_{\mu} \times \mathrm{U}(1)_{\tau}$ exists. In Chapter 2, we will see that, according to neutrino oscillations, neutrinos are massive and a lepton mixing matrix must exist, leading to lepton flavor violation (LFV).

1.5 Anomalies in the SM

Although the Standard Model of particle physics has earned its place among the best theories ever created by humanity, it still faces some important unresolved questions that require attention. In the works on which this thesis is based, we have focused only on anomalies that are currently hinting at the presence of New Physics (NP) in the lepton sector of the SM. In the

following, we will introduce some of the most relevant anomalies. While not all of them are equally important, each one is relevant for this thesis.

Neutrino masses

First of all, neutrino oscillation experiments have clearly established that neutrinos are massive. This is arguably the most robust evidence of NP beyond the SM. Right-handed neutrinos do not exist in the model, and the scalar potential is minimal. Therefore, a neutrino mass term is not allowed by gauge invariance at the renormalizable level. This definitely calls for an extension of the SM lepton and/or scalar sectors with new degrees of freedom which, in most scenarios, lead to deviations in other observables, directly associated to leptons or not. Neutrino masses are a central topic of this thesis and will be discussed in detail in Chapter 2.

Dark matter

Another problem of the SM is related to some important astronomical observations that suggest the presence of *dark matter* (DM) [33]. One of the most important pieces of evidence of DM comes from observations of the rotation curves of galaxies [34, 35]. The stars orbit around the center of the galaxy, and the speed at which they are moving should decrease with increasing distance from the center due to the gravitational pull of the matter in the galaxy. However, observations show that the rotation curves of galaxies remain roughly constant with increasing distance from the center, indicating the presence of additional matter that has no electromagnetic interaction, hence the name of this mysterious matter. Other evidences for DM include observations of gravitacional lensing [36], the study of the cosmic microwave background radiation [37], or the fact that DM is necessary to explain the formation of galaxies and large-scale structures of the Universe [38]. However, the nature of the DM that constitutes $\sim 27\%$ of the energy content of the Universe is still a mystery [39]. Many new physics models include DM candidates, sometimes relating them to other open questions in particle physics or even being instrumental in their resolution.

Charged lepton anomalous magnetic and electric moments

The charged lepton anomalous magnetic moments (AMMs),

$$a_\ell = \frac{g_\ell - 2}{2}\,, \tag{1.48}$$

with $\ell = e, \mu, \tau$, are known to be powerful probes of NP effects, potentially hidden in loop contributions. Interestingly, there is a discrepancy between the Standard Model prediction for the electron and muon anomalous magnetic moments and their experimentally determined values [40–46]. In the case of the electron $g-2$, the significance is slightly below $\sim 3\sigma$, and hence not very notable at the moment. In contrast, the deviation has become particularly relevant in the case of the muon $g-2$, in particular after the Muon $g-2$ experiment at Fermilab has

published its long-awaited first results [47]. Their measurement of a_μ perfectly agrees with the result obtained by the E821 experiment at Brookhaven [48] and disagrees with the SM. Their combination leads to a 4.2σ discrepancy with the SM prediction compiled by the theory community in [49]. In summary, the current status of the electron and muon $g-2$ can be quantified as [8]

$$\begin{aligned}\Delta a_e &= a_e^{\rm exp} - a_e^{\rm SM} = (-87 \pm 36) \times 10^{-14}\,, \\ \Delta a_\mu &= a_\mu^{\rm exp} - a_\mu^{\rm SM} = (25.1 \pm 5.9) \times 10^{-10}\,. \end{aligned} \tag{1.49}$$

New measurements and more refined theoretical calculations are definitely required to assess the relevance of these anomalies and confirm whether these intriguing deviations are hints of NP [52], SM contributions not correctly taken into account, or just statistical fluctuations. [9] However, it is tempting to interpret them as a signal of the presence of new states beyond the SM (BSM). In this case, the $g-2$ anomalies may hide valuable information about the shape of the underlying model. In particular, the sign difference between Δa_e and Δa_μ and the sizable value of $|\Delta a_e|$ would indicate that the NP contributions do not scale with the square of the charged lepton masses [66]. This calls for a non-trivial extension of the SM.

The muon $g-2$ has been considered in a wide variety of contexts, in many cases in connection to neutrino mass generation. This includes models based on the inverse seesaw mechanism [67–75] and/or with VL leptons [76–96]. See also [97] for a recent work in the context of a radiative neutrino mass model including triplet fermions. Finally, we note that the muon $g-2$ has also been considered as a motivation for a muon collider [98–100].

In what concerns the electric dipole moments (EDMs) of the charged leptons, the SM predicts tiny values well beyond the experimental prospects in the near future. Therefore, any measurement of a non-zero charged lepton EDM would be a clear indication of CP-violating new physics effects. The current best limits for the electron and muon EDMs, at 95% C.L., are [101, 102]

$$|d_e| < 1.1 \times 10^{-29}\, e\,{\rm cm}\,, \tag{1.50}$$

$$|d_\mu| < 1.5 \times 10^{-19}\, e\,{\rm cm}\,. \tag{1.51}$$

[8] The status of the electron $g-2$ has recently changed by a new measurement of the fine-structure constant [50]. The new value differs by more than 5σ to the previous one and affects the electron $g-2$ anomaly, which gets reduced to just 1.6σ and flips sign, see [51]. We will not include these results in the chapters below. We also point out that this change in the fine-structure constant value has little impact on the muon $g-2$.

[9] The theoretical calculation of the electron and muon anomalous magnetic moments is a challenging task and has led to some controversies over the years. Indeed, the SM prediction for the muon is currently under debate due to recent lattice results [53–55]. For instance, a recent calculation of the hadronic vacuum polarization contribution by the Budapest-Marseilles-Wuppertal collaboration [53] brings the SM prediction for the muon $g-2$ into agreement with the experimental value, hence ruling out any discrepancy. However, it has been pointed out that this result, in turn, leads to some tension with electroweak data [56–59]. Other subsequent lattice calculations [60–65] go in the same direction as [53].

Both charged lepton magnetic and electric moments can be described by the effective Hamiltonian [103]

$$\mathcal{H} = c_{ij}\,\bar{\ell}_j\,\sigma_{\mu\nu}\,P_R\,\ell_i\,F^{\mu\nu} + \text{h.c.}\,, \tag{1.52}$$

where $P_R = (1+\gamma_5)/2$ is the usual right-handed chiral projector, $F^{\mu\nu}$ the electromagnetic field strength tensor and ℓ_i denote the SM charged lepton mass eigenstates. The anomalous magnetic moment is given in terms of the real components of the diagonal c coefficients as

$$a_i = -\frac{2\,m_i}{e}\,(c_{ii} + c_{ii}^*) = -\frac{4\,m_i}{e}\,\text{Re}\,c_{ii}\,, \tag{1.53}$$

whereas the imaginary components would, in turn, induce electric dipole moments as

$$d_i = i\,(c_{ii} - c_{ii}^*) = -2\,\text{Im}\,c_{ii}\,. \tag{1.54}$$

B flavor anomalies

At present, there are several measurements of observables involving B-meson decays that do not align with the predictions of the SM. These discrepancies are commonly referred to as the B flavor anomalies and are categorized into two types: the neutral-current anomalies, which arise in processes involving $b \to s\,\ell\ell$ decays, and the charged-current anomalies, observed in $b \to c\,\ell\nu_\ell$ decays.

In 2013, the LHCb Collaboration announced at the EPS conference in Stockholm the first observation of the $b \to s\,\ell\ell$ anomaly [104]. They measured a deviation from the SM prediction at the level of 3.7σ in the observable P_5', a parameter that characterizes the angular distribution of the decay products in $B^0 \to K^{*0}\mu^+\mu^-$ decays. Since this measurement, there has been a significant increase in the number of measured observables involving $b \to s\,\ell\ell$ decays, and many of these also exhibit important deviations from the predictions of the SM. Among all these discrepancies, some of them merit more attention. On the one hand, we have the possible violation of lepton flavor universality in B-meson decays [105–108] encoded in the $R_{K^{(*)}}$ ratios, defined as

$$R_{K^{(*)}} = \frac{\text{BR}(B \to K^{(*)}\mu\bar{\mu})}{\text{BR}(B \to K^{(*)}e\bar{e})}\,. \tag{1.55}$$

For these ratios, the theoretical uncertainties of the SM predictions are at the percent level [109], which strengthens the relevance of the anomalies. Indeed, in the SM, these ratios are known to be 1, except for minor electromagnetic corrections and kinematic mass effects. Another important discrepancy between theory and experiment was found in the branching ratio $\text{BR}(B_s \to \mu\bar{\mu})$ [110–113].

However, we note that very recently, some new results from the experimental collaborations have reduced the discrepancy between some of the most important neutral-current anomalies in B meson decays and the SM predictions. For instance, the recent CMS result [114] suggests that the experimental branching ratio $\text{BR}(B_s \to \mu\bar{\mu})$ is in good agreement with the SM. Also, the

LHCb collaboration announced that they have discovered misidentified hadronic backgrounds which had not been taken into account in previous R_K and R_{K^*} measurements, which affected the electron mode and pushed the results away from the SM expectations [115]. Taking these backgrounds into account resulted in values compatible with the predictions of the SM. Nevertheless, in this thesis we use the results of the global fit in [116], which was performed before the latest results on the anomalies were published.

The operators that govern the $b \to s\,\ell\ell$ transitions are collected in the effective Lagrangian

$$\mathcal{L}_{\text{eff}} = \frac{4\,G_F}{\sqrt{2}} V_{tb} V_{ts}^* \sum_i \left(C_i \mathcal{O}_i + C_i' \mathcal{O}_i'\right) + \text{h.c.}\,, \tag{1.56}$$

with V_{ij} being the elements of the CKM matrix and C_i are the Wilson coefficients of the operators

$$\begin{aligned}
&\mathcal{O}_7 = \tfrac{e}{16\pi^2} m_b \bar{s} \sigma^{\mu\nu} P_R b F_{\mu\nu}\,, && \mathcal{O}_8 = \tfrac{g_s}{16\pi^2} m_b \bar{s}_\alpha \sigma^{\mu\nu} P_R T^a_{\alpha\beta} b_\beta G^a_{\mu\nu}\,,\\
&\mathcal{O}_9 = \tfrac{\alpha_{\text{EM}}}{4\pi} \left(\bar{s}\gamma_\mu P_L b\right)\left(\bar{\mu}\gamma^\mu \mu\right)\,, && \mathcal{O}_{10} = \tfrac{\alpha_{\text{EM}}}{4\pi} \left(\bar{s}\gamma_\mu P_L b\right)\left(\bar{\mu}\gamma^\mu \gamma_5 \mu\right)\,,\\
&\mathcal{O}_S = \tfrac{\alpha_{\text{EM}}}{4\pi} \left(\bar{s} P_R b\right)\left(\bar{\mu}\mu\right), && \mathcal{O}_P = \tfrac{\alpha_{\text{EM}}}{4\pi} \left(\bar{s} P_R b\right)\left(\bar{\mu}\gamma_5 \mu\right)\,,\\
&\mathcal{O}_T = \tfrac{\alpha_{\text{EM}}}{4\pi} \left(\bar{s}\sigma_{\mu\nu} b\right)\left(\bar{\mu}\sigma^{\mu\nu} P_R \mu\right)\,,
\end{aligned} \tag{1.57}$$

where e is the electron charge, α_{EM} is the fine structure constant, and g_s is the strong coupling constant. Also, the primed operators are obtained just by interchanging P_L and P_R. Complete and general analytical 1-loop expressions for the Wilson coefficients of a given model can be found in [82]. Note that we do not aim to provide a thorough description of effective field theories. Instead, we refer to [117] for a nice introduction.

Regarding the charged-current anomalies in $b \to c\,\ell\nu_\ell$ processes, the first measurement was taken in 2012, when the BaBar Collaboration measured $R_{D^{(*)}} \equiv \text{BR}(\bar{B} \to D^{(*)}\tau\nu_\tau)/\text{BR}(\bar{B} \to D^{(*)}\ell\nu_\ell)$, with $\ell = e, \mu$. They found values for both R_D and $R_{D^{(*)}}$ that, when taken together, exceed the SM expectation by 3.4σ [118]. New measurements of these observables have been repeated over the years, with the results seemingly confirming the anomaly [119–121]. However, the latest results from the LHCb Collaboration, presented very recently, indicate a deviation of just 1.9σ from the SM [122]. Nevertheless, their measurement is not precise enough to significantly reduce the uncertainty on the combined value of the other measurements, consequently resulting in a combined deviation of 3.2σ. Subsequent measurements of additional $b \to c\,\ell\nu_\ell$ observables have been made, although far fewer in number compared to the $b \to s\,\ell\ell$ case. These have also shown other deviations from the SM predictions.

We propose a model in Chapter 5 to fit all the anomalies discussed in this Section. However, there we just focused on the neutral-current B flavor anomalies since a vector leptoquark (or a combination of two different scalar leptoquarks), as well as an extended gauge symmetry, would be required to simultaneously address both types of anomalies [123–126].

Chapter 2

Neutrino masses

"Is it not a strange fate that we should suffer so much fear and doubt for so small a thing? So small a thing!"

– J.R.R. Tolkien, The Fellowship of the Ring

2.1 Introduction

Neutrinos were first postulated in 1930 by the physicist Wolfgang Pauli in an open letter addressed to a group of *radioactive people* at the Gauverein meeting in Tübingen [127]. He proposed the existence of these particles as a theoretical solution to the apparent non-conservation of energy, momentum and spin in β decays. However, Pauli initially thought that the neutrino would never be detected because it is an electrically neutral particle with an extremely small mass that rarely interacts with other particles. Fortunately, and despite the pessimism of Pauli, the first successful detection of neutrinos occurred in 1956 [128]. The breakthrough discovery was made by Frederick Reines and Clyde Cowan, who used a detector filled with water and cadmium chloride to detect antineutrinos emitted by a nuclear reactor in Savannah River. Since then, numerous neutrino detectors have been constructed, and neutrinos have been detected from different sources, including the Sun, supernovae, and cosmic rays.

Later on, in the 1960s, John Bahcall and Ray Davis headed the Homestake experiment, which began measuring the flux of neutrinos coming from the Sun using different techniques [129]. Bahcall performed the corresponding theoretical calculations, whereas Davis designed the experiment. What is interesting about this is that the number of neutrinos predicted to be detected on Earth by Bahcall was about three times higher than what Davis observed. This discrepancy between the predicted and observed number of solar neutrinos was known as the solar neutrino problem.

Luckily, at that time, there was already a hypothesis that could solve the problem: *neutrino oscillations*. The first idea of neutrino oscillations was brightly proposed by Bruno Pontecorvo

back in 1957 and 1958, although he originally thought of $\nu-\bar{\nu}$ oscillations [130,131]. The concept was refined with time, but the idea is that neutrinos might change from one type to another as they travel through space. The first experimental evidence for neutrino oscillations came from the Super-Kamiokande experiment in Japan in 1998 [132]. They reported that atmospheric neutrinos produced in the atmosphere of the Earth were oscillating between different flavors. Further experiments, including the Sudbury Neutrino Observatory (SNO) in Canada [133] and the KamLAND experiment conducted in Japan [134], confirmed the hypothesis of the oscillation of solar neutrinos as well.

In the rest of the chapter, we provide a brief review of neutrino physics, emphasizing neutrino flavor oscillations and their impact on lepton flavor violation. We will also delve into some of the most relevant neutrino mass models. Additionally, we will explore the possibility of spontaneous lepton number violation (LNV). For a comprehensive overview of the current status of neutrino physics, see, for instance, [135].

2.2 Neutrino oscillations

The phenomenon of neutrino flavor oscillations was initially proposed by Pontecorvo in 1957. He was thinking of neutrino-antineutrino transitions, analogous to the neutral kaon oscillations, $K^0 - \bar{K^0}$. However, five years later, the muon neutrino was discovered [136], and the idea of Pontecorvo was refined by Ziro Maki, Masami Nakagawa, and Shoichi Sakata. They proposed a model that allowed for oscillations between the electron and muon neutrinos [137]. This was made possible by assuming that the mass eigenstates, ν_1 and ν_2, and the weak [1] eigenstates, ν_e and ν_μ, were not the same. Thus, the weak neutrinos needed to be redefined by the relation

$$\begin{aligned} \nu_e &= \nu_1 \cos\theta - \nu_2 \sin\theta\,, \\ \nu_\mu &= \nu_1 \sin\theta + \nu_2 \cos\theta\,, \end{aligned} \tag{2.1}$$

and the presence of the mixing parameter θ is responsible for the oscillations between the known flavor eigenstates. [2]

2.2.1 Neutrino oscillations in vacuum

The SM accounts for the presence of three different flavors of neutrinos, one for each lepton doublet. Similarly to the CKM matrix in the quark sector, the neutrino mixing between the mass and flavor basis is described by the 3×3 unitary matrix known as the Pontecorvo-Maki-Nakagawa-Sakata (PMNS) mixing matrix. Then, the mass eigenstates ν_i $(i = 1, 2, 3)$, with well-defined masses m_i, can be expressed as a linear combination of the weak eigenstates ν_α $(\alpha = e, \mu, \tau)$, or vice versa. In the basis where there is no mixing between the charged leptons,

[1] The neutrino weak eigenstates are also referred to as the neutrino gauge or flavor eigenstates.

[2] We note that a Majorana phase should be present in Eq. (2.1). However, it is irrelevant to the neutrino oscillation phenomenon and we do not consider it here.

that is, where the leptonic Yukawa matrix is diagonal, the neutrino flavor and mass eigenstates relate through

$$|\nu_\alpha\rangle = U_{\alpha i}\,|\nu_i\rangle \ , \tag{2.2}$$

where U is the PMNS mixing matrix and the convention of summing over repeated indices is assumed. Taking this into account, the leptonic charged current in Eq. (1.44) becomes

$$\mathcal{L}_{CC} = \frac{g}{\sqrt{2}} W_\mu^+ \left(\bar{u}_L \gamma^\mu V_{\rm CKM} d_L + \bar{\nu}_L \gamma^\mu U^\dagger e_L\right) + \text{ h.c. } , \tag{2.3}$$

where both the neutrinos and the charged leptons correspond to states in the mass basis.

Repeating the discussion performed in Section 1.4 for the CKM matrix and taking into account that there are just three lepton families, the PMNS mixing matrix, U, is also left with 3 angles and 6 phases. If neutrinos are Dirac particles, it is possible to rephase the charged leptons and two neutrinos to absorb five of the six phases from the PMNS mixing matrix. This is because of a global symmetry related to the conservation of lepton number. In contrast, if neutrinos are of the Majorana type, their mass terms are not invariant under the phase transformations, and the phases of the PMNS matrix cannot be eliminated by redefining the neutrino fields. In this case, we can only eliminate three of the phases by redefining the charged lepton fields. Therefore, we are left with three mixing angles and one Dirac phase (or one Dirac plus two Majorana phases). The PMNS matrix can, thus, be parametrized as [32]

$$U = \begin{pmatrix} 1 & 0 & 0 \\ 0 & c_{23} & s_{23} \\ 0 & -s_{23} & c_{23} \end{pmatrix} \cdot \begin{pmatrix} c_{13} & 0 & s_{13}e^{-i\delta_{\rm CP}} \\ 0 & 1 & 0 \\ -s_{13}e^{i\delta_{\rm CP}} & 0 & c_{13} \end{pmatrix} \cdot \begin{pmatrix} c_{12} & s_{12} & 0 \\ -s_{12} & c_{12} & 0 \\ 0 & 0 & 1 \end{pmatrix} \cdot \begin{pmatrix} e^{i\eta_1} & 0 & 0 \\ 0 & e^{i\eta_2} & 0 \\ 0 & 0 & 1 \end{pmatrix} \tag{2.4}$$

where $c_{ij} \equiv \cos\theta_{ij}$ and $s_{ij} \equiv \sin\theta_{ij}$. The angles θ_{ij} can be taken to lie in the first quadrant without loss of generality. $\delta_{\rm CP}$ is the Dirac CP phase, which is relevant for understanding CP violation in neutrino oscillations, and η_i are the Majorana phases. The latter are zero in the case of neutrinos being Dirac particles, and do not affect neutrino flavor oscillations but are important for neutrinoless double beta decay.

Now, we are prepared to see the derivation of the probability for neutrinos to oscillate. Assuming the existence of an underlying mechanism that gives mass to neutrinos, a physical neutrino, that is, a mass eigenstate, traveling in vacuum will be an eigenstate of the free Hamiltonian,

$$H_0\,|\nu_i\rangle = E_i\,|\nu_i\rangle \ , \tag{2.5}$$

with well-defined mass m_i and energy given by the relativistic relation $E_i^2 = \vec{p}_i^{\,2} + m_i^2$, where $\vec{p}_i$ are the neutrino trimomenta. As the Hamiltonian is diagonal in the neutrino mass basis, it is straightforward to obtain the time evolution of the neutrinos:

$$|\nu_i(t)\rangle = |\nu_i(t=0)\rangle\, e^{-iE_i t} \, . \tag{2.6}$$

Combining this equation with Eq. (2.2), we can express the flavor eigenstates at a time t as

$$|\nu_\alpha(t)\rangle = U_{\alpha i}\,|\nu_i(t=0)\rangle\, e^{-iE_i t}\,, \tag{2.7}$$

and we can calculate the amplitude of an initial neutrino of flavor α oscillating to a flavor β at a given time t,

$$\mathcal{A}(\nu_\alpha \to \nu_\beta)(t) = \langle \nu_\beta(t)|\nu_\alpha(0)\rangle = \langle \nu_\beta(t)|\nu_j(t)\rangle\,\langle \nu_j(t)|\nu_j(0)\rangle\,\langle \nu_j(0)|\nu_\alpha(0)\rangle = U^*_{\beta j}U_{\alpha j}e^{-i\,E_j\,t}\,, \tag{2.8}$$

where we have used the completeness relation $|\nu_i(t)\rangle\,\langle\nu_i(t)| = \mathbb{1}$ twice. In the expression above one can identify the three stages in the evolution of neutrinos. The leftmost term involves the projection of the final mass eigenstate onto the flavor neutrinos, the middle term represents the propagation of the initial energy eigenstate, and the rightmost term projects the initial neutrino onto the flavor eigenstates. Therefore, the probability of the oscillation is given by the modulus squared of the previous amplitude,

$$P(\nu_\alpha \to \nu_\beta)(t) = |\mathcal{A}(\nu_\alpha \to \nu_\beta)(t)|^2 = U^*_{\alpha i}U_{\beta i}U^*_{\beta j}U_{\alpha j}e^{-i(E_j-E_i)t}\,. \tag{2.9}$$

Note that neutrino oscillations conserve probability, satisfying $\sum_\beta P(\nu_\alpha \to \nu_\beta) = 1$. Assuming ultrarelativistic neutrinos and the equal momentum approximation, we can simplify the expression using

$$E_j - E_i = \sqrt{\vec{p}^2 + m_j^2} - \sqrt{\vec{p}^2 + m_i^2} \approx |\vec{p}| + \frac{1}{2}\frac{m_j^2}{|\vec{p}|} - |\vec{p}| - \frac{1}{2}\frac{m_i^2}{|\vec{p}|} = \frac{m_j^2 - m_i^2}{2\,E} \equiv \frac{\Delta m_{ij}^2}{2\,E}\,, \tag{2.10}$$

where we have defined $E \equiv |\vec{p}|$. Finally, given that neutrinos travel at speeds very close to that of light, we can consider t to be equal to L, in natural units, with L the total distance traveled by the neutrino since it is produced until it is detected. Therefore, Eq. (2.11) takes the form

$$P(\nu_\alpha \to \nu_\beta)(t) = |\langle \nu_\beta|\nu_\alpha(t)\rangle|^2 = U^*_{\alpha i}U_{\beta i}U^*_{\beta j}U_{\alpha j}e^{-i\frac{\Delta m_{ij}^2}{2\,E}\,L}\,. \tag{2.11}$$

Finally, the oscillation probability can be simplified to [135]

$$\begin{aligned} P\left(\nu_\alpha \to \nu_\beta\right) = \delta_{\alpha\beta} &- 4\sum_{i>j}\mathrm{Re}\left(U^*_{\alpha i}U_{\alpha j}U_{\beta i}U^*_{\beta j}\right)\sin^2\left(\frac{\Delta m_{ij}^2 L}{4E}\right) \\ &+ 2\sum_{i>j}\mathrm{Im}\left(U^*_{\alpha i}U_{\alpha j}U_{\beta i}U^*_{\beta j}\right)\sin\left(\frac{\Delta m_{ij}^2 L}{2E}\right)\,. \end{aligned} \tag{2.12}$$

Some important features can be extracted from this expression. First, these oscillations violate the conservation of lepton flavor number but still conserve the total lepton number. Second, antineutrinos can also be described by the PMNS matrix, but with the substitution of U by its complex conjugate, U^*. Therefore, the phases in the mixing matrix induce CP-violation since

$P(\nu_\alpha \to \nu_\beta)(t) \neq P(\bar{\nu}_\alpha \to \bar{\nu}_\beta)(t)$ in general. Third, neutrino oscillations are not sensitive to the absolute mass scale of neutrinos but only to the difference of the squared masses. Finally, they are not sensitive to Majorana phases.

2.2.2 Current experimental status

Currently, three different neutrino flavors have been observed. This implies that their oscillations depend on the three mixing angles θ_{12}, θ_{13}, and θ_{23}, as well as on the CP phase δ_{CP}, defined in (2.4), and also on the two mass differences Δm^2_{21} and Δm^2_{31}. While the values of the three mixing angles, the mass splitting Δm^2_{21}, and the absolute value of Δm^2_{31} have been measured with good precision, there are still important quantities that require further investigation. For instance, the sign of the mass splitting Δm^2_{31} is unknown, and the mass hierarchy of the neutrinos is compatible with two scenarios:

- Normal Ordering (NO): $m_1 < m_2 < m_3$
- Inverted Ordering (IO): $m_3 < m_1 < m_2$

As mentioned above, the absolute neutrino mass scale of neutrinos is not directly accessible through neutrino oscillation experiments. Therefore, other experiments are needed to set bounds to this value. Cosmological observations offer the most stringent limits on the neutrino mass scale by studying the large-scale structure of the Universe. The existence of massive neutrinos affects the formation and evolution of structures over time. Although the bounds depend on specific assumptions made about the expansion history of the Universe and on the data analyzed, the Planck Collaboration has set the current strongest bound on the sum of the neutrino masses, $\sum m_\nu < (0.11 - 0.54)\,\text{eV}$ (95%C.L.) [39].

Combining and exploiting the complementarity between the data samples, the authors of [138] manage to perform a global fit of neutrino oscillation data in the simplest three-neutrino framework and including all the currently available neutrino physics inputs. The numerical values of their analysis for each of the parameters are shown in Table 2.1.

2.3 Lepton Flavor Violation

In the Standard Model, lepton flavor is an accidental symmetry. However, the presence of the PMNS mixing matrix in Eq. (2.3), combined with the fact that it is not the identity matrix, implies that lepton flavor is violated. Despite this, no experimental evidence of lepton flavor violation has been observed in the leptonic charged sector. Many BSM extensions providing a theoretical explanation for neutrino masses and mixings include additional states that may enhance the LFV processes. Therefore, setting experimental bounds on these possible LFV channels is crucial to constrain the parameter space of BSM models.

Experimental searches for charged LFV are of great interest and lepton flavor physics is about to live a golden age. Several state-of-the-art experiments recently started taking data

Parameter	Best fit $\pm 1\sigma$	2σ range	3σ range
$\Delta m^2_{21}\left[10^{-5}\,\mathrm{eV}^2\right]$	$7.50^{+0.22}_{-0.20}$	$7.12 - 7.93$	$6.94 - 8.14$
$\lvert\Delta m^2_{31}\rvert\left[10^{-3}\,\mathrm{eV}^2\right]$ (NO)	$2.55^{+0.02}_{-0.03}$	$2.49 - 2.60$	$2.47 - 2.63$
$\lvert\Delta m^2_{31}\rvert\left[10^{-3}\,\mathrm{eV}^2\right]$ (IO)	$2.45^{+0.02}_{-0.03}$	$2.39 - 2.50$	$2.37 - 2.53$
$\sin^2\theta_{12}/10^{-1}$	3.18 ± 0.16	$2.86 - 3.52$	$2.71 - 3.69$
$\sin^2\theta_{23}/10^{-1}$ (NO)	5.74 ± 0.14	$5.41 - 5.99$	$4.34 - 6.10$
$\sin^2\theta_{23}/10^{-1}$ (IO)	$5.78^{+0.10}_{-0.17}$	$5.41 - 5.98$	$4.33 - 6.08$
$\sin^2\theta_{13}/10^{-2}$ (NO)	$2.200^{+0.069}_{-0.062}$	$2.069 - 2.337$	$2.000 - 2.405$
$\sin^2\theta_{13}/10^{-2}$ (IO)	$2.225^{+0.064}_{-0.070}$	$2.086 - 2.356$	$2.018 - 2.424$
δ_{CP}/π (NO)	$1.08^{+0.13}_{-0.12}$	$0.84 - 1.42$	$0.71 - 1.99$
δ_{CP}/π (IO)	$1.58^{+0.15}_{-0.16}$	$1.26 - 1.85$	$1.11 - 1.96$

Table 2.1: Neutrino oscillation parameters summary determined from the global fit [138].

and a few more are about to begin [139, 140]. These include new searches for lepton flavor violating processes, forbidden in the SM, as well as more precise measurements of lepton flavor conserving observables, such as charged lepton anomalous magnetic moments. The search for LFV in processes involving charged leptons is strongly motivated by the observation of LFV in the neutral sector. In what concerns muon observables, the search for the radiative LFV decay $\mu \to e\gamma$ was the pioneering effort in the quest for LFV processes. The strongest upper limit for its branching ratio comes from the MEG experiment at the PSI laboratory, setting $\mathrm{BR}(\mu \to e\gamma) < 4.2 \times 10^{-13}$ at 90 % C.L. [141]. The second phase of the MEG experiment, MEG-II [142,143], expects to reach a sensitivity of $\sim 10^{-14}$ with 3 years of data taking. Another interesting possibility for LFV in muon decays is the process $\mu \to eee$. Currently, the best limit, $\mathrm{BR}(\mu \to eee) < 1.0 \times 10^{-12}$ at 90 % C.L., was set by the SINDRUM experiment at PSI [144], while the long-awaited Mu3e experiment will aim at an impressive sensitivity to branching ratios for the 3-body decay as low as 10^{-16} [143, 145]. A plethora of promising experiments looking for neutrinoless $\mu - e$ conversion in nuclei is also planned [146–148].

Regarding τ leptons, they have the drawback of being produced far less frequently than muons at colliders as well as having lifetimes significantly shorter, complicating their study. Flavor factories and experiments aiming at a broad spectrum of flavor observables, such as Belle II and LHCb, will also contribute to this era of lepton flavor, mainly due to their high sensitivities in the measurement of tau lepton observables [149, 150].

In addition to the low-energy LFV observables mentioned earlier, or others such as B-meson or pion decays [139] and some exotic signatures like $\ell_\alpha \to \ell_\beta\gamma\gamma$ [151], LFV can be explored in high-energy processes as well. However, the searches mentioned above, like the

one for $\mu \to e\gamma$, put stringent limits on the LFV expectations in many BSM scenarios, usually precluding the observation of this phenomenon at high-energy colliders. Nevertheless, large LFV rates compatible with the existing bounds can be obtained in some scenarios for the Higgs boson decaying into $\tau\mu$ [152]. Another possibility consists in the production of right-handed neutrinos via a Z' portal which are only allowed to decay via small LFV couplings [153]. This leads to an unsuppressed rate that can be visible despite the stringent constraints.

2.4 Dirac or Majorana neutrinos?

Some of the most fundamental unknown questions of neutrino physics include whether neutrinos are Dirac or Majorana particles, what is the value of the CP-violating phase $\delta_{\rm CP}$, what is the real neutrino mass ordering, or how many neutrinos exist in nature. The answer to these problems is crucial for understanding the origin of the masses of these particles. In this section, however, we will focus on the Dirac or Majorana nature of neutrinos. [3]

The possible conservation of lepton number L can be used to characterize the nature of neutrinos. When L is conserved, the neutrino mass eigenstates (ν_i) and their corresponding antineutrinos ($\bar{\nu}_i$) share the same masses but have different lepton numbers: $L(\nu_i) = -L(\bar{\nu}_i) = 1$. They are, hence, distinguishable, and neutrinos are Dirac particles. On the other hand, neutrinos are of the Majorana type if there is no conserved symmetry that differentiates between particle and antiparticle. It is important to note that this discussion is specific to neutrinos and does not apply to other SM fermions, as their electric charge makes it possible to distinguish them from their antiparticles.

In the case of Majorana neutrinos, one can construct a mass term of the form

$$-\mathcal{L}_M = \frac{1}{2} m_M \left(\bar{\nu}_L^c \nu_L + \bar{\nu}_L \nu_L^c\right) , \tag{2.13}$$

where $\nu_L^c \equiv C\,\nu_L$ with $C \equiv i\,\gamma^2\,\gamma^0$ is the charge conjugated neutrino, which breaks all the U(1) symmetries but not $\mathbb{Z}_{2n}$ parities [4]. While for the Majorana case the mass term does not need a new particle to give mass to the left-handed neutrino, the Dirac neutrino scenario requires the addition of another state. This new state, which has to be right-handed, is usually denoted as ν_R or N. The mass term, in this case, is written as

$$-\mathcal{L}_D = m_D \left(\bar{\nu}_L \nu_R + \bar{\nu}_R \nu_L\right) . \tag{2.14}$$

The scientific community generally finds the Majorana neutrinos hypothesis to be more appealing for several aesthetic reasons. First, as previously discussed, Dirac neutrinos require the introduction of a right-handed partner, ν_R, to generate a mass term. However, if the addition is done without any further symmetry constraints, then a Majorana mass term is automatically

[3] See [154] for a nice review on the subject.

[4] $\mathbb{Z}_n$ parities are discrete symmetries under which the states transform as $X \to e^{\,i\,2\pi k/n}\,X$, with $k = 1, \ldots, n$.

allowed as well. The resulting Lagrangian for the neutrino mass is given by:

$$-\mathcal{L}_{m_\nu} = m_D\,\bar{\nu}_L\nu_R + \frac{1}{2}\,m_L\,\bar{\nu}_L\nu_L^c + \frac{1}{2}\,m_R\,\bar{\nu}_R\nu_R^c + \text{h.c.}\,. \tag{2.15}$$

Therefore, to ensure that neutrinos remain as Dirac particles, it is necessary to impose a protective symmetry that forbids the existence of Majorana mass terms. The most natural choice for this symmetry is lepton number, which is already a global accidental symmetry in the SM. Another concern that arises is the fact that neutrinos have extremely small masses compared to the EW scale. If neutrinos acquire their mass through the SM Higgs mechanism, then the associated Yukawa couplings would be of the order of 10^{-12}. [5] For these reasons, the Majorana neutrino hypothesis tends to be more appealing than the Dirac one, as it typically requires fewer new fields and symmetries. Furthermore, Majorana neutrinos have a richer phenomenology compared to Dirac neutrinos, mainly due to the breaking of lepton number.

Observationally, the nature of neutrinos remains a mystery. The phenomenon of neutrino oscillations is unable to distinguish between Dirac and Majorana neutrinos since the probabilities of oscillations do not depend on the Majorana phases. One potential avenue for distinguishing between these two options is to search for lepton number violating processes, with neutrinoless double beta decay being the most promising candidate. In this hypothetical nuclear process, two neutrons in a nucleus simultaneously decay into two protons, emitting two electrons and no neutrinos. If neutrinos turn out to be Majorana particles, then this decay can occur, violating lepton number conservation (LNC). However, if neutrinos are Dirac particles, then this decay process would not be possible without the emission of two neutrinos, hence conserving lepton number. Thus, the observation of neutrinoless double beta decay would provide direct evidence for the Majorana nature of neutrinos, while the non-observation of the process would not necessarily rule out the Majorana hypothesis, since its actual rate may be below the current experimental sensitivities [156].

2.5 Neutrino mass models

The experimental observation of neutrino flavor oscillations constitutes a milestone in particle physics and proves that the Standard Model is an incomplete theory. Although many questions remain open, such as the Majorana or Dirac nature of neutrinos or the possible violation of CP in the leptonic sector, the SM must certainly be extended to include a mechanism that accounts for non-zero neutrino masses and mixings. In the rest of the thesis we will work under the assumption of neutrinos being Majorana particles, implying that lepton number will be broken.

From a model-independent perspective, one of the most useful theoretical constructions that have emerged in the search for a mechanism to explain neutrino masses is the well-known

[5] This is, however, technically natural in the sense of 't Hooft [155]. This means that in the limit of the parameter going to zero, a symmetry is restored. In this case, the chiral symmetry. Therefore, any loop correction to the parameter must be proportional to the parameter itself, implying that if it is small at a certain scale, it will remain small across all scales.

Weinberg operator [157]. Proposed by Steven Weinberg in 1979, this operator, which is the lowest dimensional operator that violates lepton number, is a dimension-5 effective operator that generates Majorana masses for neutrinos. It can be expressed as:

$$\mathcal{O}_W = \frac{C_5^{\alpha\beta}}{\Lambda}\,\bar{\ell}^c_{L\alpha}\,\ell_{L\beta}\,\widetilde{H}^\dagger\,H + \text{h.c.} \tag{2.16}$$

where, as usual, $\widetilde{H} \equiv i\sigma_2 H^*$. Here, Λ is the scale at which the NP responsible for the lepton number violating effects becomes relevant, while C_5 is the model-dependent Wilson coefficients matrix, which is symmetric in flavor space. After EW symmetry breaking, the VEV of the Higgs generates the Majorana mass matrix in Eq. (2.13):

$$m_N = \frac{C_5^{\alpha\beta}\,v^2}{\Lambda}\,. \tag{2.17}$$

The smallness of neutrino masses, as implied by the Weinberg operator, corresponds to choosing a very large scale Λ. For instance, if the Wilson coefficients $C_5^{\alpha\beta}$ are of order one, we would need $\Lambda \sim O(10^{14})$ GeV to obtain $m_\nu \sim 0.1$ eV. However, it is also possible to have $C_5^{\alpha\beta}$ much smaller than one, as this would result in lower values of the energy scale Λ. This can be achieved through models in which neutrino masses are generated radiatively and the loop factors naturally suppress the coefficients. Alternatively, small couplings can be achieved due to nearly conserved symmetries in some models.

The Weinberg operator can be realized in three possible ways at tree-level, resulting in three distinct UV completions known as the type I, type II, and type III seesaw mechanisms [158–164]. These mechanisms involve different messenger fields in the generation of neutrino masses, and all of them require a large NP scale to account for the smallness of the masses, as long as we want the C_5 coefficients to be of the order of unity. However, other scenarios have to be considered when small Wilson coefficients are wanted. For instance, the inverse seesaw mechanisms are good examples of models with nearly conserved symmetries. Additionally, there are radiative neutrino mass models, with the Scotogenic model being a popular example. These models offer alternative ways to explain the smallness of neutrino masses but require different mechanisms and symmetries compared to the usual seesaw mechanisms. We will briefly review these models in the remainder of this section.

2.5.1 Tree-level scenarios

As expected, the simplest way to generate the Weinberg operator is at tree-level. We will start by introducing the standard seesaw scenarios, and then we will move to the more interesting inverse seesaws.

2.5.1.1 Type-I seesaw

The topology of the *type-I seesaw* (SS1) [158] is obtained by contracting ℓ_L and H in such a way that their product transforms as an $\mathrm{SU(2)_L}$ singlet in the Weinberg operator,

$$\mathcal{O}_W = \frac{C_5^{\alpha\beta}}{\Lambda}\left(\bar{\ell}^c_{L\alpha}\, H\right)\left(\widetilde{H}^\dagger\, \ell_{L\beta}\right) + \text{h.c.}\,. \tag{2.18}$$

Therefore, the new field involved in the neutrino mass generation must be a singlet under that symmetry, colorless and with zero hypercharge.

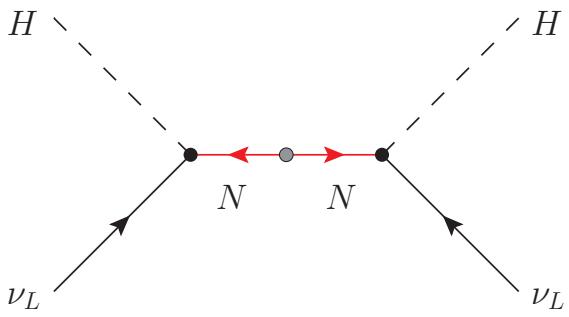

Figure 2.1: Type-I seesaw neutrino mass mechanism. This Feynman diagram shows the relevant gauge eigenstates involved in the tree-level contribution to neutrino masses.

Such a model is an extension of the SM that includes n copies of a new gauge singlet fermion, commonly known as a right-handed neutrino, N_R, with a Majorana mass term $M_R \gg v$. The number of families of the singlet lepton is arbitrary, but at least two copies are required to fit oscillation data from experiments [165]. The most general renormalizable Lagrangian is given by

$$\mathcal{L}_{\mathrm{SS1}} = \mathcal{L}_{\mathrm{SM}} + \frac{i}{2}\bar{N}_R \not{\partial} N_R - Y_\nu\, \bar{N}_R\, \widetilde{H}^\dagger\, \ell_L - \frac{1}{2} M_R\, \bar{N}_R N_R^c + \text{h.c.}\,, \tag{2.19}$$

where Y_ν is a general $n\times 3$ matrix and M_R a symmetric $n\times n$ matrix that can be chosen diagonal without loss of generality.

The right-handed neutrinos play a crucial role in generating neutrino masses through the Feynman diagram depicted in Fig. 2.1. After electroweak symmetry breaking, the neutral Majorana leptons mass term is given by

$$-\mathcal{L}_\nu = \frac{1}{2}\begin{pmatrix} \bar{\nu}^c_L & \bar{N}_R \end{pmatrix} \mathcal{M}_N \begin{pmatrix} \nu_L \\ N_R^c \end{pmatrix} + \text{h.c.}\,, \tag{2.20}$$

with the $(3+n)\times(3+n)$ symmetric matrix $\mathcal{M}_N$ defined as

$$\mathcal{M}_N = \begin{pmatrix} 0 & m_D^T \\ m_D & M_R \end{pmatrix}. \tag{2.21}$$

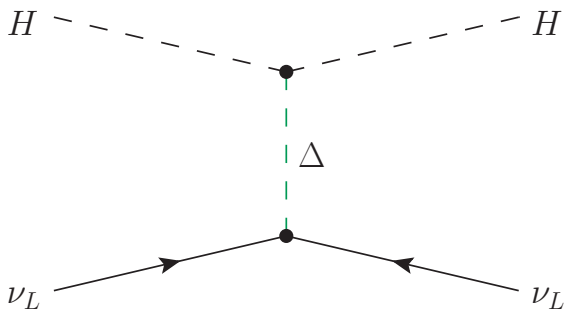

Figure 2.2: Type-II seesaw neutrino mass mechanism. This Feynman diagram shows the relevant gauge eigenstates involved in the tree-level contribution to neutrino masses.

In the previous expression, $m_D = Y_\nu v/2$. Then, the resulting Majorana mass matrix corresponds to the standard type-I seesaw matrix. If $m_D \ll M_R$, the light and heavy neutrino mass matrices are given by the well-known approximate formulae

$$\begin{aligned} m_\nu^{\text{SS1}} &\approx -m_D^T\, M_R^{-1}\, m_D\,, \\ m_R &\approx M_R\,. \end{aligned} \tag{2.22}$$

It is worth noting that the hierarchy $m_D \ll M_R$ arises naturally from $v \ll M_R$ if the Yukawa couplings are perturbative. As shown by the equation above, explaining light neutrino masses at a scale of around 0.1 eV with order one Yukawa couplings requires right-handed neutrino masses of the order of 10^{14} GeV. While this mechanism offers a natural and viable explanation for the smallness of neutrino masses, the N_R masses are well beyond the detection capabilities of current and near-future experiments.

2.5.1.2 Type-II seesaw

In the case of the *type-II seesaw* (SS2) [166], the topology is obtained by contracting both ℓ_L and H doublets, independently, such that their product transforms as a SU(2)_L triplet in the Weinberg operator,

$$\mathcal{O}_W = \frac{C_5^{\alpha\beta}}{\Lambda}\, \left(\bar{\ell}^c_{L\alpha}\, \vec{\sigma}\, \ell_{L\beta}\right) \left(\widetilde{H}^\dagger\, \vec{\sigma}\, H\right) + \text{h.c.}\,, \tag{2.23}$$

where $\vec{\sigma} \equiv (\sigma^1, \sigma^2, \sigma^3)$. This implies that, in this mechanism, the new field required for the neutrino mass generation must be an SU(2)_L triplet.

Therefore, the standard type-II seesaw extends the SM particle content with a scalar triplet with hypercharge 1, usually denoted as $\Delta = (\Delta^1, \Delta^2, \Delta^3)$. It can be conveniently written in the usual 2×2 notation,

$$\Delta = \frac{1}{\sqrt{2}}\, \sigma^i \Delta^i = \begin{pmatrix} \Delta^+/\sqrt{2} & \Delta^{++} \\ \Delta^0 & -\Delta^+/\sqrt{2} \end{pmatrix}, \tag{2.24}$$

where $\Delta^{++} \equiv (\Delta^1 - i\,\Delta^2)/\sqrt{2}$, $\Delta^+ \equiv \Delta^3$, and $\Delta^0 \equiv (\Delta^1 + i\,\Delta^2)/\sqrt{2}$. The complete Yukawa Lagrangian of the model is given by

$$\mathcal{L}_Y^{\rm SS2} = \mathcal{L}_Y^{\rm SM} + \frac{i}{2}\bar{\Delta}\not{D}\,\Delta - \left(Y_\Delta \bar{\ell}_L^c \Delta\,\ell_L + \text{h.c.}\right)\,, \tag{2.25}$$

whereas the scalar potential, which includes new terms involving the scalar triplet, can be written as

$$\begin{aligned}\mathcal{V} = {} & m_H^2 H^\dagger H + m_\Delta^2 \,\text{Tr}\left(\Delta^\dagger\Delta\right) + \lambda_H \left(H^\dagger H\right)^2 + \lambda_\Delta^1 \left[\text{Tr}\left(\Delta^\dagger\Delta\right)\right]^2 + \lambda_\Delta^2 \,\text{Tr}\left(\Delta^\dagger\Delta\right)^2 \\ & + \lambda_{H\Delta}^1 \left(H^\dagger H\right)\text{Tr}\left(\Delta^\dagger\Delta\right) + \lambda_{H\Delta}^2\, H^\dagger\Delta\,\Delta^\dagger H + \left(\mu \widetilde{H}^\dagger \Delta^\dagger\, H + \text{h.c.}\right)\,.\end{aligned} \tag{2.26}$$

Of course, since neutrinos are Majorana in this model, lepton number is broken in two units by the simultaneous presence of the new Yukawa and scalar potential trilinear terms. Also, the trilinear term is responsible for Δ acquiring an induced VEV, $\langle\Delta_0\rangle = v_\Delta/\sqrt{2}$, once the EW symmetry is broken. This can be easily seen from the tadpole equations,

$$\left.\frac{\text{d}\mathcal{V}}{\text{d}H^0}\right|_{\langle H^0\rangle=\frac{v}{\sqrt{2}},\langle\Delta^0\rangle=\frac{v_\Delta}{\sqrt{2}}} = \frac{v}{\sqrt{2}}\left[m_H^2 + \lambda_H\, v^2 + \left(\lambda_{H\Delta}^1 + \lambda_{H\Delta}^2\right)\frac{v_\Delta}{2} + \sqrt{2}\,\mu\, v_\Delta\right] = 0\,, \tag{2.27}$$

$$\left.\frac{\text{d}\mathcal{V}}{\text{d}\Delta^0}\right|_{\langle H^0\rangle=\frac{v}{\sqrt{2}},\langle\Delta^0\rangle=\frac{v_\Delta}{\sqrt{2}}} = \frac{v_\Delta}{\sqrt{2}}\left[m_\Delta^2 + \left(\lambda_\Delta^1 + \lambda_\Delta^2\right) v_\Delta^2 + \left(\lambda_{H\Delta}^1 + \lambda_{H\Delta}^2\right)\frac{v^2}{2} + \frac{\mu\, v^2}{\sqrt{2} v_\Delta}\right] = 0\,. \tag{2.28}$$

In the limit where v is much smaller than the mass of the Δ triplet,

$$v_\Delta = \frac{\mu\, v^2}{\sqrt{2} m_\Delta^2} + \mathcal{O}\left(\frac{v^4}{m_\Delta^4}\right)\,. \tag{2.29}$$

Then, from the new Yukawa interaction in Eq. (2.25), we obtain the neutrino mass matrix in the type II seesaw model

$$m_\nu^{\rm SS2} = Y_\Delta \frac{v_\Delta}{\sqrt{2}}\,. \tag{2.30}$$

This relation can also be seen from the Feynman diagram shown in Fig. 2.2. In the mass matrix, the seesaw relation is manifest: the larger the mass of the triplet is, the more the neutrino masses are suppressed. Actually, Δ being a heavy particle is well motivated by the allowed range for its VEV,

$$\mathcal{O}(1)\text{GeV} > v_\Delta > \mathcal{O}(10^{-2})\text{eV}\,. \tag{2.31}$$

The lower bound comes from the requirement of having perturbative Yukawa couplings, while the upper limit comes from electroweak precision data [167].

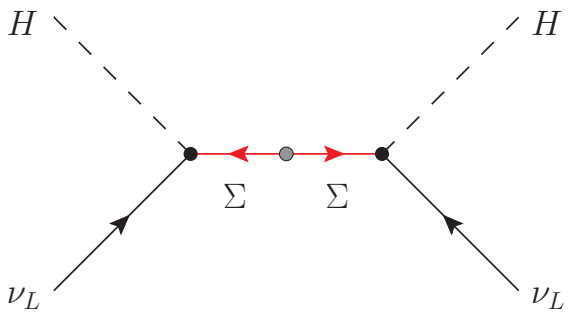

Figure 2.3: Type-III seesaw neutrino mass mechanism. This Feynman diagram shows the relevant gauge eigenstates involved in the tree-level contribution to neutrino masses.

2.5.1.3 Type-III seesaw

The topology of the *type-III seesaw* (SS3) [164] is obtained by contracting ℓ_L and H in such a way that their product transforms as an $\mathrm{SU(2)_L}$ triplet in the Weinberg operator,

$$\mathcal{O}_W = \frac{C_5^{\alpha\beta}}{\Lambda} \left(\bar{\ell}^c_{L\alpha}\, \vec{\sigma}\, H\right) \left(\widetilde{H}^\dagger\, \vec{\sigma}\, \ell_{L\beta}\right) + \text{h.c.}\,, \tag{2.32}$$

This mechanism is completely analogous to the type-I seesaw but instead of the right-handed neutrinos N_R, here we have n triplet fermions $\Sigma = (\Sigma^+, \Sigma^0, \Sigma^-)$ with hypercharge 0. As in the type-II mechanism, the triplet fermions can be written as

$$\Sigma = \begin{pmatrix} \Sigma^0/\sqrt{2} & \Sigma^+ \\ \Sigma^- & -\Sigma^0/\sqrt{2} \end{pmatrix}, \tag{2.33}$$

and the complete Lagrangian of the minimal type-III mechanism is given by

$$\mathcal{L}_{\mathrm{SS3}} = \mathcal{L}_{\mathrm{SM}} + \frac{i}{2}\bar{\Sigma}\, \not{D}\, \Sigma - \sqrt{2} Y_\Sigma\, \bar{\Sigma}\, \widetilde{H}^\dagger\, \ell_L - \frac{1}{2} M_\Sigma\, \bar{\Sigma}\Sigma^c + \text{h.c.}\,, \tag{2.34}$$

where Y_Σ is a general $n \times 3$ matrix and M_Σ a symmetric $n \times n$ matrix that can be chosen to be diagonal without losing generality.

Neutrino masses are generated here through the Feynman diagram depicted in Fig. 2.3 and after electroweak symmetry breaking, the neutral leptons mass term in the Lagrangian is given by

$$-\mathcal{L}_\nu = \frac{1}{2} \begin{pmatrix} \bar{\nu}^c_L & \bar{\Sigma}^0 \end{pmatrix} \mathcal{M}_N \begin{pmatrix} \nu_L \\ \Sigma^{0c} \end{pmatrix} + \text{h.c.}\,. \tag{2.35}$$

The $n \times n$ symmetric matrix $\mathcal{M}_N$ is defined as in Eq. (2.21) but substituting Y_ν by Y_Σ and M_R by M_Σ. Equivalently, if $m_D \ll M_\Sigma$, the light and heavy neutrino mass matrices are given by

the well-known approximations

$$\begin{aligned} m_\nu^{\text{SS3}} &\approx -m_D^T\, M_\Sigma^{-1}\, m_D\,, \\ m_R &\approx M_\Sigma\,. \end{aligned} \tag{2.36}$$

Although the results regarding the neutral fermions are the same in both type-I and type-III mechanisms, their phenomenology differs. In contrast to the right-handed neutrinos that are singlets, the triplet Σ in the type-III seesaw has gauge interactions and charged components. These charged states induce mixings of the SM charged leptons with the NP states through the new Yukawa term, which are much easier to probe experimentally compared to the mixing of neutral states. As a result, direct searches impose stringent lower bounds on the mass of the triplet [168].

2.5.1.4 Inverse type-I seesaw

The *inverse type-I seesaw* (ISS1) [169–172] was proposed to bring the standard seesaw closer to the EW scale. It is a non-minimal variant of the type-I seesaw mechanism with additional lepton singlets.

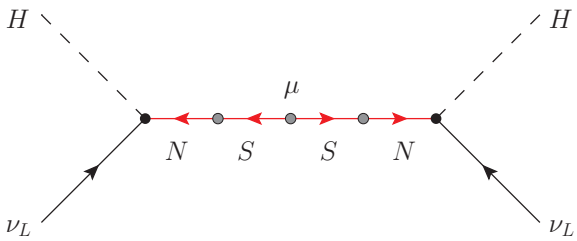

Figure 2.4: Inverse type-I seesaw neutrino mass mechanism. This Feynman diagram shows the relevant gauge eigenstates involved in the tree-level contribution to neutrino masses. The smallness of the parameter μ is closely linked to the smallness of neutrino masses.

The model extends the SM with n_N copies of a right-handed gauge singlet fermion N and with n_S extra sterile fermions S, with lepton numbers 1 and -1, respectively, although this choice is not unique. [6] The numbers of families of the singlets are, in principle, arbitrary, but at least two copies of each are required to fit oscillation data from experiments [173]. The most general renormalizable Lagrangian is given by

$$\mathcal{L}_{\text{ISS1}} = \mathcal{L}_{\text{SM}} - Y_\nu\, \bar{N}\, \widetilde{H}^\dagger\, \ell_L - Y_L\, \bar{S}\, \widetilde{H}^\dagger\, \ell_L - \frac{1}{2} m\, \bar{N} N^c - \frac{1}{2} \mu\, \bar{S} S^c - M\, \bar{N} S^c + \text{h.c.}\,, \tag{2.37}$$

where Y_ν and Y_L are general $n_N \times 3$ and $n_S \times 3$ Yukawa matrices, respectively, while m, μ, and M are symmetric $n_N \times n_N$, $n_S \times n_S$, and $n_N \times n_S$ Majorana mass matrices, respectively. The Majorana mass term for the N singlet has been included here for the sake of generality, but it

[6] Notice that in the case $n_S = 0$, we recover the standard type-I seesaw mechanism. In this case, $n_R \geq 2$ would be required for the model to be phenomenologically viable.

is normally set to zero since it does not contribute to the SM neutrino masses at leading order. Therefore, we will not include it in the following discussion. Notice, then, that both M and μ can be chosen diagonal without loss of generality. In this realization, μ and Y_L are responsible for breaking lepton number in two units. In addition, both right-handed and sterile fermions are identical in this general version of the model. The possible difference between them could only be observed in some UV theory from which this model comes. Indeed, some terms in the Lagrangian can be absent depending on the high energy theory, leading to different realizations, as we will see below.

After electroweak symmetry breaking, the neutral Majorana leptons mass term is given by

$$-\mathcal{L}_\nu = \frac{1}{2}\begin{pmatrix} \bar{\nu}_L^c & \bar{N} & \bar{S} \end{pmatrix} \mathcal{M}_N \begin{pmatrix} \nu_L \\ N^c \\ S^c \end{pmatrix} + \text{h.c.}\,, \tag{2.38}$$

with the $(3+n_N+n_S)\times(3+n_N+n_S)$ symmetric matrix $\mathcal{M}_N$ defined as

$$\mathcal{M}_N = \begin{pmatrix} 0 & m_D^T & m_L^T \\ m_D & 0 & M \\ m_L & M^T & \mu \end{pmatrix}. \tag{2.39}$$

In the previous expression, $m_D = Y_\nu\, v/2$, as usual, and $m_L = Y_L\, v/2$. However, the inverse type-I seesaw takes $m_L = 0$.[7] Considering the natural hierarchy $\mu \ll m_D \ll M$, [8] one can diagonalise the neutral leptons mass matrix, finding

$$m_\nu^{\text{ISS1}} = m_D^T \left(M^T\right)^{-1} \mu\, M^{-1} m_D\,, \tag{2.41}$$

for the light neutrinos. Their masses are generated in this realization as illustrated in the Feynman diagram in Fig. 2.4. What makes the inverse seesaw mechanism distinguish from the other seesaws is that the additional parameter μ allows us to accommodate small neutrino masses with a low seesaw scale and $\mathcal{O}(1)$ Yukawa couplings.

2.5.1.5 Inverse type-III seesaw

The *inverse type-III seesaw* model (ISS3) is obtained by replacing the fermionic SU(2)_L singlets in the original inverse type-I seesaw by SU(2)_L triplets. This variant has already been studied [177–183], although not extensively, and many of its phenomenological features are still

[7] The mechanism with $m_L \neq 0$ and $\mu = 0$ is called the *linear seesaw* (LSS) [174–176]. Here the light neutrinos mass matrix is given by

$$m_\nu^{\text{LSS}} = m_L^T M^{-1} m_D + m_D^T (M^T)^{-1} m_L\,. \tag{2.40}$$

[8] A small μ is considered to be natural in this scenario since its presence is responsible for breaking lepton number.

to be investigated. [9] In fact, there are several phenomenological directions of interest in the ISS3. The fact that triplets couple to the SM gauge bosons allows for new production mechanisms at the LHC, where one can also look for lepton number violating signatures. Lepton flavor violation might also be an interesting subject to explore in this model, which may offer some differences with respect to the more common ISS1. Finally, the potentially sizable mixing between the charged components of the type-III triplet and the SM charged leptons may also lead to observable $Z \to \ell_i^+ \ell_j^-$ decays with $i \neq j$. We refer to [190] for a recent analysis of these and other relevant observables in the presence of light fermion triplets. In Chapter 4, we will study an extension of this model along the lines of what is stated here.

Since the derivation of the neutrino masses in this mechanism is completely analogous to that shown for the inverse type-I seesaw, here we will only provide the relation between them. The singlets N and S are replaced by the triplets Σ and Σ', respectively, and the Lagrangian takes the form

$$\mathcal{L}_{\text{ISS3}} = \mathcal{L}_{\text{SM}} - \sqrt{2}\, Y_\Sigma\, \bar{\Sigma}\, \widetilde{H}^\dagger\, \ell_L - \frac{1}{2}\mu\, \bar{\Sigma}'\, \Sigma'^c - M_\Sigma\, \bar{\Sigma}\, \Sigma'^c + \text{h.c.}\,, \tag{2.42}$$

where a similar Yukawa term for Σ' has been omitted here exactly as we did in the ISS1 with $Y_L = 0$. Also, the Majorana mass term for Σ is not included either since it will not affect neutrino masses. Then, the neutral leptons and light neutrinos mass matrices will be given by Eqs.(2.39) and (2.41), respectively, with the redefinitions $m_D = Y_\Sigma\, v/2$ and $M \to M_\Sigma$.

2.5.1.6 Decoupling the small from the large seesaw scales

Sometimes it may be convenient to decouple the heavy from light fermion fields. The authors in [191] proposed a simple yet powerful method that allows decoupling the small from the large scales in the case of seesaw-type mass matrices. It allows us to obtain an approximate expression for the mass matrices to arbitrary order as well as for the unitary matrices that block-diagonalize them. We will illustrate this for the case of the neutral fields in the inverse type-I (or inverse type-III).

The mass matrix for the neutral fermions can be brought to diagonal form as

$$\widehat{\mathcal{M}}_N = V^\nu \mathcal{M}_N V^{\nu T}\,, \tag{2.43}$$

where V^ν is a unitary matrix, and the idea is to obtain an approximate expression for V^ν using a perturbative expansion in powers of the inverse of the largest scale present in $\mathcal{M}_N$. We can express the unitary matrix V^ν as

$$V^\nu = W\, D^\nu\,, \tag{2.44}$$

[9] See also [172,184] for discussions of generalized inverse seesaw models, including versions with Dirac neutrinos, [185–188] for four references studying the phenomenology of light fermion triplets and [189] for a recent work on the inverse seesaw with spontaneous violation of lepton number.

where both W and D^ν are unitary matrices. While W will be responsible for the block-diagonalization of $\mathcal{M}_N$, D^ν will diagonalize the light and heavy sub-blocks independently. The latter can be expressed as

$$D^\nu = \begin{pmatrix} D_l^\nu & 0 \\ 0 & D_h^\nu \end{pmatrix}, \tag{2.45}$$

with the non-zero entries being unitary matrices. On the other hand, we impose that W decouples the neutral states such that

$$\begin{pmatrix} \nu_L \\ N^c \\ S^c \end{pmatrix} = W \begin{pmatrix} \nu_{\text{light}} \\ N_{\text{heavy}} \end{pmatrix}, \tag{2.46}$$

and we further require that

$$W^T \mathcal{M}_N W = W^T \begin{pmatrix} M_L & M_D^T \\ M_D & M_R \end{pmatrix} W = \begin{pmatrix} M_N^{\text{light}} & 0 \\ 0 & M_N^{\text{heavy}} \end{pmatrix}, \tag{2.47}$$

where we have defined

$$M_L = 0 \quad , \quad M_D = \begin{pmatrix} m_D \\ 0 \end{pmatrix} \quad , \quad M_R = \begin{pmatrix} 0 & M \\ M^T & \mu \end{pmatrix}, \tag{2.48}$$

for our particular model. In the case of the general ISS1, with n_N copies of the right-handed singlets N and n_S sterile fermions S, the matrices M_L, M_D, and M_R are 3×3, $(n_N + n_S) \times 3$, and $(n_N + n_S) \times (n_N + n_S)$ matrices, respectively. Now, as explained in [191], we can make the ansätze

$$W = \begin{pmatrix} \sqrt{\mathbb{1}_3 - B\,B^\dagger} & B \\ -B^\dagger & \sqrt{\mathbb{1}_{(n_N+n_S)} - B^\dagger B} \end{pmatrix}, \tag{2.49}$$

where $\mathbb{1}_n$ is the $n \times n$ identity matrix and B is a $3 \times (n_N + n_S)$ matrix that can be fixed perturbatively as a function of the parameters in $\mathcal{M}_N$ by expanding in powers of m_R^{-1}, which is the scale of the eigenvalues of $\sqrt{M_R^\dagger M_R}$. Therefore,

$$B = B_1 + B_2 + B_3 + \cdots, \tag{2.50}$$

with the B_i matrices being proportional to M^{-i}. In addition, the square roots in Eq. (2.49) must also be Taylor-expanded, resulting in

$$\sqrt{\mathbb{1}_3 - B\,B^\dagger} = \mathbb{1}_3 - \frac{1}{2} B\,B^\dagger - \frac{1}{8} B\,B^\dagger\,B\,B^\dagger + \cdots, \tag{2.51}$$

$$\sqrt{\mathbb{1}_{(n_N+n_S)} - B^\dagger\,B} = \mathbb{1}_{(n_N+n_S)} - \frac{1}{2} B^\dagger\,B - \frac{1}{8} B^\dagger\,B\,B^\dagger\,B + \cdots. \tag{2.52}$$

Then, the coefficients B_i are computed recursively as indicated in [191]. At leading order, this procedure leads to

$$W = \begin{pmatrix} \mathbb{1}_3 & -m_D^\dagger \left(M^\dagger\right)^{-1} \mu^\dagger \left(M^*\right)^{-1} & m_D^\dagger \left(M^\dagger\right)^{-1} \\ \left(M^T\right)^{-1} \mu\, M^{-1} m_D & \mathbb{1}_{n_N} & 0 \\ -M^{-1} m_D & 0 & \mathbb{1}_{n_S} \end{pmatrix} + \mathcal{O}\left(m_R^{-2}\right) , \quad (2.53)$$

where we have used that $B \approx B_1 = M_D^\dagger \left(M_R^\dagger\right)^{-1}$. In addition, the light and heavy neutral fermion mass matrices are approximated, again at leading order, to

$$\begin{aligned} M_N^{\text{light}} &= -\, M_D^T \left(M_R\right)^{-1} M_D + \mathcal{O}\left(m_R^{-2}\right) = m_D^T \left(M^T\right)^{-1} \mu M^{-1} m_D + \mathcal{O}\left(m_R^{-2}\right) , \\ M_N^{\text{heavy}} &= M_R + \frac{1}{2}\left(M_D\, M_D^\dagger \left(M_R^*\right)^{-1} + \left(M_R^*\right)^{-1} M_D^* M_D^T\right) + \mathcal{O}\left(m_R^{-2}\right) . \end{aligned} \quad (2.54)$$

It can be seen that $M_N^{\text{light}} \equiv m_\nu^{\text{ISS1}}$ coincides at leading order with the previous result in Eq. (2.41).

A similar procedure can be followed for the charged lepton mass matrix, as indicated in [191]. We will follow that method in Chapter 6 for a variant of the type-I seesaw.

2.5.2 Radiative scenarios: The Scotogenic model

Among all the neutrino mass models that have been proposed over the years, radiative models are particularly appealing. After the pioneer models developed in the 80's [192–195], countless radiative models have been proposed and extensively studied [196]. These models offer several advantages over traditional tree-level scenarios: the suppression introduced by the loop factors allows for the accommodation of the observed solar and atmospheric mass scales with sizable couplings and relatively light (TeV scale) mediators. This typically leads to a richer phenomenology, with the new mediators possibly accessible to current colliders. Furthermore, some radiative models provide a straightforward solution to a completely independent problem: the nature of the dark matter in the Universe. Discrete symmetries, linked to the radiative origin of neutrino masses, may be utilized to stabilize viable DM candidates, resulting in very economical scenarios [197].

Arguably, the most popular model of this class is the Scotogenic model [198, 199].[10] It is a famous extension of the Standard Model that addresses two of the currently most important open questions in physics: the origin of neutrino masses and the nature of the dark matter of the Universe. Its popularity stems from its simplicity. The model extends the SM particle content with three singlet fermions, $N_{1,2,3}$, and a scalar doublet, η, all odd under a new *dark* $\mathbb{Z}_2$ symmetry under which the SM fields are even. These ingredients suffice to induce Majorana

[10] While the Scotogenic model is widely credited to Ernest Ma in 2006 [199], it has been noted recently that the first person linking neutrino masses to DM in this scenario was Zhijian Tao in 1996 [198].

Field	**Generations**	$\mathrm{SU(3)_c}$	$\mathrm{SU(2)_L}$	$\mathrm{U(1)_Y}$	$\mathbb{Z}_\mathbf{2}$
ℓ_L	3	**1**	**2**	-1/2	+
e_R	3	**1**	**1**	-1	+
N	3	**1**	**1**	0	−
H	1	**1**	**2**	1/2	+
η	1	**1**	**2**	1/2	−

Table 2.2: Lepton and scalar particle content and representations under the gauge and discrete symmetries in the Scotogenic model. ℓ_L and e_R are the SM left- and right-handed leptons, respectively, and H is the SM Higgs doublet.

neutrino masses at the 1-loop level and provide a viable DM candidate, namely the lightest $\mathbb{Z}_2$-odd state. The lepton and scalar particle content of the model are shown in Table 2.2.

The model contains two scalar doublets: the usual Higgs doublet H and the new doublet η, only distinguished by their $\mathbb{Z}_2$ charges. They can be decomposed in terms of their $\mathrm{SU(2)_L}$ components as

$$H = \begin{pmatrix} H^+ \\ H^0 \end{pmatrix}, \quad \eta = \begin{pmatrix} \eta^+ \\ \eta^0 \end{pmatrix}. \tag{2.55}$$

Once specified the particle content and symmetries of the model, we can write down the Lagrangian, which contains the terms

$$\mathcal{L}_\mathrm{Y} = y\,\overline{N}\,\widetilde{\eta}^\dagger\,\ell_L + \frac{1}{2}M_N\,\overline{N}^c N + \mathrm{h.c.}\,, \tag{2.56}$$

where y is a general complex 3×3 matrix and M_N is a symmetric 3×3 mass matrix. The scalar potential of the model is given by

$$\begin{aligned}\mathcal{V}_\mathrm{UV} = {} & m_H^2 H^\dagger H + m_\eta^2 \eta^\dagger\eta + \frac{\lambda_1}{2}(H^\dagger H)^2 + \frac{\lambda_2}{2}(\eta^\dagger\eta)^2 \\ & + \lambda_3(H^\dagger H)(\eta^\dagger\eta) + \lambda_4(H^\dagger\eta)(\eta^\dagger H) + \left[\frac{\lambda_5}{2}(H^\dagger\eta)^2 + \mathrm{h.c.}\right],\end{aligned} \tag{2.57}$$

where all the parameters are real except for λ_5, which is complex. Also, m_H^2 and m_η^2 are parameters with dimensions of mass^2. We assume that the minimization of the scalar potential leads to a vacuum defined by

$$\langle H^0\rangle = \frac{v}{\sqrt{2}}, \quad \langle\eta^0\rangle = 0\,. \tag{2.58}$$

This may be achieved with a proper choice of the parameters of the scalar potential, certainly requiring $m_H^2 < 0$ and $m_\eta^2 > 0$. This vacuum configuration breaks the electroweak symmetry in the usual way but preserves the $\mathbb{Z}_2$ symmetry of the model. As a consequence, the lightest $\mathbb{Z}_2$-odd state (either N_1 or η^0) is completely stable and can play the role of the DM of the Universe. Furthermore, neutrinos acquire non-zero Majorana masses at the 1-loop level, as

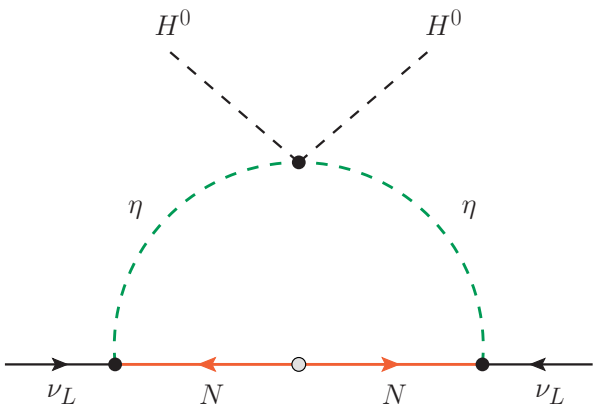

Figure 2.5: Neutrino mass generation in the Scotogenic model. This Feynman diagram shows the relevant gauge eigenstates involved in the 1-loop contribution to neutrino masses.

shown in Fig. 2.5. The resulting 3×3 neutrino mass matrix is given by

$$(m_\nu)_{\alpha\beta} = \frac{\lambda_5\, v^2}{32\pi^2} \sum_n \frac{y_{n\alpha}\, y_{n\beta}}{M_{N_n}} \left[\frac{M_{N_n}^2}{m_0^2 - M_{N_n}^2} + \frac{M_{N_n}^4}{\left(m_0^2 - M_{N_n}^2\right)^2} \log \frac{M_{N_n}^2}{m_0^2} \right] , \tag{2.59}$$

where $m_0^2 = m_\eta^2 + (\lambda_3 + \lambda_4)\, v^2/2$ and M_{N_n} are the diagonal elements of the M_N matrix, with $n = 1, 2, 3$. For the derivation of Eq. (2.59), we have assumed that all the scalar potential parameters are real, hence conserving CP in the scalar sector. We note that the stability of DM and the radiative origin of neutrino masses are both a consequence of the $\mathbb{Z}_2$ conservation. One can easily estimate that in order to obtain neutrino masses of the order of 0.1 eV with Scotogenic states in the TeV scale and Yukawas of order 1, λ_5 must be of order $\sim 10^{-10}$. The smallness of this parameter is protected by lepton number and thus is technically natural [155]. However, it is not explained in the context of the Scotogenic model. In Chapter 8, we will provide a set of ultraviolet extensions of the model in which the smallness of this parameter is naturally explained.

2.5.3 Casas-Ibarra parametrization

In Majorana neutrino mass models, the neutrino mass matrices are generated through the Yukawa interaction between the left-handed neutrinos of the Standard Model and other states. The precise form of these Yukawa couplings plays a crucial role in determining the neutrino mixing parameters and masses, ensuring that they are consistent with experimental oscillation data. However, while it is often not complicated to find isolated points in the parameter space of a given model that explain the data, a comprehensive exploration of the complete parameter space can be a challenging task in many cases.

Luckily, in 2001, Alberto Casas and Alejandro Ibarra proposed a powerful parametrization, currently known as the Casas-Ibarra parametrization [200], which provides a convenient and intuitive way to describe the neutrino Yukawa couplings. Their parametrization allows for a direct connection between the observed neutrino mixing angles and masses and the neutrino Yukawa couplings. Although it was originally presented in the framework of the type-I seesaw mechanism, it can be easily adapted to any model including a neutrino mass matrix of the form

$$m_\nu = y^T M y \,, \tag{2.60}$$

with M a symmetric matrix and y the Yukawa couplings [201, 202]. On the other hand, the authors of [203, 204] generalized the parametrization to apply it to any Majorana mass model where the contributions to the neutrino mass matrix can always be expressed in the form:

$$m_\nu = y_1^T M y_2 + y_2^T M^T y_1 \,, \tag{2.61}$$

where $y_1 \neq y_2$ in general.

The cases we are interested in always lie in the $y_1 = y_2$ scenario, and then it is enough to present here the results for the adapted Casas-Ibarra parametrization. As explained in [201–204], the Yukawa matrices can be written in full generality as

$$y = i\, V^\dagger \Sigma^{-1/2} R\, D_{\sqrt{m}}\, U^\dagger \,. \tag{2.62}$$

Here, U is the 3×3 PMNS unitary matrix, defined by the Takagi decomposition of the neutrino mass matrix

$$U^T m_\nu U = \mathrm{diag}\,(m_1, m_2, m_3) \,, \tag{2.63}$$

with m_i the three physical neutrino masses. R is a general orthogonal matrix whose dimensions are model dependent, and we have defined $D_{\sqrt{m}} = \mathrm{diag}\,(\sqrt{m_1}, \sqrt{m_2}, \sqrt{m_3})$. Finally, Σ and V are determined by the matrix M, defined implicitly by the general expression $m_\nu = y^T M y$. $\Sigma = \mathrm{diag}\,(\sigma_1, \sigma_2, \sigma_3)$ is a diagonal matrix containing the eigenvalues of M, while V is a unitary matrix such that $M = V^T \Sigma V$. With these definitions, Eq. (2.62) ensures compatibility with neutrino oscillation data.

As an example, we can consider the neutrino mass matrix in the Scotogenic model that we showed in Eq. (2.59). In this framework, the matrix M will be a 3×3 diagonal matrix given by

$$M_{mn} = \frac{\lambda_5\, v_H^2}{32\pi^2} \frac{1}{M_{N_n}} \left[\frac{M_{N_n}^2}{m_0^2 - M_{N_n}^2} + \frac{M_{N_n}^4}{\left(m_0^2 - M_{N_n}^2\right)^2} \log \frac{M_{N_n}^2}{m_0^2} \right] \delta_{mn} \,, \tag{2.64}$$

with V being the 3×3 identity matrix and

$$R = \begin{pmatrix} \cos\beta\cos\gamma & -\cos\alpha\sin\gamma - \sin\alpha\sin\beta\cos\gamma & \sin\alpha\sin\gamma - \cos\alpha\sin\beta\cos\gamma \\ \cos\beta\sin\gamma & \cos\alpha\cos\gamma - \sin\alpha\sin\beta\sin\gamma & -\sin\alpha\cos\gamma - \cos\alpha\sin\beta\sin\gamma \\ \sin\beta & \sin\alpha\cos\beta & \cos\alpha\cos\beta \end{pmatrix}, \quad (2.65)$$

where α, β, and γ are arbitrary complex angles.

2.6 Spontaneous Lepton Number Breaking: The Majoron

In Section 2.4, we saw that neutrino masses may be non-zero due to the violation of lepton number, in which case, neutrinos are Majorana particles. The literature contains numerous Majorana neutrino mass models which simply add explicit lepton number violating interactions or mass terms to the Lagrangian. However, it is also possible for the violation of $\mathrm{U(1)_L}$ to be spontaneous in origin. The spontaneous breaking of a global continuous quantum number generates a massless Goldstone boson, in the case of lepton number usually called the *majoron* [205, 206], J. The original majoron of [205, 206] is a gauge singlet. Nonetheless, it is also possible to break lepton number spontaneously using larger multiplets, resulting in the doublet and triplet majorons [207–209]. In general, the majoron can be an admixture of these three representations or even more exotic possibilities exist.

The presence of a massless boson in the particle spectrum certainly will affect phenomenology. However, the extent to which these changes are relevant for explicit lepton number violating models depends strongly on the specific model and on the nature of the majoron. For instance, the pure singlet majoron interacts so weakly with all of the SM particles that it is highly unlikely it will ever be observed experimentally. In the other extreme, *pure* doublet and triplet majorons have been ruled out by LEP [210]. Nevertheless, majorons with a sufficiently large singlet admixture can escape this constraint.

The interaction of the majoron with charged leptons can be described in a model-independent way as [211],

$$\mathcal{L}_{\ell\ell J} = J\,\bar{\ell}_\beta \left(S_L^{\beta\alpha}\,P_L + S_R^{\beta\alpha}\,P_R\right)\ell_\alpha + \text{h.c.}\,, \quad (2.66)$$

where $\ell_{\alpha,\beta}$ are the standard light charged leptons and $P_{L,R}$ are the usual chiral projectors. The $S_{L,R}$ couplings are dimensionless coefficients, and we consider all flavor combinations: $\beta\alpha = \{ee, \mu\mu, \tau\tau, e\mu, e\tau, \mu\tau\}$. Due to the pseudoscalar nature of majorons, the diagonal $S^{\beta\beta} = S_L^{\beta\beta} + S_R^{\beta\beta *}$ couplings are purely imaginary. In Chapter 3, we will derive upper bounds to these couplings.

While the values of the couplings between the majoron and the charged leptons have to be obtained for one particular model realization, it is possible to discuss some general features qualitatively. The $S_{L,R}$ couplings of the majoron with the charged leptons, introduced in Eq. (2.66),

can be generically written as

$$S_{L,R} \sim a\,\frac{\widehat{m}_e}{v} + b\,Y\,. \tag{2.67}$$

Here, Y is a general matrix in flavor space and $\widehat{m}_e$ is the diagonal charged lepton mass matrix, $\widehat{m}_e = \mathrm{diag}(m_e, m_\mu, m_\tau)$. The coefficients a and b depend on the model under consideration. In the case of a type-I seesaw and a pure singlet (or doublet) majoron, both a and b are zero at tree-level but generated at 1-loop [206, 212, 213]. The 1-loop diagram is further suppressed by the small mixing between the right-handed neutrinos and the active states, and one expects that decays such as $\mu \to e\,J$ are unobservable. For the triplet majoron, on the other hand, a is non-zero at tree-level. It is generated via the mixing of the triplet with the SM Higgs due to a coupling of the form $\lambda\,\sigma H \Delta H$, where σ is the scalar singlet, H the SM Higgs, and Δ the triplet scalar. b again can be generated only radiatively, and LFV interactions with majorons are expected to be tiny. How about the type-III seesaw? In the type-III seesaw, the charged leptons of the SM are mixed with the charged components of the fermionic triplet Σ. In the spontaneous version of this setup, one would thus expect some non-diagonal coupling of the majoron to charged leptons to appear in the mass eigenstate basis [214]. However, the corresponding mixing is related to the small neutrino masses and, in the end, the rates for $\ell_\alpha \to \ell_\beta\,J$ decays are typically very small.

This discussion can serve as a basis to establish the criteria a model has to fulfill in order to have sizeable off-diagonal couplings between the majoron and charged leptons. First of all, if the majoron couplings to charged leptons are induced via majoron mixing with the SM Higgs doublet, they will be exactly diagonal in the charged lepton mass basis. Therefore, in order to obtain sizable off-diagonal couplings, the majoron must couple directly to the charged lepton sector. This coupling can be either to the light charged leptons themselves or to some additional heavy charged leptons which, after symmetry breaking, mix with them. In the first case, sizeable off-diagonal couplings can be obtained with a non-universal lepton number assignment, whereas in the second case, it is crucial that the light-heavy mixing is not suppressed by neutrino masses. We refer to [215] for a discussion along similar lines.

Part II

Leptonic Observables and Standard Model Anomalies

Chapter 3

Ultralight scalars in leptonic observables

In the realm of particle physics, the quest to discover new physics effects beyond the Standard Model is both an exciting and ongoing endeavor. From a theoretical perspective, one interesting avenue consists in exploring the potential contributions of new states and interactions to different observables. If these observables are predicted by the Standard Model, two scenarios emerge: either the theory agrees with the experimental results, limiting the new contributions, or the model is in tension with the measured values, indicating the possibility of using these new fields to reconcile both outcomes. Additionally, the new states may contribute to observables strictly forbidden in the Standard Model, motivating the need to search for them experimentally to probe the hypotheses.

3.1 Introduction

There is an exciting experimental perspective in the near future, as hinted in Section 2.3, so it is natural to question the potential for new physics discoveries. In this Chapter, based on [211], we will focus on the study of ultralight scalars that couple to charged leptons and examine their impact on leptonic observables. In this context, the term *ultralight scalar* refers to a generic scalar ϕ much lighter than the electron, such that $m_\phi \ll m_e$, allowing ϕ to be produced on-shell in charged lepton decays. In practice, the scalar can be treated as an approximately massless particle in all the physical processes considered here. In the following, we will adopt a model-independent approach and neglect the mass m_ϕ in our analytical computations. This is, however, not an approximation in the case of an exactly massless scalar such as a Goldstone boson whose mass is protected by a spontaneously broken global continuous symmetry.

Many physics scenarios contain these ultralight scalars. Majorons, which are the Goldstone bosons associated to the breaking of global lepton number [206–209], as discussed above in Section 2.6, constitute a well-motivated example of this type of particle. Besides majorons, the

apparent absence of CP violation in the strong interactions may be explained by the Peccei-Quinn mechanism [216], suggesting the existence of a new ultralight pseudoscalar: the axion [217, 218]. Nevertheless, the mass of the axion is not predicted by the theory and can range over a broad spectrum [219], although a significant portion of the parameter space (corresponding to large axion decay constants) results in an ultralight axion. Interestingly, this low mass axion could potentially play a role as a component of the DM of the Universe [220–222]. Axion-like particles (ALPs) generalize this scenario by allowing the mass and decay constant to be two independent parameters. This expands the parameter space, including again a large portion with really low-mass ALPs. An alternate ultralight scalar is the familon, a Goldstone boson resulting from the spontaneous breaking of global family symmetry. Additionally, the Universe may contain ultralight scalars as fuzzy cold dark matter [223].

While the examples mentioned previously are pseudoscalar states, the ultralight scalar we are interested in can also have scalar couplings. This would be the case for a massless Goldstone boson if the associated broken symmetry is non-chiral. Consequently, limiting the phenomenological exploration just to pseudoscalars would exclude many well-motivated scenarios. This has frequently been the situation in recent works [224–234], which were mainly interested in the phenomenological implications of flavored axions (or ALPs) and majorons [213].

Driven by the principle of generalization, we consider a generic scenario not determining the CP nature of the scalar and exploring several leptonic observables of interest. In most of the cases, we will generalize previous results present in the literature, commonly obtained for pure pseudoscalars or for the case of a massive ϕ. Some examples of the observables include the possibility of ϕ being produced in the final state, as in $\ell_\alpha \to \ell_\beta\, \phi$ or $\ell_\alpha \to \ell_\beta\, \phi\, \gamma$. In other processes that we will study, ϕ will not be produced but act as a mediator. One of the finest examples of this category is $\ell_\alpha^- \to \ell_\beta^- \ell_\beta^- \ell_\beta^+$. To the extent of our knowledge, the mediation of this decay by an ultralight scalar has only been previously considered in [224]. Here we will extend the previous work to a more general scalar state, providing an analytical expression for the decay width of the process. The analogous processes $\ell_\alpha^- \to \ell_\beta^- \ell_\gamma^- \ell_\gamma^+$ and $\ell_\alpha^- \to \ell_\beta^+ \ell_\gamma^- \ell_\gamma^-$ will be addressed as well, though for the first time here. Finally, other interesting examples of observables induced by the ultralight ϕ can be found in the anomalous magnetic and electric moments of charged leptons.

3.2 Effective Lagrangian

We are interested in studying low-energy charged leptons processes in the presence of the ultralight real scalar ϕ. Even though we treat ϕ as exactly massless for practical purposes, our results apply for a massive ϕ, as long as $m_\phi \ll m_e$ holds. This is a natural situation for Goldstone or pseudo Nambu-Goldstone bosons, but it may require fine-tuning in the case of CP-even scalars. The interaction between ϕ and a pair of charged leptons ℓ_α and ℓ_β, where $\alpha, \beta = e, \mu, \tau$, can be

generally parametrized by

$$\mathcal{L}_{\ell\ell\phi} = \phi\, \bar{\ell}_\beta \left(S_L^{\beta\alpha} P_L + S_R^{\beta\alpha} P_R \right) \ell_\alpha + \text{h.c.}\,, \tag{3.1}$$

where $P_{L,R} = \frac{1}{2}(1 \mp \gamma_5)$ are the standard chiral projectors, and no sum over the α and β charged lepton flavor indices is performed. Lastly, S_L and S_R are dimensionless coefficients and we consider all possible flavor combinations: $\beta\alpha = \{ee, \mu\mu, \tau\tau, e\mu, e\tau, \mu\tau\}$. Eq. (3.1) describes the most general effective interaction between the ultralight scalar ϕ and a pair of charged leptons, including both scalar and pseudoscalar interactions as well as flavor violating and flavor conserving interactions. It is a generalization of Eq. (2.66), since the diagonal interactions are allowed to have here pure scalar couplings. In Appendix A, we present an alternative parametrization for this effective Lagrangian based on the introduction of derivative interactions, only applicable to the case of pseudoscalar interactions.

Some of the observables that we analyze below receive contributions from the usual dipole and 4-fermion operators. Therefore, the full effective Lagrangian [1] we have to use is given by

$$\mathcal{L} = \mathcal{L}_{\ell\ell\phi} + \mathcal{L}_{\ell\ell\gamma} + \mathcal{L}_{4\ell}\,, \tag{3.2}$$

with

$$\mathcal{L}_{\ell\ell\gamma} = \frac{e\, m_\alpha}{2}\, \bar{\ell}_\beta\, \sigma^{\mu\nu} \left[\left(K_2^L \right)^{\beta\alpha} P_L + \left(K_2^R \right)^{\beta\alpha} P_R \right] \ell_\alpha F_{\mu\nu} + \text{h.c.}\,, \tag{3.3}$$

$$\mathcal{L}_{4\ell} = \sum_{\substack{I=S,V,T \\ X,Y=L,R}} \left(A_{XY}^I \right)^{\beta\alpha\delta\gamma}\, \bar{\ell}_\beta \Gamma_I P_X \ell_\alpha\, \bar{\ell}_\delta \Gamma_I P_Y \ell_\gamma + \text{h.c.}\,, \tag{3.4}$$

where $F_{\mu\nu}$ is the electromagnetic field strength tensor introduced in Eq. (1.10), and we have defined $\Gamma_S = 1$, $\Gamma_V = \gamma_\mu$ and $\Gamma_T = \sigma_{\mu\nu}$. No sum over the α, β, γ and δ charged lepton flavor indices is performed in Eqs. (3.3) and (3.4). The coefficients K_2^X and A_{XY}^I, with $I = S, V, T$ and $X, Y = L, R$, have dimensions of mass^{-2}. We assume $m_\alpha > m_\beta$ and therefore normalize the Lagrangian in Eq. (3.3) by including the mass of the heaviest charged lepton in the process of interest. Eq. (3.3) contains the usual photonic dipole operators, which contribute to $\ell_\alpha \to \ell_\beta \gamma$ and lead to

$$\Gamma\left(\ell_\alpha \to \ell_\beta \gamma\right) = \frac{e^2\, m_\alpha^5}{16\,\pi} \left[\left| \left(K_2^L \right)^{\beta\alpha} \right|^2 + \left| \left(K_2^R \right)^{\beta\alpha} \right|^2 \right], \tag{3.5}$$

while Eq. (3.4) contains 4-lepton operators. To summarize, the effective Lagrangian shown in Eq. (3.2) corresponds to the one in [235], but including the new operators with the ultralight scalar ϕ introduced in Eq. (3.1).

In the following, we will focus on purely leptonic observables and ignore interactions of ϕ with quarks. These processes include the LFV decays $\ell_\alpha \to \ell_\beta\, \phi$ or $\ell_\alpha \to \ell_\beta \ell_\beta \ell_\beta$, and the electron

[1] In this context, we use the term *effective* to refer to generic operators not necessarily of dimension larger than 4.

and muon anomalous magnetic and electric dipole moments. Although ϕ couplings to quarks are possible in specific realizations of our general scenario, for instance, for the QCD axion, they introduce a significant model dependence. Nevertheless, leptophilic ultralight scalars, such as the majoron, are also well-motivated possibilities that naturally appear in models with spontaneous violation of global lepton number.

3.3 Bounds on leptonic flavor conserving couplings

Before moving to the computation of the observables, let us comment on the current experimental constraints on the lepton flavor conserving couplings of the scalar ϕ. We will start by discussing the stellar cooling mechanism. Since this subject has been extensively studied in the literature, and we do not want to delve further into the topic, we will only present a brief outline. Then we will discuss another source of constraints, the 1-loop coupling between ϕ and a pair of photons.

3.3.1 Stellar cooling

The production of scalar particles inside stars, followed by their subsequent emission, may constitute a powerful stellar cooling mechanism. If this process occurs at a high rate, it may alter star evolution, eventually leading to conflict with astrophysical observations [236]. This sets stringent constraints on the ϕ couplings. The dominant cooling mechanisms are scalar bremsstrahlung in lepton-nucleus scattering, $\ell^- + N \to \ell^- + N + \phi$, and the Compton process $\gamma + \ell^- \to \ell^- + \phi$, with their relative importance depending on the density and temperature of the medium, that is, on the astrophysical scenario. In particular, the Compton process dominates only in low-density and high-temperature environments, like red giants. Limits can also be derived from ultralight scalar production in supernovae. In these astrophysical scenarios, the scalar ϕ can be efficiently produced and, since it will typically escape without interacting with the medium, it will take place a net transport of energy out of the supernova. Such an energy loss may dramatically affect other processes that may take place in the supernova, such as neutrino production.

Plenty of works have recently studied the question of astrophysical cooling by the emission of ultralight scalars [219, 234, 237–239]. However, to the best of our knowledge, all of them consider axions or ALPs. These are low-mass pseudoscalars and thus, their impact on stellar evolution can only be used to constrain pseudoscalar couplings. Even though we will not provide a detailed calculation to support this statement, we will argue that similar bounds can be set on the scalar couplings.

To make the pure scalar and pseudoscalar interactions explicit, we can use a redefinition of our Lagrangian in Eq. (3.1) which, for the diagonal terms, can be written as

$$\mathcal{L}^{\text{diag}}_{\ell\ell\phi} = \phi\,\bar{\ell}_\beta \left(S^{\beta\beta} P_L + S^{\beta\beta *} P_R\right) \ell_\beta = \phi\,\bar{\ell}_\beta \left[\text{Re}\, S^{\beta\beta} - i\,\text{Im}\, S^{\beta\beta}\,\gamma_5\right] \ell_\beta\,, \tag{3.6}$$

with $S^{\beta\beta} = S_L^{\beta\beta} + S_R^{\beta\beta *}$. For a pure pseudoscalar, only $\mathrm{Im}\, S^{\beta\beta}$ is present.

Currently the most stringent limit on the pseudoscalar couplings to electrons is derived from white dwarfs. Specifically, the limit is obtained by considering the bremsstrahlung process, which can be very efficient in the dense core of a white dwarf. Using data from the Sloan Digital Sky Survey and the SuperCOSMOS Sky Survey, Ref. [234] found (at 90% C.L.)

$$\mathrm{Im}\, S^{ee} < 2.1 \times 10^{-13}\,. \tag{3.7}$$

The coupling with muons has been recently studied in some works [234, 237, 238]. In this case the process ultimately used to set the constraint is neutrino production, clearly suppressed if energy is transported out of the supernova by scalars produced in $\mu + \gamma \to \mu + \phi$. Using the famous supernova SN1987A, Ref. [238] has found

$$\mathrm{Im}\, S^{\mu\mu} < 2.1 \times 10^{-10}\,. \tag{3.8}$$

Setting precise limits for the scalar parts of the couplings would require a complete analysis implying the calculation of the cross sections and the energy-loss rates per unit mass. Instead, one can gauge the relevance of the bounds on the scalar couplings by making the following arguments. First, we note that if we neglect the charged lepton mass, the scalar and pseudoscalar couplings contribute exactly in the same way to the relevant cross sections. However, this is not an accurate approximation due to the low energies involved in the astrophysical scenarios that set the limits. Hence, one must keep the charged lepton mass. We have numerically integrated the cross sections for a wide range of low energies and found that, for the same numerical value of $\mathrm{Re}\, S$ and $\mathrm{Im}\, S$, the scalar interaction always results in larger cross sections. Therefore, the constraints on the scalar couplings will be stronger and we can conclude that

$$\mathrm{Re}\, S^{\beta\beta} \lesssim \left[\mathrm{Im}\, S^{\beta\beta}\right]_{\mathrm{max}}\,, \tag{3.9}$$

with $\beta = e, \mu$. Nevertheless, we point out again that a detailed analysis of the cooling mechanism with pure scalars is required to fully determine the corresponding bounds.

As a final remark, one should note that these limits are based on the (reasonable) assumption that the scalar properties are not altered in the astrophysical medium. In particular, its mass and couplings are assumed to be the same as in vacuum. However, some mechanisms have been recently proposed [240, 241] (see also previous work in [242]) that would render this assumption invalid. These works were mainly motivated by the XENON1T results, which included a $3.5\,\sigma$ excess of low-energy electron recoil events [243]. An axion explaining this excess would violate the astrophysical constraints, since the required coupling to electrons would be larger than the limit in Eq. (3.7), see for instance [239]. This motivates the consideration of mechanisms that alter the effective couplings to electrons or the axion mass in high-density scenarios. If any of these mechanisms are at work, larger diagonal couplings would be allowed. However, we note

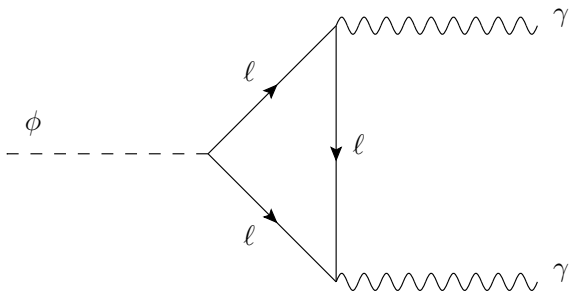

Figure 3.1: Loop induced coupling of ϕ to a pair of photons.

that additional bounds, not derived from astrophysical observations, can be set on the diagonal couplings. This is precisely what we proceed to discuss.

3.3.2 1-loop coupling to photons

The interaction of the scalar ϕ with a pair of photons is described by the effective Lagrangian

$$\mathcal{L}_{\phi\gamma\gamma} = g_{S\gamma\gamma}\,\phi\,F_{\mu\nu}F^{\mu\nu} + g_{A\gamma\gamma}\,\phi\,F_{\mu\nu}\widetilde{F}^{\mu\nu}\,, \tag{3.10}$$

where $g_{S\gamma\gamma}$ and $g_{A\gamma\gamma}$ are the couplings for a pure scalar and a pure pseudoscalar, respectively, and $\widetilde{F}^{\mu\nu}$ is the dual electromagnetic tensor, defined as

$$\widetilde{F}^{\mu\nu} = \frac{1}{2}\,\varepsilon^{\mu\nu\alpha\beta}\,F_{\alpha\beta}\,. \tag{3.11}$$

The couplings $g_{S\gamma\gamma}$ and $g_{A\gamma\gamma}$ can be generated at the 1-loop level from diagrams involving charged leptons, as depicted in Fig. 3.1. Since $g_{S\gamma\gamma}$ and $g_{A\gamma\gamma}$ are constrained by a variety of experimental sources, this can be used to set indirect constraints on the ϕ couplings to charged leptons introduced in Eq. (3.1). In particular, we will exploit this connection to impose additional limits on the lepton flavor conserving couplings of ϕ. The 1-loop analytical expression for $g_{S\gamma\gamma}$ and $g_{A\gamma\gamma}$ can be written as [244] [2]

$$|g_{I\gamma\gamma}|^2 = \frac{\alpha^2}{64\,\pi^2}\left|\sum_\beta \frac{g_{I\beta\beta}}{m_\beta}\,A^I_{1/2}\left(\tau_\beta\right)\right|^2\,, \tag{3.12}$$

where $I = S, A$ and we sum over $\beta = e, \mu, \tau$. Here $g_{I\beta\beta}$ denote the ϕ couplings to the charged leptons, and their relation to S_L and S_R is given below. $A^S_{1/2}$ and $A^A_{1/2}$ are 1-loop fermionic functions defined as

$$A^S_{1/2}(\tau_\beta) = 2\left[\tau_\beta + (\tau_\beta - 1)\,f\left(\tau_\beta\right)\right]\tau_\beta^{-2} \tag{3.13}$$

[2] It is important to highlight the disagreement between the results presented in Ref. [244] and Ref. [245]. Nevertheless, the latter work obtains the 1-loop couplings to photons under the assumption that the scalar is much heavier than the QCD scale, so the ultralight scalar limit cannot be recovered.

for the scalar coupling and

$$A_{1/2}^{A}(\tau_\beta) = 2\tau_\beta^{-1} f(\tau_\beta) \tag{3.14}$$

for the pseudoscalar case, with $\tau_\beta = m_\phi^2/4m_\beta^2$. The function $f(\tau)$ can be found for instance in [246]. It is given by

$$f(\tau) \equiv \begin{cases} \arcsin^2\sqrt{\tau} & \tau \leq 1 \\ -\frac{1}{4}\left[\log\frac{1+\sqrt{1-\tau^{-1}}}{1-\sqrt{1-\tau^{-1}}} - i\pi\right]^2 & \tau > 1 \end{cases} . \tag{3.15}$$

In this work, we consider the case of an ultralight scalar. In the limit $m_\phi \to 0$, the loop functions reduce simply to $A_{1/2}^{S}(0) = \frac{4}{3}$ and $A_{1/2}^{A}(0) = 2$, and then we can write

$$\begin{aligned} |g_{S\gamma\gamma}|^2 &= \frac{\alpha^2}{36\,\pi^2}\left|\sum_\beta \frac{g_{S\beta\beta}}{m_\beta}\right|^2 , \\ |g_{A\gamma\gamma}|^2 &= \frac{\alpha^2}{16\,\pi^2}\left|\sum_\beta \frac{g_{A\beta\beta}}{m_\beta}\right|^2 , \end{aligned} \tag{3.16}$$

with the couplings to the charged leptons being given by

$$\begin{aligned} g_{S\beta\beta} &= \mathrm{Re}\, S^{\beta\beta} , \\ g_{A\beta\beta} &= \mathrm{Im}\, S^{\beta\beta} . \end{aligned} \tag{3.17}$$

We are now in a position to compare to the current experimental limits on the coupling to photons, which are of two types. First, let us consider astrophysical limits. Magnetic fields around astrophysical sources of photons may cause the photons to transform into scalars, providing a way to set constraints on their coupling. Ref. [247] provides a comprehensive overview of limits from astrophysical observations. Ref. [248] finds that for scalar masses in the range $m_\phi \ll 1\,\mathrm{peV}\,(1\,\mathrm{neV})$, astrophysical constraints imply

$$g_{I\gamma\gamma} \lesssim 10^{-12}\left(10^{-11}\right)\ \mathrm{GeV}^{-1} \tag{3.18}$$

for both scalar and pseudoscalar couplings. Taking this into account, we can find the relations

$$\begin{aligned} \left|\sum_\beta \frac{\mathrm{Re}\, S^{\beta\beta}}{m_\beta}\right|^2 &= \frac{36\,\pi^2}{\alpha^2}\, g_{S\gamma\gamma}^2 < 6.7\times 10^{-16}\,\mathrm{GeV}^{-2} , \\ \left|\sum_\beta \frac{\mathrm{Im}\, S^{\beta\beta}}{m_\beta}\right|^2 &= \frac{16\,\pi^2}{\alpha^2}\, g_{A\gamma\gamma}^2 < 3.0\times 10^{-16}\,\mathrm{GeV}^{-2} , \end{aligned} \tag{3.19}$$

which translate into very stringent bounds on the diagonal couplings to charged leptons, $S^{ee} \lesssim 10^{-11}$ and $S^{\mu\mu} \lesssim 10^{-9}$. The OSQAR experiment [249], a light-shining-through-a-wall experiment, has also derived limits for massless scalars. Again, these are valid for both scalar and

pseudoscalar couplings,

$$g_{I\gamma\gamma} < 5.76 \times 10^{-8}\,\text{GeV}^{-1}\,, \tag{3.20}$$

and therefore,

$$\begin{aligned} \left|\sum_\beta \frac{\text{Re}\,S^{\beta\beta}}{m_\beta}\right|^2 &= \frac{36\,\pi^2}{\alpha^2}\,g_{S\gamma\gamma}^2 < 3.8 \times 10^{-8}\,\text{GeV}^{-2}\,, \\ \left|\sum_\beta \frac{\text{Im}\,S^{\beta\beta}}{m_\beta}\right|^2 &= \frac{16\,\pi^2}{\alpha^2}\,g_{A\gamma\gamma}^2 < 1.7 \times 10^{-8}\,\text{GeV}^{-2}\,. \end{aligned} \tag{3.21}$$

These relations also imply strong constraints on the diagonal couplings to charged leptons, but milder than in the previous case with astrophysical observations, $S^{ee} \lesssim 10^{-7}$ and $S^{\mu\mu} \lesssim 10^{-5}$.

Finally, we point out that these indirect limits are strictly only valid if the diagrams in Fig. 3.1 are the sole contributions to the ϕ coupling to photons. If additional contributions exist, possible cancellations among them may reduce the total coupling so that the constraints are satisfied for larger couplings to charged leptons. We should also note that astrophysical constraints are subject to the same limitations discussed above. They rely on the assumption that the properties of ϕ in the astrophysical medium are the same as in vacuum.

3.4 Leptonic observables

3.4.1 $\ell_\alpha \to \ell_\beta\,\phi$

Using the effective Lagrangian in Eq. (3.1), it is straightforward to obtain the branching ratio of the LFV decays $\ell_\alpha \to \ell_\beta\,\phi$,

$$\Gamma\left(\ell_\alpha \to \ell_\beta\,\phi\right) = \frac{m_\alpha}{32\,\pi}\left(\left|S_L^{\beta\alpha}\right|^2 + \left|S_R^{\beta\alpha}\right|^2\right)\,, \tag{3.22}$$

where terms proportional to the small ratio m_β/m_α have been neglected. [3] The off-diagonal $S_A^{\beta\alpha}$ scalar couplings, with $A = L, R$, can be directly constrained from these processes.

3.4.2 $\ell_\alpha \to \ell_\beta\,\gamma\,\phi$

The decay width for the 3-body LFV process $\ell_\alpha \to \ell_\beta\,\gamma\,\phi$ can be written as

$$\Gamma\left(\ell_\alpha \to \ell_\beta\,\gamma\,\phi\right) = \frac{\alpha\,m_\alpha}{64\pi^2}\left(\left|S_L^{\beta\alpha}\right|^2 + \left|S_R^{\beta\alpha}\right|^2\right)\mathcal{I}\left(x_{\text{min}}, y_{\text{min}}\right)\,, \tag{3.23}$$

[3] We must notice that this approximation is not equally good for all $\ell_\alpha \to \ell_\beta\,\phi$ cases. This is because the ratio $m_\mu/m_\tau \sim 0.1$ is not completely negligible. Therefore, while the approximation is very good for $\mu \to e\,\phi$ and $\tau \to e\,\phi$, it may lead to an error of the order of 20% in $\tau \to \mu\,\phi$. This deviation is acceptable, but can be accounted for by including additional terms proportional to m_μ/m_τ, hence leading to a much more complicated analytical expression. Completely analogous comments can be made for the rest of the observables discussed in this section.

where terms proportional to m_β/m_α have been neglected. Here $\mathcal{I}(x_{\min}, y_{\min})$ is a phase space integral given by

$$\mathcal{I}(x_{\min}, y_{\min}) = \int \mathrm{d}x\, \mathrm{d}y\, \frac{(x-1)(2-xy-y)}{y^2(1-x-y)}\,, \tag{3.24}$$

and we have introduced the usual dimensionless parameters x and y, defined as

$$x = \frac{2E_\beta}{m_\alpha} \quad , \quad y = \frac{2E_\gamma}{m_\alpha}\,, \tag{3.25}$$

which, together with $z = 2E_\phi/m_\alpha$, must fulfill the kinematical condition $x+y+z = 2$. We point out that our analytical results match those in [250], except for redefinitions in the couplings. [4]

The phase space integral in Eq. (3.24) depends on $x_{\min}$ and $y_{\min}$, the minimal values of the x and y parameters. While one could naively think that kinematics dictate their values, they are actually determined by the minimal ℓ_β lepton and photon energies measured in a given experiment. This properly adapts the calculation of the phase space integral to the physical region explored in a real experiment and also eliminates the kinematical divergences that would otherwise appear. In fact, we note that the integral in Eq. (3.24) becomes divergent when the photon energy vanishes ($y \to 0$) as, in this case, the photon would not be observable by any detector. This is the well-known infrared divergence that also appears, for instance, in the radiative SM decay $\mu \to e\nu\bar{\nu}\gamma$. Another divergence appears when the photon and the ℓ_β lepton in the final state are emitted in the same direction. The angle between their momenta is given by

$$\cos\theta_{\beta\gamma} = 1 + \frac{2-2(x+y)}{xy}\,. \tag{3.26}$$

Since we work in the limit $m_\beta = 0$, one finds a colinear divergence in configurations in which the photon and the ℓ_β lepton have their momenta aligned ($\theta_{\beta\gamma} \to 0$). Again, if these two particles are emitted parallel to each other, the lack of energy resolution in the detector makes it impossible to distinguish between them. Therefore, infrared and collinear divergences can be effectively canceled by considering other processes that are not distinguishable in practice. This includes both processes in which soft photons are emitted and those where the massless particles are produced in parallel. This approach provides a more comprehensive treatment of the interactions and ensures that the final result is free from infrared divergences. However, any experimental setup has a finite resolution, which implies a non-zero minimum measurable E_γ and a non-zero minimum $\theta_{\beta\gamma}$ angle. Therefore, by restricting the phase space integration to the kinematical region explored in a realistic situation, all divergences disappear.

On the other hand, direct comparison with Eq. (3.22) allows one to establish the relation

$$\Gamma(\ell_\alpha \to \ell_\beta\, \gamma\, \phi) = \frac{\alpha}{2\pi}\, \mathcal{I}(x_{\min}, y_{\min})\, \Gamma(\ell_\alpha \to \ell_\beta\, \phi)\,, \tag{3.27}$$

[4] In the model considered in [250], the right-handed coupling was suppressed and hence neglected.

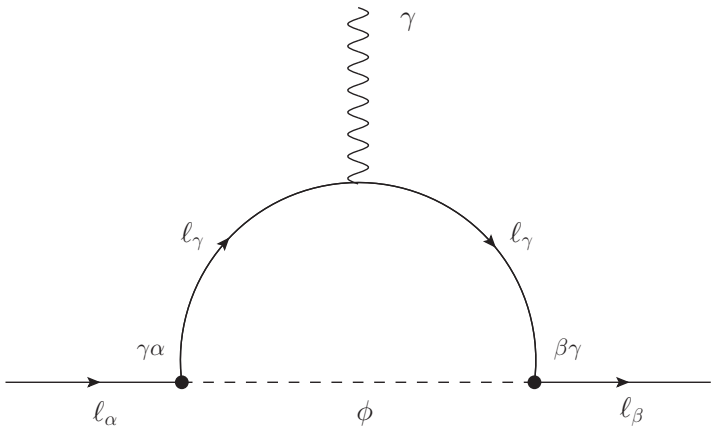

Figure 3.2: 1-loop Feynman diagram contributing to the process $\ell_\alpha \to \ell_\beta\gamma$ described by the effective Lagrangian in Eq. (3.1). The flavor indices of the couplings contributing to the diagram have been specified in the vertices.

which tells us that $\ell_\alpha \to \ell_\beta\,\gamma\,\phi$ is suppressed with respect to $\ell_\alpha \to \ell_\beta\,\phi$ due to an additional α coupling and a phase space factor. In fact, the latter turns out to be the main source of suppression.

3.4.3 $\ell_\alpha \to \ell_\beta\,\gamma$

The amplitude for the $\ell_\alpha \to \ell_\beta\,\gamma$ radiative decay only receives contributions from dipole operators and takes the general form

$$\mathcal{M}_\phi = -e\,\bar{u}_\beta \left\{ m_\alpha\,\sigma^{\mu\nu} q_\nu \left[\left(K_2^L\right)^{\beta\alpha} P_L + \left(K_2^R\right)^{\beta\alpha} P_R \right] \right\} u_\alpha\,\varepsilon_\mu^*\,, \tag{3.28}$$

where u and v are spinors and q_μ and ε_μ are the photon 4-momentum and polarization vector, respectively. The K_2^L and K_2^R coefficients are induced at the 1-loop level, as shown in Fig. 3.2, and we find the expressions

$$\begin{aligned}\left(K_2^L\right)^{\beta\alpha} =& \frac{1}{32\pi^2\,m_\alpha^5\,m_\beta^3\,(m_\alpha+m_\beta)\,(m_\alpha-m_\beta)^2}\left[C_L^{\gamma\alpha}\,C_L^{\beta\gamma}\,f_1\,(m_\alpha,m_\beta,m_\gamma)\right.\\ &\left.+\,C_L^{\gamma\alpha}\,C_R^{\beta\gamma}\,f_2\,(m_\alpha,m_\beta,m_\gamma)+C_R^{\gamma\alpha}\,C_L^{\beta\gamma}\,f_2\,(m_\beta,m_\alpha,m_\gamma)\right]\,,\end{aligned} \tag{3.29}$$

$$\begin{aligned}\left(K_2^R\right)^{\beta\alpha} =& \frac{1}{32\pi^2\,m_\alpha^5\,m_\beta^3\,(m_\alpha+m_\beta)\,(m_\alpha-m_\beta)^2}\left[C_R^{\gamma\alpha}\,C_R^{\beta\gamma}\,f_1\,(m_\beta,m_\alpha,m_\gamma)\right.\\ &\left.+\,C_L^{\gamma\alpha}\,C_R^{\beta\gamma}\,f_2\,(m_\beta,m_\alpha,m_\gamma)+C_R^{\gamma\alpha}\,C_L^{\beta\gamma}\,f_2\,(m_\alpha,m_\beta,m_\gamma)\right]\,,\end{aligned} \tag{3.30}$$

where a sum over γ is implicit and the f_i loop functions are defined as

$$\begin{aligned} f_1\left(m_\alpha, m_\beta, m_\gamma\right) = & \, 2\, m_\alpha\, m_\beta\, m_\gamma \left[m_\beta^2 \left(m_\alpha^2 - m_\beta^2\right)\left(m_\alpha^2 - m_\gamma^2\right) \log \frac{m_\gamma^2}{m_\gamma^2 - m_\alpha^2} \right. \\ & + m_\alpha^2 \left(m_\beta^2 - m_\alpha^2\right)\left(m_\beta^2 - m_\gamma^2\right) \log \frac{m_\gamma^2}{m_\gamma^2 - m_\beta^2} \\ & \left. + m_\alpha^2\, m_\beta^2 \left(m_\alpha^2 - m_\beta^2\right)^2 C_0\left(0, m_\alpha^2, m_\beta^2, m_\gamma, m_\gamma, 0\right) \right] , \end{aligned} \tag{3.31}$$

$$\begin{aligned} f_2\left(m_\alpha, m_\beta, m_\gamma\right) = & \, m_\alpha^3 \left(m_\beta^2 - m_\gamma^2\right)\left[2\, m_\beta^2\, m_\gamma^2 + m_\alpha^2\left(m_\beta^2 - m_\gamma^2\right)\right] \log \frac{m_\gamma^2}{m_\gamma^2 - m_\beta^2} \\ & - m_\alpha^3\, m_\beta^2 \left(m_\alpha^2 - m_\beta^2\right)\left(m_\beta^2 + m_\gamma^2\right) - m_\alpha\, m_\beta^4 \left(m_\alpha^4 - m_\gamma^4\right) \log \frac{m_\gamma^2}{m_\gamma^2 - m_\alpha^2} \\ & - 2\, m_\alpha^3\, m_\beta^4\, m_\gamma^2 \left(m_\alpha^2 - m_\beta^2\right) C_0\left(0, m_\alpha^2, m_\beta^2, m_\gamma, m_\gamma, 0\right) , \end{aligned} \tag{3.32}$$

and we have introduced here the usual scalar Passarino-Veltman three-point function

$$\begin{aligned} C_0\left(0, m_\alpha^2, m_\beta^2, m_\gamma, m_\gamma, 0\right) = & \frac{1}{2\left(m_\alpha^2 - m_\beta^2\right)} \left[\log^2\left(-\frac{m_\gamma^2}{m_\alpha^2}\right) \right. \\ & \left. - \log^2\left(-\frac{m_\gamma^2}{m_\beta^2}\right) + 2\,\mathrm{Li}_2\,\frac{m_\gamma^2}{m_\alpha^2} - 2\,\mathrm{Li}_2\,\frac{m_\gamma^2}{m_\beta^2} \right] . \end{aligned} \tag{3.33}$$

The $C_{L,R}$ couplings that appear in Eqs. (3.29) and (3.30) are related to the $S_{L,R}$ couplings introduced in the effective Lagrangian in Eq. (3.1). The relation depends on the particular diagram under consideration:

$$C_L^{\eta\rho} = \begin{cases} S_L^{\eta\rho} & m_\eta < m_\rho \\ S_R^{\rho\eta *} & m_\eta > m_\rho \\ S^{\eta\eta} & \eta = \rho \end{cases} , \tag{3.34}$$

and

$$C_R^{\eta\rho} = \begin{cases} S_R^{\eta\rho} & m_\eta < m_\rho \\ S_L^{\rho\eta *} & m_\eta > m_\rho \\ S^{\eta\eta *} & \eta = \rho \end{cases} . \tag{3.35}$$

It proves convenient to find approximate expressions for the $K_2^{L,R}$ coefficients, obtained at leading order in m_β. We find

$$\left(K_2^L\right)^{\beta\alpha} = \frac{S^{\beta\beta}\, S_R^{\beta\alpha}}{32\pi^2\, m_\alpha^2} - \frac{S_L^{\beta\alpha}\left[S^{\alpha\alpha}\left(\pi^2-6\right) + S^{\alpha\alpha *}\left(\pi^2-9\right)\right]}{96\pi^2\, m_\alpha^2} + \frac{1}{32\pi^2\, m_\alpha} \begin{cases} \frac{S_L^{\beta\gamma}\, S_R^{\gamma\alpha}}{m_\alpha} & m_\alpha \gg m_\gamma \gg m_\beta \\ \frac{S_R^{\gamma\beta *}\, S_R^{\gamma\alpha}}{m_\alpha} & m_\alpha \gg m_\beta \gg m_\gamma \\ -\frac{S_L^{\beta\gamma}\, S_R^{\alpha\gamma *}}{m_\gamma} & m_\gamma \gg m_\alpha \end{cases} \tag{3.36}$$

and

$$\left(K_2^R\right)^{\beta\alpha} = \frac{S^{\beta\beta *}\, S_L^{\beta\alpha}}{32\pi^2\, m_\alpha^2} - \frac{S_R^{\beta\alpha}\left[S^{\alpha\alpha}\left(\pi^2-9\right) + S^{\alpha\alpha *}\left(\pi^2-6\right)\right]}{96\pi^2\, m_\alpha^2} + \frac{1}{32\pi^2\, m_\alpha} \begin{cases} \frac{S_R^{\beta\gamma}\, S_L^{\gamma\alpha}}{m_\alpha} & m_\alpha \gg m_\gamma \gg m_\beta \\ \frac{S_L^{\gamma\beta *}\, S_L^{\gamma\alpha}}{m_\alpha} & m_\alpha \gg m_\beta \gg m_\gamma \\ -\frac{S_R^{\beta\gamma}\, S_L^{\alpha\gamma *}}{m_\gamma} & m_\gamma \gg m_\alpha \end{cases} . \tag{3.37}$$

We must emphasize, however, that these approximate expressions may only serve as a rough estimate for the order of magnitude of the $K_2^{L,R}$ coefficients, as large errors ($\sim 50\%$) are obtained in some cases due to the presence of large logs. Finally, upon substitution in Eq. (3.5), one obtains the total decay width of the process. [5] Then, we can compare our analytical results with those found in [227]. Assuming that the only non-vanishing couplings are the ones involving the $\mu\mu$ and $e\mu$ flavor combinations, and making the replacements

$$S^{\mu\mu} = i\frac{m_\mu\, c_{\mu\mu}}{f} \quad , \quad S_L^{e\mu} = i\frac{m_\mu\, (k_e)_{e\mu}}{f} \quad , \quad S_R^{e\mu} = i\frac{m_\mu\, (k_E)_{e\mu}}{f} \, , \tag{3.38}$$

full agreement is recovered.

3.4.4 $\ell_\alpha^- \to \ell_\beta^-\ell_\beta^-\ell_\beta^+$

Complete expressions for the $\ell_\alpha^- \to \ell_\beta^-\ell_\beta^-\ell_\beta^+$ decay width in the absence of ϕ can be found in [251]. Here we are interested in the new contributions mediated by the scalar ϕ, which are given by the Feynman diagrams shown in Fig. 3.3. The relative sign is due to the interchange of charged

[5] For completeness, we note that the expression for the $\ell_\alpha \to \ell_\beta\, \gamma$ decay width without neglecting m_β^2 is

$$\Gamma\left(\ell_\alpha \to \ell_\beta \gamma\right) = \frac{e^2\, \left(m_\alpha^2 - m_\beta^2\right)^3}{16\, \pi\, m_\alpha} \left[\left|\left(K_2^L\right)^{\beta\alpha}\right|^2 + \left|\left(K_2^R\right)^{\beta\alpha}\right|^2\right] .$$

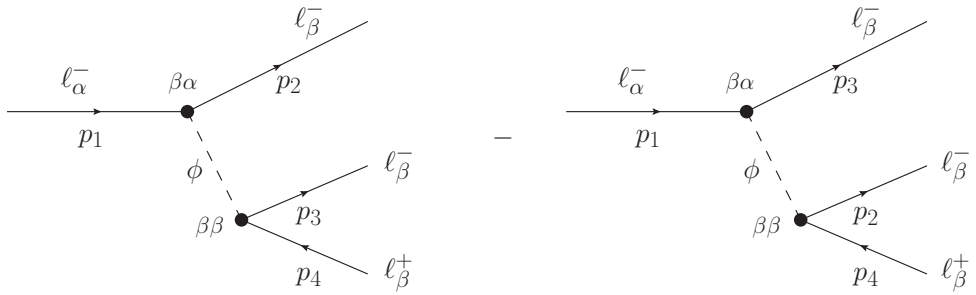

Figure 3.3: Tree-level Feynman diagrams contributing to the process $\ell_\alpha^- \to \ell_\beta^-\ell_\beta^-\ell_\beta^+$ described by the effective Lagrangian in Eq. (3.1).

leptons. It is straightforward to derive the associated amplitude, given by

$$\begin{aligned}\mathcal{M}_\phi = &\,\bar{u}\,(p_3)\,i\left(S^{\beta\beta}P_L + S^{\beta\beta *}P_R\right)v\,(p_4)\,\frac{i}{q^2+i\varepsilon}\,\bar{u}\,(p_2)\,i\left(S_L^{\beta\alpha}P_L + S_R^{\beta\alpha}P_R\right)u\,(p_1)\\ &-\bar{u}\,(p_2)\,i\left(S^{\beta\beta}P_L + S^{\beta\beta *}P_R\right)v\,(p_4)\,\frac{i}{k^2+i\varepsilon}\,\bar{u}\,(p_3)\,i\left(S_L^{\beta\alpha}P_L + S_R^{\beta\alpha}P_R\right)u\,(p_1)\,.\end{aligned} \tag{3.39}$$

Here $q = p_1 - p_2$ and $k = p_1 - p_3$ are the ϕ virtual momenta and we have explicitly indicated the flavor indices of the $S_{L,R}$ coefficients. The total decay width can then be written as

$$\Gamma\left(\ell_\alpha^- \to \ell_\beta^-\ell_\beta^-\ell_\beta^+\right) = \Gamma_{\bar{\phi}}\left(\ell_\alpha^- \to \ell_\beta^-\ell_\beta^-\ell_\beta^+\right) + \Gamma_\phi\left(\ell_\alpha^- \to \ell_\beta^-\ell_\beta^-\ell_\beta^+\right)\,, \tag{3.40}$$

where $\Gamma_{\bar{\phi}}$ is the decay width in the absence of ϕ, given in [251], and

$$\begin{aligned}&\Gamma_\phi\left(\ell_\alpha^- \to \ell_\beta^-\ell_\beta^-\ell_\beta^+\right) =\\ &\frac{m_\alpha}{512\pi^3}\Bigg\{\left(\left|S_L^{\beta\alpha}\right|^2 + \left|S_R^{\beta\alpha}\right|^2\right)\left\{\left|S^{\beta\beta}\right|^2\left(4\log\frac{m_\alpha}{m_\beta} - \frac{49}{6}\right) - \frac{2}{6}\left[\left(S^{\beta\beta *}\right)^2 + \left(S^{\beta\beta}\right)^2\right]\right\}\\ &-\frac{m_\alpha^2}{6}\Big\{S_L^{\beta\alpha}S^{\beta\beta}A_{LL}^{S*} + 2S_L^{\beta\alpha}S^{\beta\beta *}A_{LR}^{S*} + 2S_R^{\beta\alpha}S^{\beta\beta}A_{RL}^{S*} + S_R^{\beta\alpha}S^{\beta\beta *}A_{RR}^{S*}\\ &-12\left(S_L^{\beta\alpha}S^{\beta\beta}A_{LL}^{T*} + S_R^{\beta\alpha}S^{\beta\beta *}A_{RR}^{T*}\right) - 4\left(S_R^{\beta\alpha}S^{\beta\beta}A_{RL}^{V*} + S_L^{\beta\alpha}S^{\beta\beta *}A_{LR}^{V*}\right)\\ &+6e^2\left[S_R^{\beta\alpha}S^{\beta\beta}\left(K_2^L\right)^{\beta\alpha *} + S_L^{\beta\alpha}S^{\beta\beta *}\left(K_2^R\right)^{\beta\alpha *}\right] + \text{c.c.}\Big\}\Bigg\}\,,\end{aligned} \tag{3.41}$$

where in this expression $A_{XY}^I = \left(A_{XY}^I\right)^{\beta\beta\beta\alpha}$. In writing Eq. (3.41) we have only kept the lowest order terms in powers of m_β for each possible combination of couplings. This is equivalent to the 0^{th} order for all terms, except for the ones in the first line, where the factor $\log\frac{m_\alpha}{m_\beta}$ avoids the appearance of an infrared divergence. An expression including terms up to first order in m_β is given in Appendix A.

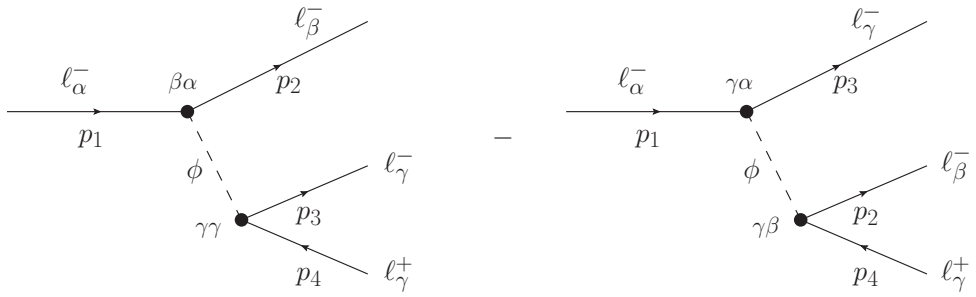

Figure 3.4: Tree-level Feynman diagrams contributing to the process $\ell_\alpha^- \to \ell_\beta^- \ell_\gamma^- \ell_\gamma^+$ described by the effective Lagrangian in Eq. (3.1).

3.4.5 $\ell_\alpha^- \to \ell_\beta^- \ell_\gamma^- \ell_\gamma^+$

Again, complete expressions for the $\ell_\alpha^- \to \ell_\beta^- \ell_\gamma^- \ell_\gamma^+$ decay width in the absence of ϕ can be found in [251]. The new contributions mediated by the scalar ϕ are obtained from the Feynman diagrams shown in Fig. 3.4. The relative sign is due to the interchange of charged leptons. While the diagram on the left involves a flavor conserving ($\gamma\gamma$) and a flavor violating ($\beta\alpha$) vertex, both vertices in the diagram on the right violate flavor ($\gamma\alpha$ and $\gamma\beta$). The associated amplitude is slightly different from that of the previous process and is given by

$$\begin{aligned}\mathcal{M}_\phi = {} & \bar{u}\left(p_3\right) i \left(S^{\gamma\gamma} P_L + S^{\gamma\gamma *} P_R\right) v\left(p_4\right) \frac{i}{q^2 + i\varepsilon} \bar{u}\left(p_2\right) i \left(S_L^{\beta\alpha} P_L + S_R^{\beta\alpha} P_R\right) u\left(p_1\right) \\ & - \bar{u}\left(p_2\right) i \left(S_L^{\gamma\beta} P_L + S_R^{\gamma\beta} P_R\right) v\left(p_4\right) \frac{i}{k^2 + i\varepsilon} \bar{u}\left(p_3\right) i \left(S_L^{\gamma\alpha} P_L + S_R^{\gamma\alpha} P_R\right) u\left(p_1\right) .\end{aligned} \tag{3.42}$$

Finally, the total decay width can be written as

$$\Gamma\left(\ell_\alpha^- \to \ell_\beta^- \ell_\gamma^- \ell_\gamma^+\right) = \Gamma_{\bar{\phi}}\left(\ell_\alpha^- \to \ell_\beta^- \ell_\gamma^- \ell_\gamma^+\right) + \Gamma_\phi\left(\ell_\alpha^- \to \ell_\beta^- \ell_\gamma^- \ell_\gamma^+\right) , \tag{3.43}$$

where $\Gamma_{\bar{\phi}}$ is the decay width in the absence of ϕ, given in [251], and

$$\begin{aligned}&\Gamma_\phi\left(\ell_\alpha^- \to \ell_\beta^- \ell_\gamma^- \ell_\gamma^+\right) = \\ &\frac{m_\alpha}{512\pi^3}\Bigg\{\left(\left|S_L^{\beta\alpha}\right|^2 + \left|S_R^{\beta\alpha}\right|^2\right)\left\{|S^{\gamma\gamma}|^2\left(4\log\frac{m_\alpha}{m_\gamma} - \frac{23}{3}\right) - \frac{1}{3}\left[(S^{\gamma\gamma *})^2 + (S^{\gamma\gamma})^2\right]\right\} \\ &+ \left(|S_L^{\gamma\alpha}|^2 + |S_R^{\gamma\alpha}|^2\right)\left(\left|S_L^{\gamma\beta}\right|^2 + \left|S_R^{\gamma\beta}\right|^2\right)\left(2\log\frac{m_\alpha}{m_f^{\max}} - 3\right) \\ &- \frac{1}{2}\left[S^{\gamma\gamma}\left(S_L^{\beta\alpha} S_L^{\gamma\alpha *} S_L^{\gamma\beta *} + S_R^{\beta\alpha *} S_R^{\gamma\alpha} S_R^{\gamma\beta}\right) + \text{c.c.}\right] + \frac{m_\alpha^2}{6}\Big\{S_L^{\gamma\alpha} S_L^{\gamma\beta} A_{LL}^{S*} \\ &+ S_R^{\gamma\alpha} S_R^{\gamma\beta} A_{RR}^{S*} - 2S^{\gamma\gamma}\left(S_L^{\beta\alpha} A_{LL}^{S*} + S_L^{\beta\alpha *} A_{LR}^{S} + S_R^{\beta\alpha} A_{RL}^{S*} + S_R^{\beta\alpha *} A_{RR}^{S}\right) \\ &+ 4\left(S_L^{\gamma\alpha} S_R^{\gamma\beta} A_{LR}^{V*} + S_R^{\gamma\alpha} S_L^{\gamma\beta} A_{RL}^{V*}\right) + 12\left(S_L^{\gamma\alpha} S_L^{\gamma\beta} A_{LL}^{T*} + S_R^{\gamma\alpha} S_R^{\gamma\beta} A_{RR}^{T*}\right) \\ &-6e^2\left[S_L^{\gamma\alpha} S_R^{\gamma\beta}\left(K_2^R\right)^{\beta\alpha *} + S_R^{\gamma\alpha} S_L^{\gamma\beta}\left(K_2^L\right)^{\beta\alpha *}\right] + \text{c.c.}\Big\}\Bigg\},\end{aligned} \tag{3.44}$$

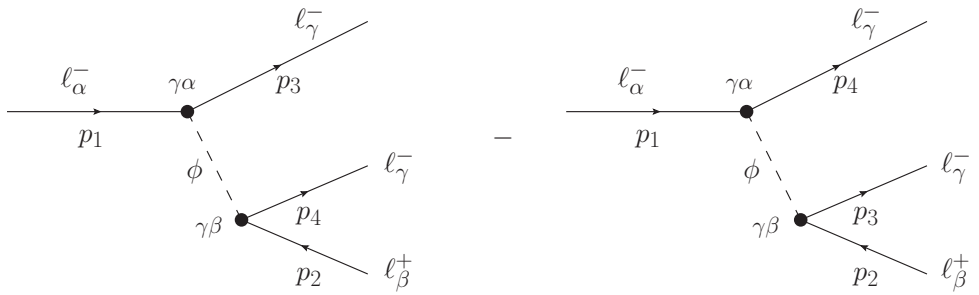

Figure 3.5: Tree-level Feynman diagrams contributing to the process $\ell_\alpha^- \to \ell_\beta^+ \ell_\gamma^- \ell_\gamma^-$ described by the effective Lagrangian in Eq. (3.1).

where in this expression $A_{XY}^I = \left(A_{XY}^I\right)^{\gamma\gamma\beta\alpha}$. Also, here $m_f^{\max} = \max(m_\beta, m_\gamma)$ and then the expression depends on the process in question. Once again, we have only kept the lowest order terms in powers of m_β and m_γ for each possible combination of couplings.

3.4.6 $\ell_\alpha^- \to \ell_\beta^+ \ell_\gamma^- \ell_\gamma^-$

Also for this process, complete expressions for the $\ell_\alpha^- \to \ell_\beta^+ \ell_\gamma^- \ell_\gamma^-$ decay width in the absence of ϕ can be found in [251]. The relative sign is due to the interchange of charged leptons. The new contributions mediated by the scalar ϕ are given by the Feynman diagrams shown in Fig. 3.5. We note that both vertices are necessarily flavor violating. The associated amplitude is given in this case by

$$\begin{aligned}\mathcal{M}_\phi = {} & \bar{u}(p_4)\, i \left(S_L^{\gamma\beta} P_L + S_R^{\gamma\beta} P_R\right) v(p_2)\, \frac{i}{q^2 + i\varepsilon}\, \bar{u}(p_3)\, i \left(S_L^{\gamma\alpha} P_L + S_R^{\gamma\alpha} P_R\right) u(p_1) \\ & - \bar{u}(p_3)\, i \left(S_L^{\gamma\beta} P_L + S_R^{\gamma\beta} P_R\right) v(p_2)\, \frac{i}{k^2 + i\varepsilon}\, \bar{u}(p_4)\, i \left(S_L^{\gamma\alpha} P_L + S_R^{\gamma\alpha} P_R\right) u(p_1)\ .\end{aligned} \tag{3.45}$$

Here $q = p_1 - p_3$ and $k = p_1 - p_4$ are different from their definitions in the processes above. Writing one more time the decay width as the sum of two contributions,

$$\Gamma\left(\ell_\alpha^- \to \ell_\beta^+ \ell_\gamma^- \ell_\gamma^-\right) = \Gamma_{\bar{\phi}}\left(\ell_\alpha^- \to \ell_\beta^+ \ell_\gamma^- \ell_\gamma^-\right) + \Gamma_\phi\left(\ell_\alpha^- \to \ell_\beta^+ \ell_\gamma^- \ell_\gamma^-\right)\ , \tag{3.46}$$

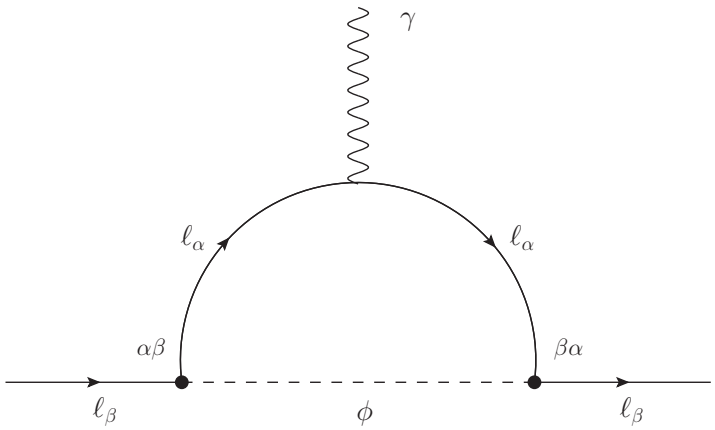

Figure 3.6: Feynman diagram for the 1-loop contribution to the anomalous magnetic moment of charged leptons given by the interaction in Eq. (3.1). The flavor indices of the couplings contributing to the diagram have been specified in the vertices. The relation between these couplings, which we generically denote as $C_{L,R}$ and $\widetilde{C}_{L,R}$, and the $S_{L,R}$ couplings in the effective Lagrangian of Eq. (3.1) depends on the flavor states involved in the diagram. See the text for a detailed explanation.

where $\Gamma_{\bar{\phi}}$ is the decay width in the absence of ϕ, given in [251], we find that

$$\begin{aligned}
&\Gamma_\phi\left(\ell_\alpha^- \to \ell_\beta^+ \ell_\gamma^- \ell_\gamma^-\right) = \\
&\frac{m_\alpha}{512\pi^3}\left\{\left(|S_L^{\gamma\alpha}|^2 + |S_R^{\gamma\alpha}|^2\right)\left(\left|S_L^{\gamma\beta}\right|^2 + \left|S_R^{\gamma\beta}\right|^2\right)\left(2\log\frac{m_\alpha}{m_f^{\max}} - 3\right)\right. \\
&-\frac{1}{2}\left(|S_L^{\gamma\alpha}|^2\left|S_L^{\gamma\beta}\right|^2 + |S_R^{\gamma\alpha}|^2\left|S_R^{\gamma\beta}\right|^2\right) \\
&+\frac{m_\alpha^2}{6}\left[-S_L^{\gamma\alpha}S_L^{\gamma\beta}A_{LL}^{S*} - S_R^{\gamma\alpha}S_R^{\gamma\beta}A_{RR}^{S*} - 2\left(S_L^{\gamma\alpha}S_R^{\gamma\beta}A_{RL}^{S*} + S_R^{\gamma\alpha}S_L^{\gamma\beta}A_{LR}^{S*}\right)\right. \\
&\left.\left.+4\left(S_L^{\gamma\alpha}S_R^{\gamma\beta}A_{RL}^{V*} + S_R^{\gamma\alpha}S_L^{\gamma\beta}A_{LR}^{V*}\right) + 12\left(S_L^{\gamma\alpha}S_L^{\gamma\beta}A_{LL}^{T*} + S_R^{\gamma\alpha}S_R^{\gamma\beta}A_{RR}^{T*}\right) + \text{c.c.}\right]\right\},
\end{aligned} \tag{3.47}$$

where in this expression $A_{XY}^I = \left(A_{XY}^I\right)^{\gamma\beta\gamma\alpha}$ and $m_f^{\max} = \max\left(m_\beta, m_\gamma\right)$.

3.4.7 Lepton magnetic and electric dipole moments

We finally consider the magnetic and electric dipole moments of the charged leptons, which can be described by the effective Lagrangians

$$\mathcal{L}_{\text{AMM}} = \frac{e}{2\,m_\alpha} a_\alpha\, \bar{\ell}_\alpha\, \sigma^{\mu\nu} F_{\mu\nu}\, \ell_\alpha\,, \tag{3.48}$$

$$\mathcal{L}_{\text{EDM}} = -\frac{i}{2} d_\alpha\, \bar{\ell}_\alpha\, \sigma^{\mu\nu} F_{\mu\nu}\, \gamma_5\, \ell_\alpha\,. \tag{3.49}$$

The charged lepton dipole moments receive contributions mediated by the scalar ϕ, as shown in Fig. 3.6. [6] In the following we denote the chiral couplings in the $\bar{\ell}_\alpha - \ell_\beta - \phi$ vertex as $C_L^{\alpha\beta}$ and $C_R^{\alpha\beta}$, whereas the chiral couplings in the $\bar{\ell}_\beta - \ell_\alpha - \phi$ vertex are denoted as $\widetilde{C}_L^{\beta\alpha}$ and $\widetilde{C}_R^{\beta\alpha}$. The $C_{L,R}$ and $\widetilde{C}_{L,R}$ couplings are related to the $S_{L,R}$ couplings in the effective Lagrangian of Eq. (3.1), but this relation depends on the flavor states involved in the diagram, as discussed below. The amplitude associated to the diagram in Fig. 3.6 can be written as

$$
\begin{aligned}
i\mathcal{M} = \int \frac{\mathrm{d}^4 q}{(2\pi)^4} \overline{u}_\ell\left(p', m_\alpha\right) \left[i\left(C_L^{\alpha\beta} P_L + C_R^{\alpha\beta} P_R\right)\right] \frac{i\left(\not{p}' + \not{q} + m_\beta\right)}{\left(p'+q\right)^2 - m_\beta^2} \left(-i\, e\, \gamma^\mu\right) \\
\frac{i\left(\not{p} + \not{q} + m_\beta\right)}{\left(p+q\right)^2 - m_\beta^2} \left[i\left(\widetilde{C}_L^{\beta\alpha} P_L + \widetilde{C}_R^{\beta\alpha} P_R\right)\right] \frac{i}{q^2} u_\ell\left(p, m_\alpha\right) \varepsilon_\mu^*\left(k\right),
\end{aligned}
\tag{3.50}
$$

where m_α and m_β are the masses of the external and internal leptons, respectively, and we sum over the index β. One must now compare to the equivalent amplitude obtained with the effective Lagrangians in Eqs. (3.48) and (3.49). After some algebra, one finds that the scalar ϕ induces the contributions to the anomalous magnetic moments and electric dipole moments of the charged leptons

$$
\Delta a_\alpha = \frac{-1}{32\,\pi^2\, m_\alpha^4} \tag{3.51}
$$

$$
\begin{aligned}
&\left\{\left[m_\alpha^2\left(m_\alpha^2 - 2\,m_\beta^2\right) - 2\,m_\beta^2\left(m_\alpha^2 - m_\beta^2\right)\log\frac{m_\beta^2}{\left|m_\beta^2 - m_\alpha^2\right|}\right]\left(C_L^{\alpha\beta}\,\widetilde{C}_R^{\beta\alpha} + C_R^{\alpha\beta}\,\widetilde{C}_L^{\beta\alpha}\right)\right. \\
&\left.-2\,m_\alpha\,m_\beta\left[m_\alpha^2 + \left(m_\alpha^2 - m_\beta^2\right)\log\frac{m_\beta^2}{\left|m_\beta^2 - m_\alpha^2\right|}\right]\left(C_L^{\alpha\beta}\,\widetilde{C}_L^{\beta\alpha} + C_R^{\alpha\beta}\,\widetilde{C}_R^{\beta\alpha}\right)\right\},
\end{aligned}
\tag{3.52}
$$

and

$$
d_\alpha = \frac{i\,e\,m_\beta}{32\,\pi^2\,m_\alpha^4}\left(C_L^{\alpha\beta}\,\widetilde{C}_L^{\beta\alpha} - C_R^{\alpha\beta}\,\widetilde{C}_R^{\beta\alpha}\right)\left[m_\alpha^2 + \left(m_\alpha^2 - m_\beta^2\right)\log\frac{m_\beta^2}{\left|m_\beta^2 - m_\alpha^2\right|}\right]. \tag{3.53}
$$

These analytical results have been checked with the help of `Package-X` [253]. We note again that a sum over the index β is performed in Eqs. (3.52) and (3.53). Therefore, they include both flavor diagonal as well as flavor off-diagonal contributions to the dipole moments. We now consider these contributions separately and study their behavior in specific limits:

1. Flavor off-diagonal contribution with $m_\beta \ll m_\alpha$

[6] Two-loop Barr-Zee contributions [252] to the charged leptons AMMs and EDMs can also be considered. However, while these might be relevant in some cases, we will assume that the $S_{L,R}$ couplings can at most have mild hierarchies among different flavors, hence making them numerically irrelevant compared to the 1-loop contributions considered here.

In this case the $C_{L,R}$ and $\widetilde{C}_{L,R}$ couplings are related to the $S_{L,R}$ couplings in Eq. (3.1) as $\widetilde{C}^{\beta\alpha}_{L,R} = S^{\beta\alpha}_{L,R}$ and $C^{\alpha\beta}_{L,R} = S^{\beta\alpha *}_{R,L}$ and the expressions simplify to

$$\Delta a_\alpha = \frac{1}{32\,\pi^2\,m_\alpha}\left[-m_\alpha\left(\left|S_L^{\beta\alpha}\right|^2+\left|S_R^{\beta\alpha}\right|^2\right) + 4\,m_\beta\,\mathrm{Re}\left(S_R^{\beta\alpha}\,S_L^{\beta\alpha *}\right)\left(1+\log\frac{m_\beta^2}{m_\alpha^2}\right)\right]+\mathcal{O}\left(m_\beta^2\right), \tag{3.54}$$

and

$$d_\alpha = \frac{e\,m_\beta}{16\,\pi^2\,m_\alpha^2}\,\mathrm{Im}\left(S_R^{\beta\alpha}\,S_L^{\beta\alpha *}\right)\left(1+\log\frac{m_\beta^2}{m_\alpha^2}\right)+\mathcal{O}\left(m_\beta^3\right). \tag{3.55}$$

2. Flavor off-diagonal contribution with $m_\beta \gg m_\alpha$

   In this case the generic $C_{L,R}$ and $\widetilde{C}_{L,R}$ couplings are related to the $S_{L,R}$ couplings as $\widetilde{C}^{\beta\alpha}_{L,R} = S^{\alpha\beta *}_{R,L}$ and $C^{\alpha\beta}_{L,R} = S^{\alpha\beta}_{L,R}$, giving us

$$\Delta a_\alpha = \frac{m_\alpha}{16\,\pi^2\,m_\beta}\left[\mathrm{Re}\left(S_R^{\alpha\beta}\,S_L^{\alpha\beta *}\right)+\frac{m_\alpha}{6\,m_\beta}\left(\left|S_L^{\beta\alpha}\right|^2+\left|S_R^{\beta\alpha}\right|^2\right)\right]+\mathcal{O}\left(m_\alpha^3\right), \tag{3.56}$$

   and

$$d_\alpha = \frac{e}{32\,\pi^2\,m_\beta}\,\mathrm{Im}\left(S_R^{\alpha\beta}\,S_L^{\alpha\beta *}\right)+\mathcal{O}\left(m_\alpha^2\right). \tag{3.57}$$

3. Flavor diagonal contribution, i.e. $m_\beta = m_\alpha$

   Finally, in this case we have $C_L^{\alpha\alpha} = \widetilde{C}_L^{\alpha\alpha} = S^{\alpha\alpha}$ and $C_R^{\alpha\alpha} = \widetilde{C}_R^{\alpha\alpha} = S^{\alpha\alpha *}$, and we find the simple expression

$$\Delta a_\alpha = \frac{1}{16\pi^2}\left[3\,(\mathrm{Re}\,S^{\alpha\alpha})^2-(\mathrm{Im}\,S^{\alpha\alpha})^2\right] \tag{3.58}$$

   for the AMM of the charged lepton ℓ_α, which agrees with previous results in the literature. In particular, it matches exactly the expression given in [254] in the limit of a massless scalar, with the equivalence

$$-\frac{m_\alpha}{v}\,a_\alpha^S = \frac{1}{2}\,(S^{\alpha\alpha}+S^{\alpha\alpha *})\,, \quad -i\,\frac{m_\alpha}{v}\,b_\alpha^S = -\frac{1}{2}\,(S^{\alpha\alpha}-S^{\alpha\alpha *})\,. \tag{3.59}$$

   Regarding the expression for the EDM, it also acquires a very simple form in this case,

$$d_\alpha = -\frac{e}{8\,\pi^2\,m_\alpha}\,(\mathrm{Re}\,S^{\alpha\alpha})\,(\mathrm{Im}\,S^{\alpha\alpha})\,. \tag{3.60}$$

   This expression agrees with the one given in [255] just by identifying $\mathrm{Re}\,S^{\alpha\alpha} = -\lambda_S^\ell$ and $\mathrm{Im}\,S^{\alpha\alpha} = \lambda_P^\ell$. Notice that Eqs. (3.58) and (3.60) are both exact results for the diagonal contributions to the dipole moments.

3.5 Phenomenological discussion

After deriving analytical expressions for several leptonic observables of interest, we now discuss their associated phenomenology.

3.5.1 Searches for $\ell_\alpha \to \ell_\beta\, \phi$

Several searches for $\ell_\alpha \to \ell_\beta\, \phi$ have been performed and used to set experimental constraints on the off-diagonal $S_A^{\beta\alpha}$ effective couplings. Let us start with muon decays. The strongest limit on the branching ratio for the 2-body decay $\mu^+ \to e^+\, \phi$ was obtained at TRIUMF, finding $\text{BR}\,(\mu \to e\, \phi) < 2.6 \times 10^{-6}$ at 90% C.L. [256]. However, as explained in [250], this experimental limit must be applied with care to the general scenario considered here. The reason is that the experimental setup in [256] uses a muon beam that is highly polarized in the direction opposite to the muon momentum and concentrates the search in the forward region. This reduces the background from the SM process $\mu^+ \to e^+ \nu_e\, \bar{\nu}_\mu$, which is strongly suppressed in this region, but also reduces the $\mu^+ \to e^+\, \phi$ signal unless the $\phi - e - \mu$ coupling is purely right-handed. Therefore, we obtain a limit valid only when $S_L^{e\mu} = 0$:

$$S_L^{e\mu} = 0 \quad \Rightarrow \quad |S_R^{e\mu}| < 2.7 \times 10^{-11}\,. \tag{3.61}$$

A more general limit can also be derived from [256]. Using the spin processed data shown in Fig.(7) of [256], the authors of [250] obtained the conservative bound $\text{BR}\,(\mu \to e\, \phi) \lesssim 10^{-5}$, valid for any chiral structure of the $S_A^{e\mu}$ couplings. This bound is similar to the more recent limit obtained by the TWIST collaboration [257], also in the $\sim 10^{-5}$ ballpark. With this value, one finds an upper limit on the $e - \mu$ flavor violating couplings of [7]

$$|S^{e\mu}| < 5.3 \times 10^{-11}\,. \tag{3.62}$$

where we have defined the convenient combination

$$\left|S^{\beta\alpha}\right| = \left(\left|S_L^{\beta\alpha}\right|^2 + \left|S_R^{\beta\alpha}\right|^2\right)^{1/2}\,. \tag{3.63}$$

Several strategies can be followed for newer $\mu \to e\, \phi$ searches. The authors of [234] advocate for a new phase of the MEG-II experiment, reconfigured to search for $\mu \to e\, \phi$ by placing a Lyso calorimeter in the forward direction. Also, as pointed out in [258, 259] and recently discussed in [234] as well, the limit in Eq. (3.62) can be substantially improved by the Mu3e experiment by looking for a bump in the continuous Michel spectrum, that is, in the $\mu \to e\, \bar{\nu}_e\, \nu_\mu$ spectrum. The detailed analysis in [259] shows that $\mu \to e\, \phi$ branching ratios above 7.3×10^{-8} can be

[7] See also the recent [234] for a comprehensive discussion of the experimental limit of [256] and how this gets altered for different chiral structures of the $S_A^{e\mu}$ couplings.

ruled out at 90% C.L.. This would imply a sensitivity to an $|S^{e\mu}|$ effective coupling as low as 4.5×10^{-12}, improving an order of magnitude with respect to the limit in Eq. (3.62).

Turning to τ decays, the previous best experimental limits were set by the ARGUS collaboration [260]. Currently, these bounds have been improved by Belle II [261], which found

$$\begin{aligned} \frac{\mathrm{BR}\,(\tau \to e\,\phi\,)}{\mathrm{BR}\,(\tau \to e\,\nu\,\bar{\nu})} &< 5.3 \times 10^{-3}\,, \\ \frac{\mathrm{BR}\,(\tau \to \mu\,\phi)}{\mathrm{BR}\,(\tau \to \mu\,\nu\,\bar{\nu})} &< 3.4 \times 10^{-3}\,, \end{aligned} \tag{3.64}$$

at 95% C.L.. These limits are weaker than those for muon decays, but still lead to stringent constraints on the LFV τ couplings with the scalar ϕ. It is straightforward to find

$$\begin{aligned} |S^{e\tau}| &< 3.5 \times 10^{-7}\,, \\ |S^{\mu\tau}| &< 2.7 \times 10^{-7}\,. \end{aligned} \tag{3.65}$$

In addition, new methods for $\tau \to \ell\,\phi$ searches at this experiment have been recently proposed [262].

3.5.2 $\ell_\alpha \to \ell_\beta\,\gamma\,\phi$ at the MEG experiment

In order to illustrate the calculation of the phase space integral for a specific case, let us focus on the $\mu \to e\,\gamma\,\phi$ decay and consider the MEG experiment [263]. This experiment has been designed to search for $\mu \to e\,\gamma$ and therefore concentrates on $E_e \simeq m_\mu/2$ and $\cos\theta_{e\gamma} \simeq -1$ (positron and photon emitted back to back). However, due to the finite experimental resolution, these cuts cannot be imposed with full precision, which makes MEG also sensitive to $\mu \to e\,\gamma\,\phi$. The final MEG results were obtained with the cuts [263]

$$\cos\theta_{e\gamma} < -0.99963 \quad , \quad 51.0 < E_\gamma < 55.5\,\mathrm{MeV} \quad , \quad 52.4 < E_e < 55.0\,\mathrm{MeV}\,. \tag{3.66}$$

This defines the MEG kinematical region for the calculation of the phase space integral in Eq. (3.24) since $\mu \to e\,\gamma\,\phi$ events that fall in this region can be detected by the experiment. For instance, events with $\cos\theta_{e\gamma} < -0.99963$, or equivalently $\theta_{e\gamma} > \theta_{e\gamma}^{\mathrm{min}} = 178.441^\circ$, were at the reach of MEG. The kinematical region can be divided into two subregions:

$$\begin{aligned} y_{\mathrm{min}} = \frac{2\,E_\gamma^{\mathrm{min}}}{m_\mu} < y < y_{\mathrm{int}}\,, \\ x_{\mathrm{inf}} < x < x_{\mathrm{max}} = 1\,, \end{aligned} \tag{3.67}$$

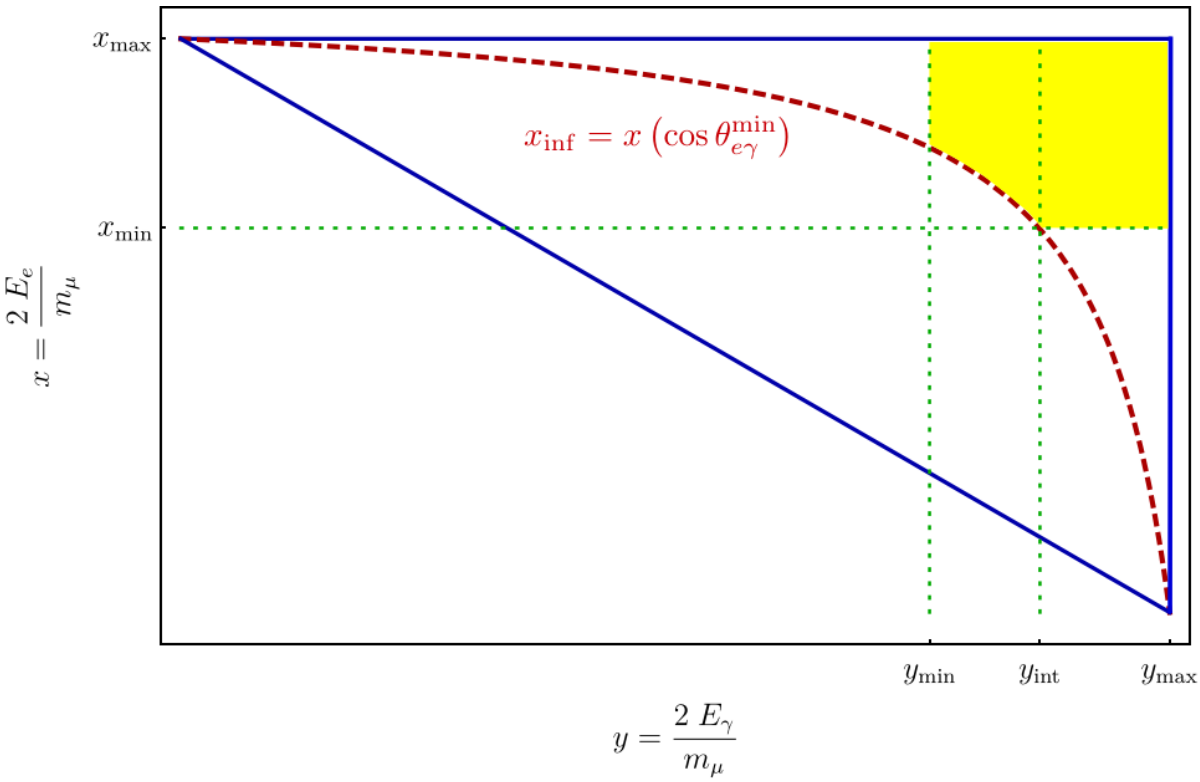

Figure 3.7: Illustration of the allowed phase space region for the process $\mu \to e\,\gamma\,\phi$ in a given experiment. The blue continuous lines correspond to $\cos\theta_{e\gamma} = \pm 1$ and therefore delimit the total phase space that would be, in principle, available due to kinematics. The red dashed line represents $x_{\inf}(y)$ and corresponds to the minimal $\theta_{e\gamma}$ angle measurable by the experiment, excluding the region below it. The green dotted straight lines at $x_{\min}$ and $y_{\min}$ are the minimal positron and photon energy, respectively, that the experiment can measure, while $y_{\inf}$ is the value of y for which $x_{\min}$ and $x_{\inf}$ intersect. Finally, the yellow surface is the region where we must integrate.

and

$$\begin{aligned} y_{\inf} < y < y_{\max} = 1\,, \\ x_{\min} = \frac{2\,E_e^{\min}}{m_\mu} < x < x_{\max}\,, \end{aligned} \tag{3.68}$$

where $x_{\inf} = x_{\inf}(y)$ is the value of x such that $\cos\theta_{e\gamma} = \cos\theta_{e\gamma}^{\min}$ for each value of y. This can be easily found by solving Eq. (3.26):

$$x_{\inf} = \frac{2\,(1-y)}{2 - y\left(1 - \cos\theta_{e\gamma}^{\min}\right)}\,. \tag{3.69}$$

Finally $y_{\inf}$ is the value of y for which $x_{\min}$ and $x_{\inf}$ coincide. These two subregions are illustrated in Fig. 3.7, where the experimental restrictions have been modified for the sake of clarity by enlarging the kinematical region of interest. A realistic representation obtained with the MEG

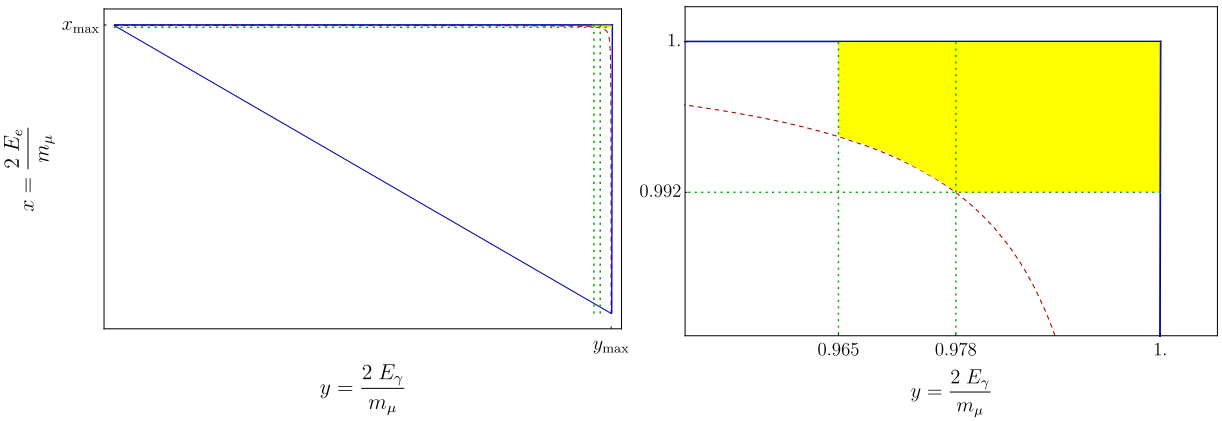

Figure 3.8: Realistic version of the phase space region limited by the experimental cuts of the MEG experiment, given in Eq. (3.66). The figure on the right shows a zoom of the figure on the left, centered on the colored surface.

cuts in Eq. (3.66) is shown in Fig. 3.8. This clearly illustrates the strong suppression due to the phase space integral.

Having explained how to compute the phase space integral and illustrated the strong suppression it introduces, we can obtain results for the MEG experiment. Using the cuts in Eq. (3.66), the phase space integral in Eq. (3.24) can be numerically computed to find

$$\mathcal{I}\left(x_{\min}, y_{\min}\right)_{\text{MEG}} = 3.8 \times 10^{-8}\,. \tag{3.70}$$

Combining this result with Eq. (3.23), we obtain the branching ratio of $\mu \to e\,\gamma\,\phi$ restricted to the MEG phase space, obtaining

$$\text{BR}_{\text{MEG}}\left(\mu \to e\,\gamma\,\phi\right) = 1.5 \times 10^{5} \left(|S_L^{e\mu}|^2 + |S_R^{e\mu}|^2\right)\,. \tag{3.71}$$

MEG results require $\text{BR}\left(\mu \to e\,\gamma\right) < 4.2 \times 10^{-13}$ [263], a bound that must also be satisfied by $\text{BR}_{\text{MEG}}\left(\mu \to e\,\gamma\,\phi\right)$. This leads to

$$|S^{e\mu}| < 1.6 \times 10^{-9}\,. \tag{3.72}$$

This bound is notably worse than the one given in Eq. (3.62), as expected due to the strong phase space suppression at MEG, an experiment that is clearly not designed to search for $\mu \to e\,\gamma\,\phi$. Similarly, a dedicated run of the MEG-II experiment with a modified trigger should yield a sensitivity that surpasses the current bounds by one order of magnitude [264].

More stringent bounds were obtained at the Crystal Box experiment at LAMPF [265–267]. They performed several searches with different experimental cuts and branching ratio bounds. These result in different limits on the $|S^{e\mu}|$ effective coupling, as shown in Table 3.1. Adapting the limit from the $\mu \to e\gamma$ search in [265] along the lines followed in the previous discussion for

References	$\theta_{e\gamma}^{\min}$	$E_\gamma^{\min}$ [MeV]	$E_e^{\min}$ [MeV]	$\mathcal{I}(x_{\min}, y_{\min})$	BR bound	Limit on $\lvert S^{e\mu}\rvert$
[265]	160°	40	44	1.3×10^{-3}	4.9×10^{-11}	9.5×10^{-11}
[266, 267]	140°	38	38	1.1×10^{-2}	1.1×10^{-9}	1.6×10^{-10}

Table 3.1: Results in the search for $\mu \to e\,\gamma\,\phi$ at the Crystal Box experiment.

MEG, we find

$$|S^{e\mu}| < 9.5 \times 10^{-11}\,. \tag{3.73}$$

This bound is still not better than the one given in Eq. (3.62), but it is in the same ballpark. A very similar bound is obtained with the results of a later analysis, in this case, more specific to $\mu \to e\,\gamma\,\phi$ [266, 267].

Finally, the Mu3e experiment is not well equipped to detect the photon in $\mu \to e\,\gamma\,\phi$ and therefore cannot improve on these limits. As explained in [259], a future *Mu3e-Gamma experiment* including a photon conversion layer could increase the sensitivity to $\mu \to e\,\gamma\,\phi$.

3.5.3 $\ell_\alpha \to \ell_\beta\gamma$ vs $\ell_\alpha \to \ell_\beta\ell_\beta\ell_\beta$

The LFV decays $\ell_\alpha \to \ell_\beta\,\gamma$ and $\ell_\alpha \to \ell_\beta\ell_\beta\ell_\beta$ constitute complementary probes of the nature of the underlying physics [139, 268]. While $\ell_\alpha \to \ell_\beta\,\gamma$ only receives contributions from dipole operators, $\ell_\alpha \to \ell_\beta\ell_\beta\ell_\beta$ is induced by dipole as well as non-dipole operators. Their relative importance can be studied through the ratio

$$R_{\alpha\beta} = \frac{\mathrm{BR}(\ell_\alpha \to \ell_\beta\ell_\beta\ell_\beta)}{\mathrm{BR}(\ell_\alpha \to \ell_\beta\,\gamma)}\,. \tag{3.74}$$

In models in which the $\ell_\alpha \to \ell_\beta\ell_\beta\ell_\beta$ amplitude is dominated by dipole contributions, the two branching ratios are strongly correlated, and one can make a definite prediction for $R_{\mu e}$. In fact, since $\ell_\alpha \to \ell_\beta\ell_\beta\ell_\beta$ involves an additional electromagnetic coupling constant, one expects $R_{\alpha\beta} \ll 1$. Departures from this prediction would clearly point towards a non-dipole dominant contribution. We now consider this issue in the presence of an ultralight scalar, which contributes at tree-level to $\ell_\alpha \to \ell_\beta\ell_\beta\ell_\beta$ via scalar (and hence non-dipole) operators. Contrary to the above-mentioned dipole-dominated scenarios, in this case, one generally expects $R_{\alpha\beta} \gg 1$, as shown below.

However, before we move on to the discussion of the interplay between $\ell_\alpha \to \ell_\beta\,\gamma$ and $\ell_\alpha \to \ell_\beta\ell_\beta\ell_\beta$, we would like to point out that light scalars may offer additional experimental handles in $\ell_\alpha \to \ell_\beta\ell_\beta\ell_\beta$. In particular, the authors of [269] showed that a light scalar produced on-shell in $\ell_\alpha^- \to \ell_\beta^-\phi$ that later decays as $\phi \to \ell_\beta^-\ell_\beta^+$ may lead to observable displaced vertices. This interesting possibility is, however, not possible in the ultralight scalar scenario considered here because ϕ is considered to be much lighter than the electron.

General dipole contributions

First, we consider the general case of a scenario in which dipole contributions are independent of the non-dipole ones induced by the ultralight scalar ϕ. This would be the case of a model containing additional LFV sources not related to ϕ. To evaluate the relevance of the new contributions to $\ell_\alpha \to \ell_\beta \ell_\beta \ell_\beta$ mediated by the scalar ϕ, we drop the 4-fermion operators in Eq. (3.4) and consider a simplified effective Lagrangian containing only left-handed photonic dipole and scalar-mediated operators

$$\mathcal{L}_{\rm LFV}^{\rm simp} = \frac{e\, m_\alpha \left(K_2^L\right)^{\beta\alpha}}{2}\, \bar{\ell}_\beta\, \sigma^{\mu\nu}\, P_L\, \ell_\alpha F_{\mu\nu} + S_L^{\beta\alpha}\, \phi\, \bar{\ell}_\beta\, P_L\, \ell_\alpha + \text{h.c.}\,. \tag{3.75}$$

Then, inspired by [270], we parametrize the K_2^L and S_L coefficients as

$$e\left(K_2^L\right)^{\beta\alpha} \equiv \frac{1}{(\kappa+1)\,\Lambda^2}\,, \qquad S_L^{\beta\alpha} \equiv m_\alpha\, \frac{\kappa}{(\kappa+1)\,\Lambda}\,. \tag{3.76}$$

Λ is a dimensionful parameter that represents the NP energy scale at which these coefficients are induced, while κ is a dimensionless parameter that accounts for the relative intensity of these two interactions. [8] In the case of $\kappa \ll 1$, the dipole operator dominates, while the scalar mediated contribution dominates for $\kappa \gg 1$. We point out that m_α in Eqs. (3.75) and (3.76) is a global factor given by the mass of the heaviest charged lepton in the process and that Eq. (3.76) assumes $S_L^{\beta\alpha} = S_L^{\beta\beta}$.

Fig. 3.9 shows contours of $\text{BR}(\mu \to e\gamma)$ and $\text{BR}(\mu \to eee)$ in the κ-Λ plane. Our results are compared to the current bounds and the future sensitivities for the MEG-II and Mu3e experiments. We observe that for $\kappa \gg 1$ and $\text{BR}(\mu \to eee) > 10^{-16}$, Λ must be necessarily below ~ 3000 TeV. A slightly lower upper limit for Λ is found when $\kappa \ll 1$ and $\text{BR}(\mu \to e\gamma) > 10^{-14}$. These are precisely the final expected sensitivities in MEG-II and Mu3e. Furthermore, we note that the search for the scalar mediated contribution in Mu3e will actually be very constraining in all the parameter space. Similar results are shown for τ decays in Fig. 3.10. In this case, the current experimental limits are expected to be improved by about one order of magnitude by the LHCb and Belle II collaborations, which will search for the $\tau \to \ell_\beta \gamma$ and $\tau \to \ell_\beta \ell_\beta \ell_\beta$ decays, with $\ell_\beta = e, \mu$. This figure has been obtained using the expected sensitivities by the Belle II experiment presented in [150]. We find that for low values of κ, i.e. $\kappa \ll 1$, the current limit on $\text{BR}(\tau \to e\gamma)$ implies the non-observation of $\tau \to eee$ at Belle II. This would therefore require a larger value of κ, to enhance the relative weight of the 3-body decay. Qualitatively similar results are obtained for $\tau \to \mu$ transitions.

[8] We normalize S_L by introducing the mass of the heaviest charged lepton involved in each process. However, this is done only for the purpose of this analysis. In the rest of the section, we do not assume any hierarchy among the couplings proportional to the charged lepton masses.

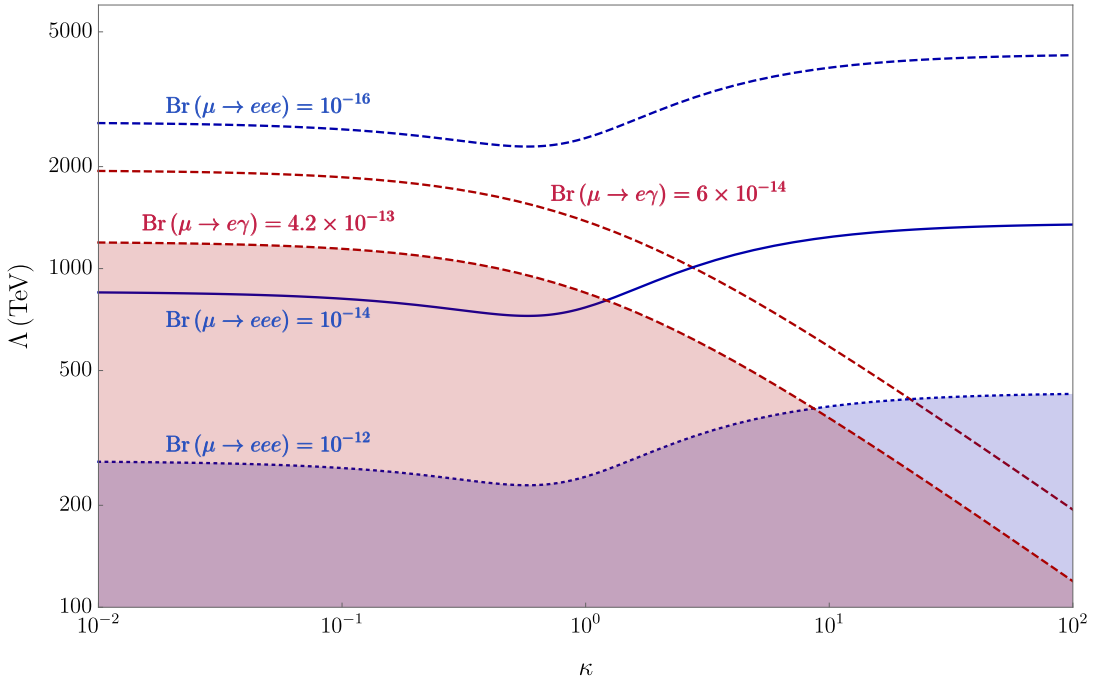

Figure 3.9: Contours of BR($\mu \to e\gamma$) and BR($\mu \to eee$) in the κ-Λ plane. The lowest values correspond to the future sensitivities for the MEG-II and Mu3e experiments, while colored regions are excluded due to the current bounds BR($\mu \to e\gamma$) $< 4.2 \cdot 10^{-13}$ and BR($\mu \to eee$) $< 10^{-12}$ [271]. These results have been obtained with the effective Lagrangian in Eq. (3.1) and the parametrization in Eq. (3.76).

ϕ-induced dipole contributions

We now consider the generation of dipole operators by loops involving the ultralight scalar ϕ, as discussed in Section 3.4.3 and shown in Fig. 3.2. In this scenario, we assume that ϕ provides the dominant (or, of course, the only) contribution to dipole operators. For the sake of simplicity, the couplings S^{ee} and $S^{e\mu}_{L,R}$ will be the only ones allowed to be different from zero in the analysis that follows. They will also be taken to be real. In this case, the general expressions for K_2^L and K_2^R given in Eqs. (3.29) and (3.30) lead to

$$\begin{aligned}\left(K_2^L\right)^{e\mu} =& \frac{S^{ee}}{96\pi^2\, m_\mu^3}\Big\{3\, m_\mu\, S_R^{e\mu} + m_e\left(-6\, S_L^{e\mu} + 2\,\pi^2\, S_L^{e\mu} + 3\, S_R^{e\mu}\right) \\ &+ 3\, m_e S_L^{e\mu} \log\left(-\frac{m_e^2}{m_\mu^2}\right)\left[1 + \log\left(-\frac{m_e^2}{m_\mu^2}\right)\right]\Big\}, \end{aligned} \tag{3.77}$$

$$\begin{aligned}\left(K_2^R\right)^{e\mu} =& \frac{S^{ee}}{96\pi^2\, m_\mu^3}\Big\{3\, m_\mu\, S_L^{e\mu} + m_e\left(-6\, S_R^{e\mu} + 2\,\pi^2\, S_R^{e\mu} + 3\, S_L^{e\mu}\right) \\ &+ 3\, m_e S_R^{e\mu} \log\left(-\frac{m_e^2}{m_\mu^2}\right)\left[1 + \log\left(-\frac{m_e^2}{m_\mu^2}\right)\right]\Big\}, \end{aligned} \tag{3.78}$$

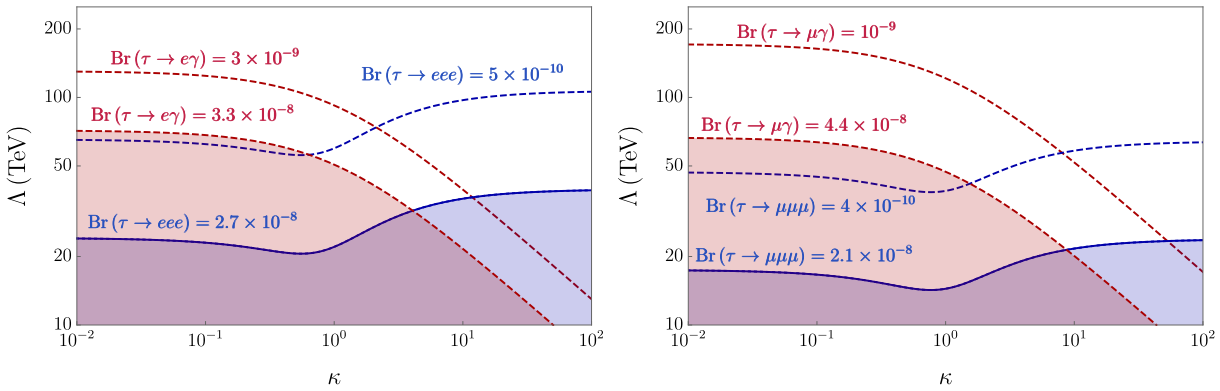

Figure 3.10: Contours of BR($\tau \to e\gamma$) and BR($\tau \to eee$), on the left, and BR($\tau \to \mu\gamma$) and BR($\tau \to \mu\mu\mu$), on the right, in the κ-Λ plane. The lowest values correspond to the expected future sensitivities of the Belle II experiment [150], while colored regions are excluded due to the current bounds BR($\tau \to e\gamma$) $< 3.3 \cdot 10^{-8}$, BR($\tau \to \mu\gamma$) $< 4.4 \cdot 10^{-8}$, BR($\tau \to eee$) $< 2.7 \cdot 10^{-8}$ and BR($\tau \to \mu\mu\mu$) $< 2.1 \cdot 10^{-8}$ [271]. These results have been obtained with the effective Lagrangian in Eq. (3.1) and the parametrization in Eq. (3.76).

where we have expanded at first order in m_e. These expressions allow us to compute the $R_{\mu e}$ ratio defined in Eq. (3.74). Defining the mass ratio $r = \frac{m_\mu^2}{m_e^2}$, we do that for some simplified scenarios:

- Scenario 1: $S_L^{e\mu} = 0$ or $S_R^{e\mu} = 0$

$$R_{\mu e}^{(1)} \approx \frac{4\,\pi\,r}{3\,\alpha}\,\frac{12\,\log r - 53}{|\log(-r)|^4 + r} \approx 3.2 \cdot 10^4\,. \tag{3.79}$$

- Scenario 2: $S_L^{e\mu} = S_R^{e\mu}$

$$R_{\mu e}^{(2)} \approx \frac{4\,\pi\,r}{3\,\alpha}\,\frac{12\,\log r - 53}{|\log^2(-r) + \sqrt{r}|} \approx 1.9 \cdot 10^4\,. \tag{3.80}$$

- Scenario 3: $S_L^{e\mu} = -S_R^{e\mu}$

$$R_{\mu e}^{(3)} \approx \frac{4\,\pi\,r}{3\,\alpha}\,\frac{12\,\log r - 53}{|\log^2(-r) - \sqrt{r}|} \approx 1.1 \cdot 10^5\,. \tag{3.81}$$

We find that $R_{\mu e} \gg 1$ in these scenarios. This, however, was expected, since $\ell_\alpha \to \ell_\beta \ell_\beta \ell_\beta$ is induced at tree-level by ϕ exchange, while $\ell_\alpha \to \ell_\beta\,\gamma$ can only take place at loop order. More interestingly, different scenarios for the ϕ couplings lead to very different predictions for $R_{\mu e}$. This would, in principle, allow us to determine the nature of the scalar ϕ if positive signals are observed for both $\mu \to e\gamma$ and $\mu \to eee$ processes.

3.5.4 Lepton magnetic and electric dipole moments

As discussed in Section 1.5, the deviation observed in the experimental determination of the electron and muon AMMs compared to their SM predicted values has attracted the attention of the physics community. On the other hand, the SM predicts tiny values for the charged leptons EDMs, so any non-zero measurement of these observables would be a clear signal of new physics effects.

Fig. 3.11 shows favored regions for the diagonal coupling S^{ee} due to the electron AMM and EDM. As shown on the left panel, the bound on the electron EDM strongly constrains the S^{ee} coupling, which must be essentially purely real or purely imaginary. However, one can find regions in the parameter space that explain the $(g-2)_e$ anomaly, compatible with the bound on the electron EDM. Given the low significance of the $(g-2)_e$ anomaly, one stays within the $3\,\sigma$ region even if $S^{ee}=0$, but if $\mathrm{Re}\,S^{ee} \lesssim 10^{-13}$, a value of about $\mathrm{Im}\,S^{ee} \sim 10^{-5}$ would actually achieve agreement at the $1\,\sigma$ level. The deviation in $(g-2)_\mu$ is more significant, implying that one must introduce larger $S^{\mu\mu}$ values in order to reconcile the theoretical prediction with the experimental measurement. This is shown in Fig. 3.12. In this case, the bound from the muon EDM does not impose strong restrictions on the parameter space, as can be seen in the left panel. However, larger $S^{\mu\mu}$ couplings, of the order of 10^{-4}, are necessary to explain the current deviation between theory and experiment. In both cases, the required values for S^{ee} and $S^{\mu\mu}$ are in conflict with the bounds discussed in Section 3.3, see Eqs. (3.7) and (3.8), and therefore a mechanism to suppress the processes from which they are derived would be necessary for the ultralight scalar ϕ to be able to explain the current $g-2$ anomalies.

Finally, we have explored whether the electron and muon AMM anomalies can be explained by purely off-diagonal contributions. In the following, we consider vanishing diagonal couplings and real non-zero off-diagonal couplings. In this scenario, the contribution to the charged leptons EDMs vanish and the AMMs strongly correlate with LFV observables. The bounds derived in Section 3.4.7 from the non-observation of $\ell_\alpha \to \ell_\beta\,\phi$ imply that an explanation to the observed deviations cannot be achieved. In particular, we find that $S_L^{e\mu} \sim -S_R^{e\mu} \sim 2\times10^{-4}$ or $S_L^{e\tau} \sim -S_R^{e\tau} \sim 7\times10^{-4}$ are needed in order to explain the $(g-2)_e$ deviation. Regarding the muon AMM anomaly, only with the $\mu-\tau-\phi$ coupling one can obtain a positive contribution, requiring $S_L^{\mu\tau} \sim S_R^{\mu\tau} \sim 3\times10^{-3}$ to explain the $(g-2)_\mu$ deviation. In all cases, the required off-diagonal couplings are several orders of magnitude larger than the limits in Eqs. (3.62) and (3.65). We therefore conclude that the explanation of the electron and muon AMMs anomalies must come from diagonal contributions, whereas the off-diagonal ones can only play a subdominant role.

3.6 Conclusions

Ultralight scalars appear in a wide variety of SM extensions, either as very light states or as exactly massless particles, like Goldstone bosons. These states can be produced in many leptonic processes or act as their mediators, leading to many exotic signatures. Examples of such scalars

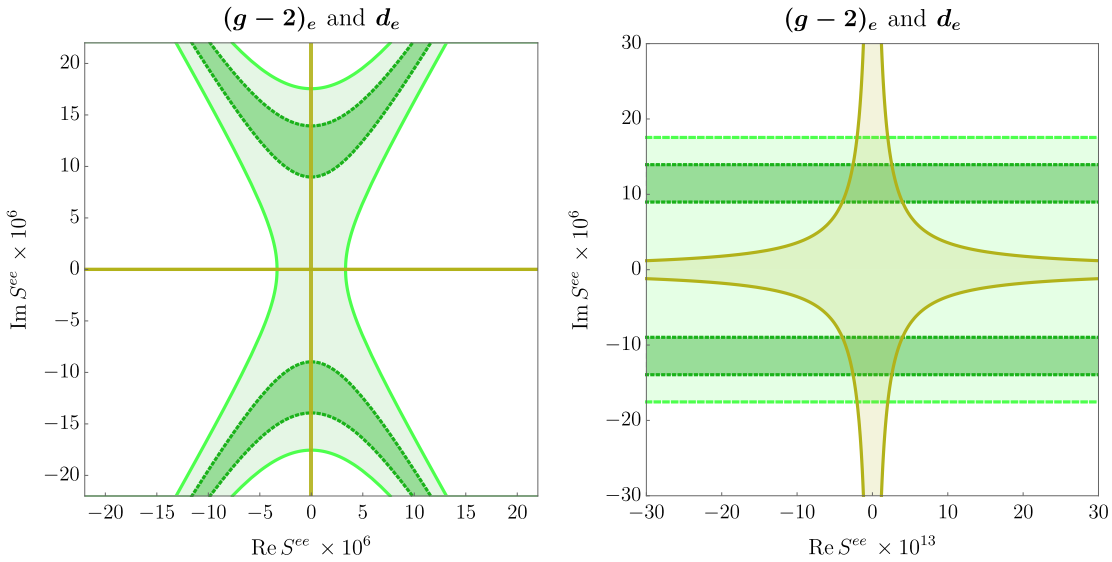

Figure 3.11: Favored region for the diagonal coupling S^{ee}, due to the electron anomalous magnetic and electric dipole moments. Within the light (dark) green region, the deviation in the electron AMM is explained at the $3\,\sigma$ ($1\,\sigma$) level. The region delimited by the orange continuous lines is the parameter space allowed by the current experimental upper bound of the electron EDM. In the figure on the right, the abscissa axis has been zoomed.

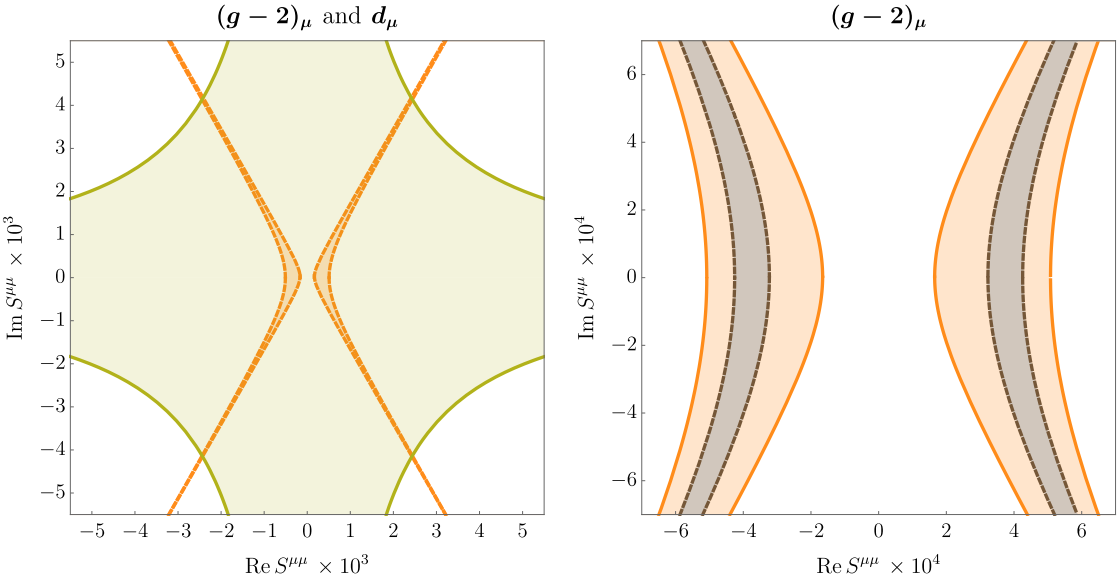

Figure 3.12: Favored regions for the diagonal coupling $S^{\mu\mu}$, due to the muon anomalous magnetic and electric dipole moments. In the figure on the left, it is seen that the bound from the muon EDM (yellow continuous curves) does not restrict too much the AMM of the muon (orange dashed curves). On the right figure, only the muon AMM is represented and within the light (dark) region, the current experimental deviation is explained at the $3\,\sigma$ ($1\,\sigma$) level.

include the majoron and the axion, two well-motivated hypothetical particles at the core of

Coupling	Upper limit	References
$\mathrm{Im}\, S^{ee}$	2.1×10^{-13}	[234]
$\mathrm{Re}\, S^{ee}$	$[\mathrm{Im}\, S^{ee}]_{\mathrm{max}}$	
$\mathrm{Im}\, S^{\mu\mu}$	2.1×10^{-9}	[238]
$\mathrm{Re}\, S^{\mu\mu}$	$[\mathrm{Im}\, S^{\mu\mu}]_{\mathrm{max}}$	
$\lvert S^{e\mu}\rvert$	5.3×10^{-11}	[211]
$\lvert S^{e\tau}\rvert$	3.5×10^{-7}	[211]
$\lvert S^{\mu\tau}\rvert$	2.7×10^{-7}	[211]

Table 3.2: Current limits on the ultralight scalar couplings to charged leptons. The limit on $\mathrm{Im}\, S^{ee}$ is at 90% C.L. [234]. The limit on $\mathrm{Im}\, S^{\mu\mu}$ has been obtained by performing a simulation of the supernova SN1987A [238]. An alternative and more stringent limit $\mathrm{Im}\, S^{\mu\mu} < 2.1 \times 10^{-10}$ can be derived with more aggressive assumptions in the simulation.

two fundamental problems: the origin of neutrino masses and the conservation of CP in strong interactions.

In this Chapter, we delve into the effects of ultralight scalars in many leptonic observables using a model-independent general approach. Our analysis takes into account both scalar and pseudoscalar interactions to charged leptons, therefore going beyond most existing studies. First, we briefly reviewed the current bounds imposed by stellar cooling on the diagonal couplings and discussed indirect limits from the 1-loop generation of a coupling to photons. Then, we derived analytical expressions for a wide variety of leptonic observables. We have revisited the decays $\ell_\alpha \to \ell_\beta\, \phi$ and $\ell_\alpha \to \ell_\beta\, \gamma\, \phi$, in which the scalar ϕ is produced, and provided complete expressions for the radiative LFV decays $\ell_\alpha \to \ell_\beta\, \gamma$, as well as for the 3-body decays $\ell_\alpha^- \to \ell_\beta^- \ell_\beta^- \ell_\beta^+$, $\ell_\alpha^- \to \ell_\beta^- \ell_\gamma^- \ell_\gamma^+$ and $\ell_\alpha^- \to \ell_\beta^+ \ell_\gamma^- \ell_\gamma^-$, in which ϕ contributes as a mediator. The effect of ultralight scalars on the charged leptons anomalous magnetic and electric dipole moments was also discussed. Finally, several phenomenological aspects of this scenario have been explored. After deriving limits on the off-diagonal couplings from lepton flavor violating observables, we have shown that an explanation to the $(g-2)_e$ and $(g-2)_\mu$ anomalies is possible in this scenario. Furthermore, we have also shown that the observables discussed in this Chapter are indeed complementary. A compilation of the current limits on the ultralight scalar couplings to charged leptons can be found in Table 3.2.

The phenomenology of ultralight scalars is very rich since they are kinematically accessible in most high- and low-energy processes. We have discussed many purely leptonic observables, but if ϕ couples to quarks too, many hadronic and semi-leptonic channels open. This could give rise to many signatures at kaon factories [272]. Furthermore, ultralight scalars may leave their footprints in other processes. For instance, they can be produced and emitted in tritium beta decay [273] or $\mu - e$ conversion in nuclei [274], have a strong impact in leptogenesis [275], and give rise to non-resonant phenomena at colliders [276]. In our opinion, this diversity of

experimental signatures and their potential to unravel some of the most important problems in particle physics through their connection to ultralight scalars merits further investigation.

Chapter 4

$(g-2)_{e,\mu}$ in an extended inverse type-III seesaw

The electron and muon $g-2$ experiments have yielded results that are at odds with the Standard Model theoretical predictions (see Section 1.5 for a detailed discussion). This is particularly relevant in the case of the muon $g-2$, which has attracted a remarkable interest in the community after the long-awaited announcement of the first results by the Muon $g-2$ collaboration at Fermilab, which confirms a previous measurement by the E821 experiment at Brookhaven and enlarges the statistical significance of the discrepancy, now at 4.2σ. Therefore, the development of BSM models to address the discrepancy, if finally confirmed, may be required. Actually, it is crucial for these models not only to explain the anomalous magnetic moments of the charged leptons but also to provide solutions to other open questions within the Standard Model while remaining consistent with all relevant experimental constraints.

4.1 Introduction

Although the main motivation of the inverse type-III seesaw model is to induce non-zero masses for neutrinos, it is natural to investigate whether the model can also account for the experimental values of the electron and muon anomalous magnetic moments in regions of the parameter space that reproduce the measured neutrino masses and leptonic mixing angles while being compatible with the bounds obtained at colliders and low-energy experiments. In this chapter, however, we show that the latter constraints preclude the ISS3 from inducing large contributions to $(g-2)_{e,\mu}$. More importantly, the ISS3 contributions are negative, making it impossible to address the existing discrepancy in the muon $g-2$. This motivates a minimal extension of the model that introduces a pair of vector-like (VL) lepton doublets with sizable couplings to electrons and muons. This extension provides the necessary ingredients to generate the required contributions to both $g-2$ anomalies while keeping the relevant features of the original model

and satisfying all the experimental constraints. The aim of this chapter, which is based on [277], is, then, to study the electron and muon $g-2$ in this model, which we denote as the ISS3VL.

4.2 The model

The ISS3VL is an extension of the leptonic sector of the SM with the addition of six right-handed Weyl fermion $\mathrm{SU(2)_L}$ triplets with vanishing hypercharge, Σ_A and Σ'_A ($A=1,2,3$), and VL copies of the SM lepton doublet, L_L and L_R. The Σ_A and Σ'_A triplets are introduced in order to generate neutrino masses via the inverse type-III seesaw mechanism. [1] They can be distinguished by their different lepton numbers, with $L(\Sigma)=+1$ and $L(\Sigma')=-1$. Nevertheless, lepton number will be explicitly broken in the ISS3VL and, therefore, this lepton number assignment is arbitrary. The new fermionic fields L_L and L_R have the same representations under the $\mathrm{SU(3)\times SU(2)\times U(1)}$ gauge group, and both are doublets under $\mathrm{SU(2)_L}$. The scalar and lepton particle content of the ISS3VL model and the representations of all fields under the $\mathrm{SU(3)\times SU(2)\times U(1)}$ gauge group are shown in Table 4.1.

The Σ and Σ' triplets can be decomposed into $\mathrm{SU(2)_L}$ components. With $\Sigma_A=(\Sigma^1,\Sigma^2,\Sigma^3)_A$, they can be conveniently written in the usual 2×2 matrix notation according to

$$\Sigma_A=\frac{1}{\sqrt{2}}\,\vec{\sigma}\cdot\vec{\Sigma}_A=\begin{pmatrix}\Sigma_A^0/\sqrt{2} & \Sigma_A^+\\ \Sigma_A^- & -\Sigma_A^0/\sqrt{2}\end{pmatrix}, \tag{4.1}$$

where σ_A are the usual Pauli matrices and the states with well-defined electric charge are given by

$$\Sigma_A^0=\Sigma_A^3\,,\qquad \Sigma_A^\pm=\frac{\Sigma_A^1\mp i\,\Sigma_A^2}{\sqrt{2}}\,. \tag{4.2}$$

The same holds for the primed states. Finally, the VL leptons $L_{L,R}$ can be decomposed as

$$L_{L,R}=\begin{pmatrix}N\\ E\end{pmatrix}_{L,R}. \tag{4.3}$$

Under the above working assumptions, the most general Yukawa Lagrangian allowed by all symmetries can be written as

$$\mathcal{L}_Y=\mathcal{L}_Y^{\mathrm{SM}}+\mathcal{L}_Y^{\mathrm{ISS3}}+\mathcal{L}_Y^{\mathrm{VL}}\,, \tag{4.4}$$

where $\mathcal{L}_Y^{\mathrm{SM}}$ is the usual SM Lagrangian that we defined in Eq. (1.38). The terms in

$$-\mathcal{L}_Y^{\mathrm{ISS3}}=\sqrt{2}\,\overline{\Sigma}\,Y_\Sigma\,\ell_L\,\widetilde{H}^\dagger+M_\Sigma\,\overline{\Sigma}\,\Sigma'^c+\frac{1}{2}\,\mu\,\overline{\Sigma'}\,\Sigma'^c+\text{h.c.}\,, \tag{4.5}$$

[1] In order to simplify the notation, we will not denote the chirality of the $\Sigma_A\equiv\Sigma_{R_A}$ and $\Sigma'_A\equiv\Sigma'_{R_A}$ fermions explicitly.

Field	Generations	$SU(3)_c$	$SU(2)_L$	$U(1)_Y$
ℓ_L	3	**1**	**2**	$-1/2$
e_R	3	**1**	**1**	-1
Σ	3	**1**	**3**	0
Σ'	3	**1**	**3**	0
L_L	1	**1**	**2**	$-1/2$
L_R	1	**1**	**2**	$-1/2$
H	1	**1**	**2**	$1/2$

Table 4.1: Scalar and lepton particle content of the ISS3VL. ℓ_L, e_R, and H are the usual SM fields.

correspond to the usual ISS3 extension. Y_Σ, M_Σ and μ are 3×3 matrices, the latter two with dimensions of mass. Here and in the following we omit $SU(2)_L$ contractions and flavor indices to simplify the notation. Finally, the VL leptons allow for additional Lagrangian terms, given by

$$-\mathcal{L}_Y^{\rm VL} = \sqrt{2}\,\overline{\Sigma}\,\lambda_L\,L_L\,\widetilde{H}^\dagger + \overline{e}_R\,\lambda_R\,L_L\,\widetilde{H}^\dagger + \overline{L}_L\,M_L\,L_R + \overline{\ell}_L\,\epsilon\,L_R + \text{h.c.}\,, \tag{4.6}$$

where λ_L and λ_R are dimensionless 3×1 vectors, and M_L is a parameter with dimensions of mass. The 1×3 vector ϵ has dimensions of mass and will be assumed to vanish for simplicity. [2] The guiding principle when writing the Yukawa Lagrangian in Eq. (6.2), in particular the piece in Eq. (4.5), is the conservation of lepton number, only allowed to be broken by the $\overline{\Sigma'}\,\mu\,\Sigma'^c$ term. In fact, in the absence of the Majorana mass μ, the Lagrangian would have an additional $U(1)_L$ global symmetry. In the following, we will consider $\mu \ll M_\Sigma$, corresponding to a *slightly broken lepton number*, in the spirit of the original inverse seesaw mechanism. [3]

The scalar potential of the model is the same as in the SM, and it was defined in Eq. (1.26). [4] After electroweak symmetry breaking, several terms in the Yukawa Lagrangian in Eq. (6.2) induce mixings in the neutral and charged lepton sectors. In the bases $n \equiv n_L = \left(\nu_L, (\Sigma^0)^c, (\Sigma'^0)^c, N_L, N_R^c\right)$, $f_L = (e_L, (\Sigma^+)^c, (\Sigma'^+)^c, E_L)$ and $f_R = (e_R, \Sigma^-, \Sigma'^-, E_R)$, the neutral and charged fermion mass terms read

$$-\mathcal{L}_m = \frac{1}{2}\overline{n^c}\,\mathcal{M}_N\,n + \overline{f_L}\,\mathcal{M}_C\,f_R + \text{ h.c.}\,, \tag{4.7}$$

[2] The ϵ term contributes to the electron, muon, and tau masses and is therefore constrained to be small.

[3] In principle, a term of the form $\overline{\Sigma}\,\mu'\,\Sigma^c$ is also allowed by all symmetries. However, it is well known that such a term would contribute to neutrino masses in a subdominant way if μ and μ' are of the same order, see for instance [172]. Therefore, we neglect this term in the following.

[4] Note that the symbol μ has been used in both Eqs. (1.26) and (4.5). However, the Higgs potential is not relevant to the discussion of this chapter, and, in the remainder of it, μ will refer to the mass parameter in Eq. (4.5).

with the mass matrices given by

$$\mathcal{M}_N = \begin{pmatrix} 0 & m_D^T & 0 & 0 & 0 \\ m_D & 0 & M_\Sigma & m_L & 0 \\ 0 & M_\Sigma^T & \mu & 0 & 0 \\ 0 & m_L^T & 0 & 0 & M_L \\ 0 & 0 & 0 & M_L & 0 \end{pmatrix}, \tag{4.8}$$

and

$$\mathcal{M}_C = \begin{pmatrix} m_e & \sqrt{2}\, m_D^T & 0 & 0 \\ 0 & 0 & M_\Sigma & 0 \\ 0 & M_\Sigma^T & \mu & 0 \\ m_R^T & \sqrt{2}\, m_L^T & 0 & -M_L \end{pmatrix}. \tag{4.9}$$

Here we have defined

$$m_D = \frac{v}{\sqrt{2}}\, Y_\Sigma\,, \quad m_e = \frac{v}{\sqrt{2}}\, Y_e\,, \quad m_L = \frac{v}{\sqrt{2}}\, \lambda_L \quad \text{and} \quad m_R = \frac{v}{\sqrt{2}}\, \lambda_R\,. \tag{4.10}$$

We note that the neutral lepton mass matrix $\mathcal{M}_N$ is 11×11, whereas the charged lepton mass matrix $\mathcal{M}_C$ is 10×10. They can be brought to diagonal form by means of the unitary transformations $\mathcal{U}$, $\mathcal{V}^L$, and $\mathcal{V}^R$, defined by

$$\mathcal{U}^*\, \mathcal{M}_N\, \mathcal{U}^\dagger = \text{diag}\,(m_{N_i})\,, \tag{4.11}$$

$$\mathcal{V}^{L\,*}\, \mathcal{M}_C\, \mathcal{V}^{R\,\dagger} = \text{diag}\,(m_{\chi_i})\,, \tag{4.12}$$

resulting in the 11 neutral (Majorana) fermion masses m_{N_i} and the 10 charged (Dirac) fermion masses m_{χ_j}, with $i = 1, \ldots, 11$ and $j = 1, \ldots, 10$. In the following, we will assume the hierarchy of energy scales

$$\mu \ll m_D, m_L, m_R \ll M_\Sigma, M_L\,, \tag{4.13}$$

which allows one to obtain approximate expressions for the physical lepton masses. We note that a small μ parameter is justified through 't Hooft naturalness criterion [155]. In the case of the charged leptons, we fix the Y_e Yukawa matrix to its SM values, neglecting the corrections from the mixings with the NP states, as we will comment below. On the other hand, for the neutral leptons, one finds 3 light states, to be identified with the standard light neutrinos, whereas the other states are heavy BSM particles. Their mass matrix in this extension is obtained in the same way as in the original ISS3 model. Using Eq.(2.48), with the new definition of M_R,

$$M_R = \begin{pmatrix} 0 & M_\Sigma & m_L & 0 \\ M_\Sigma^T & \mu & 0 & 0 \\ m_L^T & 0 & 0 & M_L \\ 0 & 0 & M_L & 0 \end{pmatrix}, \tag{4.14}$$

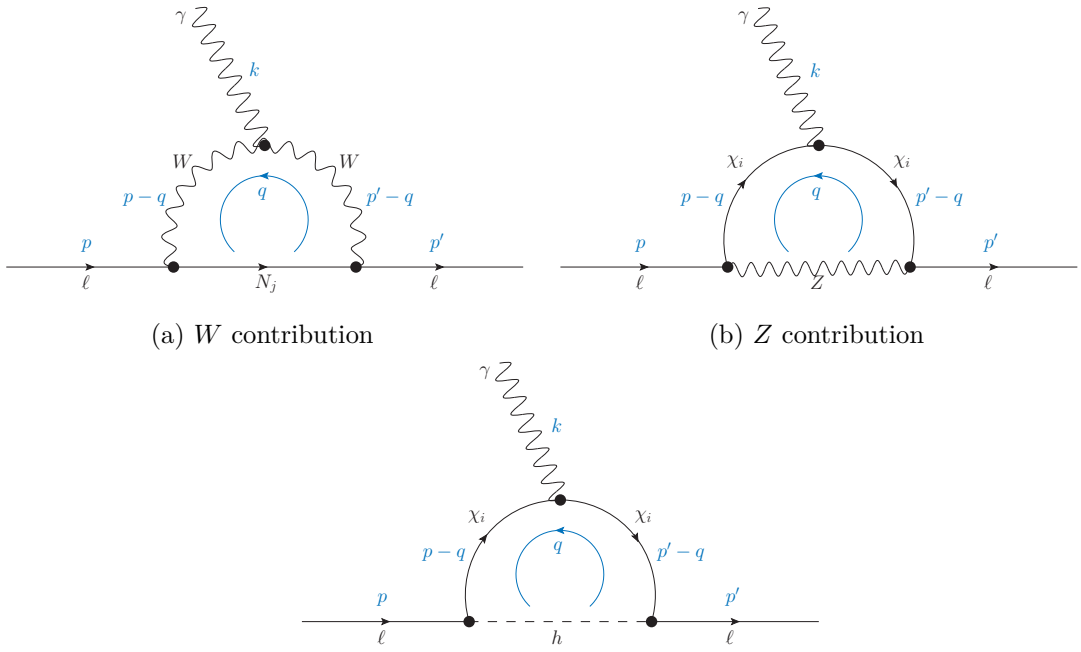

(a) W contribution

(b) Z contribution

(c) h contribution

Figure 4.1: Feynman diagrams that contribute to the charged lepton anomalous magnetic moment at the 1-loop level in the ISS3VL. Here χ_i and N_j denote any of the charged and neutral lepton mass eigenstates, respectively. Momenta are shown in blue.

the neutrino mass matrix is approximately given by

$$m_\nu \approx m_D^T \left(M_\Sigma^T\right)^{-1} \mu\, M_\Sigma^{-1}\, m_D\,, \tag{4.15}$$

with corrections of the order of the small ratios $(m_D/M_\Sigma)^2$ and $(m_L/M_L)^2$. As expected, this result is proportional to the μ parameter. It is then clear that sizable Y_Σ Yukawa couplings and triplets at the TeV scale are consistent with light neutrino masses due to the suppression by the μ term. This is the inverse seesaw mechanism.

4.3 Charged lepton anomalous magnetic moments

The ISS3VL has the ingredients to induce large charged lepton anomalous magnetic moments, namely, relatively light new particles with sizable couplings to the charged leptons. In the ISS3VL, new contributions to the charged lepton anomalous magnetic moments are induced at the 1-loop level, as shown in Fig. 4.1. While these diagrams also exist in the SM, in the ISS3VL, the mass eigenstates N_i and χ_i include new heavy states beyond the SM leptons. Moreover, the couplings of the SM states get modified due to mixings with the new BSM states, changing

their SM contributions. The amplitudes of these Feynman diagrams are given by [5]

$$
\begin{aligned}
i\,\mathcal{M}_{\ell}^{W} = & \int \frac{d^4q}{(2\pi)^4} \bar{u}_{\ell}\left(p'\right)\, i\,\gamma^{\beta}\left[\left(g_{\chi NW}^{L}\right)_{\ell j} P_L + \left(g_{\chi NW}^{R}\right)_{\ell j} P_R\right] i\frac{\not{q}+m_{N_j}}{q^2-m_{N_j}^2} \\
& i\,\gamma^{\alpha}\left[\left(g_{\chi NW}^{L}\right)_{j\ell} P_L + \left(g_{\chi NW}^{R}\right)_{j\ell} P_R\right] \frac{-i\left(g_{\alpha\tilde{\alpha}} - \frac{(p-q)_{\alpha}(p-q)_{\tilde{\alpha}}}{m_W^2}\right)}{(p-q)^2-m_W^2}\, i\,\Gamma^{\mu\tilde{\alpha}\tilde{\beta}} \\
& \frac{-i\left(g_{\beta\tilde{\beta}} - \frac{(p'-q)_{\beta}(p'-q)_{\tilde{\beta}}}{m_W^2}\right)}{(p'-q)^2-m_W^2} u_{\ell}\left(p\right)\varepsilon_{\mu}\,,
\end{aligned}
\tag{4.16}
$$

$$
\begin{aligned}
i\,\mathcal{M}_{\ell}^{Z} = & \int \frac{d^4q}{(2\pi)^4} \bar{u}_{\ell}\left(p'\right)\, i\,\gamma^{\beta}\left[\left(g_{\chi Z}^{L}\right)_{i\ell} P_L + \left(g_{\chi Z}^{R}\right)_{i\ell} P_R\right] i\frac{\left(\not{p}'-\not{q}\right)+m_{\chi_i}}{(p'-q)^2-m_{\chi_i}^2} \\
& i\,\gamma^{\mu}\left[\left(g_{\chi\gamma}^{L}\right)_{ii} P_L + \left(g_{\chi\gamma}^{R}\right)_{ii} P_R\right] i\frac{\left(\not{p}-\not{q}\right)+m_{\chi_i}}{(p-q)^2-m_{\chi_i}^2}\, i\,\gamma^{\alpha}\left[\left(g_{\chi Z}^{L}\right)_{\ell i} P_L + \left(g_{\chi Z}^{R}\right)_{2i} P_R\right] \\
& \frac{-i\left(g_{\alpha\beta} - \frac{q_{\alpha}q_{\beta}}{m_Z^2}\right)}{q^2-m_Z^2} u_{\ell}\left(p\right)\varepsilon_{\mu}\,,
\end{aligned}
\tag{4.17}
$$

$$
\begin{aligned}
i\,\mathcal{M}_{\ell}^{h} = & \int \frac{d^4q}{(2\pi)^4} \bar{u}_{\ell}\left(p'\right)\, i\,\left[\left(g_{\chi h}^{L}\right)_{i\ell} P_L + \left(g_{\chi h}^{R}\right)_{i\ell} P_R\right] i\frac{\left(\not{p}'-\not{q}\right)+m_{\chi_i}}{(p'-q)^2-m_{\chi_i}^2} \\
& i\,\gamma^{\mu}\left[\left(g_{\chi\gamma}^{L}\right)_{ii} P_L + \left(g_{\chi\gamma}^{R}\right)_{ii} P_R\right] i\frac{\left(\not{p}-\not{q}\right)+m_{\chi_i}}{(p-q)^2-m_{\chi_i}^2}\, i\,\left[\left(g_{\chi h}^{L}\right)_{\ell i} P_L + \left(g_{\chi h}^{R}\right)_{\ell i} P_R\right] \\
& \frac{i}{q^2-m_h^2} u_{\ell}\left(p\right)\varepsilon_{\mu}\,.
\end{aligned}
\tag{4.18}
$$

Here ε_{μ} is the photon polarization 4-vector and the couplings $g_{\chi NW}^{L,R}$, $g_{\chi Z}^{L,R}$, $g_{\chi\gamma}^{L,R}$, $g_{\chi h}^{L,R}$ and Γ are defined in Appendix B. A sum over the indices i, j is implicit in these expressions, while ℓ is the index of the external charged lepton. We have computed the amplitudes in Eqs. (4.16)-(4.18) with the help of `Package-X` [253]. After projecting onto the operator in Eq. (1.52), one obtains analytical expressions for the contributions to the c coefficient, which can then be translated into contributions to the charged leptons $g-2$ thanks to the relation in Eq. (1.53). The total ISS3VL contribution to Δa_{ℓ} can be written as [6]

$$
\Delta a_{\ell} = \Delta a_{\ell}\left(W\right) + \Delta a_{\ell}\left(Z\right) + \Delta a_{\ell}\left(h\right)\,. \tag{4.19}
$$

[5] In order to obtain the correct sign for the ISS3VL contributions to the electron and muon $g-2$ one must use a consistent set of sign conventions for the Feynman rules of the model. We used the useful Ref. [278] to guarantee the consistency of the amplitudes in Eqs. (4.16)-(4.18).

[6] Higher-order contributions, such as those induced by 2-loop Barr-Zee diagrams [252], will be neglected in the following.

Assuming that the ISS3VL states N_i and χ_i are much heavier than the SM states (assuming the mass hierarchy $m_{N_i}, m_{\chi_i} \gg m_h, m_W, m_Z \gg m_\ell$ with $i > 3$), one can find approximate expressions for the three contributions:

$$\Delta a_\ell\,(W) \simeq \frac{m_\ell}{32\,\pi^2\,m_W^2}\left\{\frac{4}{3}\,m_\ell\left[1-\frac{3\,m_W^2}{4\,m_{N_i}^2}\left(11+6\log\frac{m_W^2}{m_{N_i}^2}\right)\right]\left(C_{\chi NW}^2\right)_{i\ell}\right.$$
$$\left.-\,m_{N_i}\left[1-\frac{3\,m_W^2}{m_{N_i}^2}\left(3+2\log\frac{m_W^2}{m_{N_i}^2}\right)\right]\left(D_{\chi NW}^2\right)_{i\ell}\right\}, \tag{4.20}$$

$$\Delta a_\ell\,(Z) \simeq \frac{m_\ell}{32\,\pi^2\,m_Z^2}\left\{-\frac{5}{3}\,m_\ell\left(C_{\chi Z}^2\right)_{i\ell}+\,m_{\chi_i}\left(D_{\chi Z}^2\right)_{i\ell}\right\}, \tag{4.21}$$

$$\Delta a_\ell\,(h) \simeq \frac{m_\ell}{32\,\pi^2\,m_{\chi_i}^2}\left\{\frac{1}{3}\,m_\ell\left(C_{\chi h}^2\right)_{i\ell}+m_{\chi_i}\left(D_{\chi h}^2\right)_{i\ell}\right\}. \tag{4.22}$$

Here we have defined the coupling combinations

$$\left(C_Y^2\right)_{i\ell} \equiv \left|\left(g_Y^L\right)_{i\ell}\right|^2+\left|\left(g_Y^R\right)_{i\ell}\right|^2 \qquad \text{and} \qquad \left(D_Y^2\right)_{i\ell} \equiv \left(g_Y^L\right)_{i\ell}\left(g_Y^R\right)_{i\ell}^*+\left(g_Y^L\right)_{i\ell}^*\left(g_Y^R\right)_{i\ell}, \tag{4.23}$$

with $Y = \chi NW, \chi Z, \chi h$. Again, the indices i and ℓ denote the BSM particle running in the loop and the charged lepton, respectively. We have checked that Eqs. (4.20), (4.21) and (4.22) reproduce the ISS3VL contributions to the charged leptons anomalous magnetic moments in very good approximation. Nevertheless, full expressions are given in Appendix C and used in the numerical analysis presented in the next section. In fact, the approximated expressions can not be used in the case of SM fermions running in the loop, and the exact formulae must be employed. We note that $\Delta a_\ell(W)$, $\Delta a_\ell(Z)$ and $\Delta a_\ell(h)$ contain contributions proportional to $m_N\,g_{\chi NW}^L\,g_{\chi NW}^R$, $m_\chi\,g_{\chi Z}^L\,g_{\chi Z}^R$, and $m_\chi\,g_{\chi h}^L\,g_{\chi h}^R$, respectively, that is, proportional to the mass of the fermion in the loop. These terms are usually called *chirally-enhanced contributions*, and they typically dominate due to the large masses of the heavy fermions running in the loop. Although it may look like particles with masses well above the EW scale will not decouple, this is not the case. Small mixings between the SM charged leptons and the BSM particles would appear, resulting in the new physics contributions vanishing.

4.4 Phenomenological discussion

We proceed now to present our phenomenological exploration of the parameter space of the ISS3VL.

4.4.1 Experimental constraints

Let us first discuss how we fix the parameters of the model in order to reproduce the measured lepton masses and mixings. The Y_e Yukawa matrix will be fixed to the same values as in the SM, hence neglecting corrections from the mixing between the SM charged lepton states and

the charged components of the Σ and Σ' triplets. These corrections are multiplicative and enter at order $\sim (m_D/M_\Sigma)^2$ and can thus be safely neglected. The same argument applies to the mixing with the charged components of the VL leptons, which enter at order $\sim (m_R/M_L)^2$. Without loss of generality, we will work in the basis in which M_Σ is diagonal and μ is a general complex symmetric matrix. In this case, Y_Σ and μ must be properly fixed in order to reproduce neutrino oscillation data [138]. In principle, one can set the entries of μ to some input values and express the Y_Σ Yukawa matrix by means of the master parametrization [203, 204], which in this case reduces to a modified Casas-Ibarra parametrization [200]. While this is perfectly valid, one generically obtains Y_Σ matrices with sizable off-diagonal entries unless some input parameters are very finely tuned. Due to the strong constraints from the non-observation of lepton flavor violating processes, this excludes most of the parameter points. Therefore, we take the alternative choice of fixing Y_Σ to specific input values, diagonal for simplicity, and computing μ by inverting Eq. (4.15) as

$$\mu = M_\Sigma^T \left(m_D^T\right)^{-1} m_\nu \, m_D^{-1} \, M_\Sigma \,, \tag{4.24}$$

where $m_\nu = U_\nu^* \, \widehat{m}_\nu \, U_\nu^\dagger$.

Here U_ν is the leptonic mixing matrix measured in oscillation experiments, given in terms of 3 mixing angles and 3 CP-violating phases, while $\widehat{m}_\nu$ is a diagonal matrix containing the physical neutrino mass eigenvalues. Eq. (4.24) guarantees that all the parameter points considered in our numerical analysis are compatible with neutrino oscillation data. In our analysis, we use the results of the global fit in [138], and we consider both normal and inverted neutrino mass orderings.

In order to ensure compatibility with constraints from flavor and electroweak precision data, we use the bounds derived in [190], where a global analysis is performed in the context of general type-III seesaw models. The limits provided in this reference are given for the 3×3 matrix η, defined in our case in terms of the matrices

$$M_D = \begin{pmatrix} m_D \\ 0 \end{pmatrix} \quad \text{and} \quad M = \begin{pmatrix} 0 & M_\Sigma \\ M_\Sigma^T & \mu \end{pmatrix} , \tag{4.25}$$

as

$$\begin{aligned} \eta &= \frac{1}{2} M_D^\dagger \left(M^\dagger\right)^{-1} M^{-1} \, M_D \\ &= \frac{1}{2} m_D^\dagger \left(M_\Sigma^\dagger\right)^{-1} \left[\mathbb{I}_3 + \mu^* \, (M_\Sigma^*)^{-1} \left(M_\Sigma^T\right)^{-1} \mu\right] M_\Sigma^{-1} \, m_D \\ &\approx \frac{1}{2} m_D^\dagger \left(M_\Sigma^\dagger\right)^{-1} M_\Sigma^{-1} \, m_D \,. \end{aligned} \tag{4.26}$$

In our analysis, we make sure that the bounds are respected by computing the η matrix in all the parameter points considered. As we will explain below, these limits imply very small BSM contributions in the ISS3, thus motivating our ISS3VL extension. Furthermore, we also consider

the decay widths for the processes $Z \to \ell^+\ell^-$ and $h \to \ell^+\ell^-$, with $\ell = e, \mu$, which are also affected due to the mixing of the light charged leptons with the heavy states in our model. They are computed as

$$\Gamma(Z \to \ell^+\ell^-) = \frac{m_Z^3}{12\pi v^2}\left[\left|\left(g_{\chi Z}^V\right)_{\ell\ell}\right|^2 + \left|\left(g_{\chi Z}^A\right)_{\ell\ell}\right|^2\right], \tag{4.27}$$

$$\Gamma(h \to \ell^+\ell^-) = \frac{m_h}{8\pi}\left[\left|\left(g_{\chi h}^L\right)_{\ell\ell}\right|^2 + \left|\left(g_{\chi h}^R\right)_{\ell\ell}\right|^2\right], \tag{4.28}$$

with $g_{\chi Z}^V = g_{\chi Z}^L + g_{\chi Z}^R$ and $g_{\chi Z}^A = g_{\chi Z}^R - g_{\chi Z}^L$. The $Z \to \ell^+\ell^-$ decay turns out to provide an important constraint in our setup. In fact, it has been recently pointed out that this process potentially correlates with the charged leptons $g-2$ [279]. We define the ratios

$$R_{Z\ell\ell} = \frac{\Gamma(Z \to \ell^+\ell^-)}{\Gamma_{\rm SM}(Z \to \ell^+\ell^-)}, \tag{4.29}$$

with $\Gamma_{\rm SM}(Z \to \ell^+\ell^-)$ the SM predicted decay width, and impose that $R_{Z\ell\ell}$ lies within the 95% CL range, which we estimate to be $0.995 < R_{Zee} < 1.003$ and $0.993 < R_{Z\mu\mu} < 1.006$ [31]. Regarding the Higgs boson decays, no constraints are actually obtained from them since, at present, there is no hint for $h \to e^+e^-$ and evidence for $h \to \mu^+\mu^-$ was only obtained recently [280]. Therefore, they will be considered as predicted observables, potentially correlated with Δa_ℓ [279, 281].

Finally, we also impose bounds from collider searches. The type-III seesaw triplets have been searched for at the LHC in multilepton final states, both by ATLAS [282] and CMS [283, 284]. No excess above the expected SM backgrounds has been found, hence allowing the experimental collaborations to set limits on the triplet mass and couplings. Using a data sample obtained with proton collisions at $\sqrt{s} = 13$ TeV and an integrated luminosity of 35.9 fb^{-1}, CMS reports a lower bound on the triplet mass of 840 GeV at 95% confidence level if the triplet couplings are assumed to be lepton flavor universal [284]. While the flavor structure of the triplet couplings to leptons does not affect the heavy triplet pair production cross-sections, driven by gauge interactions, it has an impact on the flavor composition of the multilepton signature. The limit changes if the assumption of lepton flavor universal couplings is dropped, resulting in a more stringent bound when the triplet couples mainly to electrons and a more relaxed bound when the triplet couples mainly to taus, with values ranging between 390 and 930 GeV. The bounds from the CMS collaboration in [284] are applied in our analysis. However, since the CMS analysis focuses on the standard type-III seesaw scenario, and does not consider the particular features of the ISS3VL model, several simplifying assumptions must be made. We define

$$B_{A\alpha} = \frac{\Gamma(\Sigma_A^0 \to \ell_\alpha + \text{boson}) + \Gamma(\Sigma_A^+ \to \ell_\alpha + \text{boson})}{\sum_\alpha \left[\Gamma(\Sigma_A^0 \to \ell_\alpha + \text{boson}) + \Gamma(\Sigma_A^+ \to \ell_\alpha + \text{boson})\right]}, \tag{4.30}$$

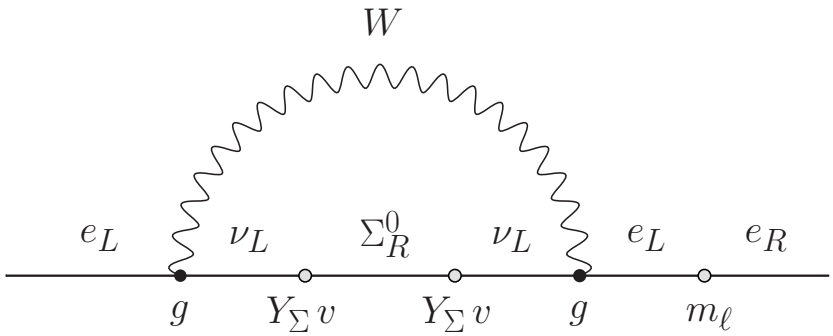

Figure 4.2: Dominant W contribution in the ISS3. Mass insertions are represented by white blobs.

where Σ_A^0 and Σ_A^+ are the quasi-Dirac pairs approximately formed by the mass eigenstates $N_i + N_j$ and $\chi_i + \chi_j$, respectively. An implicit sum over the bosons in the final states is also assumed, including decays to $W^\pm$, Z, and h. For instance, in a parameter point in which the lightest BSM states are mainly composed of the components of the Σ_1 triplet, we have $i = 4$, $j = 5$ and $\Gamma(\Sigma_1^0 \to \ell_\alpha + \text{boson}) \equiv \Gamma(N_4 \to W^\pm \ell^\mp) + \Gamma(N_4 \to Z\nu_\alpha) + \Gamma(N_4 \to h\nu_\alpha) + \Gamma(N_5 \to W^\pm \ell^\mp) + \Gamma(N_5 \to Z\nu_\alpha) + \Gamma(N_5 \to h\nu_\alpha)$. We note that $B_{Ae} + B_{A\mu} + B_{A\tau} = 1$. This is the quantity that we use to confront each quasi-Dirac pair with the limits given in Figure 3 of [284]. Our approach approximates the total heavy triplet pair production to $pp \to \Sigma_A^0 \Sigma_A^+$, which is known to give the dominant contribution at the LHC [285]. Furthermore, we apply two additional simplifications. First, since CMS assumes the neutral and charged components of the triplet to be mass degenerate, we adopt a conservative approach and take the lowest of them as the triplet mass to be used in the analysis. And second, we do not apply the CMS bounds to quasi-Dirac triplet pairs that are largely mixed with the VL leptons, since their production cross-section is clearly reduced with respect to the pure triplet case. [7] We believe that our assumptions conservatively adapt the CMS limits in [284] to our scenario. We note that ATLAS finds a similar bound on the triplet mass in the flavor universal scenario, ruling out (at 95% confidence level) values below 790 GeV [282]. Finally, LHC limits on VL leptons strongly depend on their decay modes, namely the flavor of the charged leptons produced in the final states [286]. In our analysis, we will consider $M_L \geq 500$ GeV, a conservative value that guarantees compatibility with current LHC searches. These limits are expected to be improved by the end of the LHC Run-III [287].

4.4.2 $(g-2)_{e,\mu}$ in the ISS3

Before studying the electron and muon $g-2$ in the ISS3VL, let us discuss these observables in the context of the *pure* ISS3 and show that this model is unable to address the existing discrepancies.

[7] In practice, we do not apply the CMS bounds in cases with large mixings. For instance, they are not applied to χ_i Dirac states that combine a left-handed fermion that is mostly a type-III triplet with a right-handed fermion that is mostly a VL lepton, or vice versa.

One can easily reach this conclusion by estimating the size of the dominant contributions to the charged lepton $g-2$. Fig. 4.2 shows the dominant W contribution. Assuming that the chirally-enhanced term in Eq. (4.20) dominates, one finds the estimate

$$\Delta a_\ell(W) \sim -\frac{1}{32\pi^2}\frac{m_N\, m_\ell}{m_W^2}\, g^2 \left(\frac{m_D}{M_\Sigma}\right)^2_{\ell\ell} \frac{m_\ell}{v} \sim -10^{-3}\,\frac{m_N\, m_\ell^2}{m_W^3}\,\eta_{\ell\ell}\,. \tag{4.31}$$

First of all, we notice that this contribution is always negative since $\eta_{\ell\ell} > 0$. Therefore, it cannot accommodate the muon $g-2$ anomaly, which requires $\Delta a_\mu > 0$. This result was already found in early studies of the charged leptons anomalous magnetic moments in seesaw scenarios [288–290], as well as in [291]. Furthermore, the absolute value of $\Delta a_\ell(W)$ is also too small to account for the anomalies. This implies that the electron $g-2$ cannot be explained either in the ISS3. In this regard, we highlight the relevance of the m_ℓ/v factor in Eq. (4.31). This factor is not apparent when inspecting the analytical expressions for the couplings in Appendix B. In fact, the individual contributions to $\Delta a_\ell(W)$ by the neutral fermions in the loop are larger than their sum, $\Delta a_\ell(W)$, by a factor $\sim v/m_\ell$. Therefore, a strong cancellation among them takes place. This cancellation can be easily understood due to the chirality-flipping nature of the dipole moment operator in Eq. (1.52). The factor m_ℓ/v is required to flip the chirality of the fermion line and induce a contribution to a dipole moment. One can now consider $m_N = 1$ TeV to obtain

$$\Delta a_e(W) \sim -5\cdot 10^{-13}\,\eta_{ee}\,, \tag{4.32}$$

$$\Delta a_\mu(W) \sim -2\cdot 10^{-8}\,\eta_{\mu\mu}\,. \tag{4.33}$$

Since η_{ee} and $\eta_{\mu\mu}$ are constrained to be smaller than $\sim 10^{-4}$ [190], these contributions fail to address the electron and muon $g-2$ anomalies by several orders of magnitude. The same argument can be applied to the Z and h contributions to find that they are actually even more suppressed. In summary, the suppression by the m_ℓ/m_W chirality flip and the stringent bounds on $\eta_{\ell\ell}$ imply that the ISS3 cannot induce sizable contributions. This, added to the fact that the contributions to the muon $g-2$ have the wrong sign, implies that the ISS3 cannot explain the deviations in the electron and muon anomalous magnetic moments.[8] We now proceed to show that the additional ingredients in our extended model can alter this conclusion.

4.4.3 $(g-2)_{e,\mu}$ in the ISS3VL

As already discussed, the ISS3 cannot explain the experimental anomalies in the electron and muon anomalous magnetic moments. Therefore, we now consider its ISS3VL extension. In this case, one has W contributions such as the one shown in Fig. 4.3. We can now derive an

[8] One should note, however, that if the calculations of the hadronic vacuum polarization by lattice collaborations turn out to be correct, the muon $g-2$ prediction will not be in tension with the experimental measurements. Therefore, the ISS3 will be a viable model.

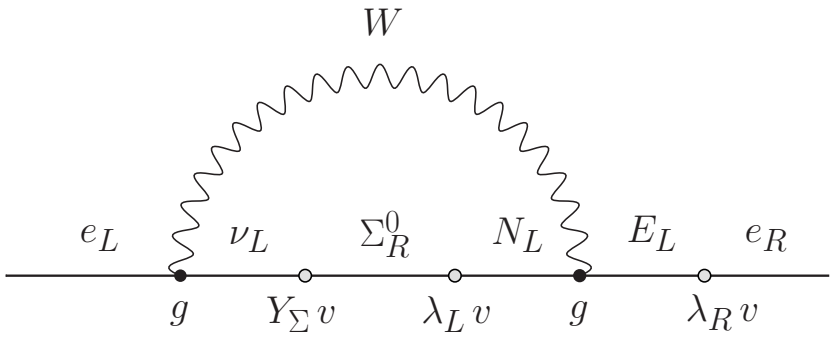

Figure 4.3: Dominant W contribution in the ISS3VL. Mass insertions are represented by white blobs.

analogous estimate along the same lines as in the case of the ISS3. One finds

$$|\Delta a_\ell(W)| \sim \frac{1}{32\pi^2}\frac{m_N\, m_\ell}{m_W^2}\, g^2 \left(\frac{m_D}{M_\Sigma}\right)_{\ell\ell} \frac{m_L}{M_L}\, \frac{m_R}{M_L} \sim 10^{-3}\, \frac{m_N\, m_\ell\, m_L\, m_R}{m_W^2\, M_L^2}\, \sqrt{\eta_{\ell\ell}}\,. \tag{4.34}$$

Note that in this scenario, the contributions to the magnetic moments are not proportional to m_ℓ^2 but m_ℓ. This is because in the ISS3VL, the chirality-flip takes place thanks to the VL lepton. One can now choose $m_N = 1$ TeV, $M_L = 500$ GeV, $m_L = 200$ GeV, and $m_R = 10$ GeV to obtain

$$|\Delta a_e(W)| \sim 6 \cdot 10^{-10}\, \sqrt{\eta_{ee}}\,, \tag{4.35}$$

$$|\Delta a_\mu(W)| \sim 10^{-7}\, \sqrt{\eta_{\mu\mu}}\,. \tag{4.36}$$

Therefore, even after the suppression given by $\sqrt{\eta_{\ell\ell}} \lesssim 10^{-2}$ these W contributions can address the current discrepancies with the electron and muon $g-2$ measurements. Furthermore, the signs of these contributions are not fixed and can be properly adjusted by fixing the signs of the relevant Yukawa couplings. We note that the loop in Fig. 4.3 is proportional to the product $Y_\Sigma\, \lambda_L\, \lambda_R$, which, as shown below, will be crucial for the resulting values for Δa_ℓ in the ISS3VL model. Similar h contributions are also found, again proportional to the $Y_\Sigma\, \lambda_L\, \lambda_R$ product. Therefore, the model is, in principle, capable of producing sizable contributions to the electron and muon $g-2$. We now proceed to confirm this by performing a detailed numerical analysis of the parameter space of the model. Since we are interested in Δa_e and Δa_μ, we fix $(\lambda_L)_3 = (\lambda_R)_3 = 0$ and randomly scan within the following parameter ranges:

Parameter	Min	Max
$(M_\Sigma)_{ii}$	850 GeV	1.5 TeV
M_L	500 GeV	1.5 TeV
$(Y_\Sigma)_{ii}$	0.05	0.2
$(\lambda_L)_1$	$-\sqrt{4\pi}$	-0.1
$(\lambda_L)_2$	0.1	$\sqrt{4\pi}$
$(\lambda_R)_1$	0.05	0.5
$(\lambda_R)_2$	0.05	0.5

Some comments about the chosen ranges are in order. First, the ranges for the mass parameters $(M_\Sigma)_{ii}$ and M_L have been selected following the discussion on LHC bounds of Section 4.4.1. Many of the parameter points in our scan were ruled out due to LHC searches for triplets, but we also find that a substantial fraction pass the test. The ranges for the Yukawa couplings have been chosen in order to maximize the resulting Δa_ℓ. The usual ISS3 Yukawas $(Y_\Sigma)_{ii}$ have been scanned around their maximal values compatible with the η_{ii} bounds. A relative sign between $(\lambda_L)_1$ and $(\lambda_L)_2$ has been introduced in order to obtain $\Delta a_e < 0$ and $\Delta a_\mu > 0$, as required by the experimental hints. Also, the corrections to $\Gamma(Z \to \ell^+\ell^-)$ tend to be too large unless $(\lambda_R)_{1,2} \lesssim 0.5$. Finally, we emphasize again that these ranges allow us to neglect the corrections to the SM charged lepton masses. As we mentioned in Section 4.4.1, those corrections coming from the mixing to the triplets and the VL leptons would enter at most at order $\sim (m_D/M_\Sigma)^2 \approx 0.002$ and $\sim (m_R/M_L)^2 \approx 0.03$, respectively.

Our results are obtained through a private code in `Wolfram Mathematica`. They are based on a random scan with 50.000 parameter points, out of which about $12\% - 13\%$ pass all the experimental tests. We have selected normal neutrino mass ordering. However, we have also run a second scan with inverted ordering and found the same qualitative results. As already explained, we consider a scenario with diagonal Y_Σ and M_Σ matrices. In this case, the lepton mixing angles encoded in the matrix U_ν are generated by the off-diagonal entries of the μ matrix, and all lepton flavor violating processes are strongly suppressed. For this reason, the bounds on the η_{ij} entries, with $i \neq j$, are easily satisfied. In contrast, the bounds on the diagonal elements of the η matrix turn out to be very important, removing a significant amount of the parameter points considered and implying the approximate bounds $(Y_\Sigma)_{11} \lesssim 0.2$ and $(Y_\Sigma)_{22} \lesssim 0.15$ for triplet masses of the order of the TeV. These limits come from constraints imposed by various phenomena, such as the decay rate of $\mu \to e\nu_i\bar{\nu}_j$, the invisible decay of the Z boson, the decay of the Z boson into charged leptons, measurements of the Z-pole asymmetries, tests of weak interaction universality, and the unitarity of the CKM matrix [190]. Another very important constraint in our setup is provided by the decay $Z \to \ell^+\ell^-$. The mixing between the SM charged leptons and the new charged BSM states from the Σ and Σ' triplets and $L_{L,R}$ VL doublets reduces $\Gamma(Z \to \ell^+\ell^-)$ with respect to its SM value. This has a strong impact on

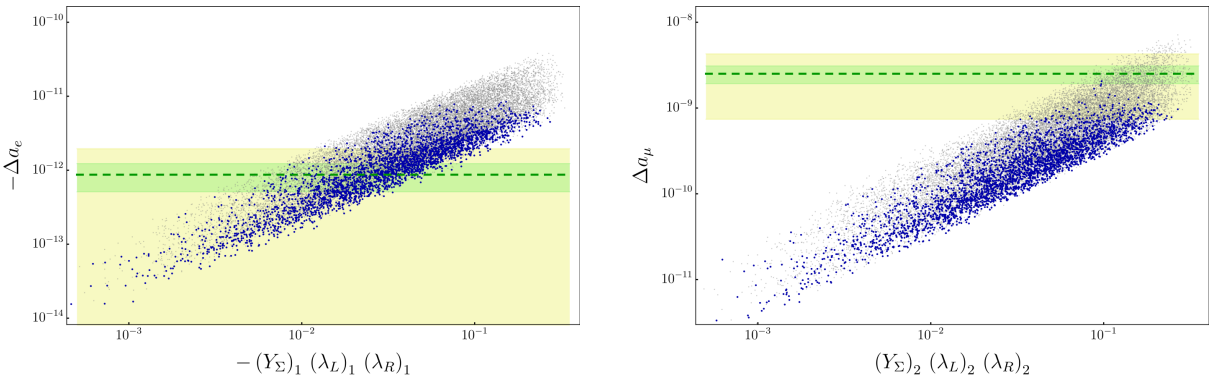

Figure 4.4: Δa_e (left) and Δa_μ (right) as a function of the product $(Y_\Sigma)_{ii}\ (\lambda_L)_i\ (\lambda_R)_i$. Blue dots correspond to parameter points that pass all the experimental constraints, whereas gray points are experimentally excluded. The horizontal dashed lines represent the central values for Δa_e and Δa_μ, whereas 1σ (3σ) regions are displayed as yellow (green) bands.

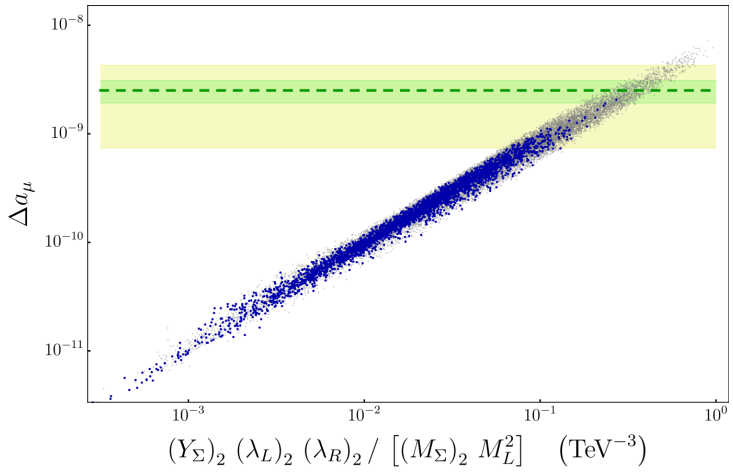

Figure 4.5: Δa_μ as a function of the combination $(Y_\Sigma)_{22}\ (\lambda_L)_2\ (\lambda_R)_2\,/\,\left[(M_\Sigma)_2\ M_L^2\right]$. Dashed line, horizontal bands and color code as in Fig. 4.4.

the m_D/M_Σ and m_R/M_L ratios. Since these ratios must be sizable in order to induce large contributions to Δa_ℓ, see Fig. 4.3, this limit is crucial for the correct evaluation of our scenario. Finally, the CMS limits discussed in Section 4.4.1 also have an impact, discarding some of the parameter points in our scan.

Our choice of a diagonal Y_Σ (in the basis in which M_Σ is diagonal too) implies that the mixing among different triplets is typically very small. In this case, and unless there is a large mixing with the VL neutral leptons, two of the heavy neutral mass eigenstates are given in good approximation by the $\Sigma_1 - \Sigma_1'$ quasi-Dirac pair and couple mainly to electrons. Similarly, two of the heavy neutral mass eigenstates are approximately given by the $\Sigma_2 - \Sigma_2'$ quasi-Dirac pair and couple mainly to muons. Therefore, the discussion in the previous section implies that one expects a strong correlation between Δa_e and the product $(Y_\Sigma)_{11}\ (\lambda_L)_1\ (\lambda_R)_1$, as well as between Δa_μ and the product $(Y_\Sigma)_{22}\ (\lambda_L)_2\ (\lambda_R)_2$. This is clearly shown in Fig. 4.4. The

left side of this figure shows Δa_e, whereas the right side displays results for Δa_μ, in both cases, as a function of the said parameter combinations. Here, and in the following figures, parameter points that pass all the experimental constraints are displayed in blue color, whereas gray points are excluded for one or several of the reasons explained above, but included in the figure for illustration purposes. The horizontal dashed line represents the central value for Δa_ℓ, while 1σ (3σ) regions are displayed as yellow (green) bands. The first and most important result shown in this figure is that the ISS3VL can indeed explain the electron and muon $g-2$ anomalies. In the case of the electron, one can easily find fully valid parameter points within the 1σ region, corresponding to values of $-(Y_\Sigma)_{11}\ (\lambda_L)_1\ (\lambda_R)_1$ in the ballpark of $\sim 0.01-0.05$. In fact, one can even exceed the experimental hint. In contrast, the muon $g-2$ can only be explained within 1σ in a narrow region of the parameter space, with $(Y_\Sigma)_{22}\ (\lambda_L)_2\ (\lambda_R)_2 \sim 0.1$. This is due to the combination of constraints that apply to our setup. Fig. 4.4 also confirms the correlations with the product $(Y_\Sigma)_{ii}\ (\lambda_L)_i\ (\lambda_R)_i$, as we expected from the arguments given in the previous section. The correlation is even more pronounced in terms of the combination $(Y_\Sigma)_{ii}\ (\lambda_L)_i\ (\lambda_R)_i\,/\,[(M_\Sigma)_i\ M_L^2]$, as shown in Fig. 4.5 for the case of the muon $g-2$. This implies that the Feynman diagram in Fig. 4.3 indeed provides one of the dominant contributions to Δa_ℓ.

An example parameter point that achieves Δa_e and Δa_μ values in the 1σ regions indicated in Eq. (1.49) is given by

$$(M_\Sigma)_{ii} = 1\,\text{TeV}\,, \quad M_L = 630\,\text{GeV}\,, \tag{4.37}$$

and

$$(Y_\Sigma)_{ii} = 0.117\,, \quad (\lambda_L)_1 = -0.6\,, \quad (\lambda_L)_2 = \sqrt{4\pi}\,, \quad (\lambda_R)_1 = 0.1\,, \quad (\lambda_R)_2 = 0.25\,. \tag{4.38}$$

We note that a large $(\lambda_L)_2$, close to the non-perturbativity regime, is required to obtain a muon $g-2$ close to the measured central value. While, in principle, this is perfectly fine, one can relax this restriction with additional contributions to the muon $g-2$. For instance, we expect this to happen in a non-minimal version of our model with more than just one generation of VL leptons or including singlet VL leptons.

Fig. 4.6 shows the dependence of Δa_ℓ on $(M_\Sigma)_{ii}$. On the left side, Δa_e is shown as a function of $(M_\Sigma)_{11}$, whereas the right side panel shows Δa_μ as a function of $(M_\Sigma)_{22}$. As explained above, these are the parameters determining the masses of the triplets that couple mainly to electrons and muons, respectively. Therefore, as expected, the NP contributions decrease for larger values of $(M_\Sigma)_{ii}$. However, given the limited range over which these parameters were scanned, the reduction is not very strong. A lower bound $(M_\Sigma)_{11} \gtrsim 930$ GeV is clearly visible on the left-side panel. This is due to the fact that lower $(M_\Sigma)_{11}$ values would lead to lighter triplets, excluded by CMS searches. The dependence on M_L, the VL mass, is shown in Fig. 4.7 for the case of the muon $g-2$. One can clearly see in this plot, as well as in the previous ones, that the density of valid parameter points gets reduced for low masses. This is because low $(M_\Sigma)_{ii}$ and/or M_L often lead to exclusion due to the $\Gamma(Z \to \ell^+\ell^-)$ constraints.

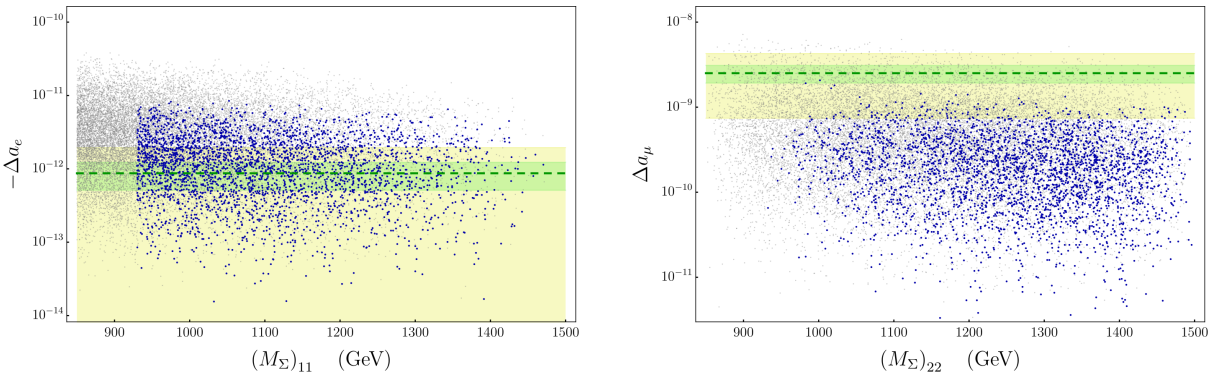

Figure 4.6: Δa_e (left) and Δa_μ (right) as a function of $(M_\Sigma)_{11}$ and $(M_\Sigma)_{22}$, respectively. Dashed line, horizontal bands and color code as in Fig. 4.4.

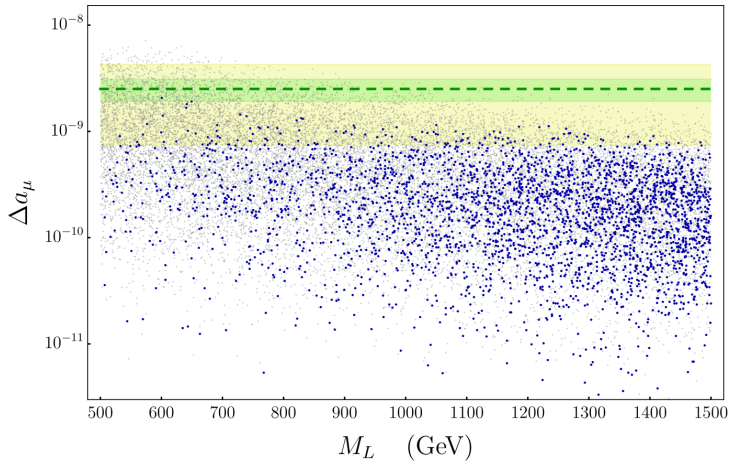

Figure 4.7: Δa_μ as a function of M_L. Dashed line, horizontal bands and color code as in Fig. 4.4.

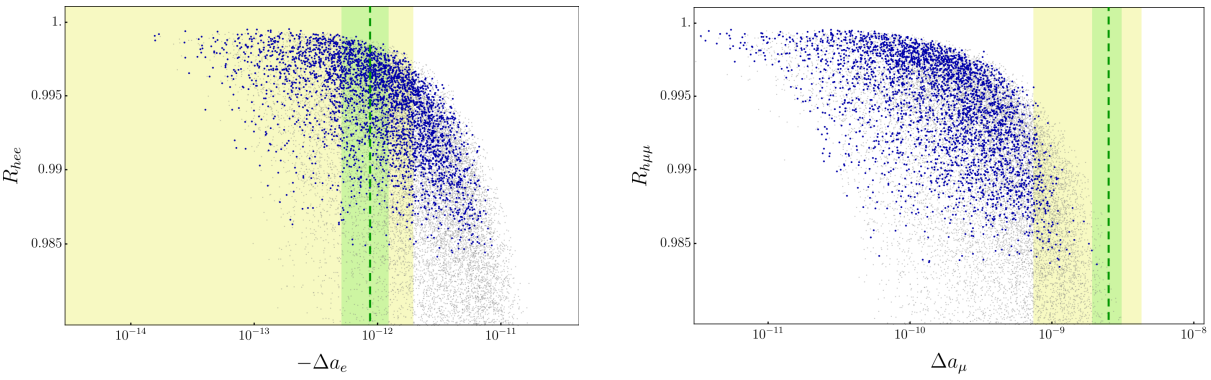

Figure 4.8: R_{hee} (left) and $R_{h\mu\mu}$ (right) as a function of Δa_e and Δa_μ, respectively. The vertical dashed lines represent the central values for Δa_e and Δa_μ, whereas 1σ (3σ) regions are displayed as yellow (green) bands.

We now turn our attention to the predictions of our setup. Fig. 4.8 shows the predicted values for the ratios

$$R_{h\ell\ell} = \frac{\Gamma(h \to \ell^+\ell^-)}{\Gamma_{\rm SM}(h \to \ell^+\ell^-)}\,, \tag{4.39}$$

where $\Gamma_{\rm SM}(h \to \ell^+\ell^-)$ is the SM decay width, as a function of Δa_ℓ. In both cases, the reductions are small, at most of about $\sim 2\%$ in the parameter points that pass all the experimental bounds. This is due the fact that the $R_{h\ell\ell}$ ratios correlate with the corresponding $R_{Z\ell\ell}$ ratios, and are thus strongly constrained. Therefore, our setup predicts SM-like Higgs boson decays into charged leptons.

Finally, we have focused on a scenario with diagonal Y_Σ couplings, as this enhances the contributions to the muon $g-2$ from diagonal entries. By doing so, we are able to strongly suppress all lepton flavor violating signals, which can only take place via the off-diagonal entries of the small μ parameter. We believe this to be a generic prediction of our model when the muon $g-2$ anomaly is addressed. However, we cannot discard the possibility of very fine-tuned parameter regions with large off-diagonal Y_Σ couplings that accidentally suppress flavor violating transitions.

4.5 Discussion

The recent announcement of the first results of the Muon $g-2$ collaboration at Fermilab has sparked a renewed interest in a long-standing anomaly. Together with the analogous discrepancy in the anomalous magnetic moment of the electron, they constitute a pair of intriguing deviations with respect to the SM predictions. If confirmed, new BSM states with masses not much above the electroweak scale will be required in order to address the discrepancies.

We have analyzed the electron and muon $g-2$ in an extended version of the ISS3 model that includes a pair of VL doublet leptons. This model is motivated by the need to generate neutrino masses, which in this setup are induced at the electroweak scale. This naturally leads to a rich phenomenology in multiple fronts. Our analysis has taken into account the most relevant experimental bounds in our scenario. This includes limits from direct searches at the LHC, deviations in $Z \to \ell^+\ell^-$ decays, and a compilation of electroweak limits. These are the main conclusions of our work:

- The pure ISS3 cannot address the electron and muon $g-2$ anomalies due to the combination of the constraints on the m_D/M_Σ ratio derived from a variety of electroweak data and a strong chiral suppression of the order of m_ℓ/v. In addition, the contributions to the muon $g-2$ have the wrong sign.

- The inclusion of a VL lepton doublet pair to the ISS3 particle content suffices to enhance the contributions to the muon $g-2$, allows one to adjust its sign conveniently and fully addresses the observed discrepancy.

- The electron $g-2$ anomaly can also be explained, in this case in a wider region of the parameter space.

- No significant change in the $h \to \ell^+\ell^-$ decays is found, and then these stay SM-like.

In this Chapter, we have focused on a minimal extension of the ISS3, containing only one VL lepton doublet pair. In principle, one may introduce additional copies of $L_{L,R}$ or VL lepton singlets, see for instance [76]. These non-minimal variations may reduce the impact of some of the bounds or enlarge the parameter space compatible with the current experimental hints in the muon $g-2$. Furthermore, lepton number is explicitly broken in our model. Alternatively, one may consider the spontaneous breaking of a global $\mathrm{U(1)_L}$ lepton number symmetry, leading to the appearance of a massless Goldstone boson, the majoron. However, a pure massless pseudoscalar state gives negative (lepton flavor conserving) contributions to the electron and muon anomalous magnetic moments, as can be seen in Section 3.4.7 and 3.5.4, hence being unable to solve the tension in the case of the muon $g-2$.

Exciting times are ahead of us. The muon $g-2$ anomaly, now hinted by a second experiment, joins the list of results that have recently attracted attention to muons. It is natural to speculate about this anomaly together with the R_K and R_{K^*} anomalies found by the LHCb collaboration, as well as with the set of deviations observed in recent years in semileptonic $b \to s$ and $b \to c$ transitions. In the upcoming chapter, we will study this possibility, although excluding $b \to c$ anomalies from the discussion. New experimental results, that may finally confirm an emerging picture beyond the SM, are eagerly awaited.

Chapter 5

Neutrino masses, flavor anomalies and muon $g-2$ from dark loops

The lepton sector of the Standard Model faces a number of intriguing anomalies that demand attention. These include an emerging pattern of deviations in $b \to s\ell\ell$ processes, with hints of lepton flavor universality violation in observables like $R_{K^{(*)}}$, a discrepancy in the muon anomalous magnetic moment, and possibly the origin of dark matter. Moreover, the model fails to account for the observed phenomenon of neutrino oscillations, which implies the existence of non-zero neutrino masses and lepton mixings. While these new physics indications might have different origins, and some of them are still hints to be confirmed with further experimental data and improved theoretical calculations, it is tempting to consider a common explanation. We already had this goal in Chapter 4, but only taking into account neutrino masses and the anomalous magnetic moments of the charged leptons. Here we wanted to be more ambitious.

5.1 Introduction

In this Chapter, we introduce an economical yet powerful model that provides an explanation for all these new physics indications. This is achieved thanks to the addition of a dark sector composed by a fermion singlet N, two generations of inert doublets η, a doublet leptoquark S and a singlet scalar ϕ. The η and S doublets can be decomposed as

$$\eta_a = \begin{pmatrix} \eta_a^+ \\ \eta_a^0 \end{pmatrix} \quad , \quad S = \begin{pmatrix} S_{\frac{2}{3}} \\ S_{-\frac{1}{3}} \end{pmatrix} , \tag{5.1}$$

where $a = 1, 2$ and the subindex in the components of the S leptoquark denotes the electric charge of the state. The model also includes a dark $\mathbb{Z}_2$ parity, under which all the new fields are assumed to be odd while the SM fields are even. This characterizes the dark sector of the model.[1] The scalar and lepton particles of the model, along with their representations under the gauge

[1] We use the term *dark* to refer to any particle charged under the $\mathbb{Z}_2$ symmetry.

Field	Generations	$SU(3)_c$	$SU(2)_L$	$U(1)_Y$	$\mathbb{Z}_2$
ℓ_L	3	**1**	**2**	$-1/2$	$+$
e_R	3	**1**	**1**	-1	$+$
N	1	**1**	**1**	0	$-$
H	1	**1**	**2**	$1/2$	$+$
η	2	**1**	**2**	$1/2$	$-$
S	1	**3**	**2**	$1/6$	$-$
ϕ	1	**1**	**1**	-1	$-$

Table 5.1: Lepton and scalar particle content of the model and their representations under the gauge symmetries. ℓ_L, e_R, and H are the usual SM fields.

group $SU(3)_c \times SU(2)_L \times U(1)_Y$ and the $\mathbb{Z}_2$ parity are shown in Table 5.1. These ingredients are enough to induce neutrino masses, accommodate the $b \to s\ell\ell$ and $(g-2)_\mu$ anomalies, and provide a viable DM candidate while being compatible with all the relevant experimental constraints. To the best of our knowledge, our economical model is the first to take into account all these unresolved issues in the lepton sector *simultaneously* and, as a by-product, also address the long-standing DM problem. In our scenario, all NP contributions to the observables of interest are induced at the 1-loop level, with $\mathbb{Z}_2$-odd particles running in the loop. These *dark loops* characterize our setup.

The connection between neutrino masses and the anomalies in $b \to s$ transitions has been explored in several works. In most cases, neutrino masses are generated radiatively with leptoquarks participating in the loop. These leptoquarks are then responsible for explaining at tree-level the flavor anomalies [292–294], and the $(g-2)_\mu$ [295–302]. Ref. [303] proposes an explanation for the $b \to s\ell\ell$ anomalies via loops, also linked to the generation of neutrino masses, while Ref. [304] considers a left-right model with neutrino masses generated through an inverse seesaw. Finally, the $b \to s$ anomalies have also been discussed in connection to the dark matter problem. We would like to highlight Refs. [96, 305–307], which also address the $b \to s\ell\ell$ and $(g-2)_\mu$ anomalies via loops involving DM, and refer to the review [308] for other works in this direction.

5.2 The model

The new states in our model allow us to write the additional Lagrangian terms:

$$-\mathcal{L}_{\rm NP} = Y_N\, \overline{N}\, \ell_L\, \eta + Y_S\, \overline{q}_L\, S\, N + \kappa\, \overline{N^c}\, e_R\, \phi^\dagger + \frac{1}{2}\, M_N\, \overline{N^c}\, N + \text{h.c.}\,. \tag{5.2}$$

Here Y_N is a 3×2 matrix, Y_S and κ are both 3-components vectors, while M_N is a parameter with dimensions of mass. Additional Yukawa couplings not written here are forbidden by the dark $\mathbb{Z}_2$ parity. For instance, this is the case of the $\overline{N}\,\ell_L\,H$ or $\overline{d}_R\,\ell_L\,S$ terms. The scalar potential of the model also contains new terms involving the η, S, and ϕ fields. It can be written as

$$\mathcal{V} = \mathcal{V}_H + \mathcal{V}_\eta + \mathcal{V}_S + \mathcal{V}_\phi + \mathcal{V}_{\text{mix}}\,, \tag{5.3}$$

where $\mathcal{V}_H$ is the standard Higgs potential defined in Eq. (1.26).

$$\mathcal{V}_\eta = m_\eta^2 |\eta|^2 + \frac{\lambda_2}{2}\,|\eta|^4\,, \tag{5.4}$$

$$\mathcal{V}_S = m_S^2 |S|^2 + \frac{\lambda_S^{(1)}}{2}\,|S|^4_{(1)} + \frac{\lambda_S^{(2)}}{2}\,|S|^4_{(2)}\,, \tag{5.5}$$

$$\mathcal{V}_\phi = m_\phi^2 |\phi|^2 + \frac{\lambda_\phi}{2}\,|\phi|^4\,, \tag{5.6}$$

and

$$\begin{aligned}\mathcal{V}_{\text{mix}} = {} & \lambda_3\,|H|^2\,|\eta|^2 + \lambda_4\,H^\dagger\,\eta\,\eta^\dagger\,H + \lambda_{HS}^{(1)}\,|H|^2\,|S|^2 + \lambda_{HS}^{(2)}\,H^\dagger\,S\,S^\dagger\,H \\ & + \lambda_{\eta S}^{(1)}\,|\eta|^2\,|S|^2 + \lambda_{\eta S}^{(2)}\,\eta^\dagger\,S\,S^\dagger\,\eta + \lambda_{H\phi}\,|H|^2\,|\phi|^2 + \lambda_{\eta\phi}\,|\eta|^2\,|\phi|^2 + \lambda_{S\phi}\,|S|^2\,|\phi|^2 \\ & + \left[\frac{\lambda_5}{2}\,\left(H^\dagger\,\eta\right)^2 + \mu\,H\,\eta\,\phi + \text{h.c.}\right]\,.\end{aligned} \tag{5.7}$$

Here m_H^2, m_η^2, m_S^2 and m_ϕ^2 have dimensions of mass^2, m_η^2 is a 2×2 matrix that can be chosen diagonal without losing generality, and we note the presence of two quartic $|S|^4$ terms, due to the two possible $\text{SU}(3)_\text{c}$ invariant contractions of four S leptoquarks (denoted as $|S|^4_{(1)}$ and $|S|^4_{(2)}$). Nevertheless, only two terms will be relevant for the discussion:

$$\mathcal{V}_{\text{NP}} \supset \frac{\lambda_5}{2}\,\left(H^\dagger\,\eta\right)^2 + \mu\,H\,\eta\,\phi + \text{h.c.}\,. \tag{5.8}$$

We remind the reader that two η doublets are added to the field inventory of the model. Therefore, μ is a 2-component vector with dimensions of mass, while λ_5 is a 2×2 symmetric matrix. In the following, only the SM scalar doublet H will be assumed to acquire a non-zero vacuum expectation value, $H^0 = v/\sqrt{2}$, where $v \simeq 246$ GeV is the electroweak VEV. This preserves the $\mathbb{Z}_2$ dark parity.

Scalar masses In the following, we will assume that all the parameters in the scalar potential are real, then conserving CP in the scalar sector. In this case, the real and imaginary components of η_a^0,

$$\eta_a^0 = \frac{1}{\sqrt{2}}\,\left(\eta_{R_a} + i\,\eta_{I_a}\right)\,, \tag{5.9}$$

do not mix. After the electroweak symmetry breaking, the 2×2 mass matrices for both real and imaginary components are given by

$$\mathcal{M}_R^2 = \begin{pmatrix} (m_\eta)^2_{11} + (\lambda_3^{11}+\lambda_4^{11}+\lambda_5^{11})\,\frac{v^2}{2} & (\lambda_3^{12}+\lambda_4^{12}+\lambda_5^{12})\,\frac{v^2}{2} \\ (\lambda_3^{12}+\lambda_4^{12}+\lambda_5^{12})\,\frac{v^2}{2} & (m_\eta)^2_{22} + (\lambda_3^{22}+\lambda_4^{22}+\lambda_5^{22})\,\frac{v^2}{2} \end{pmatrix}, \tag{5.10}$$

and

$$\mathcal{M}_I^2 = \begin{pmatrix} (m_\eta)^2_{11} + (\lambda_3^{11}+\lambda_4^{11}-\lambda_5^{11})\,\frac{v^2}{2} & (\lambda_3^{12}+\lambda_4^{12}-\lambda_5^{12})\,\frac{v^2}{2} \\ (\lambda_3^{12}+\lambda_4^{12}-\lambda_5^{12})\,\frac{v^2}{2} & (m_\eta)^2_{22} + (\lambda_3^{22}+\lambda_4^{22}-\lambda_5^{22})\,\frac{v^2}{2} \end{pmatrix}, \tag{5.11}$$

respectively. Here $\lambda_X^{ab} \equiv (\lambda_X)_{ab}$ and we have used that $\lambda_{3,4}$ are Hermitian matrices. We also note that both mass matrices are the same in the limit $(\lambda_5)_{ab} \to 0$. Regarding the charged scalars, the charged components of the η doublets mix with ϕ. In the basis $\left(\eta_1^+, \eta_2^+, \phi^+\right)$, their mass matrix is written as

$$\mathcal{M}_{ch}^2 = \begin{pmatrix} (m_\eta)^2_{11} + \lambda_3^{11}\,\frac{v^2}{2} & \lambda_3^{12}\,\frac{v^2}{2} & -\frac{\mu_1\, v}{\sqrt{2}} \\ \lambda_3^{12}\,\frac{v^2}{2} & (m_\eta)^2_{22} + \lambda_3^{22}\,\frac{v^2}{2} & -\frac{\mu_2\, v}{\sqrt{2}} \\ -\frac{\mu_1\, v}{\sqrt{2}} & -\frac{\mu_2\, v}{\sqrt{2}} & m_\phi^2 + \frac{\lambda_{H\phi}\, v^2}{2} \end{pmatrix}. \tag{5.12}$$

Finally, the leptoquark masses are given by the expressions

$$m^2_{S_{-1/3}} = m_S^2 + \left(\lambda_{HS}^{(1)} + \lambda_{HS}^{(2)}\right)\frac{v}{2}\,, \tag{5.13}$$

and

$$m^2_{S_{2/3}} = m_S^2 + \lambda_{HS}^{(1)}\,\frac{v}{2}\,. \tag{5.14}$$

Neutrino masses The conservation of $\mathbb{Z}_2$ prevents the generation of neutrino masses at tree-level. However, the simultaneous presence of Y_N, M_N, and λ_5 in Eqs. (5.2) and (5.8) implies the explicit breaking of lepton number by two units. Majorana neutrino masses are induced at the 1-loop level *a la Scotogenic* [198, 199], as shown in Fig. 5.1. The states running in the loop belong to the dark sector, a feature enforced by the $\mathbb{Z}_2$ symmetry and common to all NP contributions discussed below. The resulting neutrino masses in the limit of small λ_5 is given by [309]

$$(m_\nu)_{\alpha\beta} \approx \frac{1}{32\pi^2} v^2 \sum_{a,b} (Y_N)_{\alpha a}(Y_N)_{\beta b}\,\lambda_5^{ab}\,\frac{M_N}{m_b^2 - M_N^2}\left[\frac{m_b^2}{m_a^2-m_b^2}\log\frac{m_a^2}{m_b^2} - \frac{M_N^2}{m_a^2-M_N^2}\log\frac{m_a^2}{M_N^2}\right], \tag{5.15}$$

were $m_{a,b}$ are the masses of the two η doublets. This mass matrix correesponds to the one we will obtain for the $(1,2)$ Scotogenic model in Chapter 7. We can roughly estimate $m_\nu \sim \frac{\lambda_5\, Y_N^2\, v^2}{16\pi^2\, M_N}$. Therefore, we obtain two non-zero neutrino masses with $m_\nu \sim 0.1$ eV for $M_N = 1$ TeV and $\lambda_5^{ab} \sim 10^{-10}$, if the entries of the Y_N matrix are of order 1. The smallness of the λ_5 elements is

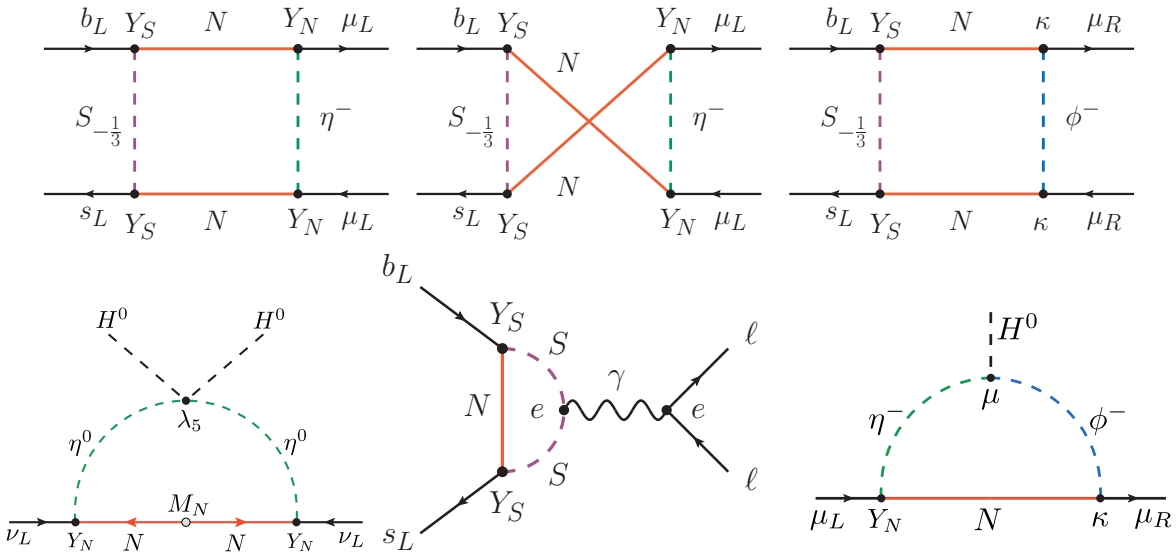

Figure 5.1: Some NP contributions to the observables of interest. Above: Box diagrams contributing to $b \to s\mu\mu$ observables. Below from left: Generation of neutrino masses at the 1-loop level, η^0 represents the real and imaginary components of all generations of η^0; flavor universal penguin contribution to the $b \to s\ell\ell$ anomalies; and 1-loop contribution to the anomalous magnetic moment of the muon (photon line should be attached to the charged scalars). Other contributions, not shown here for simplicity, were considered in the analysis.

technically natural and protected against radiative corrections [155] since in the limit $\lambda_5^{ab} \to 0$ lepton number is restored.

5.3 Observables

We now discuss the NP contributions induced by the new states in our model to the observables of interest.

***b → sℓℓ* anomalies** The model induces many 1-loop contributions to $b \to s\ell\ell$ observables. Some examples of them are shown in Fig. 5.1. We note that the charged η^- scalars mix with the charged singlet ϕ^-, and thus the states propagating in the loops are the mass eigenstates resulting from this mixing. We nevertheless show gauge eigenstates in Fig. 5.1 to better illustrate the most relevant contributions. Box diagrams are responsible for flavor universality violating contributions, central to explain observables such as the R_K ratio. In addition, one should also consider flavor universal contributions from penguin diagrams, as shown in the second row of Fig. 5.1. Our model realizes scenario b) of [310]. We highlight the presence of the crossed-diagram in Fig. 5.1, possible due to the Majorana nature of the N singlets. We do not show an analogous crossed-diagram with ϕ^- in the loop. These diagrams play a crucial role in canceling unwanted contributions to $B_s - \overline{B}_s$ mixing [82], as discussed below.

Anomalous magnetic moment of the muon The model also has new contributions to the anomalous magnetic moment of the muon, as shown in the lower row of Fig. 5.1. One should note that two different Yukawa couplings enter this diagram. While Y_N plays a role in the generation of neutrino masses, the κ Yukawa couplings do not. We also highlight the presence of the μ trilinear couplings that induce mixing between the charged component of η and ϕ and can be used to chirally enhance the associated contribution. These NP contributions were computed using the formalism described in [103].

Dark matter Last but not least, the model also provides a solution to the DM problem. The lightest $\mathbb{Z}_2$-odd state is stable and, if electrically neutral, it is a potentially valid DM candidate. Two possibilities arise: the lightest N state and one of the components (CP-even or CP-odd) of the neutral η^0 scalars. Both scenarios have been widely studied in the literature for the pure Scotogenic model [198, 199], and both have been shown to be compatible with the observed DM relic density. However, we note that the scalar candidate can achieve this more easily [311–315], since the fermionic candidate requires large Y_N Yukawa couplings and then leads to some tension with existing bounds from lepton flavor violating observables [202]. Nevertheless, our model deviates from the usual scenario with one inert η doublet, since two generations are introduced. This scenario was studied in great detail in [316], where it was shown that the richer inert sector may open up novel regions in parameter space where the relic density can match the observed value. For instance, this is achieved when both scalar doublets have similar masses since coannihilation rates get enhanced.

5.4 Numerical results

Our model faces several experimental constraints. First, we must make sure that neutrino oscillation data are correctly reproduced. We use the results of the global fit [138] and implement them by means of a Casas-Ibarra parametrization [200], properly adapted to the Scotogenic scenario [201, 203, 204], as explained in Section 2.5.3. Then, Eq. (2.62) allows us to write the Y_N Yukawa matrix in terms of the neutrino oscillation parameters, the neutrino mass matrix of the model, and the orthogonal matrix R, which, in this scenario, is a general 2×3 orthogonal matrix defined as

$$R = \begin{pmatrix} 0 & \cos\theta & -\sin\theta \\ 0 & \sin\theta & \cos\theta \end{pmatrix} . \tag{5.16}$$

Therefore, neutrino masses strongly restrict the elements of the Y_N Yukawa matrix, which play a crucial role in the resolution of the $b\to s\ell\ell$ and $(g-2)_\mu$ anomalies (see Fig. 5.1). Furthermore, as in most neutrino mass models, LFV processes are potentially dangerous, being $\mu\to e\gamma$ the most constraining one.

Regarding processes with mesons, the main constraints come from $b\to s\gamma$, $B\to K^{(*)}\nu\bar{\nu}$ and $B_s-\overline{B}_s$ mixing. The $b\to s\gamma$ decays yield strong constraints on the coefficients of dipole

operators [317]. These are induced at the 1-loop level by diagrams like the one shown in the lower middle of Fig. 5.1, with photons or gluons and without the charged leptons. The inclusive $b \to s\gamma$ branching ratio is experimentally determined to be $\text{BR}(b \to s\gamma) = (3.49 \pm 0.19) \times 10^{-4}$ [318]. As we will show below, this constrains the $(Y_S)_2 \times (Y_S)_3$ product. About $B \to K^{(*)}\nu\bar{\nu}$, note that if a contribution to $B \to K^{(*)}\ell^+\ell^-$ exists, the corresponding process with neutrinos is unavoidable due to $\text{SU}(2)_\text{L}$ invariance. Current experimental results set limits to the branching ratios of $B \to K^{(*)}\nu\bar{\nu}$ which, normalized to their SM predictions, are restricted to $R_K^{\nu\bar{\nu}} < 3.9$ and $R_{K^*}^{\nu\bar{\nu}} < 2.7$ [319]. On top of this, $B_s - \overline{B}_s$ mixing [320] is again inevitable and typically very constraining in scenarios aiming at an explanation of the $b \to s\ell\ell$ anomalies at the 1-loop level. Any model that generates a box diagram with b and s quarks and two leptons, like the ones in Fig. 5.1, will automatically produce box contributions to the four quarks operators responsible for $B_s - \overline{B}_s$ mixing. In fact, this specific constraint precludes most radiative models for $b \to s$ transitions. In our scenario, however, the Majorana nature of the N singlet can be used to suppress $B_s - \overline{B}_s$ mixing in the limit of (nearly) degenerate NP masses participating in the box, i.e., $S_{-1/3}$ and N, as pointed out in [82]. This is actually the reason to introduce just one N singlet. If the model contained more than one generation of N, the cancellation would no longer work or would require more tunings.

We present now our results. Our goal is to prove that our model can accommodate all the anomalies while being consistent with neutrino oscillation data and all the experimental constraints. In what concerns the $b \to s\ell\ell$ anomalies, a reasonable goal is to accommodate Scenario 5 of the global fit [116], characterized by

$$\begin{aligned} \mathcal{C}_{9\mu}^V &= -0.55^{+0.44}_{-0.47}\,, \\ \mathcal{C}_{10\mu}^V &= 0.49^{+0.35}_{-0.41}\,, \\ \mathcal{C}_9^U &= \mathcal{C}_{10}^U = -0.35^{+0.42}_{-0.38}\,, \end{aligned} \tag{5.17}$$

where $\mathcal{C}_9$ and $\mathcal{C}_{10}$ are the Wilson coefficients of the $\mathcal{O}_9$ and $\mathcal{O}_{10}$ effective operators, respectively, introduced in Eq. (1.57). The superindices V and U denote flavor universality violating and conserving contributions, respectively, and the flavor universality violating ones are specific to the muon flavor. This scenario provides a clear improvement with respect to the SM in what concerns the description of $b \to s\ell\ell$ data [116]. We used a private code in `Wolfram Mathematica` where we constructed a χ^2-function in the usual way, with these four Wilson coefficients and the anomalous magnetic moment of the muon. Rather than finding the global minimum of the resulting χ^2-function, which depends non-trivially on many model parameters, our goal is to prove that our model can provide a good explanation to all the anomalies. Therefore, in order to simplify the analysis, we fixed several parameters. First, the masses of the NP states were taken to be close to 1 TeV, a typical reference NP scale. We have explicitly checked that the qualitative results and the conclusions of our analysis remain the same with other choices of NP scale. Note that the $B_s - \overline{B}_s$ mixing suppression requires the masses of S and N to be degenerate or nearly degenerate [82]. The mass of η is taken to be lower, around 550 GeV. With

this hierarchy, η would be the lightest stable particle with a mass compatible with the observed DM relic density and direct detection cross-section bounds [314,315]. We assumed that the 2×2 matrix λ_5 is proportional to the identity, i.e. $\lambda_5 = \lambda_5^0\,\mathbb{I}_2$, and fix the following values:

$$\mu_1 = -\mu_2 = -1.0\,\text{TeV}\,, \qquad \kappa_1 = 0\,, \tag{5.18}$$

$$\lambda_5^0 = 2\times10^{-10}\,, \qquad \kappa_2 = 0.04\,. \tag{5.19}$$

We noticed that these two elements of the coupling vector $\kappa = (\kappa_1\ \kappa_2\ \kappa_3)$ need to be small in order to suppress the branching ratio of $\mu\to e\gamma$ below the experimental bound. Indeed, we chose to set κ_1 to zero, leading to observables with electrons being SM-like. The rest of the parameters of the model are not relevant for our discussion here, given the flavor structure of the diagrams depicted in Fig. 5.1. Note also that due to the external quark structure, Y_S always enters in the combination $(Y_S)_2\times(Y_S)_3$. For the χ^2 minimization, we are then left with $(Y_S)_2\times(Y_S)_3$ and $\sin\theta$. We found that the values of the parameters for which χ^2 was minimal were

$$(Y_S)_2\times(Y_S)_3 = 0.6\,, \quad \sin\theta = 0.25\,, \tag{5.20}$$

giving $\chi^2_{\text{min}} = 1.52$ and $\Delta\chi^2 = \chi^2_{\text{SM}} - \chi^2_{\text{min}} = 21.23$. This not only shows a remarkable improvement with respect to the SM, but the low χ^2_{min} value also guarantees that all the anomalous observables can be properly accommodated in our model. This is better illustrated on the left-hand side of Fig. 5.2, which shows the results of our χ^2 fit in the $\sin\theta - (Y_S)_2\times(Y_S)_3$ plane. We find that both parameters can substantially deviate from their best-fit values without affecting the χ^2-function notably. However, $\sin\theta$ is required to be in the 0.25 ballpark in order to reduce the $\mu\to e\gamma$ branching ratio below its experimental bound. This turns out to be a strong constraint in our model due to the connection to neutrino masses, which generically require the Y_N couplings involving the electron to be non-zero. Similarly, the $b\to s\gamma$ constraint imposes an upper bound on the $(Y_S)_2\times(Y_S)_3$ product, which has to be below ~ 1. The impact on $\mathcal{C}^V_{9\mu}$ and Δa_μ is shown on the right-hand side of Fig. 5.2. Here we see that the central values for both *observables* (we treat the $\mathcal{C}^V_{9\mu}$ coefficient as an observable here) can be easily achieved in our model and are, in fact, very close to the central value of the muon anomalous magnetic moment shown in Eq. (1.49) and to our global best-fit point in Eq. (5.17), which only deviates slightly due to the influence of other Wilson coefficients. It is also remarkable that our model does not require too large Y_S Yukawa parameters to accommodate the $b\to s\ell\ell$ anomalies. In fact, $\mathcal{O}(1)$ Y_S Yukawas are sufficient to reproduce all the anomalies at the $1\,\sigma$ level. We emphasize, once again, that all the parameter points considered in our analysis comply with the constraints from neutrino oscillation data, $b\to s\gamma$ and $B_s - \overline{B}_s$ mixing. The $B\to K^{(*)}\nu\bar{\nu}$ bounds are also easily satisfied. Finally, the mass spectrum chosen in our numerical fit also accommodates the observed DM relic density. Therefore, although a more sophisticated analysis is required to determine precisely the region of parameter space where our model can accommodate all the anomalies, we have shown that this region does exist, and the model can fully achieve its goals.

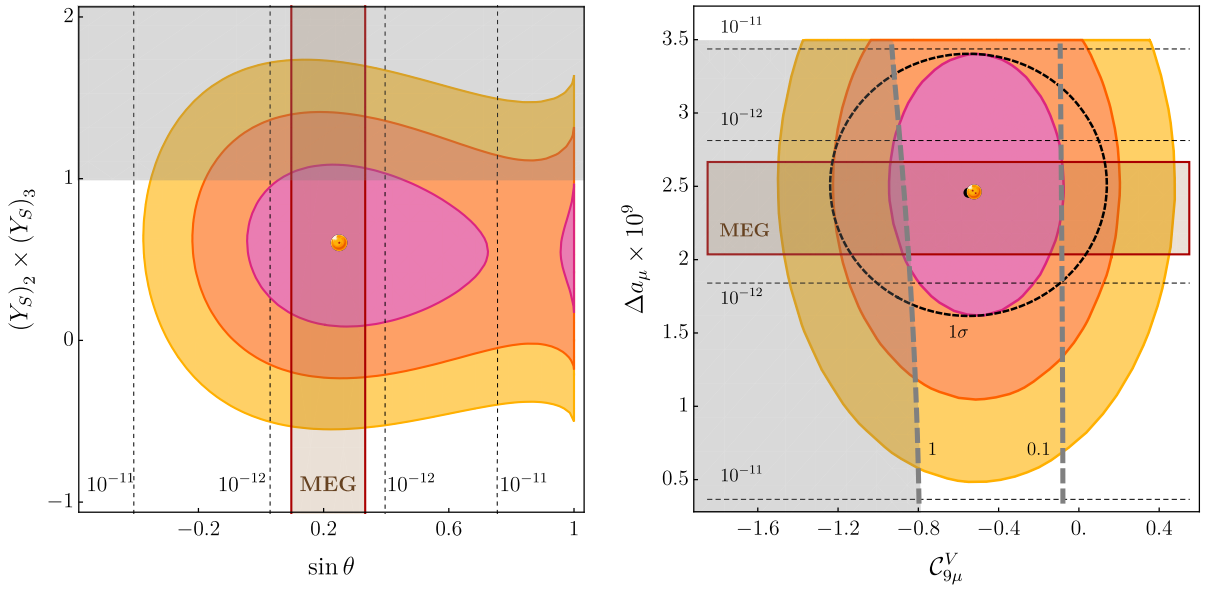

Figure 5.2: Results of our χ^2 fit of the model parameters. The colored regions correspond to $1\,\sigma$ (pink), $2\,\sigma$ (orange), and $3\,\sigma$ (yellow) regions, while the best-fit point is indicated with an orange dot. The region allowed by the MEG experiment is shown in dark red, while the dashed lines correspond to contours of $\mathrm{BR}(\mu \to e\gamma)$. The shaded region is excluded by the $b \to s\gamma$ constraint at $3\,\sigma$. In the right panel, contours of the $(Y_S)_2 \times (Y_S)_3$ product are shown with thick dashed gray lines, while the black dashed line and dot are the experimentally determined $1\,\sigma$ region and central value, respectively.

5.5 Discussion

We have proposed a novel model that accommodates the existing deviations in $b \to s\ell\ell$ observables and the muon $g-2$, induces neutrino masses and provides a weakly-interacting dark matter candidate, thanks to a dark sector including several states contributing to the observables of interest at the 1-loop level. We have shown that our simple and economical model can explain all the anomalies via these dark loops. This is achieved with renormalizable Yukawa couplings, while being compatible with neutrino oscillation data and the existing experimental bounds. The flavor violating muon decay $\mu \to e\gamma$ turns out to provide an important constraint, but this can be easily satisfied in a wide region of the parameter space. Also, we chose the scalar mass in such a way that it is a viable DM candidate.

The scenario considered in our analysis requires the existence of several states at the TeV scale. Since they are all odd under a new dark parity, their production and decay channels are modified with respect to more common scenarios. For instance, the S leptoquark must be produced in pairs at colliders and subsequently decay as $S \to j\,N \to j\,\ell\,\not{E}_T$, where the jet can be given by a 2nd or 3rd generation quark and the missing energy in the final state is due to the production of the η DM particle. The approximate mass degeneracy between S and N, introduced to suppress $B_s - \overline{B}_s$ mixing, implies very soft jets, undetectable at the LHC. Moreover, if both η generations are lighter than N, additional leptons can be produced

in the cascade. A more compressed spectrum would not affect our results in a substantial way, but would make these leptons very soft too, leading to a particularly challenging scenario at the LHC. In what concerns the heavy neutral lepton N, the conservation of the dark parity forbids its mixing with the standard neutrinos. We conclude that our scenario contains several non-standard features and a dedicated study is thus required to fully assess its observability.

Finally, we note that, as discussed in Section 1.5, the latest experimental results seem to indicate that some of the relevant neutral-current B flavor anomalies may be likely to disappear. The measurements becoming SM-like would imply that the values of the NP contributions to the Wilson coefficients would approach to zero, leading to lower model parameters to accommodate them.

Chapter 6

Observable flavor violation from spontaneous lepton number breaking

While constructing new physics models to address the anomalies in the Standard Model, as done in Chapters 4 and 5, is undoubtedly relevant, it is important to keep in mind that most of these discrepancies are only hints at present. An alternative avenue of research involves studying models that exhibit signatures that may be detected experimentally in the near future. This is the case of charged lepton flavor violation. In addition, this can be linked with the spontaneous breaking of lepton number, which implies the existence of a majoron, a particular case of the ultralight scalars we examined in Chapter 3.

6.1 Introduction

In this Chapter, based on [321], we study charged lepton flavor violation connected to the spontaneous violation of lepton number. As discussed in Section 2.6, the spontaneous breaking of the lepton number global symmetry is always accompanied by a majoron.

Here we propose a relatively simple model that induces large off-diagonal majoron couplings to charged leptons at tree-level. Our model adds a singlet and a doublet scalar to the SM, both with lepton number. It also extends the SM symmetry by imposing lepton number conservation. Finally, we introduce three right-handed neutrinos and a vector-like lepton, which we choose to be an $\mathrm{SU}(2)_\mathrm{L}$ singlet for simplicity. After the electroweak and lepton number symmetries are spontaneously broken, neutrinos acquire non-zero masses via a TeV-scale type-I seesaw mechanism, and the vector-like lepton mixes with the SM charged leptons, inducing in this way large LFV majoron couplings. Furthermore, extending the SM lepton sector with vector-like fermions will affect a number of observables, most notably the anomalous magnetic moment of the charged leptons, as well as their coupling to gauge bosons. As a by-product of our construction, the model can explain the observed anomaly in the muon anomalous magnetic

Field	Generations	$SU(3)_c$	$SU(2)_L$	$U(1)_Y$	$U(1)_L$
ℓ_L	3	**1**	**2**	$-1/2$	1
e_R	3	**1**	**1**	-1	1
ν_R	3	**1**	**1**	0	1
$F_{L,R}$	1	**1**	**1**	-1	-1
H	1	**1**	**2**	$1/2$	0
σ	1	**1**	**1**	0	2
S	1	**1**	**2**	$-1/2$	-2

Table 6.1: Particle content of the model (excluding the gauge and quark sectors) and representations under the gauge and global symmetries. ℓ_L, e_R and H are the usual SM fields.

moment [49, 322] in parts of its parameter space. It can also lead to observable effects in Higgs boson decays, most notably in $h \to \mu\mu$.

We mention in passing that branching ratios for $\mu \to e\, J$ decays as large as the experimental limit have been found in [250]. The underlying model is supersymmetric with spontaneous violation of R-parity. This provides one, albeit quite complicated, model example, where off-diagonal majoron couplings to charged leptons are induced at tree-level and can be large. Nevertheless, we note that this decay can, in principle, saturate the experimental bound also in models that generate the majoron couplings to charged leptons at the 1-loop level [213].

6.2 The model

We consider a variant of the type-I seesaw discussed in Section 2.5.1.1 with spontaneous lepton number violation. The quark sector remains as in the SM, whereas the lepton sector is extended with the addition of 3 generations of singlet right-handed neutrinos, ν_R, a pair of singlet vector-like leptons, F_L and F_R, the scalars σ and S and a $U(1)_L$ global symmetry, where L refers to lepton number. The full particle content of the model and the representations of all fields under the gauge and global groups are shown in Table 6.1.

As usual, the SM $SU(2)_L$ doublets can be decomposed as in Eqs. (1.2), (1.3), and (1.25), whereas the new S doublet can be expressed as

$$S = \begin{pmatrix} S^0 \\ S^- \end{pmatrix} . \tag{6.1}$$

Under the above working assumptions, the most general Yukawa Lagrangian allowed by all symmetries can be written as

$$\mathcal{L}_Y = \mathcal{L}_Y^{\rm SM} + \mathcal{L}_Y^{\rm extra} , \tag{6.2}$$

where $\mathcal{L}_Y^{\rm SM}$ is the usual SM Yukawa Lagrangian defined in Eq. (1.38). The new terms are given by

$$-\mathcal{L}_Y^{\rm extra} = Y_\nu\,\overline{\nu}_R\,\ell_L\,H + \frac{1}{2}\,\kappa\,\sigma\,\overline{\nu_R}\,\nu_R^c + \rho\,\sigma\,\overline{e}_R\,F_L + Y_S\,S\,\overline{F}_R\,\ell_L + M_F\,\overline{F}_R\,F_L + \text{h.c.}\,. \tag{6.3}$$

Here Y_ν and κ are 3×3 matrices, ρ is a 3×1 matrix and Y_S is a 1×3 matrix. The parameter M_F has dimensions of mass and $\mathrm{SU(2)_L}$ contractions and flavor indices have been omitted for the sake of clarity. The guiding principle when writing Eq. (6.3) is the conservation of lepton number. [1] Finally, the scalar potential of the model also includes new terms involving the σ and S fields. It can be written as

$$\mathcal{V} = \mathcal{V}_H + \mathcal{V}_\sigma + \mathcal{V}_S + \mathcal{V}_{\rm mix}\,, \tag{6.4}$$

where

$$\mathcal{V}_\phi = m_\phi^2|\phi|^2 + \frac{\lambda_\phi}{2}\,|\phi|^4\,, \tag{6.5}$$

with $\phi = H, \sigma, S$, and

$$\mathcal{V}_{\rm mix} = \lambda_{H\sigma}\,|H|^2\,|\sigma|^2 + \lambda_{HS}^{(1)}\,|H|^2\,|S|^2 + \lambda_{HS}^{(2)}\,H^\dagger\,S\,S^\dagger\,H + \lambda_{\sigma S}\,|\sigma|^2\,|S|^2 + (\mu\,H\,\sigma\,S + \text{h.c.})\,. \tag{6.6}$$

Here all m_ϕ^2 parameters have dimensions of mass^2, whereas μ is a parameter with dimensions of mass.

6.2.1 Scalar sector

The scalars of the model take the vacuum expectation values (VEVs)

$$\langle H\rangle = \frac{1}{\sqrt{2}}\begin{pmatrix} 0 \\ v_H \end{pmatrix}, \quad \langle\sigma\rangle = \frac{v_\sigma}{\sqrt{2}}, \quad \langle S\rangle = \frac{1}{\sqrt{2}}\begin{pmatrix} v_S \\ 0 \end{pmatrix}. \tag{6.7}$$

These relations define the VEVs v_H, v_σ and v_S, which break the electroweak and $\mathrm{U(1)_L}$ symmetries. [2] As a result of this, the W and Z gauge bosons acquire non-zero masses, given by

$$m_W^2 = \frac{1}{4}\,g^2\,v^2\,, \tag{6.8}$$

$$m_Z^2 = \frac{1}{4}\left(g^2 + g'^2\right)\,v^2\,, \tag{6.9}$$

where $v^2 = v_H^2 + v_S^2$ and g and g' are the $\mathrm{SU(2)_L}$ and $\mathrm{U(1)_Y}$ gauge couplings, respectively. Here $v \simeq 246$ GeV is the usual electroweak VEV, which receives contributions from both scalar

[1] For instance, we have not included a Yukawa term of the form $\sigma\,\overline{e}_R\,F_R^c$ because it would violate lepton number explicitly.

[2] In this Chapter, the VEV of the Higgs doublet H will be denoted as v_H since, in this model, we will use v to refer to the electroweak VEV.

doublets H and S. The tadpole equations obtained by minimizing the scalar potential read

$$\frac{\partial \mathcal{V}}{\partial H^0} = \frac{v_H}{\sqrt{2}}\left(m_H^2 + \frac{v_H^2\,\lambda_H}{2} + \frac{v_S^2\,\lambda_{HS}^{(1)}}{2} + \frac{v_\sigma^2\,\lambda_{H\sigma}}{2} - \frac{v_S\,v_\sigma\,\mu}{\sqrt{2}\,v_H}\right) = 0\,, \tag{6.10}$$

$$\frac{\partial \mathcal{V}}{\partial \sigma} = \frac{v_\sigma}{\sqrt{2}}\left(m_\sigma^2 + \frac{v_\sigma^2\,\lambda_\sigma}{2} + \frac{v_H^2\,\lambda_{H\sigma}}{2} + \frac{v_S^2\,\lambda_{S\sigma}}{2} - \frac{v_H\,v_S\,\mu}{\sqrt{2}\,v_\sigma}\right) = 0\,, \tag{6.11}$$

$$\frac{\partial \mathcal{V}}{\partial S^0} = \frac{v_S}{\sqrt{2}}\left(m_S^2 + \frac{v_S^2\,\lambda_S}{2} + \frac{v_H^2\,\lambda_{HS}^{(1)}}{2} + \frac{v_\sigma^2\,\lambda_{S\sigma}}{2} - \frac{v_H\,v_\sigma\,\mu}{\sqrt{2}\,v_S}\right) = 0\,. \tag{6.12}$$

The trilinear μ term in Eq. (6.6) plays an important role. In the limit $\mu \to 0$, the scalar potential has an accidental U(1) symmetry, under which all scalar fields can have arbitrary charges. Therefore, its presence is crucial to explicitly break this global symmetry and avoid the appearance of an unwanted Goldstone boson. The μ term also induces a tadpole for each of the scalar fields if the other two have non-vanishing VEVs.

Assuming that CP is not violated in the scalar sector, namely that all scalar potential parameters and VEVs are real, we can split the neutral scalar fields into their real and imaginary components as

$$H^0 = \frac{1}{\sqrt{2}}\left(S_H + i\,P_H + v_H\right)\,, \tag{6.13}$$

$$\sigma = \frac{1}{\sqrt{2}}\left(S_\sigma + i\,P_\sigma + v_\sigma\right)\,, \tag{6.14}$$

$$S^0 = \frac{1}{\sqrt{2}}\left(S_S + i\,P_S + v_S\right)\,. \tag{6.15}$$

The scalar potential contains the piece $\mathcal{V}_{\rm mass} = \mathcal{V}^N_{\rm mass} + \mathcal{V}^C_{\rm mass}$, with mass terms for the neutral ($\mathcal{V}^N_{\rm mass}$) and charged ($\mathcal{V}^C_{\rm mass}$) scalars in the model. The neutral scalars mass terms read

$$\mathcal{V}^N_{\rm mass} = \frac{1}{2}\,{\rm Re}(z_i)\,\left(\mathcal{M}_R^2\right)_{ij}\,{\rm Re}(z_j) + \frac{1}{2}\,{\rm Im}(z_i)\,\left(\mathcal{M}_I^2\right)_{ij}\,{\rm Im}(z_j)\,, \tag{6.16}$$

where $z = \{H^0, \sigma, S^0\}$ and $\mathcal{M}_R^2$ and $\mathcal{M}_I^2$ are the 3×3 squared mass matrices for the CP-even and CP-odd neutral states, respectively. The prefactors of $\frac{1}{2}$ are due to the fact that ${\rm Re}(z_i)$ and ${\rm Im}(z_i)$ are real scalar fields. It is straightforward to get the analytical expressions of the mass matrices, which can be computed as

$$\left(\mathcal{M}_R^2\right)_{ij} = \frac{1}{2}\left(\frac{\partial^2 \mathcal{V}_{\rm mass}}{\partial z_i \partial z_j} + \frac{\partial^2 \mathcal{V}_{\rm mass}}{\partial z_i^* \partial z_j^*}\right) + \frac{\partial^2 \mathcal{V}_{\rm mass}}{\partial z_i \partial z_j^*}\,, \tag{6.17}$$

$$\left(\mathcal{M}_I^2\right)_{ij} = -\frac{1}{2}\left(\frac{\partial^2 \mathcal{V}_{\rm mass}}{\partial z_i \partial z_j} + \frac{\partial^2 \mathcal{V}_{\rm mass}}{\partial z_i^* \partial z_j^*}\right) + \frac{\partial^2 \mathcal{V}_{\rm mass}}{\partial z_i \partial z_j^*}\,. \tag{6.18}$$

Then, using the expressions above, one finds [3]

$$\mathcal{M}_R^2 = \begin{pmatrix} m_H^2 + \frac{3\,v_H^2\,\lambda_H}{2} + \frac{v_S^2\,\lambda_{HS}^{(1)}}{2} + \frac{v_\sigma^2\,\lambda_{H\sigma}}{2} & v_H\,v_\sigma\,\lambda_{H\sigma} - \frac{v_S\,\mu}{\sqrt{2}} & v_H\,v_S\,\lambda_{HS}^{(1)} - \frac{v_\sigma\,\mu}{\sqrt{2}} \\ v_H\,v_\sigma\,\lambda_{H\sigma} - \frac{v_S\,\mu}{\sqrt{2}} & m_\sigma^2 + \frac{3\,v_\sigma^2\,\lambda_\sigma}{2} + \frac{v_H^2\,\lambda_{H\sigma}}{2} + \frac{v_S^2\,\lambda_{S\sigma}}{2} & v_S\,v_\sigma\,\lambda_{S\sigma} - \frac{v_H\,\mu}{\sqrt{2}} \\ v_H\,v_S\,\lambda_{HS}^{(1)} - \frac{v_\sigma\,\mu}{\sqrt{2}} & v_S\,v_\sigma\,\lambda_{S\sigma} - \frac{v_H\,\mu}{\sqrt{2}} & m_S^2 + \frac{3\,v_S^2\,\lambda_S}{2} + \frac{v_H^2\,\lambda_{HS}^{(1)}}{2} + \frac{v_\sigma^2\,\lambda_{S\sigma}}{2} \end{pmatrix}, \tag{6.19}$$

and

$$\mathcal{M}_I^2 = \begin{pmatrix} m_H^2 + \frac{v_H^2\,\lambda_H}{2} + \frac{v_S^2\,\lambda_{HS}^{(1)}}{2} + \frac{v_\sigma^2\,\lambda_{H\sigma}}{2} & \frac{v_S\,\mu}{\sqrt{2}} & \frac{v_\sigma\,\mu}{\sqrt{2}} \\ \frac{v_S\,\mu}{\sqrt{2}} & m_\sigma^2 + \frac{v_\sigma^2\,\lambda_\sigma}{2} + \frac{v_H^2\,\lambda_{H\sigma}}{2} + \frac{v_S^2\,\lambda_{S\sigma}}{2} & \frac{v_H\,\mu}{\sqrt{2}} \\ \frac{v_\sigma\,\mu}{\sqrt{2}} & \frac{v_H\,\mu}{\sqrt{2}} & m_S^2 + \frac{v_S^2\,\lambda_S}{2} + \frac{v_H^2\,\lambda_{HS}^{(1)}}{2} + \frac{v_\sigma^2\,\lambda_{S\sigma}}{2} \end{pmatrix}. \tag{6.20}$$

One can now use the tadpole equations in Eqs. (6.10)-(6.12) to evaluate these matrices at the minimum of the scalar potential. We obtain

$$\mathcal{M}_R^2 = \begin{pmatrix} v_H^2\,\lambda_H + \frac{v_S\,v_\sigma\,\mu}{\sqrt{2}\,v_H} & v_H\,v_\sigma\,\lambda_{H\sigma} - \frac{v_S\,\mu}{\sqrt{2}} & v_H\,v_S\,\lambda_{HS}^{(1)} - \frac{v_\sigma\,\mu}{\sqrt{2}} \\ v_H\,v_\sigma\,\lambda_{H\sigma} - \frac{v_S\,\mu}{\sqrt{2}} & v_\sigma^2\,\lambda_\sigma + \frac{v_H\,v_S\,\mu}{\sqrt{2}\,v_\sigma} & v_S\,v_\sigma\,\lambda_{S\sigma} - \frac{v_H\,\mu}{\sqrt{2}} \\ v_H\,v_S\,\lambda_{HS}^{(1)} - \frac{v_\sigma\,\mu}{\sqrt{2}} & v_S\,v_\sigma\,\lambda_{S\sigma} - \frac{v_H\,\mu}{\sqrt{2}} & v_S^2\,\lambda_S + \frac{v_H\,v_\sigma\,\mu}{\sqrt{2}\,v_S} \end{pmatrix}, \tag{6.21}$$

and

$$\mathcal{M}_I^2 = \begin{pmatrix} \frac{v_S\,v_\sigma\,\mu}{\sqrt{2}\,v_H} & \frac{v_S\,\mu}{\sqrt{2}} & \frac{v_\sigma\,\mu}{\sqrt{2}} \\ \frac{v_S\,\mu}{\sqrt{2}} & \frac{v_H\,v_S\,\mu}{\sqrt{2}\,v_\sigma} & \frac{v_H\,\mu}{\sqrt{2}} \\ \frac{v_\sigma\,\mu}{\sqrt{2}} & \frac{v_H\,\mu}{\sqrt{2}} & \frac{v_H\,v_\sigma\,\mu}{\sqrt{2}\,v_S} \end{pmatrix}. \tag{6.22}$$

The physical CP-even mass eigenstates $\{H_1, H_2, H_3\}$ are related to the corresponding weak eigenstates $\{S_H, S_\sigma, S_S\}$ as

$$\begin{pmatrix} H_1 \\ H_2 \\ H_3 \end{pmatrix} = W \begin{pmatrix} S_H \\ S_\sigma \\ S_S \end{pmatrix}, \tag{6.23}$$

where W is the 3×3 unitary matrix which brings the matrix $\mathcal{M}_R^2$ into diagonal form as

$$W\,\mathcal{M}_R^2\,W^T = \mathrm{diag}(m_{H_1}^2, m_{H_2}^2, m_{H_3}^2)\,. \tag{6.24}$$

The model has thus 3 CP-even neutral scalars. One of them, presumably the lightest, is to be identified with the Higgs boson discovered at the LHC, H_1, with $m_{H_1} \approx 125$ GeV. Similarly, diagonalizing the mass matrix $\mathcal{M}_I^2$, we can obtain the profile of the three CP-odd mass eigenstates. We end up with a massive state that we denote by A, and two massless states. One

[3] It proves useful to compute the matrix $\mathcal{M}_I^2$ in a general R_ξ gauge, since this allows for the proper identification of the Goldstone boson that becomes the longitudinal component of the Z boson. However, we present here the results in the Landau gauge ($\xi = 0$).

of the massless states is the Goldstone boson, z, *eaten* by the Z boson, while the other is the majoron, J, the Goldstone boson associated to the spontaneous breaking of lepton number. In the basis $\mathrm{Im}\{H^0, \sigma, S^0\} = \{P_H, P_\sigma, P_S\}$, the mass eigenstates are given in terms of the original gauge eigenstates as

$$z = \frac{1}{v}\,(v_H, 0, -v_S)\,, \tag{6.25}$$

$$J = \frac{1}{V^2}\left(\frac{v_H\, v_S^2}{v}, -v\, v_\sigma, \frac{v_H^2\, v_S}{v}\right), \tag{6.26}$$

$$A = \frac{1}{V^2}\,(v_S\, v_\sigma, v_H\, v_S, v_H\, v_\sigma)\,, \tag{6.27}$$

with their masses given by

$$m_z^2 = m_J^2 = 0\,, \quad m_A^2 = \frac{\mu\, V^4}{\sqrt{2}\, v_H\, v_S\, v_\sigma}\,. \tag{6.28}$$

We have defined the combination $V^4 = v_H^2\, v_S^2 + v_H^2\, v_\sigma^2 + v_S^2\, v_\sigma^2$. Note that while z is given by H^0 in the SM, here it is a combination of the two scalar doublets. As already discussed, the μ parameter breaks an accidental U(1) symmetry that would lead in its absence to the appearance of an additional massless Goldstone boson. This can be observed in m_A^2, which would vanish if $\mu = 0$. We have also found that the majoron has a non-vanishing component in the doublet directions. Therefore, in order to avoid phenomenological problems with a doublet majoron, such as a sizable invisible Z-boson width, we are forced to impose the hierarchy of VEVs

$$v_H, v_S \ll v_\sigma\,, \tag{6.29}$$

which guarantees that the majoron is mostly singlet. We turn now to the charged scalar mass matrix. In this case, the scalar potential contains the term

$$\mathcal{V}^C_{\text{mass}} = \begin{pmatrix} H^- & S^- \end{pmatrix} \mathcal{M}^2_\pm \begin{pmatrix} H^+ \\ S^+ \end{pmatrix}, \tag{6.30}$$

with

$$\mathcal{M}^2_\pm = \begin{pmatrix} m_H^2 + \frac{v_H^2\,\lambda_H}{2} + \frac{v_S^2}{2}\left(\lambda_{HS}^{(1)} + \lambda_{HS}^{(2)}\right) + \frac{v_\sigma^2\,\lambda_{H\sigma}}{2} & \frac{v_\sigma\,\mu}{\sqrt{2}} + \frac{\lambda_{HS}^{(2)}\, v_H\, v_S}{2} \\ \frac{v_\sigma\,\mu}{\sqrt{2}} + \frac{\lambda_{HS}^{(2)}\, v_H\, v_S}{2} & m_S^2 + \frac{v_S^2\,\lambda_S}{2} + \frac{v_H^2}{2}\left(\lambda_{HS}^{(1)} + \lambda_{HS}^{(2)}\right) + \frac{v_\sigma^2\,\lambda_{S\sigma}}{2} \end{pmatrix}. \tag{6.31}$$

Again, the application of the tadpole equations leads to

$$\mathcal{M}^2_\pm = \begin{pmatrix} \frac{v_S\, v_\sigma\,\mu}{\sqrt{2}\, v_H} + \frac{\lambda_{HS}^{(2)}\, v_S^2}{2} & \frac{v_\sigma\,\mu}{\sqrt{2}} + \frac{\lambda_{HS}^{(2)}\, v_H\, v_S}{2} \\ \frac{v_\sigma\,\mu}{\sqrt{2}} + \frac{\lambda_{HS}^{(2)}\, v_H\, v_S}{2} & \frac{v_H\, v_\sigma\,\mu}{\sqrt{2}\, v_S} + \frac{\lambda_{HS}^{(2)}\, v_H^2}{2} \end{pmatrix}. \tag{6.32}$$

One of the eigenvalues of this matrix vanishes. This corresponds to the Goldstone boson *eaten* by the W boson, w. The other state is the massive charged scalar $C^{\pm}$. In the basis $\{H^{\pm}, S^{\pm}\}$, they are given in terms of the gauge eigenstates as

$$w^{\pm} = \frac{1}{v}\,(-v_H, v_S)\,, \tag{6.33}$$

$$C^{\pm} = \frac{1}{v}\,(v_S, v_H)\,, \tag{6.34}$$

and their masses are

$$m_w^2 = 0\,, \quad m_C^2 = \frac{1}{2}\,\frac{v^2}{v_H\,v_S}\left(\sqrt{2}\,\mu\,v_\sigma + \lambda_{HS}^{(2)}\,v_H\,v_S\right)\,. \tag{6.35}$$

6.2.2 Lepton masses

The light neutrinos get their masses by means of a standard type-I seesaw mechanism, as seen in Section 2.5.1.1. However, in this model, the 3×3 matrices in generation space m_D and M_R that appear in Eq. (2.21), are defined as

$$m_D = \frac{v_H}{\sqrt{2}}\,Y_\nu\,, \quad M_R = \frac{v_\sigma}{\sqrt{2}}\,\kappa\,. \tag{6.36}$$

The resulting mass matrix, $\mathcal{M}_N$, of the neutral states corresponds to the standard type-I seesaw matrix, see Eq. (2.21). If $m_D \ll M_R$, the light neutrinos mass matrix is given by the well-known formula $m_\nu = -m_D^T\,M_R^{-1}\,m_D$. We note that the hierarchy $m_D \ll M_R$ follows naturally from the hierarchy in Eq. (6.29). On the other hand, the mass term of the charged leptons reads

$$-\mathcal{L}_C = \begin{pmatrix} \bar{e}_R & \bar{F}_R \end{pmatrix} \mathcal{M}_C \begin{pmatrix} e_L \\ F_L \end{pmatrix} + \text{h.c.}\,, \tag{6.37}$$

where the 4×4 matrix $\mathcal{M}_C$ is given by

$$\mathcal{M}_C = \begin{pmatrix} m_e & m_\rho \\ m_S & M_F \end{pmatrix}\,, \tag{6.38}$$

and we have defined

$$m_e = \frac{v_H}{\sqrt{2}}\,Y_e\,, \quad m_\rho = \frac{v_\sigma}{\sqrt{2}}\,\rho\,, \quad m_S = \frac{v_S}{\sqrt{2}}\,Y_S\,. \tag{6.39}$$

The matrices m_e, m_ρ and m_S are 3×3, 3×1 and 1×3, respectively. Also, m_e would be the SM-like charged leptons mass matrix. The mass matrices $\mathcal{M}_N$ and $\mathcal{M}_C$ can be brought to

diagonal form as

$$\widehat{\mathcal{M}}_N = \text{diag}(m_{N_i}) = V^\nu \, \mathcal{M}_N \, V^{\nu T} \,, \tag{6.40}$$

$$\widehat{\mathcal{M}}_C = \text{diag}(m_{C_i}) = V^{R\dagger} \, \mathcal{M}_C \, V^L \,, \tag{6.41}$$

where V^ν and $V^{L,R}$ are unitary matrices. [4]

It proves convenient to derive approximate expressions for the matrices involved in Eq. (6.41). Similarly to what we did in Section 2.5.1.6, we now follow [191] to obtain approximate expressions for the matrices $V^{L,R}$ by performing a perturbative expansion in powers of the inverse of the largest scale in $\mathcal{M}_C$. [5] We assume

$$m_e, m_S \ll m_\rho \ll M_F \,, \tag{6.42}$$

consistent with Eq. (6.29). Then, we can write the matrices $V^{L,R}$ as

$$V^{L(R)} = U^{L(R)} \, D^{L(R)} \,, \tag{6.43}$$

where $U^{L,R}$ and $D^{L,R}$ are unitary matrices. The matrices $U^{L,R}$ will be responsible for the block-diagonalization of $\mathcal{M}_C$ while $D^{L,R}$ will diagonalize the light and heavy sub-blocks. The matrices $D^{L,R}$ can be written in the form

$$D^{L(R)} = \begin{pmatrix} D_e^{L(R)} & 0 \\ 0 & D_F^{L(R)} \end{pmatrix} \,, \tag{6.44}$$

where $D_e^{L,R}$ are 3×3 matrices and $D_F^{L,R}$ are just complex phases. While the non-vanishing elements of the D matrices are expected to be of $\mathcal{O}(1)$, the elements of U will instead be sensitive to the hierarchy of the scales involved in $\mathcal{M}_C$. We can decompose the 4×4 unitary matrices $U^{L,R}$ in the block form

$$U^{L(R)} = \begin{pmatrix} U_{ee}^{L(R)} & U_{eF}^{L(R)} \\ U_{Fe}^{L(R)} & U_{FF}^{L(R)} \end{pmatrix} \,, \tag{6.45}$$

where $U_{ee}^{L,R}$, $U_{eF}^{L,R}$ and $U_{Fe}^{L,R}$ are 3×3, 3×1 and 1×3 matrices, respectively, and $U_{FF}^{L,R}$ are complex numbers. We impose that the following unitary transformation brings $\mathcal{M}_C$ into a block-diagonal matrix, namely that

$$U^{R\dagger} \begin{pmatrix} m_e & m_\rho \\ m_S & M_F \end{pmatrix} U^L = \begin{pmatrix} m_{\text{light}} & 0 \\ 0 & m_{\text{heavy}} \end{pmatrix} \,. \tag{6.46}$$

[4] We observe that for $v_H \ll v_\sigma$, which is required by the seesaw mechanism, and assuming the Yukawa couplings ρ and Y_S to be of $\mathcal{O}(1)$, we are forced to impose $v_S \ll v_\sigma$ in order not to have all charged lepton masses pushed towards the seesaw scale. This is in agreement with the considerations regarding the majoron profile.

[5] See also the pioneer work [207] for an alternative (but equivalent) approach for the perturbative diagonalization of a Majorana mass matrix.

Eq. (6.46) imposes constraints on the $U^{L,R}$ matrices and hence reduces their numbers of independent parameters. In particular, it requires $U^{L,R}$ to lead to two vanishing 3×1 and 1×3 submatrices. Therefore, each of them must have three degrees of freedom only. We then formulate the ansätze for U^L and U^R

$$U^L = \begin{pmatrix} \sqrt{\mathbb{1}_3 - LL^\dagger} & L \\ -L^\dagger & \sqrt{1 - L^\dagger L} \end{pmatrix}, \tag{6.47}$$

$$U^R = \begin{pmatrix} \sqrt{\mathbb{1}_3 - RR^\dagger} & R \\ -R^\dagger & \sqrt{1 - R^\dagger R} \end{pmatrix}, \tag{6.48}$$

where $\mathbb{1}_3$ is the 3×3 identity matrix and L and R are 3×1 matrices. The L and R matrices must be determined perturbatively as a function of the parameters in $\mathcal{M}_C$ by expanding in powers of $1/M_F$. One must also Taylor-expand the square root. In the case of L, the expansion is given by

$$L = L_1 + L_2 + L_3 + \cdots \tag{6.49}$$

and

$$\sqrt{\mathbb{1}_3 - LL^\dagger} = \mathbb{1}_3 - \frac{1}{2}LL^\dagger - \frac{1}{8}LL^\dagger LL^\dagger + \cdots \tag{6.50}$$

where the L_i matrices are proportional to M_F^{-i}. Analogous expansions can be given for R. The coefficients of the expansion are computed recursively, imposing that the off-diagonal sub-blocks of $\mathcal{M}_C$ vanish at each order in M_F. Using the aforementioned hierarchy among scales, this procedure leads to

$$U^L = \begin{pmatrix} \mathbb{1}_3 - \frac{1}{2}\frac{m_S^\dagger m_S}{M_F^2} - \frac{1}{2}\frac{m_e^\dagger m_\rho m_S + m_S^\dagger m_\rho^\dagger m_e}{M_F^3} & \frac{m_S^\dagger}{M_F} + \frac{m_e^\dagger m_\rho}{M_F^2} - \frac{m_S^\dagger m_\rho^\dagger m_\rho}{M_F^3} \\ -\frac{m_S}{M_F} - \frac{m_\rho^\dagger m_e}{M_F^2} + \frac{m_\rho^\dagger m_\rho m_S}{M_F^3} & 1 - \frac{1}{2}\frac{m_S m_S^\dagger}{M_F^2} - \frac{1}{2}\frac{m_S m_e^\dagger m_\rho + m_\rho^\dagger m_e m_S^\dagger}{M_F^3} \end{pmatrix} + \mathcal{O}(M_F^{-3}), \tag{6.51}$$

$$U^R = \begin{pmatrix} \mathbb{1}_3 - \frac{1}{2}\frac{m_\rho m_\rho^\dagger}{M_F^2} - \frac{1}{2}\frac{m_\rho m_S m_e^\dagger + m_e m_S^\dagger m_\rho^\dagger}{M_F^3} & \frac{m_\rho}{M_F} + \frac{m_e m_S^\dagger}{M_F^2} - \frac{m_\rho m_\rho^\dagger m_\rho}{2M_F^3} \\ -\frac{m_\rho^\dagger}{M_F} - \frac{m_S m_e^\dagger}{M_F^2} + \frac{m_\rho^\dagger m_\rho m_\rho^\dagger}{2M_F^3} & 1 - \frac{1}{2}\frac{m_\rho^\dagger m_\rho}{M_F^2} - \frac{1}{2}\frac{m_S m_e^\dagger m_\rho + m_\rho^\dagger m_e m_S^\dagger}{M_F^3} \end{pmatrix} + \mathcal{O}(M_F^{-3}), \tag{6.52}$$

where we kept only the leading order contribution in m_ρ to the $\mathcal{O}(M_F^{-3})$ coefficients L_3 and R_3. The block-diagonal masses for the light and heavy charged leptons are finally given by

$$m_{\text{light}} = m_e - \frac{m_\rho m_S}{M_F} - \frac{m_\rho m_\rho^\dagger m_e}{2\,M_F^2} - \frac{m_e m_S^\dagger m_S}{2\,M_F^2} + \frac{m_\rho m_\rho^\dagger m_\rho m_S}{2\,M_F^3} + \mathcal{O}(M_F^{-3}), \tag{6.53}$$

$$m_{\text{heavy}} = M_F + \frac{m_\rho^\dagger m_\rho}{2\,M_F} + \frac{m_S m_S^\dagger}{2\,M_F} + \frac{m_\rho^\dagger m_e m_S^\dagger + m_S m_e^\dagger m_\rho}{2\,M_F^2} - \frac{m_\rho^\dagger m_\rho m_\rho^\dagger m_\rho}{8\,M_F^3} + \mathcal{O}(M_F^{-3}). \tag{6.54}$$

In summary, $m_{\text{light}} \approx m_e$ and $m_{\text{heavy}} \approx M_F$, with corrections to these zeroth order results entering at different orders in $1/M_F$.

6.3 Majoron couplings

In the gauge basis, the interaction terms of the majoron with neutrinos and charged leptons read

$$-\mathcal{L}_{JNN} = -\frac{i\,J}{2\,v\,V^2}\begin{pmatrix}\bar{\nu}_L^c & \bar{\nu}_R\end{pmatrix}\begin{pmatrix}0 & -v_S^2\,m_D^T\\ -v_S^2\,m_D & v^2\,M_R\end{pmatrix}\begin{pmatrix}\nu_L\\ \nu_R^c\end{pmatrix} + \text{h.c.}\,, \tag{6.55}$$

$$-\mathcal{L}_{JCC} = -\frac{i\,J}{v\,V^2}\begin{pmatrix}\bar{e}_R & \bar{F}_R\end{pmatrix}\begin{pmatrix}v_S^2\,m_e & v^2\,m_\rho\\ -v_H^2\,m_S & 0\end{pmatrix}\begin{pmatrix}e_L\\ F_L\end{pmatrix} + \text{h.c.}\,. \tag{6.56}$$

The majoron profile in Eq. (6.26) has been used in the derivation of Eqs. (6.55) and (6.56). We can now focus on the interaction Lagrangian involving charged leptons and write it in the fermion mass basis. This results in

$$-\mathcal{L}_{JCC} = -\frac{i\,J}{v\,V^2}\left[\bar{X}^\beta\left(V^{R\dagger}AV^L\right)_{\beta\alpha}P_L\,X^\alpha - \bar{X}^\alpha\left(V^{L\dagger}A^\dagger V^R\right)_{\alpha\beta}P_R\,X^\beta\right], \tag{6.57}$$

where α,β are flavor indices, specified here for the sake of clarity, we have defined the four component array in flavor space $X=(e,F)$ and

$$A = \begin{pmatrix}v_S^2\,m_e & v^2\,m_\rho\\ -v_H^2\,m_S & 0\end{pmatrix} \tag{6.58}$$

is the matrix in Eq. (6.56). By comparing to Eq. (2.66), one finds a dictionary between the $S_{L,R}$ effective couplings and the parameters of the model under consideration. In the case of the flavor violating couplings, with $\beta\neq\alpha$, one finds

$$S_L^{\beta\alpha} = \frac{i}{v\,V^2}\left(V^{R\dagger}AV^L\right)^{\beta\alpha}\,, \tag{6.59}$$

$$S_R^{\beta\alpha} = -\frac{i}{v\,V^2}\left(V^{L\dagger}A^\dagger V^R\right)^{\beta\alpha}\,. \tag{6.60}$$

This matching only holds for the light charged leptons, hence $\alpha,\beta=1,2,3$ here. We note that the matching is completely specified by the charged lepton mass matrix $\mathcal{M}_C$. In the case of the flavor conserving couplings, with $\beta=\alpha$, one gets

$$S^{\beta\beta} \equiv S_L^{\beta\beta} + S_R^{\beta\beta *} = \frac{i}{v\,V^2}\left(V^{R\dagger}AV^L\right)^{\beta\beta}\,. \tag{6.61}$$

We note that there is a mismatch of a factor of 2 with the matching holding for the off-diagonal couplings, which prevents us from writing a single matching relation. The coupling in Eq. (6.61) is purely imaginary, as expected for a pure pseudoscalar. The analytic proof of this result is given in Appendix D.

Finally, one can find approximate expressions for the $S_{L,R}$ couplings by using the expressions derived for the $V^{L,R}$ matrices in the previous Section. One finds

$$S_L^{\beta\alpha} = \frac{i}{v\,V^2}\,C^{\beta\alpha}\,, \tag{6.62}$$

$$S_R^{\beta\alpha} = -\frac{i}{v\,V^2}\,C^{\alpha\beta *}\,, \tag{6.63}$$

with

$$C = D_e^{R\dagger}\left[v_S^2\,m_e - \frac{v_S^2}{M_F} m_\rho m_S - \frac{3\,v_S^2 + 2\,v_H^2}{2\,M_F^2}\,m_\rho m_\rho^\dagger m_e + \frac{2\,v_H^2 - v_S^2}{2\,M_F^2}\,m_e m_S^\dagger m_S + \mathcal{O}(M_F^{-3})\right] D_e^L\,. \tag{6.64}$$

Comparing with Eq. (6.53), it follows that the off-diagonal couplings of the Majoron are suppressed by $\mathcal{O}(M_F^{-2})$, and not by $\mathcal{O}(M_F^{-1})$ as one could naively expect. This follows from the fact that $D_e^{L,R}$ are the unitary matrices that diagonalize m_{light}.

6.4 Phenomenology of the model

The model can be probed owing to its signatures in low-energy flavor experiments and high-energy colliders.

Lepton flavor violating signatures

The first and most evident consequence of a massless majoron with tree-level LFV couplings is the existence of large LFV rates in wide regions of the parameter space. This includes the usual LFV processes, such as $\ell_\alpha \to \ell_\beta\,\gamma$ or $\ell_\alpha \to 3\,\ell_\beta$, which constitute important constraints for our model. For the radiative processes $\ell_\alpha \to \ell_\beta\,\gamma$ we use the general formulas in [323], whereas for the 3-body LFV decays $\ell_\alpha^- \to \ell_\beta^-\ell_\beta^-\ell_\beta^+$, $\ell_\alpha^- \to \ell_\beta^-\ell_\gamma^-\ell_\gamma^+$ and $\ell_\alpha^- \to \ell_\beta^+\ell_\gamma^-\ell_\gamma^-$, we use the general expressions in [251]. The effective coefficients for the 3-body decays are generated in our model at tree-level and are listed in Appendix E. In addition, we must consider processes involving the majoron in the final state. In particular, the LFV decay $\ell_\alpha \to \ell_\beta\,J$ is induced by the off-diagonal $S_A^{\beta\alpha}$ scalar couplings, with $A = L, R$, defined in Eq. (2.66). The majoron contributions to all the LFV processes of interest where calculated in Chapter 3, where a detailed discussion on the obtention of the bounds of the majoron couplings with charged leptons is presented. A summary of these limits is also provided in Table 3.2. In addition, the new massive charged scalar $C^\pm$ will also contribute to some LFV processes through its S doublet component.

Anomalous magnetic moment of the muon

The enlarged lepton sector in our model induces contributions to many leptonic observables. We have already discussed flavor violating observables, which vanish in the SM. In addition, flavor conserving observables also receive new contributions, and these may potentially induce

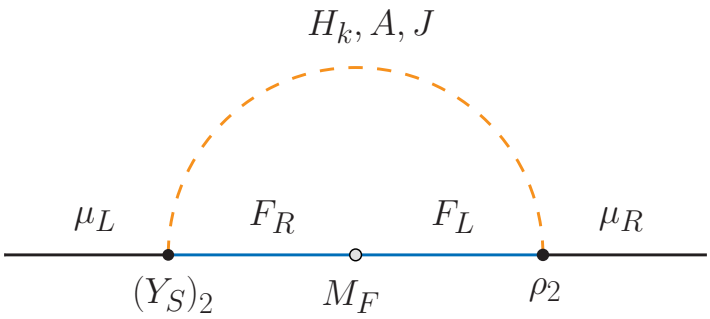

Figure 6.1: Dominant new physics contribution to the muon anomalous magnetic moment.

deviations from the SM predictions. For instance, the new states contribute to the anomalous magnetic moment of the muon, an observable that has received a lot of attention recently.

In our model, new contributions to the muon $g-2$ are induced at the 1-loop level, as shown in Fig. 6.1. This figure includes diagrams with the massive CP-even bosons H_k, with the massive CP-odd state A, and with the majoron J. For the massive states, we use the analytical expressions given in [103], whereas the majoron contribution was computed in Section 3.4.7.

Higgs boson decays

The lightest CP-even scalar mass eigenstate, $H_1 \equiv h$, can be identified with the 125 GeV state discovered at the LHC. Therefore, it is crucial that its properties and decay channels match those observed, within the ranges allowed by the experimental errors. Since the observed state resembles the Higgs boson of the SM, this is guaranteed if the mixing angles in the CP-even scalar sector are sufficiently small. In this case, h is made up mostly by the S_H state, which has the properties of a SM Higgs. Thus, decays such as $h \to ZZ, WW$ are not modified substantially.

Higgs decays into a pair of muons have been recently searched for by the ATLAS [324] and CMS [325] collaborations. Their data yields the following ratio in terms of the SM predicted value [210],

$$R_{h\mu\mu} = \frac{\mathrm{BR}(h \to \mu\mu)^{\mathrm{exp}}}{\mathrm{BR}(h \to \mu\mu)^{\mathrm{SM}}} = 1.19 \pm 0.39\,. \tag{6.65}$$

In our model, the mixing in the CP-even scalar sector may induce large deviations from the SM predicted ratio, $R_{h\mu\mu} = 1$. Even if the mixing is tiny, the large S and σ couplings to muons, required if one wants to address the experimental anomaly in the muon anomalous magnetic moment, induce sizable contributions to $R_{h\mu\mu}$, which can largely deviate from 1. An approximate analytical expression for $R_{h\mu\mu}$, valid under some simplifying assumptions, is provided in Appendix F.

Finally, h can also decay invisibly to a pair of majorons. The current ATLAS limit on the invisible Higgs branching ratio translates into $\mathrm{BR}(h \to JJ) < 0.19$ at 95% C.L. [326]. We take this constraint into account in our numerical analysis, using $\Gamma_h \approx \Gamma_h^{\mathrm{SM}} = 4.1$ MeV for the total Higgs decay width [327]. Its error is negligible.

6.5 Numerical results

In this Section, we present our numerical results. These have been obtained by randomly scanning in the wide parameter space of the model and computing the observables discussed in the previous Section. All points in our scans are compatible with current neutrino oscillation data. This is achieved by using a Casas-Ibarra parametrization [200] for the Y_ν Yukawa matrix, as explained in Section 2.5.3, considering $M = \frac{v_H^2}{2} M_R^{-1}$ in Eq. (2.62). Here, we are working in the basis in which the M_R matrix, defined in Eq. (6.36), is diagonal, with $M_R = \text{diag}\,(M_1, M_2, M_3)$. In our numerical analysis we assume normal neutrino mass ordering and randomly take neutrino oscillation parameters within the $3\,\sigma$ ranges obtained by the global fit [138]. Qualitatively similar results can be obtained assuming inverted neutrino mass ordering.

Several parameters are chosen randomly in our scans. These are v_S, v_σ, the vector-like lepton mass M_F, the trilinear coupling μ as well as the ρ and Y_S Yukawa couplings, where the ρ_2 and the $(Y_S)_2$ upper bounds are chosen below the non-perturbative regime. In addition, the κ Yukawa matrix has been taken diagonal, with κ_{ii} also chosen randomly. All Yukawa couplings have been assumed to be real for simplicity. The ranges for the parameters that have been chosen randomly in our scans are shown on Table 6.2. We have chosen the VEV v_S in the narrow range $[0.05, 0.1]$ GeV. This choice is motivated by the fact that the doublet S does not couple to quarks. A sizable v_S VEV would imply a reduction of v_H and, as a consequence of this, an increase in the Higgs boson couplings to quarks, already constrained by LHC data. Moreover, v_S is also indirectly constrained due to its impact on the diagonal majoron couplings, see Eq. (6.64), and a small value is generally required. Furthermore, a small value for v_S motivates a similarly small value for the μ trilinear coupling. Otherwise, the heavy CP-even scalars H_k and the pseudoscalar A become very heavy, and their impact on the phenomenology is negligible, see Eqs. (6.21) and (6.28). Finally, the scalar potential parameters $\lambda_\sigma = \lambda_{HS}^{(1)} = 0.1$ and $\lambda_S = \lambda_{H\sigma} = \lambda_{HS}^{(2)} = \lambda_{S\sigma} = 0.01$ have been fixed in all the scans. Note, however, that the exact choice for these quartic couplings is irrelevant for the observables we study. Also, the small values of v_S and the quartics assure that SM precision observables are not substantially changed in our model.

Our analysis has taken into account several experimental bounds. Starting with the LFV processes, we have checked that the branching ratios of the radiative processes $\ell_\alpha \to \ell_\beta \gamma$ as well as the 3-body decays $\ell_\alpha^- \to \ell_\beta^- \ell_\beta^- \ell_\beta^+$, $\ell_\alpha^- \to \ell_\beta^- \ell_\gamma^- \ell_\gamma^+$ and $\ell_\alpha^- \to \ell_\beta^+ \ell_\gamma^- \ell_\gamma^-$ satisfy the existing bounds [210]. Regarding the decays $\ell_\alpha \to \ell_\beta\, J$, we have imposed the restrictions on the flavor violating couplings instead of the branching ratios. To do so, we have defined the combination

$$|S^{\beta\alpha}| = \left(\left| S_L^{\beta\alpha} \right|^2 + \left| S_R^{\beta\alpha} \right|^2 \right)^{1/2} \tag{6.66}$$

and imposed the bounds derived in Chapter 3. On the flavor conserving side, we also consider the stringent constraints from astrophysics on the imaginary couplings. Both flavor conserving and violating bounds are collected in Table 3.2. The impact of these bounds on the phenomenology

Parameter	Range
v_S	$[0.05\,,\,0.1]$ GeV
v_σ	$[0.75\,,\,1.5]$ TeV
M_F	$[0.75\,,\,3]$ TeV
μ	$[0.01\,,\,0.1]$ GeV
κ_{ii}	$[0.1\,,\,1]$
ρ_1	$[10^{-6}\,,\,1]\times 5\cdot 10^{-3}$
ρ_2	$\left[5\cdot 10^{-4}\,,\,\sqrt{4\pi}\right]$
ρ_3	$[0.05\,,\,1]\times 10^{-7}$
$(Y_S)_1$	$[0.01\,,\,1]\times 10^{-6}$
$(Y_S)_2$	$\left[0.1\,,\,\sqrt{4\pi}\right]$
$(Y_S)_3$	$[0.001\,,\,5]\times 10^{-7}$

Table 6.2: Ranges for the parameters that are randomly taken in our numerical analysis.

of the model will be studied in detail in the discussion that follows. We have also made sure here that the ratios

$$R_{Z\ell\ell} = \frac{\Gamma\left(Z\to\ell^+\ell^-\right)}{\Gamma_{SM}\left(Z\to\ell^+\ell^-\right)}\,, \tag{6.67}$$

where $\Gamma_{SM}\left(Z\to\ell^+\ell^-\right)$ is the SM predicted decay width, lie within the 95% CL range, which is estimated to be $0.995 < R_{Zee} < 1.003$ and $0.993 < R_{Z\mu\mu} < 1.006$ [210]. With respect to Higgs decays, we have considered the very recent measurement of the process $h\to\mu\mu$, discussed in the previous Section, and we have rejected the points in our analysis outside the range compatible with Eq. (6.65) at $3\,\sigma$. Finally, points with $\mathrm{BR}\left(h\to JJ\right) > 0.19$ [326] have been discarded as well.

Our results for the LFV processes $\mu\to e\,\gamma$ and $\mu\to e\,J$ are shown in Fig. 6.2, which shows $\mathrm{BR}(\mu\to e\,\gamma)$ as a function of $\mathrm{BR}(\mu\to e\,J)$. The vertical line corresponds to the bound $\mathrm{BR}(\mu\to e\,J) < 10^{-5}$, already discussed in Chapter 3, while the horizontal line is the current limit $\mathrm{BR}(\mu\to e\,\gamma) < 4.2\times 10^{-13}$, obtained by the MEG experiment [141]. Red points correspond to parameter points that respect all astrophysical bounds, namely the bounds on S^{ee} and $S^{\mu\mu}$ in Eqs. (3.7) and (3.8), while the astrophysical bound on the majoron coupling to muons is violated in the blue points. Finally, the clear points are excluded due to one or several of the other experimental constraints mentioned above. First, as can be seen in this figure, our model is able to attain the current experimental bounds on $\mathrm{BR}(\mu\to e\,\gamma)$ and $\mathrm{BR}(\mu\to e\,J)$. Moreover, one finds no difference at all between blue and red points. This implies that the astrophysical bounds on the flavor conserving couplings S^{ee} and $S^{\mu\mu}$ have no impact on the results for the flavor

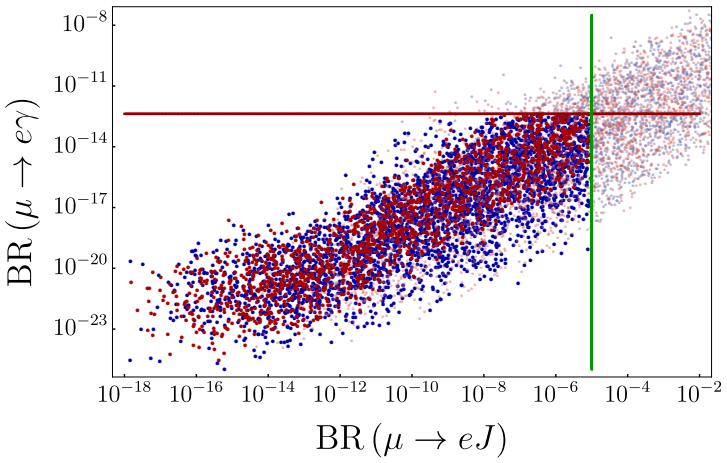

Figure 6.2: BR$(\mu \to e\,\gamma)$ as a function of BR$(\mu \to e\,J)$.

violating observables. We also observe that a correlation between BR$(\mu \to e\,\gamma)$ and BR$(\mu \to e\,J)$ exists, although these two observables depend on different combinations of parameters. However, it is easy to understand that they are not completely independent. In the limit $\rho_1 = (Y_S)_1 = 0$, the vector-like fermion F does not couple to electrons. In this case, the only contributions to $\mu - e$ LFV observables come from the Y_ν Yukawa matrix, which has entries of the size of $\sim 10^{-7} - 10^{-6}$ and then leads to tiny LFV branching ratios. Therefore, sizable ρ_1 or $(Y_S)_1$ couplings are required in order to have observable LFV, and this applies both to $\mu \to e\,J$ and $\mu \to e\,\gamma$. Regarding other LFV processes, our numerical results also show that dipole contributions dominate the amplitude of the 3-body decay $\mu^- \to e^- e^+ e^-$. This leads to strong correlations with $\mu \to e\,\gamma$, which always has a much larger branching ratio.

Furthermore, in the region of parameter space covered by our numerical scan, it is easy to show that BR$(\mu \to e\,J)$ clearly correlates with the combination of parameters $v_\sigma\,\rho_1\,\rho_2\,M_F^{-2}$. From the expression of the majoron couplings to charged leptons in Eqs. (6.62) and (6.63) and the charged lepton mass matrix in Eq. (6.53), derived under the assumption $m_\rho \ll M_F$, and assuming $v_S \ll v_H$ and a large ρ_2 coupling, as motivated by the explanation of the muon $g-2$ anomaly, one can obtain the approximation for the off-diagonal $e - \mu$ coupling

$$|S^{e\mu}| \approx \frac{m_\mu\, v_\sigma}{M_F^2}\,\rho_1\,\rho_2\,. \tag{6.68}$$

We observe that, as long as the condition $m_\rho < M_F$ is satisfied, $|S^{e\mu}|$ actually grows when the $\mathrm{U(1)_L}$ symmetry breaking scale v_σ increases. This result seems to go against the usual decoupling behavior expected when the new physics scale becomes larger. However, when v_σ is increased, the mixing between the SM-like charged leptons and the vector-like lepton F increases as well, hence enhancing the $\mu - e - J$ coupling. Eventually, when v_σ is pushed above M_F, Eq. (6.68) becomes invalid and BR$(\mu \to e\,J)$ starts to decrease.

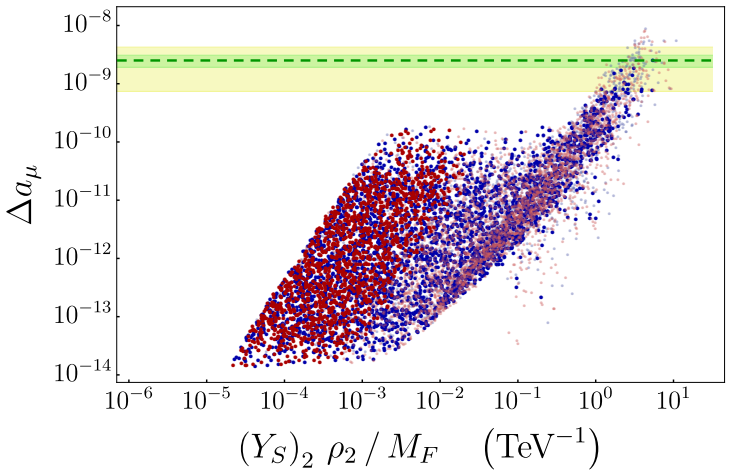

Figure 6.3: Δa_μ as a function of the combination $(Y_S)_2\,\rho_2/M_F$. Gray points are excluded due to one or several experimental bounds, but are shown for illustration.

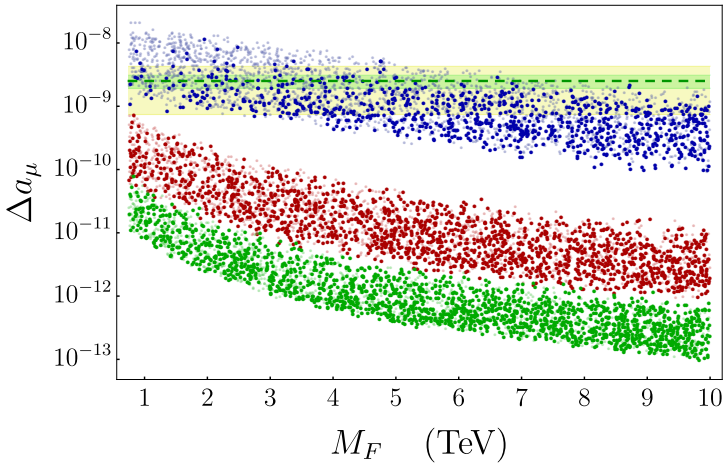

Figure 6.4: Δa_μ as a function of the vector-like mass M_F for $\rho_2 = (Y_S)_2 = \sqrt{4\pi}$ (blue), $\rho_2 = (Y_S)_2 = 1$ (red) and $\rho_2 = (Y_S)_2 = 0.5$ (green).

In what concerns τ decays, our choice of parameters suppresses all the LFV amplitudes. Since experimental limits in the τ sector are much weaker than for the muon, we do not show plots for LFV τ decays. We note, however, that one can saturate (some of) the experimental bounds also for τ's in our model, for the appropriate choice of (large) parameters in the 3rd generation. On the other hand, in our model it is not possible to have both, $\tau \to e\,\gamma$ and $\tau \to \mu\,\gamma$, with large rates at the same time, without running into conflict with $\mu \to e\,\gamma$.

Our model can also induce large contributions to the muon anomalous magnetic moment and address the current experimental anomaly. [6] This is shown in Fig. 6.3. This figure displays Δa_μ as a function of the combination of parameters $(Y_S)_2\,\rho_2/M_F$, which enters the Feynman diagram

[6] We notice that an explanation for the anomalous magnetic moment of the electron is not possible due to the ranges chosen for the Yukawa couplings of the electron. The motivation for this was that we wanted to avoid too large $\mu \to e\,\gamma$ decaying rates.

in Fig. 6.1. The horizontal dashed line represents the experimental central value, while the green and yellow bands correspond to the 1σ and 3σ ranges, respectively. [7] As in the previous figure, the red points respect the astrophysical bounds on S^{ee} and $S^{\mu\mu}$, while the blue points only respect the constraint on S^{ee}. Clear points are excluded due to one or several constraints but are shown for illustration. We have found numerically that all diagrams, with massive scalars or with the majoron in the loop, may have comparable sizes. Interestingly, some points are found within the 1σ interval, hence providing a good explanation for the experimental value of the muon anomalous magnetic moment. These points require relatively light F fermions (with masses of the order of $\sim 1-2$ TeV) and large (order 1) ρ_2 and $(Y_S)_2$ Yukawa couplings. However, they violate the bound on $S^{\mu\mu}$ obtained from the supernova SN1987A, since this constraint necessarily implies a low value of ρ_2. In fact, we note that this figure displays a large concentration of points with low values of Δa_μ in a region where all the red points are found. This region is characterized by $\rho_2 \ll 1$, and hence the dominant contributions to the muon $g-2$ do not come from the diagram in Fig. 6.1 but are mostly induced by diagrams proportional to $(Y_S)_2^2/M_F^2$. These diagrams have an external chirality flip that introduces an m_μ suppressing factor and then, as is generically found in a large class of models with this feature, Δa_μ can be at most $\sim 10^{-10}$.

Complementary information is provided by Fig. 6.4, which shows Δa_μ as a function of the vector-like mass M_F for three different values of $\rho_2 = (Y_S)_2$. Blue points corresponds to $\rho_2 = (Y_S)_2 = \sqrt{4\pi}$, red points to $\rho_2 = (Y_S)_2 = 1$ and green points to $\rho_2 = (Y_S)_2 = 0.5$. This figure has been obtained with a specific parameter scan in which $M_F \in [0.75\,,\,10]$ TeV, while the ranges for the other randomly chosen parameters are as in Table 6.2. As expected, all new physics contributions decrease for large M_F and strongly depend on the value of the ρ_2 and $(Y_S)_2$ couplings. When $\rho_2 = (Y_S)_2 = 0.5$, these are not large enough to address the muon $g-2$ anomaly, while when $\rho_2 = (Y_S)_2 = 1$ this happens in a narrow region of the parameter space characterized by very light vector-like leptons, with masses $\lesssim 1$ TeV. Only when $\rho_2 = (Y_S)_2 = \sqrt{4\pi}$, one can find an explanation for the anomaly in a wide M_F range. And even in this case, they eventually become too small to account for the measured muon $g-2$. However, this happens for very large vector-like masses. In fact, one finds that vector-like masses as large as 10 TeV still allow for a 3σ explanation of the muon $g-2$ anomaly. Such a large mass would make the F fermions unobservable at the LHC.

We turn our attention to Higgs boson decays. As already explained, the mixing in the CP-even scalar sector can induce large deviations from the SM predicted Higgs branching ratios. In particular, a large effective coupling to muons is induced in parameter points in which the muon $g-2$ anomaly is explained. This is shown in Fig. 6.5. Here we plot the ratio $R_{h\mu\mu}$, defined in Eq. (6.65), as a function of the lepton number breaking scale v_σ. The horizontal line represents the current central value, $R_{h\mu\mu} = 1.19$ [210], while the green and yellow bands correspond to

[7] We note that the 1σ and 3σ intervals are symmetric with respect to the central value, but they look asymmetric in this figure since we are using a logarithmic scale for the y-axis.

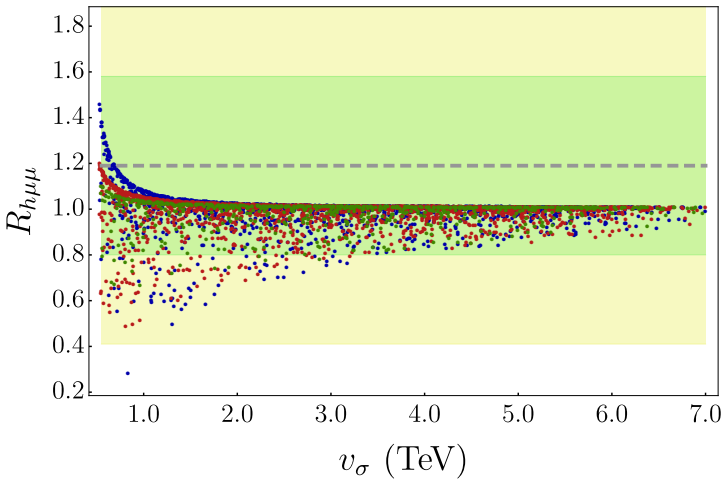

Figure 6.5: $R_{h\mu\mu}$ as a function of v_σ for three fixed values of the vector-like mass M_F: $M_F = 1$ TeV (blue), $M_F = 3$ TeV (red) and $M_F = 5$ TeV (green). The horizontal line represents the current central value, $R_{h\mu\mu} = 1.19$ [210], while the green and yellow bands correspond to the 1σ and 2σ ranges, respectively.

the 1σ and 2σ ranges, respectively. As in the previous plot, the vector-like mass M_F is fixed to specific values in this figure: $M_F = 1$ TeV (blue points), $M_F = 3$ TeV (red points), and $M_F = 5$ TeV (green points). In addition, $v_S = 0.1$ GeV and $\rho_2 = (Y_S)_2 = \sqrt{4\pi}$ are fixed in this plot, while $\mu \in [0.05\,,\,50]$ GeV, $\rho_1 \in [0.002\,,\,1.2] \times 10^{-6}$ and $(Y_S)_1 \in [0.1\,,\,5] \times 10^{-7}$ are randomly varied and the rest of parameters are taken as in Table 6.2. Due to the large value chosen for ρ_2, the astrophysical bound on $S^{\mu\mu}$ is not respected in this plot. Imposing this constraint would imply $R_{h\mu\mu} \approx 1$. We observe that for large v_σ and M_F, the new physics contributions become negligibly small, and one finds $R_{h\mu\mu} = 1$. However, for lower scales one finds many parameter points leading to large deviations from the SM predicted value. In particular, for $M_F = 1$ TeV our scan reveals points with $R_{h\mu\mu}$ as large ~ 1.4 or as low as ~ 0.3. These extreme points are, of course, ruled out by the existing data but serve as an example of how easily Higgs decays into muons can deviate from the SM predictions in our setup.

We finally note that the $R_{h\mu\mu}$ ratio does not correlate with other observables due to the large number of independent contributions to the $h-\mu-\mu$ coupling, see Appendix F. For this reason, a definite prediction cannot be made. For instance, Eqs. (F.7)-(F.9) imply that for vanishing mixing in the scalar sector, $c_{\mu\mu}^{S_\sigma} = c_{\mu\mu}^{S_S} = 0$ and $c_{\mu\mu}^{S_H} > c_{\mu\mu}^{\rm SM}$, hence predicting $R_{h\mu\mu} > 1$. However, the α and β angles never vanish and in fact, one can find $R_{h\mu\mu} < 1$ as well.

6.6 Summary

In this Chapter, we have proposed a simple model that leads to sizable majoron flavor violating couplings to charged leptons. The particle spectrum is extended with the addition of two new scalar multiplets as well as three right-handed neutrino singlets and a vector-like lepton. The

SM symmetry is also extended with a continuous lepton number global symmetry. As a result of spontaneous symmetry breaking, neutrinos acquire non-zero Majorana masses via a type-I seesaw mechanism, and a massless Goldstone boson appears in the spectrum, the majoron.

Thanks to sufficiently large mixings between the SM charged leptons and the vector-like lepton, sizable majoron LFV couplings are generated at tree-level. Therefore, our model constitutes a simple example of a model with tree-level off-diagonal majoron couplings not suppressed by neutrino masses. This induces plenty of signatures in experiments looking for LFV processes. In particular, we have shown that the decay $\mu \to e\, J$ can have large rates close to the experimental limit. In fact, it already excludes part of the parameter space of the model.

As a by-product of our construction, other interesting phenomenological possibilities emerge: (i) an explanation to the current muon $g-2$ discrepancy can be provided in large parts of the parameter space of the model, easily finding points that address the anomaly even within 1σ, and (ii) sizable deviations with respect to the SM predicted Higgs decay rates can be obtained, most notably in $h \to \mu\mu$. These two phenomenological possibilities provide additional handles on the model. We note, however, that an explanation of the muon $g-2$ anomaly would lead to tension with recent astrophysical bounds on the majoron coupling to muons.

Here we have shown that as soon as the lepton sector is extended beyond the minimal models, exotic signatures appear, such as those including a massless majoron in the final state. This motivates the experimental search for processes like $\mu \to e\, J$ and stimulates the construction of new theoretical scenarios that, in addition to neutrino masses, provide an understanding to other open questions.

Part III

Model Building

Chapter 7

Generalizing the Scotogenic model

In particle physics, *model building* refers to the construction of novel quantum field theories that extend the Standard Model. These new theories have specific features that make them theoretically appealing. While in the previous chapters the models were motivated by phenomenology, in this part of the thesis we adopt a model building perspective.

7.1 Introduction

In Section 2.5.2, we discussed the Scotogenic model, which is a well-known radiative neutrino mass model [198, 199]. The original version of the model was proposed in 1996 by Zhijian Tao and later, independently, in 2006 by Ernest Ma. Since then, many variations and extensions have been developed. These include colored versions of the model [328–331] and versions with additional states and/or symmetries, both in Dirac [332–340] and Majorana fashion [341–385]. The $\mathbb{Z}_2$ parity can also be promoted to a local [386, 387] or global U(1) symmetry [388–391], or to a Peccei-Quinn quasi-symmetry [392–394]. Finally, Scotogenic-like scenarios have also been combined with, or even obtained from, extended gauge symmetries [395–398].

In the original version of the Scotogenic model, a single copy of the inert doublet and three generations of singlet fermions were included. [1] However, this choice was not unique, and the Scotogenic model can be generalized to include alternative numbers of generations [399, 400]. In this chapter, based on [309], we introduce the *general Scotogenic model*, which allows for arbitrary numbers of generations of the Scotogenic states, and explore its more relevant features.

7.2 The general Scotogenic model

The particle content of the SM is expanded by an unspecified number, n_N, of singlet fermions N, and also an arbitrary number, n_η, of inert scalar doublets η. Particular cases of this particle spectrum can be labeled by their (n_N, n_η) values. Furthermore, the symmetry group of the SM

[1] Even though this version of the Scotogenic model is often referred to as *the minimal Scototogenic model*, we note that more minimal setups can be built [343, 374, 375].

is enlarged with a *dark* $\mathbb{Z}_2$ parity, under which all the new fields are odd, while the SM particles are even. The scalar and lepton particles of the model, along with their representations under the gauge group $\mathrm{SU(3)_c} \times \mathrm{SU(2)_L} \times \mathrm{U(1)_Y}$ and the $\mathbb{Z}_2$ parity are given in Table 7.1.

Field	Generations	$\mathrm{SU(3)_c}$	$\mathrm{SU(2)_L}$	$\mathrm{U(1)_Y}$	$\mathbb{Z}_2$
ℓ_L	3	**1**	**2**	$-1/2$	$+$
e_R	3	**1**	**1**	-1	$+$
H	1	**1**	**2**	$1/2$	$+$
η	n_η	**1**	**2**	$1/2$	$-$
N	n_N	**1**	**1**	0	$-$

Table 7.1: Scalar and lepton particle content of the model and their representations under the gauge and global symmetries. ℓ_L and e_R are the SM left- and right-handed leptons, respectively, and H is the SM Higgs doublet.

The relevant Yukawa and bare mass terms for our discussion are

$$\mathcal{L}_N \supset y_{na\alpha}\, \overline{N}_n\, \eta_a\, \ell_L^\alpha + \frac{1}{2}\, M_{N_n}\, \overline{N^c}_n\, N_n + \text{h.c.}\,, \tag{7.1}$$

where $n = 1, \ldots, n_N$, $a = 1, \ldots, n_\eta$ and $\alpha = 1, 2, 3$ are generation indices and y is a general complex $n_N \times n_\eta \times 3$ object. Besides, M_N is a symmetric $n_N \times n_N$ Majorana mass matrix that has been chosen diagonal without loss of generality. Furthermore, one can also write the scalar potential

$$\begin{aligned}\mathcal{V} = {} & m_H^2 H^\dagger H + \left(m_\eta^2\right)_{ab} \eta_a^\dagger \eta_b + \frac{1}{2}\,\lambda_1 \left(H^\dagger H\right)^2 + \frac{1}{2}\,\lambda_2^{abcd} \left(\eta_a^\dagger \eta_b\right)\left(\eta_c^\dagger \eta_d\right) \\ & + \lambda_3^{ab} \left(H^\dagger H\right)\left(\eta_a^\dagger \eta_b\right) + \lambda_4^{ab} \left(H^\dagger \eta_a\right)\left(\eta_b^\dagger H\right) \\ & + \frac{1}{2}\left[\lambda_5^{ab} \left(H^\dagger \eta_a\right)\left(H^\dagger \eta_b\right) + \text{h.c.}\right].\end{aligned} \tag{7.2}$$

Here all the indices are η generation indices and can take the values $1, \ldots, n_\eta$. Therefore, m_η^2 and $\lambda_{3,4,5}$ are $n_\eta \times n_\eta$ matrices while λ_2 is an $n_\eta \times n_\eta \times n_\eta \times n_\eta$ object. Note that λ_5 must be symmetric whereas $\lambda_{3,4}$ must be Hermitian. Again, m_η^2 will be assumed to be diagonal without loss of generality. Finally, we highlight the presence of the scalar potential quartic couplings λ_5^{ab}, which play a major role in the neutrino mass generation mechanism, as shown in Section 7.3.

Similar to the minimal Scotogenic model, we will assume that the minimization of the scalar potential in Eq. (7.2) leads to the vacuum configuration

$$\left\langle H^0 \right\rangle = \frac{v}{\sqrt{2}} \quad , \quad \left\langle \eta_a^0 \right\rangle = 0\,, \tag{7.3}$$

with $a = 1, \ldots, n_\eta$. Therefore, only the neutral component of H acquires a non-zero vacuum expectation value, which breaks the electroweak symmetry in the standard way, while the η_a scalars are inert doublets with vanishing VEVs. In this way, the $\mathbb{Z}_2$ symmetry remains unbroken and the stability of the lightest $\mathbb{Z}_2$-charged particle is guaranteed. We will explore the possibility of $\mathbb{Z}_2$ breaking due to Renormalization Group Equations (RGEs) effects later.

In the following we will assume that all the parameters in the scalar potential are real, hence conserving CP in the scalar sector. In this case, the real and imaginary components of η_a^0,

$$\eta_a^0 = \frac{1}{\sqrt{2}} \left(\eta_{R_a} + i\, \eta_{I_a}\right) , \tag{7.4}$$

do not mix. After electroweak symmetry breaking, the $n_\eta \times n_\eta$ mass matrices for the real and imaginary components are given by

$$(\mathcal{M}_R^2)_{ab} = (m_\eta)_{aa}^2\, \delta_{ab} + \left(\lambda_3^{ab} + \lambda_4^{ab} + \lambda_5^{ab}\right) \frac{v^2}{2} \tag{7.5}$$

and

$$(\mathcal{M}_I^2)_{ab} = (m_\eta)_{aa}^2\, \delta_{ab} + \left(\lambda_3^{ab} + \lambda_4^{ab} - \lambda_5^{ab}\right) \frac{v^2}{2} , \tag{7.6}$$

respectively. We note that $\mathcal{M}_R^2 = \mathcal{M}_I^2$ in the limit $\lambda_5 \to 0$, in which all the elements of λ_5 vanish. This will be crucial in the calculation of neutrino masses, as shown below. Both mass matrices can be brought into diagonal form by means of a change of basis. The gauge eigenstates, η_{A_a}, are related to the mass eigenstates, $\hat{\eta}_{A_b}$, where $A = R, I$, by

$$\eta_A = V_A\, \hat{\eta}_A \, . \tag{7.7}$$

Here η_A and $\hat{\eta}_A$ are n_η-component vectors. In general, the $n_\eta \times n_\eta$ matrices V_A are unitary, such that $V_A V_A^\dagger = V_A^\dagger V_A = \mathbb{I}_{n_\eta}$, where $\mathbb{I}_{n_\eta}$ is the $n_\eta \times n_\eta$ identity matrix. However, in the simplified scenario of CP conservation in the scalar sector, $\mathcal{M}_R^2$ and $\mathcal{M}_I^2$ are real symmetric matrices, and then the V_A matrices are orthogonal, such that $V_A V_A^T = V_A^T V_A = \mathbb{I}_{n_\eta}$. With these transformations, the diagonal mass matrices are given by

$$\widehat{\mathcal{M}}_A^2 = \begin{pmatrix} m_{A_1}^2 & & 0 \\ & \ddots & \\ 0 & & m_{A_{n_\eta}}^2 \end{pmatrix} = V_A^T \mathcal{M}_A^2 V_A \, . \tag{7.8}$$

The resulting analytical expressions for the mass eigenvalues $m_{A_a}^2$ and mixing matrices V_A involve complicated combinations of the scalar potential parameters. However, under the assumptions[2]

[2]Note that this assumption is technically natural [155]: the smallness of λ_5 is not dynamically explained but is stable against RGE flow. This is due to the fact that the limit $\lambda_5 \to 0$ increases the symmetry of the model by restoring lepton number. Therefore, if λ_5 is set small at one scale it will remain small at all scales.

$$\lambda_{3,4}^{aa}\,\frac{v^2}{2} \ll \left(m_\eta^2\right)_{aa} \quad \text{and} \quad \lambda_5^{ab} \ll \lambda_{3,4}^{ab} \ll 1\,, \tag{7.9}$$

where $a \neq b$, one can find simple expressions. The $m^2_{A_a}$ mass eigenvalues are approximated by

$$m^2_{R_a} = \left(m_\eta^2\right)_{aa} + \left(\lambda_3^{aa} + \lambda_4^{aa} + \lambda_5^{aa}\right)\,\frac{v^2}{2}\,, \tag{7.10}$$

$$m^2_{I_a} = \left(m_\eta^2\right)_{aa} + \left(\lambda_3^{aa} + \lambda_4^{aa} - \lambda_5^{aa}\right)\,\frac{v^2}{2}\,. \tag{7.11}$$

We note that the mass splitting $m^2_{R_a} - m^2_{I_a} = \lambda_5^{aa}\,v^2$ vanishes in the limit $\lambda_5 \to 0$. In what concerns the V_A orthogonal matrices, each of them can be expressed as a product of $n_\eta(n_\eta-1)/2$ rotation matrices, with the scalar mixing angles given by

$$\tan 2\,\theta_A^{ab} = \frac{2\,(\mathcal{M}_A^2)_{ab}}{(\mathcal{M}_A^2)_{bb} - (\mathcal{M}_A^2)_{aa}} = \left(\lambda_3^{ab} + \lambda_4^{ab} + \kappa_A^2\,\lambda_5^{ab}\right)\,\frac{v^2}{m^2_{A_b} - m^2_{A_a}}\,, \tag{7.12}$$

where $a \neq b$ and the κ_A^2 sign ($\kappa_R^2 = +1$ and $\kappa_I^2 = -1$) has been introduced.

7.3 Neutrino masses

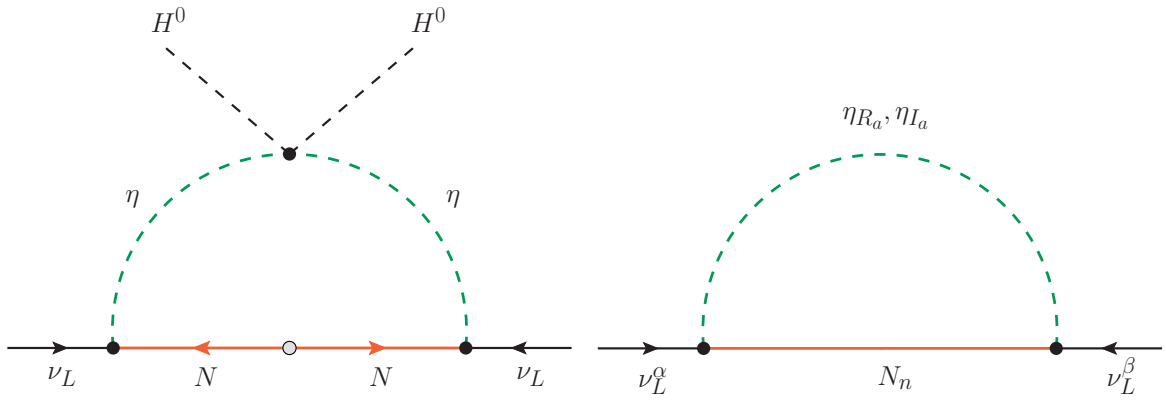

Figure 7.1: Neutrino mass generation. To the left, Feynman diagram with gauge eigenstates. To the right, the analogous Feynman diagram with the physical mass eigenstates that propagate in the loop.

The generation of neutrino masses takes place at the 1-loop level *à la scotogenic* [198, 199]. In the presence of the terms given in Eqs. (7.1) and (7.2), lepton number is explicitly broken by two units, hence inducing Majorana neutrino masses. Assuming that the potential is such that the η_a scalars do not get VEVs, see Eq. (7.3), neutrino masses are forbidden at tree-level. Nevertheless, they are induced at the 1-loop level, as shown in Fig. 7.1. Several diagrams contribute to the

neutrino mass matrix. Therefore, one can write

$$(m_\nu)_{\alpha\beta} = \sum_{A,a,n} \left(m_\nu^A\right)_{\alpha\beta}^{an} , \tag{7.13}$$

where $\left(m_\nu^A\right)_{\alpha\beta}^{an}$ is the contribution to $(m_\nu)_{\alpha\beta}$ generated by the $N_n - \eta_{A_a}$ loop, given by

$$-i\left(m_\nu^A\right)_{\alpha\beta}^{an} = C_{na\alpha}^A \int \frac{\mathrm{d}^D k}{(2\pi)^D} \frac{i}{k^2 - m_{A_a}^2} \frac{i\,(\not{k} + M_{N_n})}{k^2 - M_{N_n}^2}\, C_{na\beta}^A , \tag{7.14}$$

where $D = 4 - \varepsilon$ is the number of space-time dimensions, the external neutrinos are taken at rest and k is the momentum running in the loop. We note that the term proportional to $\not{k}$ does not contribute because it is odd in the loop momentum. $C_{na\alpha}^A$ is the $N_n - \eta_{A_a} - \nu_L^\alpha$ coupling, given by

$$C_{na\alpha}^A = i\,\frac{\kappa_A}{\sqrt{2}} \sum_b (V_A)_{ba}^*\, y_{nb\alpha} , \tag{7.15}$$

with $\kappa_R = 1$ and $\kappa_I = i$. Since we assume real parameters in the scalar sector, complex conjugation in V_A will be dropped in the following. Replacing Eq. (7.15) into Eq. (7.14) and introducing the standard Passarino-Veltman loop function B_0 [401],

$$B_0\left(0, m_{A_a}^2, M_{N_n}^2\right) = \Delta_\varepsilon + 1 - \frac{m_{A_a}^2 \log m_{A_a}^2 - M_{N_n}^2 \log M_{N_n}^2}{m_{A_a}^2 - M_{N_n}^2} , \tag{7.16}$$

where Δ_ε diverges in the limit $\varepsilon \to 0$, Eq. (7.13) becomes

$$(m_\nu)_{\alpha\beta} = -\frac{1}{32\pi^2} \sum_{A,a,b,c,n} M_{N_n}\, \kappa_A^2\, (V_A)_{ba}\, (V_A)_{ca}\, y_{nb\alpha}\, y_{nc\beta}\, B_0(0, m_{A_a}^2, M_{N_n}) . \tag{7.17}$$

Equation (7.17) constitutes our central result for the exact 1-loop neutrino mass matrix in the model. It is important to note that the divergent pieces cancel exactly. Indeed, the κ_A^2 factor implies that the term proportional to Δ_ε in Eq. (7.17) (see Eq. (7.16)) involves the combination

$$\sum_a \left[(V_R)_{ba}\ (V_R)_{ca} - (V_I)_{ba}\ (V_I)_{ca}\right] = \left(V_R\, V_R^T\right)_{bc} - \left(V_I\, V_I^T\right)_{bc} = \delta_{bc} - \delta_{bc} = 0 , \tag{7.18}$$

which vanishes due to the orthogonality of the V_A matrices, ensuring the cancellation of the divergent part of the B_0 functions. This was expected since the neutrino mass matrix is physical and therefore finite.

Equation (7.17) provides a simple analytical expression for the neutrino mass matrix. However, the dependence on the fundamental parameters of the model is not explicit. The neutrino mass matrix involves a product of V_A matrices and B_0 functions, both in general depending on the scalar potential parameters in a non-trivial way. Therefore, to clearly identify the role of these parameters, we will work under the assumptions in Eq. (7.9) and derive an approximate form for the neutrino mass matrix, valid for small values of the λ_5^{ab} couplings and small mixing

angles in the scalar sector. First, it is convenient to expand in powers of $\lambda_5^{ab} \ll 1$. One can write

$$(m_\nu)_{\alpha\beta} = -\frac{1}{32\pi^2}\sum_n M_{N_n} \sum_{a,b,c} y_{nb\alpha}\, y_{nc\beta} \Big\{ [(V)_{ba}\ (V)_{ca}]^{(0)} \left[B_0^{(1)}(0, m_{R_a}^2, M_{N_n}) - B_0^{(1)}(0, m_{I_a}^2, M_{N_n})\right] + [(V_R)_{ba}\ (V_R)_{ca} - (V_I)_{ba}\ (V_I)_{ca}]^{(1)}\ B_0^{(0)}(0, m_a^2, M_{N_n})\Big\} + \mathcal{O}\left(\lambda_5^2\right) , \tag{7.19}$$

where the superindex $^{(i)}$, with $i = 0, 1$, denotes the order in λ_5^{ab}. We highlight that since $\lambda_5 = 0$ would imply the restoration of lepton number and then massless neutrinos, the expansion begins at 1^{st} order in λ_5. With this in mind, the origin of the two terms in Eq. (7.19) is easy to understand. In the first term, the λ_5^{ab} couplings are neglected in the V_A matrices but kept at leading order in the B_0 functions. This term is proportional to the $B_0(0, m_{R_a}^2, M_{N_n}) - B_0(0, m_{I_a}^2, M_{N_n})$ difference, which would vanish for $\lambda_5^{aa} = 0$, see Eqs. (7.10) and (7.11). The mass matrices for the real and imaginary components of η^0 are equal at 0^{th} order in λ_5, $\widehat{\mathcal{M}}_R^{2\,(0)} = \widehat{\mathcal{M}}_I^{2\,(0)}$, and then we can define $V \equiv V_R^{(0)} = V_I^{(0)}$. In the second term, the λ_5^{ab} couplings are neglected in the B_0 functions but kept at leading order in the V_A mixing matrices. Since $m_{R_a}^{(0)} = m_{I_a}^{(0)} \equiv m_a$ at 0^{th} order in λ_5^{aa}, then the $B_0^{(0)}$ function has the argument

$$m_a^2 = \left(m_\eta^2\right)_{aa} + (\lambda_3^{aa} + \lambda_4^{aa})\ \frac{v^2}{2} . \tag{7.20}$$

We note that this term will only be non-zero when the λ_5 matrix contains non-vanishing off-diagonal entries, since this is the only way the $(V_R)_{ba}\ (V_R)_{ca} - (V_I)_{ba}\ (V_I)_{ca}$ would not vanish at 1st order in λ_5. Next, we find approximate expressions for the V_A mixing matrices. This is only feasible by assuming small scalar mixing angles, in agreement with Eq. (7.9). In this case one can expand V not only in powers of λ_5, but also in powers of the small parameter

$$s_{ab} = \frac{1}{2}\left(\lambda_3^{ab} + \lambda_4^{ab}\right)\frac{v^2}{m_b^2 - m_a^2} \ll 1 , \tag{7.21}$$

which is defined for $a \neq b$ and corresponds to $\sin\theta_R^{ab}$ or $\sin\theta_I^{ab}$ at 0^{th} order in λ_5, see Eq. (7.12). Note that the scenario we are considering does not include the possibility of degenerate masses in the scalar sector. With this definition, one finds the general expression $(V)_{ab} = \delta_{ab} + (1 - \delta_{ab})\, s_{ab} + \mathcal{O}\left(s^2\right)$. Analogous expressions are found for V_R and V_I replacing s by $\sin\theta_R$ and $\sin\theta_I$, respectively. With all these ingredients, Eq. (7.19) can be written as

$$(m_\nu)_{\alpha\beta} = \frac{v^2}{32\pi^2}\sum_{n,a,b}\frac{y_{na\alpha}\, y_{nb\beta}}{M_{N_n}}\,\Gamma_{abn} + \mathcal{O}\left(\lambda_5^2\right) + \mathcal{O}\left(\lambda_5\, s^2\right) , \tag{7.22}$$

where we have defined the dimensionless quantity

$$\Gamma_{abn} = \delta_{ab}\,\lambda_5^{aa}\, f_{an} - (1 - \delta_{ab})\left[\left(\lambda_5^{aa}\, f_{an} - \lambda_5^{bb}\, f_{bn}\right) s_{ab} - \frac{M_{N_n}^2}{m_b^2 - m_a^2}\,\lambda_5^{ab}\, g_{abn}\right] \tag{7.23}$$

and the loop functions

$$f_{an} = \frac{M_{N_n}^2}{m_a^2 - M_{N_n}^2} + \frac{M_{N_n}^4}{\left(m_a^2 - M_{N_n}^2\right)^2} \log \frac{M_{N_n}^2}{m_a^2} \,, \tag{7.24}$$

$$g_{abn} = \frac{m_a^2}{m_a^2 - M_{N_n}^2} \log \frac{M_{N_n}^2}{m_a^2} - \frac{m_b^2}{m_b^2 - M_{N_n}^2} \log \frac{M_{N_n}^2}{m_b^2} \,. \tag{7.25}$$

Eq. (7.22) involves the quantity Γ_{abn}, which we have written in Eq. (7.23) as the sum of two terms. The first term in Γ_{abn} contributes only for $a = b$ and involves only diagonal elements of λ_5. The second term, which involves diagonal as well as off-diagonal elements of λ_5, only contributes for $a \neq b$. We also note that $g_{abn} = -g_{ban}$.

Eq. (7.22) is the main analytical result of this chapter. Under the assumptions of Eq. (7.9), it reproduces the neutrino mass matrix in very good approximation. It is valid for any n_N and n_η values. We will now show how in some particular cases it reduces to well-known expressions in the literature.

7.3.1 Particular case 1: $(n_N, n_\eta) = (3, 1)$

Of course, the first example we consider is the standard Scotogenic model, which is obtained for $(n_N, n_\eta) = (3, 1)$. In this case, only one inert doublet η is introduced, resulting in all the matrices in the scalar sector becoming just scalar parameters. In particular, $V_A = 1$, $\lambda_5^{ab} \equiv \lambda_5^{11} \equiv \lambda_5$ and $(m_\eta^2)_{aa} \equiv (m_\eta^2)_{11} \equiv m_\eta^2$. Besides, the Yukawa couplings become 3×3 matrices: $y_{na\alpha} \equiv y_{n1\alpha} \equiv y_{n\alpha}$. Similarly, $f_{an} \equiv f_{1n} \equiv f_n$, and the second term in Eq. (7.23) does not contribute. These simplifications result in the general Γ_{abn} reducing to $\Gamma_n^{(3,1)}$, which is given by

$$\Gamma_{abn}^{(3,1)} \equiv \Gamma_{11n}^{(3,1)} \equiv \Gamma_n^{(3,1)} = \lambda_5 \, f_n \,. \tag{7.26}$$

Replacing this into Eq. (7.22), one obtains the well-known Scotogenic neutrino mass matrix that we derived in Section 2.5.2,

$$(m_\nu)_{\alpha\beta}^{(3,1)} = \frac{\lambda_5 \, v^2}{32\pi^2} \sum_n \frac{y_{n\alpha} \, y_{n\beta}}{M_{N_n}} \left[\frac{M_{N_n}^2}{m_0^2 - M_{N_n}^2} + \frac{M_{N_n}^4}{\left(m_0^2 - M_{N_n}^2\right)^2} \log \frac{M_{N_n}^2}{m_0^2} \right] , \tag{7.27}$$

with $m_0^2 = m_\eta^2 + (\lambda_3 + \lambda_4) \, v^2/2$.

7.3.2 Particular case 2: $(n_N, n_\eta) = (1, 2)$

Our second example is a variation of the Scotogenic model featuring one singlet fermion and two inert doublets, denoted by $(n_N, n_\eta) = (1, 2)$. This particular model has been previously explored in [399, 400]. Since the model contains only one singlet fermion N, $M_{N_n} \equiv M_N$ is just a parameter and the Yukawa couplings become 2×3 matrices: $y_{na\alpha} \equiv y_{1a\alpha} \equiv y_{a\alpha}$. Finally, $f_{na} \equiv f_{1a} \equiv f_a$ and $g_{abn} \equiv g_{ab1} \equiv g_{ab}$. Both references work in the basis in which the m_η^2 matrix

is diagonal. However, they take different simplifying assumptions about the scalar potential parameters.

In [399] the matrix $\lambda_3 + \lambda_4$ was assumed to be diagonal. In this case, which we denote as scenario $(1,2)_{\rm I}$, $(1-\delta_{ab})s_{ab} = 0$ and the general Γ_{abn} reduces to

$$\Gamma^{(1,2)\,\rm I}_{abn} \equiv \Gamma^{(1,2)\,\rm I}_{ab1} \equiv \Gamma^{(1,2)\,\rm I}_{ab} = \delta_{ab}\,\lambda_5^{aa}\,f_{an} + (1-\delta_{ab})\,\frac{M^2_{N_n}}{m_b^2 - m_a^2}\,\lambda_5^{ab}\,g_{abn}\,. \tag{7.28}$$

Replacing this expression into Eq. (7.22) and arranging the different pieces properly, one obtains

$$(m_\nu)^{(1,2)\,\rm I}_{\alpha\beta} = \frac{v^2}{32\pi^2}\sum_{a,b} y_{a\alpha}\,y_{b\beta}\,\lambda_5^{ab}\,\frac{M_N}{m_b^2 - M_N^2}\left[\frac{m_b^2}{m_a^2 - m_b^2}\log\frac{m_a^2}{m_b^2} - \frac{M_N^2}{m_a^2 - M_N^2}\log\frac{m_a^2}{M_N^2}\right], \tag{7.29}$$

which agrees with the result in [399] up to a global factor of 1/4.

On the other hand, a diagonal λ_5 matrix was taken in [400]. We denote this as scenario $(1,2)_{\rm II}$. Again, this simplifies Γ_{abn}, which becomes

$$\Gamma^{(1,2)\,\rm II}_{abn} \equiv \Gamma^{(1,2)\,\rm II}_{ab1} \equiv \Gamma^{(1,2)\,\rm II}_{ab} = \delta_{ab}\,\lambda_5^{aa}\,f_{an} - (1-\delta_{ab})\left(\lambda_5^{aa}\,f_{an} - \lambda_5^{bb}\,f_{bn}\right)\,s_{ab}\,. \tag{7.30}$$

With this result, one can easily use Eq. (7.22) to derive

$$(m_\nu)^{(1,2)\,\rm II}_{\alpha\beta} = \frac{v^2}{32\pi^2 M_N}\sum_{a,b,c} y_{a\alpha}\,y_{b\beta}\,\lambda_5^{cc}\,f_c\,X_{abc}\,, \tag{7.31}$$

with

$$X_{abc} = \delta_{ab}\delta_{bc} + \frac{1}{2}\,(1-\delta_{ab})\,(\delta_{c2} - \delta_{c1})\left(\lambda_3^{ab} + \lambda_4^{ab}\right)\frac{v^2}{m_b^2 - m_a^2}\,, \tag{7.32}$$

which agrees with the expression given in [400] if terms of order s_{12}^2 are neglected.

7.4 High-energy behavior

The conservation of the $\mathbb{Z}_2$ parity is a crucial aspect of the consistency of the Scotogenic model. In the absence of this symmetry, neutrinos would get masses at tree-level, and the DM candidate would no longer be stable. This motivates the study of the conservation of $\mathbb{Z}_2$ at high energies. This research was initiated in [402], which identified that the RGE flow in the Scotogenic model might alter the shape of the scalar potential at high energies leading to the breaking of $\mathbb{Z}_2$. Later works [403, 404] have extensively explored this issue, demonstrating that the $\mathbb{Z}_2$ parity breaking occurs in significant regions of the parameter space.

At the 1-loop order, the RGEs of a model can be written as

$$\frac{dx(t)}{dt} = \frac{1}{16\pi^2}\,\beta_x\,, \tag{7.33}$$

where $t \equiv \log \mu$, μ is the renormalization scale and β_x is the 1-loop β function for the parameter x. In our analysis, the full 1-loop running in the Scotogenic model with arbitrary numbers of N and η generations has been considered. Analytical expressions for all the 1-loop β functions have been derived with the help of `SARAH` [405–409]. [3] These have been included in a private code that solves the complete set of RGEs numerically.

We can understand some general features of the high-energy behavior of the model, and in particular of the possible breaking of the $\mathbb{Z}_2$ symmetry, by inspecting the 1-loop β functions for the m_η^2 matrix,

$$\left(\beta_{m_\eta^2}\right)_{ab} = -\frac{9}{10}\, g_1^2 \left(m_\eta^2\right)_{ab} - \frac{9}{2}\, g_2^2 \left(m_\eta^2\right)_{ab} + \sum_{c,d=1}^{n_\eta} \left[4\,\lambda_2^{abcd} \left(m_\eta^2\right)_{dc} + 2\,\lambda_2^{acdb} \left(m_\eta^2\right)_{cd}\right] + \left[4\,\lambda_3^{ab} + 2\,\lambda_4^{ab}\right] m_H^2 + \left(m_\eta^2\right)_{ab} \sum_{n=1}^{n_N} \sum_{\alpha=1}^{3} \left(|y_{na\alpha}|^2 + |y_{nb\alpha}|^2\right) - 4\,\mathrm{Tr}\left[y_a^\dagger M_N^* M_N y_b\right] . \tag{7.34}$$

Here $y_a \equiv [y_{na\alpha}]$ is a $n_N \times 3$ matrix, being the first index a singlet fermion family index and the third one a charged lepton family index. We have explicitly checked that for $n_N = 3$ and $n_\eta = 1$, Eq. (7.34) reduces to the m_η^2 β function in the standard Scotogenic model [402].

Eq. (7.34) extends the result previously derived in [402] and provides a general expression for the 1-loop β function for the m_η^2 matrix, valid for any combination of (n_N, n_η) values. To study the potential breaking of the $\mathbb{Z}_2$ symmetry, we need to examine the sign (positive or negative) of the individual contributions to the running of m_η^2. In this regard, the negative contribution of the term proportional to $\mathrm{Tr}\left[y_a^\dagger M_N^* M_N y_b\right]$ turns out to be crucial. In the following, we will refer to this term as *the trace term*. As demonstrated in [402] for the standard Scotogenic model, in cases where there are large Yukawa couplings (equivalent to $\lambda_5 \ll 1$) and $M_N^2 \gtrsim m_\eta^2$, the trace term dominates the m_η^2 running, causing it to decrease towards negative values. Eventually, this results in the breaking of the $\mathbb{Z}_2$ symmetry at high energies, once $m_\eta^2 < 0$ induces a minimum of the scalar potential with $\langle \eta \rangle \neq 0$. The general Scotogenic model is expected to exhibit the same behavior. However, other terms in Eq. (7.34) may counteract this effect. In particular, the quartic scalar coupling terms may do so if their signs are appropriately chosen. The contribution to the m_η^2 running will be positive for $\lambda_2 > 0$ and $\lambda_{3,4} < 0$ (since $m_H^2 < 0$), while their impact will otherwise reinforce that of the trace term.

We will now explore the scalar potential of the model at high energies by solving the full set of RGEs numerically. In order to do that we will concentrate on two specific (but representative) versions of the general Scotogenic model:

- The **(3, 1) model**, with three singlet fermions and one inert doublet. This is the original Scotogenic model [198, 199].
- The **(1, 3) model**, with one singlet fermion and three inert doublets.

[3] See [410] for a pedagogical introduction to the use of `SARAH` in the context of non-supersymmetric models.

To analyze the high energy behavior of our model parameters, we fix all their values at the electroweak scale, which we take to be the mass of the Z-boson, denoted as m_Z. Therefore, the inputs of all the parameters must be understood to hold at $\mu = m_Z$. We determine m_H^2 by solving the tadpole equations of the model and set the value of λ_1 to reproduce the measured Higgs boson mass. The remaining scalar potential parameters are chosen freely, but always to values that guarantee that the potential is bounded from below (BFB) at the electroweak scale. This is a non-trivial constraint due to the complexity of the scalar potential in the general Scotogenic model. For a detailed discussion on how we ensure boundedness from below, we refer to Appendix G. Finally, we must accommodate the neutrino squared mass differences and the leptonic mixing angles measured in neutrino oscillation experiments by properly fixing the Yukawa couplings of the model. In the two variants of the general Scotogenic model considered, the Yukawa couplings become 3×3 matrices, and then they can be obtained using a Casas-Ibarra parametrization properly adapted to both variants of the Scotogenic model, as explained in Section 2.5.3. The difference between both parametrizations lies in the definition of the matrix M introduced in Eq. (2.60). The case $(3,1)$, the standard Scotogenic model, was already discussed there and $M_{(3,1)}$ was defined in Eq. (2.64), while in the $(1,3)$ model, the matrix takes the form

$$M_{(1,3)} = \frac{v^2}{32\,\pi^2}\frac{\Gamma_{ab1}}{M_{N_1}}\,. \tag{7.35}$$

With these definitions, Eq. (2.62) ensures compatibility with neutrino oscillation data. We consider neutrino normal mass ordering and the $1\,\sigma$ ranges for the oscillation parameters obtained in the global fit [411], including the CP-violating phase δ, hence allowing for complex Yukawa couplings. For simplicity, we take $m_1 = 0$ and $R = \mathbb{1}_3$, with $\mathbb{1}_1$ the 3×3 identity matrix. We note, however, that in variants of the general Scotogenic model with both $n_N, n_\eta > 1$, which can be regarded as *hybrid scenarios*, the *master parametrization* [203, 204] must be used to parametrize the Yukawa tensor couplings, as can be seen in Appendix F of [204].

Some comments are in order before presenting our numerical results. In what follows, we explore several regions of the parameter spaces of the $(3,1)$ and $(1,3)$ Scotogenic models, with our focus on the behavior of these models at high energies. While there are many phenomenological directions of interest, our work is specifically motivated by the effects associated to the trace term. This motivates us to consider small λ_5 values ($\lambda_5^{aa} \leq 10^{-8}$). Larger λ_5 entries would require smaller y Yukawa couplings to accommodate the mass scales observed in neutrino oscillation experiments, see Eq. (7.22), hence making the trace term less relevant numerically. For this reason, all scenarios considered below have $y \sim \mathcal{O}(1)$. It should be noted that this choice of y may conflict with the current bounds on charged lepton flavor violating processes. However, there are many free parameters in the y Yukawa matrices. This freedom can be used to cancel the most constraining observables, for instance by choosing specific R matrices, without any impact on our discussion. Similarly, the scenarios considered below, and in particular the values chosen for the masses of the $\mathbb{Z}_2$-odd states, may not be compatible with the measured dark matter relic density.

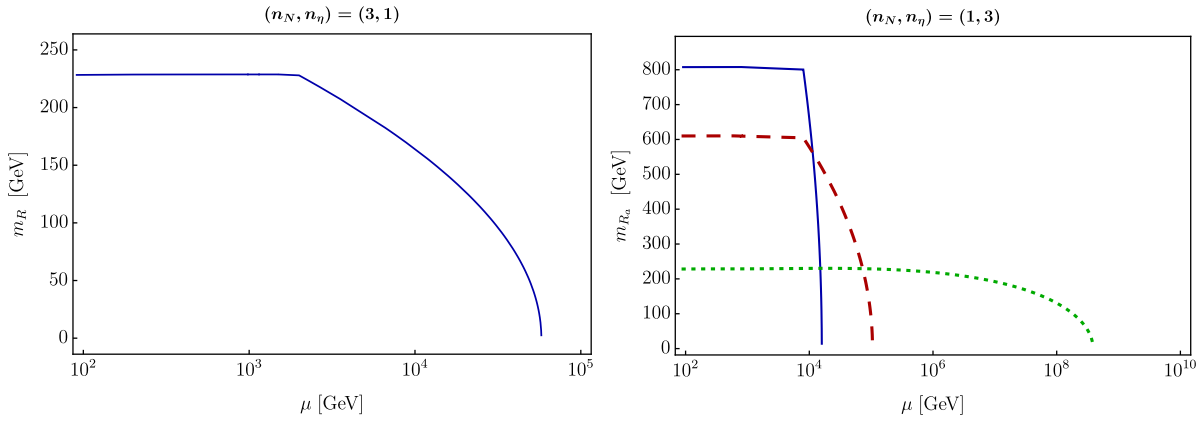

Figure 7.2: Evolution of the CP-even scalar masses as a function of the energy scale μ in the $(3,1)$ and $(1,3)$ Scotogenic models. To the left, the CP-even scalar mass m_R in the standard $(3,1)$ model with $M_N = (1, 1.5, 2)$ TeV, $\lambda_2 = \lambda_3 = \lambda_4 = 0.1$, $\lambda_5 = 10^{-9}$ and $m_\eta^2 = (200 \text{ GeV})^2$. To the right, the three CP-even scalar masses m_{R_a} in the $(1,3)$ model with $M_N = 8$ TeV, $\lambda_2^{aaaa} = \lambda_3^{aa} = \lambda_4^{aa} = 0.1$, $\lambda_5^{aa} = 10^{-9}$ and $m_\eta^2 = (200^2, 600^2, 800^2)$ GeV^2, with the remaining scalar parameters set to zero.

First, we have *rediscovered* the parity problem in the standard $(3,1)$ Scotogenic model. This is shown on the left-hand side of Fig. 7.2, which displays the RGE evolution of the CP-even scalar mass m_R with the energy scale μ. This is the most convenient parameter to study the breaking of the $\mathbb{Z}_2$ symmetry. When m_R^2 becomes negative, the lightest CP-even scalar becomes tachyonic, a clear sign that $\langle \eta \rangle = 0$ is not the minimum of the potential. We have checked that the scalar potential is BFB at all energy scales in this figure. We note that due to our parameter choices, the lightest singlet fermion, N_1, has vanishing Yukawa couplings. In particular, this is due to our choice $m_{\nu_1} = 0$. For the same reason, $y_{2\alpha} \ll y_{3\alpha}$ and the breaking of the parity is driven predominantly by N_3. This explains the drastic change in the evolution of m_R at $\mu = 2$ TeV when N_3 becomes active. Below this scale, N_3 effectively decouples and does not contribute to the RGE running. We point out that a much less pronounced change occurs at $\mu = 1.5$ TeV, when N_2 becomes active, but this is not visible in the figure. The $\mathbb{Z}_2$ parity gets broken at $\mu \simeq 60$ TeV, after which the η_R state becomes tachyonic. These results agree well with those found in [402] and confirm the possible breaking of $\mathbb{Z}_2$ in the original Scotogenic model. We found a very similar behavior for the $(1,3)$ model, which only has one singlet fermion, as shown on the right-hand side of Fig. 7.2. In this case, the three CP-even scalar masses m_{R_a} are displayed. Again, we have checked that the scalar potential is BFB at all energy scales in this figure. As in the case of the standard Scotogenic model, when one of the CP-even scalar masses reaches zero, the $\mathbb{Z}_2$ symmetry gets broken. As we can see in this figure, this happens at $\mu \simeq 15$ TeV, where one of the scalar masses (the one receiving the largest contribution from the trace term) goes very sharply towards zero due to the effect of the large $M_N = 8$ TeV value. This is clearly the same behavior observed in the standard $(3,1)$ Scotogenic model.

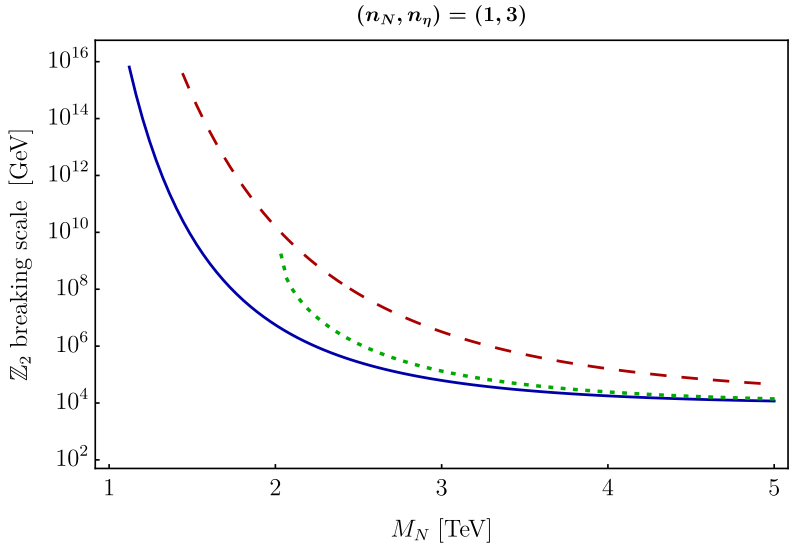

Figure 7.3: $\mathbb{Z}_2$ breaking scale as a function of the singlet fermion mass M_N in the $(1, 3)$ Scotogenic model for three different scenarios: $\lambda_2^{aaaa} = \lambda_3^{aa} = \lambda_4^{aa} = 0.1$ and $m_\eta^2 = (200^2, 300^2, 400^2)$ GeV^2 (blue), $\lambda_2^{aaaa} = \lambda_3^{aa} = \lambda_4^{aa} = 0.1$ and $m_\eta^2 = (200^2, 600^2, 800^2)$ GeV^2 (red, dashed), and $\lambda_2^{aaaa} = \lambda_2^{aabb} = \lambda_3^{aa} = \lambda_4^{aa} = 0.3$ and $m_\eta^2 = (200^2, 300^2, 400^2)$ GeV^2 (green, dotted). In the three cases $\lambda_5^{aa} = 10^{-9}$ and the remaining quartic parameters are set to zero.

In the following, we concentrate only on the $(1, 3)$ model. As already discussed, the singlet fermion mass M_N drives the scalar masses towards negative values via the trace term, breaking the $\mathbb{Z}_2$ parity at high energies. Fig. 7.3 shows the $\mathbb{Z}_2$ breaking scale as a function of M_N for several scalar parameter sets. The blue and red lines correspond to moderate values for the quartic couplings, $\lambda_2^{aaaa} = \lambda_3^{aa} = \lambda_4^{aa} = 0.1$, while the green line has increased (and additional) quartics, $\lambda_2^{aaaa} = \lambda_2^{aabb} = \lambda_3^{aa} = \lambda_4^{aa} = 0.3$. The λ_5 matrix is taken to be diagonal, with $\lambda_5^{aa} = 10^{-9}$. We have explicitly checked that the scalar potential is BFB at the electroweak scale in all scenarios. [4] As expected, the $\mathbb{Z}_2$ breaking scale decreases for larger M_N since the effect of the trace term becomes stronger. While different scalar potential couplings may alter the outcome, this generic behavior is found in large portions of the parameter space. One should notice, however, that the green curve begins at $M_N \simeq 2$ TeV. For this specific scenario, lower values of M_N do not break the $\mathbb{Z}_2$ symmetry, as we now proceed to discuss.

Fig. 7.4 shows the evolution of the lightest scalar mass m_{R_1} as a function of the energy for the parameter values corresponding to the green curve in Fig. 7.3. The results have been obtained for several values of M_N. It is important to note that this figure shows the mass of the lightest scalar at each energy scale and not the mass of a single mass eigenstate at all energies.

[4] We have allowed for (possible) non-BFB potentials at high energies, where some of the quartic couplings become negative due to running effects. We note that our algorithm gives us only sufficient (and not necessary) boundedness from below conditions, and in principle some of the possibly non-BFB potentials might actually be BFB. Moreover, even non-BFB potentials may be realistic if the electroweak vacuum is metastable and has a large enough lifetime. This issue is already present in the SM and is clearly beyond the scope of our analysis, which focuses on the possible breaking of the $\mathbb{Z}_2$ symmetry.

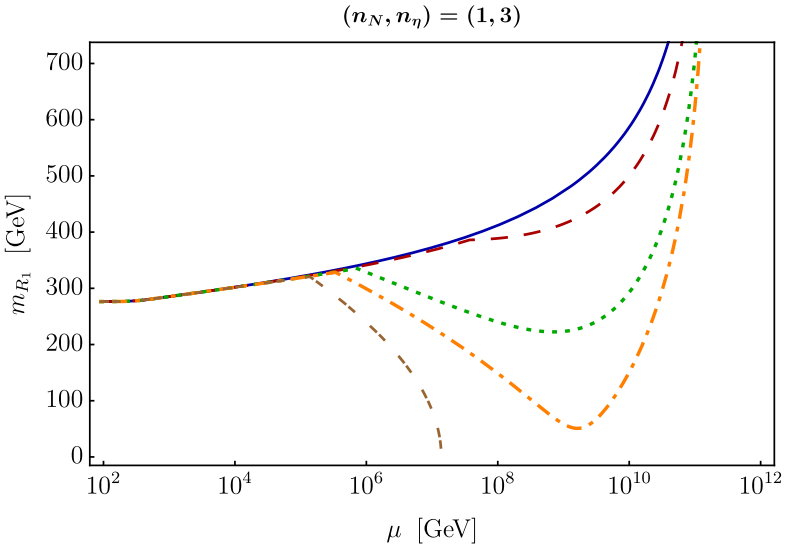

Figure 7.4: Evolution of the lightest scalar mass m_{R_1} as a function of the energy scale μ in the $(1,3)$ Scotogenic model. The scalar parameters are set to $\lambda_2^{aaaa} = \lambda_2^{aabb} = \lambda_3^{aa} = \lambda_4^{aa} = 0.3$, $\lambda_5^{aa} = 10^{-9}$ and $m_\eta^2 = (200^2, 300^2, 400^2)$ GeV^2, while M_N takes the values 1 TeV (blue), 1.5 TeV (red, dashed), 1.9 TeV (green, dotted), 2.025 TeV (orange, dash-dotted) and 2.2 TeV (brown, double dashed).

For $M_N = 2.2$ TeV one observes that m_{R_1} reaches zero and the $\mathbb{Z}_2$ symmetry gets broken at $\mu \simeq 10^7$ GeV, in accordance with Fig. 7.3. For lower M_N values, however, m_{R_1} never reaches zero. Although m_{R_1} gets initially decreased due to the effect of the trace term, it eventually increases at higher energies. The reason is the appearance of a Landau pole in the λ_2 quartic couplings. In this figure, $\lambda_2^{aaaa} = \lambda_2^{aabb} = 0.3$ at the electroweak scale, and this value grows with the energy until it completely dominates the m_η^2 β function with a positive contribution, see Eq. (7.34). The high multiplicity of λ_2 couplings reinforces the effect. We note that this Landau pole is present at very high energies, well above the $\mathbb{Z}_2$ breaking scale, for many choices of the parameters at the electroweak scale.

We conclude our exploration of the high-energy behavior of the $(1,3)$ model with Fig. 7.5. In this case, we plot the $\mathbb{Z}_2$ breaking scale as a function of one of the λ_2 parameters, namely λ_2^{2233}. This is done for three scenarios: the blue curve corresponds to $\lambda_2^{aaaa} = \lambda_3^{aa} = \lambda_4^{aa} = 0.1$, $\lambda_5^{aa} = 10^{-8}$, $m_\eta^2 = (200^2, 300^2, 400^2)$ GeV^2 and $M_N = 5$ TeV, in red we show the results for $\lambda_2^{aaaa} = \lambda_3^{aa} = \lambda_4^{aa} = 0.1$, $\lambda_5^{aa} = 10^{-9}$, $m_\eta^2 = (200^2, 250^2, 300^2)$ GeV^2 and $M_N = 1.25$ TeV, while the green line is for $\lambda_2^{aaaa} = \lambda_2^{aabb} = \lambda_3^{aa} = \lambda_4^{aa} = 0.3$, $\lambda_5^{aa} = 10^{-8}$, $m_\eta^2 = (200^2, 600^2, 800^2)$ GeV^2 and $M_N = 9$ TeV. In all cases, we have checked that the scalar potential is BFB at the electroweak scale. For the blue and green lines, the impact of λ_2^{2233} is relatively mild. This is because the high values of M_N (5 and 9 TeV, respectively) make the trace term completely dominant and break the $\mathbb{Z}_2$ symmetry at relatively low energies. In contrast, the $\mathbb{Z}_2$ breaking scale has a much stronger dependence on λ_2^{2233} in the red scenario, which has a lower $M_N = 1.25$ TeV. For $\lambda_2^{2233} \gtrsim 0.6$, a Landau pole is found *before* the $\mathbb{Z}_2$ symmetry gets broken.

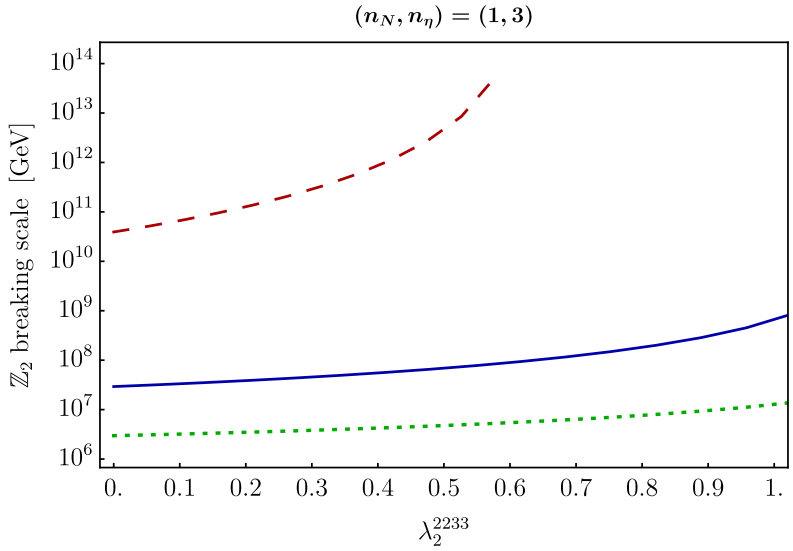

Figure 7.5: $\mathbb{Z}_2$ breaking scale as a function of the λ_2^{2233} parameter in the $(1,3)$ Scotogenic model for three different scenarios: $\lambda_2^{aaaa} = \lambda_3^{aa} = \lambda_4^{aa} = 0.1$, $\lambda_5^{aa} = 10^{-8}$, $m_\eta^2 = (200^2, 300^2, 400^2)$ GeV^2 and $M_N = 5$ TeV (blue), $\lambda_2^{aaaa} = \lambda_3^{aa} = \lambda_4^{aa} = 0.1$, $\lambda_5^{aa} = 10^{-9}$, $m_\eta^2 = (200^2, 250^2, 300^2)$ GeV^2 and $M_N = 1.25$ TeV (red, dashed), and $\lambda_2^{aaaa} = \lambda_2^{aabb} = \lambda_3^{aa} = \lambda_4^{aa} = 0.3$, $\lambda_5^{aa} = 10^{-8}$, $m_\eta^2 = (200^2, 600^2, 800^2)$ GeV^2 and $M_N = 9$ TeV (green, dotted). In the three cases the remaining quartic parameters are set to zero.

7.5 Summary and discussion

The Scotogenic model is a well-known radiative scenario to generate neutrino masses. The introduction of three singlet fermions and one inert scalar doublet, all charged under a new $\mathbb{Z}_2$ parity, leads to 1-loop Majorana neutrino masses and, as a bonus, provides a viable weakly-interacting dark matter candidate. In this chapter, we have considered a generalization of this setup to any number of generations of singlet fermions and inert doublets. After computing the 1-loop neutrino mass matrix in the general version of the model, both exactly and approximately, we have studied its high-energy behavior, focusing on two specific variants: the original Scotogenic model with $(n_N, n_\eta) = (3, 1)$ and a new multi-scalar variant with $(n_N, n_\eta) = (1, 3)$. Our main conclusion is that all the features of the original model are kept in the multi-scalar version, with some particularities due to the presence of a more involved scalar sector.

Our generalization of the Scotogenic model offers several novel possibilities. For instance, flavor model building could benefit from an interesting feature of multi-scalar versions of the model. In the $(n_N, n_\eta) = (1, 3)$ model, one obtains three massive neutrinos and leptonic mixing can be fully explained even if the Yukawa matrices are completely diagonal. In this case, the leptonic mixing matrix would be generated by mixing in the scalar sector. This could be relevant in some flavor models. For example, it may be a crucial ingredient to rescue models where lepton mixing is predicted to be similar to quark mixing. Novel phenomenological signatures might exist as well. The η doublets can be produced at the Large Hadron Collider due to their couplings to

the SM gauge bosons. Exotic signatures might be possible in models with many η generations, such as the $(n_N, n_\eta) = (1, 3)$ model. Cascade decays initiated by the production of the heaviest η doublets would lead to striking multilepton signatures, including missing energy due to the production of the lightest $\mathbb{Z}_2$-odd state at the end of the decay chain. Finally, the dark matter production rates in the early Universe might be affected as well by the presence of additional scalar degrees of freedom. These interesting questions certainly deserve further study.

Chapter 8

Ultraviolet extensions of the Scotogenic model

At this point in the thesis, we are rather familiar with the Scotogenic model [198, 199]. It is a well-founded and economical theory, and since its appearance, numerous models have been constructed based on it. Often just incorporating additional fields and/or symmetries to enhance its phenomenological appeal. This was precisely the case of the model proposed in Chapter 7, where we generalized it to include an arbitrary number of generations of the Scotogenic states. However, the minimal version of the theory encounters certain theoretical issues that can be accounted for by considering an ultraviolet completion of the model, as we will see below.

8.1 Introduction

In Chapter 2, we saw that radiative neutrino mass models provide a natural suppression for neutrino masses through loop factors. This is one of the main motivations in favor of this class of models. Moreover, some models introduce further suppression by assuming an approximate lepton number symmetry broken to a small extent by the presence of a Lagrangian term with a suppressed coefficient. This is the case of the Scotogenic model, which requires a small $\lambda_5 \ll 1$ quartic parameter to generate the correct size for neutrino masses with sizable Yukawa couplings. While this is technically valid and natural in the sense of 't Hooft [155], it also calls for an extension that explains the smallness of the λ_5 parameter, possibly relating it to the breaking of lepton number. The Scotogenic model was introduced in Section 2.5.2, and here we will follow the conventions that were set there.

In this chapter, based on [412,413], we consider ultraviolet (UV) extensions of the Scotogenic model that provide a natural explanation for the smallness of the λ_5 parameter and in which the $\mathbb{Z}_2$ parity of the model emerges at low energies from a spontaneously broken global U(1) lepton number symmetry. Here we classify all possible models with these features in which a low-energy Scotogenic model is obtained after integrating out a heavy field at tree-level. Besides one or

several massive scalars, the particle spectrum of the theory will contain a massless Goldstone boson, the *majoron* [206–209], induced by the spontaneous breaking of lepton number. These new states are not present in the original Scotogenic model and lead to novel phenomenological predictions that allow one to probe our setup.

8.2 Ultraviolet extensions of the Scotogenic model

8.2.1 General considerations

The Scotogenic model has two features that call for a refinement, namely, the origin of the $\mathbb{Z}_2$ symmetry and $\lambda_5 \ll 1$. Although these features do not pose any theoretical problem, they can be regarded as ad-hoc ingredients in an otherwise very natural framework. We are thus interested in an UV extension of the Scotogenic model that provides an explanation for them. More specifically, we want to classify all possible UV scenarios that lead to the Scotogenic model at low energies after integrating out a heavy scalar field S, with $m_S \gg v$, and that satisfy the following two requirements:

(A) The Scotogenic $\mathbb{Z}_2$ is obtained as a remnant after the spontaneous breaking of a $\mathrm{U}(1)_\mathrm{L}$ lepton number symmetry by the VEV of one or several singlet scalar fields σ:

$$\mathrm{U}(1)_\mathrm{L} \xrightarrow{\langle\sigma\rangle} \mathbb{Z}_2$$

(B) The $(H^\dagger\eta)^2$ operator is forbidden in the UV theory due to $\mathrm{U}(1)_\mathrm{L}$ conservation, but an operator of the form $(H^\dagger\eta)^2\sigma^n$, with $n \geq 1$, is generated after integrating out S. After the singlets get VEVs and $\mathrm{U}(1)_\mathrm{L}$ is spontaneously broken, this will induce an effective λ_5 coupling, which will be naturally suppressed by the large m_S energy scale.

Here we will concentrate on global $\mathrm{U}(1)_\mathrm{L}$ lepton number symmetries, tree-level completions of the λ_5 operator, and UV models with one or two σ singlets. Gauged versions of the lepton number symmetry, higher-order completions, and models with additional singlets are left for future work.

The models we are looking for induce neutrino masses *à la Scotogenic*, with variations of the neutrino mass diagram in Fig. 2.5. This diagram has an internal scalar line (with η^0) and an internal fermion line (with N). The analogous diagrams in the UV extended models will include the heavy scalar S in the loop and one or several external legs with σ singlets (or σ insertions, for short). After these considerations, there are two classes of models that can be already discarded:

- Models without σ insertions in the scalar line. These models can be discarded because the $(H^\dagger\eta)^2$ operator would be allowed in the UV theory. This would preclude an explanation of $\lambda_5 \ll 1$. In addition, $H^\dagger\eta$ would also be allowed and η would acquire a VEV.

- Models without σ insertions in the fermion line. The $\mathrm{U}(1)_{\mathrm{L}}$ charge of the N singlet fermions must necessarily vanish if the $\sigma\overline{N}^{c}N$ operator is absent and their Majorana masses are explicitly introduced in the Lagrangian. However, in this case, N will be even under the $\mathbb{Z}_2$ symmetry obtained after spontaneous $\mathrm{U}(1)_{\mathrm{L}}$ breaking. This scenario does not correspond to the Scotogenic model. Nevertheless, an additional accidental $\mathbb{Z}_2$ symmetry may appear, as explained in Appendix H.

Topology	Diagram	Required operators
I	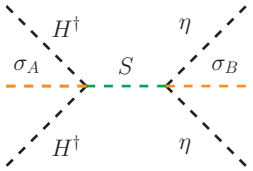	$(\sigma_A H^\dagger S\tilde{H}),(\sigma_B\tilde{\eta}^\dagger S^\dagger\eta)$
II	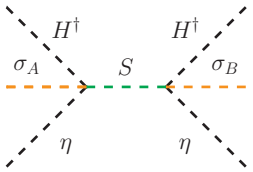	$(\sigma_A H^\dagger S\eta),(\sigma_B H^\dagger S^\dagger\eta)$
III	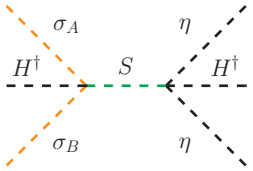	$(\sigma_A\sigma_B H^\dagger S),(H^\dagger\eta S^\dagger\eta)$
IV	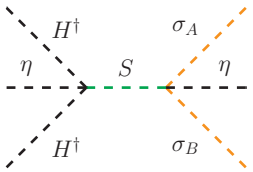	$(H^\dagger S H^\dagger\eta),(\sigma_A\sigma_B S^\dagger\eta)$
V	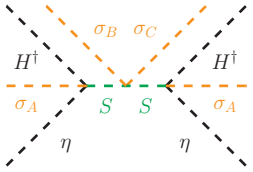	$(\sigma_A H^\dagger S\eta),((S^\dagger)^2\sigma_B\sigma_C)$

Table 8.1: λ_5 operator in the UV theory.

We are thus left with neutrino mass topologies with σ insertions in both internal lines. The scalar line leads to an operator $(H^\dagger\eta)^2\sigma^n$ after the heavy S is integrated out. All possible topologies are shown in Table 8.1. Topologies I – IV include one S propagator and lead to a λ_5 operator of the form

$$\mathcal{O}_{\lambda_5} = (H^\dagger\eta)^2\sigma_A\sigma_B\,, \tag{8.1}$$

suppressed by $1/m_S^2$, while topology V includes two S propagators and induces the operator

$$\mathcal{O}_{\lambda_5} = (H^\dagger \eta)^2 \sigma_A^2 \sigma_B \sigma_C \,, \tag{8.2}$$

suppressed by $1/m_S^4$. These two generic expressions for the λ_5 operator include cases in which one of the σ insertions is missing (for instance, $\sigma_B = \emptyset$, where $\emptyset$ indicates that no σ enters the corresponding vertex) and cases in which several σ insertions in the scalar line correspond to the same field (for instance, $\sigma_A = \sigma_B$). Finally, the fermion line simply corresponds to a $\sigma - N - N$ Yukawa interaction. In the following, we will always assume the presence of the operator $\sigma \overline{N}^c N$ (for models with one σ field) or $\sigma_1 \overline{N}^c N$ (for models with two σ fields), and we will not draw it. The coefficient of this operator will be denoted by κ. Therefore, once the singlet scalar gets a VEV, $\langle \sigma_{(1)} \rangle = \frac{v_{\sigma_{(1)}}}{\sqrt{2}}$, the Majorana mass matrix for the singlet fermions N is generated, [1]

$$M_N = \sqrt{2}\, \kappa\, v_{\sigma_{(1)}} \,. \tag{8.3}$$

In the following, we classify all possible UV extensions of the Scotogenic model compatible with our requirements (A) and (B). Given their qualitative differences, we discuss topologies I − IV and V separately.

8.2.2 Topologies I-IV

We first discuss the models based on topologies I−IV. We will refer to a specific model using the notation $\xi(A, B)$, where $\xi = \{\mathrm{I}, \mathrm{II}, \mathrm{III}, \mathrm{IV}\}$ denotes the topology for the $(H^\dagger \eta)^2 \sigma_A \sigma_B$ operator, as listed in Table 8.1, and A and B denote the singlets involved in the vertices where $\sigma_{A,B}$ are coupled. Since we only consider UV theories with at most two different singlets, A and B can only take the values $\emptyset, 1, 2, 1^*$, where $\sigma_{1^*} \equiv \sigma_1^*$. It is important to mention that we do not consider scenarios with $A, B = 2^*$ because they lead to a redefinition of the charge $q_{\sigma_2} \to -q_{\sigma_2}$. [2] Therefore, in principle each topology has 16 different variations depending on the way the $\sigma_{A,B}$ singlets are coupled. However, we can reduce this number by taking into account the following arguments:

- $A \neq B$ is required to forbid the term $(H^\dagger \eta\, \sigma_A)^2$ in the effective Lagrangian. If this specific combination is allowed, then the term $(H^\dagger \eta\, \sigma_A)$ is too. This trilinear interaction induces a non-zero VEV for η after both H and σ_A acquire their VEVs, hence breaking the Scotogenic $\mathbb{Z}_2$ symmetry.
- $A \neq B^*$ is also required. Otherwise, $(H^\dagger \eta)^2 \sigma_A \sigma_A^*$ is allowed by the $\mathrm{U}(1)_\mathrm{L}$ symmetry and then the operator $(H^\dagger \eta)^2$ is present in the UV theory.

[1] In models with two σ fields such that $q_{\sigma_1} = q_{\sigma_2}$ or $q_{\sigma_1} = -q_{\sigma_2}$, an additional Yukawa term $\sigma_2 \overline{N}^c N$ or $\sigma_2^* \overline{N}^c N$ would be present. Here q_{σ_1} and q_{σ_2} denote the $\mathrm{U}(1)_\mathrm{L}$ charges of σ_1 and σ_2, respectively. This would lead to $M_N = \sqrt{2}\,(\kappa_1\, v_{\sigma_1} + \kappa_2\, v_{\sigma_2})$ without affecting our discussion. We note, however, that in such models, both σ singlets are essentially copies of the same field.

[2] In the following, we will denote the $\mathrm{U}(1)_\mathrm{L}$ charge of the field X as q_X. Furthermore, $q_{\ell_L} = q_{e_R} = 1$ and $q_H = 0$, as usual.

	Topology	A	B	q_N	q_η	q_{σ_1}	q_{σ_2}	q_S	$(\mathrm{SU(2)_L, U(1)_Y})_S$
1	I	1^*	$\emptyset$	$\frac{1}{2}$	$-\frac{1}{2}$	-1	-	-1	$(\mathbf{3},1)$
2	I	$\emptyset$	1^*	$\frac{1}{2}$	$-\frac{1}{2}$	-1	-	0	$(\mathbf{3},1)$
3	I	2	$\emptyset$	q_N	q_N-1	$-2q_N$	$2-2q_N$	$2q_N-2$	$(\mathbf{3},1)$
4	I	$\emptyset$	2	q_N	q_N-1	$-2q_N$	$2-2q_N$	0	$(\mathbf{3},1)$
5	I	1	2	q_N	q_N-1	$-2q_N$	2	$2q_N$	$(\mathbf{3},1)$
6	I	2	1	q_N	q_N-1	$-2q_N$	2	-2	$(\mathbf{3},1)$
7	I	1^*	2	q_N	q_N-1	$-2q_N$	$2-4q_N$	$-2q_N$	$(\mathbf{3},1)$
8	I	2	1^*	q_N	q_N-1	$-2q_N$	$2-4q_N$	$4q_N-2$	$(\mathbf{3},1)$
9-10	II	1^*	$\emptyset$	$\frac{1}{2}$	$-\frac{1}{2}$	-1	-	$-\frac{1}{2}$	$(\mathbf{3},0)$ or $(\mathbf{1},0)$
11-12	II	2	$\emptyset$	q_N	q_N-1	$-2q_N$	$2-2q_N$	q_N-1	$(\mathbf{3},0)$ or $(\mathbf{1},0)$
13-14	II	1	2	q_N	q_N-1	$-2q_N$	2	$1+q_N$	$(\mathbf{3},0)$ or $(\mathbf{1},0)$
15-16	II	1^*	2	q_N	q_N-1	$-2q_N$	$2-4q_N$	$1-3q_N$	$(\mathbf{3},0)$ or $(\mathbf{1},0)$
17	III	1^*	$\emptyset$	$\frac{1}{2}$	$-\frac{1}{2}$	-1	-	-1	$(\mathbf{2},1/2)$
18	III	2	$\emptyset$	q_N	q_N-1	$-2q_N$	$2-2q_N$	$2q_N-2$	$(\mathbf{2},1/2)$
19	III	1	2	q_N	q_N-1	$-2q_N$	2	$2q_N-2$	$(\mathbf{2},1/2)$
20	III	1^*	2	q_N	q_N-1	$-2q_N$	$2-4q_N$	$2q_N-2$	$(\mathbf{2},1/2)$
21	IV	1^*	$\emptyset$	$\frac{1}{2}$	$-\frac{1}{2}$	-1	-	$\frac{1}{2}$	$(\mathbf{2},1/2)$
22	IV	2	$\emptyset$	q_N	q_N-1	$-2q_N$	$2-2q_N$	$1-q_N$	$(\mathbf{2},1/2)$
23	IV	1	2	q_N	q_N-1	$-2q_N$	2	$1-q_N$	$(\mathbf{2},1/2)$
24	IV	1^*	2	q_N	q_N-1	$-2q_N$	$2-4q_N$	$1-q_N$	$(\mathbf{2},1/2)$

Table 8.2: UV extended models satisfying conditions (A) and (B). For each model we show the $\mathrm{U(1)_L}$ charges of N, η, σ_1, σ_2 and S, as well as the $(\mathrm{SU(2)_L, U(1)_Y})$ representation of S. Models that become any of the models in this list after renaming the fields or redefining their $\mathrm{U(1)_L}$ charges are not included, as explained in the text.

- In all $\xi(1,\emptyset)$ and $\xi(\emptyset,1)$ models the effective operator leading to the λ_5 coupling is $\mathcal{O}_{\lambda_5} = (H^\dagger\eta)^2\sigma$. This implies the relation $2q_\eta + q_\sigma = 0$. In addition, the Yukawa coupling $\sigma\overline{N}^c N$ implies $2q_N + q_\sigma = 0$. Hence, the charges for η and N must satisfy $q_\eta = q_N$ and then the $\overline{N}\tilde{\eta}^\dagger\ell_L$ Yukawa term is forbidden by $\mathrm{U(1)_L}$. Similarly, in all $\xi(1^*,\emptyset)$ and $\xi(\emptyset,1^*)$ models one finds $q_\eta = -q_N$ and then $q_N = \frac{1}{2}$ is required in order to allow the term $\overline{N}\tilde{\eta}^\dagger\ell_L$.

With these considerations, there are only 8 possibilities left in each of the four topologies. However, there are duplicities. Models based on topologies III and IV are symmetric with respect to the exchange $\sigma_A \leftrightarrow \sigma_B$ (i.e. $\xi(A,B) = \xi(B,A)$ with $\xi = \mathrm{III, IV}$). Similarly, $\mathrm{II}(A,B) \sim$

II(B,A) by redefining $q_S \to -q_S$. This further reduces the number of fundamentally different UV models. In total, we find 24 (20 + 4, because in II-models, S can be an $\mathrm{SU}(2)_\mathrm{L}$ singlet or triplet) different UV theories. They are listed in Table 8.2, where the $\mathrm{U}(1)_\mathrm{L}$ charges of N, η, $\sigma_{A,B}$ and S, as well as the $(\mathrm{SU}(2)_\mathrm{L}, \mathrm{U}(1)_\mathrm{Y})$ representation of S in each model, are shown. Some comments are in order:

(i) The $(\mathrm{SU}(2)_\mathrm{L}, \mathrm{U}(1)_\mathrm{Y})$ representation of the heavy scalar S depends on the topology. In I-models S transforms as $(\mathbf{3}, 1)$, in II-models we have two possibilities, $(\mathbf{3}, 0)$ or $(\mathbf{1}, 0)$, while in III- and IV-models S transforms as $(\mathbf{2}, 1/2)$.

(ii) In all the models in Table 8.2, the global $\mathrm{U}(1)_\mathrm{L}$ symmetry may be spontaneously broken to a $\mathbb{Z}_2$ parity, under which N and η are odd. In all the $\xi(1^*, \emptyset)$ models and in I$(\emptyset, 1^*)$, the conservation of $\mathrm{U}(1)_\mathrm{L}$ restricts the lepton number charges of N, η, $\sigma_{A,B}$ and S, which must take precise values, and this automatically implies a remnant $\mathbb{Z}_2$ that corresponds to the usual Scotogenic parity. In the rest of the models, the conservation of $\mathrm{U}(1)_\mathrm{L}$ leaves one of the charges to be chosen freely. We decided to choose q_N. In this case, these are the restrictions to recover the *dark* $\mathbb{Z}_2$ parity from $\mathrm{U}(1)_\mathrm{L}$ breaking:

- q_N cannot be an integer.
- If $q_N = \frac{\alpha}{\beta}$, with $\alpha, \beta \in \mathbb{Z}$, then α and β have to be odd and even, respectively.
- $\mathrm{GCD}(\alpha, \beta) = 1$, where GCD stands for Greatest Common Divisor. Therefore, α and β must be coprime.

The first restriction comes from the requirement of N and η being both odd under the remnant Scotogenic $\mathbb{Z}_2$. The relation $q_\eta = q_N - 1$ implies that if q_N is even, then q_η must be odd, and vice versa. Then, N and η will transform differently under the remnant $\mathbb{Z}_2$ symmetry. As an example of this, consider the model I$(1, 2)$ with $q_N = 2$. In this case, the solution for the rest of the $\mathrm{U}(1)_\mathrm{L}$ charges in the model is $q_\eta = 1, q_{\sigma_1} = -4, q_{\sigma_2} = 2$ and $q_S = 4$. The global lepton number symmetry gets spontaneously broken as $\mathrm{U}(1)_\mathrm{L} \to \mathbb{Z}_2$, but with N and η charged under $\mathbb{Z}_2$ as $+$ and $-$, respectively, and this does not reproduce the Scotogenic model. Similarly, if $q_N = \frac{\alpha}{\beta}$, after normalizing all $\mathrm{U}(1)_\mathrm{L}$ charges so that they become integer numbers (multiplying by β) we obtain $\tilde{q}_\eta = \beta - \alpha$ and $\tilde{q}_N = \alpha$. Hence, for η and N to be odd under $\mathbb{Z}_2$, α and β must be odd and even, respectively. Finally, the third restriction is required to guarantee that $n = 2$ after $\mathrm{U}(1)_\mathrm{L}$ breaks to the discrete symmetry $\mathbb{Z}_n$. As an example we take model I(1,2), where $n \equiv \mathrm{GCD}(\tilde{q}_{\sigma_1}, \tilde{q}_{\sigma_2}, \tilde{q}_S) = \mathrm{GCD}(-2\alpha, 2\beta, 2\alpha) = 2\,\mathrm{GCD}(\alpha, \beta) = 2$. We checked for all the working models that $\mathrm{GCD}(\tilde{q}_{\sigma_1}, \tilde{q}_{\sigma_2}, \tilde{q}_S)$ or $\mathrm{GCD}(\tilde{q}_{\sigma_1}, \tilde{q}_{\sigma_2})$, depending on whether S acquires a VEV or not, always reduces to $\mathrm{GCD}(\alpha, \beta) = 1$. Also, we want $q_N = \frac{\alpha}{\beta}$ to be irreducible.

(iii) In all models, and for all possible values of q_N in agreement with the restrictions listed in the previous item, η never acquires an induced VEV. This is crucial for the consistency of the Scotogenic model.

(iv) It is clear that in all models of the form $\xi(A,\emptyset)$ or $\xi(\emptyset,B)$, a trilinear coupling μ participates in the generation of the λ_5 coupling, induced after the breaking of $\mathrm{U}(1)_\mathrm{L}$. This is perfectly consistent but requires the assumption $\mu \ll m_S$ to justify $\lambda_5 \ll 1$. This poses a theoretical issue, since μ is a parameter of the UV theory. In contrast, in models of the form $\xi(A,B)$ with $A,B \neq \emptyset$, the λ_5 coupling will only depend on the $\sigma_{A,B}$ VEVs, induced at low energies and naturally small compared to m_S.

(v) Finally, we note that in I-models, the $\mathrm{U}(1)_\mathrm{L}$ charges of the particles N, η and $\sigma_{A,B}$ remain the same after the non-trivial change $A \leftrightarrow B$. For instance, this is the case in models $\mathrm{I}(1,2)$ and $\mathrm{I}(2,1)$.

8.2.3 Topology V

Topology V contains an internal line with a double S propagator and thus induces the λ_5 coupling at order $1/m_S^4$. This is two orders higher than the corresponding contributions from topologies $\mathrm{I}-\mathrm{IV}$. Therefore, in order for a diagram with topology V to be dominant, other topologies must be absent (or highly suppressed due to a specific parameter choice). In fact, many models leading to topology V also generate other topologies, and they have been already included in the previous discussion. Nevertheless, there are also some models in which the symmetries allow for topology V but forbid other topologies, as we proceed to show.

Topology V requires the presence of the operators $H^\dagger \eta\, S\, \sigma_A$ and $\left(S^\dagger\right)^2 \sigma_B \sigma_C$ to produce a λ_5 operator as in Eq. (8.2). A model based on this topology will be denoted as $\mathrm{V}(A,B,C)$, where A, B, and C can take the values $\emptyset, 1, 2, 1^*$, as in the previous topologies. Again, we do not consider models with $A,B,C = 2^*$. The reason, however, is twofold. On the one hand, in scenarios involving 2^* but not 2, this is again due to the existence of a redefinition of the charges that allows showing equivalence to models without 2^*. On the other hand, models combining 2 and 2^* do not lead to a solution for the $U(1)_\mathrm{L}$ charges or their solutions are compatible with topology II, which is naturally dominant. [3] In conclusion, topology V leads to $4 \times 4 \times 4 = 64$ different variations depending on the way the $\sigma_{A,B,C}$ singlets are coupled. However, we can reduce this number by taking into account the following arguments:

- All V models are symmetric under $B \leftrightarrow C$, $\mathrm{V}(A,B,C) = \mathrm{V}(A,C,B)$. Then, for each of the 4 possible values of A, this removes $(4^2-4)/2 = 6$ possibilities, leaving 40 variations.

- $B \neq C$ and $B \neq C^*$. The former is required to forbid the operator $S^\dagger \sigma_B$. This would induce a VEV for S, which, in turn, would induce a VEV for η due to the operator $H^\dagger \eta\, S\, \sigma_A$. The latter restriction avoids having $S^\dagger S^\dagger$ in the Lagrangian since this term would imply that S is a singlet under every symmetry of the model, hence leading to an induced VEV for η as well. This condition, together with the previous one, leaves $4 \times [(4^2+4)/2 - 4 - 1] = 20$ possibilities.

[3] This is the case of models $\mathrm{V}(2,2^*,C)$ and $\mathrm{V}(2,B,2^*)$. These are not equivalent to models $\mathrm{V}(2,2,C)$ and $\mathrm{V}(2,B,2)$, respectively, so they do not lead to just a redefinition of the charges.

	Topology	A	B	C	q_N	q_η	q_{σ_1}	q_{σ_2}	q_S	$(\mathrm{SU(2)_L}, \mathrm{U(1)_Y})_S$
25-26	V	1	1	$\emptyset$	$-\frac{1}{2}$	$-\frac{3}{2}$	1	-	$\frac{1}{2}$	$(\mathbf{3},0)$ or $(\mathbf{1},0)$
27-28	V	1^*	1^*	$\emptyset$	$\frac{1}{4}$	$-\frac{3}{4}$	$-\frac{1}{2}$	-	$\frac{1}{4}$	$(\mathbf{3},0)$ or $(\mathbf{1},0)$
29-30	V	$\emptyset$	1	2	q_N	q_N-1	$-2q_N$	2	$1-q_N$	$(\mathbf{3},0)$ or $(\mathbf{1},0)$
31-32	V	$\emptyset$	1^*	2	q_N	q_N-1	$-2q_N$	$2-4q_N$	$1-q_N$	$(\mathbf{3},0)$ or $(\mathbf{1},0)$
33-34	V	1	2	$\emptyset$	q_N	q_N-1	$-2q_N$	$2q_N+2$	$1+q_N$	$(\mathbf{3},0)$ or $(\mathbf{1},0)$
35-36	V	1^*	2	$\emptyset$	q_N	q_N-1	$-2q_N$	$2-6q_N$	$1-3q_N$	$(\mathbf{3},0)$ or $(\mathbf{1},0)$
37-38	V	1	1	2	q_N	q_N-1	$-2q_N$	$4q_N+2$	$1+q_N$	$(\mathbf{3},0)$ or $(\mathbf{1},0)$
39-40	V	1^*	1^*	2	q_N	q_N-1	$-2q_N$	$2-8q_N$	$1-3q_N$	$(\mathbf{3},0)$ or $(\mathbf{1},0)$
41-42	V	2	1	$\emptyset$	q_N	q_N-1	$-2q_N$	1	$-q_N$	$(\mathbf{3},0)$ or $(\mathbf{1},0)$
43-44	V	2	1^*	$\emptyset$	q_N	q_N-1	$-2q_N$	$1-2q_N$	q_N	$(\mathbf{3},0)$ or $(\mathbf{1},0)$
45-46	V	2	2	$\emptyset$	q_N	q_N-1	$-2q_N$	$\frac{2}{3}-\frac{2}{3}q_N$	$\frac{1}{3}-\frac{1}{3}q_N$	$(\mathbf{3},0)$ or $(\mathbf{1},0)$
47-48	V	2	1	2	q_N	q_N-1	$-2q_N$	$\frac{2}{3}$	$\frac{1}{3}-q_N$	$(\mathbf{3},0)$ or $(\mathbf{1},0)$
49-50	V	2	1^*	2	q_N	q_N-1	$-2q_N$	$\frac{2}{3}-\frac{4}{3}q_N$	$\frac{1}{3}+\frac{1}{3}q_N$	$(\mathbf{3},0)$ or $(\mathbf{1},0)$

Table 8.3: UV extended models leading to topology V and satisfying conditions (A) and (B). For each model we show the $\mathrm{U(1)_L}$ charges of N, η, σ_1, σ_2 and S, as well as the $(\mathrm{SU(2)_L}, \mathrm{U(1)_Y})$ representation of S. Models that become any of the models in this list after renaming the fields or redefining their $\mathrm{U(1)_L}$ charges are not included, as explained in the text.

- $A \neq B^*$ (or C^*) leads either to models for which the equations for the charges are incompatible with the original assumptions or to models for which the solutions for the charges are compatible with topology II. Here $\mathcal{O}_{\lambda_5}$ takes the form $(\sigma_A^*\sigma_A)\sigma_A\sigma_C(H^\dagger\eta)^2$, which means that the term $\sigma_A\sigma_C(H^\dagger\eta)^2$ would be allowed by lepton number and, in turn, $\sigma_C(H^\dagger S^\dagger\eta)$ too, with $C \neq A$ in order to satisfy the above requirements. Given that, by construction, we have the operator $\sigma_A(H^\dagger S\eta)$ within the model, the diagram for the scalar line of II-models (shown in Table 8.1) would appear, leaving this new topology as a subdominant effect in the generation of the λ_5 coupling. From the remaining 20 variations, this removes 2 for each $A = 1$ and $A = 1^*$, and 3 more for the models $\mathrm{V}(\emptyset, B, \emptyset)$, leaving 13 possibilities.

Notice that S can be a singlet and a triplet in all the models, so we have the 26 models shown in Table 8.3. Again, we note that if only one of the three A, B, or C labels is equal to 2, then the same model but with 2^* instead, is equivalent to the former with $q_{\sigma_2} \to -q_{\sigma_2}$.

Again, in all the models in Table 8.3, the global $\mathrm{U(1)_L}$ symmetry may be spontaneously broken to a $\mathbb{Z}_2$ parity, under which N and η are odd. In the models $\mathrm{V}(1,1,\emptyset)$ and $\mathrm{V}(1^*,1^*,\emptyset)$, the conservation of $\mathrm{U(1)_L}$ restricts the lepton number charges of N, η, $\sigma_{A,B,C}$ and S, which must

take precise values, and this automatically implies a remnant $\mathbb{Z}_2$ that corresponds to the usual Scotogenic parity. In the rest of the models, the conservation of $\mathrm{U}(1)_\mathrm{L}$ leaves one of the charges to be chosen freely. We decided to choose q_N. In this case, these are the restrictions to recover the *dark* $\mathbb{Z}_2$ parity from $\mathrm{U}(1)_\mathrm{L}$ breaking:

- q_N cannot be an integer.
- If $q_N = \frac{\alpha}{\beta}$, with $\alpha, \beta \in \mathbb{Z}$, then α and β have to be odd and even, respectively.
- $\mathrm{GCD}(\alpha, \beta) = 1$. Therefore, α and β must be coprime.

Additionally, some models have extra conditions for the $\mathbb{Z}_2$ to appear:

- In $\mathrm{V}(2,2,0)$, we further require $\mathrm{GCD}(3\,\alpha, \alpha-\beta) = 1$ if $\frac{\alpha-\beta}{3}$ is not an integer, or $\mathrm{GCD}(\alpha, \frac{\alpha-\beta}{3}) = 1$ if $\frac{\alpha-\beta}{3}$ is an integer.
- In $\mathrm{V}(2,1^*,2)$, we further require $\mathrm{GCD}(3\,\alpha, 2\,\alpha - \beta) = 1$ if $\frac{2\,\alpha-\beta}{3}$ is not an integer, or $\mathrm{GCD}(\alpha, \frac{2\,\alpha-\beta}{3}) = 1$ if $\frac{2\,\alpha-\beta}{3}$ is an integer.
- In $\mathrm{V}(2,1,2)$, we further require $\mathrm{GCD}(3\,\alpha, \beta) = 1$ if $\frac{\beta}{3}$ is not an integer, or $\mathrm{GCD}(\alpha, \frac{\beta}{3}) = 1$ if $\frac{\beta}{3}$ is an integer.

We note that all the formal conditions for the five topologies have been derived individually for each of the models. This concludes our classification of all possible UV extensions of the Scotogenic model satisfying our requirements (A) and (B). We will now illustrate it with three specific example models.

8.3 An UV extended Scotogenic model with one σ field: First example

We will begin with an example model that is an UV extension of the Scotogenic model with one σ field. It is based on the work [413]. We will provide more details in this example than in the subsequent ones.

8.3.1 Ultraviolet theory

We consider an extension of the Scotogenic model with two new particles: the $\mathrm{SU}(2)_\mathrm{L}$ triplet S and the singlet σ, both scalars. The $\mathbb{Z}_2$ Scotogenic parity is replaced by a global $\mathrm{U}(1)_\mathrm{L}$ lepton number symmetry. Table 8.4 shows the scalar and leptonic fields of the model and their representations under the gauge and global symmetries.

We aim to explain the smallness of the Scotogenic's λ_5 coupling. Our strategy will be to forbid it in our original Lagrangian and make it arise effectively at low energies once the scalar σ acquires a VEV and we integrate out S. We also impose that, after symmetry breaking, the

Field	**Generations**	$SU(3)_c$	$SU(2)_L$	$U(1)_Y$	$U(1)_L$
ℓ_L	3	**1**	**2**	-1/2	1
e_R	3	**1**	**1**	-1	1
N	3	**1**	**1**	0	q_N
H	1	**1**	**2**	1/2	0
η	1	**1**	**2**	1/2	q_η
σ	1	**1**	**1**	0	q_σ
S	1	**1**	**3**	1	q_S

Table 8.4: Lepton and scalar particle content and representations under the gauge and global symmetries in the first example of an UV extension of the Scotogenic model with one σ field.

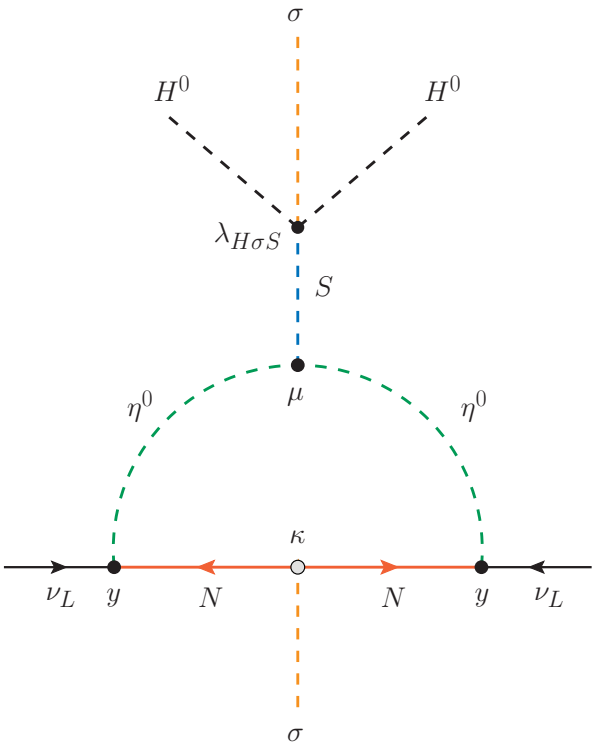

Figure 8.1: Neutrino mass generation in the first example of an extended Scotogenic model with one σ field. This Feynman diagram shows the relevant gauge eigenstates involved in the 1-loop contribution to neutrino masses. In our notation, this corresponds to a $I(1^*, \emptyset)$ model.

effective λ_5 coupling induces neutrino masses as shown in Fig. 8.1. In our notation, this is a $I(1^*, \emptyset)$ model. It requires the presence of the operators

$$\overline{N}\widetilde{\eta}^\dagger \ell_L \quad , \quad \sigma \overline{N}^c N \quad , \quad \sigma^* H^\dagger S \widetilde{H} \quad , \quad \widetilde{\eta}^\dagger S^\dagger \eta \,, \tag{8.4}$$

which in turn imply the following set of equations for the $\mathrm{U(1)_L}$ charges of the model:

$$-q_N + q_\eta + 1 = 0\,, \tag{8.5}$$
$$q_\sigma + 2\,q_N = 0\,, \tag{8.6}$$
$$q_S - q_\sigma = 0\,, \tag{8.7}$$
$$2\,q_\eta - q_S = 0\,. \tag{8.8}$$

This system of linear equations has a unique solution:

$$q_N = \frac{1}{2}\,, \tag{8.9}$$
$$q_\eta = -\frac{1}{2}\,, \tag{8.10}$$
$$q_\sigma = -1\,, \tag{8.11}$$
$$q_S = -1\,. \tag{8.12}$$

With this solution, the operators

$$\overline{N}^c N \quad , \quad \overline{N}\widetilde{H}^\dagger \ell_L \quad , \quad \left(H^\dagger \eta\right)^2 \tag{8.13}$$

are automatically forbidden due to $\mathrm{U(1)_L}$ conservation. One should note that if we choose the operator $\sigma H^\dagger S \widetilde{H}$ instead of $\sigma^* H^\dagger S \widetilde{H}$, no solution for the resulting system of equations would exist. Indeed, if one replaces $-q_\sigma$ by q_σ in Eq. (8.7), the combination of the resulting equation with Eqs. (8.6) and (8.8) leads to $q_N = q_\eta$, which is incompatible with Eq. (8.5). This illustrates why $\xi(1, \emptyset)$ models are not compatible with our requirements.

Having fixed the quantum numbers of all the particles in the model, we proceed to write its Lagrangian. The new Yukawa interactions are given by

$$\mathcal{L}_\mathrm{Y} = y\,\overline{N}\,\widetilde{\eta}^\dagger\,\ell_L + \kappa\,\sigma\overline{N}^c N + \mathrm{h.c.}\,, \tag{8.14}$$

where y is a general complex 3×3 matrix and κ is a complex symmetric 3×3 matrix. The scalar potential of the model can be written as

$$\begin{aligned}
\mathcal{V}_\mathrm{UV} = {} & m_H^2 H^\dagger H + m_S^2 \mathrm{Tr}(S^\dagger S) + m_\sigma^2 \sigma^*\sigma + m_\eta^2 \eta^\dagger\eta + \frac{\lambda_1}{2}(H^\dagger H)^2 + \frac{\lambda_2}{2}(\eta^\dagger\eta)^2 \\
& + \frac{\lambda_{S1}}{2}\,\mathrm{Tr}\,(S^\dagger S)^2 + \frac{\lambda_{S2}}{2}(\,\mathrm{Tr}\,S^\dagger S)^2 + \frac{\lambda_\sigma}{2}\,(\sigma^*\sigma)^2 + \lambda_3(H^\dagger H)(\eta^\dagger\eta) \\
& + \lambda_3^{HS}(H^\dagger H)\,\mathrm{Tr}\,(S^\dagger S) + \lambda_3^{H\sigma}(H^\dagger H)(\sigma^*\sigma) + \lambda_3^{\eta S}(\eta^\dagger\eta)\,\mathrm{Tr}\,(S^\dagger S) + \lambda_3^{\eta\sigma}(\eta^\dagger\eta)(\sigma^*\sigma) \\
& + \lambda_3^{\sigma S}(\sigma^*\sigma)\,\mathrm{Tr}\,(S^\dagger S) + \lambda_4(H^\dagger\eta)(\eta^\dagger H) + \lambda_4^{HS}(H^\dagger S^\dagger S\,H) + \lambda_4^{\eta S}(\eta^\dagger S^\dagger S\,\eta) \\
& + \left[\lambda_{H\sigma S}\,\sigma^*(H^\dagger S\,\widetilde{H}) + \mu\,(\eta^\dagger S\,\widetilde{\eta}\,) + \mathrm{h.c.}\right]\,.
\end{aligned} \tag{8.15}$$

Here μ is a trilinear parameter with dimensions of mass while m_H^2, m_η^2, m_S^2, and m_σ^2 have dimensions of mass^2. Other Lagrangian terms, like $(H^\dagger\,\eta)^2$, $H^\dagger S\,\eta^\dagger$, $H^\dagger S\eta^\dagger\sigma$, and $H^\dagger\eta\,\sigma$, are allowed by the gauge symmetries of the model but forbidden by $\mathrm{U}(1)_\mathrm{L}$.

8.3.2 Effective theory

Assuming that m_S is much larger than any other mass scale in the model, we can properly describe all physical processes at energies well below m_S using an effective field theory in which the heavy field S has been integrated out and expanding the resulting theory in powers of $1/m_S$. For our purposes, we only need to work at tree-level and keep operators up to dimension 6. We can easily achieve this by following the method outlined in [414]. We now present how this effective theory is obtained.

In order to integrate out the S triplet, we need to solve its classical equation of motion and insert the solution into the UV Lagrangian. We will consider the 2×2 representation of the triplet,

$$S=\begin{pmatrix} S^+/\sqrt{2} & S^{++} \\ S^0 & -S^+/\sqrt{2}\end{pmatrix}. \tag{8.16}$$

In addition, we can simplify the derivation of the equations of motion by integrating by parts $(D_\mu S)^\dagger\,(D^\mu S)$ and substituting it by $-S^\dagger D^2 S$. This way, the Euler-Lagrange equation becomes

$$\begin{aligned}\frac{\partial\mathcal{L}}{\partial\,(S^\dagger)_{ba}} =& -D^2 S_{ba} - m_S^2\,S_{ba} - \lambda_3^{HS}\,(H^\dagger H)\,S_{ba} - \lambda_3^{\eta S}\,(\eta^\dagger\eta)\,S_{ba} - \lambda_3^{\sigma S}\,(\sigma^*\sigma)\,S_{ba}\\ &- \lambda_4^{HS}\,(H^\dagger)_a\,(\Delta H)_b - \lambda_4^{\eta S}\,(\eta^\dagger)_a\,(S\eta)_b - \lambda^*_{H\sigma S}\,\sigma\,(\widetilde{H}^\dagger)_a H_b - \mu^*\,(\widetilde{\eta}^\dagger)_a\,\eta_b = 0\,,\end{aligned} \tag{8.17}$$

where we have not included quartic S terms as they would contribute at higher orders in $1/m_S$. Now, we can factor out the S_{ab} field from the terms in which it appears explicitly,

$$\begin{aligned}m_S^2\,[1 +&\frac{D^2}{m_S^2} + \frac{\lambda_3^{HS}}{m_S^2}(H^\dagger H) + \frac{\lambda_3^{\eta S}}{m_S^2}(\eta^\dagger\eta) + \frac{\lambda_3^{\sigma S}}{m_S^2}(\sigma^*\sigma)\Big]\,S_{ba} =\\ &- \lambda_4^{HS}\,(H^\dagger)_a\,(S\,H)_b - \lambda_4^{\eta S}\,(\eta^\dagger)_a\,(S\,\eta)_b - \lambda^*_{H\sigma S}\,\sigma\,(\widetilde{H}^\dagger)_a\,H_b - \mu^*(\widetilde{\eta}^\dagger)_a\,\eta_b = 0\,.\end{aligned} \tag{8.18}$$

We have also extracted a factor of m_S^2 from the left side of the equation. This enables us to express the left-hand side in a form that resembles $(1+\varepsilon)$, where ε is a small term of order $1/m_S^2$. By doing so, we can use the approximation $(1+\varepsilon)^{-1}\approx(1-\varepsilon)$ to solve for S_{ab},

$$\begin{aligned}S_{ba} =&\frac{-1}{m_S^2}\Big[\lambda_4^{HS}\,(H^\dagger)_a\,(S\,H)_b + \lambda_4^{\eta S}\,(\eta^\dagger)_a\,(S\,\eta)_b + \lambda^*_{H\sigma S}\,\sigma\,(\widetilde{H}^\dagger)_a\,H_b + \mu^*\,(\widetilde{\eta}^\dagger)_a\,\eta_b\Big]\\ &+\frac{1}{m_S^4}\Big[\lambda_4^{HS}\,(H^\dagger)_a\,(S\,H)_b + \lambda_4^{\eta S}\,(\eta^\dagger)_a\,(S\,\eta)_b + \lambda^*_{H\sigma S}\,\sigma\,(\widetilde{H}^\dagger)_a H_b + \mu^*\,(\widetilde{\eta}^\dagger)_a\,\eta_b\Big]\\ &\Big[D^2 + \lambda_3^{HS}\,(H^\dagger H) + \lambda_3^{\eta S}\,(\eta^\dagger\eta) + \lambda_3^{\sigma S}\,(\sigma^*\sigma)\Big] + \mathcal{O}\left(\frac{1}{m_S^6}\right).\end{aligned} \tag{8.19}$$

Notice that S still appears on the right-hand side of the result, making it difficult to obtain an explicit solution. One strategy to address this issue is to recursively solve for S. Those terms on the right-hand side of the equation having an S will have, at least, an additional $1/m_S^2$ factor, making them smaller and potentially irrelevant for our purposes. Actually, it is enough for us to keep just the lower order terms in the solution,

$$S_{ab} = \frac{-1}{m_S^2}\left[\lambda^*_{H\sigma S}\,\sigma\,H_a\,(\widetilde{H}^\dagger)_b + \mu^*\,\eta_a\,(\widetilde{\eta}^\dagger)_b\right] + \mathcal{O}\left(\frac{1}{m_S^4}\right), \tag{8.20}$$

where we have interchanged the a and b indices. Now, it is straightforward to write Eq. (8.20) in matrix form,

$$S = \frac{-1}{m_S^2}\left[\lambda^*_{H\sigma S}\,\sigma\,(H\,\widetilde{H}^\dagger) + \mu^*\,(\eta\,\widetilde{\eta}^\dagger)\right] + \mathcal{O}\left(\frac{1}{m_S^4}\right). \tag{8.21}$$

We obtain the tree-level effective field theory by substituting this equation into the Lagrangian. Since we are interested in dimension 6 operators, it is enough to substitute S in those terms of Eq. (8.15) involving just a single triplet S and in its mass term. Therefore, the new non-renormalizable operators that are added to the effective potential at low energies are

$$\begin{aligned}\mathcal{V}_{\rm IR} \supset & - m_S^2\left(\frac{1}{m_S^2}\right)^2 \mathrm{Tr}\left\{\left[\lambda_{H\sigma S}\,\sigma^*\,(\widetilde{H}\,H^\dagger) + \mu\,(\widetilde{\eta}\,\eta^\dagger)\right]\left[\lambda^*_{H\sigma S}\,\sigma\,(H\widetilde{H}^\dagger) + \mu^*\,(\eta\,\widetilde{\eta}^\dagger)\right]\right\} \\ & + \left[\frac{|\lambda_{H\sigma S}|^2}{m_\Delta^2}\,(\sigma^*\sigma)\,H^\dagger H\,\widetilde{H}^\dagger\widetilde{H} + \frac{|\mu|^2}{m_S^2}\eta^\dagger\eta\,\widetilde{\eta}^\dagger\widetilde{\eta}\right. \\ & \left. + \frac{\lambda_{H\sigma S}\,\mu^*}{m_S^2}\,\sigma^*\,H^\dagger\eta\,\widetilde{\eta}^\dagger\widetilde{H} + \frac{\lambda^*_{H\sigma S}\,\mu}{m_S^2}\,\sigma\,\eta^\dagger H\,\widetilde{H}^\dagger\widetilde{\eta} + \text{h.c.}\right].\end{aligned} \tag{8.22}$$

Using the relations

$$\begin{aligned}&\widetilde{\psi}^\dagger\widetilde{\phi} = (i\sigma_2\psi^*)^\dagger\,(i\sigma_2\phi^*) = \psi^T\sigma_2^\dagger\,\sigma_2\,\phi^* = \psi^T\phi^* = \phi^\dagger\psi\,, \\ &\mathrm{Tr}\left(\widetilde{\psi}\,\psi^\dagger\phi\,\widetilde{\phi}^\dagger\right) = \left(\psi^\dagger\phi\right)\mathrm{Tr}\left(\widetilde{\psi}\,\widetilde{\phi}^\dagger\right) = \left(\psi^\dagger\phi\right)\mathrm{Tr}\left(\widetilde{\phi}^\dagger\,\widetilde{\psi}\right) = \left(\psi^\dagger\phi\right)^2,\end{aligned} \tag{8.23}$$

valid for any two $SU(2)$ doublets ψ and ϕ, to simplify the new terms, we get the full low energy potential of our effective field theory,

$$\begin{aligned}\mathcal{V}_{\rm IR} = & \,m_H^2 H^\dagger H + m_\sigma^2\sigma^*\sigma + m_\eta^2\eta^\dagger\eta + \left(H^\dagger H\right)^2\left[\frac{\lambda_1}{2} - \frac{|\lambda_{H\sigma S}|^2}{m_S^2}\,(\sigma^*\sigma)\right] + \frac{\lambda_\sigma}{2}\,(\sigma^*\sigma)^2 \\ & + \left(\eta^\dagger\eta\right)^2\left(\frac{\lambda_2}{2} - \frac{|\mu|^2}{m_S^2}\right) + \lambda_3\left(H^\dagger H\right)\left(\eta^\dagger\eta\right) + \lambda_3^{H\sigma}\left(H^\dagger H\right)(\sigma^*\sigma) + \lambda_3^{\eta\sigma}\left(\eta^\dagger\eta\right)(\sigma^*\sigma) \\ & + \lambda_4\left(H^\dagger\eta\right)\left(\eta^\dagger H\right) - \left[\frac{\lambda_{H\sigma S}\mu^*}{m_S^2}\sigma^*\left(H^\dagger\eta\right)^2 + \text{ h.c. }\right] + \mathcal{O}\left(\frac{1}{m_\Delta^4}\right).\end{aligned} \tag{8.24}$$

Assuming now that CP is conserved in the scalar sector, the neutral fields H^0 and σ can be decomposed as

$$H^0 = \frac{1}{\sqrt{2}}(v + \phi + i\,z)\,, \quad \sigma = \frac{1}{\sqrt{2}}(v_\sigma + \rho + i\,J)\,, \tag{8.25}$$

with $\frac{v}{\sqrt{2}}$ and $\frac{v_\sigma}{\sqrt{2}}$ the VEVs of H^0 and σ, respectively. These VEVs are determined by minimizing the scalar potential in Eq. (8.24). The resulting tadpole equations are given by

$$\left.\frac{\mathrm{d}\mathcal{V}_{\rm IR}}{\mathrm{d}H^0}\right|_{\langle H^0\rangle=\frac{v}{\sqrt{2}},\langle\sigma\rangle=\frac{v_\sigma}{\sqrt{2}}} = \frac{v}{\sqrt{2}}\left(m_H^2 + \lambda_1\frac{v^2}{2} + \lambda_3^{H\sigma}\frac{v_\sigma^2}{2} - \frac{v^2\,v_\sigma^2\,|\lambda_{H\sigma S}|^2}{2m_S^2}\right) = 0\,, \tag{8.26}$$

$$\left.\frac{\mathrm{d}\mathcal{V}_{\rm IR}}{\mathrm{d}\sigma}\right|_{\langle H^0\rangle=\frac{v}{\sqrt{2}},\langle\sigma\rangle=\frac{v_\sigma}{\sqrt{2}}} = \frac{v_\sigma}{\sqrt{2}}\left(m_\sigma^2 + \lambda_3^{H\sigma}\frac{v^2}{2} + \lambda_\sigma\frac{v_\sigma^2}{2} - \frac{v^4\,|\lambda_{H\sigma S}|^2}{4m_S^2}\right) = 0\,, \tag{8.27}$$

where we have only written the non-trivial equations, and they are evaluated at the VEVs of each scalar field. As we can see from Eq. (8.24), once σ acquires a VEV, the operator $(H^\dagger\eta)^2$ is generated, with an effective λ_5 coupling that is naturally suppressed by the mass of the heavy field S,

$$\frac{\lambda_5}{2} \equiv -\frac{\lambda_{H\sigma S}\,\mu^*\,v_S}{\sqrt{2}\,m_S^2} \ll 1\,. \tag{8.28}$$

This follows from the assumption $\mu \ll m_S$. As explained in Section 8.2, this is perfectly valid. However, it poses a theoretical problem since μ is a parameter of the UV theory. A model without this issue will be discussed below in Section 8.5. We now proceed to the computation of the scalar spectrum of the model. In the bases $\{\phi, \rho\}$ for the CP-even states and $\{z, J\}$ for the CP-odd ones, the squared mass matrices read

$$\mathcal{M}_R^2 = \begin{pmatrix} m_H^2 + \frac{3v^2}{2}\lambda_1 + \frac{v_\sigma^2}{2}\lambda_3^{H\sigma} - \frac{3\,v^2\,v_\sigma^2|\lambda_{H\sigma S}|^2}{2\,m_S^2} & v\,v_\sigma\left(\lambda_3^{H\sigma} - \frac{v^2|\lambda_{H\sigma S}|^2}{m_S^2}\right) \\ v\,v_\sigma\left(\lambda_3^{H\sigma} - \frac{v^2|\lambda_{H\sigma S}|^2}{m_S^2}\right) & m_\sigma^2 + \frac{3\,v_\sigma^2}{2}\lambda_\sigma + \frac{v^2}{2}\lambda_3^{H\sigma} - \frac{v^4|\lambda_{H\sigma S}|^2}{4\,m_S^2} \end{pmatrix}, \tag{8.29}$$

and

$$\mathcal{M}_I^2 = \begin{pmatrix} m_H^2 + \frac{v^2}{2}\lambda_1 + \frac{v_\sigma^2}{2}\lambda_3^{H\sigma} - \frac{v^2\,v_\sigma^2|\lambda_{H\sigma S}|^2}{2\,m_S^2} & 0 \\ 0 & m_\sigma^2 + \frac{v_\sigma^2}{2}\lambda_\sigma + \frac{v^2}{2}\lambda_3^{H\sigma} - \frac{v^4|\lambda_{H\sigma S}|^2}{4\,m_S^2} \end{pmatrix}, \tag{8.30}$$

respectively. Using now the tadpole equations in Eqs. (8.26) and (8.27), one can simplify these mass matrices notably. In fact, the CP-odd matrix $\mathcal{M}_I^2$ is exactly zero once the minimization equations are used. This implies the existence of two massless Goldstone bosons. One of them (z) is the would-be Goldstone boson that becomes the longitudinal component of the Z boson and makes it massive, while the other (J) is the majoron, a (physical) massless Goldstone boson associated to the spontaneous breaking of lepton number. On the other hand, after applying

Eqs. (8.26) and (8.27), $\mathcal{M}_R^2$ becomes

$$\mathcal{M}_R^2 = \begin{pmatrix} v^2\left(\lambda_1 - \frac{v_\sigma^2|\lambda_{H\sigma S}|^2}{m_S^2}\right) & v\,v_\sigma\left(\lambda_3^{H\sigma} - \frac{v^2|\lambda_{H\sigma S}|^2}{m_S^2}\right) \\ v\,v_\sigma\left(\lambda_3^{H\sigma} - \frac{v^2|\lambda_{H\sigma S}|^2}{m_S^2}\right) & v_\sigma^2\,\lambda_\sigma \end{pmatrix}. \tag{8.31}$$

This matrix can be brought to diagonal form as $V_R^T \mathcal{M}_R^2 V_R = \widehat{\mathcal{M}}_R^2 = \text{diag}(m_h^2, m_\Phi^2)$, where V_R is a unitary matrix that can be parametrized as

$$V_R = \begin{pmatrix} \cos\theta & -\sin\theta \\ \sin\theta & \cos\theta \end{pmatrix}. \tag{8.32}$$

The mixing angle θ is given by

$$\tan(2\theta) = \frac{2(\mathcal{M}_R^2)_{12}}{(\mathcal{M}_R^2)_{11} - (\mathcal{M}_R^2)_{22}} \approx \frac{2\,r\,\lambda_3^{H\sigma}}{r^2\lambda_1 - \lambda_\sigma} \approx -2r\frac{\lambda_3^{H\sigma}}{\lambda_\sigma} + \mathcal{O}(r^2)\,, \tag{8.33}$$

where we have neglected contributions proportional to $1/m_S^2$ and we have defined $r \equiv v/v_\sigma$. For $v_\sigma \sim$ TeV, $r \ll 1$ and simple approximate expressions can be obtained. The lightest of the two mass eigenstates is the well-known Higgs-like state h, with mass $m_h \approx 125$ GeV, discovered at the LHC. In addition, the model contains the heavy scalar Φ, with a mass of the order of v_σ. We focus now on the $\mathbb{Z}_2$-odd scalars η^+ and η^0. The neutral η^0 field can be decomposed as

$$\eta^0 = \frac{1}{\sqrt{2}}(\eta_R + i\,\eta_I)\,. \tag{8.34}$$

Their masses are given by

$$m_{\eta^+}^2 = m_\eta^2 + \lambda_3^{\text{eff}}\,\frac{v^2}{2}\,, \tag{8.35}$$

$$m_{\eta_R}^2 = m_\eta^2 + \left(\lambda_3^{\text{eff}} + \lambda_4^{\text{eff}} + \lambda_5\right)\frac{v^2}{2}\,, \tag{8.36}$$

$$m_{\eta_I}^2 = m_\eta^2 + \left(\lambda_3^{\text{eff}} + \lambda_4^{\text{eff}} - \lambda_5\right)\frac{v^2}{2}\,, \tag{8.37}$$

where we have defined

$$\lambda_3^{\text{eff}} \equiv \lambda_3 + \lambda_3^{\eta\sigma}\frac{v_\sigma^2}{v^2}\,, \tag{8.38}$$

$$\lambda_4^{\text{eff}} \equiv \lambda_4\,, \tag{8.39}$$

As in the usual Scotogenic model, the mass square difference between η_R and η_I is controlled by the effective λ_5 coupling,

$$m_{\eta_R}^2 - m_{\eta_I}^2 = -\frac{4\,\lambda_{HS\Delta}\,\mu\,v_S}{\sqrt{2}\,m_\Delta^2}\,\frac{v^2}{2} \equiv \lambda_5^{\text{eff}}\,v^2\,. \tag{8.40}$$

Field	**Generations**	$SU(3)_c$	$SU(2)_L$	$U(1)_Y$	$U(1)_L$
ℓ_L	3	**1**	**2**	-1/2	1
e_R	3	**1**	**1**	-1	1
N	3	**1**	**1**	0	q_N
H	1	**1**	**2**	1/2	0
η	1	**1**	**2**	1/2	q_η
σ	1	**1**	**1**	0	q_σ
S	1	**1**	**2**	1/2	q_S

Table 8.5: Lepton and scalar particle content and representations under the gauge and global symmetries in the second example of an UV extension of the Scotogenic model with one σ field.

Finally, the spontaneous breaking of $U(1)_L$ by the VEV of σ induces a Majorana mass term for the N singlets, with $M_N = \sqrt{2}\,\kappa\, v_\sigma$. This leads to Majorana neutrino masses at 1-loop, as shown in Fig. 8.1. The 3×3 neutrino mass matrix is given by the usual Scotogenic formula in Eq. (2.59), where λ_5 is the effective coupling in Eq. (8.28). Due to the additional scalar states, including a massless majoron with couplings to charged leptons, the phenomenology of this model is richer than that of the usual Scotogenic scenario. This will be discussed in Section 8.6.

8.4 An UV extended Scotogenic model with one σ field: Second example

Our second example model is a UV extension of the Scotogenic model with one σ field.

8.4.1 Ultraviolet theory

For this second example we consider an extension of the Scotogenic model with two new particles: the $SU(2)_L$ doublet S and the singlet σ, both scalars. The $\mathbb{Z}_2$ Scotogenic parity is replaced by a global $U(1)_L$ lepton number symmetry. Table 8.5 shows the scalar and leptonic fields of the model and their representations under the gauge and global symmetries.

Again, we aim at an explanation of the smallness of the Scotogenic's λ_5 coupling, and our strategy will be to forbid it in our original Lagrangian, making it arise effectively at low energies once the scalar σ acquires a VEV and we integrate out S. We also impose that, after symmetry breaking, the effective λ_5 coupling induces neutrino masses as shown in Fig. 8.2. In our notation, this is a IV$(1^*, \emptyset)$ model. This requires the presence of the operators

$$\overline{N}\widetilde{\eta}^\dagger \ell_L \quad , \quad \sigma \overline{N}^c N \quad , \quad H^\dagger S H^\dagger \eta \quad , \quad \sigma^* S^\dagger \eta\,. \tag{8.41}$$

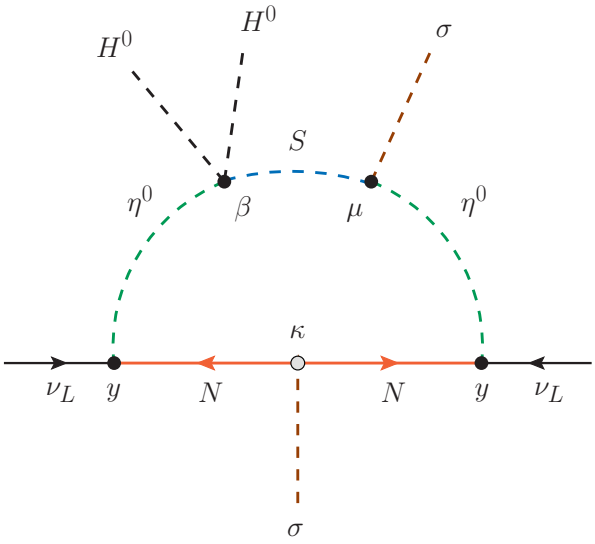

Figure 8.2: Neutrino mass generation in the second example of an extended Scotogenic model with one σ field. This Feynman diagram shows the relevant gauge eigenstates involved in the 1-loop contribution to neutrino masses. In our notation, this corresponds to a IV$(1^*, \emptyset)$ model.

As a result, the following set of equations is implied for the $\mathrm{U}(1)_\mathrm{L}$ charges of the model:

$$-q_N + q_\eta + 1 = 0\,, \tag{8.42}$$
$$q_\sigma + 2\,q_N = 0\,, \tag{8.43}$$
$$q_S + q_\eta = 0\,, \tag{8.44}$$
$$-q_\sigma - q_S + q_\eta = 0\,. \tag{8.45}$$

For this system of linear equations there is again a unique solution:

$$q_N = \frac{1}{2}\,, \tag{8.46}$$
$$q_\eta = -\frac{1}{2}\,, \tag{8.47}$$
$$q_\sigma = -1\,, \tag{8.48}$$
$$q_S = \frac{1}{2}\,. \tag{8.49}$$

This solution implies that the operators

$$\overline{N}^c N \quad , \quad \overline{N}\widetilde{H}^\dagger \ell_L \quad , \quad \left(H^\dagger \eta\right)^2 \tag{8.50}$$

are automatically forbidden due to $\mathrm{U}(1)_\mathrm{L}$ conservation, as required. As in the previous example, it should be noted that if we chose the operator $\sigma S^\dagger \eta$ instead of $\sigma^* S^\dagger \eta$, there would be no solution for the resulting system of equations. In fact, if we replace $-q_\sigma$ by q_σ in Eq. (8.45),

the resulting equation combined with Eqs. (8.43) and (8.44) leads to $q_N = q_\eta$, which contradicts Eq. (8.42). This confirms again why $\xi(1, \emptyset)$ models are not compatible with our requirements.

Once the quantum numbers of all the particles in the model are fixed, we can proceed with writing its Lagrangian. Specifically, the new Yukawa interactions are given by

$$\mathcal{L}_{\rm Y} = y\,\overline{N}\,\widetilde{\eta}^\dagger\,\ell_L + \kappa\,\sigma\overline{N}^c N + \text{h.c.}\,, \tag{8.51}$$

where y is a general complex 3×3 matrix and κ is a complex symmetric 3×3 matrix. The scalar potential in this model can be written as

$$\begin{aligned}\mathcal{V}_{\rm UV} &= m_H^2 H^\dagger H + m_S^2 S^\dagger S + m_\sigma^2 \sigma^*\sigma + m_\eta^2 \eta^\dagger\eta + \frac{\lambda_1}{2}(H^\dagger H)^2 + \frac{\lambda_2}{2}(\eta^\dagger\eta)^2 \\ &+ \frac{\lambda_S}{2}(S^\dagger S)^2 + \frac{\lambda_\sigma}{2}(\sigma^*\sigma)^2 + \lambda_3(H^\dagger H)(\eta^\dagger\eta) + \lambda_3^S(H^\dagger H)(S^\dagger S) \\ &+ \lambda_3^\sigma(H^\dagger H)(\sigma^\dagger\sigma) + \lambda_3^{\eta S}(\eta^\dagger\eta)(S^\dagger S) + \lambda_3^{\eta\sigma}(\eta^\dagger\eta)(\sigma^*\sigma) \\ &+ \lambda_3^{\sigma S}(\sigma^*\sigma)(S^\dagger S) + \lambda_4(H^\dagger\eta)(\eta^\dagger H) + \lambda_4^{HS}(H^\dagger S)(S^\dagger H) \\ &+ \lambda_4^{\eta S}(S^\dagger\eta)(\eta^\dagger S) + \Big[\beta(H^\dagger S H^\dagger\eta) + \mu(\sigma^* S^\dagger\eta) + \text{h.c.}\Big]\,.\end{aligned} \tag{8.52}$$

Here μ is a trilinear parameter with dimensions of mass while m_H^2, m_η^2, and m_σ^2 have dimensions of mass^2.

8.4.2 Effective theory

We will now assume that m_S is much larger than any other energy scale in the theory. At energies well below m_S, all physical processes can be properly described by an effective field theory in which the heavy field S has been integrated out. We now present this effective theory, obtained after integrating out S at tree-level. Following the same procedure as in Section 8.3.2, the effective potential at low energies can be written as

$$\begin{aligned}\mathcal{V}_{\rm IR} &= m_H^2 H^\dagger H + m_\eta^2 \eta^\dagger\eta + m_\sigma^2\sigma^*\sigma + \frac{\lambda_1}{2}(H^\dagger H)^2 + \frac{\lambda_2}{2}(\eta^\dagger\eta)^2 + \frac{\lambda_\sigma}{2}(\sigma^*\sigma)^2 \\ &+ \lambda_3(H^\dagger H)(\eta^\dagger\eta) + \lambda_3^\sigma(H^\dagger H)(\sigma^*\sigma) + \left(\lambda_3^{\eta\sigma} - \frac{|\mu|^2}{m_S^2}\right)(\sigma^*\sigma)(\eta^\dagger\eta) \\ &+ \left[\lambda_4 - \frac{|\beta|^2(H^\dagger H)}{m_S^2}\right](H^\dagger\eta)(\eta^\dagger H) - \left[\frac{\beta\mu}{m_S^2}\sigma^*(H^\dagger\eta)^2 + \text{h.c.}\right] + \mathcal{O}\left(\frac{1}{m_S^4}\right)\,.\end{aligned} \tag{8.53}$$

If we assume that CP is conserved in the scalar sector, we can decompose the neutral fields H^0 and σ as

$$H^0 = \frac{1}{\sqrt{2}}(v + \phi + iz)\,, \quad \sigma = \frac{1}{\sqrt{2}}(v_\sigma + \rho + iJ)\,, \tag{8.54}$$

with $\frac{v}{\sqrt{2}}$ and $\frac{v_\sigma}{\sqrt{2}}$ the VEVs of H^0 and σ, respectively. These VEVs are determined by minimizing the scalar potential in Eq. (8.53). The resulting tadpole equations are given by

$$\left.\frac{d\mathcal{V}_{\rm IR}}{dH^0}\right|_{\langle H^0,\sigma\rangle=\{\frac{v}{\sqrt{2}},\frac{v_\sigma}{\sqrt{2}}\}} = \frac{v}{\sqrt{2}}\left(m_H^2 + \frac{\lambda_1 v^2}{2} + \frac{\lambda_3^\sigma v_\sigma^2}{2}\right), \tag{8.55}$$

$$\left.\frac{d\mathcal{V}_{\rm IR}}{d\sigma}\right|_{\langle H^0,\sigma\rangle=\{\frac{v}{\sqrt{2}},\frac{v_\sigma}{\sqrt{2}}\}} = \frac{v_\sigma}{\sqrt{2}}\left(m_{\sigma^2} + \frac{\lambda_3^\sigma v^2}{2} + \frac{\lambda_\sigma v_\sigma^2}{2}\right). \tag{8.56}$$

Here we have only included the non-trivial equations, which are evaluated at the VEVs of each scalar field. As shown in Eq. (8.53), once σ gets a VEV, the operator $(H^\dagger\eta)^2$ is generated with an effective λ_5 coupling that is naturally suppressed by the mass of the heavy field S,

$$\frac{\lambda_5}{2} = -\frac{\beta\mu v_\sigma}{\sqrt{2}m_S^2} \ll 1\,. \tag{8.57}$$

As mentioned in the previous example, this follows from the assumption $\mu \ll m_S$. Next, we will compute the scalar spectrum of the model. The squared mass matrices for the CP-even and CP-odd states are expressed in the bases $\{\phi,\rho\}$ and $\{z,J\}$, respectively. They read

$$\mathcal{M}_R^2 = \begin{pmatrix} m_H^2 + \frac{1}{2}\left(3\lambda_1 v^2 + \lambda_3^\sigma v_\sigma^2\right) & \lambda_3^\sigma v v_\sigma \\ \lambda_3^\sigma v v_\sigma & m_\sigma^2 + \frac{1}{2}\left(\lambda_3^\sigma v_H^2 + 3\lambda_\sigma v_\sigma^2\right) \end{pmatrix}, \tag{8.58}$$

for the former, and

$$\mathcal{M}_I^2 = \begin{pmatrix} m_H^2 + \frac{\lambda_1 v_H^2}{2} + \frac{\lambda_3^\sigma v_\sigma^2}{2} & 0 \\ 0 & m_\sigma^2 + \frac{\lambda_\sigma^2 v^2}{2} + \frac{\lambda_\sigma v_\sigma^2}{2} \end{pmatrix}, \tag{8.59}$$

for the latter. The above expressions can be reduced using Eqs. (8.55) and (8.56). When this is done, the resulting $\mathcal{M}_I^2$ becomes identically zero, implying the existence of two massless Goldstone bosons. One of them (z) corresponds to the state that is *eaten up* by the Z boson and becomes its longitudinal component, while the other (J) is associated to the spontaneous breaking of the global $\mathrm{U(1)_L}$ symmetry, the so-called majoron. On the other hand, the reduction of $\mathcal{M}_R^2$ with Eqs. (8.55) and (8.56) leads to

$$\mathcal{M}_R^2 = \begin{pmatrix} \lambda_1 v^2 & \lambda_3^{H\sigma} v\, v_\sigma \\ \lambda_3^{H\sigma} v\, v_\sigma & \lambda_\sigma v_\sigma^2 \end{pmatrix}. \tag{8.60}$$

Which is the same mass matrix as the one in Eq.(8.31), although in the limit $m_S \to \infty$. Therefore, it will be diagonalized by the same matrix V_R defined in Eq. (8.32) with the mixing angle in Eq. (8.33). Again, the lightest of the two mass eigenstates is to be identified with the well-known Higgs-like state h, and the model contains a heavy scalar Φ, with a mass of the order of v_σ. Regarding the $\mathbb{Z}_2$-odd scalars η^+, η_R, and η_I, their masses are given by the expressions in

Eqs. (8.35), (8.36), and (8.37), but with the new definitions of λ_5 and

$$\lambda_3^{\text{eff}} \equiv \lambda_3 + \lambda_3^{\eta\sigma}\frac{v_\sigma^2}{v^2} - \mu^2\frac{v_\sigma^2}{v^2 m_S^2}\,, \tag{8.61}$$

$$\lambda_4^{\text{eff}} \equiv \lambda_4 - \frac{\beta^2 v^2}{2m_S^2}\,. \tag{8.62}$$

The mass square difference between η_R and η_I is given by

$$m_{\eta_R}^2 - m_{\eta_I}^2 = -\sqrt{2}\,\frac{\beta\mu v_\sigma}{m_S^2}v^2 = \lambda_5 v^2\,, \tag{8.63}$$

as in the original Scotogenic model. Finally, the VEV of σ induces a Majorana mass term for the N singlets, with $M_N = \sqrt{2}\,\kappa\, v_\sigma$. This results in Majorana neutrino masses at 1-loop, as shown in Fig. 8.1. The 3×3 neutrino mass matrix is given by the usual Scotogenic formula in Eq. (2.59), where λ_5 is the effective coupling in Eq. (8.57). As this model includes additional scalar states, including a massless majoron with couplings to charged leptons, its phenomenology is richer than that of the standard Scotogenic scenario. This will be illustrated in Section 8.6.

8.5 An UV extended Scotogenic model with two σ fields

We consider now an UV extension of the Scotogenic model with two σ fields.

8.5.1 Ultraviolet theory

We enlarge the Scotogenic particle content with three new particles: the scalar $\text{SU}(2)_\text{L}$ singlets S, σ_1, and σ_2. Again, instead of the usual $\mathbb{Z}_2$ Scotogenic parity, a global $\text{U}(1)_\text{L}$ lepton number symmetry is introduced. Table 8.5 shows the scalar and leptonic fields of the model and their representations under the gauge and global symmetries.

We consider the 1-loop generation of neutrino masses by the diagram in Fig. 8.3. In our notation, this corresponds to a II$(1,2)$ model. For this mechanism to take place, the operators

$$\overline{N}\tilde{\eta}^\dagger \ell_L \quad , \quad \sigma_1 \overline{N}^c N \quad , \quad \sigma_1 H^\dagger S \eta \quad , \quad \sigma_2 H^\dagger S^* \eta \tag{8.64}$$

must be allowed by the symmetries of the model. This restricts the $\text{U}(1)_\text{L}$ charges of the fields in the model. In particular, one can write the following set of equations for them:

$$-q_N + q_\eta + 1 = 0\,, \tag{8.65}$$

$$q_{\sigma_1} + 2\,q_N = 0\,, \tag{8.66}$$

$$q_{\sigma_1} + q_S + q_\eta = 0\,, \tag{8.67}$$

$$q_{\sigma_2} - q_S + q_\eta = 0\,. \tag{8.68}$$

Field	**Generations**	$SU(3)_c$	$SU(2)_L$	$U(1)_Y$	$U(1)_L$
ℓ_L	3	**1**	**2**	-1/2	1
e_R	3	**1**	**1**	-1	1
N	3	**1**	**1**	0	q_N
H	1	**1**	**2**	1/2	0
η	1	**1**	**2**	1/2	q_η
σ_1	1	**1**	**1**	0	q_{σ_1}
σ_2	1	**1**	**1**	0	q_{σ_2}
S	1	**1**	**1**	0	q_S

Table 8.6: Lepton and scalar particle content and representations under the gauge and global symmetries in an UV extension of the Scotogenic model with two σ fields.

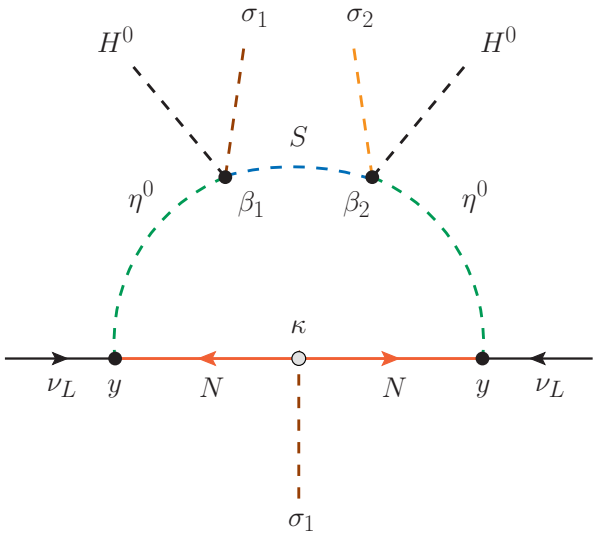

Figure 8.3: Neutrino mass generation in an extended Scotogenic model with two σ fields. This Feynman diagram shows the relevant gauge eigenstates involved in the 1-loop contribution to neutrino masses. In our notation, this corresponds to a II$(1,2)$ model.

They can be solved in terms of q_N to obtain

$$q_\eta = q_N - 1\,, \tag{8.69}$$

$$q_{\sigma_1} = -2\,q_N\,, \tag{8.70}$$

$$q_{\sigma_2} = 2\,, \tag{8.71}$$

$$q_S = q_N + 1\,. \tag{8.72}$$

In addition, we want the operators

$$\overline{N}^c N \quad , \quad \overline{N}\widetilde{H}^\dagger \ell_L \quad , \quad \left(H^\dagger \eta\right)^2 \tag{8.73}$$

to be forbidden. In order to forbid the first operator, a Majorana mass term for N, we just require $q_N \neq 0$. The second operator would lead to ν_L-N Dirac mass terms, and we can forbid it by requiring $q_N \neq 1$. Then, Eq. (8.69) implies $q_\eta \neq 0$ too. Finally, with these considerations, we choose

$$q_N = \frac{1}{2}\,, \tag{8.74}$$

which implies

$$q_\eta = -\frac{1}{2} \quad , \quad q_S = \frac{3}{2} \quad , \quad q_{\sigma_1} = -1 \quad , \quad q_{\sigma_2} = 2\,. \tag{8.75}$$

Some comments are in order. First, the diagram in Fig. 8.3 has two different σ singlets attached to the scalar internal line, σ_1 and σ_2. In principle, one may wonder why we did not consider the same σ singlet in both vertices as starting point for constructing our model. That would imply $q_S = 0$ and reduce the number of couplings in the model. However, such a construction would lead to an effective operator $(H^\dagger\eta)^2\sigma^2$ after integrating out the S field. If this operator is allowed by all symmetries of the model, so is the trilinear $(H^\dagger\eta)\,\sigma$ term. We will assume that the σ singlets acquire non-zero VEVs, breaking the original $\mathrm{U(1)_L}$. In the presence of the trilinear $(H^\dagger\eta)\,\sigma$, this would induce a tadpole for η, hence breaking the $\mathbb{Z}_2$ parity of the Scotogenic model. This forces us to discard this possibility and consider different σ_1 and σ_2 attached to the internal scalar line. It also illustrates why models with $\sigma_A = \sigma_B$ are not compatible with our requirements. Furthermore, one may consider a third σ_3 singlet field coupled to the internal fermion line. While this is possible, we preferred to choose a charge assignment that allows us to identify $\sigma_3 \equiv \sigma_1$ and reduce the number of fields in the model. Finally, once σ_1 and σ_2 acquire non-zero VEVs, the original $\mathrm{U(1)_L}$ symmetry will get broken to one of its $\mathbb{Z}_n$ subgroups. Here n is the GCD of $|q_{\sigma_1}|$ and $|q_{\sigma_2}|$ after being normalized to become integer numbers, hence $n = 2$ and the remnant symmetry is $\mathbb{Z}_2$.

Once we know the quantum numbers of all the particles in the model, we can write its Lagrangian. The new Yukawa interactions are given by

$$\mathcal{L}_\mathrm{Y} = y\,\overline{N}\,\widetilde{\eta}^\dagger\,\ell_L + \kappa\,\sigma_1\overline{N}^c N + \mathrm{h.c.}\,, \tag{8.76}$$

where y is a general complex 3×3 matrix and κ is a complex symmetric 3×3 matrix. The scalar potential of the model is given by

$$\begin{aligned}\mathcal{V}_{\rm UV} &= m_H^2 H^\dagger H + m_S^2 S^* S + m_{\sigma_i}^2 \sigma_i^* \sigma_i + m_\eta^2 \eta^\dagger \eta + \frac{\lambda_1}{2}(H^\dagger H)^2 + \frac{\lambda_2}{2}(\eta^\dagger \eta)^2 \\ &+ \frac{\lambda_S}{2}(S^* S)^2 + \frac{\lambda_{\sigma_i}}{2}(\sigma_i^* \sigma_i)^2 + \lambda_3 (H^\dagger H)(\eta^\dagger \eta) + \lambda_3^S (H^\dagger H)(S^* S) \\ &+ \lambda_3^{\sigma_i} (H^\dagger H)(\sigma_i^* \sigma_i) + \lambda_3^{\eta S} (\eta^\dagger \eta)(S^* S) + \lambda_3^{\eta \sigma_i} (\eta^\dagger \eta)(\sigma_i^* \sigma_i) \\ &+ \lambda_3^{\sigma\sigma} (\sigma_1^* \sigma_1)(\sigma_2^* \sigma_2) + \lambda_3^{\sigma_i S} (\sigma_i^* \sigma_i)(S^* S) + \lambda_4 (H^\dagger \eta)(\eta^\dagger H) \\ &+ \left[\beta_1 (\sigma_1 H^\dagger S \eta) + \beta_2 (\sigma_2 H^\dagger S^\dagger \eta) + \frac{\mu}{\sqrt{2}}(\sigma_2 \sigma_1 \sigma_1) + \lambda_0 (S S \sigma_1 \sigma_2^*) + \text{h.c.}\right],\end{aligned} \tag{8.77}$$

where we sum over $i = 1, 2$. Here μ is a trilinear parameter with dimensions of mass while m_H^2, m_η^2 and $m_{\sigma_i}^2$ have dimensions of mass^2. Other Lagrangian terms are allowed by the gauge symmetries of the model but forbidden by $\mathrm{U}(1)_{\rm L}$.

8.5.2 Effective theory

In the following we will assume that m_S is much larger than any other energy scale in the model and integrate out the heavy scalar S. If we do this at tree-level, the effective scalar potential at low energies can be written as

$$\begin{aligned}\mathcal{V}_{\rm IR} &= m_H^2 (H^\dagger H) + m_\eta^2 (\eta^\dagger \eta) + m_{\sigma_i}^2 (\sigma_i^* \sigma_i) + \frac{\lambda_1}{2}(H^\dagger H)^2 + \frac{\lambda_2}{2}(\eta^\dagger \eta)^2 + \frac{\lambda_{\sigma_i}}{2}(\sigma_i^* \sigma_i)^2 \\ &+ \lambda_3 (H^\dagger H)(\eta^\dagger \eta) + \lambda_3^{\sigma_i} (H^\dagger H)(\sigma_i^* \sigma_i) + \lambda_3^{\eta \sigma_i} (\eta^\dagger \eta)(\sigma_i^* \sigma_i) + \lambda_3^{\sigma\sigma} (\sigma_1^* \sigma_1)(\sigma_2^* \sigma_2) \\ &+ \left[\lambda_4 - \frac{|\beta_i|^2}{m_S^2}(\sigma_i^* \sigma_i)\right](H^\dagger \eta)(\eta^\dagger H) \\ &+ \left[\frac{\mu}{\sqrt{2}}(\sigma_2 \sigma_1 \sigma_1) - \frac{\beta_1 \beta_2}{m_S^2}\sigma_1 \sigma_2 (H^\dagger \eta)^2 + \text{h.c.}\right] + \mathcal{O}\left(\frac{1}{m_S^4}\right).\end{aligned} \tag{8.78}$$

Now, we decompose the neutral fields H^0 and $\sigma_{1,2}$ as

$$H^0 = \frac{1}{\sqrt{2}}(v + \phi + i\, z)\,, \quad \sigma_i = \frac{1}{\sqrt{2}}(v_{\sigma_i} + \rho_i + i\, J_i)\,, \tag{8.79}$$

where we defined $\frac{v}{\sqrt{2}}$ and $\frac{v_{\sigma_i}}{\sqrt{2}}$ as the VEVs of the corresponding fields. After this, we can compute the tadpole equation resulting from the effective potential in Eq. (8.78), evaluated at the VEVs

of each scalar field. The non-trivial tadpole equations are

$$\left.\frac{d\mathcal{V}_{\rm IR}}{dH^0}\right|_{\langle H^0,\sigma_i\rangle=\{\frac{v_H}{\sqrt{2}},\frac{v_{\sigma_i}}{\sqrt{2}}\}} = \frac{v_H}{\sqrt{2}}\left(m_H^2+\lambda_1\frac{v_H^2}{2}+\lambda_3^{\sigma_1}\frac{v_{\sigma_1}^2}{2}+\lambda_3^{\sigma_2}\frac{v_{\sigma_2}^2}{2}\right)=0, \tag{8.80}$$

$$\left.\frac{d\mathcal{V}_{\rm IR}}{d\sigma_1}\right|_{\langle H^0,\sigma_i\rangle=\{\frac{v_H}{\sqrt{2}},\frac{v_{\sigma_i}}{\sqrt{2}}\}} = \frac{v_{\sigma_1}}{\sqrt{2}}\left(m_{\sigma_1}^2+\mu\, v_{\sigma_2}+\lambda_3^{\sigma_1}\frac{v_H^2}{2}+\lambda_{\sigma_1}\frac{v_{\sigma_1}^2}{2}+\lambda_3^{\sigma\sigma}\frac{v_{\sigma_2}^2}{2}\right)=0, \tag{8.81}$$

$$\left.\frac{d\mathcal{V}_{\rm IR}}{d\sigma_2}\right|_{\langle H^0,\sigma_i\rangle=\{\frac{v_H}{\sqrt{2}},\frac{v_{\sigma_i}}{\sqrt{2}}\}} = \frac{v_{\sigma_2}}{\sqrt{2}}\left(m_{\sigma_2}^2+\mu\frac{v_{\sigma_1}^2}{2v_{\sigma_2}}+\lambda_3^{\sigma_2}\frac{v_H^2}{2}+\lambda_{\sigma_2}\frac{v_{\sigma_2}^2}{2}+\lambda_3^{\sigma\sigma}\frac{v_{\sigma_1}^2}{2}\right)=0. \tag{8.82}$$

As already explained, as a result of σ_i acquiring a VEV, lepton number gets spontaneously broken, leaving a discrete $\mathbb{Z}_2$ symmetry, under which all the particles in the model are even except for N and η, which are odd. Another important consequence of the spontaneous breaking of lepton number is the generation of the $(H^\dagger\eta)^2$ operator, with a naturally suppressed λ_5 coupling due to the $1/m_S^2$ factor. One finds

$$\frac{\lambda_5}{2}=-\frac{v_{\sigma_1}v_{\sigma_2}\beta_1\beta_2}{2m_S^2}\ll 1\,, \tag{8.83}$$

where β_i are dimensionless parameters of the UV theory and $v_{\sigma_i}\ll m_S$ by construction. This expression clearly corresponds to a II$(1,2)$ model, following the classification of Section 8.2. We now consider the scalar spectrum of the model. We will assume that CP is conserved in the scalar sector, just for the sake of simplicity. In this case, the spectrum contains three CP-even and three CP-odd gauge eigenstates. In the bases $\{\phi,\rho_1,\rho_2\}$ and $\{z,J_1,J_2\}$, their mass matrices are given by

$$\mathcal{M}_R^2=\begin{pmatrix}\lambda_1 v_H^2 & \lambda_3^{\sigma_1}v_H v_{\sigma_1} & \lambda_3^{\sigma_2}v_H v_{\sigma_2}\\ \lambda_3^{\sigma_1}v_H v_{\sigma_1} & \lambda_{\sigma_1}v_{\sigma_1}^2 & v_{\sigma_1}(\mu+\lambda_3^{\sigma\sigma}v_{\sigma_2})\\ \lambda_3^{\sigma_2}v_H v_{\sigma_2} & v_{\sigma_1}(\mu+\lambda_3^{\sigma\sigma}v_{\sigma_2}) & \lambda_2 v_{\sigma_2}^2-\frac{\mu v_{\sigma_1}^2}{2v_{\sigma_2}}\end{pmatrix} \tag{8.84}$$

and

$$\mathcal{M}_I^2=\begin{pmatrix}0 & 0 & 0\\ 0 & -2\mu v_{\sigma_2} & -\mu v_{\sigma_1}\\ 0 & -\mu v_{\sigma_1} & -\frac{\mu v_{\sigma_1}^2}{2v_{\sigma_2}}\end{pmatrix}, \tag{8.85}$$

respectively. The tadpole equations (8.80)-(8.82) were used in the derivation of Eqs. (8.84) and (8.85). The CP-even and CP-odd physical mass eigenstates can be written as linear combinations of $\{\phi,\rho_1,\rho_2\}$ and $\{z,J_1,J_2\}$, respectively, obtained after the diagonalization of the matrices $\mathcal{M}_R^2$ and $\mathcal{M}_I^2$. Out of the three CP-even mass eigenstates, one can be identified with the Higgs boson. In addition, two massive CP-even scalar fields exist. In what concerns the CP-odd mass eigenstates, their mass matrix in Eq. (8.85) can be readily diagonalized as $V_I^T\,\mathcal{M}_I^2\,V_I=\widehat{\mathcal{M}}_I^2$,

where

$$V_I = \begin{pmatrix} 1 & 0 & 0 \\ 0 & \cos\theta & -\sin\theta \\ 0 & \sin\theta & \cos\theta \end{pmatrix} \tag{8.86}$$

is a unitary matrix and $\widehat{\mathcal{M}}_I^2$ is a diagonal matrix. One obtains

$$\widehat{\mathcal{M}}_I^2 = \begin{pmatrix} 0 & 0 & 0 \\ 0 & 0 & 0 \\ 0 & 0 & -\frac{\mu(v_{\sigma_1}^2+4v_{\sigma_2}^2)}{2v_{\sigma_2}} \end{pmatrix}, \tag{8.87}$$

thus leading to two massless pseudoscalar bosons. The first one is the Goldstone boson that becomes the longitudinal component of the Z boson (z), while the second one (a linear combination of fields J_1 and J_2) is associated to the spontaneous breaking of $\mathrm{U}(1)_\mathrm{L}$ and is the so-called majoron, denoted as J. The $J_1 - J_2$ mixing angle is given by

$$\tan(2\theta) = \frac{2\,(\mathcal{M}_I^2)_{23}}{(\mathcal{M}_I^2)_{22} - (\mathcal{M}_I^2)_{33}} = \frac{4v_{\sigma_1}v_{\sigma_2}}{4v_{\sigma_2}^2 - v_{\sigma_1}^2}\,. \tag{8.88}$$

We finally turn our attention to the $\mathbb{Z}_2$-odd scalars and decompose the neutral field η^0 as

$$\eta^0 = \frac{1}{\sqrt{2}}(\eta_R + i\,\eta_I)\,. \tag{8.89}$$

The mass of the charged η^+ and the neutral $\eta_{R,I}$ fields are given by Eqs. (8.35), (8.36), and (8.37), respectively, with the new definitions of λ_5 and

$$\lambda_3^{\text{eff}} \equiv \lambda_3 + \lambda_3^{\eta\sigma_1}\frac{v_{\sigma_1}^2}{v^2} + \lambda_3^{\eta\sigma_2}\frac{v_{\sigma_2}^2}{v^2} \tag{8.90}$$

$$\lambda_4^{\text{eff}} \equiv \lambda_4 - \frac{\beta_1^2 v_{\sigma_1}^2}{2m_S^2} - \frac{\beta_2^2 v_{\sigma_2}^2}{2m_S^2}\,. \tag{8.91}$$

As in the Scotogenic model, the mass difference between η_R and η_I is proportional to the λ_5 coupling:

$$m_{\eta_R}^2 - m_{\eta_I}^2 = -\frac{v_{\sigma_1}v_{\sigma_2}\beta_1\beta_2}{m_S^2}v^2 = \lambda_5 v^2\,. \tag{8.92}$$

Finally, the breaking of $\mathrm{U}(1)_\mathrm{L}$ also induces a Majorana mass term for the N singlets, with $M_N = \sqrt{2}\,\kappa\,v_{\sigma_1}$. This leads to Majorana neutrino masses at 1-loop, as shown in Fig. 8.3. The resulting neutrino mass matrix is given by Eq. (2.59), with the effective λ_5 of Eq. (8.83). Furthermore, contrary to the minimal Scotogenic model, this UV extension induces a 1-loop interaction between the majoron and a pair of charged leptons. This enriches the phenomenology of the model, as we discuss in the next Section.

8.6 Phenomenology

All UV scenarios discussed in our classification of Section 8.2 and illustrated with the three examples of Secs. 8.3, 8.4, and 8.5 share some common features. They are characterized at low energies by a Scotogenic model extended with a massless pseudoscalar, the majoron J, and one or several massive scalars and pseudoscalars. While some phenomenological implications may be specific to particular models, there are also some general expectations that we may highlight.

8.6.1 Majoron coupling to charged leptons

The presence of a massless majoron dramatically affects the phenomenology of this class of models. In fact, models including a majoron are strongly constrained by a variety of experimental limits, such as those originated by the majoron coupling to a pair of charged leptons, as discussed in Chapter 3. The relevance of these limits depends on the flavor structure of the couplings [215], which necessarily depends on the specific model. Stringent constraints exist for both flavor conserving and flavor violating couplings. Let us write the majoron interaction with charged leptons as,

$$\mathcal{L}_{\ell\ell J} = J\,\bar{\ell}_\beta \left(S_L^{\beta\alpha}\,P_L + S_R^{\beta\alpha}\,P_R\right)\ell_\alpha + \text{h.c.}\,, \tag{8.93}$$

which is a particularization of Eq. (3.1) for the majoron. Due to the pseudoscalar nature of majorons, the diagonal $S^{\beta\beta} = S_L^{\beta\beta} + S_R^{\beta\beta *}$ couplings are purely imaginary. As discussed in Chapter 3, they receive strong constraints from astrophysical observations due to the cooling effects induced by the majoron in dense astrophysical media. Flavor off-diagonal couplings are constrained by the null searches of lepton flavor violation in processes involving charged leptons. In particular, searches for $\ell_\alpha \to \ell_\beta\, J$ can be used to set bounds on the combinations

$$|S^{\beta\alpha}| = \left(\left|S_L^{\beta\alpha}\right|^2 + \left|S_R^{\beta\alpha}\right|^2\right)^{1/2}\,. \tag{8.94}$$

A compilation of the current limits on the majoron couplings to charged leptons can be found in Table 3.2.

While in some scenarios the majoron couplings to charged leptons appear at tree-level [250, 321], in many cases the leading order contribution is induced at the 1-loop level. For instance, this is the case of the popular type-I seesaw with spontaneous lepton number violation [206,212,213]. Similarly, in the Scotogenic scenarios discussed in this chapter, the majoron coupling to charged leptons is also induced at 1-loop [413, 415] by the Feynman diagram in Fig. 8.4. Here g_{JNN} is the $J-N-N$ coupling, which depends on the specific model. It is given by

$$g_{JNN} = \begin{cases} i\frac{\kappa}{\sqrt{2}} & \text{in models with one } \sigma \text{ singlet} \\ i\frac{\kappa}{\sqrt{2}}\cos\theta & \text{in models with two } \sigma \text{ singlets} \end{cases}\,, \tag{8.95}$$

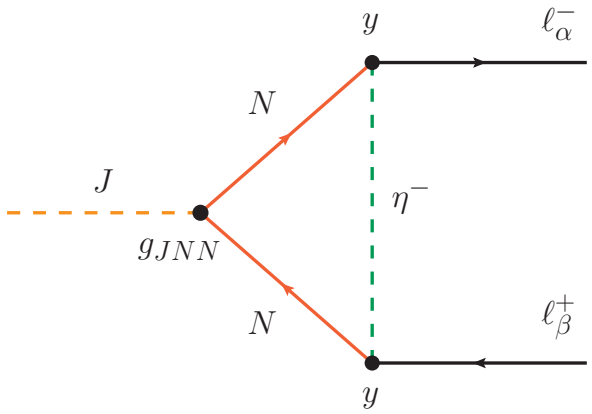

Figure 8.4: 1-loop generation of the majoron coupling to a pair of charged leptons in the Scotogenic scenarios discussed in this work.

where the mixing angle θ is defined in Eq. (8.86). The prefactor $\cos\theta$ in models with two σ singlets is due to the fact that only σ_1 has a coupling to $\overline{N}^c N$. No other contributions to the majoron coupling to charged leptons exist at 1-loop. One may wonder about a Feynman diagram with two scalar lines in the loop induced by a $J\,\eta^+\eta^-$ coupling. However, this contribution vanishes exactly. The reason is the pseudoscalar nature of the majoron. The $J\bar{\ell}_\alpha\ell_\alpha$ vertex must be proportional to γ_5, but the Lorentz structure of this contribution does not generate such pseudoscalar couplings. Indeed, in the case of the η scalars running in the loop, the contribution cannot exist because the combination $\eta^+\eta^-$ is real, while J always comes with an i factor due to its pseudoscalar nature. Thus, a Lagrangian with this vertex would not be Hermitian, and the term is not allowed. Also, diagrams with gauge bosons vanish due to the pure singlet nature of N. Therefore, one can find the $S_{L,R}$ couplings introduced in Eq. (8.93) by direct computation of the diagram in Fig. 8.4. The result can be written as [413, 415]

$$S_L^{\beta\alpha} = -\frac{m_{\ell_\beta}}{8\pi^2}\left(y^\dagger g_{JNN}\,\Gamma\,y\right)_{\beta\alpha}\,, \tag{8.96}$$

$$S_R^{\beta\alpha} = \frac{m_{\ell_\alpha}}{8\pi^2}\left(y^\dagger g_{JNN}\,\Gamma\,y\right)_{\beta\alpha}\,, \tag{8.97}$$

for the non-diagonal couplings and

$$S^{\beta\beta} = -\frac{m_{\ell_\beta}}{8\pi^2}\left(y^\dagger g_{JNN}\,\Gamma\,y\right)_{\beta\beta}\,, \tag{8.98}$$

for the diagonal ones. Here $m_{\ell_\beta} = \{m_e, m_\mu, m_\tau\}$ and we have defined

$$\Gamma_{mn} = \frac{M_{N_n}}{\left(M_{N_n}^2 - m_{\eta^+}^2\right)^2}\left(M_{N_n}^2 - m_{\eta^+}^2 + m_{\eta^+}^2\,\log\frac{m_{\eta^+}^2}{M_{N_n}^2}\right)\delta_{mn}\,. \tag{8.99}$$

We can now study how the bounds on these couplings restrict the parameter space of the models considered in our classification. In the following, we will focus on the 2-body decay $\mu \to eJ$, for

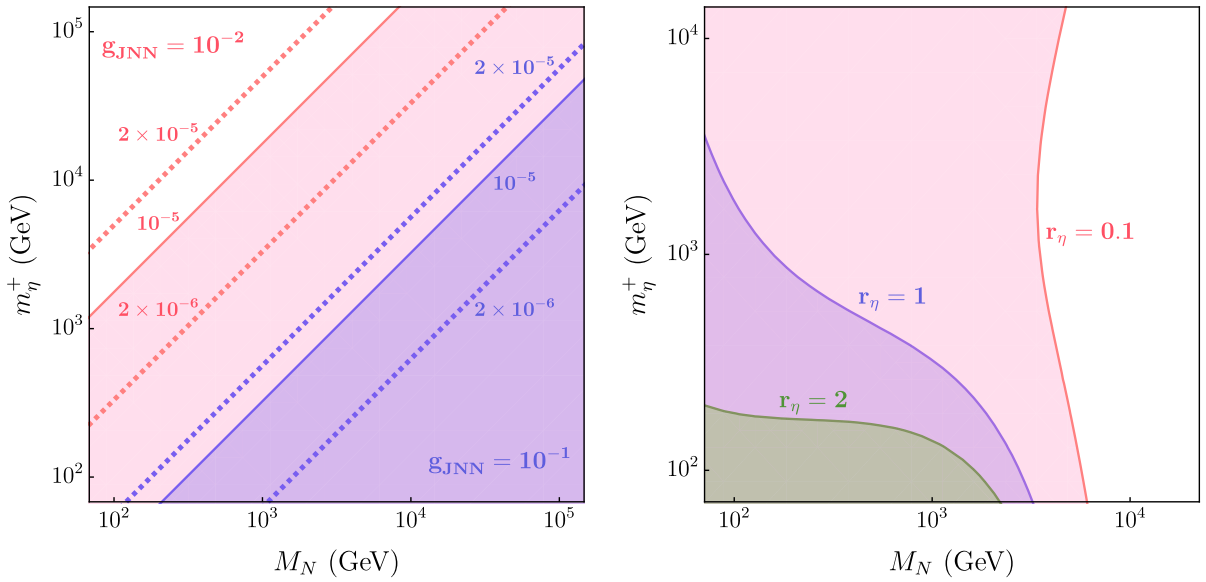

Figure 8.5: Contours of BR $(\mu \to eJ)$ in the $\left(M_N, m_{\eta^+}\right)$ plane. The colored regions correspond to the regions allowed by the current experimental bound on the branching ratio. On the left, g_{JNN} has been fixed to 10^{-1} (blue) and to 10^{-2} (pink), while $r_\eta = 1$ has been used. On the right, the coupling g_{JNN} was not fixed, and three different values of the r_η ratio have been considered, 0.1 (pink), 1 (blue), and 2 (green).

which

$$\mathrm{BR}\,(\mu \to eJ) = \frac{m_\mu}{32\,\pi\,\Gamma_\mu}\left(|S_L^{e\mu}|^2 + |S_R^{e\mu}|^2\right)\,, \tag{8.100}$$

where $\Gamma_\mu \approx 3 \times 10^{-19}$ GeV is the total decay width of the muon. We used a Casas-Ibarra parametrization [200] properly adapted to the Scotogenic model [201,203,204], see Section 2.5.3, and the best-fit values obtained in the global fit [138] to neutrino oscillation data in order to express the Yukawa matrix y in terms of experimentally measured quantities. We assumed that the three singlet fermions are degenerate, that is, $M_{N_1} = M_{N_2} = M_{N_3} = M_N$ and we fixed $\lambda_5 = 5 \times 10^{-8}$. Notice that lower values of this parameter would imply larger values of the Yukawas, thus further restricting the parameter space of the model. It also proves convenient to define

$$r_\eta = \frac{m_0}{m_{\eta^+}}\,. \tag{8.101}$$

Our results are shown in Fig. 8.5. On the left-hand side we fixed the coupling g_{JNN} to 10^{-1} (blue), and to 10^{-2} (pink), and we considered $r_\eta = 1$ in both scenarios. The colored regions correspond to regions allowed by the experimental bound on the $\mu \to eJ$ decay, which implies $\mathrm{BR}\,(\mu \to eJ) < 10^{-5}$ [250]. As expected, the larger the $J - N - N$ coupling is, the smaller the allowed region of the parameter space becomes. We also find that light Scotogenic states can be made compatible with the $\mu \to eJ$ bound. This can be easily understood by inspecting the non-trivial relation between the masses m_{η^+} and M_N and the Yukawa couplings y. Under the

assumptions mentioned above one finds

$$S_{L,R} \propto g_{JNN}\Gamma_{ii}\left(y^\dagger y\right)_{12}\,, \tag{8.102}$$

where Γ_{ii} is any of the diagonal entries of Γ, given by

$$\Gamma_{ii} \propto M_N \frac{M_N^2 - m_{\eta^+}^2 + m_{\eta^+}^2 \log\frac{m_{\eta^+}^2}{M_N^2}}{\left(M_N^2 - m_{\eta^+}^2\right)^2}\,. \tag{8.103}$$

Eq. (2.59) implies that the Yukawa product $\left(y^\dagger y\right)_{12}$ is proportional to

$$\left(y^\dagger y\right)_{12} \propto \frac{1}{M_N}\frac{\left(M_N^2 - m_0^2\right)^2}{M_N^2 - m_0^2 + M_N^2 \log\frac{m_0^2}{M_N^2}}\,. \tag{8.104}$$

Therefore, in the limit $r_\eta = 1$ one finds

$$S_{L,R} \propto g_{JNN}\frac{M_N^2 - m_{\eta^+}^2 + m_{\eta^+}^2 \log\left(\frac{m_{\eta^+}^2}{M_N^2}\right)}{M_N^2 - m_{\eta^+}^2 + M_N^2 \log\left(\frac{m_{\eta^+}^2}{M_N^2}\right)}\,. \tag{8.105}$$

For a fixed g_{JNN} value two possibilities arise: (i) if we fix m_{η^+}, the $\Gamma_{ii}\left(y^\dagger y\right)_{12}$ combination decreases if M_N increases, and (ii) if we fix M_N, the $\Gamma_{ii}\left(y^\dagger y\right)_{12}$ combination increases if m_{η^+} increases. Essentially, the involved couplings strongly depend on m_{η^+} and M_N, and this dependence may lead to an apparent non-decoupling behavior that explains the results for the $\mu \to eJ$ branching ratio observed in Fig. 8.5. Finally, the right-hand side of this figure provides complementary information. Here we considered $g_{JNN} = i\frac{\kappa}{\sqrt{2}} = i\frac{M_N}{2\,v_\sigma}$ and fixed $v_\sigma = 5$ TeV. Since the g_{JNN} coupling grows with M_N, for each m_{η^+} there is a maximum value of M_N for which $\mathrm{BR}\,(\mu \to eJ) < 10^{-5}$. This can be clearly seen in our results.

8.6.2 Collider signatures

Since the spontaneous breaking of $\mathrm{U(1)_L}$ requires the introduction of additional scalar multiplets, all models in our classification have extended scalar sectors containing several states besides the ones in the Scotogenic model. This can be used to probe them at colliders.

One of the CP-even scalars, presumably the lightest, is to be identified with the 125 GeV state discovered at the LHC. The production cross-section and decay rates of this state, denoted generally as h, must agree with the values measured by the ATLAS and CMS collaborations. Since these are very close to those predicted for a pure SM Higgs, $h \approx \mathrm{Re}(H^0)$ is generally required. In particular, mixings with the σ states are strongly constrained since they would affect its decay rates in a twofold way. First, the σ states do not couple to the SM gauge bosons

or quarks. Thus, any mixing would induce a universal reduction of the h partial decay widths into these states. And second, h can have additional decay modes. It can decay invisibly to a pair of singlet fermions ($h \to N_1 N_1$) or a pair of majorons ($h \to JJ$). The former can only take place if $m_{N_1} \leq m_h/2$. In contrast, since the majoron is massless, the latter is always kinematically available. We can write the interaction Lagrangian of h with a pair of majorons as $\mathcal{L}_{hJJ} = \frac{1}{2}\, g_{hJJ}\, h\, J^2$, where g_{hJJ} is a dimensionful coupling that depends on the specific model. This interaction induces the invisible decay $h \to JJ$, with the decay width given by

$$\Gamma(h \to JJ) = \frac{g_{hJJ}^2}{32\,\pi\, m_h}\,. \tag{8.106}$$

If we assume a total Higgs decay width in agreement with the SM expectation, $\Gamma_h \approx \Gamma_h^{\rm SM} = 4.1$ MeV [327], the bound on the invisible Higgs branching ratio $\mathrm{BR}(h \to JJ) < 0.19$ at 95% C.L. [326], implies $g_{hJJ} < 3.1$ GeV. This translates into constraints on the parameters of the scalar potential of the model, which are encoded in g_{hJJ}. For instance, in the model discussed in 8.3, the dimensionful coupling g_{hJJ} is given by

$$g_{hJJ} = v_\sigma\, \lambda_\sigma\, \sin\theta + \left(\lambda_3^{H\sigma} - \frac{v^2\, |\lambda_{H\sigma S}|^2}{m_S^2}\right) v\, \cos\theta\,, \tag{8.107}$$

where the mixing angle θ is defined in Eq. (8.32). Therefore, the previous bound on the coupling g_{hJJ} implies that the $\lambda_3^{H\sigma}$ parameter must be $\lesssim 10^{-2}$. We note, however, that stronger constraints can be derived by combining invisible and visible channels, as recently pointed out in [416].

Finally, all models in our classification also contain additional heavy states. They can also be searched for at colliders. Their production cross-sections and decay models strongly depend on the specific realization of our setup and, more specifically, on their gauge composition. If they have sizable doublet components, they can, in principle, be produced at high rates at the LHC via Drell–Yan processes. In contrast, heavy scalars with a dominant component in the singlet direction have tiny production cross-sections at the LHC. Due to the constraints discussed above, which imply suppressed mixing between the SM Higgs doublet and the σ states, this is the most likely scenario in all models discussed in our classification.

8.6.3 Dark matter

In all the UV models studied in this chapter, a remnant $\mathbb{Z}_2$ symmetry is obtained as a result of the spontaneous breaking of lepton number. This is the Scotogenic $\mathbb{Z}_2$ parity, under which only the usual Scotogenic states N and η are charged. The conservation of $\mathbb{Z}_2$ implies that the lightest of them is completely stable and, in principle, a valid DM candidate. Both options have been widely studied in the literature. In the case of a scalar candidate, the DM phenomenology resembles that of the Inert Doublet model [311–313, 315, 417], with the DM production in the early Universe set by gauge interactions. We note that in this scenario, there is no connection

between lepton flavor violation and DM phenomenologies. In contrast, the case of a fermion candidate typically requires large Yukawa couplings. This leads to tension with bounds from lepton flavor violation [201], although the observed DM relic density can be achieved [202, 418–421].

The low energy theories resulting from our UV extended models do not correspond *exactly* to the original Scotogenic model. As explained above and illustrated in Secs. 8.3 - 8.5, additional scalar states are present: the massless majoron and one or several massive scalars. These new degrees of freedom couple to the $\mathbb{Z}_2$-odd states and may affect the resulting DM phenomenology, which may have some differences with respect to the one in the original Scotogenic scenario. This has recently been studied in [391, 422] for the case of fermion DM. The main conclusion from these works is that the new scalar states open up new regions in parameter space in which the DM relic density can match the observed value. In particular, annihilations become very efficient when the mass of the DM candidate, m_{N_1}, is about half of the mass of a new scalar state. This implies that one can find the correct DM abundance for any value of m_{N_1} without resorting to coannihilations, in contrast to the original Scotogenic model. These models are also expected to have a rich phenomenology at direct and indirect detection experiments [422].

8.7 Summary and discussion

The Scotogenic model is a very popular scenario for neutrino masses and dark matter. In this chapter, we have considered extensions of this scenario that naturally explain the smallness of the quartic λ_5 coupling and the origin of the Scotogenic $\mathbb{Z}_2$ parity. This is achieved in UV extensions including a conserved global lepton number symmetry, spontaneously broken by the VEVs of one or several scalar singlets, and a new heavy state that suppresses all lepton number violating effects at low energies. We explored all possible models with these assumptions and found 50 variations. They are all characterized at low energies by the presence of a massless Goldstone boson, the majoron, as well as other massive scalars besides the usual Scotogenic states. Three specific example models are discussed in detail in order to illustrate the basic ingredients of our setup. In these models, as well as in all the variants in our classification, a rich phenomenology is expected, with potential signatures in collider and lepton flavor violating searches, and implications for dark matter.

Out of the 50 models identified by our analysis, none of them have been studied in the literature, except for the examples in Sections 8.3, 8.4, and 8.5. This illustrates the vast model space beyond the original Scotogenic model, which is yet to be explored. In fact, there are many variations of the fundamental setup that keep all the positive features and include additional ingredients. While many of these modified Scotogenic scenarios may contain unnecessary or redundant ingredients, others may offer novel ways to address open questions in current particle physics [423]. This is the main motivation behind the classification presented in this chapter.

There are several ways in which our analysis can be extended. First of all, we have considered UV theories that realize the λ_5 coupling at tree-level. In this case, the only source of suppression is given by the large energy scale m_S, assumed to lie well above the electroweak scale. Alternatively, the λ_5 coupling can also be realized at loop order, as recently explored in [424]. This possibility leads to many novel extensions of the Scotogenic setup with, at least potentially, new phenomenological expectations. Another way in which our analysis can be extended is by considering a local lepton number symmetry. In this case, the massless majoron that was characteristic in our setup would be replaced by a heavy Z' boson, with a dramatic impact on the low-energy phenomenology. However, we note that this direction requires non-trivial extensions of the fermion particle content in order to cancel out the usual triangle gauge anomalies. Therefore, a general classification of all possible gauge models becomes more cumbersome, although interesting too. Finally, variations with non-universal lepton charges for the N fermions or featuring alternative numbers of generations for the Scotogenic states can be explored as well.

Part IV

Collider Searches

Chapter 9

Collider Searches for Heavy Neutral Leptons: Beyond Simplified Scenarios

"There is nothing like looking, if you want to find something. You certainly usually find something, if you look, but it is not always quite the something you were after."

– J.R.R. Tolkien, The Hobbit

This Chapter, based on [425], is the final part of the thesis and will take a different path. Many neutrino mass models predict the existence of Heavy Neutral Leptons that mix with the Standard Model neutrinos. Here we will be interested in Heavy Neutral Lepton searches at high-energy colliders, mainly at the LHC due to its current extensive program dedicated to them, see, for instance, Ref. [426], and the numerous dedicated works and analyses [427–468].

9.1 Introduction

With very few exceptions, the large amount of available Heavy Neutral Lepton (HNL) bounds have been derived relying on the assumption of a single (usually Majorana) HNL that mixes with only one lepton flavor. Most of the BSM scenarios involving new neutral leptons address the lepton mixing as a whole, as it impacts flavor physics studies and lepton properties (such as the Dirac or Majorana nature of neutrinos) through different lepton number conserving/violating processes. The mixing pattern in these scenarios is expected to be quite complex, making it inadequate to apply bounds derived from negative HNL searches based on simplified hypotheses on the HNL parameter space. Indeed, as we will see, using these limits directly will in general

overconstrain the parameter space. Consequently, most of the experimental bounds for HNL need to be recast before being applied to a generic BSM scenario.

The motivation for reinterpreting LHC bounds is, in general, a well-established topic. See, for example, Ref. [469] and references therein. In the context of HNL searches, the reinterpretation of the obtained bounds on the HNL mixings to active flavors has been addressed in previous works. This is the case of Ref. [460], which discussed searches for Heavy Neutral Leptons with Displaced Vertices, and, more recently, of Ref. [468], focusing on HNLs decaying promptly to a tri-lepton final state. In the latter, the single-flavor mixing results obtained by ATLAS were recast to a low-scale seesaw model with a quasi-degenerate pair of HNLs, which is the most minimal and simple extension in order to accommodate neutrino oscillation data (the lightest neutrino being massless). Due to the simplicity of this model, the active neutrino masses and mixings determine the flavor pattern of the HNLs [178,470], and it is possible to define benchmark points beyond the single-flavor scenario [471]. While being an interesting scenario, this approach has the drawback of being model dependent. For example, considering other sources for light neutrino masses, [1] such as additional HNLs not necessarily within the LHC range, could spoil the correlation between light and heavy sectors that motivated the definition of these scenarios.

For this reason, in this chapter, we will follow a different approach. We will work with physical HNL states with independent mixings and masses, with the motivation of covering every scenario that could be realized at generic BSM models. We will also discuss how to go beyond the simplest single-flavor mixing scenario. However, we will not attempt to explain light neutrino masses and mixings. This idea is actually the most straightforward extension to what is usually assumed at LHC searches. In doing so, we will discuss what the most relevant quantities to be bounded experimentally would be in order to easily reinterpret the results.

Furthermore, we will also extend the study to the case where more than one HNL is present and take into account possible interference effects when at least two heavy neutral leptons are in the same mass regime (nearly degenerate or possibly forming a pseudo-Dirac neutrino pair). This potential interference can lead to different bounds on the active-sterile mixings, see, for instance, Ref. [472–474].

Notice that those models where there is no mixing between the HNLs and the active neutrinos are out of the scope of this Chapter. This is, for instance, the case of the Scotogenic model. The $\mathbb{Z}_2$ parity present in this model prevents the N singlets (which are odd) from mixing with the SM neutrinos (that are even).

9.2 Status of HNL searches at high-energy colliders

Heavy Neutral Leptons can be searched for in a wide variety of processes and experiments, being the HNL mass the key parameter to decide which is the optimal one. HNLs lighter than the GeV scale can lead to signatures in nuclear β decays or in leptonic or semileptonic meson

[1] This would actually be needed in order to relax the hypothesis of the lightest active neutrino being massless and, thus, to have three massive active neutrinos.

and tau decays. On the other hand, heavy HNLs above the TeV are better explored indirectly by electroweak precision observables or rare flavor processes. For a detailed review of all these signals and experimental status, see, for instance, Refs. [475–477].

Here, we are interested in the intermediate regime, with HNL masses M_N ranging from a few to hundreds of GeVs. Such HNLs could be directly produced at high-energy colliders with lifetimes usually short enough to decay within the detectors, enabling us to discover them looking for their decay products. Since these decays are weak processes, the relevant scale to compare to is defined by the masses of the SM gauge bosons. Throughout this Chapter, we refer to HNLs lighter than the W boson as *light HNLs*, and to those with $M_N > M_W$ as *heavy HNLs*. These definitions are in the context of high-energy collider searches. Detailed reviews of HNL searches at colliders can be found in Refs. [478–480]. Here we update and summarize the list of experimental analyses and highlight the most relevant aspects that we will use in our discussion in the following sections.

As in any collider search looking for heavy unstable particles, we need to consider both the production and the decay channels of the HNLs. At a hadronic collider such as the LHC, the main production channel comes from Drell-Yan W and Z bosons,

$$pp \to W^{(*)} \to N\ell^{\pm} \quad \text{and} \quad pp \to Z^{(*)} \to N\nu\,, \tag{9.1}$$

where the gauge bosons could be on- or off-shell, depending on whether the HNL is lighter or heavier than the W or Z bosons. Additional production channels could also arise from the Higgs boson decays, which could be motivated in several models providing large neutrino Yukawa couplings. Unfortunately, Higgs bosons are produced less abundantly than weak bosons, so they are usually neglected. Moreover, the W channel has the additional prompt charged lepton that can help triggering the process and reducing backgrounds, and thus experimental searches focused mostly on this channel. Nevertheless, it is worth mentioning that for very heavy masses, at around the TeV scale, vector boson fusion channels such as $W\gamma$ or WW become important and could even dominate the production of HNLs [435,437,467]. Indeed, the latest CMS analysis [481] already included the $W\gamma$ channel in order to enhance their sensitivity to high HNL masses.

After being produced, a HNL of several GeVs, but still lighter than M_W, will decay dominantly via off-shell W or Z bosons to a 3-body final state

$$N \to \ell^{\pm}_{\alpha} jj\,, \tag{9.2}$$
$$N \to \ell^{\pm}_{\alpha} \ell^{\mp}_{\beta} \nu_{\beta}\,, \tag{9.3}$$
$$N \to \nu_{\alpha} jj\,, \tag{9.4}$$
$$N \to \nu_{\alpha} \ell^{\pm}_{\beta} \ell^{\mp}_{\beta}\,, \tag{9.5}$$
$$N \to 3\nu\,. \tag{9.6}$$

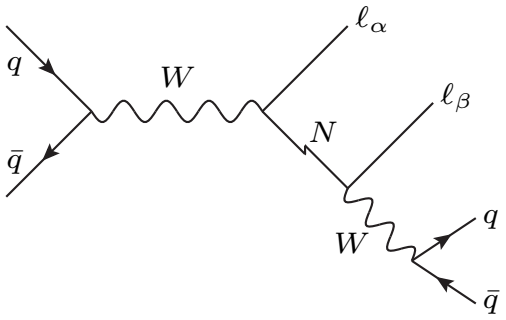

Figure 9.1: Drell-Yann HNL production leading to a dilepton signature. The thunder-shaped arrow indicates that the HNL could be of Dirac or Majorana nature, short- or long-lived.

On the other hand, if M_N is above the EW scale, the dominant decays will be to on-shell W, Z, and H bosons, i.e., $N \to \ell^\pm W^\mp, \nu Z, \nu H$. These 2-body decays will be followed by the decay of the heavy bosons, leading in the end to the same final states as before. Nevertheless, it is important to keep in mind that the kinematics in these two mass regimes will be different.

Combining both production and decay channels, we get a full process such as the example shown in Fig. 9.1. Depending on the relative size of M_N and M_W, either the first or the second W boson will be on-/off-shell, distinguishing the light and heavy HNL regimes. A complete catalog of HNL signatures, combining the different production and decay processes, can be found in Ref. [482]. Here we focus only on those that have been already searched for at the LHC, and we collect them in Table 9.1. Similar searches considering the existence of right-handed currents have also been performed [483–490], and could, in principle, be recast to our setup. Nevertheless, one would naively expect lower sensitivities, as they are optimized for heavy right-handed gauge bosons.

Most of the LHC searches focused on the *smoking gun* signature for Majorana neutrinos, the same sign (SS) dilepton final state:

$$pp \to \ell_\alpha^\pm N \to \ell_\alpha^\pm \ell_\beta^\pm + nj\,. \tag{9.7}$$

Here, the lepton pair is accompanied by at least two jets (see Fig. 9.1) unless M_N is much lighter or heavier than M_W, which leads to boosted objects and collimated jets that are reconstructed as a single one. Being a LNV process, the SS dilepton does not suffer from severe SM backgrounds. Unfortunately, current collider searches are sensitive only to relatively large mixings between the HNL and the active neutrinos, too large to explain the masses of the light neutrinos unless a symmetry protected scenario is invoked. More specifically, this symmetry is an approximated conservation of lepton number [491], which may suppress the expected LNV signal from HNLs, although sizable SS decaying rates can be obtained in some regions of the parameter space (see Refs. [492–495]).

From this point of view, searching for opposite sign (OS) dileptons, as done by LHCb [496], seems more relevant to explore theoretically motivated scenarios. The drawback is the large amount of background from $Z \to \ell^+\ell^-$ decays, which reduces the sensitivity. A possible alternative would be focusing on LFV channels to reduce backgrounds [442, 462].

Yet another alternative considers the fully leptonic process

$$pp \to \ell^\pm_\alpha N \to \ell^\pm_\alpha \ell^\pm_\beta \ell^\mp_\gamma \nu \,. \tag{9.8}$$

This channel has a trilepton signature, rather clean in a hadronic collider. Nevertheless, it also has a source of MET, which might spoil the complete reconstruction of M_N. The trilepton channel offers the possibility to search for both LNV and LNC signals, although most of the experimental analyses still focus only on the LNV channels to reduce backgrounds, again from $Z \to \ell^+\ell^-$. For example, ATLAS searched for $e^\pm e^\pm \mu^\mp$ and $\mu^\pm \mu^\pm e^\mp$ channels, [2] but not for $e^\pm e^\mp \mu^\pm$ and $\mu^\pm \mu^\mp e^\pm$ [497]. CMS did something similar for light HNLs, although they also included channels with OS but same flavor lepton pairs in the heavy HNL regime, removing only those events with lepton pairs compatible with a decay of a Z boson [481]. As stated before for the SS dilepton channel, searching for HNLs without assuming their Majorana nature will be helpful to probe scenarios compatible with neutrino oscillation data and thus with potentially suppressed LNV signals.

Finally, it is important to stress that improving the experimental sensitivities to smaller values of mixings implies exploring HNL with longer lifetimes, which can travel macroscopic distances before decaying. Such long-lived HNLs would avoid the searches mentioned so far, as they all assumed prompt decaying HNLs and, therefore, we need a dedicated search for this kind of topologies. Recently, both ATLAS [498] and CMS [499] have searched for displaced vertex signatures for light HNLs, setting the strongest constraints for GeV masses up to 20 GeV. This can be seen in Fig. 9.2, where we summarize all the relevant LHC constraints explained in this section.

Searches at lepton colliders

Even though our current most powerful high-energy collider is a hadronic one, it is important to stress that lepton colliders are extremely relevant for HNL searches. Not only due to the impressive sensitivities expected at future leptonic colliders such as the FCCee [506], but also because HNL searches at LEP still provide the most relevant limits for some M_N hypotheses.

The great advantage of a leptonic collider is its clean environment, in contrast with the hadronic ones. In the case of LEP, they combined this cleanliness with the huge amount of Z bosons they collected to search for HNLs produced in $Z \to \nu N$ processes. Moreover, they

[2] Having an undetected (anti)neutrino, it is not always possible to define a LNV or LNC process unambiguously. Assuming the presence of a HNL that mixes only to electrons or to muons, as ATLAS did, the $e^\pm e^\pm \mu^\mp$ and $\mu^\pm \mu^\pm e^\mp$ channels are originated only from LNV processes. However, this is not true anymore if the HNL mixes to both flavors [468].

Channel	Lepton Flavor	Experiment	$\sqrt{s}$ [TeV]	$\mathcal{L}$ [fb^{-1}]	M_N [GeV]
Prompt SS dilepton $pp \to \ell_\alpha^\pm N \to \ell_\alpha^\pm \ell_\beta^\pm + nj$	$ee/\mu\mu$	CMS'12 [500]	7	4.98	(50, 210)
	$\mu\mu$	CMS'15 [501]	8	19.7	(40, 500)
	$ee/e\mu$	CMS'16 [502]	8	19.7	(40, 500)
	$ee/\mu\mu$	ATLAS'15 [503]	8	20.3	(100, 500)
	$ee/e\mu/\mu\mu$	CMS'18 [481]	13	35.9	(20, 1600)
	$\mu\mu$	LHCb'20 [496]	7-8	3.0	(5, 50)
Prompt OS dilepton $pp \to \ell_\alpha^\pm N \to \ell_\alpha^\pm \ell_\beta^\mp + nj$	$\mu\mu$	LHCb'20 [496]	7-8	3.0	(5, 50)
Prompt trilepton $pp \to \ell_\alpha^\pm N \to \ell_\alpha^\pm \ell_\beta^\pm \ell_\gamma^\mp \nu$	$eee + ee\mu/\mu\mu\mu + \mu\mu e$	CMS'18 [504]	13	35.9	(1, 1200)
	$ee\mu/\mu\mu e$	ATLAS'19 [497]	13	36.1	(5, 50)
Displaced trilepton $pp \to \ell_\alpha N,\ N \to \ell_\beta \ell_\gamma \nu$	$\mu - e\mu/\mu - \mu\mu$	ATLAS'19 [497]	13	32.9	(4.5, 10)
	6 combinations of e, μ	ATLAS'22 [498]	13	139	(3, 15)
	6 combinations of e, μ	CMS'22 [499]	13	138	(1, 20)

Table 9.1: HNL searches at the LHC, classified according to the type of signal searched for. OS/SS are for opposite/same sign for the charges of final leptons and nj for a number n of final jets.

considered both visible and semi-invisible HNL decays, such as monojet final states [507]:

$$e^+e^- \to \nu N \to \nu\nu q\bar{q}\,, \tag{9.9}$$

with the $q\bar{q}$ pair clustered as a single jet due to the large HNL boost (efficient for $M_N \lesssim 30$ GeV). For heavier masses, $M_N \in (30, 80)$ GeV, the signature is composed of two jets with or without a charged lepton. Such a search would be very challenging at a hadronic collider. However, it has the advantage of being sensitive to all flavors, including the mixing to the τ lepton, not explored so far by LHC searches. The DELPHI results [507], derived for both long-lived and prompt light HNLs, were not improved (for mixings to e and μ flavors) by LHC until very recently and still dominate for some mass ranges (cf. Fig. 9.2).

Additionally, the L3 collaboration explored the heavy HNL regime by considering their production via the t-channel W diagram [508]. This process dominates the heavy HNL production at a e^+e^- collider running above the Z pole, although it is sensitive only to mixings to electrons. The results by L3 still provide the strongest limits for masses between 100 and 200 GeV.

Despite the great effort in the search for HNLs by both LEP and LHC, it is important to analyze their implications for realistic models introducing and motivating the existence of HNLs. A common feature of all these searches is the assumption of a simplified scenario, most of the time consisting on a single HNL mixing to a single lepton flavor, which is not the standard hypothesis one would use from the theory side. To our knowledge, the only exceptions to these simplifications are provided by the recent ATLAS search for long-lived HNLs that also considered a minimal but realistic 2HNL scenario [498], and CMS searches for SS $e\mu$ final states [481, 502],

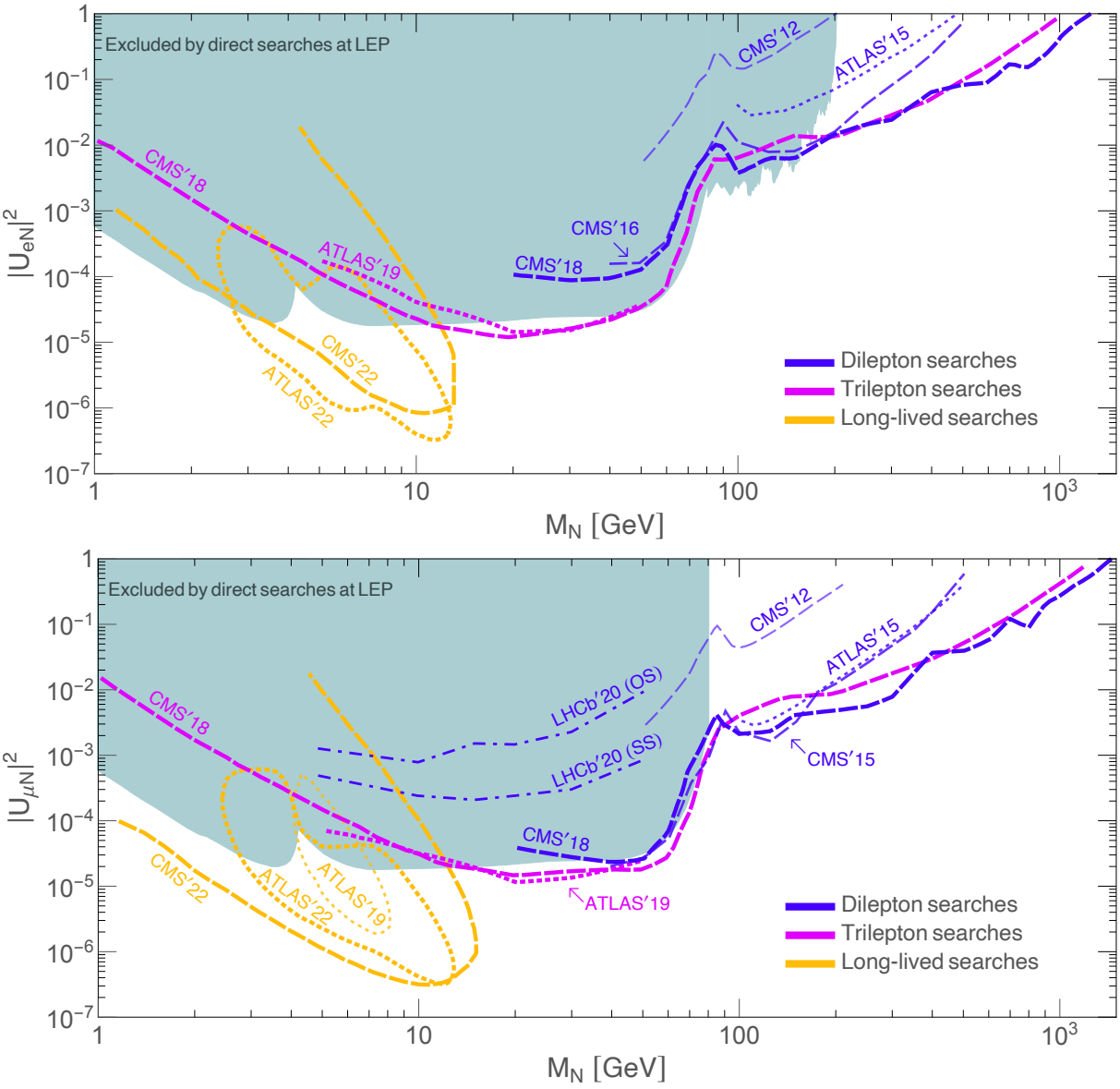

Figure 9.2: Summary of direct HNL searches performed at the LHC so far either by CMS (dashed), ATLAS (dotted), or LHCb (dot-dashed), and grouped by colors for different kinds of searches as given in Table 9.1. In the upper (lower) panel, a single mixing scenario to electrons (muons) is assumed. The shadowed region covers the area excluded by direct searches at LEP. Notice that below 2 GeV and above (approx.) 100 GeV, bounds from meson decays and from non-unitarity of the lepton mixing [505] dominate respectively over current LHC bounds, although we do not show them explicitly for easier reading of the collider results.

although still neglecting the mixing to taus. In the two following sections, we discuss the importance of going beyond these simplified scenarios to explore more realistic scenarios.

9.3 Beyond the single mixing assumption

As explained in the previous section, most of the LHC analyses are done assuming the existence of just one HNL that mixes to a single flavor. We refer to this hypothesis as the single mixing scenario. In this section, we consider deviations from this simplification and discuss their implications for reinterpreting the LHC bounds summarized in Fig. 9.2. In particular, we focus only on prompt searches, while the implications for long-lived HNL were discussed in, for instance, Ref. [460].

For simplicity, we still consider the presence of a single HNL (we will discuss deviations from this hypothesis in the next section). However, we open the room for generic mixing patterns. Moreover, we will follow a bottom-up approach where the SM is extended by *ad-hoc* masses for the three active neutrinos, as required by oscillation phenomena and by the presence of the additional HNL N. In particular, this framework is useful to study the collider phenomenology of HNLs without assuming any specific underlying model or mechanism of light neutrino mass and leptonic mixing generation. [3]

In such a framework, the lepton mixing matrix is thus enlarged to a 4×4 unitary matrix

$$U_\nu = \begin{pmatrix} U_{\nu\nu}^{3\times 3} & U_{\nu N}^{3\times 1} \\ U_{N\nu}^{1\times 3} & U_{NN}^{1\times 1} \end{pmatrix} , \tag{9.10}$$

so the would-be-PMNS matrix $U_{\nu\nu}$ is no longer a unitary matrix, a feature which is indeed used to constrain these models [505]. The fourth column contains the HNL mixings to each flavor:

$$U_{\nu N}^T = (U_{eN}, U_{\mu N}, U_{\tau N}) . \tag{9.11}$$

For our discussion, it is interesting to parametrize this column as

$$U_{\nu N}^T = \sqrt{U^2}\,(\varepsilon_e, \varepsilon_\mu, \varepsilon_\tau) , \tag{9.12}$$

where U^2 represents the total (squared) mixing of the HNL and the ε_α its flavor strengths, with $|\varepsilon_e|^2 + |\varepsilon_\mu|^2 + |\varepsilon_\tau|^2 = 1$. Notice that this framework is precisely the one considered by most LHC analyses, the only difference being that they simplify it by setting the a priori non-relevant mixings to zero. Here, we are interested in knowing how these bounds need to be modified in a generic mixing pattern scenario.

The reason why we expect the bounds to be modified is twofold. The first reason is the importance of the HNL decay width, which depends on every mixing $U_{\alpha N}$, and which plays a major role in the resonant searches (on-shell produced HNL) we are interested in. This means that the final cross sections will depend on all of the mixings, even on those flavors that are not explicitly present in the charged leptons involved in the processes. The second reason is that

[3] Notice, however, that reproducing oscillation data in a given framework may introduce relations between the HNL mass and mixings, shrinking the parameter space we will consider.

for some channels, considering generic mixings could open new contributing diagrams which could modify the distributions and thus the efficiencies of the searches as discussed thoroughly in Ref. [468]. Complete expressions for the computation of the total decay width Γ_N can be found in Ref. [509]. For our purposes, we parameterize it as

$$\Gamma_N = |U_{eN}|^2 \, \Gamma_N^e + |U_{\mu N}|^2 \, \Gamma_N^\mu + |U_{\tau N}|^2 \, \Gamma_N^\tau \,, \tag{9.13}$$

where Γ_N^α stands for the sum of partial decay widths depending on the mixing $U_{\alpha N}$, after factorizing the $|U_{\alpha N}|^2$ dependence itself. Thus, Γ_N^α are independent of the mixings (at leading order) and depend only on the HNL mass. Moreover, when the HNL is heavy enough so that we can neglect charged lepton masses, we get $\Gamma_N^e \simeq \Gamma_N^\mu \simeq \Gamma_N^\tau$ and thus

$$\Gamma_N \propto \sum_\alpha \left|U_{\alpha N}\right|^2 = U^2 \,. \tag{9.14}$$

With this discussion in mind, we can now study how the different processes displayed in Table 9.1 depend on the HNL mixings. Let us start focusing on the dilepton channels, which are the most straightforward cases, as we only need to track the effect of the HNL total decay width.

In the narrow width approximation (NWA), the processes with SS and same flavor dileptons can be factorized in the production of the HNL together with a charged lepton, times its subsequent decay to the same lepton plus jets. The first part depends only on the mixing to the flavor of that lepton, but the second one involves all the mixings due to the HNL decay width. More explicitly, we have

$$\sigma(pp \to \ell_\alpha^\pm N \to \ell_\alpha^\pm \ell_\alpha^\pm + nj) \propto |U_{\alpha N}|^2 \, \mathrm{BR}(N \to \ell_\alpha^\pm jj) \propto \frac{|U_{\alpha N}|^4}{\Gamma_N} \,, \tag{9.15}$$

or, assuming a heavy enough HNL,

$$\sigma(pp \to \ell_\alpha^\pm N \to \ell_\alpha^\pm \ell_\alpha^\pm + nj) \propto U^2 \, |\varepsilon_\alpha|^4 \,. \tag{9.16}$$

Then, we clearly see that those bounds obtained in the single mixing benchmark ($\varepsilon_\alpha = 1$) will be relaxed in a general flavor scenario with a fixed U^2 since, in general, we will have $|\varepsilon_\alpha|^2 \leq 1$. This is actually the expected behavior, as switching on other mixings opens for new decay channels, so not every produced HNL will decay to the final state we are searching for.

We can repeat the exercise for the different flavor SS dilepton processes. Obviously, the minimal setup in this case requires to have two non-zero mixings, leading to two diagrams that, in principle, interfere. Nevertheless, using the narrow width approximation, we can see that both diagrams cannot resonate at the same time, so we can neglect the interference and add

process (prompt)	Relevant parameters (Majorana HNL)	
	approx.	complete dependence
$pp \to \ell_\alpha^\pm \ell_\alpha^\pm + nj$	$U^2 \lvert\varepsilon_\alpha\rvert^4$	$\lvert U_{\alpha N}\rvert^2 \,\mathrm{BR}(N \to \ell_\alpha^\pm jj)$
$pp \to \ell_\alpha^\pm \ell_\beta^\pm + nj$	$U^2 \lvert\varepsilon_\alpha\rvert^2 \lvert\varepsilon_\beta\rvert^2$	$\lvert U_{\alpha N}\rvert^2 \,\mathrm{BR}(N \to \ell_\beta^\pm jj) + \lvert U_{\beta N}\rvert^2 \,\mathrm{BR}(N \to \ell_\alpha^\pm jj)$
$pp \to \ell_\alpha^+ \ell_\alpha^+ \ell_\alpha^- + \not{E}_T$	$U^2 \lvert\varepsilon_\alpha\rvert^4$	$\lvert U_{\alpha N}\rvert^2 \,\mathrm{BR}(N \to \ell_\alpha^+ \ell_\alpha^- \bar{\nu}_\alpha) + \lvert U_{\alpha N}\rvert^2 \,\mathrm{BR}(N \to \ell_\alpha^- \ell_\alpha^+ \nu_\alpha)$
$pp \to \ell_\alpha^+ \ell_\alpha^+ \ell_\beta^- + \not{E}_T$	$U^2 \lvert\varepsilon_\alpha\rvert^2 (\lvert\varepsilon_\alpha\rvert^2 + \lvert\varepsilon_\beta\rvert^2)$	$\lvert U_{\alpha N}\rvert^2 \,\mathrm{BR}(N \to \ell_\alpha^+ \ell_\beta^- \bar{\nu}_\beta) + \lvert U_{\alpha N}\rvert^2 \,\mathrm{BR}(N \to \ell_\beta^- \ell_\alpha^+ \nu_\alpha)$
$pp \to \ell_\alpha^+ \ell_\alpha^- \ell_\beta^+ + \not{E}_T$	$U^2 \lvert\varepsilon_\alpha\rvert^2 (\lvert\varepsilon_\alpha\rvert^2 + 3\lvert\varepsilon_\beta\rvert^2)$	$\lvert U_{\alpha N}\rvert^2 \,\mathrm{BR}(N \to \ell_\alpha^- \ell_\beta^+ \nu\ ) + \lvert U_{\beta N}\rvert^2 \,\mathrm{BR}(N \to \ell_\alpha^- \ell_\alpha^+ \nu\ )$
$pp \to \ell_\alpha^+ \ell_\beta^+ \ell_\gamma^- + \not{E}_T$	$U^2 \sum_{i=\alpha,\beta} \lvert\varepsilon_i\rvert^2 \left(1 - \lvert\varepsilon_i\rvert^2\right)$	$\lvert U_{\alpha N}\rvert^2 \,\mathrm{BR}(N \to \ell_\beta^+ \ell_\gamma^- \nu\ ) + \lvert U_{\beta N}\rvert^2 \,\mathrm{BR}(N \to \ell_\alpha^+ \ell_\gamma^- \nu\ )$

Table 9.2: Summary table for generic flavor dependences of dilepton and trilepton channels at the LHC assuming a single Majorana HNL with generic mixing patterns. Flavor indices are to be understood as different, i.e. $\alpha \neq \beta \neq \gamma$. For trileptons, we are neglecting the effects of differential distributions, as discussed in the text.

both processes incoherently:

$$\begin{aligned}\sigma(pp \to \ell_\alpha^\pm \ell_\beta^\pm + nj) &\propto \left(\lvert U_{\alpha N}\rvert^2 \,\mathrm{BR}(N \to \ell_\beta^\pm jj) + \lvert U_{\beta N}\rvert^2 \,\mathrm{BR}(N \to \ell_\alpha^\pm jj)\right) \\ &\propto \frac{\lvert U_{\alpha N}\rvert^2 \lvert U_{\beta N}\rvert^2}{\Gamma_N} \propto U^2 \lvert\varepsilon_\alpha\rvert^2 \lvert\varepsilon_\beta\rvert^2 . \end{aligned} \tag{9.17}$$

The case of the trilepton channels can be more involved, mainly because we cannot know the lepton number and the flavor carried by the missing (anti)neutrino. Let us consider first the case of same flavor trileptons. There are two contributing diagrams, one with a neutrino and one with an antineutrino, which we can add incoherently. [4] Then, considering for simplicity a W^+ Drell-Yan channel, we have

$$\sigma(pp \to \ell_\alpha^+ \ell_\alpha^+ \ell_\alpha^- + \not{E}_T) \propto \left(\lvert U_{\alpha N}\rvert^2 \,\mathrm{BR}(N \to \ell_\alpha^+ \ell_\alpha^- \bar{\nu}_\alpha) + \lvert U_{\alpha N}\rvert^2 \,\mathrm{BR}(N \to \ell_\alpha^- \ell_\alpha^+ \nu_\alpha)\right) . \tag{9.18}$$

Notice that the first contribution is mediated by the Majorana nature of the HNL, while the second one is of Dirac type. In principle, both contributions are identical when integrated over the full phase space. However, different spin-correlations induce different angular distributions, which might translate into different acceptances under a given experimental analysis. Still, both channels have the same flavor dependence, and we can write

$$\sigma(pp \to \ell_\alpha^+ \ell_\alpha^+ \ell_\alpha^- + \not{E}_T) \propto \lvert U_{\alpha N}\rvert^2 \,\mathrm{BR}(N \to \ell_\alpha \ell_\alpha \nu_\alpha) \propto \frac{\lvert U_{\alpha N}\rvert^4}{\Gamma_N} \propto U^2 \lvert\varepsilon_\alpha\rvert^4 . \tag{9.19}$$

[4] If light neutrinos are of Majorana nature, then there is an interference term, which is, however, negligible as it is proportional to light neutrino masses.

When the trilepton signal involves leptons of two different flavors, we need to consider two subcases: the same-sign same-flavor (SSSF) and opposite-sign same-flavor (OSSF). These channels are trickier because in a generic flavor pattern, there are new diagrams not present in the single mixing scenario. For instance, in the case of the SSSF, we have two types of contributions:

$$\begin{aligned} &\text{Majorana-like:} \quad pp \to \ell_\alpha^+ N\,, N \to \ell_\alpha^+ \ell_\beta^- \bar{\nu}_\beta\,, \\ &\text{Dirac-like:} \qquad\quad pp \to \ell_\alpha^+ N\,, N \to \ell_\beta^- \ell_\alpha^+ \nu_\alpha\,. \end{aligned} \tag{9.20}$$

It is clear that the first process requires a Majorana HNL, while the second one needs mixings to both flavors. As before, the interference is negligible, so we have

$$\sigma(pp \to \ell_\alpha^+ \ell_\alpha^+ \ell_\beta^- + \not{E}_T) \propto \left(|U_{\alpha N}|^2 \,\mathrm{BR}(N \to \ell_\alpha^+ \ell_\beta^- \bar{\nu}_\beta) + |U_{\alpha N}|^2 \,\mathrm{BR}(N \to \ell_\beta^- \ell_\alpha^+ \nu_\alpha) \right). \tag{9.21}$$

Due to the missing (anti)neutrino, both processes are almost identical at the LHC, with the only difference coming again from the different distributions and acceptances of the experimental analysis. This was studied in detail in Ref. [468] for the case of light HNLs. Nevertheless, in order to get a first rough estimate, we can neglect these differences and write

$$\sigma(pp \to \ell_\alpha^+ \ell_\alpha^+ \ell_\beta^- + \not{E}_T) \propto |U_{\alpha N}|^2 \, \frac{|U_{\alpha N}|^2 + |U_{\beta N}|^2}{\Gamma_N} \propto U^2 \, |\varepsilon_\alpha|^2 \, (|\varepsilon_\alpha|^2 + |\varepsilon_\beta|^2)\,. \tag{9.22}$$

The case of OSSF is similar, although now the roles of Majorana and Dirac HNLs are flipped:

$$\begin{aligned} &\text{Majorana-like:} \quad pp \to \ell_\alpha^+ N\,, N \to \ell_\beta^+ \ell_\alpha^- \bar{\nu}_\alpha\,, \\ &\text{Dirac-like:} \qquad\quad pp \to \ell_\alpha^+ N\,, N \to \ell_\alpha^- \ell_\beta^+ \nu_\beta\,. \end{aligned} \tag{9.23}$$

Moreover, since we are working in the prompt HNL regime, we can also have $pp \to \ell_\beta^+ N, N \to \ell_\alpha^+ \ell_\alpha^- \nu_\alpha$. This means that a proper recasting of this kind of signals would require to compute the efficiencies for all these diagrams. If, for the sake of this discussion, we neglect these effects again, we get:

$$\begin{aligned} \sigma(pp \to \ell_\alpha^+ \ell_\alpha^- \ell_\beta^+ + \not{E}_T) &\propto \Big(|U_{\alpha N}|^2 \,\mathrm{BR}(N \to \ell_\alpha^- \ell_\beta^+ \nu_\beta) + |U_{\alpha N}|^2 \,\mathrm{BR}(N \to \ell_\beta^+ \ell_\alpha^- \bar{\nu}_\alpha) \\ &\quad + |U_{\beta N}|^2 \,\mathrm{BR}(N \to \ell_\alpha^- \ell_\alpha^+ \nu_\alpha) + |U_{\beta N}|^2 \,\mathrm{BR}(N \to \ell_\alpha^+ \ell_\alpha^- \bar{\nu}_\alpha) \Big) \\ &\propto |U_{\alpha N}|^2 \, \frac{|U_{\alpha N}|^2 + 3|U_{\beta N}|^2}{\Gamma_N} \propto U^2 \, |\varepsilon_\alpha|^2 \, (|\varepsilon_\alpha|^2 + 3|\varepsilon_\beta|^2)\,. \end{aligned} \tag{9.24}$$

process (prompt)	Relevant parameters (Dirac HNL)	
	approx.	complete dependence
$pp \to \ell_\alpha^\pm \ell_\alpha^\mp + nj$	$U^2 \lvert\varepsilon_\alpha\rvert^4$	$\lvert U_{\alpha N}\rvert^2 \,\mathrm{BR}(N \to \ell_\alpha^\pm jj)$
$pp \to \ell_\alpha^\pm \ell_\beta^\mp + nj$	$U^2 \lvert\varepsilon_\alpha\rvert^2 \lvert\varepsilon_\beta\rvert^2$	$\lvert U_{\alpha N}\rvert^2 \,\mathrm{BR}(N \to \ell_\beta^\pm jj) + \lvert U_{\beta N}\rvert^2 \,\mathrm{BR}(N \to \ell_\alpha^\pm jj)$
$pp \to \ell_\alpha^+ \ell_\alpha^+ \ell_\alpha^- + \not{E}_T$	$U^2 \lvert\varepsilon_\alpha\rvert^4$	$\lvert U_{\alpha N}\rvert^2 \,\mathrm{BR}(N \to \ell_\alpha^- \ell_\alpha^+ \nu_\alpha)$
$pp \to \ell_\alpha^+ \ell_\alpha^+ \ell_\beta^- + \not{E}_T$	$U^2 \lvert\varepsilon_\alpha\rvert^2 \lvert\varepsilon_\beta\rvert^2$	$\lvert U_{\alpha N}\rvert^2 \,\mathrm{BR}(N \to \ell_\beta^- \ell_\alpha^+ \nu_\alpha)$
$pp \to \ell_\alpha^+ \ell_\alpha^- \ell_\beta^+ + \not{E}_T$	$U^2 \lvert\varepsilon_\alpha\rvert^2 (\lvert\varepsilon_\alpha\rvert^2 + \lvert\varepsilon_\beta\rvert^2)$	$\lvert U_{\alpha N}\rvert^2 \,\mathrm{BR}(N \to \ell_\alpha^- \ell_\beta^+ \nu_\beta) + \lvert U_{\beta N}\rvert^2 \,\mathrm{BR}(N \to \ell_\alpha^- \ell_\alpha^+ \nu_\alpha)$
$pp \to \ell_\alpha^+ \ell_\beta^+ \ell_\gamma^- + \not{E}_T$	$U^2 \lvert\varepsilon_\gamma\rvert^2 \left(1 - \lvert\varepsilon_\gamma\rvert^2\right)$	$\lvert U_{\alpha N}\rvert^2 \,\mathrm{BR}(N \to \ell_\gamma^- \ell_\beta^+ \nu_\beta) + \lvert U_{\beta N}\rvert^2 \,\mathrm{BR}(N \to \ell_\gamma^- \ell_\alpha^+ \nu_\alpha)$

Table 9.3: Same as Table 9.2, but for Dirac HNL. We give the OS dileptons in this case since the SS ones are not sensitive to Dirac HNLs.

Finally, and even if no LHC searches have been performed so far, we can also consider the case with three different flavors. Following the same steps, we get

$$\begin{aligned}\sigma(pp \to \ell_\alpha^+ \ell_\beta^+ \ell_\gamma^- + \not{E}_T) \propto \Big(&\lvert U_{\alpha N}\rvert^2 \,\mathrm{BR}(N \to \ell_\beta^+ \ell_\gamma^- \bar{\nu}_\gamma) + \lvert U_{\alpha N}\rvert^2 \,\mathrm{BR}(N \to \ell_\gamma^- \ell_\beta^+ \nu_\beta) \\ &+ \lvert U_{\beta N}\rvert^2 \,\mathrm{BR}(N \to \ell_\alpha^+ \ell_\gamma^- \bar{\nu}_\alpha) + \lvert U_{\beta N}\rvert^2 \,\mathrm{BR}(N \to \ell_\alpha^- \ell_\alpha^+ \nu_\alpha)\Big) \\ \propto\ & U^2 \left\{\lvert\varepsilon_\alpha\rvert^2 \left(1 - \lvert\varepsilon_\alpha\rvert^2\right) + \lvert\varepsilon_\beta\rvert^2 \left(1 - \lvert\varepsilon_\beta\rvert^2\right)\right\}. \end{aligned} \tag{9.25}$$

We summarize our discussion in Table 9.2. Here, we assume a Majorana HNL, although a similar table can be easily obtained for a Dirac HNL just by switching off the LNV channels we discussed above. This is done in Table 9.3. Notice that some channels that were designed for Majorana HNLs are also sensitive to Dirac HNLs in the case of generic mixing patterns, as was already discussed in Ref. [468].

These tables are to be compared with the minimal mixing scenario where all of the processes scale as $|U_{\alpha N}|^2$, or $|U_{\alpha N}|^2|U_{\beta N}|^2/(|U_{\alpha N}|^2 + |U_{\beta N}|^2)$ for $\alpha \neq \beta$. However, we see that, in general, each process is sensitive to different combinations of mixing strengths. This means that, in order to generalize the bounds to a generic pattern, it is better to set bounds on the quantity on the last columns of Tables 9.2 and 9.3, since then we only need to recompute the new BRs for each mixing hypothesis.

While there are some experimental works presenting bounds in the $(M_N, |U_{\alpha N}|^2 \times \mathrm{BR})$ plane, most of the results are given directly in the $(M_N, |U_{\alpha N}|^2)$ one. Translating the latter to the former is straightforward in most of the cases since the experimental collaborations usually assume a constant BR [5] for the channel under study. Although not always specifying the precise value they used. Nevertheless, this recasting to $|U_{\alpha N}|^2 \times \mathrm{BR}$ is not possible when the experimental results on $|U_{\alpha N}|^2$ are presented after combining different channels. This is the case, for instance,

[5] This is a well-justified approximation, but still an approximation that could be avoided by setting bounds directly on $|U_{\alpha N}|^2 \times \mathrm{BR}$.

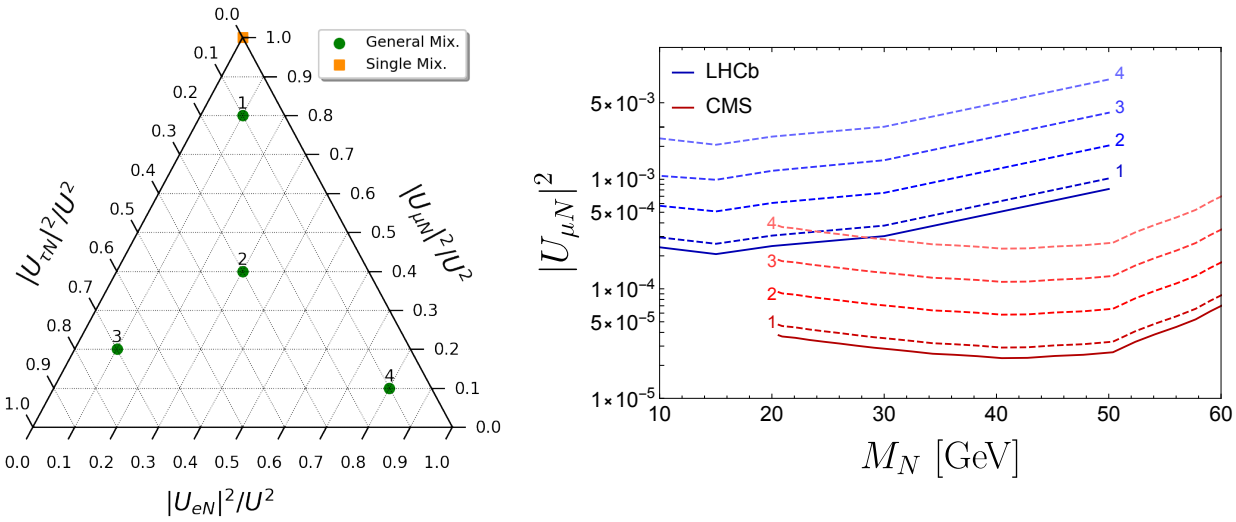

Figure 9.3: Rescaling of the bounds on $|U_{\mu N}|^2$ from CMS [481] (solid red line) and LHCb [496] (solid blue line), fixing the active−sterile mixings to the values corresponding to the green points $1-4$ in the ternary plot on the left. The orange squared point represents the single mixing case.

of the latest CMS searches for trileptons [504], where they combined channels like $e^\pm e^\pm e^\mp$ and $e^\pm e^\mp \mu^\mp$ (see Table 9.1). While in the single mixing scenario both channels depend only on $|U_{eN}|^2$, they have a different dependence in the case of a generic mixing scenario (see Table 9.2), and thus it is not easy to recast the obtained bounds without a dedicated analysis. For this reason, together with the potential efficiency differences discussed above, we will focus the rest of our discussion only on the dilepton channels.

As a case of study for the use of Table 9.2, let us consider the CMS [481] and LHCb [496] searches for the LNV dimuon channel $\mu^\pm\mu^\pm$. For a given total active-sterile mixing U^2, we can display the full flavor mixing space in a ternary diagram, as in the left panel of Fig. 9.3. Then, the single mixing scenario constraints by both CMS and LHCb lie in the top corner. As we move along the ternary diagram, we decrease the flavor strength to muons, so the bounds are relaxed, as shown in the right panel (dashed lines). Here we chose just a few benchmark points for the light HNL mass regime, although the same logic applies to the heavy one.

As discussed above, the physical reason for the relaxation of these bounds is due to the new HNL decay channels in the generic mixing scenario. On the other hand, this also implies that the experimental searches for other channels with different flavors might become relevant. In order to show the interplay between different flavor channels, let us consider a ternary diagram again. We can understand it as a subspace of the parameter space with fixed values of M_N and U^2, which is dissected in flavor space. Then, searches for dimuon channels will cover the area close to the $\varepsilon_\mu = 1$ corner, becoming weaker as we move further away. Equivalently, dielectron searches will cover the ternary from the $\varepsilon_e = 1$ corner, while the $e^\pm\mu^\pm$ channel will cover the area in between. This is depicted in Fig. 9.4 for two benchmark points, one in the light regime ($M_N = 30$ GeV) and one in the heavy regime ($M_N = 300$ GeV).

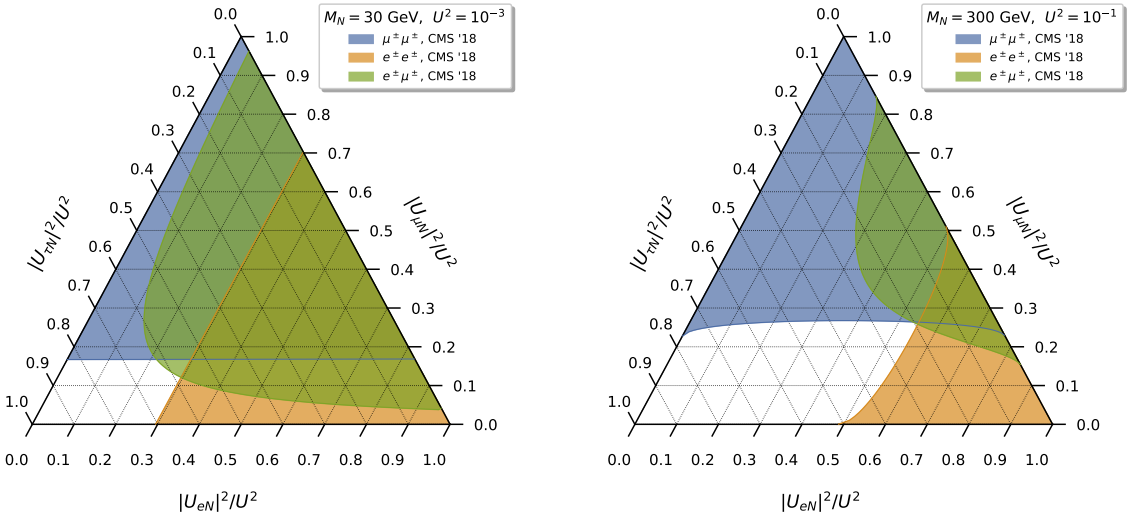

Figure 9.4: Combination of several bounds in a general mixing pattern for two benchmark points of mass M_N and total mixing U^2. Each bound corresponds to the latest SS dilepton searches by CMS (Table 9.1), which were derived within a single mixing scenario (or assuming $U_{\tau N}$ for the $e^\pm\mu^\pm$ channel). The white area is still allowed by LHC searches.

Fig. 9.4 clearly shows the complementarity of the different dilepton searches, to which we could supplementarily add the bounds from trilepton channels if the above mentioned concerns are solved. If the combination of every channel covered all the area of the ternary, we could say that this (M_N, U^2) point is excluded no matter which flavor mixing pattern we were considering. This is not the case in any of the two examples in the figure since the bottom left corner is still allowed by LHC. Notice that this is always the case at present, since there are no LHC searches for HNLs mixing to the tau lepton, so the corner of $\varepsilon_\tau = 1$ will always be allowed. Although we already discussed that a single mixing scenario does not seem very natural for a realistic model including HNLs, closing this gap still motivates the need of performing dedicated searches in the tau sector.

On the other hand, it is important to stress that the benchmark points in Fig. 9.4 are chosen just for illustrative purposes since they are already excluded by LEP searches or global fit bounds. Indeed, this is actually the case in a large part of the parameter space for the current LHC bounds discussed in Section 9.2. Nevertheless, it is worth emphasizing that LHC sensitivities are expected to improve during the currently ongoing runs, pushing our knowledge about HNLs beyond present limits. Therefore, combining the different LHC channels, as we discussed here, will become crucial in order to determine whether a heavy neutral lepton with a given mass and mixing is completely excluded or not.

9.4 Beyond the single HNL

Should HNLs exist in Nature, there is a priori no bound on their number, and, in general, BSM models involving HNLs do not introduce just one of them. For example, in the standard type-I seesaw model, at least two HNLs are needed to explain neutrino oscillation data. In this work, in order to explore deviations from the single HNL hypothesis, we extend the framework considered in the previous section to include more neutral fermions focusing here on the minimal case of SM extension via two HNLs. In this case, the lepton mixing matrix is now a 5×5 unitary matrix

$$U_\nu = \begin{pmatrix} U_{\nu\nu}^{3\times3} & U_{\nu N}^{3\times2} \\ U_{N\nu}^{2\times3} & U_{NN}^{2\times2} \end{pmatrix}, \tag{9.26}$$

with the fourth and fifth columns encoding the mixings of both HNLs to the active leptons

$$U_{\nu N} = \begin{pmatrix} U_{eN_1} & U_{eN_2} \\ U_{\mu N_1} & U_{\mu N_2} \\ U_{\tau N_1} & U_{\tau N_2} \end{pmatrix}. \tag{9.27}$$

For the sake of simplicity, we will assume in this section that the two HNLs mix with just a single flavor. In a sense, it can be seen as extending the interpretation of the bounds of Fig. 9.2 in horizontal in $U_{\nu N}$, to additional columns, while in Section 9.3 we extended them in vertical, to additional flavors. The most general case with several HNLs and arbitrary mixing patterns can then be inferred as a combination of these two discussions.

In the case where only one of these HNLs is within experimental reach or when there are several HNLs but with well-separated mass regimes, our conclusions derived following the single HNL scenario will apply to each of the HNLs. Nevertheless, if two HNLs happen to be close in mass (as motivated by low-scale seesaw models [173, 178, 510], resonant leptogenesis [511] or ARS leptogenesis [512]), they could lead to interference effects and modify the results and the bounds obtained in the single HNL hypothesis. Moreover, these modifications might affect both LNV and LNC branching ratios, and thus studying their correlation could shed light on the nature of the HNL (see [473] and references therein).

In this section, we discuss how these effects could affect the LHC bounds obtained in the single HNL scenario from searches for LNV and LNC channels and provide a recipe to combine both results (on LNV and LNC searches) in order to bring forth more robust bounds on the HNLs parameter space. The recipe is also applicable to the case where HNLs interfere. We mostly focus on the LHCb [496] results for the prompt dimuon channel, since this is the only available analysis addressing both SS and OS dilepton channels (cf. Table 9.1). More specifically, this search considers light HNLs which are dominantly produced from on-shell DY W bosons in Fig. 9.1, that is,

$$pp \to W^+ \to \ell_\alpha^+ N_i \to \ell_\alpha^+ \ell_\beta^+ \, q\,\overline{q}', \quad pp \to W^+ \to \ell_\alpha^+ N_i \to \ell_\alpha^+ \ell_\beta^- \, q\,\overline{q}'. \tag{9.28}$$

In the presence of just a single Majorana HNL, although the angular distributions will be different (see Appendix I for more details), the predictions for the total rates of these two processes are of similar size: equal for channels with $\alpha = \beta$ and twice as large for $\alpha \neq \beta$. The reason for this difference is that the channel with crossed ℓ_α and ℓ_β is also contributing in the case of the LNV process. However, it must be added incoherently to the process since the rate is dominated by on-shell HNLs, fixing the momentum of the first lepton with the 2-body decay kinematics, and thus the interference becomes subdominant. This means that for channels with $\alpha \neq \beta$, the total rate for the LNV process is enhanced by a factor of 2 with respect to the LNC one. On the other hand, in channels with $\alpha = \beta$, there is an additional 1/2 factor from having two identical particles, and thus we obtain the same total rate for both LNV and LNC.

When assuming the existence of two HNLs, we have two identical contributions to the total amplitude of the processes, one for each N_i. The squared amplitude is, then, given as a sum of the individual contributions of each HNL plus a potential interference between the N_1 and N_2 contributions. For each individual contribution to the amplitudes, we find that they are proportional to $U^*_{\alpha N_i} U^*_{\beta N_i}$ for the SS process and to $U^*_{\alpha N_i} U_{\beta N_i}$ for the OS one, proving convenient to define

$$U_{\alpha N_i} = |U_{\alpha N_i}|\, e^{i\phi_{\alpha i}}\,, \tag{9.29}$$

with $\phi_{\alpha i} \in [0, 2\pi]$, $\alpha = e, \mu, \tau$ and $i = 1, 2$. In this way, the interference term resulting from both amplitudes will be proportional to

$$|U_{\alpha N_1}|\,|U_{\alpha N_2}|\,|U_{\beta N_1}|\,|U_{\beta N_2}|\, e^{i\delta\phi^\pm}\,, \tag{9.30}$$

where we have defined $\delta\phi^\pm$ as follows:

$$\delta\phi^\pm = (\phi_{\alpha 2} - \phi_{\alpha 1}) \pm (\phi_{\beta 2} - \phi_{\beta 1})\ \,, \tag{9.31}$$

with $+/-$ for the SS/OS channel. Details with the complete analytical amplitude and decay rates, which we have additionally checked with `WHIZARD` [513], can be found in Appendix I, both for the case with just one HNL and with two HNLs.

As already stated, when the mass difference between the two HNLs is large (compared to their decay width), the contribution of each HNL resonates independently, and the interference is negligible. In this case, the total rates for the LNV and LNC rates are related as in the case of the single HNL scenario. Therefore, in the following, we will assume the scenario where the interference effects can modify considerably the relative predictions between LNV and LNC rates, which corresponds to the case where both HNLs are close in mass. More specifically, we assume that the individual contribution of each HNL is of similar size, $M_{N_1} \simeq M_{N_2} \equiv M_N, \Gamma_{N_1} \simeq \Gamma_{N_2} \equiv \Gamma_N$, and also that $|U_{\alpha N_2}|\,|U_{\beta N_2}| = |U_{\alpha N_1}|\,|U_{\beta N_1}|$. However, we consider that the two HNL mass splitting $\Delta M_N \equiv M_{N_2} - M_{N_1}$ could be different from zero as long as it is small compared to the decay width Γ_N. Notice that this kind of scenario appears naturally in low-scale seesaws due to the approximate lepton number conservation. The only differences are

that, in these models, the phases of the HNLs are fixed to be opposite, i.e., $\delta\phi^+ = \pi$ and $\delta\phi^- = 0$ (the heavy neutrinos forming a pseudo-Dirac neutrino pair), and that ΔM_N is somehow related to light neutrino masses [494, 495], while in the following we will let them free, in the spirit of the bottom-up approach described before.

Under these conditions, we can write the total decay rate driven by the two HNLs in the case of the W^+ channel as

$$\Gamma\left(W^+ \to \ell_\alpha^+ \ell_\beta^\pm q\bar{q}'\right)\Big|_{N_1 \& N_2} = 2\,\mathcal{K}_+\left(y, \delta\phi^\pm\right)\,\Gamma\left(W^+ \to \ell_\alpha^+ \ell_\beta^\pm q\bar{q}'\right)\Big|_{N_1}\,, \tag{9.32}$$

and equivalently for the W^- channel with $\mathcal{K}_-\left(y, \delta\phi^\pm\right)$. Here, we have factorized the total rate in presence of only one HNL and defined the modulation function

$$\mathcal{K}_\pm\left(y, \delta\phi^\pm\right) \equiv \left(1 + \cos\delta\phi^\pm \frac{1}{1+y^2} \mp \sin\delta\phi^\pm \frac{y}{1+y^2}\right), \tag{9.33}$$

with

$$y \simeq \frac{\Delta M_N}{\Gamma_N}\,. \tag{9.34}$$

The function $\mathcal{K}_\pm$ codifies the role of the interference. In the limit of $\Delta M_N \gg \Gamma_N$, the two HNL are too separated in mass, coherence is lost, and the total contribution is just twice the single HNL contribution for both LNV and LNC. On the other hand, for $\Delta M_N < \Gamma_N$, the modulation function can take values from 0 (maximally destructive interference) to 2 (maximally constructive). Thus, we are maximizing the effects of the interference between the two HNLs. Moreover, these effects will be different for LNV and LNC, breaking the equal size prediction in the single HNL scenario.

These modulation functions can be used to simply recast the bounds derived by LHCb [496] under the assumption of a single HNL. Noticing that LHCb searched only for the W^+ channel and given Eq. (9.15), to recast these bounds to our scenario with two HNLs, we need to rescale the mixing as

$$|U_{\mu N}|^2 \to |U_{\mu N}|^2 \times 2\mathcal{K}_+\left(y, \delta\phi^\pm\right)\,, \tag{9.35}$$

with $\delta\phi^- = 0$ in this channel with $\alpha = \beta$. Following this modulation, we show in the left panel of Fig. 9.5 how the LHCb bounds might vary, depending on the values of y and the relative phases $\delta\phi^+$, for both LNV and LNC searches, which defines the green and blue bands, respectively. The vertical axis needs to be understood now as the (squared) mixing of each of the HNLs to muons, which in absence of interference ($y \gg 1$), is just a factor of two stronger with respect to the single HNL scenario. For $y \ll 1$, however, constructive interference can strengthen the bounds by up to an additional factor of two, while destructive interference could relax it, even avoid it completely in the case of LNV signals. The latter corresponds to the case where $\delta\phi^+ = \pi$, which is precisely when the two HNLs have opposite phases (thus forming a pseudo-Dirac pair), as required by low-scale seesaws with approximate lepton number conservation. Interestingly, the same choice of parameters that maximizes the destructive interference of LNV channels also

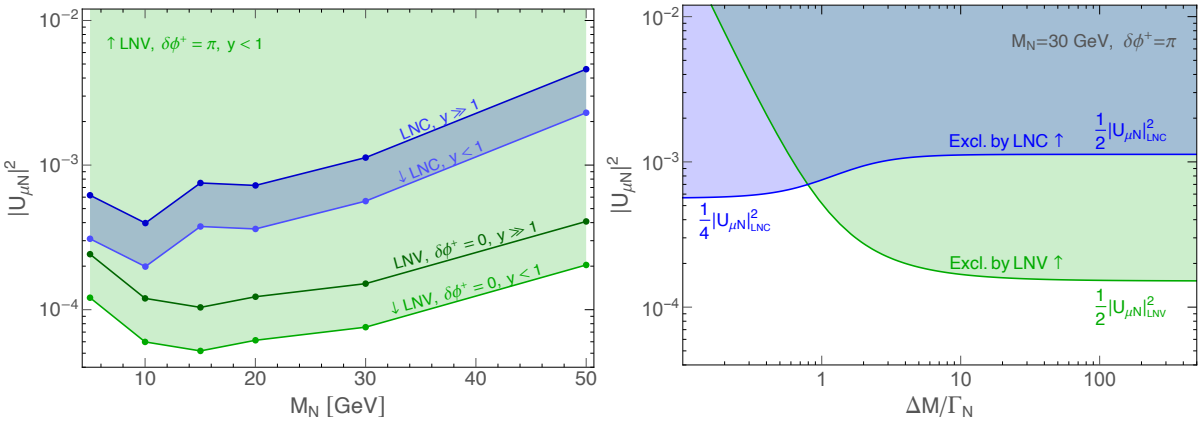

Figure 9.5: Left: rescaling of the bounds on $|U_{\mu N}|^2$ from LHCb [496] in the presence of two HNLs. The dark blue line is the LHCb bound in the LNC searches, while in lighter blue (lower curve) is the rescaled bound for $y = \Delta M_N/\Gamma_N < 1$. The dark green line is the bound in the LNV searches, which can be relaxed (upper green region) if the $N_{1,2}$ form a pseudo−Dirac pair ($\delta\phi^+ = \pi$, $y \ll 1$), or strengthened (lower green region) if $\delta\phi^+ = 0$. Right: $|U_{\mu N}|^2$ as a function of y, with $M_N = 30$ GeV and $\delta\phi^+ = \pi$. The blue (green) region is for the LNC (LNV) channel with the thick lines corresponding to the (rescaled) LHCb bounds to the case of a low-scale seesaw with pseudo-Dirac HNL pair.

maximizes the constructive interference for the LNC ones, making the bounds from the latter stronger.

This interplay prompts us to consider both channels at the same time, using their complementarity to set absolute bounds on the mixings that could not be avoided even with *ad-hoc* values of the parameters that maximize the interference. We show this in the right panel of Fig. 9.5 for a particular example of $M_N = 30$ GeV and opposite phases, $\delta\phi^+ = \pi$, as required by low-scale seesaws. When the contributions of the two HNLs are maximally coherent ($y \ll 1$), the LNV searches are avoided at the price of maximizing the LNC bounds. If coherence is lost ($y \gg 1$), then the stronger LNV bounds always dominate over the LNC ones. We see then that the largest possible mixing could be obtained between the two cases when the two tendencies cross over, which we can consider as an absolute bound on the mixing that cannot be avoided even with two interfering HNLs.

To summarize, searches for LNC and LNV processes are important and complementary since they can cover different areas of the parameter space even in cases where there is some interference (partially) canceling any of the two channels. This strongly motivates the need to search for both LNC and LNV channels in parallel, even if the latter is more challenging experimentally since combining both of them could set more robust bounds on generic scenarios, including more than one heavy neutral lepton.

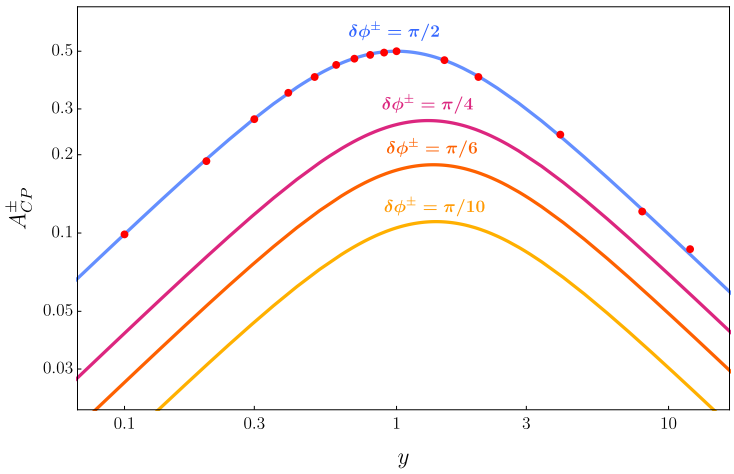

Figure 9.6: CP violating ratio $A^{\pm}_{\rm CP}$, defined in Eq. (9.37), as function of the relevant ratio $y = \Delta M_N/\Gamma_N$ and for different choices of the relative phases $\delta\phi^{\pm}$. Red dots were obtained with `WHIZARD` as a cross-check of our analytical results.

CP violation

When a quasi-degenerated pair of HNLs is considered, new CP-violating phases are introduced, which can induce differences in the decays of these particles to leptons over antileptons. If HNLs were discovered in processes such as those in Eq. (9.28) and provided that enough events were collected, one way of measuring this potential CP asymmetry would be by defining the ratio [474]

$$A^{\pm}_{\rm CP} = \frac{\text{BR}\left(W^- \to \ell^-_\alpha \ell^{\mp}_\beta \bar{q} q'\right) - \text{BR}\left(W^+ \to \ell^+_\alpha \ell^{\pm}_\beta q \bar{q}'\right)}{\text{BR}\left(W^- \to \ell^-_\alpha \ell^{\mp}_\beta \bar{q} q'\right) + \text{BR}\left(W^+ \to \ell^+_\alpha \ell^{\pm}_\beta q \bar{q}'\right)} \,. \tag{9.36}$$

Using our previous results for the W decays, see Eq. (9.32), it is straightforward to see that $A^{\pm}_{\rm CP}$ takes the simple form

$$A^{\pm}_{\rm CP} = \frac{y \, \sin\delta\phi^{\pm}}{1 + y^2 + \cos\delta\phi^{\pm}} \,, \tag{9.37}$$

where $+/-$ denotes again LNV/LNC processes.

As one can see, this equation does not depend on the HNL masses but on their mass difference ΔM_N (through $y = \Delta M_N/\Gamma_N$). It vanishes for the obvious case of $\delta\phi^{\pm} = 0$, since then there is no difference in both the W decay and its CP equivalent; notice that it is also the case when y is close to zero or too large. This is shown in Fig. 9.6 where we display the CP asymmetry for different values of $\delta\phi^{\pm}$.

Notice that a similar computation was performed in Ref. [474] with which our results agree but with some slight differences. On the one hand, we find a discrepancy when applying the narrow width approximation for the interference term (see Appendix I for more details). On the other hand, we performed the computation considering very prompt heavy neutral leptons, so we did not take into account their time evolution and their possible oscillations before decaying. Our approach is appropriate for heavy HNLs, while one should take into account the evolution

effect for very light HNLs with longer decay lifetimes, as it was done in Ref. [474]. Finally, we also point out that, in order to measure A_{CP} at a proton-proton collider, we must take into account that the production rates for W^+ and W^- are not the same [474].

9.5 Conclusions

In this chapter, we focused on LHC searches of heavy neutral leptons that decay promptly (short-lived). In most of the searches, which we summarized in Section 9.2, the obtained bounds were derived under the hypothesis of the existence of a single (usually Majorana) HNL that mixes with only one lepton flavor, while most of the BSM scenarios involving new neutral fermions require more than one HNL. Moreover, unless some specific symmetries are present, the mixing pattern in these BSM scenarios is more complex, each HNL mixing in general with all charged leptons, and thus, the bounds derived from negative searches on the HNL parameter space have to be recast before being applied to a generic BSM scenario.

In this study, we discussed how to recast the present experimental bounds on the parameter space of HNLs, to the case of generic mixing to all active flavors as well as to the case with several HNLs. The former was covered in Section 9.3, where we inspected the flavor dependencies of each of the channels searched for by the LHC and stressed the importance of setting bounds not only on the mixings but on the relevant combination of $|U_{\alpha N}|^2 \times \mathrm{BR}$ (see Tables 9.2 and 9.3). Considering the bounds on this combination, we proposed a method to combine the results in flavor space, using the ternary diagrams in Fig. 9.4 to conclude whether that area of parameter space is fully excluded, regardless of the assumed mixing pattern.

In the case with several heavy neutral leptons, we focused on the scenario when two HNLs are in the same mass regime, nearly degenerate or possibly forming a pseudo-Dirac neutrino pair, paying special attention to the non-trivial role of the interference between their contributions. To illustrate its importance, we focused on dilepton channels and moreover considered both channels with the same and opposite charge of the final leptons, as it was done by LHCb [496]. We showed the complementarity of the LNC and LNV searches and the importance of performing both of them in parallel. We stressed that, by doing this, we are not only taking into account the two possible natures of a single HNL, Dirac or Majorana, but also covering the case when, for example, two Majorana HNLs exist and however they interfere destructively, suppressing the expected LNV signature.

To summarize, we have discussed the importance of going beyond simplified scenarios such as the single mixing hypothesis. While they are useful for simplifying experimental analyses, they are not directly applicable to BSM models introducing HNLs. Unfortunately, recasting the current bounds of each experiment to a given BSM scenario can be tedious. In this work, we have proposed an alternative way of presenting the constraints on the parameter space of the HNLs, which, under some approximations, can be directly constrained by experimental analyses and easily recast to a generic BSM scenario.

Part V

Final Remarks

Final Thoughts

The prediction of the Standard Model that neutrinos are massless stands as one of its most significant limitations. The experimental observation of neutrino flavor oscillations directly contradicts this theoretical result and constitutes the clearest evidence of physics beyond the model. This phenomenon unequivocally confirms the existence of neutrino masses, although tiny, and reveals the presence of mixing between them, implying that lepton flavor is violated. Nevertheless, the mechanism responsible for generating their masses, as well as determining their Dirac or Majorana nature, remains elusive, leaving researchers with a compelling motivation to unravel these mysteries.

In Chapters 1 and 2, we have thoroughly discussed the need for going beyond the Standard Model of particle physics due to the existence of several anomalies that we present there. However, the number of unresolved questions that the model cannot answer is vast, making it impractical to address them all in a thesis. Instead, we have focused on selected problems that are hinting at the presence of new physics in the lepton sector of the SM.

Most of the works presented in this thesis have focused on studying and proposing neutrino mass models. In particular, neutrinos can acquire Majorana masses if the lepton number symmetry, L, is violated. This can happen both explicitly, just by adding lepton number violating interactions or mass terms to the Lagrangian, or spontaneously. If the symmetry is global, the latter includes a massless Goldstone boson, usually called the *majoron*, J. Motivated by this possibility, in Chapter 3, we studied the possible impact of an ultralight scalar, a scalar much lighter than the electron, on leptonic observables. Considering a model independent approach that included both scalar and pseudoscalar interactions, we computed the leptonic observables of interest analytically, including several 2- and 3-body charged lepton decays and the lepton magnetic and electric dipole moments. However, the ultralight scalars that we considered were leptophilic and it may also be interesting to allow these particles to have couplings with quarks.

Besides neutrino masses, more anomalies are currently demanding an explanation. One example of these other anomalies is the long-standing discrepancy between experiments and the SM prediction for the anomalous magnetic moments of the electron and the muon. Both deviations can be accommodated by considering an extension of the inverse type-III seesaw with a pair of vector-like leptons, as we have shown in Chapter 4. Although these deviations may be due to a problem with the theoretical calculations, their possible connection to the neutrino mass mechanism could shed light on the neutrino mass problem. The anomaly in the case of the muon

was also addressed, although as a by-product, in Chapter 6. In this case, with a variation of the type-I seesaw with a vector-like lepton and spontaneous Lepton Number Violation. However, this model aimed to motivate the experimental search for charged lepton flavor violating processes, proving that large rates for them, close to the experimental sensitivities, are common to some neutrino mass models.

Other interesting deviations are the B flavor anomalies, with hints of lepton flavor universality violation. In Chapter 5, thanks to the introduction of a dark sector contributing to the observables of interest, we achieved an economical explanation for these anomalies as well as for the anomalous magnetic moment of the muon while generating neutrino masses and providing a weakly-interacting dark matter candidate. However, in this Chapter, we just focused on the $b \to s\ell\ell$ processes, leaving the anomalies in $b \to c\ell\nu$ observables aside. Alternative versions of this model, including a vector leptoquark and extending the gauge symmetry, may address both deviations from the SM predictions at the same time.

Among the plethora of neutrino mass models, an appealing possibility are radiative models. That is, models that induce neutrino masses at the loop level. What makes these models interesting is that the suppression introduced by the loop factors allows us to accommodate the observed neutrino mass scales with sizable couplings and relatively light mediators. In addition, some of these radiative models include discrete symmetries connected to the generation of neutrino masses that can be used to obtain a viable dark matter candidate. Regarding this class of models, one of the first and (possibly) the most popular one is the Scotogenic model. Many variations and extensions have been proposed since its appearance, and in Chapter 7, we introduced the *general Scotogenic model* with arbitrary numbers of generations of the original Scotogenic states. After computing the analytical expression for the neutrino mass matrix in the general version of the model, we also studied its high-energy behavior. Also, in Chapter 8, we proposed ultraviolet completions for the Scotogenic model in order to address some open questions of it. Specifically, neutrino masses in this model are proportional to a small parameter in the scalar potential, the so-called λ_5 quartic term, and even though it is naturally small in the sense of 't Hooft, its smallness is not explained in the context of the model. In addition, the *dark* $\mathbb{Z}_2$ parity is an *ad-hoc* symmetry. Therefore, in our completions, an explanation for the smallness of the λ_5 parameter is provided and the $\mathbb{Z}_2$ is obtained as a residual symmetry from the spontaneous breaking of the lepton number symmetry $U(1)_L$, which also implies the existence of a majoron.

Finally, out of all the possibilities to generate neutrino masses, Heavy Neutral Leptons are often present as building blocks of the mechanisms. The presence of these particles may modify the charged and neutral currents if the leptonic mixing matrix not only includes the usual PMNS matrix but also the active-HNL mixings. Of course, these modifications would imply an impact on numerous observables, leading to abundant constraints on the new mixings. However, and with very few exceptions, the large amount of available experimental bounds on HNLs have been derived under the assumption of the existence of just a single (usually Majorana) sterile

fermion which only mixes with one lepton flavor. And this is not the case in most of the new physics scenarios involving these particles, which usually have a complex mixing pattern involving several HNLs. Therefore, in Chapter 9, we discussed how the available bounds on the active-HNL mixings from LHC searches can be reinterpreted when it comes to considering more generic mixing patterns. The main result was that the experimental constraints should be presented in a particular way in order for them to be easily recast to any new physics scenario.

Summing up, along the thesis, we have presented and discussed several tree-level and radiative neutrino mass models with both model building and phenomenological motivations. Particularly interesting are those models that connect the neutrino mass generation with explanations for other important anomalies, such as those in the leptonic sector of the Standard Model or the dark matter problem. In addition, numerous models that generate neutrino masses also predict important lepton flavor violating rates. This emphasizes the importance of conducting searches not only for potential particles that could explain the anomalies but also for processes that violate lepton flavor.

Summary of the Thesis

In this part of the thesis, we will present a comprehensive overview of the work. It will include an introduction and an outline of the research objectives, a description of the methodology used, a summary of the main findings in each chapter, and the conclusions drawn from the thesis as a whole.

Introduction

Physicists in the latter half of the 20th century developed what is now considered the most precise and successful theoretical framework, the Standard Model of particle physics. This model describes three of the four fundamental forces found in Nature: electromagnetism, weak, and strong interactions. It is a relativistic quantum field theory that remains invariant under the Lorentz group transformations, and it is based on gauge invariance under the symmetry group

$$\mathrm{SU(3)_C} \times \mathrm{SU(2)_L} \times \mathrm{U(1)_Y}\,. \tag{1}$$

The forces are mediated by the exchange of spin-1 gauge bosons. The strong force is described by the $\mathrm{SU(3)_C}$ group and its 8 massless gauge fields, called gluons. In contrast, the electroweak force is governed by the symmetry group $\mathrm{SU(2)_L} \times \mathrm{U(1)_Y}$. This force is carried by 3 $\mathrm{SU(2)_L}$ W gauge bosons and 1 $\mathrm{U(1)_Y}$ B gauge boson. Together, these four gauge bosons provide the framework for the electroweak force, which unifies electromagnetism and weak forces.

Regarding the fermion content of the model, they can be grouped in different $\mathrm{SU(2)_L}$ multiplets depending on the chirality of the fields. The left-handed particles are organized as $\mathrm{SU(2)_L}$ doublets while the right-handed ones are $\mathrm{SU(2)_L}$ singlets:

$$\begin{pmatrix} \nu_e \\ e \end{pmatrix}_L \quad , \quad \begin{pmatrix} u \\ d \end{pmatrix}_L \quad , \quad e_R \quad , \quad u_R \quad , \quad d_R\,. \tag{2}$$

In addition, in the SM, the quarks and leptons have three families (or flavors) and the structure of multiplets above is replicated three times.

The gauge group given by Eq. (1) represents the symmetry group of the SM, which forbids any of the particles in the model from having mass terms in the Lagrangian. However, we know from experiments that particles possess masses, necessarily implying that the symmetry must

be broken. One can break a symmetry explicitly or spontaneously, but in the case of a gauge symmetry, only the latter option is viable.

In the SM, spontaneous symmetry breaking is achieved through the Higgs mechanism. This mechanism introduces a new scalar field with a scalar potential preserving the gauge symmetry, but the ground state of the theory does not. [1] Since the electroweak symmetry is meant to be spontaneously broken down to electromagnetism, $\mathrm{U(1)_Q}$, the simplest way to achieve this is by introducing a doublet under $\mathrm{SU(2)_L}$ with hypercharge $Y = 1/2$, known as the Higgs doublet:

$$H = \begin{pmatrix} H^+ \\ H^0 \end{pmatrix} . \tag{3}$$

The ground state of the SM is obtained once the Higgs doublet gets the appropriately chosen Vacuum Expectation Value

$$\langle H \rangle = \frac{1}{\sqrt{2}} \begin{pmatrix} 0 \\ v \end{pmatrix} , \tag{4}$$

breaking the gauge symmetry of the standard model spontaneously such that

$$\mathrm{SU(3)_C \times SU(2)_L \times U(1)_Y} \quad \rightarrow \quad \mathrm{SU(3)_C \times U(1)_Q} . \tag{5}$$

After the process of electroweak symmetry breaking, the gauge bosons of the weak interaction and the fermion fields successfully and naturally get masses, as desired. However, the SM does not include right-handed neutrinos, and as a result, neutrinos are predicted to be massless in the theory. This leads to the conservation of lepton flavors within the model.

Although the SM is a highly successful theory that obeys a complex set of symmetries and has earned its place among the greatest achievements of humanity, it still has some gaps that need to be addressed. Some of the important issues that the theory faces include:

Neutrino masses Neutrinos in the SM are massless by construction, but neutrino oscillation experiments have clearly established that this is not correct. This evidence is considered by many to be the most robust indication of new physics beyond the Standard Model. As a result, there is a need for an extension of the SM lepton sector with new degrees of freedom, which typically lead to deviations in other observables, whether directly associated with leptons or not.

Dark matter The observation of the rotation curves of galaxies provides evidence for the existence of dark matter, which is additional matter that we can not see but makes up approximately 25 % of the energy content of the Universe. However, the nature of this matter is still a mystery.

[1] The ground state of any theory is the state of minimum energy.

Charged leptons anomalous magnetic moments The electron and muon anomalous magnetic moments have a long-standing discrepancy between the Standard Model predictions and their experimental values. This suggests the presence of new states beyond the SM and calls for a non-trivial extension of the model. The muon $g-2$ has been considered in various contexts, including models for neutrino mass generation and as a motivation for a muon collider. Further measurements and refined theoretical calculations are needed to confirm the relevance of these anomalies.

***B* flavor anomalies** The B flavor anomalies refer to a set of observations involving B-meson decays that do not match the theoretical predictions of the Standard Model. They are divided into two types: neutral-current anomalies, which occur in $b \to s\ell\ell$ decays, and charged-current anomalies, which are seen in $b \to c\ell\nu_\ell$ decays. The first observation of these anomalies was made about a decade ago, and since then, there has been an increase in the number of measurements, which also showed significant deviations from the SM. Nevertheless, recent results from experimental collaborations have reduced the discrepancies between the experimental measurements and the SM predictions.

This first anomaly presented here is, perhaps, the most urgent problem of the model, so we will delve further into the issue. Neutrino oscillations occur due to the fact that neutrino mass eigenstates do not coincide with neutrino flavor eigenstates, and ones can be expressed as a superposition of the others. Then, a neutrino traveling through space changes from one flavor to another with a probability depending on the distance traveled, the neutrino energy, the mass differences, and the mixing parameters. The values of the parameters that are measured, with good precision, in neutrino oscillation experiments are summarized in Table 2.1, although there are still some unknown questions in neutrino physics. For instance, we do not know the precise number of neutrinos that exist, nor have we determined the neutrino mass ordering. Additionally, the nature of neutrinos remains an unresolved question: specifically, whether they are Dirac or Majorana particles.

From a model-independent point of view, the Weinberg operator $\mathcal{O}_W$ is the lowest dimensional operator, violating lepton number, that can be added to the SM Lagrangian in order to generate Majorana masses for the neutrinos. There are three possible ways to generate the Weinberg operator at tree-level in a renormalizable theory: through the well-known type I, type II, and type III seesaw mechanisms. Thanks to the addition of a singlet fermion, a triplet scalar, or a triplet fermion, respectively, these models can generate tiny neutrino masses by means of huge new physics scales. Nevertheless, there are extensions of these scenarios, such as the inverse seesaw mechanisms, where nearly conserved symmetries are used to relax the large mass scales required. An interesting alternative to tree-level mechanisms are radiative neutrino mass models, such as the famous Scotogenic model. In spite of requiring different mechanisms and symmetries compared to the usual seesaw mechanisms, the suppression introduced by the

loop factors allows us to accommodate the observed neutrino masses and mixings with sizable couplings and relatively light mediators, typically leading to a richer phenomenology.

An interesting possibility for neutrino mass models is that non-zero masses for the neutrinos can be originated due to the violation of lepton number, which can result in neutrinos being Majorana particles. While it is possible to add explicit lepton number violating terms to the Lagrangian of the model, it is also possible for the violation of lepton number to be spontaneous in origin. This spontaneous symmetry breaking would generate a massless Goldstone boson called the majoron. The presence of this boson in the particle spectrum of the theory may affect the phenomenology.

Objectives

The main objective of this thesis has been to study BSM models primarily designed to explain the origin of neutrino masses. Throughout the majority of the thesis, we have assumed that neutrinos are Majorana particles, as is common in the scientific literature. In many of the chapters, we have proposed variations of some of the standard seesaw and inverse seesaw mechanisms, as well as explored the Scotogenic mechanism, which has played a significant role in constructing several models in this thesis. In some cases, we aimed to connect the neutrino mass generation to other anomalies mentioned above, while also considering the potential for sizable LFV rates in the leptonic charged sector which is predicted by many extensions of the SM that generate neutrino masses, even though there is no experimental evidence for such rates. This must be used to constrain the parameter space of any model. This has been done in Chapters 4, 5, and 6.

In Chapter 3, we wanted to fulfill a minor objective of the thesis. As mentioned earlier, when lepton number is spontaneously broken in a Majorana neutrino mass model, a massless majoron appears. The presence of this particle can significantly impact the phenomenology of the model and, depending on the nature of the majoron, lead to relevant lepton flavor violating effects. Therefore, we aimed to study the potential contributions of this massless scalar to several important observables considering a model-independent approach and generalizing the problem to any ultralight scalar with arbitrary scalar and pseudoscalar couplings to the SM charged leptons.

Chapters 7 and 8 had a slightly different objective than the previous ones. Here, we followed an approach with a model building perspective. In the former, what we wanted to achieve was to generalize the neutrino mass matrix of the Scotogenic model but for arbitrary numbers of the Scotogenic states and also to study how different versions of the model could affect the high energy behavior. On the other hand, in the latter, our goal was to list all the possible ultraviolet completions, satisfying some conditions, of the Scotogenic model that could provide a natural explanation to two open questions of the model.

Finally, many neutrino mass models predict the existence of Heavy Neutral Leptons that mix with the active neutrinos. However, most of the experiments searching for these particles

have set bounds assuming that only one HNL exists and it mixes just with one lepton flavor. Therefore, in Chapter 9, we aimed to reinterpret the available bounds to a generic scenario with more than one HNL mixing with all the lepton flavors.

Methodology

To conduct the study performed in this thesis, several tools and techniques, both theoretical and computational, have been fundamental. In the following, we will be examining some of them.

First of all, being a thesis on theoretical particle physics, an advanced understanding of quantum field theory is essential. Quantum field theory unifies the principles of special relativity, which is the framework describing phenomena involving velocities close to that of light, and quantum mechanics, which is the branch of mechanics studying the interactions of subatomic particles at a microscopic scale. This, in combination with proficient mathematical skills, enables us to accurately calculate the physical observables required for the research presented in this thesis.

In terms of computer tools, `Wolfram Mathematica` has been the most important program for the obtention of the results. Not only it has been useful for complex analytical manipulations or obtention of numerical results, but it also has a number of integrated packages that make the life of a particle physicist way easier. For example, the package `Sym2Int` is used to get all the valid interactions permitted by the gauge and global symmetries and particle content of a given theory. Then, once the Lagrangian of a model is known, the `SARAH` package helps you to build it. It is able to calculate for you the vertices, mass matrices, tadpole equations, or the RGEs of your model. It can also generate the source code needed for `SPheno`, a `Fortran`-based code that allows for the numerical evaluation of analytical expressions obtained from `SARAH`. Additionally, `FeynCalc` and `PackageX` are used for the symbolic evaluation of Feynman diagrams and algebraic calculations in quantum field theory. The development of `PackageX`, however, has been recently terminated due to insufficient funding. Occasionally, other programs such as `WHIZARD`, which efficiently calculates multi-particle scattering cross sections and simulated event samples, and the well-known `Python` have also been used.

Leptonic Observables and Standard Model Anomalies

Many physics scenarios contain scalar states, ϕ, that are either exactly massless or much lighter than the electron. We refer to those particles as ultralight scalars. In Majorana neutrino mass models including spontaneous lepton number violation, the majoron plays this role. While in most scenarios including Goldstone bosons, they are pure pseudoscalar particles, in Chapter 3, we took a model-independent approach, allowing for ϕ to have both scalar and pseudoscalar couplings with the SM charged leptons. Motivated by generalization, we studied the possible impact of these ultralight scalars on several purely leptonic observables. In most of the cases, we

generalized previous results present in the literature, which frequently considered massive scalars or just pure pseudoscalars. We revisited the decays $\ell_\alpha \to \ell_\beta\, \phi$ and $\ell_\alpha \to \ell_\beta\, \gamma\, \phi$, where the scalar ϕ is produced, and presented complete expressions for the radiative LFV decays $\ell_\alpha \to \ell_\beta\, \gamma$, as well as for the 3-body decays $\ell_\alpha^- \to \ell_\beta^- \ell_\beta^- \ell_\beta^+$, $\ell_\alpha^- \to \ell_\beta^- \ell_\gamma^- \ell_\gamma^+$ and $\ell_\alpha^- \to \ell_\beta^+ \ell_\gamma^- \ell_\gamma^-$, where ϕ acts as a mediator. Furthermore, we discussed the effect of ultralight scalars on anomalous magnetic and electric dipole moments of charged leptons.

The effective Lagrangian parametrizing the most general interaction between the ultralight scalar ϕ and a pair of charged leptons is given by

$$\mathcal{L}_{\ell\ell\phi} = \phi\, \bar{\ell}_\beta \left(S_L^{\beta\alpha} P_L + S_R^{\beta\alpha} P_R \right) \ell_\alpha + \text{h.c.}\,, \tag{6}$$

where no sum over the α and β charged lepton indices is performed, and all the possible flavor combinations are considered: $\beta\alpha = \{ee, \mu\mu, \tau\tau, e\mu, e\tau, \mu\tau\}$. Also, $S_{L,R}$ are dimensionless coefficients and most of the observables that we considered receive contributions from the usual dipole and 4-fermion operators defined in Eqs. (3.2), (3.3), and (3.4).

Before computing the observables we were interested in, we wanted to derive experimental bounds on the lepton flavor conserving interactions, whose couplings can be redefined as

$$\mathcal{L}_{\ell\ell\phi}^{\text{diag}} = \phi\, \bar{\ell}_\beta \left[\text{Re}\, S^{\beta\beta} - i\, \text{Im}\, S^{\beta\beta}\, \gamma_5 \right] \ell_\beta\,, \tag{7}$$

with $S^{\beta\beta} = S_L^{\beta\beta} + S_R^{\beta\beta *}$. The most stringent bounds on the diagonal couplings, shown in Table 3.2, come from the phenomenon of stellar cooling. Scalar particles generated within stars and subsequently emitted could act as a potent cooling mechanism, potentially leading to discrepancies with astrophysical observations by altering the evolution of stars. Previous works that studied astrophysical cooling by the emission of ultralight scalars have only considered pure pseudoscalar couplings. However, one can estimate $\text{Re}\, S^{\beta\beta} \lesssim \left[\text{Im}\, S^{\beta\beta}\right]_{\text{max}}$ by numerically integrating the relevant cross sections for the cooling. It is worth noting that less stringent bounds can be set on the lepton flavor conserving couplings through the 1-loop interaction of ϕ with two photons.

After establishing the bounds on the diagonal couplings, we proceeded to compute analytical expressions for the leptonic observables of interest and discussed possible phenomenological directions. Of particular interest are the processes $\ell_\alpha \to \ell_\beta \phi$, as the most powerful bounds on the lepton flavor violating couplings of the ultralight scalar come from experimental searches for these decays. These upper limits are shown in Table 3.2. Furthermore, searches for these processes can also be used to set bounds on the couplings when the same observable with an additional photon in the final state is considered. Due to the experimental finite resolution, it is possible to integrate the phase space over the region that can be detected by the experiment, allowing to set limits on the couplings, although milder.

On the other hand, the observables considered in the Chapter are indeed complementary. For example, both LFV $\mu \to e\gamma$ and $\mu \to eee$ branching ratios can be used to determine the nature

of the scalar ϕ by using the ratio defined in Eq. (3.74) if they are experimentally determined. Additionally, these observables can shed light on the energy scale at which the new physics effects are relevant or even on the relative intensity between the dipole interactions and those of the ultralight scalar with charged leptons. Furthermore, we have found that the lepton flavor conserving couplings $S^{\beta\beta}$ could explain the electron and muon anomalous magnetic moments. However, the values required for these couplings would conflict with astrophysical observations, necessitating a mechanism to suppress the processes that gave rise to those constraints. Finally, we have concluded that off-diagonal contributions would have only a minor impact.

Then, in Chapter 4, we were interested in whether the inverse type-III seesaw model, initially designed to explain neutrino masses and mixings, could also account for the deviation of the experimental values of the electron and muon anomalous magnetic moments from their theoretically predicted values. However, we found that this scenario fails to explain the anomalies due to a few reasons, and an alternative is required. Therefore, to address this issue, we proposed a minimal extension to the model that introduced a pair of vector-like lepton doublets with sizable couplings to electrons and muons. Our proposal had the necessary components to produce the required contributions to both the electron and muon $g-2$ anomalies while maintaining the relevant features of the original model.

To confirm that the new version of the model was capable of explaining the $g-2$ anomalies while remaining compatible with neutrino oscillation data, we conducted a thorough analysis of the parameter space of the model using a random scan approach. During the scan, we ensured that all the accepted points were in agreement with constraints from both flavor and electroweak precision data. Additionally, we checked that the decay widths for the processes $Z \to \ell^+\ell^-$ and $h \to \ell^+\ell^-$, with $\ell = e, \mu$, remained within the allowed range, with the former decay being a strong constraint for our scenario. We also imposed bounds from collider searches on the masses and couplings of the triplets, as no excess has been observed in searches for type-III seesaw triplets at the LHC.

Fig. 4.4 demonstrates that our model can explain both electron and muon anomalies. In the case of the electron, we can find valid points within the 1σ region allowed by all the experimental constraints easily. In contrast, the muon $g-2$ can only be addressed at the 1σ level in narrow regions of the parameter space. Furthermore, Fig. 4.5 shows that the Δa_μ correlates clearly with the combination $(Y_\Sigma)_{ii}\ (\lambda_L)_i\ (\lambda_R)_i\ /\ [(M_\Sigma)_i\ M_L^2]$, implying that the W contribution to the anomalous magnetic moment of the muon is the dominant one. Lastly, our model predicts no significant change in the Higgs decays to the charged leptons compared to their results in the SM.

Next, in Chapter 5, we presented an efficient model that provides a unified explanation for various indications of new physics, including non-zero neutrino masses, $b \to s$ transitions, the anomalous magnetic moment of the muon, and the potential origin of dark matter. Our proposal introduces several new fields: a singlet fermion N, two scalar doublets η, a singlet scalar ϕ, and a doublet leptoquark S that is necessary to accommodate the $b \to s\ell\ell$ anomalies. In this scenario,

all these new particles are odd under a dark $\mathbb{Z}_2$ parity that is added to the model, while the SM fields are even. One remarkable feature of this model is the presence of dark loops, with $\mathbb{Z}_2$-odd states running within them, that induce all the new physics contributions to the anomalous observables we aim to explain. Moreover, Majorana neutrino masses are generated at the 1-loop level through a variation of the Scotogenic mechanism, as tree-level contributions are forbidden by the presence of the $\mathbb{Z}_2$ symmetry.

In addition to explaining the aforementioned anomalies, the model must satisfy several experimental constraints. Of course, neutrino oscillation data has to be correctly reproduced, although this can be easily achieved by considering a properly adapted Casas-Ibarra parametrization to our scenario. Another common concern in neutrino mass models is the risk of lepton flavor violating processes. The model also faces constraints from various processes involving mesons, the most relevant ones being $b \to s\gamma$, $B \to K^{(*)}\nu\bar{\nu}$, and $B_s - \bar{B}_s$ mixing.

The goal of this Chapter was to demonstrate that our model can account for all the anomalies while satisfying all the experimental constraints. To achieve this, we constructed a χ^2-funcion including the anomalous magnetic moment of the muon and the Wilson coefficients of the effective operators involved in the $b - s$ anomalies. After fixing several parameters for simplicity, we found the minimum value of the χ^2-function to be $\chi^2_{\text{min}} = 1.52$, to be compared with the SM value: $\Delta\chi^2 = \chi^2_{\text{SM}} - \chi^2_{\text{min}} = 21.23$. The left-hand side of Fig. 5.2 shows the results of the fit, revealing that the model parameters that were left free in the fit can vary significantly from their best-fit values without causing a significant change in the χ^2-function. However, $\mu \to e\gamma$ turns out to be a strong constraint in the model. Furthermore, the right-hand side of the Figure shows that the model can easily achieve the central value of the observables fitted.

Chapter 6 concludes this part of the thesis. It was devoted to the study of charged lepton flavor violation in a model with spontaneous lepton number breaking and, therefore, with a majoron J. In this Chapter, we present a relatively simple model that generates significant off-diagonal majoron couplings to charged leptons at tree-level. In addition to the SM symmetries, this model imposes lepton number conservation and extends the particle content with a singlet and a doublet scalars, three right-handed neutrinos, and an $\text{SU}(2)_{\text{L}}$ singlet vector-like lepton, all of them with non-zero lepton number. After the spontaneous breaking of the EW and lepton number symmetries, neutrinos acquire masses through a TeV-scale type-I seesaw mechanism.

As a consequence of the tree-level LFV couplings, the model exhibits sizable LFV rates covering large regions of its parameter space, including the usual $\ell_\alpha \to \ell_\beta\gamma$ and $\ell_\alpha \to 3\ell_\beta$ processes. This implies the existence of important constraints. Moreover, the inclusion of vector-like fermions to the lepton sector of the SM has an impact on several observables, particularly on the anomalous magnetic moment of the charged leptons and on their coupling to gauge bosons. As a result, the model induces new contributions to the muon magnetic moment at the 1-loop level that can account for the observed anomaly in some ranges of its parameter space. Regarding the couplings of the charged leptons to the Z boson, we made sure during the analysis

that they lie within the allowed ranges. Lastly, the model can also lead to observable effects in Higgs boson decays, especially in $h \to \mu\mu$, and allows for Higgs decay in a pair of majorons.

Similarly to Chapter 4, here we randomly scanned the wide parameter space of the model while computing the relevant observables for each point of the scan. Thanks to a Casas-Ibarra parametrization, all the points were compatible with the current neutrino oscillation observations. As depicted in Fig. 6.2, our model can reach the experimental upper bounds on $\mathrm{BR}(\mu \to e\gamma)$ and $\mathrm{BR}(\mu \to eJ)$, which are actually correlated. Additionally, the muon $g-2$ can be explained in large parts of the parameter space of the model, even within 1σ, as shown in Fig. 6.4, and we found significant deviations of the $h \to \mu\mu$ branching ratio with respect to its SM prediction, as illustrated in Fig. 6.5.

Model Building

In this part of the thesis, we adopted a model building perspective while relegating phenomenology to a secondary role. It consists of two chapters, both of them centered on the Scotogenic model.

The Scotogenic model, in its original version, features an inert scalar doublet η and three copies of singlet fermions N in addition to the particles of the SM. The model is also characterized by a dark $\mathbb{Z}_2$ parity under which the new states are odd and the SM particles are even. However, the choice for the number of generations of each new field is not unique, and to address this, we have presented the general Scotogenic model in Chapter 7. This model allows for arbitrary numbers of generations of the Scotogenic states.

The relevant Yukawa and bare mass terms for the discussion are

$$\mathcal{L}_N \supset y_{na\alpha}\, \overline{N}_n\, \eta_a\, \ell_L^\alpha + \frac{1}{2}\, M_{N_n}\, \overline{N^c}_n\, N_n + \text{h.c.}\,, \tag{8}$$

where $n = 1, \ldots, n_N$, $a = 1, \ldots, n_\eta$ and $\alpha = 1, 2, 3$ are generation indices and n_N and n_η are the number of copies of N and η, respectively, in the general version of the model. Particular cases of the model can be labeled by their (n_N, n_η) values. Furthermore, one can also write the important scalar potential terms

$$\mathcal{V} \supset \left(m_\eta^2\right)_{ab} \eta_a^\dagger \eta_b + \lambda_3^{ab} \left(H^\dagger H\right) \left(\eta_a^\dagger \eta_b\right) + \lambda_4^{ab} \left(H^\dagger \eta_a\right) \left(\eta_b^\dagger H\right) + \frac{1}{2} \left[\lambda_5^{ab} \left(H^\dagger \eta_a\right) \left(H^\dagger \eta_b\right) + \text{h.c.}\right]. \tag{9}$$

The main result of this Chapter is the derivation of the neutrino mass matrix in the general version of the model. To simplify the computation, we made the assumption that CP is conserved in the scalar sector of the model by considering that all the parameters in the scalar potential are real. By doing this, we obtained an exact analytical expression for the mass matrix:

$$(m_\nu)_{\alpha\beta} = -\frac{1}{32\pi^2} \sum_{A,a,b,c,n} M_{N_n}\, \kappa_A^2\, (V_A)_{ba}\, (V_A)_{ca}\, y_{nb\alpha}\, y_{nc\beta}\, B_0(0, m_{A_a}^2, M_{N_n})\,. \tag{10}$$

Here, $A = R, I$ and b and c can take the same values as a. $B_0(0, m^2_{A_a}, M_{N_n})$ is the standard Passarino-Veltman loop function introduced in Eq. (7.16), $\kappa_R = 1$, $\kappa_I = i$, and $m^2_{R(I)_a}$ and $V_{R(I)}$ are the mass eigenvalues and diagonalization matrix of the mass matrix of the real (imaginary) components of the neutral parts of η_a, respectively.

Although the exact dependence on the parameters of the model is not explicit in the exact neutrino mass matrix, we can still obtain a useful approximate form by making reasonable assumptions. Specifically, we assume that $\lambda^{aa}_{3,4} v^2/2 \ll (m^2_\eta)_{aa}$ and $\lambda^{ab}_5 \ll \lambda^{ab}_{3,4} \ll 1$, with $a \neq b$. By doing so, we have derived an approximate form for the neutrino mass matrix, which is the main analytical result of the Chapter:

$$(m_\nu)_{\alpha\beta} = \frac{v^2}{32\pi^2} \sum_{n,a,b} \frac{y_{na\alpha}\, y_{nb\beta}}{M_{N_n}} \Gamma_{abn} + \mathcal{O}\left(\lambda_5^2\right) + \mathcal{O}\left(\lambda_5\, s^2\right) , \tag{11}$$

where $s_{ab} = 1/2(\lambda^{ab}_3 + \lambda^{ab}_4)v^2/(m^2_b - m^2_a)$ and $m^2_a = (m^2_\eta)_{aa} + (\lambda^{aa}_3 + \lambda^{aa}_4)v^2/2$. We also defined the dimensionless quantity

$$\Gamma_{abn} = \delta_{ab}\, \lambda^{aa}_5\, f_{an} - (1 - \delta_{ab}) \left[\left(\lambda^{aa}_5\, f_{an} - \lambda^{bb}_5\, f_{bn} \right) s_{ab} - \frac{M^2_{N_n}}{m^2_b - m^2_a}\, \lambda^{ab}_5\, g_{abn} \right] \tag{12}$$

with the loop functions

$$f_{an} = \frac{M^2_{N_n}}{m^2_a - M^2_{N_n}} + \frac{M^4_{N_n}}{\left(m^2_a - M^2_{N_n}\right)^2} \log \frac{M^2_{N_n}}{m^2_a} , \tag{13}$$

$$g_{abn} = \frac{m^2_a}{m^2_a - M^2_{N_n}} \log \frac{M^2_{N_n}}{m^2_a} - \frac{m^2_b}{m^2_b - M^2_{N_n}} \log \frac{M^2_{N_n}}{m^2_b} . \tag{14}$$

After demonstrating that our expression reduces to the mass matrices obtained in two previously published results, the standard Scotogenic model and a variant that includes two η and one N, we studied the high-energy behavior of the model.

The conservation of the $\mathbb{Z}_2$ symmetry is essential for any version of the general Scotogenic model to be consistent. Otherwise, neutrinos would acquire masses at tree-level, and the dark matter candidate would no longer be stable. However, the running of the RGEs can alter the shape of the scalar potential at high energies, leading to the breaking of $\mathbb{Z}_2$. This motivates the study of the high energy behavior of the theory. We computed all the 1-loop β functions and used them to numerically solve the complete set of RGEs. We focused on two specific versions of the general Scotogenic model: the $(3, 1)$ and $(1, 3)$ models, where the former is the original version of the model. Despite some particularities due to the different numbers of generations, our main conclusion is that all the features of the original Scotogenic model are present in other specific variants of the general model.

On the other hand, in the Scotogenic model, a small $\lambda_5 \ll 1$ quartic parameter is required to generate the correct scale of neutrino masses while having sizable Yukawa couplings and

relatively light mediators. The smallness of this parameter is technically natural in the sense of 't Hooft, but it asks for an extension explaining it. In addition, the $\mathbb{Z}_2$ symmetry in the Scotogenic model is considered an *ad-hoc* symmetry. Therefore, in Chapter 8, we wanted to classify the possible ultraviolet completions leading to the Scotogenic model at low energies when integrating out a heavy scalar field S and addressing these two issues. Specifically, we were interested in UV scenarios where the $\mathbb{Z}_2$ appears as a remnant symmetry after the spontaneous breaking of a $\mathrm{U}(1)_\mathrm{L}$ symmetry, where the L stands for lepton number. We also wanted the operator $(H^\dagger\eta)^2$, which is the λ_5 term, to be forbidden in the UV theory due to lepton number. In contrast, an operator of the form $(H^\dagger\eta)^2\sigma^n$, with $n \geq 1$, must be generated after integrating out the heavy field. This operator induces an effective λ_5 coupling, naturally suppressed by the large mass of the scalar S, after the singlets acquire VEVs.

Focusing on possible tree-level completions of the λ_5 operator using one or two different σ singlets, we identified all the possible topologies in the UV theory that generate this operator, as shown in Table 8.1. Of the five possible topologies, four include just one S propagator, leading to a λ_5 operator of the form $\mathcal{O}_{\lambda_5} = (H^\dagger\eta)^2\sigma_A\sigma_B$, suppressed by a factor $1/m_S^2$. In contrast, the remaining topology has two S propagators and generates the operator $\mathcal{O}_{\lambda_5} = (H^\dagger\eta)^2\sigma_A^2\sigma_B\sigma_C$, now suppressed by $1/m_S^4$. It is worth noting that these generic expressions include cases where some σ insertions correspond to the same field, as well as cases where one of the σ insertions is missing. We explored all the possibilities and found 50 different variations that satisfy the previous requirements. However, it is important to note that the lepton numbers of the fields in all these variations must take specific values to prevent η from acquiring a VEV and to generate the correct $\mathbb{Z}_2$ parity.

In this Chapter, we discussed three illustrative example models. The phenomenology of these models, as well as of the rest of variations, is expected to be very rich. Due to the spontaneous breaking of lepton number, the models predict the existence of a massless majoron and other new massive scalars. We derived analytical expressions for the couplings of the majoron to the charged leptons, including both lepton flavor conserving and violating interactions. Furthermore, the models have potential signatures in collider searches and offer interesting implications for dark matter compared to the standard Scotogenic model, as they contain additional states.

Collider Searches

Chapter 9 was the final chapter of the thesis, and there we focused on short-lived heavy neutral lepton searches at high-energy colliders, primarily at the LHC. Our interest was in the fact that the HNL bounds, with very few exceptions, are derived by experimental collaborations under the assumption of a single HNL that mixes with only one lepton flavor. However, this is not the case in most of the BSM scenarios involving this kind of particles, where the mixing pattern can be quite complex. In this Chapter, we aimed to address this issue by discussing how to recast

the existing experimental limits on HNLs to a scenario that involves generic mixings to all the lepton flavors and with several HNLs.

Initially, we explored the scenario of a single HNL but allowing it to mix with all three lepton flavors. Typically, the experimental limits on HNL searches are presented in the $\left(M_N, |U_{\alpha N}|^2\right)$ plane, where $U_{\alpha N}$, with $\alpha = e, \mu, \tau$ represents the active-sterile mixings, and M_N denotes the HNL mass. However, we wanted to emphasize that to generalize the bounds, it is better to present them in the $\left(M_N, |U_{\alpha N}|^2 \times \mathrm{BR}\right)$ plane. This is because, this way, one only has to compute the new branching ratios for their particular mixing hypothesis. While most of the works present their results using the former possibility, translating it to the latter is straightforward when the experimental collaboration assumes a constant BR for the channel they study, although they do not always specify its value. Nevertheless, the recasting is not possible when the results are obtained after combining different channels.

In principle, there is no restriction on the number of HNLs that a model can have. If only one of the HNLs is within the reach of current experiments, or if there are multiple HNLs but with distinct mass regimes, then the conclusions drawn from the analysis of the single HNL scenario can be applied to each of the HNLs. However, when two HNLs have similar masses, interference effects may occur, potentially altering the results and bounds obtained under the assumption of just one HNL. For simplicity, we focused on the scenario with two HNLs close in mass. To better illustrate the importance of the interference, we focus on the LHCb results for the prompt dimuon channel, considering both same sign and opposite sign dilepton channels. This way, we were able to show that LNC and LNV searches are important and complementary, and they should be performed in parallel.

Conclusions

Neutrino mass models are arguably the best motivated extensions of the Standard Model of particle physics. Although neutrino oscillation experiments have confirmed that they are massive, the mechanism behind the generation of their masses is a mystery. In this thesis, we have presented several models specially focused on generating neutrino masses, both at tree-level and radiatively. Of particular interest are those models that not only provide masses to neutrinos but also connect them with explanations for other outstanding issues in particle physics, such as the origin of dark matter, the anomalous magnetic moment of the charged leptons, or the B flavor anomalies. Moreover, many neutrino mass models predict substantial lepton flavor violating interactions, highlighting the importance of searching not only for the possible particles involved in generating neutrino masses but also for lepton flavor violating processes.

Resum de la Tesi

En aquesta part de la tesi, oferirem una visió general i completa del treball. Inclourà una introducció i una descripció dels objectius de la investigació, una explicació detallada de la metodologia utilitzada, un resum de les principals troballes en cada capítol i les conclusions extretes de la tesi com un tot.

Introducció

Els físics de la segona meitat del segle XX van desenvolupar el que ara es considera el marc teòric més precís i reeixit, el Model Estàndard (ME) de la física de partícules. Aquest model descriu tres de les quatre forces fonamentals que es troben en la naturalesa: electromagnetisme, interaccions febles i fortes. És una teoria de camps quàntics relativista que roman invariant sota les transformacions del grup de Lorentz, i es basa en la invariància de *gauge* sota el grup de simetria.

$$\mathrm{SU(3)_C} \times \mathrm{SU(2)_L} \times \mathrm{U(1)_Y}\,. \tag{1}$$

Les forces són mediades per l'intercanvi de bosons de gauge de *spin*-1. La força forta es descriu pel grup $\mathrm{SU(3)_C}$ i els seus 8 camps de gauge sense massa, anomenats gluons. D'altra banda, la força electrofeble està governada pel grup de simetria $\mathrm{SU(2)_L} \times \mathrm{U(1)_Y}$. Aquesta força és transmesa per 3 bosons de gauge W de $\mathrm{SU(2)_L}$ i 1 bosó de gauge B de $\mathrm{U(1)_Y}$. Junts, aquests quatre bosons de gauge proporcionen el marc per a la força electrofeble, que unifica l'electromagnetisme i les forces febles.

Pel que fa al contingut fermiònic del model, es poden agrupar en diferents multiplets de $\mathrm{SU(2)_L}$ depenent de la quiralitat dels camps. Les partícules esquerres s'organitzen en doblets de $\mathrm{SU(2)_L}$, mentre que les dretes són singlets de $\mathrm{SU(2)_L}$:

$$\begin{pmatrix} \nu_e \\ e \end{pmatrix}_L \quad , \quad \begin{pmatrix} u \\ d \end{pmatrix}_L \quad , \quad e_R \quad , \quad u_R \quad , \quad d_R\,. \tag{2}$$

A més a més, en el ME, els quarks i leptons tenen tres famílies (o sabors) i l'estructura dels multiplets anteriorment descrits es replica tres vegades.

El grup de gauge donat per l'Eq. (1) representa el grup de simetria del ME, el qual prohibeix que cap partícula del model puga tindre termes de massa al lagrangià. No obstant això, sabem

per experiments que les partícules tenen masses, el que implica necessàriament que la simetria ha de ser trencada. Un pot trencar una simetria explícitament o espontàniament, però en el cas d'una simetria de gauge, només la segona opció és viable.

En el ME, la ruptura espontània de la simetria s'aconsegueix a través del mecanisme de Higgs. Aquest mecanisme introdueix un nou camp escalar amb un potencial escalar que preserva la simetria de gauge, però l'estat fonamental de la teoria no ho fa. [1] Donat que es pretén que la simetria electrofeble es trenque de manera espontània fins a l'electromagnetisme, $\mathrm{U(1)_Q}$, la manera més senzilla d'aconseguir-ho és introduint un doblet sota $\mathrm{SU(2)_L}$ amb hipercàrrega $Y = 1/2$, conegut com el doblet de Higgs:

$$H = \begin{pmatrix} H^+ \\ H^0 \end{pmatrix} . \tag{3}$$

L'estat fonamental del ME s'obté quan el doblet de Higgs adquireix l'adequadament triat Valor d'Expectació del Buit (VEB)

$$\langle H \rangle = \frac{1}{\sqrt{2}} \begin{pmatrix} 0 \\ v \end{pmatrix} , \tag{4}$$

trencant la simetria de gauge del ME de manera espontània, de tal manera que

$$\mathrm{SU(3)_C \times SU(2)_L \times U(1)_Y} \quad \rightarrow \quad \mathrm{SU(3)_C \times U(1)_Q} \, . \tag{5}$$

Després del procés de ruptura de simetria electrofeble, els bosons de gauge de la interacció feble i els camps fermiònics adquireixen masses amb èxit i de manera natural, com es desitjava. No obstant això, el ME no inclou neutrins drets i, per tant, els neutrins són predits com no massius en la teoria. Això porta a la conservació dels sabors leptònics dins del model.

Encara que el ME és una teoria altament exitosa que compleix un conjunt complex de simetries i ha guanyat el seu lloc entre els grans èxits de la humanitat, encara té algunes llacunes que cal abordar. Algunes de les qüestions importants a les que s'enfronta la teoria inclouen:

Masses dels neutrins Els neutrins en el ME són sense massa per construcció, però els experiments d'oscil·lacions de neutrins han establert clarament que això no és correcte. Aquesta evidència és considerada per molts com la indicació més robusta de nova física més enllà del ME. Com a resultat, hi ha la necessitat d'una extensió del sector leptònic del model amb nous graus de llibertat, que típicament porten a desviacions en altres observables, ja siguen directament associats amb leptons o no.

Matèria fosca L'observació de les corbes de rotació de galàxies proporciona evidència de l'existència de matèria fosca, que és una matèria addicional que no podem veure, però que

[1] L'estat fonamental de qualsevol teoria és l'estat d'energia mínima.

constitueix aproximadament el 25 % del contingut energètic de l'Univers. No obstant això, la naturalesa d'aquesta matèria encara és un misteri.

Moments magnètics anòmals dels leptons carregats Els moments magnètics anòmals de l'electró i el muó tenen una discrepància que ha persistit durant molt de temps entre les prediccions del ME i els seus valors experimentals. Això suggereix la presència d'estats nous més enllà del ME i demana una extensió no trivial del model. El valor del $g-2$ del muó ha estat considerat en diversos contextos, incloent models per a la generació de la massa del neutrí i com a motivació per a un col·lisionador de muons. Són necessàries mesures addicionals i càlculs teòrics refinats per confirmar la rellevància d'aquestes anomalies.

Anomalies de sabor dels B Les anomalies de sabor B es refereixen a un conjunt d'observacions que involucren desintegracions de mesons B que no coincideixen amb les prediccions teòriques del ME. Es divideixen en dos tipus: anomalies de corrent neutral, que es produeixen en les desintegracions $b \to s\ell\ell$, i anomalies de corrent carregat, que es veuen en les desintegracions $b \to c\ell\nu_\ell$. La primera observació d'aquestes anomalies es va fer fa una dècada, de llavors ençà hi ha hagut un augment en el nombre de mesures, que també van mostrar desviacions significatives del ME. No obstant, resultats recents de col·laboracions experimentals han reduït les discrepàncies entre les mesures experimentals i les prediccions del ME.

La primera anomalia presentada ací és, potser, el problema més urgent del model, així que aprofundirem més en el tema. Les oscil·lacions de neutrins es produeixen pel fet que els estats propis de neutrins de massa no coincideixen amb els estats propis de sabor de neutrins, i els uns es poden expressar com una superposició dels altres. Així, un neutrí que viatja pel espai canvia d'un sabor a un altre amb una probabilitat que depén de la distància recorreguda, l'energia del neutrí, les diferències de massa i els paràmetres de mescla. Els valors dels paràmetres que es mesuren, amb bona precisió, en experiments d'oscil·lacions de neutrins es resumixen a la Taula 2.1, tot i que encara hi ha preguntes sense resposta en la física de neutrins. Per exemple, no sabem el nombre exacte de neutrins que existeixen, ni hem determinat l'ordre de massa dels neutrins. A més, la naturalesa dels neutrins segueix sent una qüestió sense resoldre: específicament, si són partícules de Dirac o de Majorana.

Des d'una perspectiva independent del model, l'operador de Weinberg $\mathcal{O}_W$ és l'operador de menor dimensió que viola el nombre leptònic i que es pot afegir al lagrangià del ME per a generar masses de Majorana per als neutrins. Hi ha tres maneres possibles de generar l'operador de Weinberg a nivell d'arbre en una teoria renormalitzable: a través dels mecanismes ben coneguts del tipus I, tipus II i tipus III de balancí. Gràcies a l'addició d'un fermió singlet, un escalar triplet o un fermió triplet, respectivament, aquests models poden generar masses de neutrins minúscules mitjançant grans escales de nova física. No obstant això, hi ha extensions d'aquests escenaris, com els mecanismes de balancí invers, on s'utilitzen simetries quasi conservades per relaxar les grans escales de masses requerides. Per altra banda, una alternativa interessant als mecanismes

a nivell d'arbre són els models de masses radiatives de neutrins, com el famós model *Scotogenic*. Malgrat requerir mecanismes i simetries diferents en comparació amb els mecanismes de balancí habituals, la supressió introduïda pels factors de bucle ens permet acomodar les masses i les barreges de neutrins observades amb acoblaments grans i mediadors relativament lleugers, que típicament porten a una fenomenologia més rica.

Una possibilitat interessant per als models de massa dels neutrins és que les masses no nul·les dels neutrins puguen originar-se per la violació del nombre leptònic, el que pot resultar en neutrins sent partícules de Majorana. Tot i que és possible afegir termes explícits que violen el nombre leptònic al lagrangià del model, també és possible que la violació del nombre leptònic siga d'origen espontani. Aquesta simetria trencada espontàniament generaria un bosó de Goldstone sense massa anomenat *majoron*. La presència d'aquest bosó en l'espectre de partícules de la teoria pot afectar la fenomenologia.

Objectius

L'objectiu principal d'aquesta tesi ha estat estudiar models més enllà del ME dissenyats principalment per explicar l'origen de les masses dels neutrins. Durant la major part de la tesi, hem assumit que els neutrins són partícules de Majorana, com és comú en la literatura científica. En molts dels capítols, hem proposat variants dels mecanismes estàndard de balancí i de balancí invers, així com explorat el mecanisme Scotogenic, que ha jugat un paper important en la construcció de diversos models d'aquesta tesi. En alguns casos, hem buscat connectar la generació de masses dels neutrins amb altres anomalies esmentades anteriorment, considerant també els ràtios potencialment grans de processos que violen la simetria de sabor leptònic en el sector leptònic carregat, cosa que és predita per moltes extensions del ME que generen masses per als neutrins, encara que no hi ha evidència experimental d'aquestes ràtios. Això s'ha d'utilitzar per a restringir l'espai de paràmetres de qualsevol model. Tot això s'ha realitzat en els capítols 4, 5, i 6.

Al Capítol 3, volguérem aconseguir un objectiu menor de la tesi. Com s'ha esmentat anteriorment, quan la ruptura espontània del nombre leptònic es produeix en un model de massa de neutrins de Majorana, apareix un majoron sense massa. La presència d'aquesta partícula pot impactar significativament la fenomenologia del model i, depenent de la naturalesa del majoron, portar a efectes rellevants de violació de sabor leptònic. Per això, vam estudiar les possibles contribucions d'aquest escalar no massiu a diversos observables importants, considerant una enfocament independent del model i generalitzant el problema a qualsevol escalar ultralleuger amb acoblaments escalars i pseudescalars arbitraris amb els leptons carregats del SM.

Els capítols 7 i 8 tenien un objectiu lleugerament diferent als anteriors. Ací, seguírem un enfocament amb una perspectiva de construcció de models. En el primer, el que volíem aconseguir era generalitzar la matriu de massa dels neutrins del model Scotogenic per a nombres arbitraris d'estats *scotogenics* i també estudiar com diferents versions del model podrien afectar

al comportament a altes energies. D'altra banda, en el segon capítol, la nostra meta era llistar totes les possibles extensions ultravioleta, satisfent certes condicions, del model Scotogenic que podrien proporcionar una explicació natural a dos preguntes obertes del model.

Finalment, molts models de masses de neutrins prediuen l'existència de Leptons Neutrals Pesats (HNL per les sigles en anglés) que es barregen amb els neutrins actius. No obstant això, la majoria dels experiments que busquen aquestes partícules han establert límits suposant que només existeix un HNL i que es barreja només amb un sabor de leptons. Per això, al Capítol 9, vam proposar com reinterpretar els límits disponibles per al cas genèric amb més d'un HNL que es barreja amb tots els sabors de leptons.

Metodologia

Per dur a terme l'estudi realitzat en aquesta tesi, diverses eines i tècniques, tant teòriques com computacionals, han estat fonamentals. A continuació, examinarem algunes d'elles.

Primer de tot, com que aquesta tesi és de física teòrica de partícules, és essencial tenir un coneixement avançat de la teoria quàntica de camps. Aquesta unifica els principis de la relativitat especial, que és el marc que descriu fenòmens que involucren velocitats properes a la de la llum, i la mecànica quàntica, que és la branca de la mecànica que estudia les interaccions de les partícules subatòmiques a escala microscòpica. Això, combinat amb habilitats matemàtiques competents, ens permet calcular amb precisió els observables físics necessàris per a la recerca presentada en aquesta tesi.

Pel que fa a les eines informàtiques, `Wolfram Mathematica` ha estat el programa més important per a l'obtenció dels resultats. No només ha sigut útil per a la manipulacións analítiques complexes o l'obtenció de resultats numèrics, sinó que també té bastants paquets integrats que fan la vida d'un físic de partícules molt més fàcil. Per exemple, el paquet `Sym2Int` s'utilitza per obtenir totes les interaccions vàlides que permeten les simetries locals i globals i el contingut de partícules d'una teoria determinada. A continuació, una vegada es coneix el lagrangià d'un model, el paquet `SARAH` t'ajuda a construir-lo. És capaç de calcular per a tu els vèrtexs, les matrius de masses, les equacions de *tadpole* o les RGEs del teu model. També pot generar el codi font necessari per a `SPheno`, un programa basat en `Fortran` que permet l'avaluació numèrica d'expressions analítiques obtingudes de `SARAH`. A més, `FeynCalc` i `PackageX` s'utilitzen per a l'avaluació simbòlica de diagrames de Feynman i càlculs algebraics en teoria quàntica de camps. No obstant, el desenvolupament de `PackageX` ha estat recentment interromput a causa d'una manca de finançament. Ocasionalment, també s'han utilitzat altres programes com `WHIZARD`, que calcula eficientment seccions eficaces de dispersió de múltiples partícules i mostres d'esdeveniments simulats, i el ben conegut `Python`.

Observables Leptònics i Anomalies del Model Estàndard

Molts escenaris de física contenen estats escalars, ϕ, que són o bé exactament no massius o molt més lleugers que l'electró. Ens referim a aquestes partícules com a escalars ultralleugers. En models de masses de neutrins de Majorana que inclouen violació espontània del nombre leptònic, el majoron exerceix aquest paper. Mentre que en la majoria d'escenaris que inclouen bosons de Goldstone, aquestes partícules són pseudoescalars purs, al Capítol 3, vam adoptar una perspectiva independent del model, permetent que ϕ tinga acoblaments tant escalars com pseudoescalars amb els leptons carregats del ME. Motivats per la generalització, vam estudiar el possible impacte d'aquests escalars ultralleugers en diversos observables purament leptònics. En la majoria dels casos, vam generalitzar resultats anteriors presents a la literatura, que sovint consideraven escalars massius o només pseudoescalars purs. Revisitàrem les desintegracions $\ell_\alpha \to \ell_\beta\, \phi$ i $\ell_\alpha \to \ell_\beta\, \gamma\, \phi$, on es produeix l'escalar ϕ, i presentàrem expressions completes per a les desintegracions radiatives $\ell_\alpha \to \ell_\beta\, \gamma$, així com per a les desintegracions de 3 cossos $\ell_\alpha^- \to \ell_\beta^- \ell_\beta^- \ell_\beta^+$, $\ell_\alpha^- \to \ell_\beta^- \ell_\gamma^- \ell_\gamma^+$ i $\ell_\alpha^- \to \ell_\beta^+ \ell_\gamma^- \ell_\gamma^-$, on ϕ actua com a mediador. A més, vam discutir l'efecte dels escalars ultralleugers en els moments dipolars magnètics i elèctrics anòmals dels leptons carregats.

El lagrangià efectiu que parametritza la interacció més general entre l'escalar ultralleuger ϕ i un parell de leptons carregats ve donat per

$$\mathcal{L}_{\ell\ell\phi} = \phi\, \bar{\ell}_\beta \left(S_L^{\beta\alpha} P_L + S_R^{\beta\alpha} P_R \right) \ell_\alpha + \text{h.c.}\,, \tag{6}$$

on no es fa cap suma sobre els índexs dels leptons carregats α i β, i es consideren totes les combinacions de sabor possibles: $\beta\alpha = \{ee, \mu\mu, \tau\tau, e\mu, e\tau, \mu\tau\}$. A més, $S_{L,R}$ són coeficients adimensionals i la majoria dels observables que vam considerar reben contribucions dels operadors usuals de dipol i 4-fermions definits a les Eqs. (3.2), (3.3), i (3.4).

Abans de calcular els observables que ens interessaven, volíem obtenir lligams experimentals per a les interaccions que conserven el sabor dels leptons, les quals es poden redefinir com a

$$\mathcal{L}_{\ell\ell\phi}^{\text{diag}} = \phi\, \bar{\ell}_\beta \left[\text{Re}\, S^{\beta\beta} - i\, \text{Im}\, S^{\beta\beta}\, \gamma_5 \right] \ell_\beta\,, \tag{7}$$

amb $S^{\beta\beta} = S_L^{\beta\beta} + S_R^{\beta\beta *}$. Els límits més exigents per als acoblaments diagonals, que es mostren a la Taula 3.2, provenen del fenomen del refredament estel·lar. Les partícules escalars generades dins les estreles i posteriorment emeses podrien actuar com a mecanisme potent de refredament, el que podria portar a discrepàncies amb les observacions astrofísiques en alterar l'evolució de les estreles. Treballs anteriors que van estudiar el refredament astrofísic per l'emissió d'escalars ultralleugers només consideraren acoblaments purament pseudescalars. No obstant això, es pot estimar $\text{Re}\, S^{\beta\beta} \lesssim \left[\text{Im}\, S^{\beta\beta}\right]_{\text{max}}$ mitjançant la integració numèrica de les seccions eficaces rellevants per al refredament. Cal destacar que lligams alternatius menys exigents es poden

establir en els acoblaments que conserven el sabor dels leptons a través de la interacció d'1-bucle de ϕ amb dos fotons.

Després d'establir els límits en els acoblaments diagonals, vam procedir a calcular expressions analítiques per als observables leptònics d'interès i discutírem possibles direccions fenomenològiques. D'interès particular són els processos $\ell_\alpha \to \ell_\beta \phi$, ja que els límits superiors més potents en els acoblaments de l'escalar ultralleuger que violen sabor leptònic provenen de les recerques experimentals per a aquestes desintegracions. Aquests límits superiors es mostren en la Taula 3.2. A més, les recerques d'aquests processos també es poden utilitzar per establir límits quan s'estudia el mateix observable amb un fotó addicional en l'estat final. Degut a la resolució finita experimental, és possible integrar l'espai de fases en la regió que es pot detectar per l'experiment, permetent establir límits en els acoblaments, tot i que més suaus.

D'altra banda, els observables considerats al Capítol són complementaris. Per exemple, tant les tases de decaïment de $\mu \to e\gamma$ com de $\mu \to eee$, que violen sabor leptònic, es poden utilitzar per determinar la naturalesa de l'escalar ϕ utilitzant la relació definida a l'Eq. (3.74) si ambdues es determinen experimentalment. A més a més, aquests observables poden aclarir l'escala energètica en què són rellevants els efectes de nova física o fins i tot la intensitat relativa entre les interaccions dipol i aquelles de l'escalar ultralleuger amb els leptons carregats. Adicionalment, hem trobat que els acoblaments que conserven el sabor dels leptons $S^{\beta\beta}$ podrien explicar els moments magnètics anòmals de l'electró i del muó. No obstant això, els valors necessaris per a aquests paràmetres entrarien en conflicte amb les observacions astrofísiques, i seria necessari un mecanisme per suprimir els processos que van donar lloc a aquestes restriccions. Finalment, hem conclòs que les contribucions fora de la diagonal tindrien només un impacte menor.

A continuació, al Capítol 4, estiguérem interessats a saber si el model de balancí invers de tipus III, dissenyat inicialment per explicar les masses i mescles dels neutrins, també podria explicar la desviació dels valors experimentals dels moments magnètics anòmals de l'electró i el muó respecte dels seus valors teòricament predits. No obstant, vam trobar que aquest escenari no és capaç d'explicar les anomalies per diverses raons, i és necessària una alternativa. Per abordar aquesta qüestió, vam proposar una extensió mínima del model que introduïa un parell de doblets de leptons vectorials amb acoblaments considerables a electrons i muons. La nostra proposta tenia els components necessaris per produir les contribucions requerides a les anomalies del moment magnètic anòmal tant de l'electró com del muó mantenint les característiques rellevants del model original.

Per confirmar que la nova versió del model era capaç d'explicar les anomalies del $g-2$ alhora que era compatible amb les dades d'oscil·lacions de neutrins, realitzàrem una anàlisi exhaustiva de l'espai de paràmetres del model utilitzant un apropament d'escaneig aleatori. Durant l'escaneig, vam assegurar-nos que tots els punts acceptats concordaven amb les restriccions de les mesures de precisió electrofeble i de sabor. A més, vam comprovar que les amplades de desintegració dels processos $Z \to \ell^+\ell^-$ i $h \to \ell^+\ell^-$, amb $\ell = e, \mu$, romangueren dins del rang permès, sent el primer procés una restricció forta per al nostre escenari. També vam imposar els

límits de les cerques de col·lisionadors sobre les masses i els acoblaments dels triplets, ja que no s'ha observat cap excés en la cerca de triplets del balancí de tipus-III en el Gran Col·lisionador d'Hadrons (LHC per les sigles en anglés).

La Figura 4.4 demostra que el nostre model pot explicar tant l'anomalia de l'electró com la del muó. En el cas de l'electró, podem trobar punts vàlids dins de la regió 1σ permesos per totes les restriccions experimentals fàcilment. En canvi, el $g-2$ del muó només es pot explicar a 1σ en regions estretes de l'espai de paràmetres. A més, la Figura 4.5 mostra que Δa_μ es correlaciona clarament amb la combinació $(Y_\Sigma)_{ii}\ (\lambda_L)_i\ (\lambda_R)_i\,/\,\left[(M_\Sigma)_i\ M_L^2\right]$, el que implica que la contribució del W a l'anomalia magnètica del muó és la dominant. Finalment, el nostre model prediu que no hi haurà cap canvi significatiu en les desintegracions del bosó de Higgs als leptons carregats en comparació amb els resultats del ME.

A continuació, al Capítol 5, vam presentar un model eficient que proporciona una explicació unificada per a diverses indicacions de nova física, incloent les masses no nul·les dels neutrins, les transicions $b \to s$, l'anomalia magnètica del muó i l'origen potencial de la matèria fosca. La nostra proposta introdueix diversos camps nous: un fermió singlet N, dos doblets escalars η, un escalar singlet ϕ i un leptoquark doblet S que és necessari per a acomodar les anomalies $b \to s\ell\ell$. En aquest escenari, totes aquestes noves partícules són imparells sota una paritat fosca $\mathbb{Z}_2$ que s'afegeix al model, mentre que els camps del Model Estàndard són parells. Una característica notable d'aquest model és la presència de bucles foscos, amb estats imparells de $\mathbb{Z}_2$ dins ells, que indueixen totes les contribucions de nova física als observables anòmals que volem explicar. A més, les masses dels neutrins de Majorana es generen al nivell d'1-bucle per mitjà d'una variació del mecanisme Scotogenic, ja que les contribucions a nivell d'arbre estan prohibides per la presència de la simetria $\mathbb{Z}_2$.

A més d'explicar les anomalies esmentades anteriorment, el model ha de satisfer diverses restriccions experimentals. És clar que les dades d'oscil·lacions de neutrins han de ser reproduïdes correctament, tot i que això es pot aconseguir fàcilment considerant una parametrització de Casas-Ibarra adequadament adaptada al nostre escenari. Una altra preocupació habitual en models de masses de neutrins és el risc de tindre processos on es viole sabor leptònic. El model també es veu sotmès a condicionants que venen de diversos processos que involucren mesons, sent els més rellevants $b \to s\gamma$, $B \to K^{(*)}\nu\bar{\nu}$, i la mescla $B_s - \bar{B}_s$.

L'objectiu d'aquest capítol era demostrar que el nostre model pot explicar totes les anomalies mentre satisfà totes les restriccions experimentals. Per aconseguir-ho, vam construir una funció χ^2 que inclou l'anomalia del moment magnètic del muó i els coeficients de Wilson dels operadors efectius involucrats en les anomalies $b-s$. Després de fixar diversos paràmetres per simplicitat, trobàrem que el valor mínim de la funció χ^2 és $\chi^2_{\text{min}} = 1,52$, que es pot comparar amb el valor del SM: $\Delta\chi^2 = \chi^2_{\text{SM}} - \chi^2_{\text{min}} = 21,23$. La part esquerra de la Figura 5.2 mostra els resultats de l'ajust, revelant que els paràmetres del model que es van deixar lliures a l'ajust poden variar significativament respecte dels seus valors millor ajustats sense causar un canvi significatiu en la funció χ^2. No obstant això, $\mu \to e\gamma$ resulta ser una forta restricció en el model. A més, el

costat dret de la figura mostra que el model pot assolir fàcilment el valor central dels observables ajustats.

El Capítol 6 conclou aquesta part de la tesi. S'ha dedicat a l'estudi de la violació de la simetria de sabor dels leptons carregats en un model amb ruptura espontània del nombre leptònic i, per tant, amb un majoron J. En aquest capítol, presentem un model relativament simple que genera acoblaments del majoró amb els leptons carregats no diagonals grans a nivell d'arbre. A més de les simetries del ME, aquest model imposa la conservació del nombre leptònic i amplia el contingut de partícules amb un singlet i un doblet d'escalars, tres neutrins drets i un leptó vectorial singlet de $\mathrm{SU(2)_L}$, tots amb nombre leptònic no nul. Després de la ruptura espontània de les simetries electrofeble i nombre leptònic, els neutrins adquireixen masses a través d'un mecanisme de balancí de tipus-I amb escala de TeV.

Com a conseqüència dels acoblaments que violen sabor leptònic a nivell d'arbre, el model exhibeix taxes de violació de sabor leptònic significatives que cobreixen regions grans del seu espai de paràmetres, incloent els processos habituals $\ell_\alpha \to \ell_\beta\gamma$ i $\ell_\alpha \to 3\ell_\beta$. Això implica l'existència de restriccions importants. A més, la inclusió de fermions vectorials al sector de leptons del ME té un impacte en diversos observables, particularment en el moment magnètic anòmal dels leptons carregats i en el seu acoblament als bosons gauge. Com a resultat, el model indueix noves contribucions al moment magnètic del muó a nivell d'1-bucle que poden explicar l'anomalia observada en algunes regions del seu espai de paràmetres. Pel que fa als acoblaments dels leptons carregats amb el bosó Z, ens hem assegurat durant l'anàlisi que es troben dins dels rangs permesos. Finalment, el model també pot portar a efectes observables en els decaïments del bosó de Higgs, especialment en $h \to \mu\mu$, i també permet la desintegració del Higgs en un parell de majorons.

De manera similar al Capítol 4, ací escanejàrem aleatòriament l'ample espai de paràmetres del model mentre calculàvem els observables rellevants per a cada punt de l'escaneig i gràcies a una parametrització de Casas-Ibarra, tots els punts eren compatibles amb les observacions actuals d'oscil·lacions de neutrins. Com es mostra a la Figura 6.2, el nostre model pot arribar als límits experimentals de $\mathrm{BR}(\mu \to e\gamma)$ i $\mathrm{BR}(\mu \to eJ)$, que en realitat estan correlacionats. A més a més, el moment magnètic del múon $g-2$ es pot explicar en gran part de l'espai de paràmetres del model, fins i tot dins de la regió d'1σ, com es mostra a la Figura 6.4, i vam trobar desviacions significatives de la tasa de decaïment de $h \to \mu\mu$ respecte a la seua predicció del ME, com s'il·lustra a la Figura 6.5.

Construcció de Models

En aquesta part de la tesi, vam adoptar una perspectiva centrada en la construcció de models mentre relegàvem la fenomenologia a un segon pla. Consisteix en dos capítols, tots dos centrats en el model Scotogenic.

El model Scotogenic, en la seua versió original, inclou un doblet escalar η i tres còpies de fermions singlets N, a més de les partícules del ME. El model es caracteritza també per una paritat fosca $\mathbb{Z}_2$, segons la qual les noves partícules són imparells i les partícules del ME són parells. No obstant, l'elecció del nombre de generacions de cada camp nou no és única i, per abordar això, hem presentat el model Scotogenic general al Capítol 7. Aquest model permet un nombre arbitrari de generacions dels estats Scotogenic.

Els termes de Yukawa i de massa rellevants per a la discussió són

$$\mathcal{L}_N \supset y_{na\alpha}\,\overline{N}_n\,\eta_a\,\ell_L^\alpha + \frac{1}{2}\,M_{N_n}\,\overline{N^c}_n\,N_n + \text{h.c.}\,, \tag{8}$$

on $n = 1, \ldots, n_N$, $a = 1, \ldots, n_\eta$ i $\alpha = 1, 2, 3$ són índexs de generació, i n_N i n_η són el nombre de còpies de les partícules N i η, respectivament, en la versió general del model. Els casos particulars del model es poden etiquetar segons els seus valors (n_N, n_η). A més, també es poden escriure els termes escalars importants del potencial com

$$\mathcal{V} \supset \left(m_\eta^2\right)_{ab}\,\eta_a^\dagger\eta_b + \lambda_3^{ab}\left(H^\dagger H\right)\left(\eta_a^\dagger\eta_b\right) + \lambda_4^{ab}\left(H^\dagger\eta_a\right)\left(\eta_b^\dagger H\right) + \frac{1}{2}\left[\lambda_5^{ab}\left(H^\dagger\eta_a\right)\left(H^\dagger\eta_b\right) + \text{h.c.}\right]\,. \tag{9}$$

El resultat principal d'aquest capítol és la derivació de la matriu de massa dels neutrins en la versió general del model. Per simplificar els càlculs, es va assumir que la simetria CP es conserva en el sector escalar del model considerant que tots els paràmetres del potencial escalar són reals. Amb això, es va obtenir una expressió analítica exacta per a la matriu de massa:

$$(m_\nu)_{\alpha\beta} = -\frac{1}{32\pi^2}\sum_{A,a,b,c,n} M_{N_n}\,\kappa_A^2\,(V_A)_{ba}\,(V_A)_{ca}\,y_{nb\alpha}\,y_{nc\beta}\,B_0(0, m_{A_a}^2, M_{N_n})\,. \tag{10}$$

Ací, $A = R, I$ i b i c poden prendre els mateixos valors que a. $B_0(0, m_{A_a}^2, M_{N_n})$ és la funció de bucle estàndard de Passarino-Veltman introduïda a l'Eq. (7.16), $\kappa_R = 1$, $\kappa_I = i$, i $m_{R(I)_a}^2$ i $VR(I)$ són els valors propis de la matriu de massa de les components reals (imaginàries) de les parts neutres de η_a, respectivament.

Tot i que la dependència exacta dels paràmetres del model no és explícita en la matriu de massa exacta, encara podem obtenir una forma aproximada útil fent assumpcions raonables. Específicament, assumírem que $\lambda_{3,4}^{aa}v^2/2 \ll (m\eta^2)aa$ i $\lambda_5^{ab} \ll \lambda_{3,4}^{ab} \ll 1$, amb $a \neq b$. D'aquesta manera, derivàrem una forma aproximada per a la matriu de massa dels neutrins, que és el principal resultat analític del capítol:

$$(m_\nu)_{\alpha\beta} = \frac{v^2}{32\pi^2}\sum_{n,a,b}\frac{y_{na\alpha}\,y_{nb\beta}}{M_{N_n}}\,\Gamma_{abn} + \mathcal{O}\left(\lambda_5^2\right) + \mathcal{O}\left(\lambda_5\,s^2\right)\,, \tag{11}$$

on $s_{ab} = 1/2(\lambda_3^{ab} + \lambda_4^{ab})v^2/(m_b^2 - m_a^2)$ i $m_a^2 = (m_\eta^2)aa + (\lambda 3^{aa} + \lambda_4^{aa})v^2/2$. També hem definit la quantitat adimensional:

$$\Gamma_{abn} = \delta_{ab}\,\lambda_5^{aa}\,f_{an} - (1-\delta_{ab})\left[\left(\lambda_5^{aa}\,f_{an} - \lambda_5^{bb}\,f_{bn}\right)\,s_{ab} - \frac{M_{N_n}^2}{m_b^2 - m_a^2}\,\lambda_5^{ab}\,g_{abn}\right] \tag{12}$$

amb les funcions de bucle

$$f_{an} = \frac{M_{N_n}^2}{m_a^2 - M_{N_n}^2} + \frac{M_{N_n}^4}{\left(m_a^2 - M_{N_n}^2\right)^2}\log\frac{M_{N_n}^2}{m_a^2}\,, \tag{13}$$

$$g_{abn} = \frac{m_a^2}{m_a^2 - M_{N_n}^2}\log\frac{M_{N_n}^2}{m_a^2} - \frac{m_b^2}{m_b^2 - M_{N_n}^2}\log\frac{M_{N_n}^2}{m_b^2}\,. \tag{14}$$

Després de demostrar que la nostra expressió es redueix a les matrius de massa obtingudes en dos resultats prèviament publicats, el model Scotogenic estàndard i una variant que inclou dos η i un N, vam estudiar el comportament a altes energies del model.

La conservació de la simetria $\mathbb{Z}_2$ és essencial perquè qualsevol versió del model Scotogenic general siga coherent. Si no, els neutrins adquiririen masses a nivell d'arbre, i el candidat a matèria fosca ja no seria estable. No obstant això, l'evolució de les RGEs pot alterar la forma del potencial escalar a altes energies, conduint al trencament de la $\mathbb{Z}_2$. Això motiva l'estudi del comportament a altes energies de la teoria. Computàrem totes les funcions β d'1 bucle i les varem utilitzar per a resoldre numèricament el conjunt complet d'RGEs. Ens vam centrar en dues versions específiques del model Scotogenic general: els models $(3,1)$ i $(1,3)$, on el primer és la versió original del model. Malgrat algunes particularitats a causa dels diferents nombres de generacions, la nostra principal conclusió és que totes les característiques del model Scotogenic original es presenten en altres variants específiques del model general.

D'altra banda, al model Scotogenic es requereix un petit paràmetre quartic $\lambda_5 \ll 1$ per a generar l'escala correcta de les masses dels neutrins mentre es tenen acoblaments de Yukawa considerables i mediadors relativament lleugers. La petitesa d'aquest paràmetre és tècnicament natural en el sentit de 't Hooft, però requerix una extensió que la explique. A més, la simetria $\mathbb{Z}_2$ al model Scotogenic és considerada una simetria *ad hoc*. Per això, al Capítol 8, vam voler classificar les possibles extensions ultravioleta que porten al model Scotogenic a baixes energies quan s'integra un camp escalar pesat S i que aborden aquests dos problemes. Específicament, estàvem interessats en escenaris UV als quals la simetria $\mathbb{Z}_2$ apareix com una simetria remanent després de la ruptura espontània d'una simetria $\mathrm{U}(1)_\mathrm{L}$, on L significa nombre leptònic. També volguérem que l'operador $(H^\dagger\eta)^2$, que és el terme λ_5, estiguera prohibit en la teoria UV a causa del nombre leptònic. D'altra banda, un operador de la forma $(H^\dagger\eta)^2\sigma^n$, amb $n \geq 1$, ha de ser generat després d'integrar el camp pesat. Aquest operador induïx un acoblament efectiu λ_5, naturalment suprimit per la gran massa de l'escalar S, després que els singlets adquireixin VEBs.

Centrant-nos en les possibles extensions a nivell d'arbre de l'operador λ_5 utilitzant un o dos singlets σ diferents, vam identificar totes les topologies possibles en la teoria UV que generen aquest operador, com es mostra a la Taula 8.1. De les cinc topologies possibles, quatre inclouen només un propagador S, portant a un operador λ_5 de la forma $\mathcal{O}\lambda_5 = (H^\dagger\eta)^2\sigma_A\sigma_B$, suprimit per un factor $1/m_S^2$. Per l'altra banda, la topologia restant té dos propagadors S i genera l'operador $\mathcal{O}\lambda_5 = (H^\dagger\eta)^2\sigma_A^2\sigma_B\sigma_C$, ara suprimit per $1/m_S^4$. Cal destacar que aquestes expressions genèriques inclouen casos on algunes insercions de σ corresponen al mateix camp, així com casos on una de les insercions de σ està absenta. Vam explorar totes les possibilitats i vam trobar 50 variacions diferents que compleixen els requisits anteriors. No obstant, és important destacar que els números leptònics dels camps en totes aquestes variacions han de prendre valors específics per a evitar que η adquirisca un VEB i per a generar la paritat $\mathbb{Z}_2$ correcta.

En aquest Capítol, hem discutit tres models exemplificatius i s'espera que la fenomenologia d'aquestos models, així com la de la resta, siga molt rica. A causa de la ruptura espontània del nombre leptònic, els models preveuen l'existència d'un majoró sense mass, a més d'altres escalars massius nous. Hem derivat expressions analítiques per als acoblaments del majoró als leptons carregats, incloent-hi interaccions tant que conserven com que violes sabor leptònic. A més, els models tenen signatures potencials en recerques de col·lisionadors i ofereixen implicacions interessants per a la matèria fosca en comparació amb el model estàndard Scotogènic, ja que contenen estats addicionals.

Recerques de Col·lisionadors de Partícules

El Capítol 9 va ser l'últim capítol de la tesi, i allí ens centràrem en les recerques de leptons neutres pesats de vida mitjana curta en col·lisionadors d'alta energia, principalment al LHC. El nostre interès es va centrar en el fet que les restriccions a l'espai de fàsic dels HNL, amb molt poques excepcions, es deriven per les col·laboracions experimentals sota l'assumpció d'un únic HNL que es mescla amb només un sabor dels leptons. No obstant això, aquest no és el cas en la majoria dels escenaris de nova física que involucren aquest tipus de partícules, on el patró de mescla pot ser bastant complex. En aquest capítol, vam proposar abordar aquesta qüestió discutint com reinterpretar els límits experimentals existents sobre els HNL per a un escenari que implica mescles genèriques amb tots els sabors de leptons i amb diversos HNLs.

Inicialment, explorarem l'escenari d'un únic HNL però permetent que es mesclara amb els tres sabors leptònics. Normalment, els límits experimentals en la cerca de HNL es presenten en el pla $\left(M_N, |U_{\alpha N}|^2\right)$, on $U_{\alpha N}$, amb $\alpha = e, \mu, \tau$, representa les mescles entre els neutrins i els HNLs i M_N denota la massa dels darrers. No obstant això, vam voler destacar que per generalitzar els límits, és millor presentar-los al pla $\left(M_N, |U_{\alpha N}|^2 \times \mathrm{BR}\right)$. Això és perquè d'aquesta manera només cal calcular les noves taxes de desintegració per a l'hipòtesi particular de mescla. Tot i que la majoria dels treballs presenten els seus resultats utilitzant la primera opció, traduir-los a la segona és senzill quan les col·laboracions experimentals assumeixen una BR constant

per al canal que estudien, encara que no sempre especifiquen el seu valor. No obstant això, la reescritura no és possible quan els resultats s'obtenen després de combinar diferents canals.

En principi, no hi ha cap restricció en el nombre de HNLs que pot tindre un model. Si només un d'ells està dins de l'abast dels experiments actuals, o si hi ha diversos HNLs però amb règims de massa diferents, llavors les conclusions extretes de l'anàlisi de l'escenari d'un sol HNL es poden aplicar a cadascun dels HNLs. No obstant això, quan dos HNLs tenen masses similars, poden produir-se efectes d'interferència, alterant potencialment els resultats i els límits obtinguts sota l'assumpció d'un sol HNL. Per simplicitat, ens vam centrar en l'escenari amb dos HNLs propers en massa. Per il·lustrar millor la importància de la interferència, ens vam centrar en els resultats de LHCb per al canal *prompt* de dimuons, considerant tant els canals de dileptons de mateix signe com els de signe oposat. D'aquesta manera, vam poder demostrar que les cerques d'ambdós canals que violen i conserven sabor leptònic són importants i complementàries, i que s'han de realitzar en paral·lel.

Conclusions

Els models de massa de neutrins són probablement les extensions del Model Estàndard de física de partícules més ben motivades. Encara que els experiments d'oscil·lacions de neutrins han confirmat que són massius, el mecanisme que hi ha darrere de la generació de les seues masses és un misteri. En aquesta tesi, hem presentat diversos models especialment centrats en la generació d'aquestes masses, tant a nivell d'arbre com radiativament. D'interès especial són aquells models que no només proporcionen masses als neutrins, sinó que també les connecten amb explicacions per a altres qüestions pendents en física de partícules, com ara l'origen de la matèria fosca, el moment magnètic anòmal dels leptons carregats o les anomalies de sabor B. A més, molts models de massa de neutrins prediuen interaccions importants que violen el sabor dels leptons, destacant l'importància de buscar no només les possibles partícules involucrades en la generació de masses de neutrins, sinó també els processos de violació de sabor de leptons.

Part VI

Appendices

Appendix A

Ultralight scalar parametrization in terms of derivative interactions

This appendix is related to Chapter 3. The Lagrangian in Eq. (3.1) is completely general and includes both scalar and pseudoscalar interactions of the field ϕ with a pair of charged leptons. An alternative parametrization in terms of derivative interactions is given by

$$\mathcal{L}_{\ell\ell\phi} = (\partial_\mu \phi)\ \bar{\ell}_\beta \gamma^\mu \left(\widetilde{S}_L^{\beta\alpha} P_L + \widetilde{S}_R^{\beta\alpha} P_R\right) \ell_\alpha + \text{h.c.}\,. \tag{A.1}$$

The coefficients $\widetilde{S}_{L,R}$ have dimensions of mass^{-1} and we consider all possible flavor combinations: $\beta\alpha = \{ee, \mu\mu, \tau\tau, e\mu, e\tau, \mu\tau\}$. Notice that the diagonal $\ell_\beta - \ell_\beta - \phi$ vertex is proportional to $(\widetilde{S}_L + \widetilde{S}_L^*)^{\beta\beta} P_L + (\widetilde{S}_R + \widetilde{S}_R^*)^{\beta\beta} P_R$, and, therefore, the diagonal couplings can be taken to be real without loss of generality. As we will shown below, Eq. (A.1) only includes pseudoscalar interactions for ϕ. Therefore, it can be thought of as a particularization of Eq. (3.1). [1]

Physical observables must be independent of the parametrization chosen. We proceed to show now that the two parametrizations considered here are equivalent for a pure pseudoscalar in processes involving on-shell leptons. First, we recall the equations of motion for the lepton fields ℓ_α and its conjugate $\bar{\ell}_\alpha$

$$\begin{aligned} i\,\gamma^\mu \partial_\mu \ell_\alpha - m_\alpha \ell_\alpha &= 0\,, \\ i\,\partial_\mu \bar{\ell}_\alpha \gamma^\mu + m_\alpha \bar{\ell}_\alpha &= 0\,, \end{aligned} \tag{A.2}$$

valid for on-shell leptons. One can now rewrite Eq. (A.1) as the sum of a total derivative and a derivative acting on the lepton fields. The total derivative does not contribute to the action,

[1] The parametrization in Eq. (A.1) is completely general if ϕ is a pure pseudoscalar, usually the case of the Goldstone bosons in many models. In such scenarios, the two parametrizations for the effective Lagrangian $\mathcal{L}_{\ell\ell\phi}$ introduced here are related to two possible ways to parametrize the Goldstone boson. Eq. (3.1) follows from a *cartesian parametrization*, that splits a complex scalar field in terms of its real and imaginary components. Alternatively, the parametrization in terms of derivative interactions in Eq. (A.1) would follow from a *polar parametrization*, that splits a complex scalar field in terms of its modulus and phase. As we will prove below, they lead to the same results for observables involving on-shell leptons.

whereas the derivative on the lepton fields can be replaced using the equations of motion in Eq. (A.2). This leads to

$$\begin{aligned}\mathcal{L}_{\ell\ell\phi} &= -i\,\phi\,\bar{\ell}_\beta\left[\left(m_\beta\,\widetilde{S}_L^{\beta\alpha} - m_\alpha\,\widetilde{S}_R^{\beta\alpha}\right)P_L + \left(m_\beta\,\widetilde{S}_R^{\beta\alpha} - m_\alpha\,\widetilde{S}_L^{\beta\alpha}\right)P_R\right]\ell_\alpha + \text{h.c.}\\ &\equiv \phi\,\bar{\ell}_\beta\left(S_L^{\beta\alpha}P_L + S_R^{\beta\alpha}P_R\right)\ell_\alpha + \text{h.c.}\,. \end{aligned} \tag{A.3}$$

Therefore we find a *dictionary* between the S_X and $\widetilde{S}_X$ coefficients

$$S_L^{\beta\alpha} = i\left(m_\alpha\,\widetilde{S}_R^{\beta\alpha} - m_\beta\,\widetilde{S}_L^{\beta\alpha}\right), \tag{A.4}$$

$$S_R^{\beta\alpha} = i\left(m_\alpha\,\widetilde{S}_L^{\beta\alpha} - m_\beta\,\widetilde{S}_R^{\beta\alpha}\right), \tag{A.5}$$

which for the diagonal couplings reduces to

$$S^{\beta\beta} = S_L^{\beta\beta} + S_R^{\beta\beta *} = 2\,i\,m_\beta\left(\widetilde{S}_R^{\beta\beta} - \widetilde{S}_L^{\beta\beta}\right). \tag{A.6}$$

Since both $\widetilde{S}_X^{\beta\beta}$ are real parameters, Eq. (A.6) implies that the diagonal $S^{\beta\beta}$ couplings must be purely imaginary. It is straightforward to show that, in this case, the flavor conserving interactions of ϕ in Eq. (3.1) are proportional to γ_5 (see Eq. (3.6)). This proves that Eq. (A.1) is not general but only includes pseudoscalar interactions, and there is no one-to-one correspondence between the two parametrizations. Given a set of $\widetilde{S}_X$ couplings, one can always find the corresponding S_X couplings using Eqs. (A.4) and (A.5). However, certain sets of S_X couplings, namely those with non-vanishing real parts, cannot be expressed in terms of $\widetilde{S}_X$ couplings. This stems from the fact that purely scalar interactions are not included in Eq. (A.1).

The equivalence for the case of a pure pseudoscalar can be explicitly illustrated by comparing the analytical expressions obtained with Eqs. (3.1) and (A.1) for a given observable. We can start with a trivial example, the process $\ell_\alpha \to \ell_\beta\phi$, discussed in Section 3.4.1. Using the parametrization in Eq. (A.1), one can easily derive the decay width of this 2-body decay,

$$\widetilde{\Gamma}\left(\ell_\alpha \to \ell_\beta\,\phi\right) = \frac{m_\alpha^3}{32\,\pi}\left(\left|\widetilde{S}_L^{\beta\alpha}\right|^2 + \left|\widetilde{S}_R^{\beta\alpha}\right|^2\right), \tag{A.7}$$

where terms proportional to m_β have been neglected. This result differs from Eq. (3.22) only by a factor m_α^2, as one would obtain from the direct application of the dictionary in Eqs. (A.4) and (A.5). Let us now consider a less trivial example: $\ell_\alpha^- \to \ell_\beta^-\ell_\beta^+\ell_\beta^-$. The computation of its amplitude with the Lagrangian in Eq. (A.1) makes use of the same Feynman diagrams shown in Fig. 3.3. In this case one obtains

$$\begin{aligned}&\widetilde{\mathcal{M}}_\phi = \\ &\bar{u}\left(p_3\right)2\left(-\not{q}\right)\left(\widetilde{S}_L^{\beta\beta}P_L + \widetilde{S}_R^{\beta\beta}P_R\right)v\left(p_4\right)\frac{i}{q^2+i\varepsilon}\bar{u}\left(p_2\right)\left(\not{q}\right)\left(\widetilde{S}_L^{\beta\alpha}P_L + \widetilde{S}_R^{\beta\alpha}P_R\right)u\left(p_1\right)\\ &-\bar{u}\left(p_2\right)2\left(-\not{k}\right)\left(\widetilde{S}_L^{\beta\beta}P_L + \widetilde{S}_R^{\beta\beta}P_R\right)v\left(p_4\right)\frac{i}{k^2+i\varepsilon}\bar{u}\left(p_3\right)\left(\not{k}\right)\left(\widetilde{S}_L^{\beta\alpha}P_L + \widetilde{S}_R^{\beta\alpha}P_R\right)u\left(p_1\right),\end{aligned} \tag{A.8}$$

where the factor of 2 preceding the diagonal coupling is due to the addition of the Hermitian conjugate, as explicitly shown in Eq. (A.1). Again, explicit flavor indices have been introduced. The decay width is computed to be

$$
\begin{aligned}
&\widetilde{\Gamma}_\phi\left(\ell_\alpha^- \to \ell_\beta^-\ell_\beta^+\ell_\beta^-\right) = \\
&\frac{m_\alpha^5}{512\pi^3}\Bigg\{4\left(\left|\widetilde{S}_L^{\beta\alpha}\right|^2+\left|\widetilde{S}_R^{\beta\alpha}\right|^2\right)\left(\widetilde{S}_L^{\beta\beta}-\widetilde{S}_R^{\beta\beta}\right)^2\frac{m_\beta^2}{m_\alpha^2}\left(4\log\frac{m_\alpha}{m_\beta}-\frac{15}{2}\right) \\
&+\frac{m_\beta}{3\,m_\alpha}\Bigg\{\left(\widetilde{S}_L^{\beta\beta}-\widetilde{S}_R^{\beta\beta}\right)\Bigg\{\widetilde{S}_R^{\beta\alpha}\left(A_{LL}^{S*}-2A_{LR}^{S*}\right)-\widetilde{S}_L^{\beta\alpha}\left(A_{RR}^{S*}-2A_{RL}^{S*}\right) \\
&+\frac{m_\beta}{m_\alpha}\Bigg\{\widetilde{S}_L^{\beta\alpha}\left[2A_{LL}^{S*}+\left(12\log\frac{m_\alpha}{m_\beta}-25\right)A_{LR}^{S*}\right]-\widetilde{S}_R^{\beta\alpha}\left[2A_{RR}^{S*}+\left(12\log\frac{m_\alpha}{m_\beta}-25\right)A_{RL}^{S*}\right]\Bigg\} \\
&+12\left[A_{RR}^{T*}\left(\widetilde{S}_L^{\beta\alpha}+2\frac{m_\beta}{m_\alpha}\widetilde{S}_R^{\beta\alpha}\right)-A_{LL}^{T*}\left(\widetilde{S}_R^{\beta\alpha}+2\frac{m_\beta}{m_\alpha}\widetilde{S}_L^{\beta\alpha}\right)\right]+4\left(\widetilde{S}_R^{\beta\alpha}A_{LR}^{V*}-\widetilde{S}_L^{\beta\alpha}A_{RL}^{V*}\right) \\
&+2\frac{m_\beta}{m_\alpha}\Bigg\{\widetilde{S}_L^{\beta\alpha}\left[\left(25-12\log\frac{m_\alpha}{m_\beta}\right)A_{LR}^{V*}-\left(42-24\log\frac{m_\alpha}{m_\beta}\right)A_{LL}^{V*}\right] \\
&-\widetilde{S}_R^{\beta\alpha}\left[\left(25-12\log\frac{m_\alpha}{m_\beta}\right)A_{RL}^{V*}-\left(42-24\log\frac{m_\alpha}{m_\beta}\right)A_{RR}^{V*}\right]\Bigg\} \\
&+6e^2\left[\left(K_2^L\right)^{\beta\alpha*}\widetilde{S}_L^{\beta\alpha}-\left(K_2^R\right)^{\beta\alpha*}\widetilde{S}_R^{\beta\alpha}\right] \\
&+4e^2\frac{m_\beta}{m_\alpha}\left(\frac{3}{2}+\pi^2+6\log^2 2-6\log^2\frac{m_\alpha}{m_\beta}\right)\left[\left(K_2^R\right)^{\beta\alpha*}\widetilde{S}_L^{\beta\alpha}-\left(K_2^L\right)^{\beta\alpha*}\widetilde{S}_R^{\beta\alpha}\right]\Bigg\}+\text{c.c.}\Bigg\}\Bigg\},
\end{aligned}
\tag{A.9}
$$

where in this expression $A_{XY}^I = \left(A_{XY}^I\right)^{\beta\beta\beta\alpha}$. We note that infrared divergences also occur in interference terms at this order in $\frac{m_\beta}{m_\alpha}$. This explains the appearance of several log factors. We can compare the decay width in Eq. (A.9) to a previous result in the literature. The authors of [224] drop all the interference terms in their calculation, and then their result must be compared to the first line in Eq. (A.9). One can easily relate the $\widetilde{S}_{L,R}$ coefficients to the ones in [224] as

$$
V_{\beta\alpha}^e \equiv -\frac{1}{2}\left(\widetilde{S}_L^{\beta\alpha}+\widetilde{S}_R^{\beta\alpha}\right), \qquad A_{\beta\alpha}^e \equiv \frac{1}{2}\left(\widetilde{S}_R^{\beta\alpha}-\widetilde{S}_L^{\beta\alpha}\right), \tag{A.10}
$$

for the flavor violating terms, and

$$
A_{\beta\beta}^e \equiv \left(\widetilde{S}_R^{\beta\beta}-\widetilde{S}_L^{\beta\beta}\right), \tag{A.11}
$$

for the flavor conserving ones. With this translation, it is easy to check that both results agree up to a global factor of 1/2.

In order to compare the $\ell_\alpha^- \to \ell_\beta^- \ell_\beta^+ \ell_\beta^-$ decay widths obtained with both parametrizations we need an expanded version of Eq. (3.41) that includes terms up to $\mathcal{O}\left(\frac{m_\beta}{m_\alpha}\right)$. This is given by

$$
\begin{aligned}
&\Gamma_\phi\left(\ell_\alpha^- \to \ell_\beta^- \ell_\beta^+ \ell_\beta^-\right) = \\
&\frac{m_\alpha}{512\pi^3}\Bigg\{\left(\left|S_L^{\beta\alpha}\right|^2+\left|S_R^{\beta\alpha}\right|^2\right)\Bigg\{\left|S^{\beta\beta}\right|^2\left(4\log\frac{m_\alpha}{m_\beta}-\frac{49}{6}\right)-\frac{2}{6}\left[\left(S^{\beta\beta*}\right)^2+\left(S^{\beta\beta}\right)^2\right]\Bigg\} \\
&-\frac{m_\alpha^2}{6}\Bigg\{S_L^{\beta\alpha}S^{\beta\beta}A_{LL}^{S*}+2S_L^{\beta\alpha}S^{\beta\beta*}A_{LR}^{S*}+2S_R^{\beta\alpha}S^{\beta\beta}A_{RL}^{S*}+S_R^{\beta\alpha}S^{\beta\beta*}A_{RR}^{S*} \\
&-12\left(S_L^{\beta\alpha}S^{\beta\beta}A_{LL}^{T*}+S_R^{\beta\alpha}S^{\beta\beta*}A_{RR}^{T*}\right)-4\left(S_R^{\beta\alpha}S^{\beta\beta}A_{RL}^{V*}+S_L^{\beta\alpha}S^{\beta\beta*}A_{LR}^{V*}\right) \\
&+6e^2\left(S_R^{\beta\alpha}S^{\beta\beta}K_2^{L*}+S_L^{\beta\alpha}S^{\beta\beta*}K_2^{R*}\right)-\frac{36m_\beta}{m_\alpha}\left(S_R^{\beta\alpha}S^{\beta\beta}A_{LL}^{T*}+S_L^{\beta\alpha}S^{\beta\beta*}A_{RR}^{T*}\right) \\
&+\frac{3m_\beta}{2m_\alpha}\Big[S^{\beta\beta}\left(11S_L^{\beta\alpha}A_{RL}^{S*}+2S_R^{\beta\alpha}A_{LL}^{S*}-7S_R^{\beta\alpha}A_{LR}^{S*}\right) \\
&+S^{\beta\beta*}\left(11S_R^{\beta\alpha}A_{LR}^{S*}+2S_L^{\beta\alpha}A_{RR}^{S*}-7S_L^{\beta\alpha}A_{RL}^{S*}\right)\Big] \\
&-\frac{6m_\beta}{m_\alpha}\left(S_L^{\beta\alpha}A_{RL}^{S*}-S_R^{\beta\alpha}A_{LR}^{S*}\right)\left(S^{\beta\beta}-S^{\beta\beta*}\right)\log\frac{m_\alpha}{m_\beta} \\
&+\frac{12m_\beta}{m_\alpha}\left(S_L^{\beta\alpha}A_{RL}^{V*}-2S_L^{\beta\alpha}A_{RR}^{V*}+2S_R^{\beta\alpha}A_{LL}^{V*}-S_R^{\beta\alpha}A_{LR}^{V*}\right)\left(S^{\beta\beta}-S^{\beta\beta*}\right)\log\frac{m_\alpha}{m_\beta} \\
&+\frac{3m_\beta}{m_\alpha}\Big[S^{\beta\beta}\left(-11S_L^{\beta\alpha}A_{RL}^{V*}+14S_L^{\beta\alpha}A_{RR}^{V*}-14S_R^{\beta\alpha}A_{LL}^{V*}+7S_R^{\beta\alpha}A_{LR}^{V*}\right) \\
&+S^{\beta\beta*}\left(-11S_R^{\beta\alpha}A_{LR}^{V*}+14S_R^{\beta\alpha}A_{LL}^{V*}-14S_L^{\beta\alpha}A_{RR}^{V*}+7S_L^{\beta\alpha}A_{RL}^{V*}\right)\Big] \\
&-4\,e^2\,\frac{m_\beta}{m_\alpha}\Bigg\{\left[S_L^{\beta\alpha}\left(K_2^L\right)^{\beta\alpha*}+S_R^{\beta\alpha}\left(K_2^R\right)^{\beta\alpha*}\right]\left(S^{\beta\beta}+S^{\beta\beta*}\right)\left(6\log\frac{m_\alpha}{m_\beta}-\frac{21}{2}\right) \\
&+\left[S_L^{\beta\alpha}S^{\beta\beta}\left(K_2^L\right)^{\beta\alpha*}+S_R^{\beta\alpha}S^{\beta\beta*}\left(K_2^R\right)^{\beta\alpha*}\right]\left(\pi^2+6\log^2 2-6\log^2\frac{m_\alpha}{m_\beta}\right)\Bigg\}+\text{c.c.}\Bigg\}\Bigg\},
\end{aligned}
\tag{A.12}
$$

where in this expression $A_{XY}^I = \left(A_{XY}^I\right)^{\beta\beta\beta\alpha}$. Replacing Eqs. (A.4) and (A.5) into Eq. (A.12) one finds full agreement with Eq. (A.9) to order $\mathcal{O}\left(\frac{m_\beta}{m_\alpha}\right)$. This proves explicitly the equivalence between both parametrizations in the calculation of $\ell_\alpha^- \to \ell_\beta^- \ell_\beta^+ \ell_\beta^-$ mediated by a pure pseudoscalar.

Appendix B

Extended inverse type-III seesaw couplings

The couplings of the model introduced in Chapter 4 that are involved in the calculation of the charged lepton anomalous magnetic moments are shown in the Feynman diagrams of Fig. 4.1 and have been computed with the help of SARAH [405–409]. We define them and list their analytical expressions here:

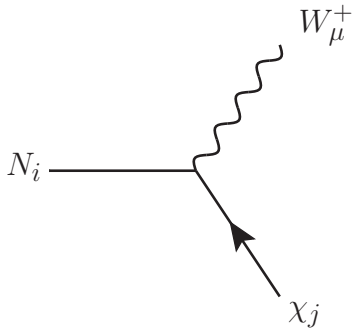

$$\mathcal{L}_{\chi NW} = \bar{N}_i \, \gamma^\mu \left[\left(g^L_{\chi NW} \right)_{ij} P_L + \left(g^R_{\chi NW} \right)_{ij} P_R \right] \chi_j \, W_\mu + \text{h.c.} \tag{B.1}$$

$$\left(g^L_{\chi NW} \right)_{ij} = -g \left(\frac{1}{\sqrt{2}} \sum_{a=1}^{3} \mathcal{V}^{L\,*}_{ja} \mathcal{U}_{ia} + \sum_{a=4}^{9} \mathcal{V}^{L\,*}_{ja} \mathcal{U}_{ia} + \frac{1}{\sqrt{2}} \mathcal{V}^{L\,*}_{j10} \mathcal{U}_{i10} \right) \tag{B.2}$$

$$\left(g^R_{\chi NW} \right)_{ij} = -g \left(\sum_{a=4}^{9} \mathcal{V}^{R}_{ja} \mathcal{U}^{*}_{ia} - \frac{1}{\sqrt{2}} \mathcal{V}^{R}_{j10} \mathcal{U}^{*}_{i11} \right) \tag{B.3}$$

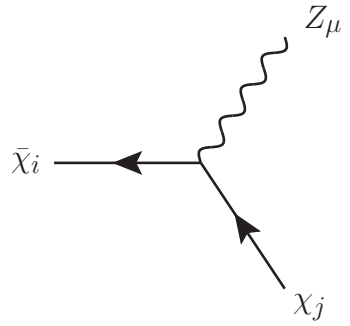

$$\mathcal{L}_{\chi Z} = \bar{\chi}_i \, \gamma^\mu \left[\left(g^L_{\chi Z} \right)_{ij} P_L + \left(g^R_{\chi Z} \right)_{ij} P_R \right] \chi_j \, Z_\mu + \text{h.c.} \tag{B.4}$$

$$\left(g^L_{\chi Z} \right)_{ij} = \frac{1}{2} \left(g \cos\theta_W - g' \sin\theta_W \right) \left(\sum_{a=1}^{3} \mathcal{V}^{L\,*}_{ja} \, \mathcal{V}^L_{ia} + \mathcal{V}^{L\,*}_{j10} \, \mathcal{V}^L_{i10} \right) + g \cos\theta_W \sum_{a=4}^{9} \mathcal{V}^{L\,*}_{ja} \, \mathcal{V}^L_{ia} \tag{B.5}$$

$$\left(g^R_{\chi Z} \right)_{ij} = -g' \sin\theta_W \sum_{a=1}^{3} \mathcal{V}^{R\,*}_{ia} \, \mathcal{V}^R_{ja} + g \cos\theta_W \sum_{a=4}^{9} \mathcal{V}^{R\,*}_{ia} \, \mathcal{V}^R_{ja} + \frac{1}{2} \left(g \cos\theta_W - g' \sin\theta_W \right) \, \mathcal{V}^{R\,*}_{i10} \, \mathcal{V}^R_{j10} \tag{B.6}$$

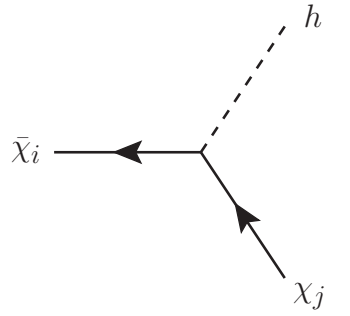

$$\mathcal{L}_{\chi h} = \bar{\chi}_i \left[\left(g^L_{\chi h} \right)_{ij} P_L + \left(g^R_{\chi h} \right)_{ij} P_R \right] \chi_j \, h + \text{h.c.} \tag{B.7}$$

$$\begin{aligned} \left(g^L_{\chi h} \right)_{ij} = & -\frac{1}{\sqrt{2}} \sum_{a,b=1}^{3} \mathcal{V}^{L\,*}_{jb} \, \mathcal{V}^{R\,*}_{ia} \, \left(Y_e \right)_{ab} - \sum_{a=1}^{3} \sum_{b=1}^{3} \mathcal{V}^{L\,*}_{jb} \, \mathcal{V}^{R\,*}_{i\,a+3} \, \left(Y_\Sigma \right)_{ab} \\ & - \mathcal{V}^{L\,*}_{j10} \left[\sum_{a=1}^{3} \mathcal{V}^{R\,*}_{i\,a+3} \, \left(\lambda_L \right)_a + \frac{1}{\sqrt{2}} \sum_{a=1}^{3} \mathcal{V}^{R\,*}_{ia} \, \left(\lambda_R \right)_a \right] \end{aligned} \tag{B.8}$$

$$\begin{aligned} \left(g^R_{\chi h} \right)_{ij} = & -\frac{1}{\sqrt{2}} \sum_{a,b=1}^{3} \mathcal{V}^{L}_{ib} \, \mathcal{V}^{R}_{ja} \, \left(Y_e \right)^*_{ab} - \sum_{a=1}^{3} \sum_{b=1}^{3} \mathcal{V}^{L}_{ib} \, \mathcal{V}^{R}_{j\,a+3} \, \left(Y_\Sigma \right)^*_{ab} \\ & - \left[\sum_{a=1}^{3} \mathcal{V}^{R}_{j\,a+3} \, \left(\lambda^*_L \right)_a + \frac{1}{\sqrt{2}} \sum_{a=1}^{3} \mathcal{V}^{R}_{ja} \, \left(\lambda^*_R \right)_a \right] \mathcal{V}^L_{i10} \end{aligned} \tag{B.9}$$

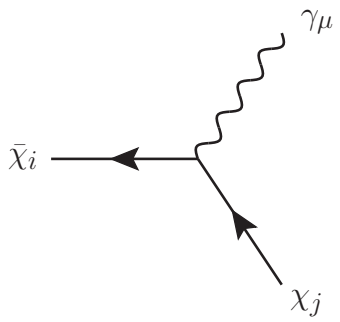

$$\mathcal{L}_{\chi\gamma} = \bar{\chi}_i \, \gamma^\mu \, \left[\left(g^L_{\chi\gamma} \right)_{ij} P_L + \left(g^R_{\chi\gamma} \right)_{ij} P_R \right] \chi_j \, A_\mu + \text{h.c.} \tag{B.10}$$

$$\left(g^L_{\chi\gamma} \right)_{ij} = \left(g^R_{\chi\gamma} \right)_{ij} = -e \, \delta_{ij} \tag{B.11}$$

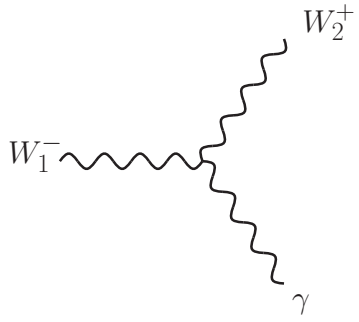

$$\mathcal{L}_{W\gamma} = \Gamma^{\mu\alpha\beta} \, W_\alpha W_\beta A_\mu \tag{B.12}$$

$$\Gamma^{\mu\alpha\beta} = g \, \sin\theta_W \left[g^{\alpha\beta} \left(p^\mu_{W_1} + p^\mu_{W_2} \right) + g^{\mu\beta} \left(-p^\alpha_{W_2} - p^\alpha_\gamma \right) + g^{\alpha\mu} \left(p^\beta_\gamma - p^\beta_{W1} \right) \right] \tag{B.13}$$

Appendix C

Charged lepton anomalous magnetic moments: full expressions

Following the notation used in Chapter 4, we define the dimensionless quantities

$$\epsilon_{\ell i} = \frac{m_\ell}{m_{\chi_i}}\,, \quad \delta_{\ell i} = \frac{m_\ell}{m_{N_i}}\,, \quad \omega_{ai} = \frac{m_a}{m_{\chi_i}} \quad \text{and} \quad \omega_{Wi} = \frac{m_W}{m_{N_i}}\,, \tag{C.1}$$

with $a = Z,\, h$.

W contribution

The W contribution to the charged lepton anomalous magnetic moments can be written as

$$\Delta a_\ell\,(W) = \frac{1}{32\pi^2\,\omega_{Wi}^2\delta_{\ell i}^4}\left[\left(C_{\chi NW}^2\right)_{i\ell}\, f_W(\delta_{\ell i}^2,\omega_{Wi}^2) - \delta_{\ell i}\,\left(D_{\chi NW}^2\right)_{i\ell}\, g_W(\delta_{\ell i}^2,\omega_{Wi}^2)\right]\,, \tag{C.2}$$

where a sum over the repeated index i is implicit and f_W and g_W are two loop functions given by

$$\begin{aligned}
f_W(x,y) &= x^3 + x^2\,(8\,y-1) + 2\,x\,\left(1+y-2\,y^2\right) \\
&\quad + \left[3\,x^2\,y - x\left(1-3\,y+5\,y^2\right) - 3\,y^2 + 2\,y^3 + 1\right]\log y \\
&\quad + \frac{2}{\Delta(x,y)}\left[3\,x^3\,y + x^2\left(1-8\,y^2\right) + x\left(7\,y^3 - 7\,y^2 + 2\,y - 2\right)\right. \\
&\quad \left. + (1-y)^3\,(1+2\,y)\right]\log\frac{1+y-x+\Delta(x,y)}{2\,\sqrt{y}}\,,
\end{aligned} \tag{C.3}$$

$$\begin{aligned}
g_W(x,y) &= 2\,x\,(1+2\,y) + \left[x\,(3\,y-1) - 2\,y^2\,+y+1\right]\,\log y \\
&\quad + \frac{2}{\Delta(x,y)}\left[x^2\,(3\,y+1) - x\left(2-y+5\,y^2\right) + 2\,y^3 - 3\,y^2 + 1\right]\log\frac{1+y-x+\Delta(x,y)}{2\,\sqrt{y}}\,.
\end{aligned} \tag{C.4}$$

Here we have defined the auxiliary function

$$\Delta(x,y) = \sqrt{x^2 - 2\,x\,(1+y) + (1-y)^2}\,. \tag{C.5}$$

Z contribution

The Z contribution can be written as

$$\Delta a_\ell\,(Z) = \frac{1}{32\pi^2\,\omega_{Zi}^2\epsilon_{\ell i}^4}\left[\left(C_{\chi Z}^2\right)_{i\ell}\,f_Z(\epsilon_{\ell i}^2,\omega_{Zi}^2) + \epsilon_{\ell i}\,\left(D_{\chi Z}^2\right)_{i\ell}\,g_Z(\epsilon_{\ell i}^2,\omega_{Zi}^2)\right]\,. \tag{C.6}$$

Again, there is a sum over the repeated index i, whereas f_Z and g_Z are the loop functions

$$\begin{aligned}
f_Z(x,y) &= -x\left[x^2 + x\,(3-4\,y) + 4\,y^2 - 2\,y - 2\right] \\
&\quad + \left[x^2 - x\left(2 - 2\,y + 3\,y^2\right) + 2\,y^3 - 3\,y^2 + 1\right]\log y \\
&\quad - \frac{2}{\Delta(x,y)}\left[x^3 + x^2\left(3\,y^2 + y - 3\right) - x\left(5\,y^3 - 4\,y^2 + 2\,y - 3\right)\right. \\
&\quad \left. - (1-y)^3\,(1+2\,y)\right]\log\frac{1+y-x+\Delta(x,y)}{2\,\sqrt{y}}\,,
\end{aligned} \tag{C.7}$$

$$\begin{aligned}
g_Z(x,y) &= 2\,x\,(2\,x - 2\,y - 1) - \left[x^2 + x\,(y-2) - 2\,y^2 + y + 1\right]\log y \\
&\quad + \frac{2}{\Delta(x,y)}\left[x^3 - 3\,x^2 + 3\,x\left(1 + y^2\right) - 2\,y^3 + 3\,y^2 - 1\right]\log\frac{1+y-x+\Delta(x,y)}{2\,\sqrt{y}}\,.
\end{aligned} \tag{C.8}$$

h contribution

Finally, the h contribution to the charged leptons $g-2$ can be written as

$$\Delta a_\ell\,(h) = \frac{1}{32\pi^2\,\epsilon_{\ell i}^4}\left[\left(C_{\chi h}^2\right)_{i\ell}\,f_h(\epsilon_{\ell i}^2,\omega_{hi}^2) + \epsilon_{\ell i}\,\left(D_{\chi h}^2\right)_{i\ell}\,g_h(\epsilon_{\ell i}^2,\omega_{hi}^2)\right]\,, \tag{C.9}$$

with an implicit sum over the repeated i index and the loop functions

$$\begin{aligned}
f_h(x,y) &= -x\,(x + 2\,y - 2) + \left[(1-y)^2 - x\right]\log y \\
&\quad + \frac{2}{\Delta(x,y)}\left[x^2 + x\left(y^2 + y - 2\right) + (1-y)^3\right]\log\frac{1+y-x+\Delta(x,y)}{2\,\sqrt{y}}\,,
\end{aligned} \tag{C.10}$$

$$\begin{aligned}
g_h(x,y) &= 2\,x - (x + y - 1)\log y \\
&\quad + \frac{2}{\Delta(x,y)}\left[(1-x)^2 + y^2 - 2\,y\right]\log\frac{1+y-x+\Delta(x,y)}{2\,\sqrt{y}}\,.
\end{aligned} \tag{C.11}$$

We have compared our results to the general expressions provided in [103], finding full agreement. Our results also match those recently presented in [93], where a model with similar contributions to the muon $g-2$ was considered. Finally, analytical expressions for the contributions to the muon $g-2$ in the limit of heavy mediators are provided in [52]. While we do not

consider this limit in our paper (since it would correspond to $m_W, m_Z, m_h \gg m_{N_i}, m_{\chi_i}$), it can be used to crosscheck our results. We find full agreement.

Appendix D

Proof of the pseudoscalar nature of the majoron couplings

This appendix is related to the model introduced in Chapter 6. Eq. (6.61) encodes the diagonal couplings of the majoron with the charged leptons of the model. Since the majoron is a pure pseudoscalar Goldstone boson, the coefficients $S^{\beta\beta}$ are purely imaginary. We are going to prove that this is indeed the case for the general scenario of n singlet vector-like lepton pairs added to the SM leptons, with the same form of the couplings as the one defined in Eq. (6.3). [1] Let

$$M = \begin{pmatrix} m_1 & m_2 \\ m_3 & m_4 \end{pmatrix} \tag{D.1}$$

be a generic complex $(3+n)\times(3+n)$ complex matrix, given by the blocks m_1, m_2, m_3 and m_4, with dimensions 3×3, $3\times n$, $n\times 3$ and $n\times n$, respectively. The singular value decomposition of the matrix M is $V_R^\dagger\, M\, V_L = \widehat{M}$, where V_R and V_L are unitary matrices and $\widehat{M} = \mathrm{diag}(M_1, M_2)$, with M_1 and M_2 3×3 and $n\times n$ real diagonal matrices, respectively, with positive entries. The interaction matrix of the majoron with the charged leptons can be written in the flavor basis as

$$N = \begin{pmatrix} x\, m_1 & (x+y)\, m_2 \\ -y\, m_3 & 0 \end{pmatrix}, \tag{D.2}$$

where N is another $(3+n)\times(3+n)$ matrix and $x, y \in \mathbb{R}$. Comparing with Eq. (6.58), the majoron coupling matrix in our model is given by $N \equiv A$ and corresponds to $m_1 \equiv m_e$, $m_2 \equiv m_\rho$, $m_3 \equiv m_S$, $x \equiv v_S^2$ and $y \equiv v_H^2$.

First of all, we block-parametrize the unitary matrices V_R and V_L as

$$V_R^\dagger = \begin{pmatrix} A & B \\ C & D \end{pmatrix}, \quad V_L^\dagger = \begin{pmatrix} E & F \\ G & H \end{pmatrix}. \tag{D.3}$$

[1] We thank Isabel Cordero-Carrión for providing the seed for this proof.

We also denote

$$e_1 = \begin{pmatrix} \mathbb{1}_3 \\ 0 \end{pmatrix}, \quad e_2 = \begin{pmatrix} 0 \\ \mathbb{1}_n \end{pmatrix}, \tag{D.4}$$

where $\mathbb{1}_n$ is the $n \times n$ identity matrix. Therefore, one obtains

$$\begin{aligned} \left(V_R^\dagger e_1\right)\left(V_R^\dagger e_1\right)^\dagger &= \begin{pmatrix} AA^\dagger & AC^\dagger \\ CA^\dagger & CC^\dagger \end{pmatrix}, \\ \left(V_R^\dagger e_2\right)\left(V_R^\dagger e_2\right)^\dagger &= \begin{pmatrix} BB^\dagger & BD^\dagger \\ DB^\dagger & DD^\dagger \end{pmatrix}. \end{aligned} \tag{D.5}$$

Analogously, one finds the following relations involving V_L:

$$\begin{aligned} \left(V_L^\dagger e_1\right)\left(V_L^\dagger e_1\right)^\dagger &= \begin{pmatrix} EE^\dagger & EG^\dagger \\ GE^\dagger & GG^\dagger \end{pmatrix}, \\ \left(V_L^\dagger e_2\right)\left(V_L^\dagger e_2\right)^\dagger &= \begin{pmatrix} FF^\dagger & FH^\dagger \\ HF^\dagger & HH^\dagger \end{pmatrix}. \end{aligned} \tag{D.6}$$

After these preliminaries, we note that the interaction matrix N can be written as

$$N = x \begin{pmatrix} m_1 & m_2 \\ 0 & 0 \end{pmatrix} + y \begin{pmatrix} 0 & m_2 \\ -m_3 & 0 \end{pmatrix}. \tag{D.7}$$

Therefore, if we prove that the combinations

$$V_R^\dagger \begin{pmatrix} m_1 & m_2 \\ 0 & 0 \end{pmatrix} V_L, \quad V_R^\dagger \begin{pmatrix} 0 & m_2 \\ -m_3 & 0 \end{pmatrix} V_L \tag{D.8}$$

have real diagonal elements, then, also $V_R^\dagger N V_L$ has real diagonal elements, and the proof is complete. Let us consider the first term. It is easy to check that

$$\begin{pmatrix} m_1 & m_2 \\ 0 & 0 \end{pmatrix} = e_1 e_1^T M. \tag{D.9}$$

Then one can obtain

$$\begin{aligned} V_R^\dagger \begin{pmatrix} m_1 & m_2 \\ 0 & 0 \end{pmatrix} V_L = V_R^\dagger e_1 e_1^T M V_L = V_R^\dagger e_1 e_1^T V_R \widehat{M} = \\ \left(V_R^\dagger e_1\right)\left(V_R^\dagger e_1\right)^\dagger \widehat{M} = \begin{pmatrix} AA^\dagger M_1 & AC^\dagger M_2 \\ CA^\dagger M_1 & CC^\dagger M_2 \end{pmatrix}. \end{aligned} \tag{D.10}$$

The diagonal terms of the resulting matrix are real because $AA^\dagger$ and $CC^\dagger$ are Hermitian matrices and M_1, M_2 are real diagonal matrices. We now have to consider the second term in Eq. (D.7).

It is possible to write

$$\begin{pmatrix} 0 & m_2 \\ -m_3 & 0 \end{pmatrix} = e_1 \left(e_1^T M e_2\right) e_2^T - e_2 \left(e_2^T M e_1\right) e_1^T \,. \tag{D.11}$$

Using similar manipulations as for the first term one finds

$$V_R^\dagger \begin{pmatrix} 0 & m_2 \\ -m_3 & 0 \end{pmatrix} V_L = \left(V_R^\dagger e_1\right)\left(V_R^\dagger e_1\right)^\dagger \widehat{M} \left(V_L^\dagger e_2\right)\left(V_L^\dagger e_2\right)^\dagger - \left(V_R^\dagger e_2\right)\left(V_R^\dagger e_2\right)^\dagger \widehat{M} \left(V_L^\dagger e_1\right)\left(V_L^\dagger e_1\right)^\dagger \,, \tag{D.12}$$

and, writing for the sake of brevity only the diagonal blocks of this expression, in the form of a column array, we obtain

$$\left[V_R^\dagger \begin{pmatrix} 0 & m_2 \\ -m_3 & 0 \end{pmatrix} V_L\right]_{\text{diag}} = \begin{pmatrix} AA^\dagger M_1 FF^\dagger + AC^\dagger M_2 HF^\dagger \\ CC^\dagger M_2 HH^\dagger + CA^\dagger M_1 FH^\dagger \end{pmatrix} - \begin{pmatrix} BB^\dagger M_1 EE^\dagger + BD^\dagger M_2 GE^\dagger \\ DD^\dagger M_2 GG^\dagger + DB^\dagger M_1 EG^\dagger \end{pmatrix} . \tag{D.13}$$

The second terms in the sum cancel for both the upper and lower diagonal blocks, using the unitarity of V_L and V_R. Then, using again unitarity in the following way

$$\begin{cases} AA^\dagger = 1 - BB^\dagger \\ EE^\dagger = 1 - FF^\dagger \\ CC^\dagger = 1 - DD^\dagger \\ GG^\dagger = 1 - HH^\dagger \,, \end{cases} \tag{D.14}$$

we finally end up with

$$\left[V_R^\dagger \begin{pmatrix} 0 & m_2 \\ -m_3 & 0 \end{pmatrix} V_L\right]_{\text{diag}} = \begin{pmatrix} M_1 FF^\dagger - BB^\dagger M_1 \\ M_2 HH^\dagger - DD^\dagger M_2 \end{pmatrix} , \tag{D.15}$$

and therefore the diagonal components of this matrix are purely real. This concludes the proof.

Appendix E

Effective coefficients for flavor violating observables

In order to use the analytical results for the flavor violating observables provided in [251] and in Chapter 3, one must match the effective Lagrangian in these references to any specific model. In particular, this appendix considers the model introduced in Chapter 6. We focus in particular on the 3-body lepton decays $\ell_\alpha^- \to \ell_\beta^- \ell_\beta^- \ell_\beta^+$, $\ell_\alpha^- \to \ell_\beta^- \ell_\gamma^- \ell_\gamma^+$ and $\ell_\alpha^- \to \ell_\beta^+ \ell_\gamma^- \ell_\gamma^-$. These processes get tree-level contributions in our model from the three CP-even scalars H_k ($k = 1, 2, 3$), the Z-boson, the CP-odd scalar A, and the majoron J. The majoron contributions have been computed in [211]. Since all the other mediators are significantly heavier than the SM charged leptons, we can then parametrize their contributions by the effective Lagrangian

$$\mathcal{L}_{4\ell} = \sum_{\substack{I=S,V,T \\ X,Y=L,R}} A_{XY}^I \bar{\ell^\beta} \Gamma_I P_X \ell^\alpha \bar{\ell^\delta} \Gamma_I P_Y \ell^\gamma + \text{h.c.}\,, \tag{E.1}$$

where we have defined $\Gamma_S = 1$, $\Gamma_V = \gamma_\mu$ and $\Gamma_T = \sigma_{\mu\nu}$ and omitted flavor indices in the effective coefficients for the sake of simplicity. The coefficients A_{XY}^I have dimensions of mass^{-2}. We will now give specific expressions for these coefficients in the model under consideration. In order to do that, it proves convenient to define the following 3-component array

$$(c_1, c_2, c_3)^{\beta\alpha} = (V_{ee}^{R\dagger} Y_e V_{ee}^L, V_{ee}^{R\dagger} \rho V_{Fe}^L, V_{Fe}^{R\dagger} Y_S V_{ee}^L)^{\beta\alpha}\,, \tag{E.2}$$

which encodes the interactions of the SM charged leptons with the CP-even scalars gauge eigenstates $\{S_H, S_\sigma, S_S\}$.

$\ell_\alpha^- \to \ell_\beta^- \ell_\beta^- \ell_\beta^+$

Recalling the definition of the 3×3 unitary matrix W given in Eq. (6.23), we get the following expressions for the effective coefficients $A_{XY}^I = (A_{XY}^I)^{\beta\beta\beta\alpha}$.

H_k contributions

$$A^S_{LL} = \frac{1}{2m^2_{H_k}} \sum_{i,j} (W_{ki} c_i^{\beta\beta})(W_{kj} c_j^{\beta\alpha}) \tag{E.3}$$

$$A^S_{LR} = \frac{1}{2m^2_{H_k}} \sum_{i,j} (W_{ki} c_i^{\beta\beta})(W_{kj} c_j^{\dagger\beta\alpha}) \tag{E.4}$$

$$A^S_{RL} = \frac{1}{2m^2_{H_k}} \sum_{i,j} (W_{ki} c_i^{\dagger\beta\beta})(W_{kj} c_j^{\beta\alpha}) \tag{E.5}$$

$$A^S_{RR} = \frac{1}{2m^2_{H_k}} \sum_{i,j} (W_{ki} c_i^{\dagger\beta\beta})(W_{kj} c_j^{\dagger\beta\alpha}) \tag{E.6}$$

Z contributions

$$A^V_{LL} = -\frac{g^2}{4m^2_W}\Big(V^{L\dagger}_{ee} V^L_{ee} - 2\sin^2\theta_W \mathbb{I}\Big)^{\beta\beta}\Big(V^{L\dagger}_{ee} V^L_{ee}\Big)^{\beta\alpha} \tag{E.7}$$

$$A^V_{LR} = 0 \tag{E.8}$$

$$A^V_{RL} = \frac{g^2}{2m^2_W}\sin^2\theta_W \Big(V^{L\dagger}_{ee} V^L_{ee}\Big)^{\beta\alpha} \tag{E.9}$$

$$A^V_{RR} = 0 \tag{E.10}$$

Actually, the parametrization $V^{L(R)} = U^{L(R)} D^{L(R)}$ greatly simplifies the expressions. Taking into account the unitarity of D^L_e one ends up with

$$A^V_{LL} = \frac{g^2}{4m^2_W M^2_F}\Big[1 - 2\sin^2\theta_W - \Big(D^{L\dagger}_e \frac{m^\dagger_S m_S}{M^2_F} D^L_e\Big)^{\beta\beta}\Big]\Big(D^{L\dagger}_e m^\dagger_S m_S D^L_e\Big)^{\beta\alpha} \tag{E.11}$$

$$A^V_{RL} = -\frac{g^2}{2m^2_W M^2_F}\sin^2\theta_W \Big(D^{L\dagger}_e m^\dagger_S m_S D^L_e\Big)^{\beta\alpha} \tag{E.12}$$

A contributions

From the profile of the massive CP-odd state A given in Eq. (6.27) one can recover the interaction Lagrangian between A and the charged leptons in the flavor basis

$$\mathcal{L}_{A\ell\ell} = -\frac{i\,A}{\sqrt{2}V^2}\begin{pmatrix} \bar{e}_R & \bar{F}_R \end{pmatrix}\begin{pmatrix} -Y_e\, v_S v_\sigma & \rho\, v_H v_S \\ Y_S\, v_H v_\sigma & 0 \end{pmatrix}\begin{pmatrix} e_L \\ F_L \end{pmatrix} + \text{h.c.}\,. \tag{E.13}$$

Denoting the matrix in the previous equation as B and transforming the Lagrangian to the mass basis, one can easily perform the matching with Eq. (E.1). We get the following expressions for the contributions of A to the effective coefficients $A^I_{XY} = (A^I_{XY})^{\beta\beta\beta\alpha}$.

$$A^S_{LL} = -\frac{1}{2V^4 m_A^2}\left(V^{R\dagger}BV^L\right)^{\beta\beta}\left(V^{R\dagger}BV^L\right)^{\beta\alpha} \tag{E.14}$$

$$A^S_{LR} = \frac{1}{2V^4 m_A^2}\left(V^{R\dagger}BV^L\right)^{\beta\beta}\left(V^{L\dagger}B^\dagger V^R\right)^{\beta\alpha} \tag{E.15}$$

$$A^S_{RL} = \frac{1}{2V^4 m_A^2}\left(V^{L\dagger}B^\dagger V^R\right)^{\beta\beta}\left(V^{R\dagger}BV^L\right)^{\beta\alpha} \tag{E.16}$$

$$A^S_{RR} = -\frac{1}{2V^4 m_A^2}\left(V^{L\dagger}B^\dagger V^R\right)^{\beta\beta}\left(V^{L\dagger}B^\dagger V^R\right)^{\beta\alpha} \tag{E.17}$$

$\ell^-_\alpha \to \ell^-_\beta \ell^-_\gamma \ell^+_\gamma$

There are two types of Feynman diagrams contributing to this process. The first class involves a flavor conserving ($\gamma\gamma$) and a flavor violating ($\beta\alpha$) vertex, while in the second class, both vertices violate flavor ($\beta\gamma$ and $\gamma\alpha$). Therefore, the matching with Eq. (E.1) would yield non vanishing contributions to both coefficients $(A^I_{XY})^{\gamma\gamma\beta\alpha}$ and $(A^I_{XY})^{\beta\gamma\gamma\alpha}$. One can actually Fierz transform the latter flavor structure into the former, thus in the following expressions, we set $A^I_{XY} = (A^I_{XY})^{\gamma\gamma\beta\alpha}$. The Fierz transformations involved in the matching are the following, where the type of parenthesis indicates the fermion field which is contracted with the gamma matrix in brackets.

$$\begin{aligned}
(P_L)[P_L] &= \frac{1}{2}(P_L][P_L) + \frac{1}{8}(\sigma^{\mu\nu}P_L][\sigma_{\mu\nu}P_L) \\
(P_R)[P_R] &= \frac{1}{2}(P_R][P_R) + \frac{1}{8}(\sigma^{\mu\nu}P_R][\sigma_{\mu\nu}P_R) \\
(P_R)[P_L] &= \frac{1}{2}(\gamma^\mu P_L][\gamma_\mu P_R) \\
(\gamma^\mu P_L)[\gamma_\mu P_L] &= -(\gamma^\mu P_L][\gamma_\mu P_L) \\
(\gamma^\mu P_R)[\gamma_\mu P_R] &= -(\gamma^\mu P_R][\gamma_\mu P_R) \\
(\gamma^\mu P_R)[\gamma_\mu P_L] &= 2(P_L][P_R)
\end{aligned} \tag{E.18}$$

H_k contributions

$$A^S_{LL} = \frac{1}{2m^2_{H_k}}\sum_{i,j}\left[(W_{ki}c_i^{\gamma\gamma})(W_{kj}c_j^{\beta\alpha}) - \frac{1}{2}(W_{ki}c_i^{\beta\gamma})(W_{kj}c_j^{\gamma\alpha})\right] \tag{E.19}$$

$$A^T_{LL} = \frac{1}{2m^2_{H_k}}\sum_{i,j}\left[-\frac{1}{8}(W_{ki}c_i^{\beta\gamma})(W_{kj}c_j^{\gamma\alpha})\right] \tag{E.20}$$

$$A_{LR}^{S} = \frac{1}{2m_{H_k}^2} \sum_{i,j} (W_{ki} c_i^{\gamma\gamma})(W_{kj} c_j^{\dagger\beta\alpha}) \tag{E.21}$$

$$A_{RL}^{S} = \frac{1}{2m_{H_k}^2} \sum_{i,j} (W_{ki} c_i^{\dagger\gamma\gamma})(W_{kj} c_j^{\beta\alpha}) \tag{E.22}$$

$$A_{RR}^{S} = \frac{1}{2m_{H_k}^2} \sum_{i,j} \Big[(W_{ki} c_i^{\dagger\gamma\gamma})(W_{kj} c_j^{\dagger\beta\alpha}) - \frac{1}{2}(W_{ki} c_i^{\dagger\beta\gamma})(W_{kj} c_j^{\dagger\gamma\alpha}) \Big] \tag{E.23}$$

$$A_{RR}^{T} = \frac{1}{2m_{H_k}^2} \sum_{i,j} \Big[-\frac{1}{8}(W_{ki} c_i^{\dagger\beta\gamma})(W_{kj} c_j^{\dagger\gamma\alpha}) \Big] \tag{E.24}$$

$$A_{LR}^{V} = \frac{1}{2m_{H_k}^2} \sum_{i,j} \Big[-\frac{1}{2}(W_{ki} c_i^{\beta\gamma})(W_{kj} c_j^{\dagger\gamma\alpha}) \Big] \tag{E.25}$$

$$A_{RL}^{V} = \frac{1}{2m_{H_k}^2} \sum_{i,j} \Big[-\frac{1}{2}(W_{ki} c_i^{\dagger\beta\gamma})(W_{kj} c_j^{\gamma\alpha}) \Big] \tag{E.26}$$

Z contributions

$$A_{LL}^{V} = -\frac{g^2}{4m_W^2} \Big[(V_{ee}^{L\dagger} V_{ee}^{L} - 2\sin^2\theta_W \mathbb{I})^{\gamma\gamma} (V_{ee}^{L\dagger} V_{ee}^{L})^{\beta\alpha} + (V_{ee}^{L\dagger} V_{ee}^{L})^{\beta\gamma} (V_{ee}^{L\dagger} V_{ee}^{L})^{\gamma\alpha} \Big] \tag{E.27}$$

$$A_{LR}^{V} = 0 \tag{E.28}$$

$$A_{RL}^{V} = \frac{g^2}{2m_W^2} \sin^2\theta_W \Big(V_{ee}^{L\dagger} V_{ee}^{L} \Big)^{\beta\alpha} \tag{E.29}$$

$$A_{RR}^{V} = 0 \tag{E.30}$$

The parametrization $V^{L(R)} = U^{L(R)} D^{L(R)}$ also simplifies the expressions in this case. Thanks to the unitarity of D_e^L, we can write

$$\begin{aligned} A_{LL}^{V} = \frac{g^2}{4m_W^2 M_F^2} \Big[\Big(1 - 2\sin^2\theta_W - \Big(D_e^{L\dagger} \frac{m_S^\dagger m_S}{M_F^2} D_e^L \Big)^{\gamma\gamma} \Big) \Big(D_e^{L\dagger} m_S^\dagger m_S D_e^L \Big)^{\beta\alpha} \\ - \frac{1}{M_F^2} \Big(D_e^{L\dagger} m_S^\dagger m_S D_e^L \Big)^{\beta\gamma} \Big(D_e^{L\dagger} m_S^\dagger m_S D_e^L \Big)^{\gamma\alpha} \Big] \end{aligned} \tag{E.31}$$

$$A_{RL}^{V} = -\frac{g^2}{2m_W^2 M_F^2} \sin^2\theta_W \Big(D_e^{L\dagger} m_S^\dagger m_S D_e^L \Big)^{\beta\alpha} \tag{E.32}$$

A contributions

$$A_{LL}^{S} = -\frac{1}{2V^4 m_A^2} \Big[(V^{R\dagger} B V^{L}\Big)^{\gamma\gamma} \Big(V^{R\dagger} B V^{L} \Big)^{\beta\alpha} - \frac{1}{2} (V^{R\dagger} B V^{L}\Big)^{\beta\gamma} \Big(V^{R\dagger} B V^{L} \Big)^{\gamma\alpha} \Big] \tag{E.33}$$

$$A_{LL}^{T} = -\frac{1}{2V^4 m_A^2}\Big[-\frac{1}{8}(V^{R\dagger}BV^{L})^{\beta\gamma}\Big(V^{R\dagger}BV^{L})^{\gamma\alpha}\Big] \tag{E.34}$$

$$A_{LR}^{S} = \frac{1}{2V^4 m_A^2}\Big(V^{R\dagger}BV^{L}\Big)^{\gamma\gamma}\Big(V^{L\dagger}B^{\dagger}V^{R}\Big)^{\beta\alpha} \tag{E.35}$$

$$A_{RL}^{S} = \frac{1}{2V^4 m_A^2}\Big(V^{L\dagger}B^{\dagger}V^{R}\Big)^{\gamma\gamma}\Big(V^{R\dagger}BV^{L}\Big)^{\beta\alpha} \tag{E.36}$$

$$A_{RR}^{S} = -\frac{1}{2V^4 m_A^2}\Big[(V^{L\dagger}B^{\dagger}V^{R}\Big)^{\gamma\gamma}\Big(V^{L\dagger}B^{\dagger}V^{R})^{\beta\alpha} - \frac{1}{2}(V^{L\dagger}B^{\dagger}V^{R}\Big)^{\beta\gamma}\Big(V^{L\dagger}B^{\dagger}V^{R})^{\gamma\alpha}\Big] \tag{E.37}$$

$$A_{RR}^{T} = -\frac{1}{2V^4 m_A^2}\Big[-\frac{1}{8}(V^{L\dagger}B^{\dagger}V^{R}\Big)^{\beta\gamma}\Big(V^{L\dagger}B^{\dagger}V^{R})^{\gamma\alpha}\Big] \tag{E.38}$$

$$A_{RL}^{V} = \frac{1}{2V^4 m_A^2}\Big[-\frac{1}{2}(V^{L\dagger}B^{\dagger}V^{R}\Big)^{\beta\gamma}\Big(V^{R\dagger}BV^{L})^{\gamma\alpha}\Big] \tag{E.39}$$

$$A_{LR}^{V} = -\frac{1}{2V^4 m_A^2}\Big[-\frac{1}{2}(V^{R\dagger}BV^{L}\Big)^{\beta\gamma}\Big(V^{L\dagger}B^{\dagger}V^{R})^{\gamma\alpha}\Big] \tag{E.40}$$

$\ell_\alpha^- \to \ell_\beta^+ \ell_\gamma^- \ell_\gamma^-$

In this process, both vertices are necessarily flavor violating ($\gamma\beta$ and $\gamma\alpha$). This allows us to easily perform the matching with Eq. (E.1) and set in the following expressions $A_{XY}^I = (A_{XY}^I)^{\gamma\beta\gamma\alpha}$.

H_k contributions

$$A_{LL}^{S} = \frac{1}{2m_{H_k}^2}\sum_{i,j}(W_{ki}c_i^{\gamma\beta})(W_{kj}c_j^{\gamma\alpha}) \tag{E.41}$$

$$A_{LR}^{S} = \frac{1}{2m_{H_k}^2}\sum_{i,j}(W_{ki}c_i^{\gamma\beta})(W_{kj}c_j^{\dagger\gamma\alpha}) \tag{E.42}$$

$$A_{RL}^{S} = \frac{1}{2m_{H_k}^2}\sum_{i,j}(W_{ki}c_i^{\dagger\gamma\beta})(W_{ki}c_j^{\gamma\alpha}) \tag{E.43}$$

$$A_{RR}^{S} = \frac{1}{2m_{H_k}^2}\sum_{i,j}(W_{ki}c_i^{\dagger\gamma\beta})(W_{kj}c_j^{\dagger\gamma\alpha}) \tag{E.44}$$

Z contributions

$$A_{LL}^{V} = -\frac{g^2}{4m_W^2}\Big(V_{ee}^{L\dagger}V_{ee}^{L}\Big)^{\gamma\beta}\Big(V_{ee}^{L\dagger}V_{ee}^{L}\Big)^{\gamma\alpha} \tag{E.45}$$

$$A_{LR}^{V} = 0 \tag{E.46}$$

$$A_{RL}^{V} = 0 \tag{E.47}$$

$$A_{RR}^{V} = 0 \tag{E.48}$$

Finally, using our previous definitions we can simplify Eq. (E.45) to

$$A_{LL}^{V} = -\frac{g^2}{4m_W^2 M_F^4}\left(D_e^{L\dagger} m_S^{\dagger} m_S D_e^{L}\right)^{\gamma\beta}\left(D_e^{L\dagger} m_S^{\dagger} m_S D_e^{L}\right)^{\gamma\alpha} \tag{E.49}$$

A contributions

$$A_{LL}^{S} = -\frac{1}{2V^4 m_A^2}\left(V^{R\dagger} B V^{L}\right)^{\gamma\beta}\left(V^{R\dagger} B V^{L}\right)^{\gamma\alpha} \tag{E.50}$$

$$A_{LR}^{S} = \frac{1}{2V^4 m_A^2}\left(V^{R\dagger} B V^{L}\right)^{\gamma\beta}\left(V^{L\dagger} B^{\dagger} V^{R}\right)^{\gamma\alpha} \tag{E.51}$$

$$A_{RL}^{S} = \frac{1}{2V^4 m_A^2}\left(V^{L\dagger} B^{\dagger} V^{R}\right)^{\gamma\beta}\left(V^{R\dagger} B V^{L}\right)^{\gamma\alpha} \tag{E.52}$$

$$A_{RR}^{S} = -\frac{1}{2V^4 m_A^2}\left(V^{L\dagger} B^{\dagger} V^{R}\right)^{\gamma\beta}\left(V^{L\dagger} B^{\dagger} V^{R}\right)^{\gamma\alpha} \tag{E.53}$$

Appendix F

$R_{h\mu\mu}$ analytical expression

In the model in Chapter 6, the $R_{h\mu\mu}$ ratio can be approximately written as

$$R_{h\mu\mu} = \frac{\mathrm{BR}(h \to \mu\mu)}{\mathrm{BR}(h \to \mu\mu)^{\mathrm{SM}}} \approx \left(\frac{c_{\mu\mu}^{S_H} + c_{\mu\mu}^{S_\sigma} + c_{\mu\mu}^{S_S}}{c_{\mu\mu}^{\mathrm{SM}}} \right)^2 , \tag{F.1}$$

where

$$c_{\mu\mu}^{\mathrm{SM}} = \frac{g m_\mu}{2 m_W} \tag{F.2}$$

is the SM Higgs coupling to a pair of muons and $c_{\mu\mu}^{S_H}$, $c_{\mu\mu}^{S_\sigma}$, and $c_{\mu\mu}^{S_S}$ denote the contributions from the gauge eigenstates S_H, S_σ, and S_S, respectively. These couplings are given by

$$c_{\mu\mu}^{S_H} \approx \frac{1}{\sqrt{2}} Y_{e_{22}} V_{22}^{R\dagger} V_{22}^{L\dagger} \tag{F.3}$$

$$c_{\mu\mu}^{S_\sigma} \approx \frac{1}{\sqrt{2}} \sin\alpha \rho_2 V_{22}^{R\dagger} V_{24}^{L\dagger} , \tag{F.4}$$

$$c_{\mu\mu}^{S_S} \approx \frac{1}{\sqrt{2}} \sin\beta Y_{S_2} V_{24}^{R\dagger} V_{22}^{L\dagger} , \tag{F.5}$$

where we have assumed $\rho_1, \rho_3 \ll \rho_2$ and $Y_{S_1}, Y_{S_3} \ll Y_{S_2}$, as motivated by the explanation of the muon $g-2$ anomaly and the stringent constraints from lepton flavor violating observables. Furthermore, we have introduced the mixing angles α, β, and γ. The CP-even scalar mass matrix $\mathcal{M}_R^2$ in Eq.(6.21) is diagonalized by the unitary matrix R, which, assuming small mixing angles, can be parametrized as

$$R = \begin{pmatrix} 1 & \sin\alpha & \sin\beta \\ -\sin\alpha & 1 & \sin\gamma \\ -\sin\beta & -\sin\gamma & 1 \end{pmatrix} , \tag{F.6}$$

where $\alpha, \beta, \gamma \ll 1$. Using now Eqs. (6.51)-(6.53) we finally obtain

$$c_{\mu\mu}^{S_H} \approx \frac{m_\mu}{v_H} + \frac{Y_{S_2} v_S \rho_2 v_\sigma}{2 M_F v_H} \left[1 - \left(\frac{\rho_2 v_\sigma}{2 M_F}\right)^2\right], \tag{F.7}$$

$$c_{\mu\mu}^{S_\sigma} \approx \frac{\rho_2 Y_{S_2} v_S}{2 M_F} \sin\alpha\,, \tag{F.8}$$

$$c_{\mu\mu}^{S_S} \approx -\frac{\rho_2 Y_{S_2} v_\sigma}{2 M_F} \left[1 - \left(\frac{\rho_2 v_\sigma}{2 M_F}\right)^2\right] \sin\beta\,. \tag{F.9}$$

Appendix G

Boundedness from below

In order to ensure the existence of a stable vacuum, the scalar potential of the theory must be BFB. There exist several approaches to analyze boundedness from below. Ideally, one would like to have a *BFB test* that provides necessary and sufficient conditions. This way, one could not only guarantee that all potentials that pass the test are BFB (sufficient condition), but also discard potentials that fail it (necessary condition). In this regard, a major step forward was given in [514] and more recently in [515]. The algorithm proposed in the second reference provides necessary and sufficient conditions for boundedness from below in a generic scalar potential using notions of spectral theory of tensors. However, applying this algorithm beyond a few simple cases turns out to be impractical due to the computational cost involved. For this reason, in phenomenological analyses, one usually resorts to less ambitious approaches which only provide sufficient conditions, but not necessary. These methods are overconstraining since one must reject potentials not passing the test, even though they might actually be BFB. Nevertheless, if the potential passes the test, one can fully trust that boundedness from below is guaranteed.

Here we will employ the *copositivity* criterion, which, combined with a recently developed mathematical algorithm, never applied to a high-energy physics scenario, will give us sufficient (but not necessary) conditions. To the best of our knowledge, the first paper relating copositivity with boundedness from below was [516]. One must first express the quartic part of the scalar potential, $\mathcal{V}_4$, as a quadratic form of the n real fields φ_a $(a = 1, 2, \ldots n)$ in the theory,

$$\mathcal{V}_4 = \Lambda_{ab}\, \varphi_a^2 \varphi_b^2 \,. \tag{G.1}$$

The scalar potential is BFB if and only if the matrix of quartic couplings Λ_{ab} is copositive. A real matrix A is said to be copositive if $x^T A\, x \geqslant 0$ for every non-negative vector $x \geqslant 0$, that is, $x^i \geqslant 0$. If the inequality is strict, the matrix is strictly copositive. Therefore, checking for the copositivity of the matrix of quartic couplings would, in principle, provide sufficient and necessary boundedness from below conditions. However, in complicated models, one cannot write $\mathcal{V}_4$ as a quadratic form without introducing mixed bilinears (scalar field combinations

involving two different fields). For this reason, this method only leads to sufficient conditions, as we now explain.

In order to write the quartic part of the scalar potential as a quadratic form we define

$$\varphi_i^\dagger \varphi_i = h_i^2 \,, \qquad \varphi_i^\dagger \varphi_j = |h_i|\,|h_j|\,\rho_{ij} e^{i\phi_{ij}} = h_{ij}^2\,\rho_{ij} e^{i\phi_{ij}} \,, \tag{G.2}$$

with $|\rho_{ij}| \in [0,1]$ by virtue of the Cauchy-Schwarz inequality. Thus, we can express the boundedness from below condition as

$$\mathcal{V}_4 = x^T\, V_4\, x \geqslant 0 \,, \tag{G.3}$$

with $x = \begin{pmatrix} h_1^2 & \dots & h_i^2 & \dots & h_{ij}^2 & \dots \end{pmatrix}$ and the matrix V_4 is given by a combination of the quartic couplings, as well as the ρ's and ϕ phases. The reason why this method provides only sufficient conditions is the presence of the mixed bilinears. Notice that the *direction* given by h_{ij}^2 is not independent of h_i^2 and h_j^2. Therefore, imposing $x^T\, V_4\, x \geqslant 0$ for every non-negative x vector is overconstraining since unphysical directions would be included in the test. Nonetheless, when the test is positive, the potential is BFB. In summary, a scalar potential is BFB if the associated V_4 matrix is copositive. However, when the matrix is not copositive nothing can be said about the potential.

One can find mathematical work showing that a symmetric matrix A of order n is (strictly) copositive if and only if every principal submatrix B of A has no eigenvector $w > 0$ with associated eigenvalue $\kappa < 0$ ($\leqslant 0$) [517]. However, these theorems have limited practical use for large matrices since the number of principal submatrices is $2^n - 1$. Luckily, we can make use of [518] instead. The authors of this work proposed an algorithm that leads to necessary and sufficient conditions for the copositivity of unit diagonal matrices (matrices with all diagonal elements equal to 1). Although the algorithm in [518] could only be applied for up to 7×7 matrices, more recent work by the same authors contains indications to extend it to higher orders [519].

After all these considerations, our procedure to check for copositivity is as follows:

1. We replace all the quartic couplings in V_4 by the numerical values in the scalar potential we want to test.

2. We transform each element of the matrix to the *worst case scenario*. This is achieved by treating the remaining ρ and ϕ parameters as independent variables and setting them to the configuration for which the term is minimal. [1]

3. We check if the matrix has null entries in the diagonal. If it does, we remove the corresponding rows and columns. The original matrix will be copositive if the remaining one is and the removed elements are non-negative.

[1] We emphasize that we do this for each element. This means that even if the same ρ parameter appears in two elements, it is treated as if each appearance is independent. This way we make sure that all the negative directions in the scalar potential are considered. However, we are again taking an overconstraining (and then very conservative) approach.

4. We need the matrix to have unit diagonal to be able to apply the algorithm in [518]. Therefore, we divide all its entries by the smallest element in the diagonal and we replace all the values greater than 1 by 1. The original matrix will be copositive if the new one is.

5. We finally check the copositivity of the resulting matrix with the algorithm in [518].

A final remark about our method is in order. The stability in charge-breaking directions is ignored in many analyses. However, since we are being overly restrictive treating all the ρ moduli and ϕ phases as independent variables in the different entries of V_4, charge-breaking directions are included as well in our BFB test. This can be easily shown for a model with scalar doublets. Let us parametrize them as

$$\phi_i = \sqrt{r_i} e^{i\gamma_i} \begin{pmatrix} \sin(\alpha_i) \\ \cos(\alpha_i)\, e^{i\beta_i} \end{pmatrix} . \tag{G.4}$$

This parametrization and an example of how to use it to explore boundedness from below is shown in [520]. Let us consider a contraction of scalar doublets

$$\left(\phi_i^\dagger \phi_j\right) = \sqrt{r_i r_j} \left[\sin\alpha_i \sin\alpha_j + \cos\alpha_i \cos\alpha_j e^{-i(\beta_i - \beta_j)}\right] , \tag{G.5}$$

and take the modulus of the term in square brackets

$$\begin{aligned} &\left|\sin\alpha_i \sin\alpha_j + \cos\alpha_i \cos\alpha_j e^{i\beta}\right|^2 \\ &\quad = \sin^2\alpha_i \sin^2\alpha_j + \cos^2\alpha_i \cos^2\alpha_j + \sin\alpha_i \sin\alpha_j \cos\alpha_i \cos\alpha_j \left(e^{i\beta} + e^{-i\beta}\right) \\ &\quad = \sin^2\alpha_i \sin^2\alpha_j + \cos^2\alpha_i \cos^2\alpha_j + 2\sin\alpha_i \sin\alpha_j \cos\alpha_i \cos\alpha_j \cos\beta \leqslant 1. \end{aligned} \tag{G.6}$$

As expected, the product is, at most, as large as the modulus of the fields, $\sqrt{r_i}$. Therefore, if we treat the factors that multiply $\sqrt{r_i r_j}$ as independent variables (that is, being overly restrictive as explained in footnote 1), $\rho_{ij} e^{i\phi_{ij}}$, and make all combinations minimal, our method will cover boundedness from below in charge-breaking directions as well.

Appendix H

UV extensions of the Scotogenic model: Accidental $\mathbb{Z}_2$ symmetries

This appendix expands the discussion in Chapter 8. The dark $\mathbb{Z}_2$ parity of the Scotogenic model can also be an accidental symmetry generated after the σ singlet (or singlets) acquires a VEV. In these scenarios, the symmetry breaking path is also $\mathrm{U}(1)_{\mathrm{L}} \to \mathbb{Z}_2$, but with ℓ_L, e_R and η as the only particles charged under the discrete symmetry. In this case, the Yukawa term $\bar{N}\tilde{\eta}^\dagger \ell_L$ and the Majorana mass $\overline{N}^c N$ are allowed by all symmetries, while $\bar{N}\tilde{H}^\dagger \ell_L$ is forbidden. Furthermore, given that η is the only $\mathbb{Z}_2$-odd scalar, it will always appear in pairs in the effective scalar potential. Therefore, although the $\mathbb{Z}_2$ Scotogenic parity does not emerge as a remnant symmetry after the breaking of $\mathrm{U}(1)_{\mathrm{L}}$, it appears *accidentally* as a consequence of it. In fact, one can see that the resulting symmetry is nothing but a non-supersymmetric version of the well-known R-parity $R_p = (-1)^{3B+L+2s}$ [521], which has its origin in a combination of the $\mathrm{U}(1)_{\mathrm{L}}$ and Lorentz symmetries. [1] These UV models are not included in the classification presented in Section 8.2 since they violate requirement (A). However, they also lead to the Scotogenic model at low energies.

Let us illustrate this possibility with a specific example. [2] Consider the particle content and charge assignment in Table H.1. The new Yukawa interactions in the model are given by

$$\mathcal{L}_{\mathrm{Y}} = y\, \overline{N}\, \widetilde{\eta}^\dagger\, \ell_L + M_N\, \overline{N}^c N + \mathrm{h.c.}\,, \tag{H.1}$$

[1] The relation between R-parity and the Scotogenic $\mathbb{Z}_2$ symmetry has been explored in [378].
[2] This model corresponds to the II′ $(1, \emptyset)$ model shown below in Table H.2.

Field	**Generations**	$SU(3)_c$	$SU(2)_L$	$U(1)_Y$	$U(1)_L$
ℓ_L	3	**1**	**2**	-1/2	1
e_R	3	**1**	**1**	-1	1
N	3	**1**	**1**	0	0
H	1	**1**	**2**	1/2	0
η	1	**1**	**2**	1/2	-1
σ	1	**1**	**1**	0	2
S	1	**1**	**1**	0	-1

Table H.1: Lepton and scalar particle content and representations under the gauge and global symmetries in an UV extension of the Scotogenic model with accidental $\mathbb{Z}_2$ symmetry.

while the scalar potential of the model is written as

$$\begin{aligned}\mathcal{V}_{\rm UV} &= m_H^2 H^\dagger H + m_S^2 S^* S + m_\sigma^2 \sigma^* \sigma + m_\eta^2 \eta^\dagger \eta + \frac{\lambda_1}{2}(H^\dagger H)^2 + \frac{\lambda_2}{2}(\eta^\dagger \eta)^2 \\ &+ \frac{\lambda_S}{2}(S^* S)^2 + \frac{\lambda_\sigma}{2}(\sigma^* \sigma)^2 + \lambda_3 (H^\dagger H)(\eta^\dagger \eta) + \lambda_3^S (H^\dagger H)(S^* S) \\ &+ \lambda_3^\sigma (H^\dagger H)(\sigma^* \sigma) + \lambda_3^{\eta S} (\eta^\dagger \eta)(S^* S) + \lambda_3^{\eta\sigma} (\eta^\dagger \eta)(\sigma^* \sigma) \\ &+ \lambda_3^{\sigma S} (\sigma^* \sigma)(S^* S) + \lambda_4 (H^\dagger \eta)(\eta^\dagger H) + \Big[\beta (\sigma H^\dagger \eta S) + \mu_1\, H^\dagger \eta S^* + \mu_2\, \sigma\, S^2 + \text{h.c.}\Big]\,.\end{aligned} \tag{H.2}$$

It is easy to check that other Lagrangian terms are forbidden by $U(1)_L$. This global symmetry gets spontaneously broken once the electroweak singlet σ acquires a non-zero VEV, leaving a remnant $\mathbb{Z}_2$ under which η, S, ℓ_L, and e_R are odd, while the rest of the fields are even. We can call this symmetry $\mathbb{Z}_2^{\rm rem}$. Since $q_N = 0$, N is even under $\mathbb{Z}_2^{\rm rem}$, and thus this symmetry cannot be identified with the Scotogenic dark parity. Nevertheless, the Lagrangian of the Scotogenic model is still obtained after decoupling the heavy scalar S. This is due to the fact that a new accidental $\mathbb{Z}_2$ parity appears. The only fields charged under this parity are η and N, while all the other fields in the effective theory are even, therefore, this accidental symmetry, that we can denote as $\mathbb{Z}_2^{\rm acc}$, is precisely the Scotogenic $\mathbb{Z}_2$. As already explained, it is a non-supersymmetric version of R-parity.

Let us now generalize the idea studied in this Appendix. We consider again the set of models in which $(H^\dagger \eta)^2$ is generated by the topologies shown in Table 8.1 with the addition of at most two different singlets $\sigma_{1,2}$. There are two possibilities to construct models in which the $\mathbb{Z}_2^{\rm acc}$ symmetry is obtained:

(i) **Models with $q_N \neq 0$.** In this case, we consider the models shown in Table 8.1 but impose that N is even under the remnant $\mathbb{Z}_2^{\rm rem}$ parity while ℓ_L, e_R, and η are odd. The Majorana masses of the N fermions are induced by the $\kappa\, \sigma_1 \overline{N}^c N$ Yukawa term.

(ii) **Models with $q_N = 0$**. This case is excluded from the classification in Section 8.2, which focuses on $q_N \neq 0$, and must be discussed independently. In these models, the Majorana mass term $M_N \overline{N}^c N$ is present in the UV theory.

We now proceed to discuss these two cases independently. Again, we find it convenient to consider topologies I – IV and V separately, since they have some qualitative differences.

H.1 Topologies I-IV

We first consider topologies I – IV. The case of $q_N \neq 0$ can be regarded as a revision of our discussion in Section 8.2, imposing now different conditions on the resulting models. In fact, the models studied in Section 8.2 could also lead to $\mathrm{U}(1)_\mathrm{L} \to \mathbb{Z}_2^{\mathrm{rem}}$, leaving the Scotogenic $\mathbb{Z}_2$ parity as an accidental symmetry. This will be the case when these conditions on q_N are satisfied:

- $q_N = 2\,z$, where z can be any integer number except zero.
- $q_N = \frac{\alpha}{\beta}$, with $\alpha, \beta \in \mathbb{Z}$ and α and β even and odd, respectively. Also, $\mathrm{GCD}(\alpha, \beta) = 1$ has to be satisfied.

Notice, however, that models with fixed charges, that is, the ones with only σ_1, always have the Scotogenic symmetry as the remnant symmetry and do not enter this discussion.

Considering now scenarios with $q_N = 0$, only 11 different models exist, and they are listed in Table H.2. Let us denote them as $\xi'(A, B)$, where $\xi = \{\mathrm{I}, \mathrm{II}, \mathrm{III}, \mathrm{IV}\}$ and the prime is used to distinguish these models from the ones studied in Section 8.2. Each of the 11 models needs to satisfy any of the following conditions on q_{σ_1} in order to generate the $\mathbb{Z}_2$ parity as an accidental symmetry:

- $q_{\sigma_1} = 2\,z$, where z can be any integer number, including zero. [3]
- $q_{\sigma_1} = \frac{\alpha}{\beta}$, with $\alpha, \beta \in \mathbb{Z}$ and α and β even and odd, respectively. Also, $\mathrm{GCD}(\alpha, \beta) = 1$ has to be satisfied.

We finally point out that in none of the above scenarios η gets an induced VEV.

H.2 Topology V

We move on to topology V. Again, for this topology, we can distinguish the same two types of models as for the previous topologies. First of all, we consider the case $q_N \neq 0$. The accidental symmetry arises for the models 29-40 in Table 8.3 when any of these conditions is satisfied:

- $q_N = 2\,z$, where z can be any integer number except zero.

[3] We note that if $q_{\sigma_1} = 0$, a second σ_2 singlet, with $q_{\sigma_2} \neq 0$, is required to break the $\mathrm{U}(1)_\mathrm{L}$ symmetry. In this case, σ_1 becomes a total singlet and is irrelevant for the model construction.

	Topology	$\boldsymbol{A}$	$\boldsymbol{B}$	$\boldsymbol{q_N}$	$\boldsymbol{q_\eta}$	$\boldsymbol{q_{\sigma_1}}$	$\boldsymbol{q_{\sigma_2}}$	$\boldsymbol{q_S}$	$\boldsymbol{(\mathrm{SU(2)_L, U(1)_Y})_S}$
1	I′	1	$\emptyset$	0	-1	2	-	-2	$(\mathbf{3},1)$
2	I′	$\emptyset$	1	0	-1	2	-	0	$(\mathbf{3},1)$
3	I′	1	2	0	-1	q_{σ_1}	$2-q_{\sigma_1}$	$-q_{\sigma_1}$	$(\mathbf{3},1)$
4-5	II′	1	$\emptyset$	0	-1	2	-	-1	$(\mathbf{3},0)$ or $(\mathbf{1},0)$
6-7	II′	1	2	0	-1	q_{σ_1}	$2-q_{\sigma_1}$	$1-q_{\sigma_1}$	$(\mathbf{3},0)$ or $(\mathbf{1},0)$
8	III′	1	$\emptyset$	0	-1	2	-	-2	$(\mathbf{2},1/2)$
9	III′	1	2	0	-1	q_{σ_1}	$2-q_{\sigma_1}$	-2	$(\mathbf{2},1/2)$
10	IV′	1	$\emptyset$	0	-1	2	-	1	$(\mathbf{2},1/2)$
11	IV′	1	2	0	-1	q_{σ_1}	$2-q_{\sigma_1}$	1	$(\mathbf{2},1/2)$

Table H.2: UV extended models leading to topologies I − IV and for which the term $\overline{N}^c N$ is allowed and the Scotogenic $\mathbb{Z}_2$ is an accidental symmetry. For each model we show the $\mathrm{U(1)_L}$ charges of N, η, σ_1, σ_2 and S, as well as the $(\mathrm{SU(2)_L, U(1)_Y})$ representation of S. Models that become any of the models in this list after renaming the fields or redefining their $\mathrm{U(1)_L}$ charges are not included.

- $q_N = \frac{\alpha}{\beta}$, with $\alpha, \beta \in \mathbb{Z}$ and α and β even and odd, respectively ($\beta \neq 1$). Also, $\mathrm{GCD}(\alpha, \beta) = 1$ has to be satisfied.

For models 41-50, we have different conditions, although in all of them, we need $q_N = \frac{\alpha}{\beta}$, with $\alpha, \beta \in \mathbb{Z}$ and α and β even and odd, respectively. Also, $\mathrm{GCD}(\alpha, \beta) = 1$ has to be satisfied and we will allow $\beta = 1$ in these models. In addition:

- In model V(2, 1, 0), we further require $q_N \neq \pm\frac{2}{3}$ if S is a singlet and $q_N \neq \frac{2}{3}$ if S is a triplet. In both cases, q_N can not be an integer (i.e., we need $\beta \neq 1$).

- In model V(2, 1*, 0), we further require $q_N \neq \frac{2}{3}, \frac{2}{5}, \frac{2}{7}$ if S is a singlet and $q_N \neq \frac{2}{3}, \frac{2}{5}$ if S is a triplet. In both cases, q_N can not be an integer (i.e., we need $\beta \neq 1$).

- In model V(2, 2, 0), we have two options depending on the nature of q_N. If $q_N \in \mathbb{Z}$, $\mathrm{GCD}(3q_N, 1 - q_N) = 1$ if $\frac{q_N - 1}{3}$ is not an integer and $\mathrm{GCD}(q_N, \frac{q_N - 1}{3}) = 1$ if $\frac{q_N - 1}{3}$ is an integer. If $q_N \notin \mathbb{Z}$, $\mathrm{GCD}(3\,\alpha, \alpha - \beta) = 1$ if $\frac{\alpha - \beta}{3}$ is not an integer and $\mathrm{GCD}(\alpha, \frac{\alpha - \beta}{3}) = 1$ if $\frac{\alpha - \beta}{3}$ is an integer.

- In model V(2, 1*, 2), we also have two options depending on the nature of q_N. If $q_N \in \mathbb{Z}$, $\mathrm{GCD}(3q_N, 1 - 2q_N) = 1$ if $\frac{1 - 2\,q_N}{3}$ is not an integer and $\mathrm{GCD}(q_N, \frac{1 - 2\,q_N}{3}) = 1$ if $\frac{1 - 2\,q_N}{3}$ is an integer. If $q_N \notin \mathbb{Z}$, $\mathrm{GCD}(3\,\alpha, 2\,\alpha - \beta) = 1$ if $\frac{2\,\alpha - \beta}{3}$ is not an integer and $\mathrm{GCD}(\alpha, \frac{2\,\alpha - \beta}{3}) = 1$ if $\frac{2\,\alpha - \beta}{3}$ is an integer.

	Topology	A	B	C	q_N	q_η	q_{σ_1}	q_{σ_2}	q_S	$(\mathbf{SU(2)_L}, \mathbf{U(1)_Y})_S$
12-13	V′	1	1	$\emptyset$	0	-1	$\frac{2}{3}$	-	$\frac{1}{3}$	$(\mathbf{3},0)$ or $(\mathbf{1},0)$
14-15	V′	$\emptyset$	1	2	0	-1	q_{σ_1}	$2-q_{\sigma_1}$	1	$(\mathbf{3},0)$ or $(\mathbf{1},0)$
16-17	V′	1	2	$\emptyset$	0	-1	q_{σ_1}	$2-2q_{\sigma_1}$	$1-q_{\sigma_1}$	$(\mathbf{3},0)$ or $(\mathbf{1},0)$
18-19	V′	1	1	2	0	-1	q_{σ_1}	$2-3q_{\sigma_1}$	$1-q_{\sigma_1}$	$(\mathbf{3},0)$ or $(\mathbf{1},0)$

Table H.3: UV extended models leading to topology V and for which the term $\overline{N}^c N$ is allowed and the Scotogenic $\mathbb{Z}_2$ is an accidental symmetry. For each model we show the $\mathrm{U(1)_L}$ charges of N, η, σ_1, σ_2 and S, as well as the $(\mathrm{SU(2)_L}, \mathrm{U(1)_Y})$ representation of S. Models that become any of the models in this list after renaming the fields or redefining their $\mathrm{U(1)_L}$ charges are not included.

- In model V$(2,1,2)$, we have again two options depending on the nature of q_N. There is no further requirement if $q_N \in \mathbb{Z}$, whereas if $q_N \notin \mathbb{Z}$, GCD$(3\,\alpha, \beta) = 1$ if $\frac{\beta}{3}$ is not an integer and GCD$(\alpha, \frac{\beta}{3}) = 1$ if $\frac{\beta}{3}$ is an integer.

Models with $q_N = 0$ based on the topology V are collected in Table H.3. Each of the 8 models needs to satisfy any of the following conditions on q_{σ_1} in order to generate the $\mathbb{Z}_2$ parity as an accidental symmetry:

- $q_{\sigma_1} = 2\,z$, where z can be any integer number, including zero.
- $q_{\sigma_1} = \frac{\alpha}{\beta}$, with $\alpha, \beta \in \mathbb{Z}$ and α and β even and odd, respectively. Also, GCD$(\alpha, \beta) = 1$ has to be satisfied.

Appendix I

W boson decays in the presence of two HNL

In this appendix, we collect the relevant details for the computation of the W boson decay into a HNL, followed by its semileptonic decays. This is the relevant process for the searches performed by LHCb [496] and that we discussed in Section 9.4 in the scenario with two heavy neutral leptons.

I.1 Same sign leptons: $W^+ \to \ell_\alpha^+ \ell_\beta^+ q' \bar{q}$

We start with the decay rate for the process $W^+ \to \ell_\alpha^+ \ell_\beta^+ q' \bar{q}$ mediated by two HNLs $N_{1,2}$ almost degenerate in mass, similar to that shown in Fig. 9.1, but without the initial quarks. The amplitude reads

$$\mathcal{M}^+ = \sum_{i=1,2} \frac{g^3}{2\sqrt{2}} U^*_{\alpha N_i} U^*_{\beta N_i} \frac{M_{N_i}}{M_W^2} \epsilon^*_\mu \frac{\overline{\ell_\alpha^c} \gamma^\mu \gamma^\nu P_L \ell_\beta \bar{q} \gamma_\nu P_L q'}{p_N^2 - M_{N_i}^2 + i \Gamma_{N_i} M_{N_i}} \,, \tag{I.1}$$

with $p_N = p_W - p_{\ell_\alpha}$. The channel with crossed ℓ_α and ℓ_β gives rise to the same amplitude, but it must be added incoherently to our process since the rate is dominated by on-shell N_i, and thus the momentum of the first lepton is fixed by the 2-body decay kinematics. Therefore, the two processes do not interfere and we can forget about the crossed channel for the moment. The only modification results in a factor of 2 in the rate.

Defining $U_{\alpha N_i} = |U_{\alpha N_i}|\, e^{i\phi_{\alpha i}}$, $\delta\phi^+ = (\phi_{\alpha 2} - \phi_{\alpha 1}) + (\phi_{\beta 2} - \phi_{\beta 1})$ and using the narrow width approximation, the squared matrix element becomes

$$\begin{aligned}
\overline{|\mathcal{M}^+|}^2 = &\left[\frac{g^3}{2\sqrt{2}M_W^2}\right]^2 \pi\left(p_{\ell_\beta}\cdot p_q\right)\left(2E_{\ell_\alpha}E_{q'} + p_{\ell_\alpha}\cdot p_{q'}\right)\times \\
&\Bigg\{ |U_{\alpha N_1}|^2\,|U_{\beta N_1}|^2\,\frac{M_{N_1}}{\Gamma_{N_1}}\delta\left(p_N^2 - M_{N_1}^2\right) + |U_{\alpha N_2}|^2\,|U_{\beta N_2}|^2\,\frac{M_{N_2}}{\Gamma_{N_2}}\delta\left(p_N^2 - M_{N_2}^2\right) \\
&+ 2\,|U_{\alpha N_1}|\,|U_{\alpha N_2}|\,|U_{\beta N_1}|\,|U_{\beta N_2}|\,M_{N_1}M_{N_2}\left[\delta\left(p_N^2 - M_{N_1}^2\right) + \delta\left(p_N^2 - M_{N_2}^2\right)\right] \\
&\left[\cos\delta\phi^+\,\frac{\Gamma_{N_1}M_{N_1} + \Gamma_{N_2}M_{N_2}}{\left(\Delta M_N^2\right)^2 + \left(\Gamma_{N_1}M_{N_1} + \Gamma_{N_2}M_{N_2}\right)^2} - \sin\delta\phi^+\,\frac{\Delta M_N^2}{\left(\Delta M_N^2\right)^2 + \left(\Gamma_{N_1}M_{N_1} + \Gamma_{N_2}M_{N_2}\right)^2}\right]\Bigg\}\,,
\end{aligned} \tag{I.2}$$

where $\Delta M_N^2 \equiv M_{N_2}^2 - M_{N_1}^2$. Notice that, for the interference term, we used the NWA as follows:

$$\begin{aligned}
&\frac{1}{\left(p_N^2 - M_{N_1}^2 + i\Gamma_{N_1}M_{N_1}\right)\left(p_N^2 - M_{N_2}^2 - i\Gamma_{N_2}M_{N_2}\right)} = \\
&\qquad\frac{\pi\left(\Gamma_{N_2}M_{N_2} + \Gamma_{N_1}M_{N_1}\right)}{\left(\Delta M_N^2\right)^2 + \left(\Gamma_{N_1}M_{N_1} + \Gamma_{N_2}M_{N_2}\right)^2}\left[\delta\left(p_N^2 - M_{N_1}^2\right) + \delta\left(p_N^2 - M_{N_2}^2\right)\right] \\
&\qquad+ \frac{i\pi\Delta M_N^2}{\left(\Delta M_N^2\right)^2 + \left(\Gamma_{N_1}M_{N_1} + \Gamma_{N_2}M_{N_2}\right)^2}\left[\delta\left(p_N^2 - M_{N_1}^2\right) + \delta\left(p_N^2 - M_{N_2}^2\right)\right],
\end{aligned} \tag{I.3}$$

which differs from the expression in Ref. [474], as discussed in Section 9.4. Assuming $M_{N_1} \simeq M_{N_2} \equiv M_N, \Gamma_{N_1} \simeq \Gamma_{N_2} \equiv \Gamma_N$ and $\Delta M_N \equiv M_{N_2} - M_{N_1} \neq 0$, and considering that $|U_{\alpha N_1}|\,|U_{\beta N_1}| = |U_{\alpha N_2}|\,|U_{\beta N_2}| \equiv |U_{\alpha N}|\,|U_{\beta N}|$, we get

$$\begin{aligned}
\overline{|\mathcal{M}^+|}^2 \simeq &\left[\frac{g^3}{2\sqrt{2}M_W^2}\right]^2 \pi\left(p_{\ell_\beta}\cdot p_q\right)\left(2E_\alpha E_{q'} + p_\alpha\cdot p_{q'}\right)\delta\left(p_N^2 - M_N^2\right)\frac{M_N}{\Gamma_N}\,|U_{\alpha N}|^2\,|U_{\beta N}|^2 \\
&\times 2\Bigg\{1 + 2\left[2\cos\delta\phi^+\,\frac{M_N^2\Gamma_N^2}{\left(\Delta M_N^2\right)^2 + 4\Gamma_N^2M_N^2} - \sin\delta\phi^+\,\frac{M_N\Gamma_N\Delta M_N^2}{\left(\Delta M_N^2\right)^2 + 4\Gamma_N^2M_N^2}\right]\Bigg\}.
\end{aligned} \tag{I.4}$$

We observe that the squared amplitude in the case of only one sterile neutrino factorizes out. Integrating over the phase space, and after factorizing the decay width in the single HNL framework, it is straightforward to obtain

$$\Gamma\left(W^+ \to \ell_\alpha^+\ell_\beta^+ q'\bar{q}\right) = 2\left(1 + \cos\delta\phi^+\,\frac{1}{1+y^2} - \sin\delta\phi^+\,\frac{y}{1+y^2}\right)\Gamma\left(W^+ \to \ell_\alpha^+\ell_\beta^+ q'\bar{q}\right)\Big|_{N_1}\,, \tag{I.5}$$

where we have defined

$$y \equiv \frac{\Delta M_N^2}{2M_N\Gamma_N} \simeq \frac{M_{N_2}^2 - M_{N_1}^2}{\left(M_{N_1} + M_{N_2}\right)\Gamma_N} = \frac{\Delta M_N}{\Gamma_N}\,. \tag{I.6}$$

Notice that we obtain the same result of Ref. [472]. This is because we are using the NWA, which corresponds to considering on-shell HNL, leading to the same result after integrating over t, the time evolution of the intermediate HNL, from 0 to ∞. In fact, the factor $1/\Gamma$ coming from the NWA is equivalent to the factor $\int_0^\infty \left| e^{-\Gamma t/2} \right|^2 = 1/\Gamma$, and the interference part of Eq. (I.4) coincides with the finding of Ref. [472].

I.2 Different sign leptons: $W^+ \to \ell_\alpha^+ \ell_\beta^- q' \bar{q}$

In this section of the appendix, the decay rate of the process $W^+ \to \ell_\alpha^+ \ell_\beta^- q' \bar{q}$ mediated by the two HNLs $N_{1,2}$, almost degenerate in mass, is computed. The amplitude of this process is given by

$$\mathcal{M}^- = \sum_{i=1,2} \frac{g^3}{2\sqrt{2} M_W^2} U_{\alpha N_i}^* U_{\beta N_i} \epsilon_\mu^* \frac{\bar{\ell}_\beta \gamma^\mu \not{p}_N \gamma^\nu P_L \ell_\alpha^+ \bar{q} \gamma_\nu P_L q'}{p_N^2 - M_{N_i}^2 + i \Gamma_{N_i} M_{N_i}} \,, \tag{I.7}$$

where, again, $p_N = p_W - p_{\ell_\alpha}$. With the help of *FeynCalc* [522], we obtain for the squared amplitude,

$$\begin{aligned} \left| \overline{\mathcal{M}^-} \right|^2 = & \left(\frac{g^3}{2\sqrt{2} M_W^2} \right)^2 \left\{ |U_{\alpha N_1}|^2 \, |U_{\beta N_1}|^2 \, \frac{K_{11}}{\left(p_N^2 - M_{N_1}^2 \right)^2 + \Gamma_{N_1}^2 \, M_{N_1}^2} \right. \\ & + |U_{\alpha N_2}|^2 \, |U_{\beta N_2}|^2 \, \frac{K_{22}}{\left(p_N^2 - M_{N_2}^2 \right)^2 + \Gamma_{N_2}^2 \, M_{N_2}^2} \\ & \left. + 2 \, \mathrm{Re} \left[U_{\alpha N_1}^* U_{\beta N_1} U_{\alpha N_2} U_{\beta N_2}^* \, \frac{K_{12}}{\left(p_N^2 - M_{N_1}^2 + i \, \Gamma_{N_1} \, M_{N_1} \right) \left(p_N^2 - M_{N_2}^2 - i \, \Gamma_{N_2} \, M_{N_2} \right)} \right] \right\} \,, \end{aligned} \tag{I.8}$$

with the K_{ij} factors defined as

$$\begin{aligned} K_{ij} = & - \frac{16}{M_W} \left(p_\beta \cdot p_{q'} \right) \left\{ M_W \, \left(p_{N_i} \cdot p_{N_j} \right) \left[\left(p_\alpha \cdot p_q \right) + 2 \, E_\alpha \, E_q \right] - 2 \, E_\alpha \left[\left(p_{N_i} \cdot p_W \right) \left(p_{N_j} \cdot p_q \right) \right. \right. \\ & \left. \left. + \left(p_{N_j} \cdot p_W \right) \left(p_{N_i} \cdot p_q \right) \right] - M_W \left[\left(p_{N_i} \cdot p_q \right) \left(p_{N_j} \cdot p_\alpha \right) + \left(p_{N_j} \cdot p_q \right) \left(p_{N_i} \cdot p_\alpha \right) \right] \right\} . \end{aligned} \tag{I.9}$$

Assuming as before that $M_{N_1} \approx M_{N_2} \equiv M_N$ and $\Gamma_{N_1} \approx \Gamma_{N_2} \equiv \Gamma_N$, then $K_{11} = K_{22} = K_{12} \equiv K$. Also, considering that $|U_{\alpha N_1}| \, |U_{\beta N_1}| = |U_{\alpha N_2}| \, |U_{\beta N_2}| \equiv |U_{\alpha N}| \, |U_{\beta N}|$, we can simplify the expression notably

$$\begin{aligned} \left| \overline{\mathcal{M}^-} \right|^2 = & \left(\frac{g^3}{2\sqrt{2} M_W^2} \right)^2 |U_{\alpha N}|^2 \, |U_{\beta N}|^2 \, 2 \left\{ \frac{K}{\left(p_N^2 - M_N^2 \right)^2 + \Gamma_N^2 \, M_N^2} \right. \\ & \left. + \mathrm{Re} \left[\frac{K \, e^{i \delta \phi^-}}{\left(p_N^2 - M_{N_1}^2 + i \, \Gamma_{N_1} \, M_{N_1} \right) \left(p_N^2 - M_{N_2}^2 - i \, \Gamma_{N_2} \, M_{N_2} \right)} \right] \right\} \,, \end{aligned} \tag{I.10}$$

with $\delta\phi^- = (\phi_{\alpha 2} - \phi_{\alpha 1}) - (\phi_{\beta 2} - \phi_{\beta 1})$. And using the narrow width approximation, we get

$$\left|\overline{\mathcal{M}^-}\right|^2 = 2\left(\frac{g^3}{2\sqrt{2}M_W^2}\right)^2 |U_{\alpha N}|^2 |U_{\beta N}|^2 \; K \, \frac{\pi}{\Gamma_N M_N} \delta\left(p_N^2 - M_N^2\right) \left\{1 + \mathrm{Re}\left[2\,\Gamma_N M_N \frac{2\,\Gamma_N M_N + i\,\Delta M_N^2}{\left(\Delta M_N^2\right)^2 + 4\,\Gamma_N^2 M_N^2} e^{i\,\delta\phi^-}\right]\right\} . \tag{I.11}$$

Finally, it is straightforward to obtain the total expression in terms of the decay width mediated by just one HNL,

$$\Gamma\left(W^+ \to \ell_\alpha^+ \ell_\beta^- q' \bar{q}\right) = 2\left(1 + \cos\delta\phi^- \frac{1}{1+y^2} - \sin\delta\phi^- \frac{y}{1+y^2}\right) \times \Gamma\left(W^+ \to \ell_\alpha^+ \ell_\beta^- q' \bar{q}\right)\Big|_{N_1} , \tag{I.12}$$

with y defined in Eq. (I.6).

Bibliography

[1] S. Weinberg, "A model of leptons," Phys. Rev. Lett. **19** (Nov, 1967) 1264–1266.

[2] S. L. Glashow, "Partial-symmetries of weak interactions," Nuclear Physics **22** no. 4, (1961) 579–588.

[3] A. Salam, "Weak and Electromagnetic Interactions," Conf. Proc. C **680519** (1968) 367–377.

[4] H. Weyl, "Gravitation und elektrizität," Sitzungsberichte der Königlich Preussischen Akademie der Wissenschaften zu Berlin **1918** no. 465, (1918) 465–480.

[5] S. Tomonaga, "On a Relativistically Invariant Formulation of the Quantum Theory of Wave Fields*," Progress of Theoretical Physics **1** no. 2, (08, 1946) 27–42.

[6] J. Schwinger, "On quantum-electrodynamics and the magnetic moment of the electron," Phys. Rev. **73** (Feb, 1948) 416–417.

[7] R. P. Feynman, "Space-time approach to nonrelativistic quantum mechanics," Rev. Mod. Phys. **20** (1948) 367–387.

[8] R. P. Feynman, "Mathematical formulation of the quantum theory of electromagnetic interaction," Phys. Rev. **80** (Nov, 1950) 440–457.

[9] C. N. Yang and R. L. Mills, "Conservation of isotopic spin and isotopic gauge invariance," Phys. Rev. **96** (Oct, 1954) 191–195.

[10] A. Salam, "Weak and electromagnetic interactions," in Elementary Particle Theory, N. Svartholm, ed., p. 367. Almquist and Wiksells, Stockholm, 1969.

[11] S. L. Glashow, J. Iliopoulos, and L. Maiani, "Weak interactions with lepton-hadron symmetry," Phys. Rev. D **2** (Oct, 1970) 1285–1292.

[12] D. J. Gross and F. Wilczek, "Ultraviolet Behavior of Nonabelian Gauge Theories," Phys. Rev. Lett. **30** (1973) 1343–1346.

[13] D. J. Gross and F. Wilczek, "Asymptotically free gauge theories. i," Phys. Rev. D **8** (Nov, 1973) 3633–3652.

[14] D. J. Gross and F. Wilczek, "Asymptotically free gauge theories. ii," Phys. Rev. D **9** (Feb, 1974) 980–993.

[15] M. Gell-Mann, "A Schematic Model of Baryons and Mesons," Phys. Lett. **8** (1964) 214–215.

[16] G. Zweig, An SU(3) model for strong interaction symmetry and its breaking. Version 2, pp. 22–101. 2, 1964.

[17] P. W. Higgs, "Broken symmetries and the masses of gauge bosons," Phys. Rev. Lett. **13** (Oct, 1964) 508–509.

[18] F. Englert and R. Brout, "Broken symmetry and the mass of gauge vector mesons," Phys. Rev. Lett. **13** (Aug, 1964) 321–323.

[19] G. S. Guralnik, C. R. Hagen, and T. W. B. Kibble, "Global conservation laws and massless particles," Phys. Rev. Lett. **13** (Nov, 1964) 585–587.

[20] **CMS** Collaboration, S. Chatrchyan et al., "Observation of a New Boson at a Mass of 125 GeV with the CMS Experiment at the LHC," Phys. Lett. B **716** (2012) 30–61, arXiv:1207.7235 [hep-ex].

[21] **ATLAS** Collaboration, G. Aad et al., "Observation of a new particle in the search for the Standard Model Higgs boson with the ATLAS detector at the LHC," Phys. Lett. B **716** (2012) 1–29, arXiv:1207.7214 [hep-ex].

[22] A. Pich, "Aspects of quantum chromodynamics," in ICTP Summer School in Particle Physics, pp. 53–102. 6, 1999. arXiv:hep-ph/0001118.

[23] M. H. Seymour, "Quantum chromodynamics," in 2004 European School of High-Energy Physics, pp. 49–94. 5, 2005. arXiv:hep-ph/0505192.

[24] H. Ruegg and M. Ruiz-Altaba, "The Stueckelberg field," Int. J. Mod. Phys. A **19** (2004) 3265–3348, arXiv:hep-th/0304245.

[25] G. Hooft, "Renormalizable lagrangians for massive yang-mills fields," Nuclear Physics B **35** no. 1, (1971) 167–188.

[26] J. Goldstone, "Field Theories with Superconductor Solutions," Nuovo Cim. **19** (1961) 154–164.

[27] J. Goldstone, A. Salam, and S. Weinberg, "Broken symmetries," Phys. Rev. **127** (Aug, 1962) 965–970.

[28] M. D. Schwartz, Quantum Field Theory and the Standard Model. Cambridge University Press, 3, 2014.

[29] M. Kobayashi and T. Maskawa, "CP-Violation in the Renormalizable Theory of Weak Interaction," Progress of Theoretical Physics **49** no. 2, (02, 1973) 652–657, https://academic.oup.com/ptp/article-pdf/49/2/652/5257692/49-2-652.pdf.

[30] N. Cabibbo, "Unitary symmetry and leptonic decays," Phys. Rev. Lett. **10** (Jun, 1963) 531–533.

[31] **Particle Data Group** Collaboration, P. A. Zyla et al., "Review of Particle Physics," PTEP **2020** no. 8, (2020) 083C01.

[32] **Particle Data Group** Collaboration, R. L. Workman et al., "Review of Particle Physics," PTEP **2022** (2022) 083C01.

[33] S. Profumo, L. Giani, and O. F. Piattella, "An Introduction to Particle Dark Matter," Universe **5** no. 10, (2019) 213, arXiv:1910.05610 [hep-ph].

[34] F. Zwicky, "Die Rotverschiebung von extragalaktischen Nebeln," Helv. Phys. Acta **6** (1933) 110–127.

[35] S. Smith, "The Mass of the Virgo Cluster," Astrophys. J. **83** (1936) 23–30.

[36] **DES** Collaboration, T. M. C. Abbott et al., "Dark Energy Survey year 1 results: Cosmological constraints from galaxy clustering and weak lensing," Phys. Rev. D **98** no. 4, (2018) 043526, arXiv:1708.01530 [astro-ph.CO].

[37] O. F. Piattella, Lecture Notes in Cosmology. UNITEXT for Physics. Springer, Cham, 2018. arXiv:1803.00070 [astro-ph.CO].

[38] M. Davis, G. Efstathiou, C. Frenk, and S. White, "The evolution of large-scale structure in a universe dominated by cold dark matter," The Astrophysical Journal **292** (06, 1985) .

[39] **Planck** Collaboration, N. Aghanim et al., "Planck 2018 results. VI. Cosmological parameters," Astron. Astrophys. **641** (2020) A6, arXiv:1807.06209 [astro-ph.CO]. [Erratum: Astron.Astrophys. 652, C4 (2021)].

[40] T. Aoyama, M. Hayakawa, T. Kinoshita, and M. Nio, "Tenth-Order QED Contribution to the Electron g-2 and an Improved Value of the Fine Structure Constant," Phys. Rev. Lett. **109** (2012) 111807, arXiv:1205.5368 [hep-ph].

[41] T. Aoyama, M. Hayakawa, T. Kinoshita, and M. Nio, "Complete Tenth-Order QED Contribution to the Muon g-2," Phys. Rev. Lett. **109** (2012) 111808, arXiv:1205.5370 [hep-ph].

[42] S. Laporta, "High-precision calculation of the 4-loop contribution to the electron g-2 in QED," Phys. Lett. B **772** (2017) 232–238, arXiv:1704.06996 [hep-ph].

[43] T. Aoyama, T. Kinoshita, and M. Nio, "Revised and Improved Value of the QED Tenth-Order Electron Anomalous Magnetic Moment," Phys. Rev. D **97** no. 3, (2018) 036001, arXiv:1712.06060 [hep-ph].

[44] **Muon g-2** Collaboration, G. Bennett et al., "Final Report of the Muon E821 Anomalous Magnetic Moment Measurement at BNL," Phys. Rev. D **73** (2006) 072003, arXiv:hep-ex/0602035.

[45] F. Jegerlehner and A. Nyffeler, "The Muon g-2," Phys. Rept. **477** (2009) 1–110, arXiv:0902.3360 [hep-ph].

[46] **RBC, UKQCD** Collaboration, T. Blum, P. Boyle, V. Gülpers, T. Izubuchi, L. Jin, C. Jung, A. Jüttner, C. Lehner, A. Portelli, and J. Tsang, "Calculation of the hadronic vacuum polarization contribution to the muon anomalous magnetic moment," Phys. Rev. Lett. **121** no. 2, (2018) 022003, arXiv:1801.07224 [hep-lat].

[47] **Muon $g-2$ Collaboration** Collaboration, B. Abi et al., "Measurement of the positive muon anomalous magnetic moment to 0.46 ppm," Phys. Rev. Lett. **126** (Apr, 2021) 141801.

[48] **Muon g-2** Collaboration, G. W. Bennett et al., "Final Report of the Muon E821 Anomalous Magnetic Moment Measurement at BNL," Phys. Rev. D **73** (2006) 072003, arXiv:hep-ex/0602035.

[49] T. Aoyama et al., "The anomalous magnetic moment of the muon in the Standard Model," Phys. Rept. **887** (2020) 1–166, arXiv:2006.04822 [hep-ph].

[50] L. Morel, Z. Yao, P. Cladé, and S. Guellati-Khélifa, "Determination of the fine-structure constant with an accuracy of 81 parts per trillion," Nature **588** no. 7836, (2020) 61–65.

[51] A. Gérardin, "The anomalous magnetic moment of the muon: status of Lattice QCD calculations," Eur. Phys. J. A **57** no. 4, (2021) 116, arXiv:2012.03931 [hep-lat].

[52] M. Lindner, M. Platscher, and F. S. Queiroz, "A Call for New Physics : The Muon Anomalous Magnetic Moment and Lepton Flavor Violation," Phys. Rept. **731** (2018) 1–82, arXiv:1610.06587 [hep-ph].

[53] S. Borsanyi et al., "Leading hadronic contribution to the muon magnetic moment from lattice QCD," Nature **593** no. 7857, (2021) 51–55, arXiv:2002.12347 [hep-lat].

[54] M. Cè et al., "Window observable for the hadronic vacuum polarization contribution to the muon g-2 from lattice QCD," Phys. Rev. D **106** no. 11, (2022) 114502, arXiv:2206.06582 [hep-lat].

[55] **Extended Twisted Mass** Collaboration, C. Alexandrou et al., "Lattice calculation of the short and intermediate time-distance hadronic vacuum polarization contributions to the muon magnetic moment using twisted-mass fermions," Phys. Rev. D **107** no. 7, (2023) 074506, arXiv:2206.15084 [hep-lat].

[56] M. Passera, W. J. Marciano, and A. Sirlin, "The Muon g-2 and the bounds on the Higgs boson mass," Phys. Rev. D **78** (2008) 013009, arXiv:0804.1142 [hep-ph].

[57] A. Crivellin, M. Hoferichter, C. A. Manzari, and M. Montull, "Hadronic Vacuum Polarization: $(g-2)_\mu$ versus Global Electroweak Fits," Phys. Rev. Lett. **125** no. 9, (2020) 091801, arXiv:2003.04886 [hep-ph].

[58] A. Keshavarzi, W. J. Marciano, M. Passera, and A. Sirlin, "Muon $g-2$ and $\Delta\alpha$ connection," Phys. Rev. D **102** no. 3, (2020) 033002, arXiv:2006.12666 [hep-ph].

[59] B. Malaescu and M. Schott, "Impact of correlations between a_μ and $\alpha_{\rm QED}$ on the EW fit," Eur. Phys. J. C **81** no. 1, (2021) 46, arXiv:2008.08107 [hep-ph].

[60] **Fermilab Lattice, HPQCD,, MILC** Collaboration, A. Bazavov et al., "Light-quark connected intermediate-window contributions to the muon g-2 hadronic vacuum polarization from lattice QCD," Phys. Rev. D **107** no. 11, (2023) 114514, arXiv:2301.08274 [hep-lat].

[61] T. Blum et al., "An update of Euclidean windows of the hadronic vacuum polarization," arXiv:2301.08696 [hep-lat].

[62] **Extended Twisted Mass** Collaboration, C. Alexandrou et al., "Lattice calculation of the short and intermediate time-distance hadronic vacuum polarization contributions to the muon magnetic moment using twisted-mass fermions," Phys. Rev. D **107** no. 7, (2023) 074506, arXiv:2206.15084 [hep-lat].

[63] C. Aubin, T. Blum, M. Golterman, and S. Peris, "Muon anomalous magnetic moment with staggered fermions: Is the lattice spacing small enough?," Phys. Rev. D **106** (Sep, 2022) 054503.

[64] **chiQCD** Collaboration, G. Wang, T. Draper, K.-F. Liu, and Y.-B. Yang, "Muon g-2 with overlap valence fermions," Phys. Rev. D **107** no. 3, (2023) 034513, arXiv:2204.01280 [hep-lat].

[65] C. Lehner and A. S. Meyer, "Consistency of hadronic vacuum polarization between lattice qcd and the r ratio," Phys. Rev. D **101** (Apr, 2020) 074515.

[66] G. Giudice, P. Paradisi, and M. Passera, "Testing new physics with the electron g-2," JHEP **11** (2012) 113, arXiv:1208.6583 [hep-ph].

[67] W. Abdallah, A. Awad, S. Khalil, and H. Okada, "Muon Anomalous Magnetic Moment and mu -> e gamma in B-L Model with Inverse Seesaw," Eur. Phys. J. C **72** (2012) 2108, arXiv:1105.1047 [hep-ph].

[68] S. Khalil and C. S. Un, "Muon Anomalous Magnetic Moment in SUSY B-L Model with Inverse Seesaw," Phys. Lett. B **763** (2016) 164–168, arXiv:1509.05391 [hep-ph].

[69] J. Cao, J. Lian, L. Meng, Y. Yue, and P. Zhu, "Anomalous muon magnetic moment in the inverse seesaw extended next-to-minimal supersymmetric standard model," Phys. Rev. D **101** no. 9, (2020) 095009, arXiv:1912.10225 [hep-ph].

[70] L. T. Hue, P. N. Thanh, and T. D. Tham, "Anomalous Magnetic Dipole Moment $(g-2)\mu$ in 3-3-1 Model with Inverse Seesaw Neutrinos," Commun. in Phys. **30** no. 3, (2020) 221–230.

[71] J. Cao, Y. He, J. Lian, D. Zhang, and P. Zhu, "Electron and muon anomalous magnetic moments in the inverse seesaw extended NMSSM," Phys. Rev. D **104** no. 5, (2021) 055009, arXiv:2102.11355 [hep-ph].

[72] T. Nomura, H. Okada, and P. Sanyal, "A radiatively induced inverse seesaw model with hidden U(1) gauge symmetry," Eur. Phys. J. C **82** no. 8, (2022) 697, arXiv:2103.09494 [hep-ph].

[73] T. Mondal and H. Okada, "Inverse seesaw and $(g-2)$ anomalies in $B-L$ extended two Higgs doublet model," Nucl. Phys. B **976** (2022) 115716, arXiv:2103.13149 [hep-ph].

[74] L. T. Hue, H. T. Hung, N. T. Tham, H. N. Long, and T. P. Nguyen, "Large $(g-2)_\mu$ and signals of decays $e_b \to e_a\gamma$ in a 3-3-1 model with inverse seesaw neutrinos," Phys. Rev. D **104** no. 3, (2021) 033007, arXiv:2104.01840 [hep-ph].

[75] A. E. C. Hernández, C. Espinoza, J. C. Gómez-Izquierdo, and M. Mondragón, "Fermion masses and mixings, dark matter, leptogenesis and $g-2$ muon anomaly in an extended 2HDM with inverse seesaw," Eur. Phys. J. Plus **137** no. 11, (2022) 1224, arXiv:2104.02730 [hep-ph].

[76] R. Dermisek and A. Raval, "Explanation of the Muon g-2 Anomaly with Vectorlike Leptons and its Implications for Higgs Decays," Phys. Rev. D **88** (2013) 013017, arXiv:1305.3522 [hep-ph].

[77] Z. Poh and S. Raby, "Vectorlike leptons: Muon g-2 anomaly, lepton flavor violation, Higgs boson decays, and lepton nonuniversality," Phys. Rev. D **96** no. 1, (2017) 015032, arXiv:1705.07007 [hep-ph].

[78] K. Kowalska and E. M. Sessolo, "Expectations for the muon g-2 in simplified models with dark matter," JHEP **09** (2017) 112, arXiv:1707.00753 [hep-ph].

[79] E. Megias, M. Quiros, and L. Salas, "$g_\mu - 2$ from Vector-Like Leptons in Warped Space," JHEP **05** (2017) 016, arXiv:1701.05072 [hep-ph].

[80] C.-W. Chiang, H. Okada, and E. Senaha, "Dark matter, muon $g-2$, electric dipole moments, and $Z \to \ell_i^+ \ell_j^-$ in a one-loop induced neutrino model," Phys. Rev. D **96** no. 1, (2017) 015002, arXiv:1703.09153 [hep-ph].

[81] L. Calibbi, R. Ziegler, and J. Zupan, "Minimal models for dark matter and the muon g−2 anomaly," JHEP **07** (2018) 046, arXiv:1804.00009 [hep-ph].

[82] P. Arnan, A. Crivellin, M. Fedele, and F. Mescia, "Generic Loop Effects of New Scalars and Fermions in $b \to s\ell^+\ell^-$, $(g-2)_\mu$ and a Vector-like 4^{th} Generation," JHEP **06** (2019) 118, arXiv:1904.05890 [hep-ph].

[83] J. Kawamura, S. Raby, and A. Trautner, "Complete vectorlike fourth family and new U(1)' for muon anomalies," Phys. Rev. D **100** no. 5, (2019) 055030, arXiv:1906.11297 [hep-ph].

[84] L. Calibbi, M. L. López-Ibáñez, A. Melis, and O. Vives, "Muon and electron $g-2$ and lepton masses in flavor models," JHEP **06** (2020) 087, arXiv:2003.06633 [hep-ph].

[85] M. Frank and I. Saha, "Muon anomalous magnetic moment in two-Higgs-doublet models with vectorlike leptons," Phys. Rev. D **102** no. 11, (2020) 115034, arXiv:2008.11909 [hep-ph].

[86] E. J. Chun and T. Mondal, "Explaining $g-2$ anomalies in two Higgs doublet model with vector-like leptons," JHEP **11** (2020) 077, arXiv:2009.08314 [hep-ph].

[87] N. Chakrabarty, "Doubly charged scalars and vector-like leptons confronting the muon g-2 anomaly and Higgs vacuum stability," Eur. Phys. J. Plus **136** no. 11, (2021) 1183, arXiv:2010.05215 [hep-ph].

[88] K.-F. Chen, C.-W. Chiang, and K. Yagyu, "An explanation for the muon and electron $g-2$ anomalies and dark matter," JHEP **09** (2020) 119, arXiv:2006.07929 [hep-ph].

[89] S. Jana, P. K. Vishnu, W. Rodejohann, and S. Saad, "Dark matter assisted lepton anomalous magnetic moments and neutrino masses," Phys. Rev. D **102** no. 7, (2020) 075003, arXiv:2008.02377 [hep-ph].

[90] R. Dermisek, K. Hermanek, N. McGinnis, and N. McGinnis, "Highly enhanced contributions of heavy Higgs bosons and new leptons to muon $g-2$ and other observables," Phys. Rev. Lett. **126** no. 19, (2021) 191801, arXiv:2011.11812 [hep-ph].

[91] P. Das, M. K. Das, and N. Khan, "A new feasible dark matter region in the singlet scalar scotogenic model," Nucl. Phys. B **964** (2021) 115307, arXiv:2001.04070 [hep-ph].

[92] M. J. Baker, P. Cox, and R. R. Volkas, "Radiative muon mass models and $(g-2)_\mu$," JHEP **05** (2021) 174, arXiv:2103.13401 [hep-ph].

[93] R. Dermisek, K. Hermanek, and N. McGinnis, "Muon g-2 in two-Higgs-doublet models with vectorlike leptons," Phys. Rev. D **104** no. 5, (2021) 055033, arXiv:2103.05645 [hep-ph].

[94] P. Das, M. K. Das, and N. Khan, "The FIMP-WIMP dark matter in the extended singlet scalar model," Nucl. Phys. B **975** (2022) 115677, arXiv:2104.03271 [hep-ph].

[95] C.-W. Chiang and K. Yagyu, "Radiative Seesaw Mechanism for Charged Leptons," Phys. Rev. D **103** no. 11, (2021) L111302, arXiv:2104.00890 [hep-ph].

[96] G. Arcadi, L. Calibbi, M. Fedele, and F. Mescia, "Muon $g-2$ and B-anomalies from Dark Matter," Phys. Rev. Lett. **127** no. 6, (2021) 061802, arXiv:2104.03228 [hep-ph].

[97] C. Arbeláez, R. Cepedello, R. M. Fonseca, and M. Hirsch, "$(g-2)$ anomalies and neutrino mass," Phys. Rev. D **102** no. 7, (2020) 075005, arXiv:2007.11007 [hep-ph].

[98] D. Buttazzo and P. Paradisi, "Probing the muon $g-2$ anomaly with the Higgs boson at a muon collider," Phys. Rev. D **104** no. 7, (2021) 075021, arXiv:2012.02769 [hep-ph].

[99] W. Yin and M. Yamaguchi, "Muon g-2 at a multi-TeV muon collider," Phys. Rev. D **106** no. 3, (2022) 033007, arXiv:2012.03928 [hep-ph].

[100] R. Capdevilla, D. Curtin, Y. Kahn, and G. Krnjaic, "A No-Lose Theorem for Discovering the New Physics of $(g-2)_\mu$ at Muon Colliders," arXiv:2101.10334 [hep-ph].

[101] **ACME** Collaboration, V. Andreev et al., "Improved limit on the electric dipole moment of the electron," Nature **562** no. 7727, (2018) 355–360.

[102] **Muon (g-2)** Collaboration, G. Bennett et al., "An Improved Limit on the Muon Electric Dipole Moment," Phys. Rev. D **80** (2009) 052008, arXiv:0811.1207 [hep-ex].

[103] A. Crivellin, M. Hoferichter, and P. Schmidt-Wellenburg, "Combined explanations of $(g-2)_{\mu,e}$ and implications for a large muon EDM," Phys. Rev. D **98** no. 11, (2018) 113002, arXiv:1807.11484 [hep-ph].

[104] **LHCb** Collaboration, R. Aaij et al., "Measurement of Form-Factor-Independent Observables in the Decay $B^0 \to K^{*0}\mu^+\mu^-$," Phys. Rev. Lett. **111** (2013) 191801, arXiv:1308.1707 [hep-ex].

[105] **LHCb** Collaboration, R. Aaij et al., "Test of lepton universality with $B^0 \to K^{*0}\ell^+\ell^-$ decays," JHEP **08** (2017) 055, arXiv:1705.05802 [hep-ex].

[106] **BELLE** Collaboration, S. Choudhury et al., "Test of lepton flavor universality and search for lepton flavor violation in $B \to K\ell\ell$ decays," JHEP **03** (2021) 105, arXiv:1908.01848 [hep-ex].

[107] **Belle** Collaboration, A. Abdesselam et al., "Test of Lepton-Flavor Universality in $B \to K^*\ell^+\ell^-$ Decays at Belle," Phys. Rev. Lett. **126** no. 16, (2021) 161801, arXiv:1904.02440 [hep-ex].

[108] **LHCb** Collaboration, R. Aaij et al., "Test of lepton universality in beauty-quark decays," Nature Phys. **18** no. 3, (2022) 277–282, arXiv:2103.11769 [hep-ex].

[109] M. Bordone, G. Isidori, and A. Pattori, "On the Standard Model predictions for R_K and R_{K^*}," Eur. Phys. J. C **76** no. 8, (2016) 440, arXiv:1605.07633 [hep-ph].

[110] **LHCb** Collaboration, R. Aaij et al., "Angular analysis and differential branching fraction of the decay $B_s^0 \to \phi\mu^+\mu^-$," JHEP **09** (2015) 179, arXiv:1506.08777 [hep-ex].

[111] **LHCb** Collaboration, R. Aaij et al., "Measurement of the $B_s^0 \to \mu^+\mu^-$ branching fraction and effective lifetime and search for $B^0 \to \mu^+\mu^-$ decays," Phys. Rev. Lett. **118** no. 19, (2017) 191801, arXiv:1703.05747 [hep-ex].

[112] **ATLAS** Collaboration, M. Aaboud et al., "Study of the rare decays of B_s^0 and B^0 mesons into muon pairs using data collected during 2015 and 2016 with the ATLAS detector," JHEP **04** (2019) 098, arXiv:1812.03017 [hep-ex].

[113] **LHCb** Collaboration, R. Aaij et al., "Analysis of Neutral B-Meson Decays into Two Muons," Phys. Rev. Lett. **128** no. 4, (2022) 041801, arXiv:2108.09284 [hep-ex].

[114] **CMS** Collaboration, A. Tumasyan et al., "Measurement of the $\mathrm{B_S^0}\to\mu^+\mu^-$ decay properties and search for the $\mathrm{B^0}\to\mu^+\mu^-$ decay in proton-proton collisions at $\sqrt{s} = 13$ TeV," Phys. Lett. B **842** (2023) 137955, arXiv:2212.10311 [hep-ex].

[115] **LHCb** Collaboration, "Measurement of lepton universality parameters in $B^+ \to K^+\ell^+\ell^-$ and $B^0 \to K^{*0}\ell^+\ell^-$ decays," arXiv:2212.09153 [hep-ex].

[116] M. Algueró, B. Capdevila, S. Descotes-Genon, J. Matias, and M. Novoa-Brunet, "$b \to s\ell^+\ell^-$ global fits after R_{K_S} and $R_{K^{*+}}$," Eur. Phys. J. C **82** no. 4, (2022) 326, arXiv:2104.08921 [hep-ph].

[117] A. V. Manohar, "Introduction to Effective Field Theories," arXiv:1804.05863 [hep-ph].

[118] **BaBar** Collaboration, J. P. Lees et al., "Evidence for an excess of $\bar{B} \to D^{(*)}\tau^-\bar{\nu}_\tau$ decays," Phys. Rev. Lett. **109** (2012) 101802, arXiv:1205.5442 [hep-ex].

[119] **BaBar** Collaboration, J. P. Lees et al., "Measurement of an Excess of $\bar{B} \to D^{(*)}\tau^-\bar{\nu}_\tau$ Decays and Implications for Charged Higgs Bosons," Phys. Rev. D **88** no. 7, (2013) 072012, arXiv:1303.0571 [hep-ex].

[120] **Belle** Collaboration, M. Huschle et al., "Measurement of the branching ratio of $\bar{B} \to D^{(*)}\tau^-\bar{\nu}_\tau$ relative to $\bar{B} \to D^{(*)}\ell^-\bar{\nu}_\ell$ decays with hadronic tagging at Belle," Phys. Rev. D **92** no. 7, (2015) 072014, arXiv:1507.03233 [hep-ex].

[121] **LHCb** Collaboration, R. Aaij et al., "Measurement of the ratio of branching fractions $\mathcal{B}(\bar{B}^0 \to D^{*+}\tau^-\bar{\nu}_\tau)/\mathcal{B}(\bar{B}^0 \to D^{*+}\mu^-\bar{\nu}_\mu)$," Phys. Rev. Lett. **115** no. 11, (2015) 111803, arXiv:1506.08614 [hep-ex]. [Erratum: Phys.Rev.Lett. 115, 159901 (2015)].

[122] G. Ciezarek, "First joint measurement of $R(D^*)$ and $R(D^0)$ at LHCb." Seminar presented at CERN, 2022.

[123] C. Cornella, J. Fuentes-Martin, and G. Isidori, "Revisiting the vector leptoquark explanation of the B-physics anomalies," JHEP **07** (2019) 168, arXiv:1903.11517 [hep-ph].

[124] L. Da Rold and F. Lamagna, "A vector leptoquark for the B-physics anomalies from a composite GUT," JHEP **12** (2019) 112, arXiv:1906.11666 [hep-ph].

[125] A. Angelescu, D. Bečirević, D. A. Faroughy, F. Jaffredo, and O. Sumensari, "Single leptoquark solutions to the B-physics anomalies," Phys. Rev. D **104** no. 5, (2021) 055017, arXiv:2103.12504 [hep-ph].

[126] M. Fernández Navarro and S. F. King, "B-anomalies in a twin Pati-Salam theory of flavour including the 2022 LHCb $R_{K^{(*)}}$ analysis," JHEP **02** (2023) 188, arXiv:2209.00276 [hep-ph].

[127] W. Pauli, "Dear radioactive ladies and gentlemen," Phys. Today **31N9** (1978) 27.

[128] C. L. Cowan, F. Reines, F. B. Harrison, H. W. Kruse, and A. D. McGuire, "Detection of the free neutrino: a confirmation," Science **124** no. 3212, (1956) 103–104.

[129] R. Davis, D. S. Harmer, and K. C. Hoffman, "Search for neutrinos from the sun," Phys. Rev. Lett. **20** (May, 1968) 1205–1209.

[130] B. Pontecorvo, "Mesonium and anti-mesonium," Sov. Phys. JETP **6** (1957) 429.

[131] B. Pontecorvo, "Inverse beta processes and nonconservation of lepton charge," Zh. Eksp. Teor. Fiz. **34** (1957) 247.

[132] **Super-Kamiokande Collaboration** Collaboration, Y. Fukuda et al., "Evidence for oscillation of atmospheric neutrinos," Phys. Rev. Lett. **81** (Aug, 1998) 1562–1567.

[133] **SNO Collaboration** Collaboration, Q. R. Ahmad et al., "Direct evidence for neutrino flavor transformation from neutral-current interactions in the sudbury neutrino observatory," Phys. Rev. Lett. **89** (Jun, 2002) 011301.

[134] **KamLAND Collaboration** Collaboration, K. Eguchi et al., "First results from kamland: Evidence for reactor antineutrino disappearance," Phys. Rev. Lett. **90** (Jan, 2003) 021802.

[135] P. Martínez-Miravé, K. Müürsepp, and M. Tortola, "Neutrino physics," PoS **CORFU2021** (2022) 321.

[136] G. Danby, J. M. Gaillard, K. A. Goulianos, L. M. Lederman, N. B. Mistry, M. Schwartz, and J. Steinberger, "Observation of High-Energy Neutrino Reactions and the Existence of Two Kinds of Neutrinos," Phys. Rev. Lett. **9** (1962) 36–44.

[137] Z. Maki, M. Nakagawa, and S. Sakata, "Remarks on the Unified Model of Elementary Particles," Progress of Theoretical Physics **28** no. 5, (11, 1962) 870–880.

[138] P. F. de Salas, D. V. Forero, S. Gariazzo, P. Martínez-Miravé, O. Mena, C. A. Ternes, M. Tórtola, and J. W. F. Valle, "2020 global reassessment of the neutrino oscillation picture," JHEP **02** (2021) 071, arXiv:2006.11237 [hep-ph].

[139] L. Calibbi and G. Signorelli, "Charged Lepton Flavour Violation: An Experimental and Theoretical Introduction," Riv. Nuovo Cim. **41** no. 2, (2018) 71–174, arXiv:1709.00294 [hep-ph].

[140] M. Ardu and G. Pezzullo, "Introduction to Charged Lepton Flavor Violation," Universe **8** no. 6, (2022) 299, arXiv:2204.08220 [hep-ph].

[141] **MEG** Collaboration, A. M. Baldini et al., "Search for the lepton flavour violating decay $\mu^+ \to e^+\gamma$ with the full dataset of the MEG experiment," Eur. Phys. J. C **76** no. 8, (2016) 434, arXiv:1605.05081 [hep-ex].

[142] **MEG II** Collaboration, A. Baldini et al., "The design of the MEG II experiment," Eur. Phys. J. C **78** no. 5, (2018) 380, arXiv:1801.04688 [physics.ins-det].

[143] A. Papa, "Towards a new generation of Charged Lepton Flavour Violation searches at the Paul Scherrer Institut: The MEG upgrade and the Mu3e experiment," EPJ Web Conf. **234** (2020) 01011.

[144] **SINDRUM** Collaboration, U. Bellgardt et al., "Search for the Decay mu+ —> e+ e+ e-," Nucl. Phys. B **299** (1988) 1–6.

[145] **Mu3e** Collaboration, N. Berger, "The Mu3e Experiment," Nucl. Phys. B Proc. Suppl. **248-250** (2014) 35–40.

[146] **COMET** Collaboration, Y. Kuno, "A search for muon-to-electron conversion at J-PARC: The COMET experiment," PTEP **2013** (2013) 022C01.

[147] **Mu2e** Collaboration, F. Abdi et al., "Mu2e Run I Sensitivity Projections for the Neutrinoless $\mu^- \to e^-$ Conversion Search in Aluminum," Universe **9** no. 1, (2023) 54, arXiv:2210.11380 [hep-ex].

[148] R. J. Barlow, "The PRISM/PRIME project," Nucl. Phys. B Proc. Suppl. **218** (2011) 44–49.

[149] T. Aushev et al., "Physics at Super B Factory," arXiv:1002.5012 [hep-ex].

[150] **Belle-II** Collaboration, D. Rodríguez Pérez, "Prospects for τ Lepton Physics at Belle II," in 17th Conference on Flavor Physics and CP Violation. 6, 2019. arXiv:1906.08950 [hep-ex].

[151] F. Fortuna, A. Ibarra, X. Marcano, M. Marín, and P. Roig, "Indirect upper limits on $\ell_i \to \ell_j \gamma\gamma$ from $\ell_i \to \ell_j \gamma$," Phys. Rev. D **107** no. 1, (2023) 015027, arXiv:2210.05703 [hep-ph].

[152] A. Vicente, "Higgs lepton flavor violating decays in Two Higgs Doublet Models," Front. in Phys. **7** (2019) 174, arXiv:1908.07759 [hep-ph].

[153] F. F. Deppisch, N. Desai, and J. W. F. Valle, "Is charged lepton flavor violation a high energy phenomenon?," Phys. Rev. D **89** no. 5, (2014) 051302, arXiv:1308.6789 [hep-ph].

[154] S. Bilenky, "Neutrinos: Majorana or Dirac?," arXiv:2008.02110 [hep-ph].

[155] G. 't Hooft, "Naturalness, chiral symmetry, and spontaneous chiral symmetry breaking," NATO Sci. Ser. B **59** (1980) 135–157.

[156] J. Schechter and J. W. F. Valle, "Neutrinoless Double beta Decay in SU(2) $\times$ U(1) Theories," Phys. Rev. D **25** (1982) 2951.

[157] S. Weinberg, "Baryon- and lepton-nonconserving processes," Phys. Rev. Lett. **43** (Nov, 1979) 1566–1570.

[158] P. Minkowski, "$\mu \to e\gamma$ at a Rate of One Out of 10^9 Muon Decays?," Phys. Lett. B **67** (1977) 421–428.

[159] T. Yanagida, "Horizontal gauge symmetry and masses of neutrinos," Conf. Proc. C **7902131** (1979) 95–99.

[160] M. Gell-Mann, P. Ramond, and R. Slansky, "Complex Spinors and Unified Theories," Conf. Proc. C **790927** (1979) 315–321, arXiv:1306.4669 [hep-th].

[161] R. N. Mohapatra and G. Senjanović, "Neutrino mass and spontaneous parity nonconservation," Phys. Rev. Lett. **44** (Apr, 1980) 912–915.

[162] J. Schechter and J. W. F. Valle, "Neutrino masses in su(2) × u(1) theories," Phys. Rev. D **22** (Nov, 1980) 2227–2235.

[163] J. Schechter and J. W. F. Valle, "Neutrino decay and spontaneous violation of lepton number," Phys. Rev. D **25** (Feb, 1982) 774–783.

[164] R. Foot, H. Lew, X. G. He, and G. C. Joshi, "Seesaw Neutrino Masses Induced by a Triplet of Leptons," Z. Phys. C **44** (1989) 441.

[165] A. Donini, P. Hernandez, J. Lopez-Pavon, and M. Maltoni, "Minimal models with light sterile neutrinos," JHEP **07** (2011) 105, arXiv:1106.0064 [hep-ph].

[166] M. Magg and C. Wetterich, "Neutrino mass problem and gauge hierarchy," Physics Letters B **94** no. 1, (1980) 61–64.

[167] S. Kanemura and K. Yagyu, "Radiative corrections to electroweak parameters in the Higgs triplet model and implication with the recent Higgs boson searches," Phys. Rev. D **85** (2012) 115009, arXiv:1201.6287 [hep-ph].

[168] **ATLAS** Collaboration, G. Aad et al., "Search for type-III seesaw heavy leptons in dilepton final states in pp collisions at $\sqrt{s} = 13$ TeV with the ATLAS detector," Eur. Phys. J. C **81** no. 3, (2021) 218, arXiv:2008.07949 [hep-ex].

[169] R. N. Mohapatra and J. W. F. Valle, "Neutrino Mass and Baryon Number Nonconservation in Superstring Models," Phys. Rev. **D34** (1986) 1642. [,235(1986)].

[170] M. C. Gonzalez-Garcia and J. W. F. Valle, "Fast Decaying Neutrinos and Observable Flavor Violation in a New Class of Majoron Models," Phys. Lett. B **216** (1989) 360–366.

[171] F. Deppisch and J. W. F. Valle, "Enhanced lepton flavor violation in the supersymmetric inverse seesaw model," Phys. Rev. D **72** (2005) 036001, arXiv:hep-ph/0406040.

[172] S. Centelles Chuliá, R. Srivastava, and A. Vicente, "The inverse seesaw family: Dirac and Majorana," JHEP **03** (2021) 248, arXiv:2011.06609 [hep-ph].

[173] A. Abada and M. Lucente, "Looking for the minimal inverse seesaw realisation," Nucl. Phys. B **885** (2014) 651–678, arXiv:1401.1507 [hep-ph].

[174] E. K. Akhmedov, M. Lindner, E. Schnapka, and J. W. F. Valle, "Left-right symmetry breaking in NJL approach," Phys. Lett. B **368** (1996) 270–280, arXiv:hep-ph/9507275.

[175] E. K. Akhmedov, M. Lindner, E. Schnapka, and J. W. F. Valle, "Dynamical left-right symmetry breaking," Phys. Rev. D **53** (1996) 2752–2780, arXiv:hep-ph/9509255.

[176] D. Fontes, J. C. Romao, and J. W. F. Valle, "Electroweak Breaking and Higgs Boson Profile in the Simplest Linear Seesaw Model," JHEP **10** (2019) 245, arXiv:1908.09587 [hep-ph].

[177] A. Abada, C. Biggio, F. Bonnet, M. B. Gavela, and T. Hambye, "Low energy effects of neutrino masses," JHEP **12** (2007) 061, arXiv:0707.4058 [hep-ph].

[178] M. B. Gavela, T. Hambye, D. Hernandez, and P. Hernandez, "Minimal Flavour Seesaw Models," JHEP **09** (2009) 038, arXiv:0906.1461 [hep-ph].

[179] D. Ibanez, S. Morisi, and J. W. F. Valle, "Inverse tri-bimaximal type-III seesaw and lepton flavor violation," Phys. Rev. **D80** (2009) 053015, arXiv:0907.3109 [hep-ph].

[180] E. Ma, "Inverse Seesaw Neutrino Mass from Lepton Triplets in the $U(1)_\Sigma$ Model," Mod. Phys. Lett. **A24** (2009) 2491–2495, arXiv:0905.2972 [hep-ph].

[181] O. J. P. Eboli, J. Gonzalez-Fraile, and M. C. Gonzalez-Garcia, "Neutrino Masses at LHC: Minimal Lepton Flavour Violation in Type-III See-saw," JHEP **12** (2011) 009, arXiv:1108.0661 [hep-ph].

[182] S. Morisi, E. Peinado, and A. Vicente, "Flavor origin of R-parity," J. Phys. **G40** (2013) 085004, arXiv:1212.4145 [hep-ph].

[183] J. A. Aguilar-Saavedra, P. M. Boavida, and F. R. Joaquim, "Flavored searches for type-III seesaw mechanism at the LHC," Phys. Rev. **D88** (2013) 113008, arXiv:1308.3226 [hep-ph].

[184] S. S. C. Law and K. L. McDonald, "Generalized inverse seesaw mechanisms," Phys. Rev. **D87** no. 11, (2013) 113003, arXiv:1303.4887 [hep-ph].

[185] A. Abada, C. Biggio, F. Bonnet, M. B. Gavela, and T. Hambye, "$\mu \to e\gamma$ and $\tau \to l\gamma$ decays in the fermion triplet seesaw model," Phys. Rev. **D78** (2008) 033007, arXiv:0803.0481 [hep-ph].

[186] R. Franceschini, T. Hambye, and A. Strumia, "Type-III see-saw at LHC," Phys. Rev. **D78** (2008) 033002, arXiv:0805.1613 [hep-ph].

[187] A. Das and S. Mandal, "Bounds on the triplet fermions in type-III seesaw and implications for collider searches," Nucl. Phys. B **966** (2021) 115374, arXiv:2006.04123 [hep-ph].

[188] S. Ashanujjaman and K. Ghosh, "Type-III see-saw: Phenomenological implications of the information lost in decoupling from high-energy to low-energy," Phys. Lett. B **819** (2021) 136403, arXiv:2102.09536 [hep-ph].

[189] S. Mandal, J. C. Romão, R. Srivastava, and J. W. F. Valle, "Dynamical inverse seesaw mechanism as a simple benchmark for electroweak breaking and Higgs boson studies," JHEP **07** (2021) 029, arXiv:2103.02670 [hep-ph].

[190] C. Biggio, E. Fernandez-Martinez, M. Filaci, J. Hernandez-Garcia, and J. Lopez-Pavon, "Global Bounds on the Type-III Seesaw," JHEP **05** (2020) 022, arXiv:1911.11790 [hep-ph].

[191] W. Grimus and L. Lavoura, "The Seesaw mechanism at arbitrary order: Disentangling the small scale from the large scale," JHEP **11** (2000) 042, arXiv:hep-ph/0008179.

[192] A. Zee, "A Theory of Lepton Number Violation, Neutrino Majorana Mass, and Oscillation," Phys. Lett. **93B** (1980) 389. [Erratum: Phys. Lett.95B,461(1980)].

[193] T. P. Cheng and L.-F. Li, "Neutrino Masses, Mixings and Oscillations in SU(2) $\times$ U(1) Models of Electroweak Interactions," Phys. Rev. **D22** (1980) 2860.

[194] A. Zee, "Quantum Numbers of Majorana Neutrino Masses," Nucl. Phys. **B264** (1986) 99–110.

[195] K. S. Babu, "Model of 'Calculable' Majorana Neutrino Masses," Phys. Lett. **B203** (1988) 132–136.

[196] Y. Cai, J. Herrero-García, M. A. Schmidt, A. Vicente, and R. R. Volkas, "From the trees to the forest: a review of radiative neutrino mass models," Front. in Phys. **5** (2017) 63, arXiv:1706.08524 [hep-ph].

[197] D. Restrepo, O. Zapata, and C. E. Yaguna, "Models with radiative neutrino masses and viable dark matter candidates," JHEP **11** (2013) 011, arXiv:1308.3655 [hep-ph].

[198] Z.-j. Tao, "Radiative seesaw mechanism at weak scale," Phys. Rev. D **54** (1996) 5693–5697, arXiv:hep-ph/9603309.

[199] E. Ma, "Verifiable radiative seesaw mechanism of neutrino mass and dark matter," Phys. Rev. **D73** (2006) 077301, arXiv:hep-ph/0601225 [hep-ph].

[200] J. Casas and A. Ibarra, "Oscillating neutrinos and $\mu \to e, \gamma$," Nucl. Phys. B **618** (2001) 171–204, arXiv:hep-ph/0103065.

[201] T. Toma and A. Vicente, "Lepton Flavor Violation in the Scotogenic Model," JHEP **01** (2014) 160, arXiv:1312.2840 [hep-ph].

[202] A. Vicente and C. E. Yaguna, "Probing the scotogenic model with lepton flavor violating processes," JHEP **02** (2015) 144, arXiv:1412.2545 [hep-ph].

[203] I. Cordero-Carrión, M. Hirsch, and A. Vicente, "Master Majorana neutrino mass parametrization," Phys. Rev. D **99** no. 7, (2019) 075019, arXiv:1812.03896 [hep-ph].

[204] I. Cordero-Carrión, M. Hirsch, and A. Vicente, "General parametrization of Majorana neutrino mass models," Phys. Rev. D **101** no. 7, (2020) 075032, arXiv:1912.08858 [hep-ph].

[205] Y. Chikashige, R. N. Mohapatra, and R. D. Peccei, "Spontaneously Broken Lepton Number and Cosmological Constraints on the Neutrino Mass Spectrum," Phys. Rev. Lett. **45** (1980) 1926.

[206] Y. Chikashige, R. N. Mohapatra, and R. Peccei, "Are There Real Goldstone Bosons Associated with Broken Lepton Number?," Phys. Lett. B **98** (1981) 265–268.

[207] J. Schechter and J. Valle, "Neutrino Decay and Spontaneous Violation of Lepton Number," Phys. Rev. D **25** (1982) 774.

[208] G. Gelmini and M. Roncadelli, "Left-Handed Neutrino Mass Scale and Spontaneously Broken Lepton Number," Phys. Lett. B **99** (1981) 411–415.

[209] C. Aulakh and R. N. Mohapatra, "Neutrino as the Supersymmetric Partner of the Majoron," Phys. Lett. B **119** (1982) 136–140.

[210] **Particle Data Group** Collaboration, P. A. Zyla et al., "Review of Particle Physics," PTEP **2020** no. 8, (2020) 083C01.

[211] P. Escribano and A. Vicente, "Ultralight scalars in leptonic observables," JHEP **03** (2021) 240, arXiv:2008.01099 [hep-ph].

[212] A. Pilaftsis, "Astrophysical and terrestrial constraints on singlet Majoron models," Phys. Rev. D **49** (1994) 2398–2404, arXiv:hep-ph/9308258.

[213] J. Heeck and H. H. Patel, "Majoron at two loops," Phys. Rev. D **100** no. 9, (2019) 095015, arXiv:1909.02029 [hep-ph].

[214] Y. Cheng, C.-W. Chiang, X.-G. He, and J. Sun, "Flavor-changing Majoron interactions with leptons," Phys. Rev. D **104** no. 1, (2021) 013001, arXiv:2012.15287 [hep-ph].

[215] J. Sun, Y. Cheng, and X.-G. He, "Structure Of Flavor Changing Goldstone Boson Interactions," JHEP **04** (2021) 141, arXiv:2101.06055 [hep-ph].

[216] R. Peccei and H. R. Quinn, "CP Conservation in the Presence of Instantons," Phys. Rev. Lett. **38** (1977) 1440–1443.

[217] S. Weinberg, "A New Light Boson?," Phys. Rev. Lett. **40** (1978) 223–226.

[218] F. Wilczek, "Problem of Strong P and T Invariance in the Presence of Instantons," Phys. Rev. Lett. **40** (1978) 279–282.

[219] L. Di Luzio, M. Giannotti, E. Nardi, and L. Visinelli, "The landscape of QCD axion models," Phys. Rept. **870** (2020) 1–117, arXiv:2003.01100 [hep-ph].

[220] J. Preskill, M. B. Wise, and F. Wilczek, "Cosmology of the Invisible Axion," Phys. Lett. B **120** (1983) 127–132.

[221] L. Abbott and P. Sikivie, "A Cosmological Bound on the Invisible Axion," Phys. Lett. B **120** (1983) 133–136.

[222] M. Dine and W. Fischler, "The Not So Harmless Axion," Phys. Lett. B **120** (1983) 137–141.

[223] W. Hu, R. Barkana, and A. Gruzinov, "Cold and fuzzy dark matter," Phys. Rev. Lett. **85** (2000) 1158–1161, arXiv:astro-ph/0003365.

[224] F. Björkeroth, E. J. Chun, and S. F. King, "Flavourful Axion Phenomenology," JHEP **08** (2018) 117, arXiv:1806.00660 [hep-ph].

[225] F. Björkeroth, L. Di Luzio, F. Mescia, and E. Nardi, "$U(1)$ flavour symmetries as Peccei-Quinn symmetries," JHEP **02** (2019) 133, arXiv:1811.09637 [hep-ph].

[226] M. Gavela, R. Houtz, P. Quilez, R. Del Rey, and O. Sumensari, "Flavor constraints on electroweak ALP couplings," Eur. Phys. J. C **79** no. 5, (2019) 369, arXiv:1901.02031 [hep-ph].

[227] M. Bauer, M. Neubert, S. Renner, M. Schnubel, and A. Thamm, "Axion-like particles, lepton-flavor violation and a new explanation of a_μ and a_e," Phys. Rev. Lett. **124** no. 21, (2020) 211803, arXiv:1908.00008 [hep-ph].

[228] Q. Bonnefoy, E. Dudas, and S. Pokorski, "Chiral Froggatt-Nielsen models, gauge anomalies and flavourful axions," JHEP **01** (2020) 191, arXiv:1909.05336 [hep-ph].

[229] C. Cornella, P. Paradisi, and O. Sumensari, "Hunting for ALPs with Lepton Flavor Violation," JHEP **01** (2020) 158, arXiv:1911.06279 [hep-ph].

[230] J. Albrecht, E. Stamou, R. Ziegler, and R. Zwicky, "Flavoured axions in the tail of $B_q \to \mu^+\mu^-$ and $B_q \to \gamma^*$ form factors," JHEP **21** (2020) 139, arXiv:1911.05018 [hep-ph].

[231] J. Martin Camalich, M. Pospelov, P. N. H. Vuong, R. Ziegler, and J. Zupan, "Quark Flavor Phenomenology of the QCD Axion," Phys. Rev. D **102** no. 1, (2020) 015023, arXiv:2002.04623 [hep-ph].

[232] M. Endo, S. Iguro, and T. Kitahara, "Probing $e\mu$ flavor-violating ALP at Belle II," JHEP **06** (2020) 040, arXiv:2002.05948 [hep-ph].

[233] S. Iguro, Y. Omura, and M. Takeuchi, "Probing $\mu\tau$ flavor-violating solutions for the muon $g-2$ anomaly at Belle II," JHEP **09** (2020) 144, arXiv:2002.12728 [hep-ph].

[234] L. Calibbi, D. Redigolo, R. Ziegler, and J. Zupan, "Looking forward to lepton-flavor-violating ALPs," JHEP **09** (2021) 173, arXiv:2006.04795 [hep-ph].

[235] W. Porod, F. Staub, and A. Vicente, "A Flavor Kit for BSM models," Eur. Phys. J. C **74** no. 8, (2014) 2992, arXiv:1405.1434 [hep-ph].

[236] G. Raffelt and A. Weiss, "Red giant bound on the axion - electron coupling revisited," Phys. Rev. D **51** (1995) 1495–1498, arXiv:hep-ph/9410205.

[237] R. Bollig, W. DeRocco, P. W. Graham, and H.-T. Janka, "Muons in Supernovae: Implications for the Axion-Muon Coupling," Phys. Rev. Lett. **125** no. 5, (2020) 051104, arXiv:2005.07141 [hep-ph]. [Erratum: Phys.Rev.Lett. 126, 189901 (2021)].

[238] D. Croon, G. Elor, R. K. Leane, and S. D. McDermott, "Supernova Muons: New Constraints on Z' Bosons, Axions and ALPs," JHEP **01** (2021) 107, arXiv:2006.13942 [hep-ph].

[239] L. Di Luzio, M. Fedele, M. Giannotti, F. Mescia, and E. Nardi, "Solar axions cannot explain the XENON1T excess," Phys. Rev. Lett. **125** no. 13, (2020) 131804, arXiv:2006.12487 [hep-ph].

[240] I. M. Bloch, A. Caputo, R. Essig, D. Redigolo, M. Sholapurkar, and T. Volansky, "Exploring new physics with O(keV) electron recoils in direct detection experiments," JHEP **01** (2021) 178, arXiv:2006.14521 [hep-ph].

[241] W. DeRocco, P. W. Graham, and S. Rajendran, "Exploring the robustness of stellar cooling constraints on light particles," Phys. Rev. D **102** no. 7, (2020) 075015, arXiv:2006.15112 [hep-ph].

[242] E. Masso and J. Redondo, "Compatibility of CAST search with axion-like interpretation of PVLAS results," Phys. Rev. Lett. **97** (2006) 151802, arXiv:hep-ph/0606163.

[243] **XENON** Collaboration, E. Aprile et al., "Excess electronic recoil events in XENON1T," Phys. Rev. D **102** no. 7, (2020) 072004, arXiv:2006.09721 [hep-ex].

[244] A. Djouadi, "The Anatomy of electro-weak symmetry breaking. II. The Higgs bosons in the minimal supersymmetric model," Phys. Rept. **459** (2008) 1–241, arXiv:hep-ph/0503173.

[245] M. Bauer, M. Neubert, and A. Thamm, "Collider Probes of Axion-Like Particles," JHEP **12** (2017) 044, arXiv:1708.00443 [hep-ph].

[246] D. Carmi, A. Falkowski, E. Kuflik, T. Volansky, and J. Zupan, "Higgs After the Discovery: A Status Report," JHEP **10** (2012) 196, arXiv:1207.1718 [hep-ph].

[247] I. Antoniou, "Constraints on scalar coupling to electromagnetism," Grav. Cosmol. **23** (2017) 171, arXiv:1508.00985 [astro-ph.CO].

[248] C. Burrage, A.-C. Davis, and D. J. Shaw, "Active Galactic Nuclei Shed Light on Axion-like-Particles," Phys. Rev. Lett. **102** (2009) 201101, arXiv:0902.2320 [astro-ph.CO].

[249] R. Ballou et al., "Latest Results of the OSQAR Photon Regeneration Experiment for Axion-Like Particle Search," in 10th Patras Workshop on Axions, WIMPs and WISPs, pp. 125–130. 2014. arXiv:1410.2566 [hep-ex].

[250] M. Hirsch, A. Vicente, J. Meyer, and W. Porod, "Majoron emission in muon and tau decays revisited," Phys. Rev. D **79** (2009) 055023, arXiv:0902.0525 [hep-ph]. [Erratum: Phys.Rev.D 79, 079901 (2009)].

[251] A. Abada, M. E. Krauss, W. Porod, F. Staub, A. Vicente, and C. Weiland, "Lepton flavor violation in low-scale seesaw models: SUSY and non-SUSY contributions," JHEP **11** (2014) 048, arXiv:1408.0138 [hep-ph].

[252] S. M. Barr and A. Zee, "Electric Dipole Moment of the Electron and of the Neutron," Phys. Rev. Lett. **65** (1990) 21–24. [Erratum: Phys.Rev.Lett. 65, 2920 (1990)].

[253] H. H. Patel, "Package-X: A Mathematica package for the analytic calculation of one-loop integrals," Comput. Phys. Commun. **197** (2015) 276–290, arXiv:1503.01469 [hep-ph].

[254] F. J. Botella, F. Cornet-Gomez, and M. Nebot, "Electron and muon $g-2$ anomalies in general flavour conserving two Higgs doublets models," Phys. Rev. D **102** no. 3, (2020) 035023, arXiv:2006.01934 [hep-ph].

[255] C.-Y. Chen, H. Davoudiasl, W. J. Marciano, and C. Zhang, "Implications of a light "dark higgs" solution to the $g_\mu - 2$ discrepancy," Phys. Rev. D **93** (Feb, 2016) 035006.

[256] A. Jodidio et al., "Search for Right-Handed Currents in Muon Decay," Phys. Rev. D **34** (1986) 1967. [Erratum: Phys.Rev.D 37, 237 (1988)].

[257] **TWIST** Collaboration, R. Bayes et al., "Search for two body muon decay signals," Phys. Rev. D **91** no. 5, (2015) 052020, arXiv:1409.0638 [hep-ex].

[258] **Mu3e** Collaboration, A.-K. Perrevoort, "The Rare and Forbidden: Testing Physics Beyond the Standard Model with Mu3e," SciPost Phys. Proc. **1** (2019) 052, arXiv:1812.00741 [hep-ex].

[259] A.-K. Perrevoort, Sensitivity Studies on New Physics in the Mu3e Experiment and Development of Firmware for the Front-End of the Mu3e Pixel Detector. PhD thesis, Ruprecht-Karls-Universität Heidelberg, 2018.

[260] **ARGUS** Collaboration, H. Albrecht et al., "A Search for lepton flavor violating decays $\tau \to e\alpha$, $\tau \to \mu\alpha$," Z. Phys. C **68** (1995) 25–28.

[261] **Belle-II** Collaboration, I. Adachi et al., "Search for Lepton-Flavor-Violating τ Decays to a Lepton and an Invisible Boson at Belle II," Phys. Rev. Lett. **130** no. 18, (2023) 181803, arXiv:2212.03634 [hep-ex].

[262] E. De La Cruz-Burelo, M. Hernandez-Villanueva, and A. De Yta-Hernandez, "New method for beyond the Standard Model invisible particle searches in tau lepton decays," Phys. Rev. D **102** no. 11, (2020) 115001, arXiv:2007.08239 [hep-ph].

[263] **MEG** Collaboration, T. Mori, "Final Results of the MEG Experiment," Nuovo Cim. C **39** no. 4, (2017) 325, arXiv:1606.08168 [hep-ex].

[264] Y. Jho, S. Knapen, and D. Redigolo, "Lepton-flavor violating axions at MEG II," JHEP **10** (2022) 029, arXiv:2203.11222 [hep-ph].

[265] R. Bolton et al., "Search for the Decay $\mu^+ \to e^+\gamma$," Phys. Rev. Lett. **56** (1986) 2461–2464.

[266] J. Goldman et al., "Light Boson Emission in the Decay of the μ^+," Phys. Rev. D **36** (1987) 1543–1546.

[267] R. Bolton et al., "Search for Rare Muon Decays with the Crystal Box Detector," Phys. Rev. D **38** (1988) 2077.

[268] S. Davidson and B. Echenard, "Reach and complementarity of $\mu \to e$ searches," Eur. Phys. J. C **82** no. 9, (2022) 836, arXiv:2204.00564 [hep-ph].

[269] J. Heeck and W. Rodejohann, "Lepton Flavor Violation with Displaced Vertices," Phys. Lett. B **776** (2018) 385–390, arXiv:1710.02062 [hep-ph].

[270] A. de Gouvea and P. Vogel, "Lepton Flavor and Number Conservation, and Physics Beyond the Standard Model," Prog. Part. Nucl. Phys. **71** (2013) 75–92, arXiv:1303.4097 [hep-ph].

[271] **Particle Data Group** Collaboration, M. Tanabashi et al., "Review of Particle Physics," Phys. Rev. D **98** no. 3, (2018) 030001.

[272] S. Gori, G. Perez, and K. Tobioka, "KOTO vs. NA62 Dark Scalar Searches," JHEP **08** (2020) 110, arXiv:2005.05170 [hep-ph].

[273] G. Arcadi, J. Heeck, F. Heizmann, S. Mertens, F. S. Queiroz, W. Rodejohann, M. Slezák, and K. Valerius, "Tritium beta decay with additional emission of new light bosons," JHEP **01** (2019) 206, arXiv:1811.03530 [hep-ph].

[274] Y. Uesaka, "Model identification in $\mu^- \to e^-$ conversion with invisible boson emission using muonic atoms," Phys. Rev. D **102** no. 9, (2020) 095007, arXiv:2005.07894 [hep-ph].

[275] D. Aristizabal Sierra, M. Tortola, J. Valle, and A. Vicente, "Leptogenesis with a dynamical seesaw scale," JCAP **07** (2014) 052, arXiv:1405.4706 [hep-ph].

[276] M. G. Folgado and V. Sanz, "On the Interpretation of Nonresonant Phenomena at Colliders," Adv. High Energy Phys. **2021** (2021) 2573471, arXiv:2005.06492 [hep-ph].

[277] P. Escribano, J. Terol-Calvo, and A. Vicente, "$(g-2)_{e,\mu}$ in an extended inverse type-III seesaw model," Phys. Rev. D **103** no. 11, (2021) 115018, arXiv:2104.03705 [hep-ph].

[278] J. C. Romao and J. P. Silva, "A resource for signs and Feynman diagrams of the Standard Model," Int. J. Mod. Phys. A **27** (2012) 1230025, arXiv:1209.6213 [hep-ph].

[279] A. Crivellin and M. Hoferichter, "Consequences of chirally enhanced explanations of $(g-2)_\mu$ for $h \to \mu\mu$ and $Z \to \mu\mu$," JHEP **07** (2021) 135, arXiv:2104.03202 [hep-ph]. [Erratum: JHEP 10, 030 (2022)].

[280] **CMS** Collaboration, A. M. Sirunyan et al., "Evidence for Higgs boson decay to a pair of muons," JHEP **01** (2021) 148, arXiv:2009.04363 [hep-ex].

[281] S. Fajfer, J. F. Kamenik, and M. Tammaro, "Interplay of New Physics Effects in $(g-2)_\ell$ and $h \to \ell^+\ell^-$ – Lessons from SMEFT," JHEP **06** (2021) 099, arXiv:2103.10859 [hep-ph].

[282] **ATLAS** Collaboration, G. Aad et al., "Search for type-III seesaw heavy leptons in dilepton final states in pp collisions at $\sqrt{s} = 13$ TeV with the ATLAS detector," Eur. Phys. J. C **81** no. 3, (2021) 218, arXiv:2008.07949 [hep-ex].

[283] **CMS** Collaboration, S. Chatrchyan et al., "Search for Heavy Lepton Partners of Neutrinos in Proton-Proton Collisions in the Context of the Type III Seesaw Mechanism," Phys. Lett. B **718** (2012) 348–368, arXiv:1210.1797 [hep-ex].

[284] **CMS** Collaboration, A. M. Sirunyan et al., "Search for Evidence of the Type-III Seesaw Mechanism in Multilepton Final States in Proton-Proton Collisions at $\sqrt{s} = 13$ TeV," Phys. Rev. Lett. **119** no. 22, (2017) 221802, arXiv:1708.07962 [hep-ex].

[285] C. Biggio and F. Bonnet, "Implementation of the Type III Seesaw Model in FeynRules/MadGraph and Prospects for Discovery with Early LHC Data," Eur. Phys. J. C **72** (2012) 1899, arXiv:1107.3463 [hep-ph].

[286] A. Falkowski, D. M. Straub, and A. Vicente, "Vector-like leptons: Higgs decays and collider phenomenology," JHEP **05** (2014) 092, arXiv:1312.5329 [hep-ph].

[287] F. F. Freitas, J. a. Gonçalves, A. P. Morais, and R. Pasechnik, "Phenomenology of vector-like leptons with Deep Learning at the Large Hadron Collider," JHEP **01** (2021) 076, arXiv:2010.01307 [hep-ph].

[288] C. Biggio, "The Contribution of fermionic seesaws to the anomalous magnetic moment of leptons," Phys. Lett. B **668** (2008) 378–384, arXiv:0806.2558 [hep-ph].

[289] W. Chao, "The Muon Magnetic Moment in the TeV Scale Seesaw Models," arXiv:0806.0889 [hep-ph].

[290] C.-K. Chua and S. S. C. Law, "Phenomenological constraints on minimally coupled exotic lepton triplets," Phys. Rev. D **83** (2011) 055010, arXiv:1011.4730 [hep-ph].

[291] A. Freitas, J. Lykken, S. Kell, and S. Westhoff, "Testing the Muon g-2 Anomaly at the LHC," JHEP **05** (2014) 145, arXiv:1402.7065 [hep-ph]. [Erratum: JHEP 09, 155 (2014)].

[292] H. Päs and E. Schumacher, "Common origin of R_K and neutrino masses," Phys. Rev. D **92** no. 11, (2015) 114025, arXiv:1510.08757 [hep-ph].

[293] S. Saad and A. Thapa, "Common origin of neutrino masses and $R_{D^{(*)}}$, $R_{K^{(*)}}$ anomalies," Phys. Rev. D **102** no. 1, (2020) 015014, arXiv:2004.07880 [hep-ph].

[294] S.-P. Li, X.-Q. Li, X.-S. Yan, and Y.-D. Yang, "Scotogenic Dirac neutrino mass models embedded with leptoquarks: one pathway to address the flavor anomalies and the neutrino masses together," Eur. Phys. J. C **82** no. 11, (2022) 1078, arXiv:2204.09201 [hep-ph].

[295] O. Popov and G. A. White, "One Leptoquark to unify them? Neutrino masses and unification in the light of $(g-2)_\mu$, $R_{D^{(*)}}$ and R_K anomalies," Nucl. Phys. B **923** (2017) 324–338, arXiv:1611.04566 [hep-ph].

[296] I. Bigaran, J. Gargalionis, and R. R. Volkas, "A near-minimal leptoquark model for reconciling flavour anomalies and generating radiative neutrino masses," JHEP **10** (2019) 106, arXiv:1906.01870 [hep-ph].

[297] S. Saad, "Combined explanations of $(g-2)_\mu$, $R_{D^{(*)}}$, $R_{K^{(*)}}$ anomalies in a two-loop radiative neutrino mass model," Phys. Rev. D **102** no. 1, (2020) 015019, arXiv:2005.04352 [hep-ph].

[298] W.-F. Chang, "One colorful resolution to the neutrino mass generation, three lepton flavor universality anomalies, and the Cabibbo angle anomaly," JHEP **09** (2021) 043, arXiv:2105.06917 [hep-ph].

[299] T. Nomura and H. Okada, "Explanations for anomalies of muon anomalous magnetic dipole moment, $b \to s\mu\mu^-$, and radiative neutrino masses in a leptoquark model," Phys. Rev. D **104** no. 3, (2021) 035042, arXiv:2104.03248 [hep-ph].

[300] J. Julio, S. Saad, and A. Thapa, "Marriage between neutrino mass and flavor anomalies," Phys. Rev. D **106** no. 5, (2022) 055003, arXiv:2203.15499 [hep-ph].

[301] T. A. Chowdhury and S. Saad, "Leptoquark-vectorlike quark model for the CDF mW, (g-2)μ, RK(*) anomalies, and neutrino masses," Phys. Rev. D **106** no. 5, (2022) 055017, arXiv:2205.03917 [hep-ph].

[302] S.-L. Chen, W.-w. Jiang, and Z.-K. Liu, "Combined explanations of B-physics anomalies, $(g-2)_{e,\mu}$ and neutrino masses by scalar leptoquarks," Eur. Phys. J. C **82** no. 10, (2022) 959, arXiv:2205.15794 [hep-ph].

[303] F. F. Freitas, J. a. Gonçalves, A. P. Morais, R. Pasechnik, and W. Porod, "On interplay between flavour anomalies and neutrino properties," arXiv:2206.01674 [hep-ph].

[304] M. Ashry, K. Ezzat, and S. Khalil, "Muon g-2 anomaly in a left-right model with an inverse seesaw mechanism," Phys. Rev. D **107** no. 5, (2023) 055044, arXiv:2207.05828 [hep-ph].

[305] D. Huang, A. P. Morais, and R. Santos, "Anomalies in B-meson decays and the muon $g-2$ from dark loops," Phys. Rev. D **102** no. 7, (2020) 075009, arXiv:2007.05082 [hep-ph].

[306] M. Becker, D. Döring, S. Karmakar, and H. Päs, "Fermionic singlet dark matter in one-loop solutions to the R_K anomaly: a systematic study," Eur. Phys. J. C **81** no. 12, (2021) 1053, arXiv:2103.12043 [hep-ph].

[307] R. Capucha, D. Huang, T. Lopes, and R. Santos, "Impact of electroweak group representation in models for B and g-2 anomalies from dark loops," Phys. Rev. D **106** no. 9, (2022) 095032, arXiv:2207.11556 [hep-ph].

[308] A. Vicente, "Anomalies in $b \to s$ transitions and dark matter," Adv. High Energy Phys. **2018** (2018) 3905848, arXiv:1803.04703 [hep-ph].

[309] P. Escribano, M. Reig, and A. Vicente, "Generalizing the Scotogenic model," JHEP **07** (2020) 097, arXiv:2004.05172 [hep-ph].

[310] P. Arnan, L. Hofer, F. Mescia, and A. Crivellin, "Loop effects of heavy new scalars and fermions in $b \to s\mu^+\mu^-$," JHEP **04** (2017) 043, arXiv:1608.07832 [hep-ph].

[311] N. G. Deshpande and E. Ma, "Pattern of Symmetry Breaking with Two Higgs Doublets," Phys. Rev. D **18** (1978) 2574.

[312] R. Barbieri, L. J. Hall, and V. S. Rychkov, "Improved naturalness with a heavy Higgs: An Alternative road to LHC physics," Phys. Rev. D **74** (2006) 015007, arXiv:hep-ph/0603188.

[313] L. Lopez Honorez, E. Nezri, J. F. Oliver, and M. H. G. Tytgat, "The Inert Doublet Model: An Archetype for Dark Matter," JCAP **02** (2007) 028, arXiv:hep-ph/0612275.

[314] L. Lopez Honorez and C. E. Yaguna, "The inert doublet model of dark matter revisited," JHEP **09** (2010) 046, arXiv:1003.3125 [hep-ph].

[315] M. A. Díaz, B. Koch, and S. Urrutia-Quiroga, "Constraints to Dark Matter from Inert Higgs Doublet Model," Adv. High Energy Phys. **2016** (2016) 8278375, arXiv:1511.04429 [hep-ph].

[316] V. Keus, S. F. King, S. Moretti, and D. Sokolowska, "Dark Matter with Two Inert Doublets plus One Higgs Doublet," JHEP **11** (2014) 016, arXiv:1407.7859 [hep-ph].

[317] M. Misiak, A. Rehman, and M. Steinhauser, "Towards $\overline{B} \to X_s\gamma$ at the NNLO in QCD without interpolation in m_c," JHEP **06** (2020) 175, arXiv:2002.01548 [hep-ph].

[318] **Heavy Flavor Averaging Group, HFLAV** Collaboration, Y. S. Amhis et al., "Averages of b-hadron, c-hadron, and τ-lepton properties as of 2021," Phys. Rev. D **107** no. 5, (2023) 052008, arXiv:2206.07501 [hep-ex].

[319] **Belle** Collaboration, J. Grygier et al., "Search for $\boldsymbol{B \to h\nu\bar{\nu}}$ decays with semileptonic tagging at Belle," Phys. Rev. D **96** no. 9, (2017) 091101, arXiv:1702.03224 [hep-ex]. [Addendum: Phys.Rev.D 97, 099902 (2018)].

[320] **Particle Data Group** Collaboration, M. Tanabashi et al., "Review of Particle Physics," Phys. Rev. D **98** no. 3, (2018) 030001.

[321] P. Escribano, M. Hirsch, J. Nava, and A. Vicente, "Observable flavor violation from spontaneous lepton number breaking," JHEP **01** (2022) 098, arXiv:2108.01101 [hep-ph].

[322] **Muon g-2** Collaboration, B. Abi et al., "Measurement of the Positive Muon Anomalous Magnetic Moment to 0.46 ppm," Phys. Rev. Lett. **126** no. 14, (2021) 141801, arXiv:2104.03281 [hep-ex].

[323] L. Lavoura, "General formulae for $f_1 \to f_2\,\gamma$," Eur. Phys. J. C **29** (2003) 191–195, arXiv:hep-ph/0302221.

[324] **ATLAS** Collaboration, G. Aad et al., "A search for the dimuon decay of the Standard Model Higgs boson with the ATLAS detector," Phys. Lett. B **812** (2021) 135980, arXiv:2007.07830 [hep-ex].

[325] **CMS** Collaboration, A. M. Sirunyan et al., "Evidence for Higgs boson decay to a pair of muons," JHEP **01** (2021) 148, arXiv:2009.04363 [hep-ex].

[326] **CMS** Collaboration, A. M. Sirunyan et al., "Search for invisible decays of a Higgs boson produced through vector boson fusion in proton-proton collisions at $\sqrt{s} = 13$ TeV," Phys. Lett. B **793** (2019) 520–551, arXiv:1809.05937 [hep-ex].

[327] **LHC Higgs Cross Section Working Group** Collaboration, D. de Florian et al., "Handbook of LHC Higgs Cross Sections: 4. Deciphering the Nature of the Higgs Sector," arXiv:1610.07922 [hep-ph].

[328] P. Fileviez Perez and M. B. Wise, "On the Origin of Neutrino Masses," Phys. Rev. **D80** (2009) 053006, arXiv:0906.2950 [hep-ph].

[329] Y. Liao and J.-Y. Liu, "Radiative and flavor-violating transitions of leptons from interactions with color-octet particles," Phys. Rev. **D81** (2010) 013004, arXiv:0911.3711 [hep-ph].

[330] M. Reig, D. Restrepo, J. W. F. Valle, and O. Zapata, "Bound-state dark matter and Dirac neutrino masses," Phys. Rev. **D97** no. 11, (2018) 115032, arXiv:1803.08528 [hep-ph].

[331] M. Reig, D. Restrepo, J. W. F. Valle, and O. Zapata, "Bound-state dark matter with Majorana neutrinos," Phys. Lett. **B790** (2019) 303–307, arXiv:1806.09977 [hep-ph].

[332] Y. Farzan and E. Ma, "Dirac neutrino mass generation from dark matter," Phys. Rev. **D86** (2012) 033007, arXiv:1204.4890 [hep-ph].

[333] W. Wang, R. Wang, Z.-L. Han, and J.-Z. Han, "The $B - L$ Scotogenic Models for Dirac Neutrino Masses," Eur. Phys. J. **C77** no. 12, (2017) 889, arXiv:1705.00414 [hep-ph].

[334] Z.-L. Han and W. Wang, "Z' Portal Dark Matter in $B - L$ Scotogenic Dirac Model," Eur. Phys. J. **C78** no. 10, (2018) 839, arXiv:1805.02025 [hep-ph].

[335] J. Calle, D. Restrepo, C. E. Yaguna, and O. Zapata, "Minimal radiative Dirac neutrino mass models," Phys. Rev. **D99** no. 7, (2019) 075008, arXiv:1812.05523 [hep-ph].

[336] E. Ma, "Scotogenic $U(1)_\chi$ Dirac neutrinos," Phys. Lett. **B793** (2019) 411–414, arXiv:1901.09091 [hep-ph].

[337] E. Ma, "Scotogenic cobimaximal Dirac neutrino mixing from $\Delta(27)$ and $U(1)_\chi$," Eur. Phys. J. **C79** no. 11, (2019) 903, arXiv:1905.01535 [hep-ph].

[338] S. Centelles Chuliá, R. Cepedello, E. Peinado, and R. Srivastava, "Scotogenic dark symmetry as a residual subgroup of Standard Model symmetries," Chin. Phys. C **44** no. 8, (2020) 083110, arXiv:1901.06402 [hep-ph].

[339] S. Jana, P. Vishnu, and S. Saad, "Minimal dirac neutrino mass models from $U(1)_R$ gauge symmetry and left–right asymmetry at colliders," Eur. Phys. J. C **79** no. 11, (2019) 916, arXiv:1904.07407 [hep-ph].

[340] S. Jana, P. Vishnu, and S. Saad, "Minimal Realizations of Dirac Neutrino Mass from Generic One-loop and Two-loop Topologies at $d = 5$," JCAP **04** (2020) 018, arXiv:1910.09537 [hep-ph].

[341] E. Ma and D. Suematsu, "Fermion Triplet Dark Matter and Radiative Neutrino Mass," Mod. Phys. Lett. **A24** (2009) 583–589, arXiv:0809.0942 [hep-ph].

[342] E. Ma, "Dark Scalar Doublets and Neutrino Tribimaximal Mixing from A(4) Symmetry," Phys. Lett. **B671** (2009) 366–368, arXiv:0808.1729 [hep-ph].

[343] Y. Farzan, "A Minimal model linking two great mysteries: neutrino mass and dark matter," Phys. Rev. **D80** (2009) 073009, arXiv:0908.3729 [hep-ph].

[344] C.-H. Chen, C.-Q. Geng, and D. V. Zhuridov, "Neutrino Masses, Leptogenesis and Decaying Dark Matter," JCAP **0910** (2009) 001, arXiv:0906.1646 [hep-ph].

[345] A. Adulpravitchai, M. Lindner, A. Merle, and R. N. Mohapatra, "Radiative Transmission of Lepton Flavor Hierarchies," Phys. Lett. **B680** (2009) 476–479, arXiv:0908.0470 [hep-ph].

[346] Y. Farzan, S. Pascoli, and M. A. Schmidt, "AMEND: A model explaining neutrino masses and dark matter testable at the LHC and MEG," JHEP **10** (2010) 111, arXiv:1005.5323 [hep-ph].

[347] M. Aoki, S. Kanemura, and K. Yagyu, "Doubly-charged scalar bosons from the doublet," Phys. Lett. **B702** (2011) 355–358, arXiv:1105.2075 [hep-ph]. [Erratum: Phys. Lett.B706,495(2012)].

[348] Y. Cai, X.-G. He, M. Ramsey-Musolf, and L.-H. Tsai, "RνMDM and Lepton Flavor Violation," JHEP **12** (2011) 054, arXiv:1108.0969 [hep-ph].

[349] C.-H. Chen and S. S. C. Law, "Exotic fermion multiplets as a solution to baryon asymmetry, dark matter and neutrino masses," Phys. Rev. **D85** (2012) 055012, arXiv:1111.5462 [hep-ph].

[350] W. Chao, "Dark matter, LFV and neutrino magnetic moment in the radiative seesaw model with fermion triplet," Int. J. Mod. Phys. **A30** no. 01, (2015) 1550007, arXiv:1202.6394 [hep-ph].

[351] E. Ma, A. Natale, and A. Rashed, "Scotogenic A_4 Neutrino Model for Nonzero θ_{13} and Large δ_{CP}," Int. J. Mod. Phys. **A27** (2012) 1250134, arXiv:1206.1570 [hep-ph].

[352] M. Hirsch, R. A. Lineros, S. Morisi, J. Palacio, N. Rojas, and J. W. F. Valle, "WIMP dark matter as radiative neutrino mass messenger," JHEP **10** (2013) 149, arXiv:1307.8134 [hep-ph].

[353] S. Bhattacharya, E. Ma, A. Natale, and A. Rashed, "Radiative Scaling Neutrino Mass with A_4 Symmetry," Phys. Rev. **D87** (2013) 097301, arXiv:1302.6266 [hep-ph].

[354] E. Ma, "Neutrino Mixing and Geometric CP Violation with Delta(27) Symmetry," Phys. Lett. **B723** (2013) 161–163, arXiv:1304.1603 [hep-ph].

[355] E. Ma, "Unified Framework for Matter, Dark Matter, and Radiative Neutrino Mass," Phys. Rev. **D88** no. 11, (2013) 117702, arXiv:1307.7064 [hep-ph].

[356] V. Brdar, I. Picek, and B. Radovcic, "Radiative Neutrino Mass with Scotogenic Scalar Triplet," Phys. Lett. **B728** (2014) 198–201, arXiv:1310.3183 [hep-ph].

[357] S. S. C. Law and K. L. McDonald, "A Class of Inert N-tuplet Models with Radiative Neutrino Mass and Dark Matter," JHEP **09** (2013) 092, arXiv:1305.6467 [hep-ph].

[358] S. Patra, N. Sahoo, and N. Sahu, "Dipolar dark matter in light of the 3.5 keV x-ray line, neutrino mass, and LUX data," Phys. Rev. **D91** no. 11, (2015) 115013, arXiv:1412.4253 [hep-ph].

[359] E. Ma and A. Natale, "Scotogenic Z_2 or $U(1)_D$ Model of Neutrino Mass with $\Delta(27)$ Symmetry," Phys. Lett. **B734** (2014) 403–405, arXiv:1403.6772 [hep-ph].

[360] S. Fraser, E. Ma, and O. Popov, "Scotogenic Inverse Seesaw Model of Neutrino Mass," Phys. Lett. **B737** (2014) 280–282, arXiv:1408.4785 [hep-ph].

[361] H. Okada and Y. Orikasa, "Radiative neutrino model with an inert triplet scalar," Phys. Rev. **D94** no. 5, (2016) 055002, arXiv:1512.06687 [hep-ph].

[362] T. A. Chowdhury and S. Nasri, "Lepton Flavor Violation in the Inert Scalar Model with Higher Representations," JHEP **12** (2015) 040, arXiv:1506.00261 [hep-ph].

[363] M. A. Díaz, N. Rojas, S. Urrutia-Quiroga, and J. W. F. Valle, "Heavy Higgs Boson Production at Colliders in the Singlet-Triplet Scotogenic Dark Matter Model," JHEP **08** (2017) 017, arXiv:1612.06569 [hep-ph].

[364] P. M. Ferreira, W. Grimus, D. Jurciukonis, and L. Lavoura, "Scotogenic model for co-bimaximal mixing," JHEP **07** (2016) 010, arXiv:1604.07777 [hep-ph].

[365] A. Ahriche, K. L. McDonald, and S. Nasri, "The Scale-Invariant Scotogenic Model," JHEP **06** (2016) 182, arXiv:1604.05569 [hep-ph].

[366] F. von der Pahlen, G. Palacio, D. Restrepo, and O. Zapata, "Radiative Type III Seesaw Model and its collider phenomenology," Phys. Rev. **D94** no. 3, (2016) 033005, arXiv:1605.01129 [hep-ph].

[367] W.-B. Lu and P.-H. Gu, "Mixed Inert Scalar Triplet Dark Matter, Radiative Neutrino Masses and Leptogenesis," Nucl. Phys. **B924** (2017) 279–311, arXiv:1611.02106 [hep-ph].

[368] A. Merle, M. Platscher, N. Rojas, J. W. F. Valle, and A. Vicente, "Consistency of WIMP Dark Matter as radiative neutrino mass messenger," JHEP **07** (2016) 013, arXiv:1603.05685 [hep-ph].

[369] P. Rocha-Moran and A. Vicente, "Lepton Flavor Violation in the singlet-triplet scotogenic model," JHEP **07** (2016) 078, arXiv:1605.01915 [hep-ph].

[370] T. A. Chowdhury and S. Nasri, "The Sommerfeld Enhancement in the Scotogenic Model with Large Electroweak Scalar Multiplets," JCAP **1701** no. 01, (2017) 041, arXiv:1611.06590 [hep-ph].

[371] E. C. F. S. Fortes, A. C. B. Machado, J. Montaño, and V. Pleitez, "Lepton masses and mixing in a scotogenic model," Phys. Lett. **B803** (2020) 135289, arXiv:1705.09414 [hep-ph].

[372] Y.-L. Tang, "Some Phenomenologies of a Simple Scotogenic Inverse Seesaw Model," Phys. Rev. **D97** no. 3, (2018) 035020, arXiv:1709.07735 [hep-ph].

[373] C. Guo, S.-Y. Guo, and Y. Liao, "Dark matter and LHC phenomenology of a scale invariant scotogenic model," Chin. Phys. **C43** no. 10, (2019) 103102, arXiv:1811.01180 [hep-ph].

[374] N. Rojas, R. Srivastava, and J. W. F. Valle, "Simplest Scoto-Seesaw Mechanism," Phys. Lett. **B789** (2019) 132–136, arXiv:1807.11447 [hep-ph].

[375] A. Aranda, C. Bonilla, and E. Peinado, "Dynamical generation of neutrino mass scales," Phys. Lett. **B792** (2019) 40–42, arXiv:1808.07727 [hep-ph].

[376] Z.-L. Han and W. Wang, "Predictive Scotogenic Model with Flavor Dependent Symmetry," Eur. Phys. J. **C79** no. 6, (2019) 522, arXiv:1901.07798 [hep-ph].

[377] D. Suematsu, "Low scale leptogenesis in a hybrid model of the scotogenic type I and III seesaw models," Phys. Rev. **D100** no. 5, (2019) 055008, arXiv:1906.12008 [hep-ph].

[378] S. K. Kang, O. Popov, R. Srivastava, J. W. F. Valle, and C. A. Vaquera-Araujo, "Scotogenic dark matter stability from gauged matter parity," Phys. Lett. **B798** (2019) 135013, arXiv:1902.05966 [hep-ph].

[379] S. Pramanick, "Scotogenic S3 symmetric generation of realistic neutrino mixing," Phys. Rev. **D100** no. 3, (2019) 035009, arXiv:1904.07558 [hep-ph].

[380] T. Nomura, H. Okada, and O. Popov, "A modular A_4 symmetric scotogenic model," Phys. Lett. **B803** (2020) 135294, arXiv:1908.07457 [hep-ph].

[381] D. Restrepo and A. Rivera, "Phenomenological consistency of the singlet-triplet scotogenic model," JHEP **04** (2020) 134, arXiv:1907.11938 [hep-ph].

[382] S. Mandal, N. Rojas, R. Srivastava, and J. W. F. Valle, "Dark matter as the origin of neutrino mass in the inverse seesaw mechanism," Phys. Lett. B **821** (2021) 136609, arXiv:1907.07728 [hep-ph].

[383] I. M. Ávila, V. De Romeri, L. Duarte, and J. W. F. Valle, "Phenomenology of scotogenic scalar dark matter," Eur. Phys. J. C **80** no. 10, (2020) 908, arXiv:1910.08422 [hep-ph].

[384] N. Kumar, T. Nomura, and H. Okada, "Scotogenic neutrino mass with large $SU(2)_L$ multiplet fields," Eur. Phys. J. C **80** no. 8, (2020) 801, arXiv:1912.03990 [hep-ph].

[385] C. A. R, G. Cottin, J. C. Helo, and M. Hirsch, "Long-lived charged particles and multi-lepton signatures from neutrino mass models," Phys. Rev. D **101** no. 9, (2020) 095033, arXiv:2003.11494 [hep-ph].

[386] E. Ma, I. Picek, and B. Radovčić, "New Scotogenic Model of Neutrino Mass with $U(1)_D$ Gauge Interaction," Phys. Lett. **B726** (2013) 744–746, arXiv:1308.5313 [hep-ph].

[387] J.-H. Yu, "Hidden Gauged U(1) Model: Unifying Scotogenic Neutrino and Flavor Dark Matter," Phys. Rev. **D93** no. 11, (2016) 113007, arXiv:1601.02609 [hep-ph].

[388] J. Kubo and D. Suematsu, "Neutrino masses and CDM in a non-supersymmetric model," Phys. Lett. **B643** (2006) 336–341, arXiv:hep-ph/0610006 [hep-ph].

[389] D. Aristizabal Sierra, M. Dhen, C. S. Fong, and A. Vicente, "Dynamical flavor origin of $\mathbb{Z}_N$ symmetries," Phys. Rev. **D91** no. 9, (2015) 096004, arXiv:1412.5600 [hep-ph].

[390] C. Hagedorn, J. Herrero-García, E. Molinaro, and M. A. Schmidt, "Phenomenology of the Generalised Scotogenic Model with Fermionic Dark Matter," JHEP **11** (2018) 103, arXiv:1804.04117 [hep-ph].

[391] C. Bonilla, L. M. G. de la Vega, J. M. Lamprea, R. A. Lineros, and E. Peinado, "Fermion Dark Matter and Radiative Neutrino Masses from Spontaneous Lepton Number Breaking," New J. Phys. **22** no. 3, (2020) 033009, arXiv:1908.04276 [hep-ph].

[392] E. Ma, D. Restrepo, and O. Zapata, "Anomalous leptonic U(1) symmetry: Syndetic origin of the QCD axion, weak-scale dark matter, and radiative neutrino mass," Mod. Phys. Lett. **A33** (2018) 1850024, arXiv:1706.08240 [hep-ph].

[393] C. D. R. Carvajal and O. Zapata, "One-loop Dirac neutrino mass and mixed axion-WIMP dark matter," Phys. Rev. **D99** no. 7, (2019) 075009, arXiv:1812.06364 [hep-ph].

[394] L. M. G. de la Vega, N. Nath, and E. Peinado, "Dirac neutrinos from Peccei-Quinn symmetry: two examples," Nucl. Phys. B **957** (2020) 115099, arXiv:2001.01846 [hep-ph].

[395] M. K. Parida, "Radiative Seesaw in SO(10) with Dark Matter," Phys. Lett. **B704** (2011) 206–210, arXiv:1106.4137 [hep-ph].

[396] J. Leite, O. Popov, R. Srivastava, and J. W. F. Valle, "A theory for scotogenic dark matter stabilised by residual gauge symmetry," Phys. Lett. B **802** (2020) 135254, arXiv:1909.06386 [hep-ph].

[397] Z.-L. Han, R. Ding, S.-J. Lin, and B. Zhu, "Gauged $U(1)_{L_\mu - L_\tau}$ scotogenic model in light of $R_{K^{(*)}}$ anomaly and AMS-02 positron excess," Eur. Phys. J. **C79** no. 12, (2019) 1007, arXiv:1908.07192 [hep-ph].

[398] W. Wang and Z.-L. Han, "$U(1)_{B-3L_\alpha}$ extended scotogenic models and single-zero textures of neutrino mass matrices," Phys. Rev. D **101** no. 11, (2020) 115040, arXiv:1911.00819 [hep-ph].

[399] D. Hehn and A. Ibarra, "A radiative model with a naturally mild neutrino mass hierarchy," Phys. Lett. **B718** (2013) 988–991, arXiv:1208.3162 [hep-ph].

[400] J. Fuentes-Martín, M. Reig, and A. Vicente, "Strong CP problem with low-energy emergent QCD: The 4321 case," Phys. Rev. **D100** no. 11, (2019) 115028, arXiv:1907.02550 [hep-ph].

[401] G. Passarino and M. J. G. Veltman, "One Loop Corrections for e+ e- Annihilation Into mu+ mu- in the Weinberg Model," Nucl. Phys. B **160** (1979) 151–207.

[402] A. Merle and M. Platscher, "Parity Problem of the Scotogenic Neutrino Model," Phys. Rev. **D92** no. 9, (2015) 095002, arXiv:1502.03098 [hep-ph].

[403] A. Merle and M. Platscher, "Running of radiative neutrino masses: the scotogenic model - revisited," JHEP **11** (2015) 148, arXiv:1507.06314 [hep-ph].

[404] M. Lindner, M. Platscher, C. E. Yaguna, and A. Merle, "Fermionic WIMPs and vacuum stability in the scotogenic model," Phys. Rev. **D94** no. 11, (2016) 115027, arXiv:1608.00577 [hep-ph].

[405] F. Staub, "SARAH," arXiv:0806.0538 [hep-ph].

[406] F. Staub, "From Superpotential to Model Files for FeynArts and CalcHep/CompHep," Comput. Phys. Commun. **181** (2010) 1077–1086, arXiv:0909.2863 [hep-ph].

[407] F. Staub, "Automatic Calculation of supersymmetric Renormalization Group Equations and Self Energies," Comput. Phys. Commun. **182** (2011) 808–833, arXiv:1002.0840 [hep-ph].

[408] F. Staub, "SARAH 3.2: Dirac Gauginos, UFO output, and more," Comput. Phys. Commun. **184** (2013) 1792–1809, arXiv:1207.0906 [hep-ph].

[409] F. Staub, "SARAH 4 : A tool for (not only SUSY) model builders," Comput. Phys. Commun. **185** (2014) 1773–1790, arXiv:1309.7223 [hep-ph].

[410] A. Vicente, "Computer tools in particle physics," arXiv:1507.06349 [hep-ph].

[411] P. de Salas, D. Forero, C. Ternes, M. Tortola, and J. Valle, "Status of neutrino oscillations 2018: 3σ hint for normal mass ordering and improved CP sensitivity," Phys. Lett. B **782** (2018) 633–640, arXiv:1708.01186 [hep-ph].

[412] D. Portillo-Sánchez, P. Escribano, and A. Vicente, "Ultraviolet extensions of the Scotogenic model," arXiv:2301.05249 [hep-ph].

[413] P. Escribano and A. Vicente, "An ultraviolet completion for the Scotogenic model," Phys. Lett. B **823** (2021) 136717, arXiv:2107.10265 [hep-ph].

[414] J. de Blas, M. Chala, M. Perez-Victoria, and J. Santiago, "Observable Effects of General New Scalar Particles," JHEP **04** (2015) 078, arXiv:1412.8480 [hep-ph].

[415] K. S. Babu and E. Ma, "Singlet fermion dark matter and electroweak baryogenesis with radiative neutrino mass," Int. J. Mod. Phys. A **23** (2008) 1813–1819, arXiv:0708.3790 [hep-ph].

[416] T. Biekötter and M. Pierre, "Higgs-boson visible and invisible constraints on hidden sectors," Eur. Phys. J. C **82** no. 11, (2022) 1026, arXiv:2208.05505 [hep-ph].

[417] L. Lopez Honorez and C. E. Yaguna, "The inert doublet model of dark matter revisited," JHEP **09** (2010) 046, arXiv:1003.3125 [hep-ph].

[418] J. Kubo, E. Ma, and D. Suematsu, "Cold Dark Matter, Radiative Neutrino Mass, $\mu \to e\gamma$, and Neutrinoless Double Beta Decay," Phys. Lett. B **642** (2006) 18–23, arXiv:hep-ph/0604114.

[419] D. Aristizabal Sierra, J. Kubo, D. Restrepo, D. Suematsu, and O. Zapata, "Radiative seesaw: Warm dark matter, collider and lepton flavour violating signals," Phys. Rev. D **79** (2009) 013011, arXiv:0808.3340 [hep-ph].

[420] D. Suematsu, T. Toma, and T. Yoshida, "Reconciliation of CDM abundance and $\mu \to e\gamma$ in a radiative seesaw model," Phys. Rev. D **79** (2009) 093004, arXiv:0903.0287 [hep-ph].

[421] A. Adulpravitchai, M. Lindner, and A. Merle, "Confronting Flavour Symmetries and extended Scalar Sectors with Lepton Flavour Violation Bounds," Phys. Rev. D **80** (2009) 055031, arXiv:0907.2147 [hep-ph].

[422] V. De Romeri, J. Nava, M. Puerta, and A. Vicente, "Dark matter in the scotogenic model with spontaneous lepton number violation," Phys. Rev. D **107** no. 9, (2023) 095019, arXiv:2210.07706 [hep-ph].

[423] R. Cepedello, P. Escribano, and A. Vicente, "Neutrino masses, flavor anomalies, and muon g-2 from dark loops," Phys. Rev. D **107** no. 3, (2023) 035034, arXiv:2209.02730 [hep-ph].

[424] A. Abada, N. Bernal, A. E. Cárcamo Hernández, S. Kovalenko, T. B. de Melo, and T. Toma, "Phenomenological and cosmological implications of a scotogenic three-loop neutrino mass model," JHEP **03** (2023) 035, arXiv:2212.06852 [hep-ph].

[425] A. Abada, P. Escribano, X. Marcano, and G. Piazza, "Collider searches for heavy neutral leptons: beyond simplified scenarios," Eur. Phys. J. C **82** no. 11, (2022) 1030, arXiv:2208.13882 [hep-ph].

[426] P. Agrawal et al., "Feebly-interacting particles: FIPs 2020 workshop report," Eur. Phys. J. C **81** no. 11, (2021) 1015, arXiv:2102.12143 [hep-ph].

[427] A. Pilaftsis, "Radiatively induced neutrino masses and large Higgs neutrino couplings in the standard model with Majorana fields," Z. Phys. C **55** (1992) 275–282, arXiv:hep-ph/9901206.

[428] F. del Águila, J. A. Aguilar-Saavedra, and R. Pittau, "Heavy neutrino signals at large hadron colliders," JHEP **10** (2007) 047, arXiv:hep-ph/0703261 [hep-ph].

[429] F. del Águila and J. A. Aguilar-Saavedra, "Distinguishing seesaw models at LHC with multi-lepton signals," Nucl. Phys. **B813** (2009) 22–90, arXiv:0808.2468 [hep-ph].

[430] F. del Águila and J. A. Aguilar-Saavedra, "Electroweak scale seesaw and heavy Dirac neutrino signals at LHC," Phys. Lett. **B672** (2009) 158–165, arXiv:0809.2096 [hep-ph].

[431] M. Nemevšek, F. Nesti, G. Senjanović, and Y. Zhang, "First Limits on Left-Right Symmetry Scale from LHC Data," Phys. Rev. **D83** (2011) 115014, arXiv:1103.1627 [hep-ph].

[432] P. S. Bhupal Dev, R. Franceschini, and R. N. Mohapatra, "Bounds on TeV Seesaw Models from LHC Higgs Data," Phys. Rev. D **86** (2012) 093010, arXiv:1207.2756 [hep-ph].

[433] C. G. Cely, A. Ibarra, E. Molinaro, and S. T. Petcov, "Higgs Decays in the Low Scale Type I See-Saw Model," Phys. Lett. B **718** (2013) 957–964, arXiv:1208.3654 [hep-ph].

[434] J. C. Helo, M. Hirsch, and S. Kovalenko, "Heavy neutrino searches at the LHC with displaced vertices," Phys. Rev. **D89** (2014) 073005, arXiv:1312.2900 [hep-ph]. [Erratum: Phys. Rev.D93,no.9,099902(2016)].

[435] P. S. B. Dev, A. Pilaftsis, and U.-k. Yang, "New Production Mechanism for Heavy Neutrinos at the LHC," Phys. Rev. Lett. **112** no. 8, (2014) 081801, arXiv:1308.2209 [hep-ph].

[436] A. Das, P. S. Bhupal Dev, and N. Okada, "Direct bounds on electroweak scale pseudo-Dirac neutrinos from $\sqrt{s} = 8$ TeV LHC data," Phys. Lett. **B735** (2014) 364–370, arXiv:1405.0177 [hep-ph].

[437] D. Alva, T. Han, and R. Ruiz, "Heavy Majorana neutrinos from $W\gamma$ fusion at hadron colliders," JHEP **02** (2015) 072, arXiv:1411.7305 [hep-ph].

[438] E. Izaguirre and B. Shuve, "Multilepton and Lepton Jet Probes of Sub-Weak-Scale Right-Handed Neutrinos," Phys. Rev. **D91** no. 9, (2015) 093010, arXiv:1504.02470 [hep-ph].

[439] F. F. Deppisch, P. S. Bhupal Dev, and A. Pilaftsis, "Neutrinos and Collider Physics," New J. Phys. **17** no. 7, (2015) 075019, arXiv:1502.06541 [hep-ph].

[440] A. Maiezza, M. Nemevšek, and F. Nesti, "Lepton Number Violation in Higgs Decay at LHC," Phys. Rev. Lett. **115** (2015) 081802, arXiv:1503.06834 [hep-ph].

[441] S. Banerjee, P. S. B. Dev, A. Ibarra, T. Mandal, and M. Mitra, "Prospects of Heavy Neutrino Searches at Future Lepton Colliders," Phys. Rev. **D92** (2015) 075002, arXiv:1503.05491 [hep-ph].

[442] E. Arganda, M. J. Herrero, X. Marcano, and C. Weiland, "Exotic $\mu\tau$jj events from heavy ISS neutrinos at the LHC," Phys. Lett. B **752** (2016) 46–50, arXiv:1508.05074 [hep-ph].

[443] A. Das and N. Okada, "Improved bounds on the heavy neutrino productions at the LHC," Phys. Rev. **D93** no. 3, (2016) 033003, arXiv:1510.04790 [hep-ph].

[444] A. M. Gago, P. Hernández, J. Jones-Pérez, M. Losada, and A. Moreno Briceño, "Probing the Type I Seesaw Mechanism with Displaced Vertices at the LHC," Eur. Phys. J. C **75** no. 10, (2015) 470, arXiv:1505.05880 [hep-ph].

[445] E. Accomando, L. Delle Rose, S. Moretti, E. Olaiya, and C. H. Shepherd-Themistocleous, "Novel SM-like Higgs decay into displaced heavy neutrino pairs in $U(1)'$ models," JHEP **04** (2017) 081, arXiv:1612.05977 [hep-ph].

[446] C. Degrande, O. Mattelaer, R. Ruiz, and J. Turner, "Fully-Automated Precision Predictions for Heavy Neutrino Production Mechanisms at Hadron Colliders," Phys. Rev. **D94** no. 5, (2016) 053002, arXiv:1602.06957 [hep-ph].

[447] M. Mitra, R. Ruiz, D. J. Scott, and M. Spannowsky, "Neutrino Jets from High-Mass W_R Gauge Bosons in TeV-Scale Left-Right Symmetric Models," Phys. Rev. **D94** no. 9, (2016) 095016, arXiv:1607.03504 [hep-ph].

[448] R. Ruiz, M. Spannowsky, and P. Waite, "Heavy neutrinos from gluon fusion," Phys. Rev. **D96** no. 5, (2017) 055042, arXiv:1706.02298 [hep-ph].

[449] S. Dube, D. Gadkari, and A. M. Thalapillil, "Lepton-Jets and Low-Mass Sterile Neutrinos at Hadron Colliders," Phys. Rev. **D96** no. 5, (2017) 055031, arXiv:1707.00008 [hep-ph].

[450] A. Caputo, P. Hernández, J. López-Pavón, and J. Salvado, "The seesaw portal in testable models of neutrino masses," JHEP **06** (2017) 112, arXiv:1704.08721 [hep-ph].

[451] S. Antusch, E. Cazzato, and O. Fischer, "Sterile neutrino searches via displaced vertices at LHCb," Phys. Lett. **B774** (2017) 114–118, arXiv:1706.05990 [hep-ph].

[452] A. Das, "Pair production of heavy neutrinos in next-to-leading order QCD at the hadron colliders in the inverse seesaw framework," Int. J. Mod. Phys. A **36** no. 04, (2021) 2150012, arXiv:1701.04946 [hep-ph].

[453] A. Das, P. Konar, and A. Thalapillil, "Jet substructure shedding light on heavy Majorana neutrinos at the LHC," JHEP **02** (2018) 083, arXiv:1709.09712 [hep-ph].

[454] F. F. Deppisch, W. Liu, and M. Mitra, "Long-lived Heavy Neutrinos from Higgs Decays," JHEP **08** (2018) 181, arXiv:1804.04075 [hep-ph].

[455] J. Liu, Z. Liu, and L.-T. Wang, "Enhancing Long-Lived Particles Searches at the LHC with Precision Timing Information," Phys. Rev. Lett. **122** no. 13, (2019) 131801, arXiv:1805.05957 [hep-ph].

[456] G. Cottin, J. C. Helo, and M. Hirsch, "Searches for light sterile neutrinos with multitrack displaced vertices," Phys. Rev. **D97** no. 5, (2018) 055025, arXiv:1801.02734 [hep-ph].

[457] G. Cottin, J. C. Helo, and M. Hirsch, "Displaced vertices as probes of sterile neutrino mixing at the LHC," Phys. Rev. **D98** no. 3, (2018) 035012, arXiv:1806.05191 [hep-ph].

[458] C. O. Dib, C. S. Kim, N. A. Neill, and X.-B. Yuan, "Search for sterile neutrinos decaying into pions at the LHC," Phys. Rev. **D97** no. 3, (2018) 035022, arXiv:1801.03624 [hep-ph].

[459] M. Nemevšek, F. Nesti, and G. Popara, "Keung-Senjanović process at the LHC: From lepton number violation to displaced vertices to invisible decays," Phys. Rev. **D97** no. 11, (2018) 115018, arXiv:1801.05813 [hep-ph].

[460] A. Abada, N. Bernal, M. Losada, and X. Marcano, "Inclusive Displaced Vertex Searches for Heavy Neutral Leptons at the LHC," JHEP **01** (2019) 093, arXiv:1807.10024 [hep-ph].

[461] S. Pascoli, R. Ruiz, and C. Weiland, "Safe Jet Vetoes," Phys. Lett. **B786** (2018) 106, arXiv:1805.09335 [hep-ph].

[462] S. Antusch, E. Cazzato, O. Fischer, A. Hammad, and K. Wang, "Lepton Flavor Violating Dilepton Dijet Signatures from Sterile Neutrinos at Proton Colliders," JHEP **10** (2018) 067, arXiv:1805.11400 [hep-ph].

[463] S. Pascoli, R. Ruiz, and C. Weiland, "Heavy neutrinos with dynamic jet vetoes: multilepton searches at $\sqrt{s} = 14$, 27, and 100 TeV," JHEP **06** (2019) 049, arXiv:1812.08750 [hep-ph].

[464] M. Drewes and J. Hajer, "Heavy Neutrinos in displaced vertex searches at the LHC and HL-LHC," JHEP **02** (2020) 070, arXiv:1903.06100 [hep-ph].

[465] J. Liu, Z. Liu, L.-T. Wang, and X.-P. Wang, "Seeking for sterile neutrinos with displaced leptons at the LHC," JHEP **07** (2019) 159, arXiv:1904.01020 [hep-ph].

[466] J. Jones-Pérez, J. Masias, and J. D. Ruiz-Álvarez, "Search for Long-Lived Heavy Neutrinos at the LHC with a VBF Trigger," Eur. Phys. J. C **80** no. 7, (2020) 642, arXiv:1912.08206 [hep-ph].

[467] B. Fuks, J. Neundorf, K. Peters, R. Ruiz, and M. Saimpert, "Majorana neutrinos in same-sign $W^{\pm}W^{\pm}$ scattering at the LHC: Breaking the TeV barrier," Phys. Rev. D **103** no. 5, (2021) 055005, arXiv:2011.02547 [hep-ph].

[468] J.-L. Tastet, O. Ruchayskiy, and I. Timiryasov, "Reinterpreting the ATLAS bounds on heavy neutral leptons in a realistic neutrino oscillation model," JHEP **12** (2021) 182, arXiv:2107.12980 [hep-ph].

[469] **LHC Reinterpretation Forum** Collaboration, W. Abdallah et al., "Reinterpretation of LHC Results for New Physics: Status and Recommendations after Run 2," SciPost Phys. **9** no. 2, (2020) 022, arXiv:2003.07868 [hep-ph].

[470] A. Ibarra and G. G. Ross, "Neutrino phenomenology: The Case of two right-handed neutrinos," Phys. Lett. B **591** (2004) 285–296, arXiv:hep-ph/0312138.

[471] M. Drewes, J. Klarić, and J. López-Pavón, "New benchmark models for heavy neutral lepton searches," Eur. Phys. J. C **82** no. 12, (2022) 1176, arXiv:2207.02742 [hep-ph].

[472] A. Das, P. S. B. Dev, and R. N. Mohapatra, "Same Sign versus Opposite Sign Dileptons as a Probe of Low Scale Seesaw Mechanisms," Phys. Rev. D **97** no. 1, (2018) 015018, arXiv:1709.06553 [hep-ph].

[473] A. Abada, C. Hati, X. Marcano, and A. M. Teixeira, "Interference effects in LNV and LFV semileptonic decays: the Majorana hypothesis," JHEP **09** (2019) 017, arXiv:1904.05367 [hep-ph].

[474] F. Najafi, J. Kumar, and D. London, "CP violation in rare lepton-number-violating W decays at the LHC," JHEP **04** (2021) 021, arXiv:2011.03686 [hep-ph].

[475] A. Atre, T. Han, S. Pascoli, and B. Zhang, "The Search for Heavy Majorana Neutrinos," JHEP **05** (2009) 030, arXiv:0901.3589 [hep-ph].

[476] A. Abada, V. De Romeri, M. Lucente, A. M. Teixeira, and T. Toma, "Effective Majorana mass matrix from tau and pseudoscalar meson lepton number violating decays," JHEP **02** (2018) 169, arXiv:1712.03984 [hep-ph].

[477] P. D. Bolton, F. F. Deppisch, and P. S. Bhupal Dev, "Neutrinoless double beta decay versus other probes of heavy sterile neutrinos," JHEP **03** (2020) 170, arXiv:1912.03058 [hep-ph].

[478] Y. Cai, T. Han, T. Li, and R. Ruiz, "Lepton Number Violation: Seesaw Models and Their Collider Tests," Front. in Phys. **6** (2018) 40, arXiv:1711.02180 [hep-ph].

[479] **nu-Test** Collaboration, B. Batell, T. Ghosh, T. Han, and K. Xie, "Heavy Neutral Lepton Searches at the Electron-Ion Collider: A Snowmass Whitepaper," in Snowmass 2021. 3, 2022. arXiv:2203.06705 [hep-ph].

[480] A. M. Abdullahi et al., "The Present and Future Status of Heavy Neutral Leptons," in 2022 Snowmass Summer Study. 3, 2022. arXiv:2203.08039 [hep-ph].

[481] **CMS** Collaboration, A. M. Sirunyan et al., "Search for heavy Majorana neutrinos in same-sign dilepton channels in proton-proton collisions at $\sqrt{s} = 13$ TeV," JHEP **01** (2019) 122, arXiv:1806.10905 [hep-ex].

[482] S. Antusch, E. Cazzato, and O. Fischer, "Sterile neutrino searches at future e^-e^+, pp, and e^-p colliders," Int. J. Mod. Phys. A **32** no. 14, (2017) 1750078, arXiv:1612.02728 [hep-ph].

[483] **ATLAS** Collaboration, G. Aad et al., "Inclusive search for same-sign dilepton signatures in pp collisions at $\sqrt{s} = 7$ TeV with the ATLAS detector," JHEP **10** (2011) 107, arXiv:1108.0366 [hep-ex].

[484] **ATLAS** Collaboration, G. Aad et al., "Search for heavy neutrinos and right-handed W bosons in events with two leptons and jets in pp collisions at $\sqrt{s} = 7$ TeV with the ATLAS detector," Eur. Phys. J. C **72** (2012) 2056, arXiv:1203.5420 [hep-ex].

[485] **CMS** Collaboration, S. Chatrchyan et al., "Search for Heavy Neutrinos and W_R Bosons with Right-Handed Couplings in a Left-Right Symmetric Model in pp Collisions at $\sqrt{s} =$ 7 TeV," Phys. Rev. Lett. **109** (2012) 261802, arXiv:1210.2402 [hep-ex].

[486] **CMS** Collaboration, V. Khachatryan et al., "Search for Heavy Neutrinos and W Bosons with Right-Handed Couplings in Proton-Proton Collisions at $\sqrt{s} = 8$ TeV," Eur. Phys. J. C **74** no. 11, (2014) 3149, arXiv:1407.3683 [hep-ex].

[487] **CMS** Collaboration, A. M. Sirunyan et al., "Search for a heavy right-handed W boson and a heavy neutrino in events with two same-flavor leptons and two jets at $\sqrt{s} = 13$ TeV," JHEP **05** (2018) 148, arXiv:1803.11116 [hep-ex].

[488] **ATLAS** Collaboration, M. Aaboud et al., "Search for heavy Majorana or Dirac neutrinos and right-handed W gauge bosons in final states with two charged leptons and two jets at $\sqrt{s} = 13$ TeV with the ATLAS detector," JHEP **01** (2019) 016, arXiv:1809.11105 [hep-ex].

[489] **CMS** Collaboration, A. M. Sirunyan et al., "Search for heavy neutrinos and third-generation leptoquarks in hadronic states of two τ leptons and two jets in proton-proton collisions at $\sqrt{s} = 13$ TeV," JHEP **03** (2019) 170, arXiv:1811.00806 [hep-ex].

[490] **ATLAS** Collaboration, M. Aaboud et al., "Search for a right-handed gauge boson decaying into a high-momentum heavy neutrino and a charged lepton in pp collisions with the ATLAS detector at $\sqrt{s} = 13$ TeV," Phys. Lett. B **798** (2019) 134942, arXiv:1904.12679 [hep-ex].

[491] K. Moffat, S. Pascoli, and C. Weiland, "Equivalence between massless neutrinos and lepton number conservation in fermionic singlet extensions of the Standard Model," arXiv:1712.07611 [hep-ph].

[492] G. Anamiati, M. Hirsch, and E. Nardi, "Quasi-Dirac neutrinos at the LHC," JHEP **10** (2016) 010, arXiv:1607.05641 [hep-ph].

[493] S. Antusch, E. Cazzato, and O. Fischer, "Resolvable heavy neutrino–antineutrino oscillations at colliders," Mod. Phys. Lett. A **34** no. 07n08, (2019) 1950061, arXiv:1709.03797 [hep-ph].

[494] M. Drewes, J. Klarić, and P. Klose, "On lepton number violation in heavy neutrino decays at colliders," JHEP **11** (2019) 032, arXiv:1907.13034 [hep-ph].

[495] E. Fernández-Martínez, X. Marcano, and D. Naredo-Tuero, "HNL mass degeneracy: implications for low-scale seesaws, LNV at colliders and leptogenesis," JHEP **03** (2023) 057, arXiv:2209.04461 [hep-ph].

[496] **LHCb** Collaboration, R. Aaij et al., "Search for heavy neutral leptons in $W^+ \to \mu^+\mu^\pm$jet decays," Eur. Phys. J. C **81** no. 3, (2021) 248, arXiv:2011.05263 [hep-ex].

[497] **ATLAS** Collaboration, G. Aad et al., "Search for heavy neutral leptons in decays of W bosons produced in 13 TeV pp collisions using prompt and displaced signatures with the ATLAS detector," JHEP **10** (2019) 265, arXiv:1905.09787 [hep-ex].

[498] **ATLAS** Collaboration, "Search for heavy neutral leptons in decays of W bosons using a dilepton displaced vertex in $\sqrt{s} = 13$ TeV pp collisions with the ATLAS detector," arXiv:2204.11988 [hep-ex].

[499] **CMS** Collaboration, A. Tumasyan et al., "Search for long-lived heavy neutral leptons with displaced vertices in proton-proton collisions at $\sqrt{s}$ =13 TeV," JHEP **07** (2022) 081, arXiv:2201.05578 [hep-ex].

[500] **CMS** Collaboration, S. Chatrchyan et al., "Search for heavy Majorana Neutrinos in $\mu^\pm\mu^\pm$+ Jets and $e^\pm e^\pm$+ Jets Events in pp Collisions at $\sqrt{s} = 7$ TeV," Phys. Lett. B **717** (2012) 109–128, arXiv:1207.6079 [hep-ex].

[501] **CMS** Collaboration, V. Khachatryan et al., "Search for heavy Majorana neutrinos in $\mu^\pm\mu^\pm$+ jets events in proton-proton collisions at $\sqrt{s} = 8$ TeV," Phys. Lett. B **748** (2015) 144–166, arXiv:1501.05566 [hep-ex].

[502] **CMS** Collaboration, V. Khachatryan et al., "Search for heavy Majorana neutrinos in $e^\pm e^\pm$+ jets and $e^\pm$ $\mu^\pm$+ jets events in proton-proton collisions at $\sqrt{s} = 8$ TeV," JHEP **04** (2016) 169, arXiv:1603.02248 [hep-ex].

[503] **ATLAS** Collaboration, G. Aad et al., "Search for heavy Majorana neutrinos with the ATLAS detector in pp collisions at $\sqrt{s} = 8$ TeV," JHEP **07** (2015) 162, arXiv:1506.06020 [hep-ex].

[504] **CMS** Collaboration, A. M. Sirunyan et al., "Search for heavy neutral leptons in events with three charged leptons in proton-proton collisions at $\sqrt{s} = 13$ TeV," Phys. Rev. Lett. **120** no. 22, (2018) 221801, arXiv:1802.02965 [hep-ex].

[505] E. Fernandez-Martinez, J. Hernandez-Garcia, and J. Lopez-Pavon, "Global constraints on heavy neutrino mixing," JHEP **08** (2016) 033, arXiv:1605.08774 [hep-ph].

[506] **FCC-ee study Team** Collaboration, A. Blondel, E. Graverini, N. Serra, and M. Shaposhnikov, "Search for Heavy Right Handed Neutrinos at the FCC-ee," Nucl. Part. Phys. Proc. **273-275** (2016) 1883–1890, arXiv:1411.5230 [hep-ex].

[507] **DELPHI** Collaboration, P. Abreu et al., "Search for neutral heavy leptons produced in Z decays," Z. Phys. C **74** (1997) 57–71. [Erratum: Z.Phys.C 75, 580 (1997)].

[508] **L3** Collaboration, P. Achard et al., "Search for heavy isosinglet neutrino in e^+e^- annihilation at LEP," Phys. Lett. B **517** (2001) 67–74, arXiv:hep-ex/0107014.

[509] K. Bondarenko, A. Boyarsky, D. Gorbunov, and O. Ruchayskiy, "Phenomenology of GeV-scale Heavy Neutral Leptons," JHEP **11** (2018) 032, arXiv:1805.08567 [hep-ph].

[510] A. Ibarra, E. Molinaro, and S. T. Petcov, "TeV Scale See-Saw Mechanisms of Neutrino Mass Generation, the Majorana Nature of the Heavy Singlet Neutrinos and $(\beta\beta)_{0\nu}$-Decay," JHEP **09** (2010) 108, arXiv:1007.2378 [hep-ph].

[511] A. Pilaftsis and T. E. J. Underwood, "Resonant leptogenesis," Nucl. Phys. B **692** (2004) 303–345, arXiv:hep-ph/0309342.

[512] E. K. Akhmedov, V. A. Rubakov, and A. Y. Smirnov, "Baryogenesis via neutrino oscillations," Phys. Rev. Lett. **81** (1998) 1359–1362, arXiv:hep-ph/9803255.

[513] S. Braß, W. Kilian, T. Ohl, J. Reuter, V. Rothe, and P. Stienemeier, "Precision Monte Carlo simulations with WHIZARD," CERN Yellow Reports: Monographs **3** (2020) 205–210.

[514] K. Kannike, "Vacuum Stability of a General Scalar Potential of a Few Fields," Eur. Phys. J. C **76** no. 6, (2016) 324, arXiv:1603.02680 [hep-ph]. [Erratum: Eur.Phys.J.C 78, 355 (2018)].

[515] I. P. Ivanov, M. Köpke, and M. Mühlleitner, "Algorithmic Boundedness-From-Below Conditions for Generic Scalar Potentials," Eur. Phys. J. **C78** no. 5, (2018) 413, arXiv:1802.07976 [hep-ph].

[516] K. Kannike, "Vacuum Stability Conditions From Copositivity Criteria," Eur. Phys. J. **C72** (2012) 2093, arXiv:1205.3781 [hep-ph].

[517] W. Kaplan, "A test for copositive matrices," Linear Algebra and its Applications **313** no. 1, (2000) 203 – 206.

[518] S.-j. Yang and X.-x. Li, "Algorithms for determining the copositivity of a given symmetric matrix," Linear Algebra and its Applications **430** no. 2, (2009) 609 – 618.

[519] S.-J. Yang, C.-Q. Xu, and X.-X. Li, "A note on algorithms for determining the copositivity of a given symmetric matrix," Journal of Inequalities and Applications **2010** (2009) 498631.

[520] F. S. Faro and I. P. Ivanov, "Boundedness from below in the $U(1) \times U(1)$ three-Higgs-doublet model," Phys. Rev. **D100** no. 3, (2019) 035038, arXiv:1907.01963 [hep-ph].

[521] G. R. Farrar and P. Fayet, "Phenomenology of the Production, Decay, and Detection of New Hadronic States Associated with Supersymmetry," Phys. Lett. B **76** (1978) 575–579.

[522] V. Shtabovenko, R. Mertig, and F. Orellana, "New Developments in FeynCalc 9.0," Comput. Phys. Commun. **207** (2016) 432–444, arXiv:1601.01167 [hep-ph].